



# Hydrothermalisme fossile dans une paléocroûte océanique associée à un centre d'expansion lent: Le complexe ophiolitique de Trinity (N. Californie, U.S.A).

Christophe Lécuyer

## ► To cite this version:

Christophe Lécuyer. Hydrothermalisme fossile dans une paléocroûte océanique associée à un centre d'expansion lent: Le complexe ophiolitique de Trinity (N. Californie, U.S.A).. Géochimie. Université Rennes 1, 1989. Français. NNT: . tel-00655957

**HAL Id: tel-00655957**

**<https://theses.hal.science/tel-00655957>**

Submitted on 3 Jan 2012

**HAL** is a multi-disciplinary open access archive for the deposit and dissemination of scientific research documents, whether they are published or not. The documents may come from teaching and research institutions in France or abroad, or from public or private research centers.

L'archive ouverte pluridisciplinaire **HAL**, est destinée au dépôt et à la diffusion de documents scientifiques de niveau recherche, publiés ou non, émanant des établissements d'enseignement et de recherche français ou étrangers, des laboratoires publics ou privés.



C. LECUYER

ISSN 0755-978X

ISBN 2-905532-32-7

hydrothermalisme fossile  
dans une paléocroûte océanique  
associée à un centre  
d'expansion lent :

LE COMPLEXE OPHIOLITIQUE  
DE TRINITY  
(N. CALIFORNIE, U.S.A.)

MEMOIRES ET DOCUMENTS

*du Centre Armoricaïn*

*d'Etude Structurale*

*des Socles*

n° 33

Rennes 1990





**MEMOIRES ET DOCUMENTS  
DU  
CENTRE ARMORICAIN D'ETUDE STRUCTURALE DES SOCLES**

**N°33**

**C. LECUYER**

**Hydrothermalisme fossile dans une paléocroûte océanique  
associée à un centre d'expansion lent :  
Le complexe ophiolitique de Trinity (N. Californie, U.S.A).**

**Thèse de l'Université de Rennes I  
soutenue le 21 Avril 1989.**

**Centre Armoricaïn d'Etude Structurale des Socles  
LP CNRS n°4661  
Université de Rennes I  
Campus de Beaulieu  
F-35042 - RENNES Cédex  
(France)**

**1989**





**ISSN : 0755-978 X**

**ISBN : 2-905532-32-7**

**1990**

**Centre Armoricaïn d'Etude Structurale des Socles  
LP CNRS n°4661  
Université de Rennes I - Campus de Beaulieu  
F-35042 - RENNES Cédex (France)**

**C. LECUYER (1989)**

**Hydrothermalisme fossile dans une paléocroûte océanique  
associée à un centre d'expansion lent :  
Le complexe ophiolitique de Trinity (N. Californie, U.S.A).**

**Mém. Docum. Centre Arm. Et. Struct. Socles, Rennes, 33 ; 342 p.**



**Je remercie, ici, les membres du Jury qui ont accepté de juger ce travail...**

**"Ayant bien vu, revu, lu, relu, paperassé et feuilleté les plaintes, ajournements, comparutions, commissions, informations, avant-procédés, productions, allégations, interdits, contredits, requêtes, enquêtes, répliques, dupliques, tripliques, écritures, reproches, griefs, salvations, récolements, confrontations, acarations, libelles, apostoles, lettres royaux, compulsoires, déclinatoires, anticipatoires, évocations, envois, renvois, conclusions, fins de non procéder, appointements, reliefs, confessions, exploits et autres telles dragées et épiceries d'une part et d'autre, comme doit faire le bon juge..."**

**Rabelais, Tiers Livre (1542)**





## **TABLE DES MATIERES**

### **INTRODUCTION - CHAPITRE 1.**

#### **1.1. Présentation du sujet.**

##### **1.1.A. Travaux antérieurs.**

##### **1.1.B. Objectifs.**

#### **1.2. Techniques analytiques.**

##### **1.2.A. Analyses des phases minérales.**

##### **1.2.B. Analyses chimiques roches totales (majeurs et traces).**

##### **1.2.C. Analyses isotopiques.**

###### **1.2.C.a. Analyses isotopiques du Sr et du Nd.**

###### **1.2.C.b. Analyses isotopiques de l'O et du C.**

#### **1.3. Cadre géologique.**

Article : Lecuyer C., Lapierre H. et Charvet J. 1989. Un exemple de collision îles océaniques - marge continentale active : les séries volcano-sédimentaires d'Yreka-Callahan (Nord Californie). Soumis aux C. R. Acad. Sci. Paris.

Article : Brouxel M., Lecuyer C. and Lapierre H. 1989. Diversity of magma types in a Lower Paleozoic island-arc marginal basin system. Accepté à Chem. Geol.

Article : Rouer O., Lecuyer C., Lapierre H., Charvet J., Coulon C. and Martin P. 1989. Significance of the Upper Paleozoic magmas from northern California and eastern Oregon in the geodynamic evolution of the Cordillera. Soumis à Geol. Soc. Am. Bull.

### **Bibliographie chapitre 1.**

### **CHAPITRE 2 - STRUCTURES ET MAGMATISMES.**

#### **2.1. Rappels.**

#### **2.2. Buts de l'étude.**

#### **2.3. La chambre magmatique de Toad Lake.**

##### **2.3.A. Géologie.**

###### **2.3.A.a. Les péridotites.**

###### **2.3.A.b. Les gabbros.**

###### **2.3.A.c. Les filons.**

###### **2.3.A.d. La chambre magmatique.**

###### **2.3.A.e. Les relations péridotites - gabbros.**

### **2.3.B. Pétrographie et Minéralogie.**

#### **2.3.B.a Les péridotites.**

#### **2.3.B.b. Les cumulats.**

#### **2.3.B.c. Les filons dans les péridotites.**

#### **2.3.B.d. Les filons dans les gabbros.**

### **2.3.C. Géochimie.**

#### **2.3.C.a. Fusion partielle et phénomènes d'imprégnation magmatique dans le manteau.**

#### **2.3.C.b. Comparaison avec les péridotites modernes : rôle du site géotectonique.**

#### **2.3.C.c. Les filons : marqueurs de l'évolution chimique du magma dans la chambre.**

- évolution des éléments majeurs et traces.
- discussion des modèles de cristallisation des magmas.

### **2.4. La chambre magmatique de Castle Lake.**

#### **2.4.A. Géologie.**

##### **2.4.A.a. Les péridotites déformées.**

##### **2.4.A.b. L'unité bréchique de base.**

##### **2.4.A.c. L'unité gabbroïque supérieure.**

#### **2.4.B. Pétrographie et Minéralogie.**

##### **2.4.B.a. L'unité bréchique basale.**

##### **2.4.B.b. L'unité gabbroïque supérieure.**

- les gabbros lités.
- les gabbros isotropes.

#### **2.4.C. Géochimie.**

##### **2.4.C.a. L'unité bréchique basale.**

##### **2.4.C.b. Comparaison des compositions chimiques des cumulats et liquides constituant les chambres magmatiques (Gray Rock et Toad Lake) de l'ophiolite de Trinity.**

Article : Lecuyer C., Brouxel M. and Lapierre H. 1989. Petrogenesis of magmas at a fossil slow-spreading center: The Lower Paleozoic Trinity ophiolite. Soumis à Contrib. Mineral. Petrol.

Article : Lecuyer C. 1989. Chemical transfer between ultrabasic xenoliths and basic magmas : evidence from oceanic magma chambers (the Trinity ophiolite, N. California). Soumis à Lithos.

Bibliographie chapitre 2.



## **CHAPITRE 3 - L'HYDROTHERMALISME OCEANIQUE. PREMIERE PARTIE (A).**

### **3.A. L'hydrothermalisme océanique.**

#### **3.A.1. Généralités.**

#### **3.A.2. Bilans géochimiques entre la croûte océanique et l'hydrosphère : les flux élémentaires.**

#### **3.A.3 L'altération basse-température des basaltes du plancher océanique.**

#### **3.A.4. Deux cas typiques de problème de bilan : le potassium et le magnésium.**

##### **3.A.4.a. Le potassium.**

##### **3.A.4.b. Le magnésium.**

#### **3.A.5. Buts de l'étude.**

#### **3.A.6. Résultats.**

## **DEUXIEME PARTIE**

### **3.B. L'hydrothermalisme océanique fossile dans l'ophiolite de Trinity Etude isotopique de l'oxygène et du carbone.**

#### **3.B.1. Rappels.**

#### **3.B.2. Buts de l'étude.**

#### **3.B.3. Comparaison de l'activité hydrothermale fossile entre un arc insulaire et un bassin océanique.**

#### **3.B.4. Les volcanites d'arcs insulaires et les roches ophiolitiques de Trinity.**

Article : Lecuyer C., Brouxel M. and Albarède F. 1989. Elemental fluxes during the hydrothermal alteration of the Trinity ophiolite (California) by seawater. Soumis à Chem. Geol.

Article : Lecuyer C. and Fourcade S. 1989. A complex history of hydrothermal alteration recorded by an ophiolitic sequence : the Trinity ophiolite. Evidence from oxygen isotopes and major elemental fluxes. Soumis à Contrib. Mineral. Petrol.

Bibliographie chapitre 3.

Conclusions générales.

Planches photos.

Remerciements.



## INTRODUCTION - CHAPITRE 1.

### I. 1. Présentation du sujet.

#### I. 1. A. Travaux antérieurs.

La première partie de ce mémoire est consacrée à l'étude du complexe ophiolitique de Trinity.

Les premiers travaux de cartographie ont été réalisés par Strand (1962; 1963), Irwin (1977) et Wagner et Saucedo (1986) mais restaient néanmoins insuffisants pour préciser les relations géométriques entre les chambres magmatiques et les péridotites mantellaires. Quick (1981) a étudié l'unité mantellaire qui a subi une histoire de déformation plastique à haute température et de fusion partielle dans un environnement analogue à celui des arcs insulaires modernes ou de bassin d'arrière-arc. Les études de la déformation dans les péridotites mantellaires (Le Sueur et al., 1984; Boudier et Nicolas, 1985-86; Cannat et Boudier, 1986; Le Sueur et Boudier, 1986) suggèrent un environnement de ride à expansion lente dans un domaine de type Mer Rouge. Le complexe ophiolitique de Trinity a été défini la première fois par Lindsley-Griffin (1977) dans la région de Lovers Leap (figure 1.1) qui correspond en fait à une unité volcano-sédimentaire d'âge ordovicien (séries d'Yreka-Callahan) recoupée par des essaims de filons Jurassique ( $149 \pm 6$  Ma par K-Ar; Brouxel, 1987) de nature calco-alcaline, chevauchant la péridotite de Trinity.

Les nouvelles données apportées par Le Sueur et al. (1984); Le Sueur et Boudier (1986) et par Brouxel et Lapierre (1984) ont permis de redéfinir l'ophiolite de Trinity comme une séquence ophiolitique complète mais de faible puissance (2 à 3Km). Les caractères pétrographiques et géochimiques de l'ensemble effusif et hypabyssal ont été étudiés en détail dans la thèse d'Université de M. Brouxel (1987) et ont donné lieu à une série de publications (Brouxel et Lapierre, 1984; 1985; Lapierre et al., 1987; Brouxel et Lapierre, 1988). Ainsi ces auteurs proposent que les séries d'arcs insulaires du Paléozoïque inférieur des Klamath orientales (Copley et Balaklala) ainsi que le cortège ophiolitique siluro-ordovicien de Trinity appartiennent à un même système arc insulaire - bassin marginal intra-océanique qui a fonctionné entre l'Ordovicien et le Dévonien inférieur.

#### I.1.B. Objectifs.

##### I.1.B.a Le complexe ophiolitique de Trinity.

Le complexe ophiolitique de Trinity offre sur le terrain une séquence crustale océanique complète associée à une vaste nappe de péridotites mantellaires. Cet objet géologique offre l'opportunité de caractériser :

1) Les relations pétrologiques et structurales entre l'unité crustale et mantellique permettant de définir la géométrie des chambres magmatiques.

2) Les bilans géochimiques invoqués au cours des processus magmatiques responsables de la genèse et de l'évolution de ces chambres magmatiques. Les marqueurs utilisés sont les phases minérales primaires et les éléments chimiques peu ou prou affectés par les processus d'altération au sens large.

3) Les bilans géochimiques invoqués au cours des processus métamorphiques et principalement l'hydrothermalisme océanique qui peut être ainsi étudié sur une séquence crustale complète. La connaissance du bilan géochimique qui s'établit au cours de l'interaction entre l'océan et la croûte océanique permet ainsi de connaître la nature et la participation des éléments chimiques recyclés dans la croûte continentale via la subduction de la croûte océanique altérée.

La caractérisation du métamorphisme passe par la reconnaissance et l'étude des différentes paragénèses minérales qui renseignent sur la température, la pression et la composition chimique du système considéré à un temps donné. Les marqueurs géochimiques utilisés sont d'abord les éléments majeurs qui vont permettre de quantifier leur mobilité, les isotopes radiogéniques du Sr et les isotopes stables de l'oxygène et du carbone



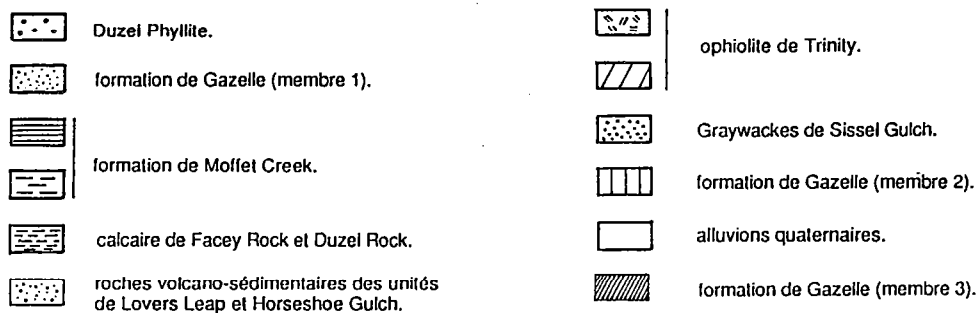
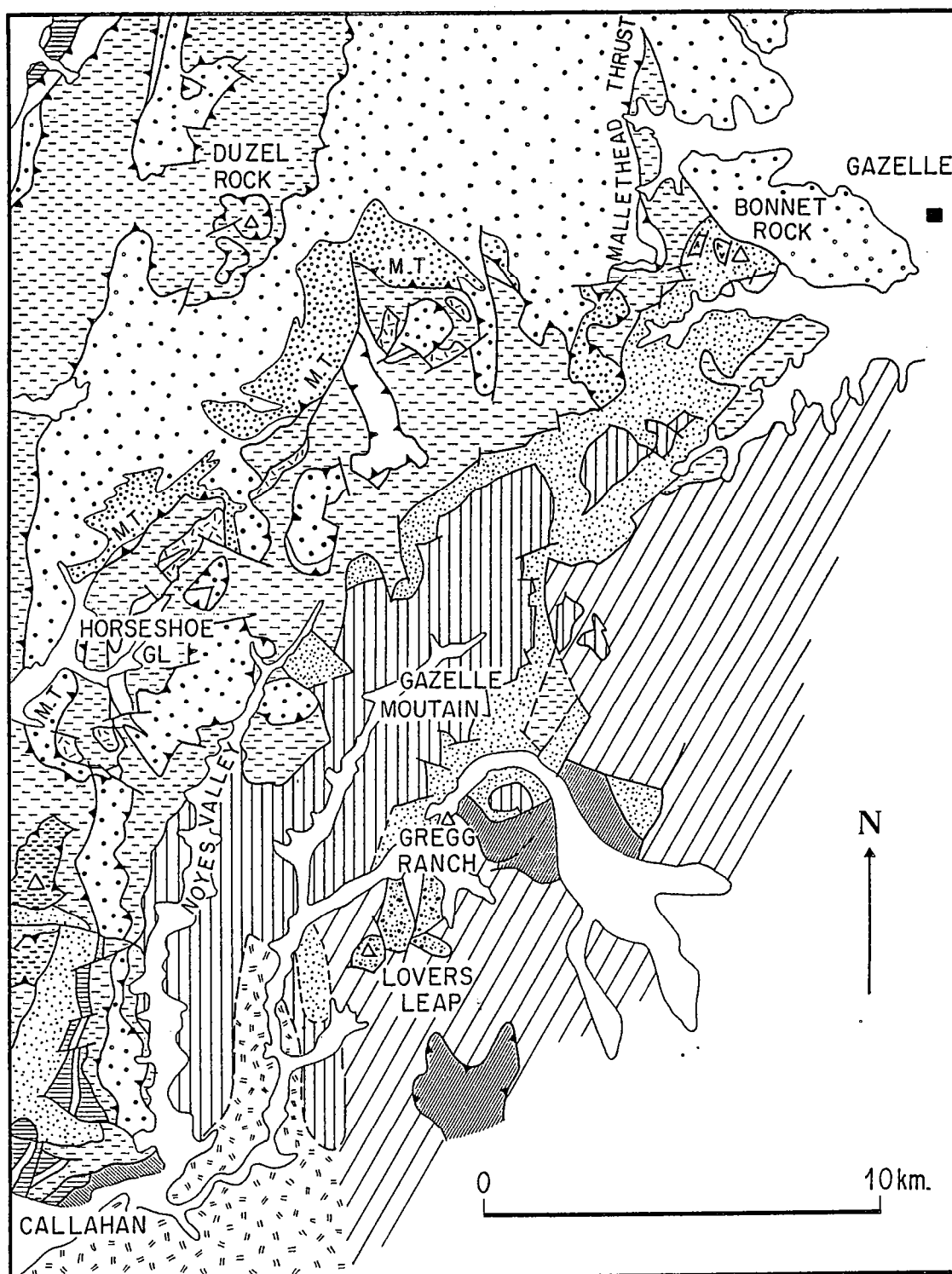
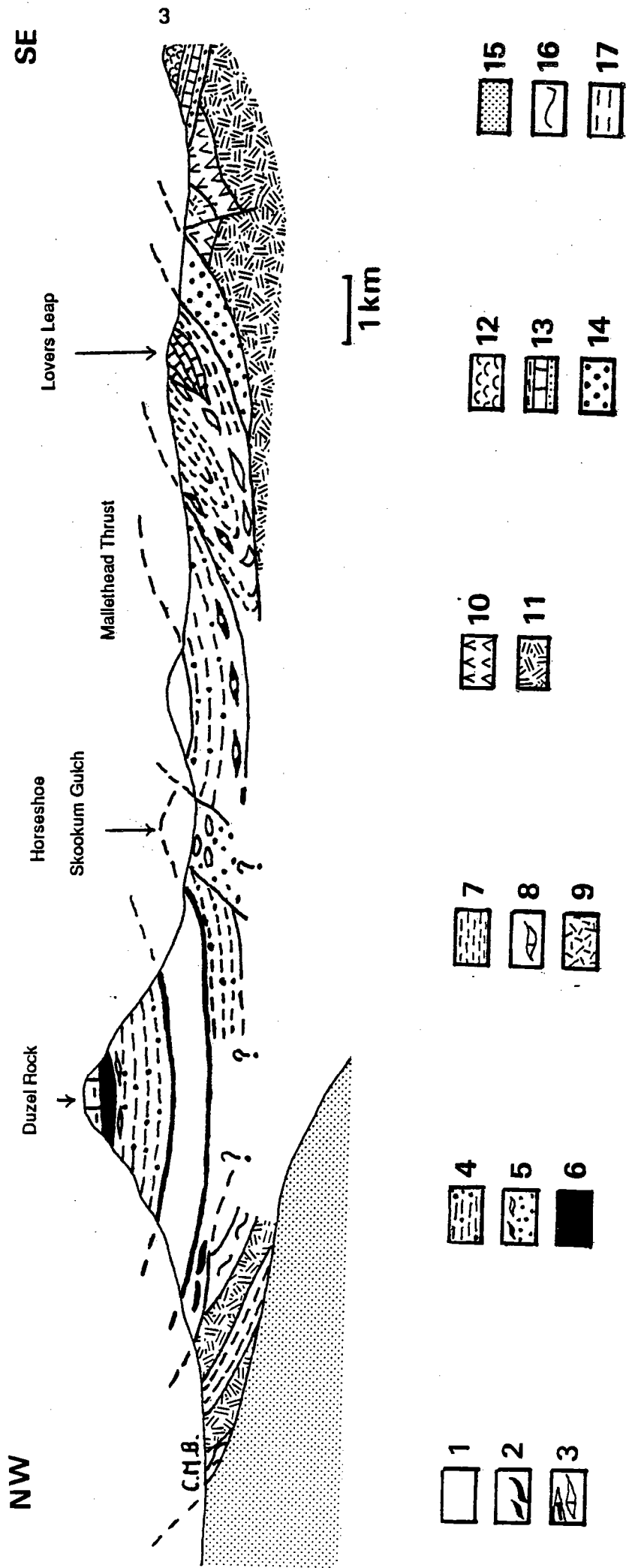


figure 1.1 : carte géologique de la région d'Yreka-Callahan (Klamath orientales)  
d'après Potter et al. (1977).

Figure 1.1 : Coupe schématique des écaïles d'Yreka-Calahan. Assemblage d'Yreka (Silurien) : (1) Phyllades de Duzel, quartzites d'Antelope; (2) Schulmeyer olistostrome. Formation de Moffett Creek (Silurien?) : olistolithes (Facey-Duzel Rock); (4) mudstones, grès; (5) olistostrome (Horseshoe et Skookum Gulch); (6) volcanites. Formation de Gazelle (Emsien) : (7) grès fins, mudstones; (8) olistolithes (Lovers Leap, Bonnett Rock, Callahan Chert). Ophiolite de Trinity (Silurien) : (9) gabbros; (10) tectonite ultramafique. Séquence de Gregg Ranch (post-emsien) : (12) basaltes en coussins; (13) calcaire et grès; (14) volcanites de Copley (anté-Dévonien à Dévonien basal). (15) Schistes bleus triasiques de Stuart Fork. Roches métamorphiques dévoniennes : (16) amphibolites; (17) schistes, marbres.

D'après Campos (1988) et Charvet et al. (1988).



qui fournissent des informations sur les rapports eau-roche (rapports massiques intégrés sur le temps), la température d'interaction et la composition isotopique de l'eau de mer initiale.

Le modèle ainsi établi peut-être comparé aux données acquises récemment dans les dorsales médio-océaniques comme la ride Pacifique Est ou la ride Médio-Atlantique (nature des roches hydrothermalisées et composition chimique des eaux chaudes hydrothermales).

Le but de cette première partie est de caractériser les bilans géochimiques enregistrés par une croûte océanique fossile créée dans un site géotectonique particulier (environnement de ride à expansion lente et croûte océanique mince).

Les différentes démarches suivies au cours de cette étude sont résumées dans la figure suivante (figure 1.2) :

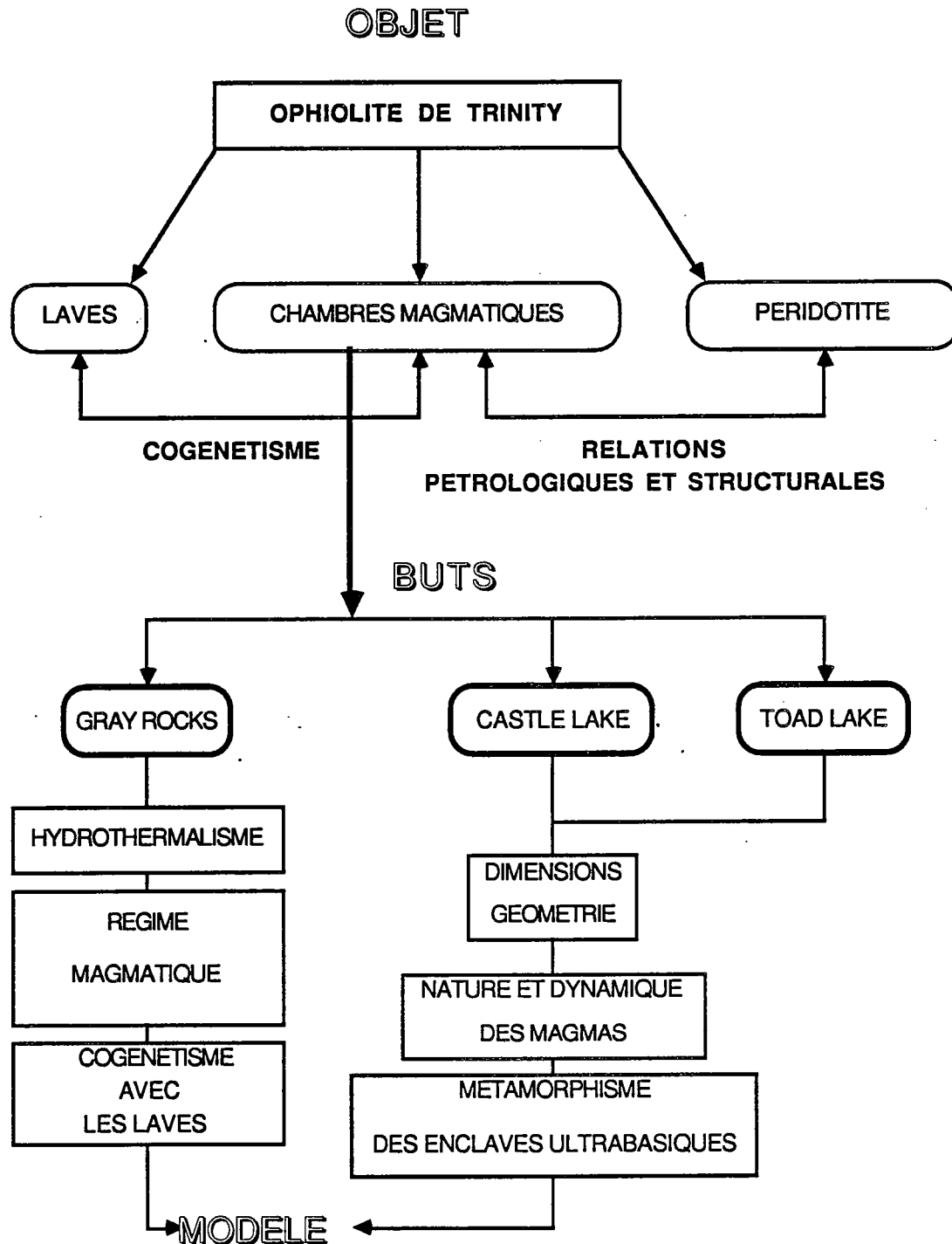


Figure 1.2



## 1.2. Techniques analytiques.

### 1.2.A Analyses des phases minérales.

Les analyses des phases minérales primaires et métamorphiques du cortège ophiolitique de Trinity (tableaux annexes et des séries volcano-sédimentaires de Yreka-Callahan (tableaux annexes) ont été répertoriées par phase minérale dans les annexes. La plupart des analyses ont été effectuées à la microsonde automatisée Camebax des Services Communs des Sciences de la Terre de Nancy I. Des analyses complémentaires ont été effectuées au Museum d'Histoire naturelle de Paris et des Services Communs B.R.G.M. - Université d'Orléans. Enfin, les minéraux mafiques des gabbros et pyroxénites pegmatitiques du complexe ophiolitique de Trinity ont été séparés à la main, nettoyés (ultrasons et HCL dilué) puis analysés (éléments majeurs et dosage du  $\text{Fe}^{2+}$  aux Services Communs des Sciences de la Terre de Nancy et les terres rares par dilution isotopique par Marc Brouxel au Centre de Recherches Péetrographiques et Géochimiques de Nancy).

#### Conditions analytiques de la microsonde CAMEBAX de l'Université de Nancy I :

*Courant échantillon* : 10A.

*Tension accélération* : 15kv.

*Temps d'analyse* : 6sec. par couples de trois éléments. Le temps a été porté à 20sec. pour les analyses de clinopyroxène des séries volcano-sédimentaires d'Yreka-Callahan.

*Taille du faisceau* : 2 à 3 $\mu\text{m}$

*Programme de correction* : MBXCOR (Henoc et Tong, 1978).

Les spectromètres utilisés sont :

LIF : fluorure de lithium, domaine d'analyse pour les raies K du Sc au Sr :

Fe K, Mn K, NiK

PET : penta érythriol :  $\text{C}_5\text{H}_{12}\text{O}_4$ , domaine d'analyse pour les raies K du Si au Fe :

Ti K, Ca K, Cr K, K K.

TAP : Phatate acide de thallium :  $\text{C}_8\text{H}_5\text{O}_4\text{Ti}$ , domaine d'analyse pour les raies K du F au P :

Si K, Al K, Mg K, Na K.

Les alcalins sont dosés en premier et les standards sont les suivants :

Na : albite

K : orthose

Al : corindon ou albite

Si : albite

Fe : hématite

Mg : forstérite

Ca : apatite

Cr : chromite

Ti : rutil

Mn : rhodonite

Ni : buésite

### 1.2.B Analyses chimiques roches totales (majeurs et traces).

Les analyses roches totales sont regroupées dans les tableaux des annexes. Les éléments majeurs et traces ont été analysés soit en Fluorescence X ou en absorption atomique au laboratoire des Services Communs des Sciences de la Terre de Nancy (conditions analytiques présentées dans Govindaraju et Montanari, 1978) soit par spectroscopie ICP (émission plasma) au C.R.P.G. de Nancy. Les analyses de terres rares des plagiogranites du complexe ophiolitique de Trinity et des laves des séries volcano-sédimentaires de Yreka-Callahan ont été effectuées par ICP au C.R.P.G. de Nancy. Les analyses de terres rares des basaltes, filons, cumulats et d'une

harzburgite mantellaire du complexe ophiolitique de Trinity ont été réalisées par dilution isotopique (M. Brouxel, C.R.P.G.). Les analyses roches totales (majeurs et éléments traces) effectuées sur les échantillons de Toad Lake et Castle Lake (complexe ophiolitique de Trinity) proviennent du laboratoire des Sciences de la Terre de l'Université de Rennes (conditions analytiques résumées dans les tableaux 1.1 et 1.2).

**Tableau 1.1**

|                               | SiO <sub>2</sub> | Al <sub>2</sub> O <sub>3</sub> | Fe <sub>2</sub> O <sub>3</sub> | MnO | MgO  | CaO  | Na <sub>2</sub> O | K <sub>2</sub> O | TiO <sub>2</sub> | P <sub>2</sub> O <sub>5</sub> |
|-------------------------------|------------------|--------------------------------|--------------------------------|-----|------|------|-------------------|------------------|------------------|-------------------------------|
| gamme (%)                     |                  |                                |                                |     |      |      |                   |                  |                  |                               |
| d'étalonnage                  | 76-38            | 30-0.3                         | 17-1                           | 0.8 | 50-0 | 16-0 | 8.5-0             | 15-0             | 2.7-0            | 1.4-0                         |
| précision sur fortes teneurs  | 1%               | 1.50%                          | 2%                             |     | 1%   | 2%   | 1.50%             | 2%               | 2%               |                               |
| précision sur faibles teneurs | 3%               | 3%                             | 10%                            | 3%  | 5%   | 3%   | 5%                | 5%               | 5%               |                               |

**Tableau 1.2**

|               | Nb  | Zr    | Y   | Sr   | Rb   | Co  | V   | Ni   | Cr    | Ba   |
|---------------|-----|-------|-----|------|------|-----|-----|------|-------|------|
| gamme (ppm)   |     |       |     |      |      |     |     |      |       |      |
| d'étalonnage  | 960 | 11000 | 150 | 4600 | 3600 | 210 | 320 | 2300 | 24000 | 2400 |
|               | à 0 | à 10  | à 0 | à 0  | à 0  | à 0 | à 0 | à 0  | à 0   | à 5  |
| précision (%) |     |       |     |      |      |     |     |      |       |      |
| < 30ppm       | 10  | 10    | 10  | 10   | 10   | 10  | 10  | 10   | 10    | 10   |
| 30 à 150ppm   | 3   | 3     | 3   | 3    | 3    | 5   | 5   | 3    | 5     | 5    |
| > à 150ppm    | 1   | 1     |     | 1    | 1    | 2   | 2   | 1    | 2     | 2    |

### **I.2.C Analyses isotopiques.**

#### **I.2.C.a Analyses Isotopiques du strontium et du néodyme.**

Les analyses isotopiques du Sr et du Nd ont été effectuées par Brouxel (1987) par dilution isotopique au C.R.P.G. Les méthodes analytiques sont décrites dans l'introduction de sa thèse (Brouxel, 1987).

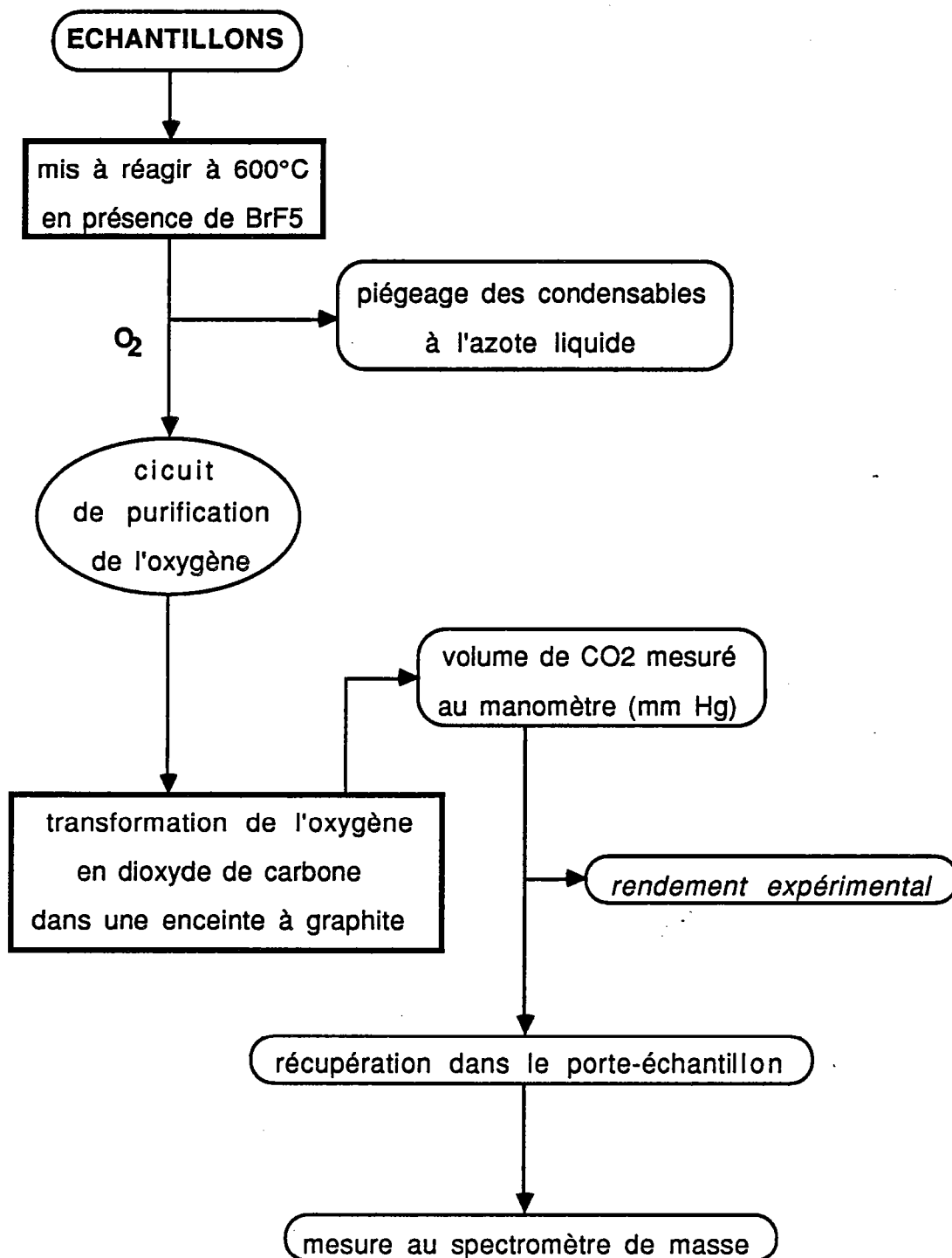
#### **I.2.C.b Analyses Isotopiques de l'oxygène et du carbone.**

Techniques d'extraction.

L'oxygène des silicates.

Le but de l'extraction consiste à récupérer théoriquement la totalité de l'oxygène contenu dans les silicates et les oxydes de la roche suivant la démarche proposée dans la figure 1.3.

# SCHEMA D'EXTRACTION DE L'OXYGENE DES SILICATES



Le rendement de l'extraction s'exprime sous la forme du rapport entre le rendement mesuré et le rendement théorique. Ce dernier est calculé à partir de la composition chimique roche totale (H<sub>2</sub>O+ compris). Les échantillons sont préalablement finement broyés. Les meilleures conditions pour effectuer la mesure au spectromètre de masse nécessitent de disposer de 100 à 200 µmoles de CO<sub>2</sub>, ainsi 6 à 8mg d'échantillon sont pesés. Les échantillons sont placés dans des tubes à nickel et mis à réagir à chaud avec du BrF<sub>5</sub> selon la méthode proposée par Clayton et Mayeda (1963). Cette attaque libère O<sub>2</sub> selon la réaction suivante :



Les produits de réaction de type  $\text{SiF}_4$ ,  $\text{KF}$ ,  $\text{AlF}_3$ ,  $\text{BrF}_5$ ,  $\text{BrF}_3$ ,  $\text{Br}_2$ ,  $\text{NiF}_2$ ,  $\text{NiBr}_2$ ...) sont soit solides soit condensables dans l'azote liquide ( $-180^\circ\text{C}$ ) et l'oxygène peut être ainsi récupéré, purifié au travers de pièges successifs au sein de la ligne d'extraction et réduit en  $\text{CO}_2$  dans une enceinte à graphite et catalyseur de platine à haute température. Le  $\text{CO}_2$  est à nouveau purifié, mesuré au manomètre et ensuite piégé avec de l'azote liquide dans un tube porte-échantillon disposé ultérieurement sur le spectromètre de masse.

Le rendement des extractions peut révéler des pertes de gaz au cours de l'extraction ou des réactions incomplètes (présence de minéraux réfractaires) s'il est inférieur à 1 ou des pollutions (par exemple de type atmosphérique), dans ce cas il est supérieur à 1.

La fréquente présence de l'épidote dans les roches de l'ophiolite de Trinity fut à l'origine de rendements insuffisants à la première extraction. Le caractère réfractaire de ce minéral est suggéré par la relation qui existe entre le pourcentage d'épidote dans la roche et le rendement mesuré à la première extraction. Des températures d'attaque plus élevées ( $640^\circ\text{C}$  au lieu de  $600^\circ\text{C}$ ), des temps de réaction plus longs (jusqu'à 48 heures) et une réextraction de l'échantillon après "recuison" ont permis finalement d'obtenir un bon rendement pour ces échantillons.

L'oxygène et le carbone des carbonates.

Le  $\text{CO}_2$  des carbonates est extrait par attaque sous vide par de l'acide phosphorique dans un bain thermostaté à  $25^\circ\text{C}$ . En effet au cours de la réaction :



seulement les 2/3 de l'oxygène sont libérés (pas de fractionnement pour le C) occasionnant un fractionnement cinétique entre l'oxygène du  $\text{CO}_2$  libéré et la calcite.

Le fractionnement  $\alpha\text{CO}_2$ -calcite (à  $25^\circ\text{C}$ ) déterminé expérimentalement par O'Neil et al. (1969) permet de faire la correction et de retrouver le  $\delta^{18}\text{O}$  du carbonate. Le  $\text{CO}_2$  extrait et piégé dans l'azote liquide et purifié par pompage des gaz résiduels puis ce  $\text{CO}_2$  est séparé de l'eau par piégeage avec de l'alcool fondant ( $-80^\circ\text{C}$ ). Le  $\text{CO}_2$  est alors stocké dans un tube porte-échantillon puis mesuré dans un manomètre à mercure pour contrôler son rendement et pouvoir calculer le pourcentage de carbonates de la roche.

Les mesures de composition ont été effectuées sur un spectromètre de masse à source gazeuse (VG SIRA10, triple collecteur). Les mesures ne présentent pas des valeurs absolues du rapport isotopique, l'échantillon est en effet mesuré en alternance avec un gaz standard de référence et le résultat signifie la déviation du rapport de l'échantillon par rapport à celui de la référence. Ce résultat est noté dans la convention  $\delta$  qui est le rapport de la différence des rapports isotopiques du standard.

$$\delta (\text{‰}) = \sqrt{(\text{R échantillon} - \text{R standard}) / \text{R standard}} \times 1000$$

$$\text{avec } R = {}^{13}\text{C} / {}^{12}\text{C}; {}^{18}\text{O} / {}^{16}\text{O}$$

La référence pour le  $\delta^{18}\text{O}$  est le SMOW ( $\delta^{18}\text{O} = 0$ ; moyenne de l'océan mondial) et pour le  $\delta^{13}\text{C}$  le PDB.

### 1.3 Cadre géologique.

La chaîne des Klamath appartient au domaine cordillérien nord-américain. Elle forme un arc à convexité ouest d'environ 300Km de long depuis Roseburg (au Sud-Ouest de l'Oregon) jusqu'à Redding en Californie du Nord. Elle couvre une superficie de 20.000Km et culmine à 2895m dans les Alpes de Trinity (figure 1.4).

Classiquement subdivisée par les géologues américains (Davis, 1966 et Irwin, 1966) en quatre ceintures (paléozoïque orientale, métamorphique centrale, paléozoïque et triasique occidentale et jurassique occidentale). Roure (1984), sur des données structurales et géochronologiques récentes, simplifie cette nomenclature en reconnaissant trois grandes unités :

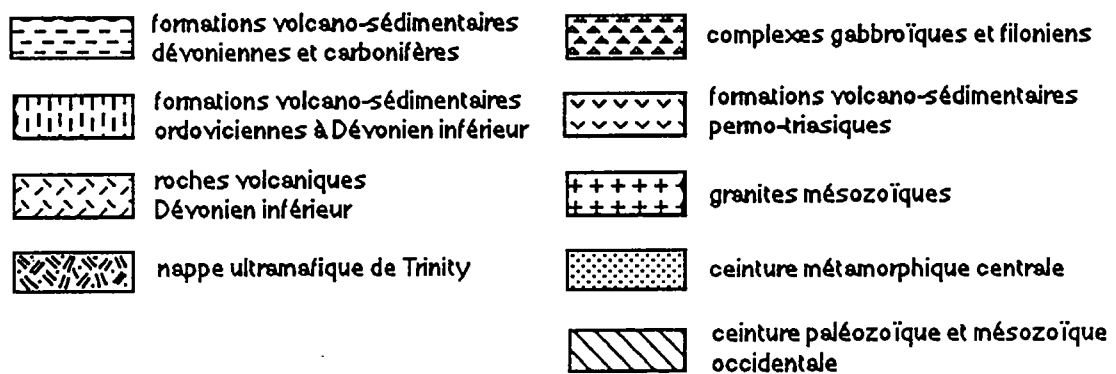
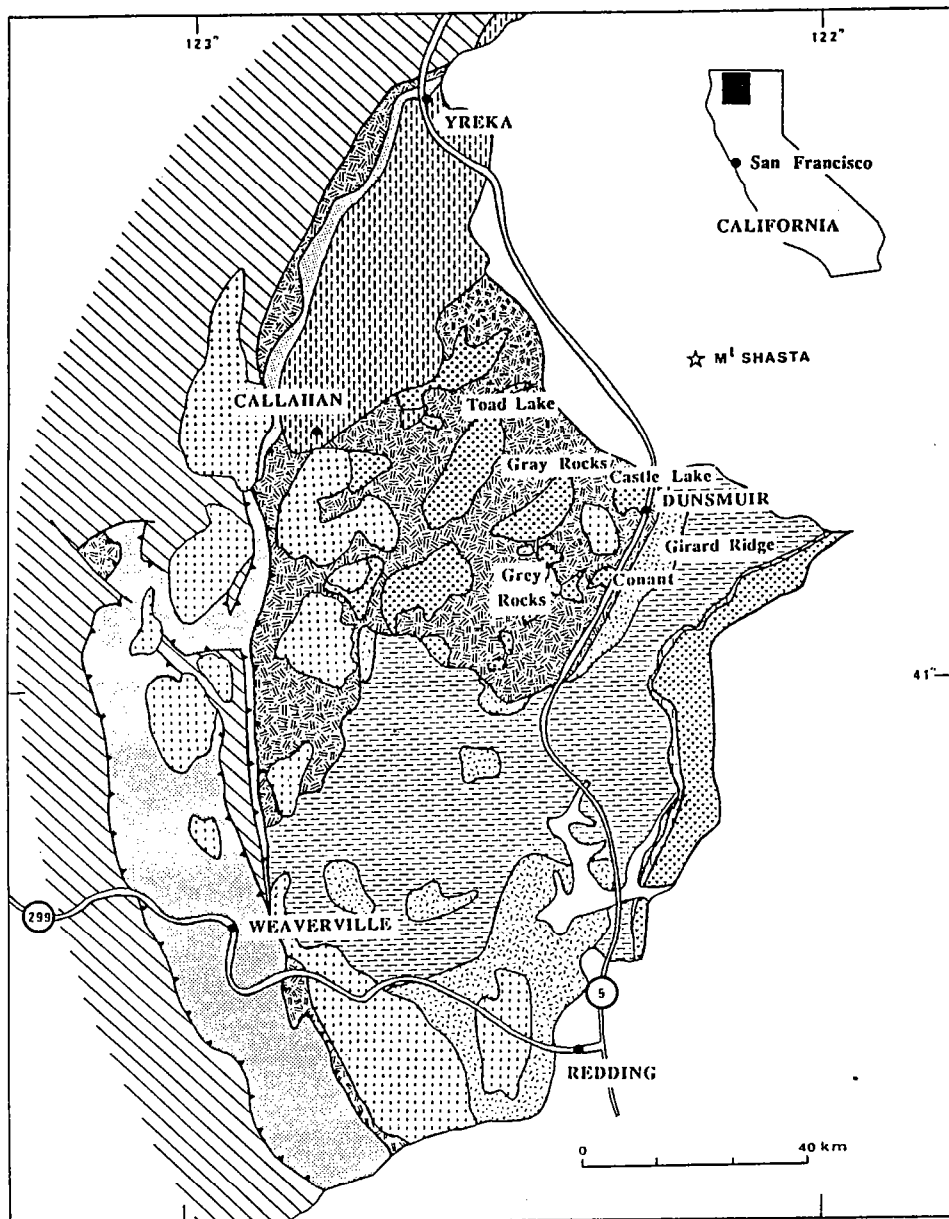


Figure 1.4 : carte géologique générale des Klamath orientales d'après Strand (1962, 1963), Irwin (1977) et Wagner et Saucedo (1986).

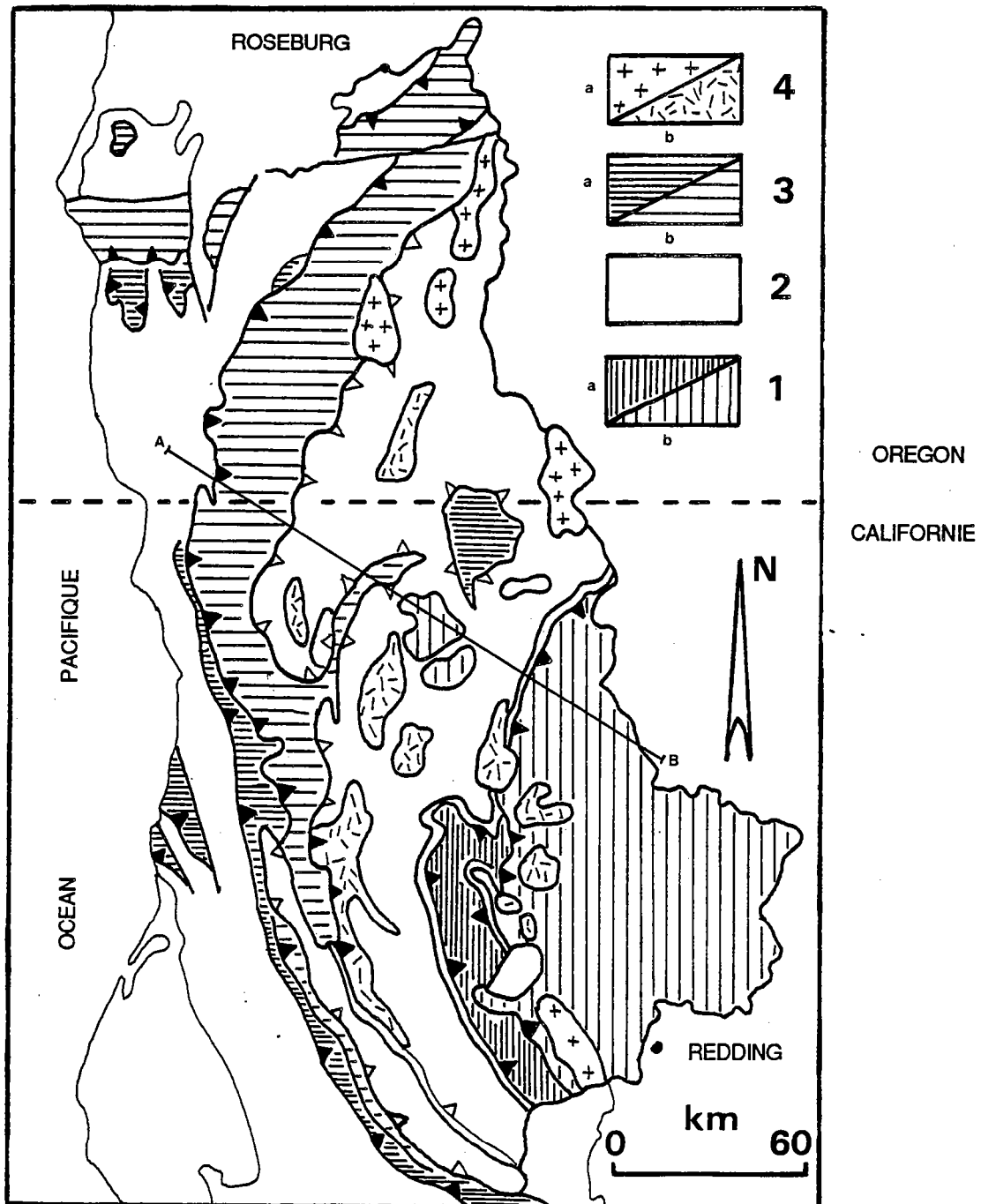


Figure 1.4b : Schéma structural des Klamath d'après Roure (1984).

1 - zone orientale : a - semelle métamorphique dévonienne.

b - Klamath orientales.

2 - zone occidentale paléozoïque et triasique.

3 - zone occidentale jurassique :

a - schistes bleus névadiens.

b - ophiolite triasique et couverture sédimentaire jurassique.

4 - plutons : a - jurassiques et b - névadiens.

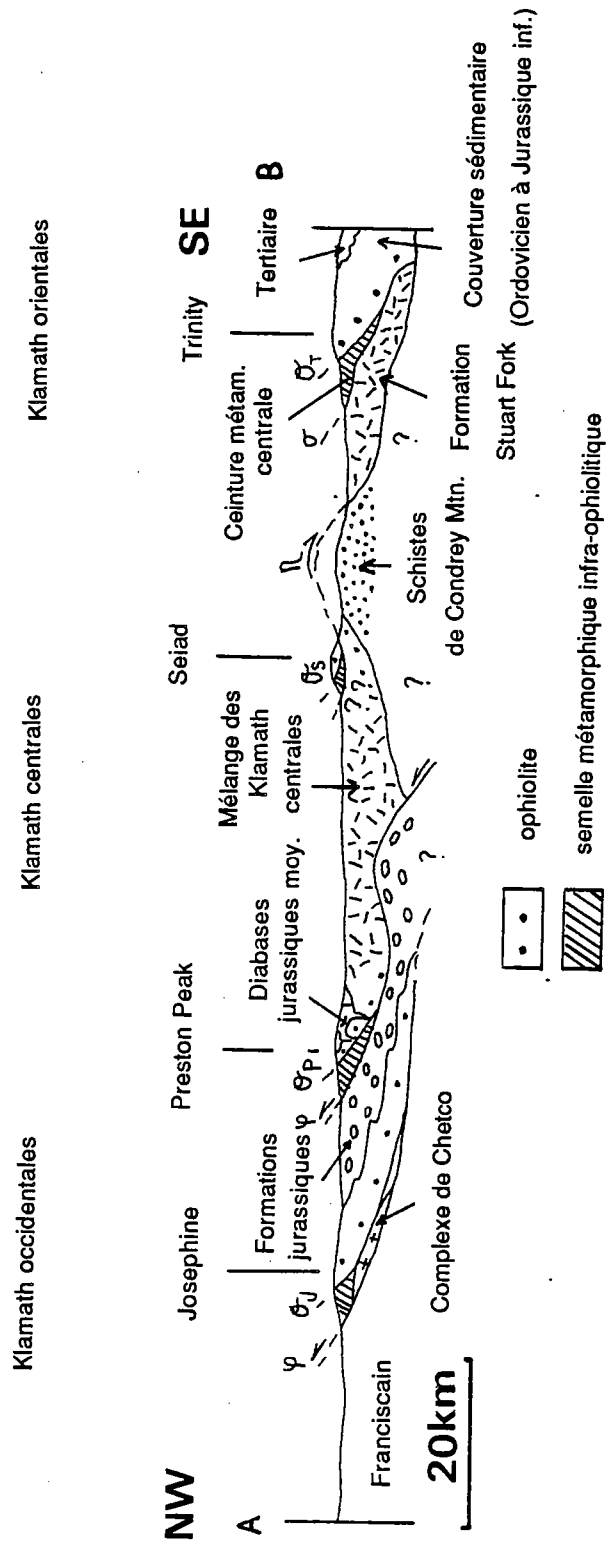


Figure 1.4c : Coupe schématique des Klamath Mountains et cinématique des charriages intra-ophiolitiques de Josephine ( $\theta_P$ ), Preston Peak ( $\theta_P$ ), Seiad ( $\theta_S$ ), Trinity ( $\theta_T$ ). ( $\varphi$ ) : contact orogénien; ( $\eta$ ) : contact névadien; ( $\sigma$ ) : contact sinémurien. Echelle verticale non respectée; plutons jurassiques et crétacés non représentés. D'après Cannat et Boudier (1986).

- une unité orientale : formations paléozoïques et métamorphiques centrales.
- une unité centrale : formations paléozoïques et triasiques.
- une unité occidentale jurassique.

L'histoire paléozoïque et mésozoïque des Klamath est jalonnée par une succession d'épisodes magmatiques qui s'apparentent à des volcanismes d'arc insulaire, des cortèges ophiolitiques et un plutonisme granodioritique Jurassique et Crétacé de marge active. Cette chaîne joue donc un rôle fondamental dans l'évolution de la marge pacifique nord-ouest américaine.

Alors que l'évolution géodynamique fini-mésozoïque des Klamath (ceinture occidentale) est marquée par la création et le développement d'un bassin marginal (ophiolite de Josephine; Harper, 1984) bordé d'arcs insulaires (Rogue et Preston Peak), celle, paléozoïque à mésozoïque inférieur (ceintures orientale et occidentale) beaucoup plus complexe, n'est pas encore complètement reconstituée.

Le complexe ophiolitique paléozoïque inférieur de Trinity constitue un des traits marquants de la géologie des Klamath orientales. Il est chevauché au Nord-Ouest (Yreka-Callahan) par un ensemble de nappes très disloquées, formées d'unités volcano-sédimentaires et métamorphiques d'âge Cambrien à Dévonien inférieur. Il s'ennoie vers le Sud et l'Est sous la couverture sédimentaire dévonienne (formation de Kennett discordante; Roure, 1984; Albers et Bain, 1985) et carbonifère (formation de Bragdon discordante; Charvet et al., 1989), sous la laquelle les séries volcaniques d'arc insulaire intra-océaniques (Kinkel et al., 1956) d'âge Paléozoïque inférieur (Copley-Balaklala) réaffleurent en boutonnière aux environs de Redding. Enfin, vers l'Est, les formations volcano-sédimentaires permo-triasiques (Albers et Robertson, 1961 et Martin et al., 1984) dessinent une vaste structure monoclinale déversée vers l'Est.

Le substratum des Klamath orientales est constitué d'une vaste nappe de péridotites mantellaires, épaisse de 2 à 3Km, qui plonge très légèrement vers l'Est et chevauche à l'Ouest des séries métamorphiques (amphibolites, quartzites et cipolins) d'âge Dévonien inférieur (380-350Ma; Cashman, 1980).

L'originalité de la nappe péridotitique de Trinity réside d'une part dans son extension (2750Km<sup>2</sup> de surface) et d'autre part dans sa diversité pétrographique. En effet, elle est constituée de harzburgites, dunites et lherzolites (localement imprégnées par du plagioclase interstitiel) datées à  $472 \pm 32$ Ma (Nd/Sm; Jacobsen et al., 1984). Le complexe ophiolitique de Trinity (localement tectonisé) est constitué de la nappe de péridotites mantellaires dite de "Trinity" et d'une mince séquence crustale en affleurements discontinus définissant de petites chambres magmatiques (Lecuyer et Cannat, 1989). La trilogie ophiolitique a pu être reconstituée (Brouxel et Lapiere, 1984) et certains contacts primaires sont préservés (Le Sueur et al., 1984; Lecuyer et Cannat, 1989) comme les contacts péridotites mantellaires - cumulats gabbroïques et l'enracinement du complexe filonien dans les gabbros de haut de chambre.

De nombreuses datations ont été réalisées sur les gabbros sans toutefois donner un âge précis pour ce complexe ophiolitique qui semble se situer à l'Ordovicien-Silurien (439-433Ma par K/Ar sur hornblende; Lanphere et al., 1968; 480-455Ma par U/Pb sur zircon; Mattinson et Hopson, 1972;  $435 \pm 21$ Ma par Nd/Sm; Jacobsen et al., 1984;  $445 \pm 50$  par Nd/Sm; Brouxel, 1988).

La présence de lherzolites à plagioclase constituant la nappe de péridotites mantellaires a conduit Boudier et Nicolas (1985-86) à considérer cette ophiolite comme appartenant au "lherzolite sub-type" qui se serait formée dans un environnement de type Mer Rouge. Les caractères pétrographiques et géochimiques des basaltes et de leurs filons nourriciers (faibles teneurs en éléments hygromagmaphiles, spectres de terres rares appauvris en terres rares légères; Lapiere et al., 1987 et Brouxel et Lapiere, 1988) semblent indiquer pour ces auteurs que le complexe ophiolitique de Trinity représente le début du fonctionnement d'un bassin océanique à proximité d'un arc insulaire intra-océanique.

Enfin, il faut noter qu'une très grande différence géologique existe entre les formations jouxtant le cortège ophiolitique sur ses frontières nord-ouest et sud-est. Alors que les séries volcaniques d'arc : basaltes - andésites - andésites riches en Mg du Copley et rhyolites pauvres en K de Balaklala (Barker et al., 1979; Lapiere, 1983; Lapiere et al., 1985 a et b) méridionales appartiennent au même environnement intra-océanique que le complexe ophiolitique de Trinity (Brouxel et Lapiere, 1988); les séries volcano-sédimentaires septentrionales d'âge cambrien à dévonien, constituées en majorité de laves alcalines, de calcaires récifaux, de sédiments détritiques à olistolithes, évoquent plutôt un environnement de "seamounts" "échoués" sur une



marge continentale (Lecuyer et al., 1989a). Les données pétrographiques et géochimiques des laves calco-alcalines associées aux calcaires ordoviciens récifaux de Lovers Leap ( figure 1.1; Lapierre et al., 1987; Brouxel et Lapierre, 1988; Brouxel et al., 1989) sont en accord avec un tel environnement.

La première partie de ce mémoire regroupe trois publications qui résultent du travail entrepris en équipe sur la géologie régionale des Klamath orientales et plus généralement qui s'inscrit dans le cadre de la géologie de la marge Nord-Ouest américaine. Les deux premiers articles traitent de la nature des séries volcano-sédimentaires des Klamath orientales et de leurs relations spatio-temporelles avec le complexe ophiolitique de Trinity dans le but de préciser le paléoenvironnement dans lequel a évolué le bassin océanique représenté par l'ophiolite de Trinity. Le troisième article témoigne des efforts de synthèse entrepris dans la géologie de la marge nord-ouest américaine par les équipes françaises avec pour exemple la distribution du volcanisme Permien et sa signification dans l'évolution géodynamique de la cordillère nord-américaine.

## Un exemple d'accrétion d'îles océaniques à une marge continentale: les séries ordoviciennes des Klamath orientales (Nord californie).

Note de Christophe Lécuyer\*, Henriette Lapierre\*\* et Jacques Charvet\*\* présentée par...

Les formations du Paléozoïque inférieur des Klamath orientales sont représentées par les séries volcano-sédimentaires très déformées de la région d'Yreka-Callahan qui chevauchent le complexe ophiolitique de Trinity. Les séries d'Yreka contiennent des coulées de basaltes semblables aux basaltes intraplaques d'îles océaniques. Ces séries témoignent de phénomènes de collisions entre des îles océaniques et une marge continentale qui suggèrent le développement de l'ophiolite de Trinity à proximité d'un continent. Les séries d'Yreka permettent de reconstruire un domaine paléogéographique similaire à celui proposé pour les séries volcano-sédimentaires ordoviciennes des "Roberts Mountain Allochthon" dans le Nord du Nevada et pourrait marquer une continuité géographique à l'Ordovicien en marge du craton nord-ouest américain.

GEOLOGY. - An example of seamount - active continental margin accretion: the Ordovician series from Eastern Klamath (Northern California).

The Lower Paleozoic formations of the eastern Klamath are illustrated by the strongly tectonized volcano-sedimentary series of Yreka-Callahan which overthrust the Trinity ophiolitic complex. These series represent accretion processes between ocean islands and an active continental margin which suggest the development of the Trinity ophiolite in the vicinity of a continent. The Yreka assemblage allows to build a paleogeographic domain similar to the model proposed for the ordovician volcano-sedimentary series of the Roberts Mountain Allochthon (Northern Nevada) and could mark a paleogeographic continuity in the vicinity of the northwestern american craton at Ordovician times.

I. INTRODUCTION - La ceinture des Klamath comprend au Nord un ensemble de nappes volcano-sédimentaires d'âge ordovicien à dévonien qui chevauchent le complexe ophiolitique de Trinity (figure 1). L'étude des relations géométriques entre les différentes unités volcano-sédimentaires, la synthèse des données géochronologiques ainsi que la nature des émissions volcaniques ont permis de proposer un modèle paléogéographique et de préciser les relations spatio-temporelles avec le complexe ophiolitique de Trinity probablement d'âge ordovicien-silurien (472-435Ma; [1], [2], [3]) qui représente soit les premiers stades d'ouverture d'un bassin marginal en milieu intra-océanique ([1], [4], [5], [6]) soit un petit océan de type Mer Rouge ([7]).

II. CADRE GEOLOGIQUE - Les formations du Paléozoïque inférieur des Klamath orientales sont représentées par les séries volcano-sédimentaires très déformées dans la région d'Yreka-Callahan (figure 1) qui chevauchent le complexe ophiolitique de Trinity.

Les unités empilées correspondent de la base au sommet, à : la "Gazelle Formation" d'âge dévonien inférieur, la formation de "Moffett Creek" d'âge silurien, la "Duzel Phyllite" et "l'Antelope Quartzite" d'âge ordovicien ([8], [9]).

La formation de Gazelle est caractérisée par la présence de marnes litées, de grès, de radiolarites et d'un olistostrome basal. Cet olistostrome contient deux types de blocs :

- des blocs de calcaires récifaux et d'andésites provenant d'un arc insulaire calco-alcalin d'âge ashgillien (séquence de Lovers Leap; figure 1) sur lesquels repose un conglomérat à galets de calcaires d'âge silurien et de diorites quartziques calco-alcalines datées à 480 Ma.

- des basaltes en coussins et des tufs surmontés par des calcaires oolitiques (Bonnet Rock; figure 1).

La formation de Moffett Creek correspond à une séquence turbiditique avec d'abondantes argiles à galets, des grauweekes et des grès. Elle contient également un horizon inférieur (Horseshoe Gulch) qui comprend des marbres déformés, des schistes bleus et verts datés Ordovicien terminal (431-432Ma), des basaltes en coussins, des coulées rhyolitiques et des calcaires récifaux. L'horizon supérieur (Duzel Rock) comprend des basaltes en coussins ([10], [11]) associés à des brèches de ces basaltes et des calcaires récifaux d'âge ordovicien moyen.

L'unité de la "Duzel Phyllite" comprend des sédiments terrigènes sous-marins profonds (siltites phylliteuses et calcareuses, marnes et grauweekes fines) étant interprétés par Potter et al. [8] et Lindsley-Griffin [9] comme un cône sous-marin ou un front de delta. L'unité "Antelope Quartzite" est considérée d'après Hotz [12] comme un faciès latéral de la "Duzel Phyllite". Elle est constituée de sédiments détritiques plus grossiers : arénites et conglomérats recouverts par des cherts avec des lits

argileux verts. Ainsi, l'assemblage sédimentaire d'Yreka correspond à des turbidites distales et profondes.

**III. PETROGRAPHIE** - Les basaltes de Duzel Rock, déformés, se présentent en coussins infradécimétriques riches en vésicules. Ces laves à texture microlitique porphyrique sont soit des basaltes à deux pyroxènes soit des basaltes à olivine avec une mésostase riche en oxydes ferrotitanés. Ces roches ont subi un métamorphisme de base de faciès schiste vert comme en témoigne la présence d'albite et de séricite en remplacement des phénocristaux de plagioclase. L'orthopyroxène est partiellement chloritisé tandis que les rares olivines sont déstabilisées en iddingsite.

Les basaltes de Horseshoe Gulch et Bonnet Rock montrent une minéralogie primaire et des conditions de métamorphisme similaires. Cependant, ils peuvent avoir des textures intersertales porphyriques ou variolitiques traduisant des degrés variables de trempe. L'ensemble des laves de ces trois séries est riche en vésicules à remplissage prédominant de calcite, chlorite et accessoirement de quartz, magnétite, zoïsite et zéolites.

**IV. GEOCHIMIE** - Les basaltes de Duzel Rock sont pauvres en  $\text{SiO}_2$  (43-47%),  $\text{Al}_2\text{O}_3$  (11,9-14,2%) et  $\text{MgO}$  (4,2-6%) tandis qu'ils présentent de fortes teneurs en  $\text{Fe}_2\text{O}_3$  total (12,7-16,7%; tableau n°1) et leurs spectres de terres rares enrichis en terres rares légères ( $(\text{La/Yb})_N = 4,5-4,7$ ) leur confèrent des affinités avec les basaltes alcalins pauvres en magnésium (figure 2).

Les basaltes de Bonnet Rock et Horseshoe Gulch sont au contraire caractérisés par des spectres de terres rares plats ou légèrement enrichis en terres rares légères ( $(\text{La/Yb})_N = 0,8-1,7\%$ ; figure 2). Leurs teneurs en  $\text{TiO}_2$  et en éléments incompatibles ( $\text{TiO}_2=1,44-2,16\%$ ;  $\text{Zr/Nb}=16,8-25,8$ ) sont davantage caractéristiques de basaltes anorogéniques tholéitiques et transitionnels (tableau n°1).

La composition en éléments majeurs et traces de ces basaltes est tout à fait similaire à celle des basaltes intraplaques des îles océaniques de Hawaï et d'Islande (tableau 2) où les associations étroites de basaltes tholéitiques et alcalins sont fréquentes ([13], [14]).

**V. DISCUSSION** - Les successions volcano-sédimentaires de Duzel Rock, Bonnet Rock et Horseshoe Gulch où s'intercalent les coulées de basaltes alcalins intraplaques suggèrent la présence de dépôts susceptibles de s'être mis en place dans un environnement d'île océanique (figure 3A) immergée sous une faible tranche d'eau (< 500m; basaltes vésiculaires, faune marine de faible profondeur). L'unité de la "Duzel Phyllite" témoigne par ses dépôts détritiques (grauwakes, silts, shales, cherts, grès et quartzites) d'une source continentale voisine [8]. Elle est intimement associée à la formation de Moffet Creek qui est interprétée comme une séquence de turbidites [8]. Ces dépôts pourraient correspondre à ceux d'un cône sous-marin ou d'un front de delta qui aurait progressivement recouvert les dépôts volcaniques à la faveur d'une marge continentale active (figure 3B). Les témoins d'une telle marge active pourraient être représentés actuellement par la succession volcano-sédimentaire ordovicienne de Lovers Leap et ses coulées calco-alcalines ([6], [15]).

Le mélange tectonique représenté par l'ensemble des séries d'Yreka serait le produit de la dislocation de ces unités dans une fosse océanique à l'aplomb d'un plan de subduction (phase Callahan, [16]). L'événement tectonique majeur anté-Carbonifère (phase Antler, [17], [18]) est responsable du recouvrement partiel du complexe ophiolitique de Trinity par les séries volcano-sédimentaires d'Yreka-Callahan. Le complexe ophiolitique de Trinity signe les premiers stades d'ouverture d'un bassin marginal en domaine intra-océanique ([4], [5], [6]) ou encore représente un océan étroit de type Mer Rouge produit à l'aplomb d'un centre d'expansion lent [7]. Les séries ordoviciennes d'Yreka qui témoignent de phénomènes d'accrétion entre des îles océaniques et une marge continentale active pourraient confirmer le développement d'un bassin océanique (l'ophiolite de Trinity) à proximité d'un continent. Toutefois pour Mattinson et Hopson [19] et Lindsley-Griffin [20] il apparaît difficile de relier spatialement et temporellement l'ophiolite de Trinity et les séries d'Yreka-Callahan.

Les séries d'Yreka permettent d'envisager un domaine paléogéographique similaire à celui proposé pour les séries volcano-sédimentaires ordoviciennes (Arénigien à Caradoc) des "Roberts Mountain Allochthon" dans le Nord du Nevada [21] et pourrait marquer une continuité géographique à l'Ordovicien en marge du craton nord-ouest américain.

(+) Remise le...

(1) M. A. LANPHERE, W. P. IRWIN et P. E. HOTZ, *Geol. Soc. Am. Bull.*, 79, 1968, p. 1027-1052.

(2) S. B. JACOBSEN, J. E. QUICK et G. J. WASSERBURG, *Earth Planet. Sci. Lett.*, 68, 1984, p. 361-378.

- (3) M. BROUXEL et H. LAPIERRE, Geol. Soc. Am. Bull., 100, 1988, p. 1111-1119.
- (4) M. BROUXEL et H. LAPIERRE, C. R. Acad. Sc. Paris, t. 299, Série II, 1984, p. 457-462.
- (5) M. BROUXEL et H. LAPIERRE, Ophioliti, 10, 1985, p. 181-202.
- (6) H. LAPIERRE, M. BROUXEL, F. ALBAREDE, C. COULON, C. LECUYER, P. MARTIN, G. MASCLE et O. ROUER, Tectonophysics, 140, 1987, p. 155-177.
- (7) F. BOUDIER et A. NICOLAS, Earth Planet. Sci. Lett., 76, 1985/86, p. 84-92.
- (8) A. W. POTTER, P. E. HOTZ et D. M. ROHR, Soc. Econom. Pal. and Mineral.. Pacific sec.. Pacific coast Paleogeography Symp., 1, 1977, p. 101.
- (9) N. LINDSLEY-GRIFFIN, Soc. Econom. Pal. and Mineral.. Pacific sec., Los Angeles, California, USA, 1983, p. 63-75.
- (10) A. W. POTTER, K. F. SCHEIDEGGER, J. B. CORLISS et E. J. DASCH, Geol. Soc. America. Abs. with Programs, 7, 1975, p. 1231.
- (11) A. W. POTTER, K. F. SCHEIDEGGER et J. B. CORLISS, Amer. Geophys. Union Trans., 57, 1976, p. 1023.
- (12) P. E. HOTZ, United States Geol. Surv. Bull., 1436, 1977, p. 1-72.
- (13) J. R. BUDAHN et R. A. SCHMITT, Geochim. Cosmochim. Acta, 49, 1985, p. 67-87.
- (14) D. A. WOOD, J. Petrol., 19, 1978, p. 393-436.
- (15) M. BROUXEL, H. LAPIERRE, A. MICHARD et F. ALBAREDE, Geol. Soc. Am. Bull., 100, 1988, p. 1111-1119.
- (16) S. J. COTKIN, M. L. COTKIN et R. L. AMSTRONG, Geology (sous presse).
- (17) J. CHARVET, H. LAPIERRE et C. CAMPOS, C. R. Acad. Sc. Paris, t. 308, Série II, 1989, p. 1629-1635.
- (18) C. CAMPOS, Diplôme d'Etudes Approfondies de l'Université d'Orléans, 41 pages.
- (19) J. M. MATTINSON et C. A. HOPSON, Carnegie Inst. Wash., Yearbook, 71, 1972, p. 578-583.
- (20) N. LINDSLEY-GRIFFIN, Geol. Soc. America. Abs. with programs, 5, 1973, p. 71-72.
- (21) M. M. MILLER et D. S. HARWOOD, Geology, 17, 1989, p. 369-372.

\* CAESS/CNRS, Laboratoire de Géochimie, 35042 Rennes CEDEX.

\*\* Université d'Orléans, Département des Sciences de la Terre, Laboratoire de Géologie structurale, B.P. 6759, 45067 Orléans CEDEX.

**LEGENDES DES FIGURES**

**figure n°1 : Carte géologique et structurale de la région d'Yreka-Callahan d'après Potter et al. (1977).**

**Geologic map and structure sections of the Yreka-Callahan area after Potter et al. (1977).**

**figure n°2 : spectres de terres rares des basaltes de HorseShoe Gulch (carrés pleins), de Bonnet Rock (carrés vides) et de Duzel Rock (ronds noirs).**

**rare earth element patterns of the Horseshoe Gulch (filled squares), Bonnet Rock (open squares) and Duzel Rock (filled circles) basalts.**

**figure n°3 : Modèle d'accrétion d'îles insulaires à une marge continentale active depuis l'Ordovicien moyen (A) jusqu'à l'Ordovicien terminal (B) des Klamath orientales.**

**Model of seamount - active continental margin accretion through Ordovician (A-B) in the eastern Klamath.**

|                                | Horseshoe<br>Gulch | Bonnet Rock |       | Duzel<br>Rock |       |       |
|--------------------------------|--------------------|-------------|-------|---------------|-------|-------|
| Echantillons                   | H12                | BO13        | BO15  | DR3           | DR4   | DR5   |
| SiO <sub>2</sub>               | 49.84              | 49.47       | 46.40 | 47.05         | 42.78 | 45.24 |
| TiO <sub>2</sub>               | 1.44               | 2.16        | 2.14  | 2.49          | 3.08  | 3.02  |
| Al <sub>2</sub> O <sub>3</sub> | 16.05              | 13.88       | 13.34 | 14.21         | 13.09 | 12.93 |
| Fe <sub>2</sub> O <sub>3</sub> | 12.46              | 11.47       | 13.60 | 12.67         | 13.42 | 13.25 |
| MnO                            | 5.78               | 5.86        | 5.54  | 4.23          | 5.35  | 4.76  |
| MgO                            | 0.20               | 0.20        | 0.21  | 0.18          | 0.19  | 0.19  |
| CaO                            | 4.24               | 8.09        | 10.38 | 10.66         | 10.73 | 10.41 |
| Na <sub>2</sub> O              | 5.45               | 4.89        | 4.23  | 3.42          | 3.94  | 3.96  |
| K <sub>2</sub> O               | 0.17               | 0.56        | 0.14  | 0.57          | 0.53  | 0.59  |
| P.F.                           | 4.20               | 2.86        | 3.84  | 4.41          | 6.66  | 5.23  |
| Total                          | 99.83              | 99.44       | 99.82 | 99.89         | 99.77 | 99.58 |
| Cr                             | 149                | 258         | 129   | 157           | 93    | 71    |
| Ni                             | 95                 | 112         | 77    | 80            | 86    | 90    |
| Nb                             | 4                  | 9           | 8     | 19            | 26    | 26    |
| Zr                             | 103                | 151         | 137   | 164           | 221   | 220   |
| Y                              | 25                 | 37          | 38    | 32            | 36    | 37    |
| Sr                             | 194                | 232         | 113   | 452           | 527   | 531   |
| Rb                             | 7                  | 16          | 16    | 15            | 14    | 14    |
| La                             | 7.58               | 7.43        | 5.25  | 17.15         | 19.46 | 19.16 |
| Ce                             | 22.80              | 22.36       | 20.53 | 45.15         | 48.08 | 48.69 |
| Nd                             | 13.63              | 15.79       | 14.32 | 26.42         | 27.78 | 28.42 |
| Sm                             | 4.23               | 5.24        | 5.22  | 7.39          | 7.41  | 7.71  |
| Eu                             | 1.29               | 1.64        | 1.76  | 2.49          | 2.54  | 2.53  |
| Gd                             | 4.31               | 5.49        | 5.90  | 7.12          | 6.75  | 6.95  |
| Dy                             | 4.92               | 6.18        | 7.02  | 6.04          | 6.15  | 6.42  |
| Er                             | 2.82               | 3.47        | 4.04  | 2.79          | 2.92  | 3.10  |
| Yb                             | 3.01               | 3.75        | 4.39  | 2.47          | 2.80  | 2.87  |

Tableau 1 : analyses chimiques sur roches totales  
des basaltes de HorseShoe Gulch, Bonnet Rock et Duzel Rock.

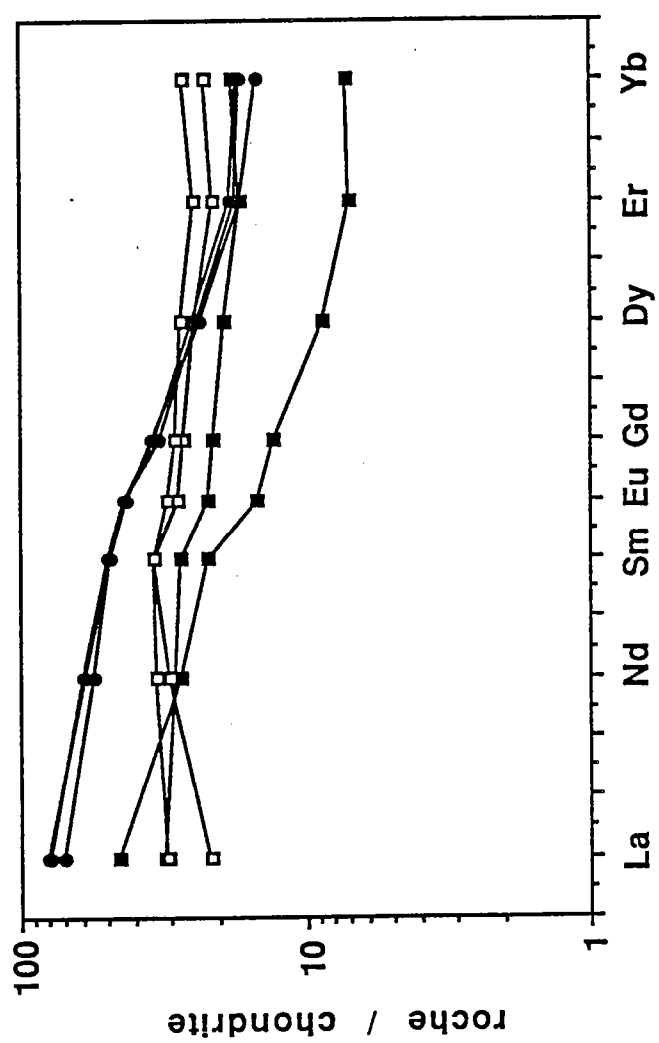
Table 1 : chemical analyses on bulk rock  
of HorseShoe Gulch, Bonnet Rock and Duzel Rock basalts.

| <b>éléments<br/>(ppm)</b> | <b>Islande<br/>(n = 4)</b> | <b>Hawaii<br/>(n = 33)</b> | <b>Yreka<br/>(n = 10)</b> |
|---------------------------|----------------------------|----------------------------|---------------------------|
| <b>Cr</b>                 | 49 - 211                   | 65-525                     | 56-258                    |
| <b>Ni</b>                 | 49-117                     | 40-305                     | 72-112                    |
| <b>V</b>                  | n.d.                       | 225-444                    | 213-375                   |
| <b>Nb</b>                 | 18-22                      | n.d.                       | 4-26                      |
| <b>Zr</b>                 | 137-224                    | 95-375                     | 103-221                   |
| <b>Y</b>                  | 38-49                      | n.d.                       | 25-40                     |
| <b>Sr</b>                 | 275-366                    | 288-628                    | 194-531                   |
| <b>Rb</b>                 | 0-12                       | n.d.                       | 7-16                      |
| <b>La</b>                 | 14-19,5                    | 8,6-20                     | 7,43-19,46                |
| <b>Sm</b>                 | 6,77-9,24                  | 4,83-7,2                   | 4,23-7,71                 |
| <b>Yb</b>                 | 2,98-3,73                  | 1,8-2,33                   | 2,47-4,39                 |

Tableau 2 : comparaison de la composition chimique des basaltes d'Yreka, d'Hawaii et d'Islande pour quelques éléments traces.

Table 2 : comparison of Yreka, Hawaii and Iceland chemical compositions for some trace elements.

Figure 1

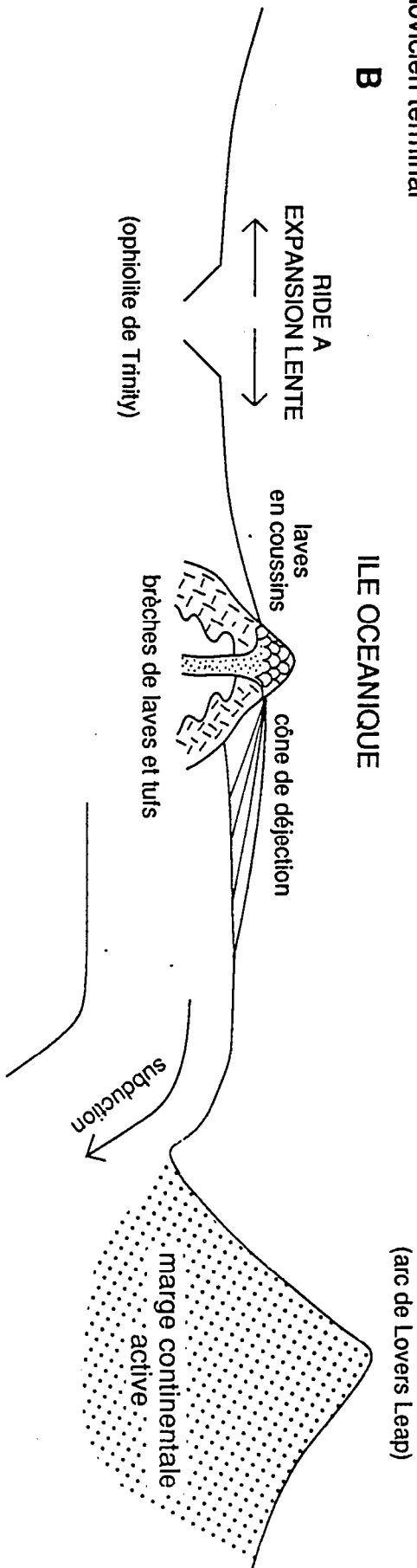




# MARGE CONTINENTALE ACTIVE

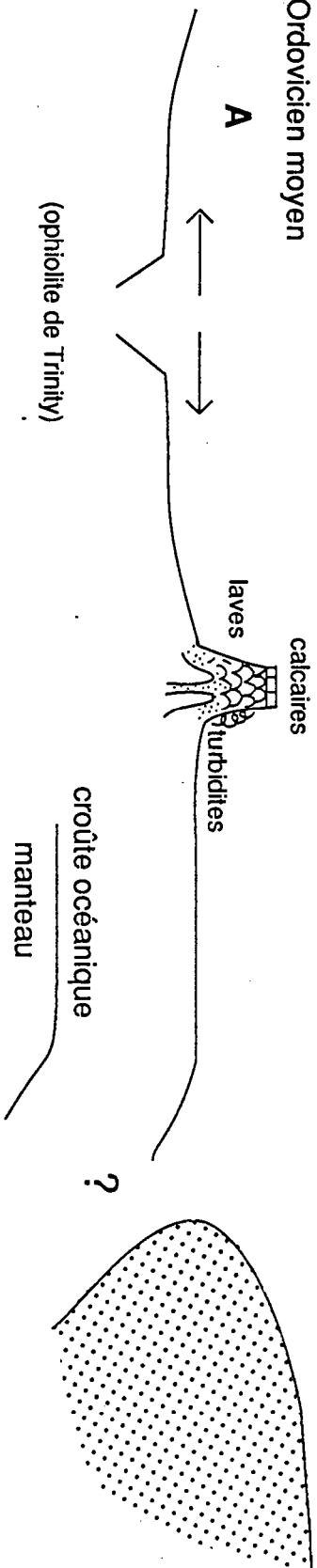
Ordovicien terminal

**B**



Ordovicien moyen

**A**



**DIVERSITY OF MAGMA TYPES IN A LOWER PALEOZOIC  
ISLAND-ARC - MARGINAL BASIN SYSTEM  
(EASTERN KLAMATH MOUNTAINS, CALIFORNIA).(\*)**

**M. Brouxel 1, C. Lecuyer 2 and H. Lapierre 3**

**1) Centre de Recherches Pétrographiques et Géochimiques  
B.P. 20, 54501 Vandœuvre-les-Nancy, France.**

**2) Laboratoire de Géochimie, CAESS/CNRS Rennes.**

**3) Laboratoire de Géologie Structurale, Université d'Orléans  
B.P. 6557, 45067 Orléans cedex 2, France.**

## ABSTRACT

A trace element investigation have been conducted on the eastern Klamath Mountains Ordovician to Devonian volcanics spatially associated to the Siluro-Ordovician Trinity peridotite and gabbros. All the studied volcanics (low-K tholeiites and calc-alkalic volcanics) present strong island-arc geochemical features (low TiO<sub>2</sub> contents, negative Nb, Zr and Ti anomalies, mild light REE enrichment and depletion). Some Lovers Leap and Copley volcanics exhibit strong immature island-arc geochemical affinities (very depleted light REE patterns and very low Nb contents) suggesting that they were formed by high degrees of partial melting (20 %) of a residual lithosphere. Diminution of the partial melting degree and addition of sediments to the source will explain the occurrence of less depleted or slightly light REE enriched volcanics.

The Grey Rocks basaltic pillow-lavas thrust on the Trinity peridotitic sheet represent likely the extrusive member of the ophiolitic sequence. Their strong island-arc geochemical affinities suggest that the ophiolite was formed during the first stages of a back-arc basin development.

Differentiation takes place in the arc by melting of the deeper basaltic layers, leading to the formation of abundant rhyolitic and trondhjemitic magmatism representing the first stages of continental accretion.

## INTRODUCTION

Studies on present day intra-oceanic island-arc volcanics reveals that an important diversity of magma types exists within a single arc (i.e. Marianas; Dixon and Batiza, 1981; Matthey et al., 1981; Wood et al., 1982). This is commonly attributed to the complex magmatic processes leading to the formation of orogenic magmas. Trace element investigations and Sr-Nd isotopic studies have stressed the probability that more than one source are involved in arc magma genesis (i.e. subducted basalts and/or sediments, subducted derived fluids, presence of an ocean-island type component; Church, 1973; Kay, 1978; Morris and Hart, 1983; Gill, 1984; White and Patchett, 1984; VonDrach et al., 1986). On the contrary, their associated marginal basin basalts appear to be more homogeneous (Matthey et al., 1981; Wood et al., 1982; Hawkins and Melchior, 1985). However, it have been shown that basalts even from well developped marginal basins (i.e. Marianas or Scotia Sea) present persistent arc-like chemical features (major and trace element chemistry transitional between mid-ocean ridge basalts and island-arc basalts; Saunders and Tarney, 1979; Hawkins and Melchior, 1985; Volpe et al., 1987). These island-arc affinities are more and more important with earlier stages of marginal basin development (Lordkipanidze et al., 1979; Hawkins and Melchior, 1985).

However, modern island-arc and marginal basin studies, biased toward subsurface sampling, reveals little as to composition at depth. Ophiolitic and paleovolcanic island-arc series, profoundly dissected by erosion and tectonic disrupting, could allow a more important overview of arc or marginal basin interior. Indeed, it is currently admitted that ophiolites could be the remnant of old oceanic lithosphere formed within an island-arc environment (Dewey and Bird, 1971; Miyashiro, 1973; Beccaluva et al., 1979; Crawford et al., 1981; Serri, 1981; Leitch, 1984). The Siluro-Ordovician Trinity ophiolite (eastern Klamath Mountains, N. California), spatially associated to more or less contemporaneous island-arc volcanic series (Ordovician to Early Devonian) have been interpreted as formed in an island-arc environment (Lindsley-Griffin, 1977; Quick, 1981; Jacobsen et al., 1984; Brouxel and Lapierre, 1985; Brouxel, 1987; Lapierre et al., 1986; 1987). The purpose of this paper is to present the petrological and geochemical features of the eastern Klamath Mountains (EKM) Ordovician to Early Devonian ophiolitic and island-arc volcanics, in order first, to define more precisely the geodynamic environment of the Trinity ophiolite, and second, to determine the different sources involved in this Paleozoic island-arc - marginal basin system.

## GEOLOGICAL SETTING

The Klamath Mountain province form an arcuate west-facing belt consisting mostly of oceanic rocks (island-arcs and ophiolites) associated with sediments (Irwin, 1981). This province have been divided in four westward younger lithologic belts : the eastern Klamath Mountains (EKM), the Central Metamorphic belt, the western Paleozoic and Triassic belt and the western Jurassic belt (Iriwin, 1966). The EKM, which is the nucleus of the province, is a long standing volcanic arc built on the Siluro-Ordovician Trinity ophiolite (Fig. 1). Volcanic series showing evidence of an intermittent volcanic activity from lower Paleozoic to Jurassic are located either to the north-west, between Yreka and

Callahan (lower Paleozoic to Devonian volcanic series), or the south and east, between Redding, Weaverville and Dunsmuir (Silurian ? and upper Paleozoic to Jurassic island arc volcanic series).

The Trinity ophiolite is composed at the base of the Ordovician Trinity peridotite ( $472 \pm 32$  My; Jacobsen et al., 1984) which is a thick ultramafic sheet (2-4 km) easterly dipping (Irwin, 1960; 1966). The Trinity sheet is overlain conformably (?) by peridotitic to gabbroic plutonic complexes. Some microgabbros, clinopyroxenites, gabbros and plagiogranite yielded K-Ar, Sm-Nd and U-Pb ages ranging between 450 and 418 My (Lanphere et al., 1968; Mattinson and Hopson, 1972; Jacobsen et al., 1984). The 480 My old quartz diorite analyzed by Mattinson and Hopson (1972) do not probably belong to the Trinity ophiolite. Indeed, their calc-alkalic affinities (presence of amphibole and biotite phenocrysts) are not in agreement with the tholeiitic nature of the Trinity ophiolite.

The eruptive and hypabyssal members of the Trinity ophiolite are apparently absent or poorly developed. Although, two or three volcanic units, which now structurally overlie the Trinity peridotite and gabbros could belong to the ophiolite. Near Dunsmuir, along the eastern part of the Trinity peridotite exposure, few outcrops of pillow-lavas and sheeted dikes have been observed (Fig. 1). The volcanics (Grey Rocks outlier, Fig. 1-II), interpreted as the extrusive member of the Trinity ophiolite (Brouxel and Lapierre, 1984; 1985), are thrust over the peridotite, while the nature of the contact between the dikes (Conant, plot n° 4 on Fig. 1-II) and the gabbros is unknown (Fig. 1). These volcanics, unconformably overlain by Carboniferous sediments (Fig. 1) do no present interbedded sediments.

Between Yreka and Callahan, in the northwestern part of the EKM, volcanic and sedimentary strata are thrust on the Trinity peridotite and gabbros (Fig. 1). Along the Lovers Leap section (Fig. 1), the Trinity gabbros are structurally overlain (thrust ?; Rohr, 1972) by a volcanic unit composed of massive flows and dikes of Ordovician or possible older age (stratigraphic correlations, Potter et al., 1977). They have been interpreted as the extrusive member of the Trinity ophiolite (Lindsley-Griffin, 1977). Along this section, where the Trinity ophiolite was first defined (Lindsley-Griffin, 1977; Fig. 1), Lindsley-Griffin and Griffin (1983) recognized three main rock assemblages : Cretaceous microdiorites and dacites (Lanphere et al., 1968) cross-cutting the Gazelle-Gregg Ranch assemblage and the Trinity ophiolite. The Gazelle-Gregg Ranch assemblage consist at Lovers Leap of the Lower Devonian Gazelle sedimentary Formation (shales, siltstones, chert ...) and the Gregg Ranch melange (mudstones, graywackes, shales, limestones, volcanic lavas and breccias), both thrust over the Trinity ophiolite (Lindsley-Griffin and Griffin, 1983; Fig. 1). According to Lindsley-Griffin and Griffin (1983), this assemblage include also volcanics and dikes intruding the Trinity peridotite and supposed to be of Devonian age (Gregg Ranch Devonian? volcano-sedimentary sequence; Fig. 1).

In the South, near Redding, the Trinity ophiolite is overlain by the volcano-sedimentary formations of the easterly dipping Redding section (Irwin, 1981). The base of this sequence is represented by the Copley mafic volcanics (Copley Greenstone, Kinkel et al., 1956) overlain by the Balaklala Rhyolite Formation. Both formations are unconformably overlain by the shales of the lower Devonian Kennett Formation (Kinkel et al., 1956). The contact between the ophiolite and the Copley Greenstone is not exposed in the Redding vicinity (gravity data, Blakely et al., 1985), however, near Dunsmuir, basic volcanics interpreted as the northernmost extension of the Copley Greenstone (Brouxel et al., 1987) are thrust over the Trinity sheet (Fig. 1). The Copley and Balaklala formations are intruded by the Early Devonian Mule Mountain trondhjemitic stock (400 My by U-Pb, Albers et al., 1981) considered as cogenetic with the Balaklala rhyolites (Barker et al., 1979; Lapierre et al., 1985a; 1985b; Kistler et al., 1985). The Copley Greenstone is therefore ante-Early Devonian in age and could be Silurian or even older.

Many different volcanic series ranging in age from Ordovician to Devonian are spatially associated to the Siluro-Ordovician Trinity ultramafic sheet and related plutonic complexes. Some of these volcanics are interpreted as the extrusive part of the Trinity ophiolite (Lovers Leap Ordovician volcanics and Grey Rocks pillow-lavas). The Copley, Balaklala and Gregg Ranch Devonian? volcanics, are likely of island-arc origin.

Various types of magmas have been recognized within these volcanic series, and their petrological and geochemical features will be developed here.

## PETROGRAPHIC AND GEOCHEMICAL FEATURES

The different lower Paleozoic to Early Devonian EKM volcanics series will be described according to their geographic distribution and age, from North to South and from Ordovician to Devonian. All the volcanics are metamorphosed to greenschist facies which as resulted in important mineralogical modifications without disturbing the original rock fabrics. Olivine and orthopyroxene, commonly altered are replaced by smectites and/or chlorites, and plagioclase is albitized. The

clinopyroxene, replaced by actinolite in the Ordovician? Lovers Leap volcanics and in the Grey Rocks pillow-lavas, is commonly fresh in the Copley Greenstone and the Devonian? volcanics of the Gazelle-Gregg Ranch assemblage. Due to the greenschist metamorphism affecting these rocks, special attention will be given to the incompatible trace elements considered as immobile during metamorphic and alteration processes : Y, Zr, Nb and rare earth elements (REE). The nomenclature used in this work follows these conventions : island-arc tholeiites (IAT) are generally low-K but Fe-enriched and have low Zr and Nb concentrations and La/Yb ratios < 2 times chondritic abundances; calc-alkaline (CA) rocks are generally medium-K but not Fe-enriched and have higher Zr and Nb concentrations and La/Yb ratios > 2 times chondritic (Gill, 1981). Incompatible trace elements are classified following Saunders et al. (1980) as low field strength (LFS : Ba, Sr and Rb) and high field strength (HFS : Zr, Ti and Nb).

#### The Ordovician? Lovers Leap dikes and volcanics

This volcanic unit has been studied along the Lovers Leap section and farther to the northwest at Negro Gulch (respectively outcrops 1 and 2 of Fig. 1-I). It consists mostly of massive flows and dikes in which three lava types can be recognized : basalts, andesites and dacites in order of increasing frequency. All the rocks are highly porphyritic with clinopyroxene and plagioclase phenocrysts. Orthopyroxene has been observed in few andesites. Hornblende phenocrysts occur in some dacitic andesites and dacites.

Geochemically speaking these rocks could be separated in two groups that could not be identified in the field.

The first one is made of low-K tholeiitic basalts, andesites and dacites characterized by low titanium ( $\text{TiO}_2 = 0.55\%$ ), HFS and RE element contents (Zr = 48 ppm, Nb = 2 ppm and La = 1.6 ppm; Tables 1 and 4). They present moreover strongly light REE depleted patterns ( $\text{La/Yb} = 0.34$  times chondritic, Fig. 2). In an extended chondrite normalized diagram (Thompson et al., 1984), they exhibit negative Nb, Zr and Ti anomalies (Fig. 3).

The second group is made of calc-alkalic basalts, andesites and dacites with low titanium contents ( $\text{TiO}_2 = 0.64\%$ ), but higher HFS and RE element contents (Zr = 97 ppm, Nb = 3 ppm and La = 6.74 ppm) than the low-K tholeiites described previously (Tables 2 and 4). They present also higher LFS element concentrations, and exhibit light REE enriched patterns ( $\text{La/Yb} = 2.21$  times chondritic, Fig. 2). Normalized to the chondrites, they exhibit negative Nb, Sr, Y and Ti anomalies (Fig. 3). Compared to the associated low-K tholeiites they present higher Zr/Y ratios and lower Ti/Zr ratios (Table 4 and Fig. 4).

#### The Gregg Ranch Devonian ? volcanics

Basalts and rare andesites have been recognized within this unit consisting of massive and pillowed flows resting on limestones, conglomerates and siliceous shales. The basalts with intersertal textures are either sub-aphyric with only few clinopyroxene microlites, or porphyritic with clinopyroxene and plagioclase phenocrysts. The andesites, always porphyritic, exhibit clinopyroxene, plagioclase and orthopyroxene phenocrysts in an intersertal texture groundmass.

The basalts and andesites are low-K titanium poor tholeiites ( $\text{TiO}_2 = 0.56\%$ ). They are characterized by high compatible trace element contents (Cr = 111-276 ppm and Ni = 62-92 ppm) contents and low HFS and RE element contents (Zr = 28 ppm, Nb = 1 ppm and La = 1.35 ppm). They present light REE depleted patterns ( $\text{La/Yb} = 0.57$  times chondritic, Tables 3 and 4 and Fig. 2). In an extended chondrite normalized diagram they present negative Nb, Sr, Zr, Ti and Y anomalies (Fig. 3).

#### The Grey Rocks pillow-lavas

The Grey Rocks outlier is a sequence of basaltic pillow-lavas and pillow breccias of 500 meters thick. Three rock types can be recognized within this succession : - uncommon clinopyroxene and plagioclase porphyritic basalts, - intersertal texture basalts with abundant plagioclase laths and clinopyroxene microphenocrysts, - subaphyric basalts with clinopyroxene microlites in an abundant cryptocrystalline groundmass.

The Grey Rocks basalts are quartz normative low-K tholeiites poor in titanium ( $\text{TiO}_2 = 0.66\%$ ;  $\text{K}_2\text{O} = 0.21\%$ ). They are characterized by high Cr (140 - 430 ppm) and Ni (90 - 190 ppm) contents, but low HFS and RE element contents (Zr = 39 ppm, Nb = 0.5 ppm and La = 1.28 ppm) and light REE depleted patterns ( $\text{La/Yb} = 0.59$  times chondritic; Tables 4; Fig. 2). In an extended chondrite normalized diagram they present negative Nb, Sr, Zr and Ti anomalies (Fig. 3).

## The Copley and Balaklala volcanics

The Copley basalts and andesites and the overlying Balaklala rhyolitic Formation represent a bimodal volcanic suite with very few rocks of intermediate composition (Kinkel et al., 1956; Barker et al., 1979; Lapierre et al., 1985a; 1985b). The Copley Greenstone consist of a sequence of massive or pillowed flows, tufs and breccias (Kinkel et al., 1956; Lapierre et al., 1985a). The volcanics, commonly highly porphyritic with plagioclase, olivine and clinopyroxene phenocrysts, are represented by picrites, basalts and andesites in order of increasing frequency. The Balaklala Rhyolite Formation consist of tufs, breccias, massive flows, dikes and sills (Kinkel et al., 1956; Lapierre et al., 1985a). The flows are commonly highly porphyritic with quartz and plagioclase phenocrysts. Uncommon amphibole microlites have been observed in the rhyolites crystallized groundmass (Lapierre et al., 1985a).

Basalts and andesites of the Copley Greenstone are low-K Ti poor tholeiites ( $\text{TiO}_2 = 0.65\%$ ). On the trace element point of view, they are characterized by an important range of variation. In some basalts, the REE and the incompatible trace elements contents are very low, and similar to those found in present day mid ocean ridge basalts (MORB), or even more depleted (Table 4; Basaltic Volcanism Study Project, 1981). A wide range of light REE concentrations, from very depleted to somewhat enriched patterns have been observed within the Copley Greenstone (La/Yb chondrite normalized ratios range between 0.21 and 2.53; Fig. 2 and Table 4). Some light REE enriched volcanics, also enriched in LFS elements (Table 4), could be considered as calc-alkalic. It must be however considered that all the types of rocks exist from incompatible trace element depleted low-K tholeiites to calc-alkalic basalts and andesites. In an extended chondrite normalized diagram, the Copley volcanics present negative Ti, Nb, Zr and Y anomalies (Fig. 3).

The Balaklala rhyolites are characterized by very low potassium ( $\text{K}_2\text{O} = 0.80\%$ ) and titanium ( $\text{TiO}_2 = 0.28\%$ ) contents. They present very low incompatible trace element contents (La = 2.90 ppm, Zr = 117 ppm and Nb = 1 ppm) and light REE depleted patterns (Fig. 2 and Table 4). In an extended chondrite normalized diagram, they exhibit strong negative Nb, Sr and Ti anomalies (Fig. 3).

## DISCUSSION

A great diversity of magma types characterized by variable La/Yb and Ti/Zr ratios (Fig. 2, 4 and 5) occur in the EKM Ordovician to Early Devonian volcanic series. Two broad categories can be defined : low-K tholeiitic and calc-alkalic volcanics. The latter, less developed, are mostly located in the northern part of the EKM, between Yreka and Callahan. It must be pointed out that all the studied volcanics present strong geochemical island-arc affinities, that is to say : low titanium contents typical of orogenic volcanism (Bébié, 1980) and low incompatible trace element concentrations, as well as Ti, Zr and Nb negative anomalies (Fig. 3; Dupuy et al., 1982; Briquet et al., 1984; Thompson et al., 1984; White and Patchett, 1984). Mild light REE depletion and enrichment is also a common feature of island-arc tholeiites (i.e. White and Patchett, 1984). Strongly light REE depleted tholeiites, as those observed in the Copley formation and Lovers Leap Ordovician? low-K tholeiites, are however less commonly described (only in the Mariana fore-arc, Crawford et al., 1986), and are interpreted as immature island-arc volcanics.

Looking to the low-K tholeiites spatially associated to the Trinity peridotite and plutonic complexes, it must be pointed out that the Ordovician? Lovers Leap low-K tholeiites, interpreted as the extrusive member of the Trinity ophiolite (Lindsley-Griffin, 1977) are typical island-arc volcanics. Indeed, porphyritic massive flows, and such highly differentiated volcanic suite have never been observed in ophiolites. On the contrary, the subaphyric basaltic pillow-lavas (very homogeneous, little vesicular and no interpillow sediments) of the Grey Rocks outlier could belong to the Trinity ophiolite. They present rather constant compatible and incompatible trace element concentrations (Table 4) more typical of basalts erupted in a spreading center rather than arc volcanics. Moreover, their geochemical features are similar to those recorded in the Trinity high level isotropic gabbros (Brouxel, 1987). They present also similar  $\epsilon\text{Nd}$  values :  $\epsilon\text{Nd}$  ( $T = 450\text{ My}$ ) = 7.3 - 7.6 in the volcanics (Brouxel, 1987) and  $\epsilon\text{Nd} = 6.6 - 7.5$  in the plutonic rocks (Jacobsen et al., 1984; Brouxel, 1987). When compared to MORB, they present similar light REE depleted patterns, but lower titanium and Zr and Nb contents suggesting strong island-arc affinities. This fact is corroborated by the  $\epsilon\text{Nd}$  values of the Trinity ophiolitic rocks. Indeed, when corrected for differential evolution relative to the bulk earth during the past 450 My, the  $\epsilon\text{Nd}$  values of the Trinity ophiolite are similar to present-day intra-oceanic island-arc and marginal basin basalts (DePaolo and Wasserburg, 1977; Hawkesworth et al., 1977; White and Patchett, 1984). We suggest therefore that the Trinity ophiolite was formed in a back-arc basin in the vicinity of an island-arc. Compared to present-day marginal basin basalts (Scotia Sea, Mariana Trough, Lau Basin; Hawkesworth et al., 1977; Saunders and Tarney, 1979; Matthey et al., 1981; Wood et al., 1982; Hawkins and Melchior, 1985), they differ by stronger island-arc geochemical

affinities : lower  $\text{TiO}_2$  and incompatible trace element contents, suggesting that they represent very early stages of back-arc basin development (Lordkipanidze et al., 1979; Hawkins and Melchior, 1985).

The Gregg Ranch Devonian? volcanics present rather similar geochemical features than the Grey Rocks pillow-lavas, with the exception of lower light REE depletion (Fig. 2 and Table 4). The occurrence of massive porphyritic flows as well as the presence of detritic and neritic carbonate sediments in this unit is more in agreement with an origin in an island-arc as suggested the intrusive character of this unit in the Trinity peridotite.

Crystal fractionation processes occur in all the studied volcanics units. This fractionation process is however only little developed in the Grey Rocks volcanic pile where only basalts have been observed. The Lovers Leap low-K tholeiitic basalts, andesites and dacites derived likely by crystal fractionation from a basaltic parent liquid (i.e. increasing of the La and decreasing of Cr and Mg contents with  $\text{SiO}_2$ ). On the contrary, the origin of the Balaklala rhyolites appears more ambiguous. Indeed, it is difficult to envisage the formation of large amounts of such incompatible trace elements depleted rhyolitic volcanics only by crystal fractionation. Moreover, no rocks of intermediate composition exists. The low trace element contents and the strong depletion in Nb, Ti and light REE of the Balaklala rhyolites suggest that their source was very depleted in incompatible trace elements. Partial melting (3-4%) of the most depleted Copley basalts or their plutonic equivalent could formed rhyolites with the required geochemical features. Such partial melting processes within an island-arc, resulting in the formation of acid rocks from mantle derived basalts represent the first stage of continental accretion.

The most important geochemical feature of the EKM low-K tholeiitic volcanic rocks is their strong incompatible trace element depletion (i.e. low Zr and Nb contents, light REE depleted patterns). These geochemical features imposed strong constraint on their source and on their petrogenesis. Indeed, their source must have been strongly depleted and important partial melting degrees (up to 20 %) are necessary to form such light REE depleted volcanics. Compared to MORB, most of the EKM low-K tholeiites are more depleted in HFS and REE elements suggesting a derivation from a source more depleted than a typical MORB source (depletion related to prior melting events). They are on the contrary enriched in alkalis, fact which is commonly interpreted by the addition of fluids derived from the subducting slab or to the partial melting of few percents (1 or 2 %) of subducted sediments (Kay, 1978; White and Patchett, 1984; VonDrach et al., 1986). The low concentration of incompatible trace elements is well explained by the residual character of the mantle source to which sediments enriched in all elements except Ti and Nb are added.

The wide range of light REE variations observed in the Copley tholeiites could not result from crystal fractionation processes ( $\text{La/Yb}$  range from 0.21 to 2.53 times chondritic), and are likely related to different partial melting degrees (Fig. 5). They present moreover an important range of variation of the  $\text{eNd}$  values ( $\text{eNd} = 4.5$  to 8) suggesting than more than one source are involved in their genesis (Brouxel et al., 1987). Diminution of the partial melting degree together with a more important addition of sediments to the source will formed the Copley light REE enriched flows (higher  $\text{La/Yb}$  ratios, lower  $\text{eNd}$  values).

Different partial melting degrees and addition of sediments could explain the geochemical features of almost all the studied volcanics. The Ordovician? Lovers Leap light REE depleted low-K tholeiites could be formed by high degrees of partial melting (20 %) of the same source than the Copley tholeiites (Fig. 5). Crystal fractionation will explain the increasing of the La concentration at constant  $\text{La/Yb}$  chondrite normalized ratio. Slightly lower partial melting degrees of the same source could form the Grey Rocks basaltic pillow-lavas and the Gregg Ranch Devonian? low-K tholeiites (Fig. 5). Lower partial melting degrees (1-5 %) and addition of subducted sediments are necessary to explain the higher alkalic contents and the light REE enrichment of the Ordovician? Lovers Leap calc-alkalic volcanics.

## CONCLUSIONS

These results lead us to suggest that all these rocks, that could derived from the same mantle source, likely belong to the same island-arc - back-arc basin system. Variable partial melting degrees and addition of different amounts of subducted sediments to the source are able to explain all the observed geochemical features.

As in present island-arc - back-arc basin system (i.e. Marianas), a great diversity of light REE depleted to light REE enriched volcanics occur in this island-arc, while back-arc basin lavas are characterized by homogeneous light REE depletion. The latter basalts present however strong island-arc geochemical affinities suggesting that they represent the first stages of back-arc basin opening. The most light REE depleted volcanics have been found in the island-arc suggesting that the first

stages of island-arc building implies high degrees of partial melting of a residual lithosphere. Differentiation takes place by melting of the island-arc deeper layers, leading to the formation of rhyolites directly from mantle derived basalts.

## REFERENCES

- Albers, J.P. and Bain, J.H., 1985. Regional setting and new information on some critical geologic features of the West Shasta District, California. *Econ. Geol.*, 80 : 2072-2091.
- Albers, J.P., Kistler, R.W. and Kwak, K.L., 1981. The Mule Mountain stock, an Early Middle Devonian pluton in northern California. *Isochron West*, 31 : 17.
- Barker, F., Millard, H.T. Jr and Knight, R.J., 1979. Reconnaissance geochemistry of Devonian island-arc volcanic and intrusive rocks, West Shasta district, California. In : F. Barker (Editor), *Trondhjemites, dacites and related rocks*, Elsevier, 2 : 531-545.
- Basaltic Volcanism Study Project, 1981. Basaltic volcanism on the terrestrial planets. Pergamon Press, Inc., New York, 1286 pp.
- Bébian, J., 1980. Magmatismes basiques dits "orogéniques" et "anorogéniques" et teneurs en  $\text{TiO}_2$  : les associations "isotitanées" et "anisotitanées". *J. Volcanol. Geotherm. Res.*, 8 : 337-342.
- Beccaluva, L., Ohnenstetter, D. and Ohnenstetter, M., 1979. Geochemical discrimination between ocean floor and island-arc tholeiites; application to some ophiolites. *Can. J. Earth Sci.*, 16 : 1874-1882.
- Blakely, R.J., Jachens, R.C., Simpson, R.W. and Couch, R.W., 1985. Tectonic setting of the southern Cascade Range as interpreted from its magnetic and gravity fields. *Geol. Soc. Am. Bul.*, 96 : 43-48.
- Briqueu, L., Bougault, H. and Joron, J.L., 1984. Quantification of Nb, Ta, Ti and V anomalies in magmas associated with subduction zones : petrogenetic implications. *Earth Planet. Sci. Lett.*, 68 : 297-308.
- Brouxel, M., 1987. Géochimie d'un arc insulaire intra-océanique fossile et son bassin marginal : les séries paléozoïques de Copley, Balaklala et le cortège ophiolitique de Trinity (Klamath orientales, Nord Californie, U.S.A.). Thèse Doct. Univ. Nancy I, 323 pp.
- Brouxel, M. and Lapierre, H., 1984. La série basaltique de Trinity (Klamath orientales, Nord California) : témoin de l'existence d'un bassin marginal au Dévonien moyen. *C. R. Acad. Sci. Paris*, 299 : 457-462.
- Brouxel, M. and Lapierre, H., 1985. Un bassin marginal dévonien dans les Klamath orientales (Californie du Nord, Etats Unis) : le cortège ophiolitique de Trinity. *Ophioliti*, 10 : 181-202.
- Brouxel, M., Lapierre, H., Michard, A. and Albarède, F., 1987. The deep layers of a Paleozoic arc : Geochemistry of the Copley-Balaklala series (Northern California). *Earth Planet. Sci. Lett.*, in press.
- Church, S.E., 1973. Limits of sediment involvement in the genesis of orogenic volcanic rocks. *Contrib. Mineral. Petrol.*, 39 : 17-32.
- Crawford, A.J., Beccaluva, L. and Serri, G., 1981. Tectono-magmatic evolution of the West Philippine-Mariana region and the origin of boninites. *Earth Planet. Sci. Lett.*, 54 : 346-356.
- Crawford, A.J., Beccaluva, L., Serri, G. and Dostal, J., 1986. Petrology, geochemistry and tectonic implications of volcanics dredged from the intersection of the Yap and Mariana trenches, *Earth Planet. Sci. Lett.*, 80 : 265-280.
- DePaolo, D.J. and Wasserburg, G.J., 1977. The sources of island arcs as indicated by Nd and Sr isotope studies. *Geophys. Res. Lett.*, 4 : 465-468.



- Dewey, J.F. and Bird, J.M., 1971. Origin and emplacement of the ophiolitic suite : Appalachians ophiolites in Newfoundland. *J. Geophys. Res.*, 76 : 3179-3206.
- Dixon, T.H. and Batiza, R., 1979. Petrology and chemistry of recent lavas in the northern Marianas; implications for the origin of island arc basalts, *Contrib. Mineral. Petrol.*, 70 : 167-181.
- Dupuy, C., Dostal, J., Marcelot, G., Bougault, H., Joron, J.L. and Treuil, M., 1982. Geochemistry of basalts from central and southern New Hebrides arc : implication for their source rock composition. *Earth Planet. Sci. Lett.*, 60 : 207-255.
- Evensen, N.M., Hamilton, P.J. and O'Nions, R.K., 1978. Rare earth abundances in chondritic meteorites. *Geochim. Cosmochim. Acta*, 42 : 1199-1212.
- Gill, J.B., 1981. *Orogenic andesites and plate tectonics*. Springer Verlag, Berlin, 390 pp.
- Gill, J.B., 1984. Sr-Pb-Nd isotopic evidence that both MORB and OIB sources contribute to oceanic island arc magmas in Fiji. *Earth Planet. Sci. Lett.*, 68 : 443-458.
- Hawkesworth, C.J., O'Nions, R.K., Pankhurst, R.J., Hamilton, P.J. and Evensen, N.M., 1977. A geochemical study of island-arc and back-arc tholeiites from the Scotia Sea. *Earth Planet. Sci. Lett.*, 36 : 253-262.
- Hawkins, J.W. and Melchior, J.T., 1985. Petrology of Mariana Trough and Lau Basin basalts. *J. Geophys. Res.*, 90 : 11431-11468.
- Irwin, W.P., 1960. Geological reconnaissance of the northern Coast Ranges and Klamath Mountains, California, with a summary of the mineral resources. *Calif. Div. Min. Geol. Bull.*, 179, 80 pp.
- Irwin, W.P., 1966. Geology of the Klamath Mountains Province. *Calif. Div. Min. Geol. Bull.*, 190 : 19-38.
- Irwin, W.P., 1977. Review of Paleozoic rocks of the Klamath Mountains. In : J.H. Stewart, C.H. Stevens and A.E. Fritsche (Editors), *Paleozoic Paleogeography of the western United States*. Soc. Econ. Paleontol. Mineral., Pac. Coast Paleogeo. Symp. 1, Pac. Sect., 441-454.
- Irwin, W.P., 1981. Tectonic accretion of the Klamath Mountains. In W.G. Ernst (Editor), *The geotectonic development of California*. Englewood Cliffs, New Jersey, Prentice-Hall, 29-49.
- Jacobsen, S.B., Quick, J.E. and Wasserburg, G.J., 1984. A Nd and Sr isotopic study of the Trinity peridotite; implications for mantle evolution. *Earth Planet. Sci. Lett.*, 68 : 361-378.
- Kay, R.W., 1978. Aleutian magnesian andesites : melts from subducted Pacific ocean crust. *J. Volcanol. Geotherm. Res.*, 4 : 117-132.
- Kinkel, A.R.J., Hall, W.E. and Albers, J.P., 1956. Geology and base metal deposits of West Shasta Copper-Zinc district, Shasta County, California. *U.S. Geol. Surv. Prof. Pap.*, 285 : 156 pp.
- Kistler, R.W., McKee, E.H., Futa, K., Peterman, Z.E. and Zartman, R.E., 1985. A reconnaissance Rb-Sr, Sm-Nd, U-Pb, and K-Ar study of some host rocks and ore minerals in the West Shasta Cu-Zn District, California. *Econ. Geol.*, 80 : 2128-2135.
- Lanphere, M.A., Irwin, W.P. and Hotz, P.E., 1968. Isotopic age of the Nevada orogeny and older plutonic and metamorphic events in the Klamath Mountains, California. *Geol. Soc. Am. Bul.*, 79 : 1027-1052.
- Lapierre, H., Albarède, F., Albers, J., Cabanis, B. and Coulon, C., 1985a. The early Devonian volcanism in the eastern Klamath Mountains, California : evidence for an immature island-arc. *Can. J. Earth Sci.*, 22 : 214-227.
- Lapierre, H., Cabanis, B., Coulon, C., Brouxel, M., and Albarède, F., 1985b. The geodynamic setting of the Early Devonian Kuroko-type sulfide deposits in the eastern Klamath Mountains (northern California) inferred by the petrological and geochemical characteristics of associated island volcanic rocks. *Econ. Geol.*, 80 : 2100-2113.

- Lapierre, H., Brouxel, M., Martin, P., Coulon, C., Mascle, G., and Cabanis, B., 1986. The Paleozoic and Mesozoic geodynamic evolution of the eastern Klamath Mountains (N. California) inferred from its magmatism. *Bull. Soc. géol. France*, 8-II : 969-980.
- Lapierre, H., Brouxel, M., Albarède, F., Coulon, C., Lecuyer, C., Martin, P., Mascle, G. and Rouer, O., 1987. Paleozoic and Lower Mesozoic magmas from the eastern Klamath Mountains (N. California) and the geodynamic evolution of the north-western America. *Tectonophysics*, in press.
- Leitch, E.C., 1984. Island arc elements and arc-related ophiolites. *Tectonophysics*, 106 : 177-203.
- Lindsley-Griffin, N., 1977. The Trinity ophiolite, Klamath Mountains, California. In : R.G. Coleman and W.P. Irwin (Editors), *North American ophiolites*. *Oreg. Dept. Geol. Min. Ind. Bull.*, 95 : 107-120.
- Lindsley-Griffin, N. and Griffin, J.R., 1983. The Trinity terrane : An Early Paleozoic microplate assemblage. In : C.H. Stevens (Editor), *Pre-Jurassic rocks in western North American suspect terranes*. *Soc. Econ. Paleontol. Mineral., Pac. Sec.*, 63-75.
- Lordkipanidze, M.B., Zakariadze, G.S. and Popolitov, E.I., 1979. Volcanic evolution of the marginal and interarc basins. *Tectonophysics*, 57 : 71-83.
- Mattey, D.P., Nicolas, N.G. and Tarney, J., 1981. The geochemistry, mineralogy, petrology of basalts from the West Philippine and Parece Vela basins and from the Palau-Kyushu and West Mariana Ridges, Deep Sea Drilling Project Leg 59. *Init. Rep. D. S. D. P.*, 59 : 753-800.
- Mattinson, J.M. and Hopson, C.A., 1972. Paleozoic ophiolitic complexes in Washington and northern California. *Can. Inst. Year. B.*, 71 : 578-583.
- Miyashiro, A., 1973. The Troodos ophiolitic complex was probably formed in an island-arc. *Earth Planet. Sci. Lett.*, 19 : 218-224.
- Morris, J.D. and Hart, S.R., 1983. Isotopic and incompatible element constraints on the genesis of arc volcanics from Cold Bay and Amak Island, Aleutians, and implications for mantle structure. *Geochim. Cosmochim. Acta*, 47 : 2015-2030.
- Potter, A.W., Hotz, P.E. and Rohr, D.M., 1977. Stratigraphy and inferred tectonic framework of lower Paleozoic rocks in the eastern Klamath Mountains, northern California. In : J.H. Stewart, C.H. Stevens and A.E. Fritsche (Editors), *Paleozoic Paleogeography of the western United States*. *Soc. Econ. Paleontol. Mineral., Pac. Coast Paleogeo. Symp.* 1, *Pac. Sect.*, 421-441.
- Quick, J.E., 1981. Petrology and petrogenesis of the Trinity peridotite, an upper mantle diapir in the eastern Klamath Mountains, northern California. *J. Geophys. Res.*, 87 : 3831-3848.
- Rohr, D.M., 1972. Geology of the Lovers Leap area, China Mountain quadrangle, California. M's Thesis, *Oreg. State Univ., Corvallis, Oregon*, 95 pp.
- Saunders, A.D. and Tarney, J., 1979. The geochemistry of basalts from a back-arc spreading center in the East Scotia Sea. *Geochim. Cosmochim. Acta*, 43 : 555-572.
- Saunders, A.D., Tarney, J., Marsh, N.G. and Wood, D.A., 1980. Ophiolites as ocean crust or marginal basin crust : a geochemical approach. In : A. Panayiotou (Editor), *Ophiolites Proceeding International Symposium, Cyprus, 1979*, 193-204.
- Serri, G., 1981. The petrochemistry of ophiolitic gabbroic complex : a key for the classification of ophiolites into low-Ti and high-Ti type. *Earth Planet. Sci. Lett.*, 52, p. 203-212.
- Strand, R.G., 1962. Geologic atlas of California, Redding sheet : 1/250,000. *Calif. Div. Min. Geol.*
- Strand, R.G., 1963. Geologic atlas of California, Weed sheet : 1/250,000. *Calif. Div. Min. Geol.*
- Thompson, R.N., Morrisson, M.A., Hendry, G.L., and Parry, S.J., 1984. An assessment of the relative roles of crust and mantle in magma genesis : an elemental approach. *Phil. Trans. Roy. Soc. London*, 310 : 549-590.

- Volpe, A.M., Macdougall, J.D. and Hawkins, J.W., 1987. Mariana Trough basalts (MTB) : trace element and Sr-Nd isotopic evidence for mixing between MORB-like and Arc-like melts. *Earth Planet. Sci. Lett.*, 82 : 241-254.
- VonDrach, V., Marsh, B.D. and Wasserburg, G.J., 1986. Nd and Sr isotopes in the Aleutians : multicomponent parenthood of island-arc magmas. *Contrib. Mineral. Petrol.*, 92 : 13-34.
- Wagner, D. and Saucedo, G.J., 1986. Geologic map of the Weed quadrangle, 1/250,000, California. *Calif. Div. Min. Geol., region. geol. map series*, 4A.
- White, W.M. and Patchett, J., 1984. Hf - Nd - Sr isotopes and incompatible element abundances in island-arcs : implications for magma origins and crust - mantle evolution. *Earth Planet. Sci. Lett.*, 67 : 167-185.
- Wood, D.A., Morsh, N.G., Tarney, J., Joron, J.L., Fryer, P. and Treuil, M., 1982. Geochemistry of igneous rocks recovered from a transect across the Mariana through, arc, fore-arc and trench. *Init. Rep. D. S. D. P.*, 60 : 611-642.

#### FIGURE CAPTIONS

- Fig. 1 : Geological map of the eastern Klamath Mountains (EKM) modified after Irwin (1977), Strand (1962; 1963) and Wagner and Saucedo (1986). The Lovers Leap area geological map and cross section (I) are slightly modified after Lindsley-Griffin and Griffin (1983). The Dunsmuir area geological map and cross section (II) are modified from Wagner and Saucedo (1986). The Redding area geological map (III) is from Albers and Bain (1985).
- Fig. 2 : Chondrite normalized REE patterns (C1 of Evensen et al., 1978) of the EKM lower Paleozoic to Devonian volcanics. See text and Fig. 1 for location of samples.
- Fig. 3 : Extended chondrite normalized trace element diagram (Thompson et al., 1984) of the EKM lower Paleozoic to Devonian volcanics. Normalized values are from Thompson et al. (1984), except REE from Evensen et al. (1978). Same symbols as in Fig. 2.
- Fig. 4 : Ti versus Zr diagram for the EKM lower Paleozoic to Devonian volcanics. Dashed lines separate the different Yreka-Callahan volcanic series. Dashed field represent the Copley volcanic. Same symbols as in Fig. 2.
- Fig. 5 : La versus La/Yb chondrite normalized ratio for the EKM lower Paleozoic to Devonian volcanics. Same symbols as in Fig. 2.

#### TABLE CAPTIONS

- Table 1 : Major and trace element concentrations of the Ordovician? Lovers Leap low-K tholeiites. Samples TR come from the Lovers Leap section (plot 1 on Fig. 1-I), and samples NG come from the Negro Gulch (plot 2 on Fig. 1-I). Major and trace element analyses (Cr, Ni, Ba, V, Sr, Rb and REE) were performed by ICP spectroscopy at the Service d'Analyses of the Centre de Recherches Pétrographiques et Géochimiques (CRPG, Nancy) ( $\text{Fe}_2\text{O}_3^*$  = total iron as  $\text{Fe}_2\text{O}_3$ ). Y, Zr and Nb have been analyzed by X-Ray Fluorescence at the Service Communs d'Analyses of the Université of Nancy I.
- Table 2 : Major and trace element concentrations of the Ordovician? Lovers Leap calc-alkaline volcanics. See Table 1 and Fig. 1-I for location of the samples.
- Table 3 : Major and trace element concentrations of the Devonian? Greeg-Ranch low-K tholeiites. Samples come from the Greeg Ranch section (plot 3 on Fig. 1-I).
- Table 4 : Mean values and trace element concentration variations of the EKM lower Paleozoic and Devonian volcanics. Grey Rocks, Copley and Balaklala analyses are from Brouxel and Lapierre (1985); Lapierre et al. (1985a; 1985b); Brouxel (1987) and Brouxel et al. (1987).

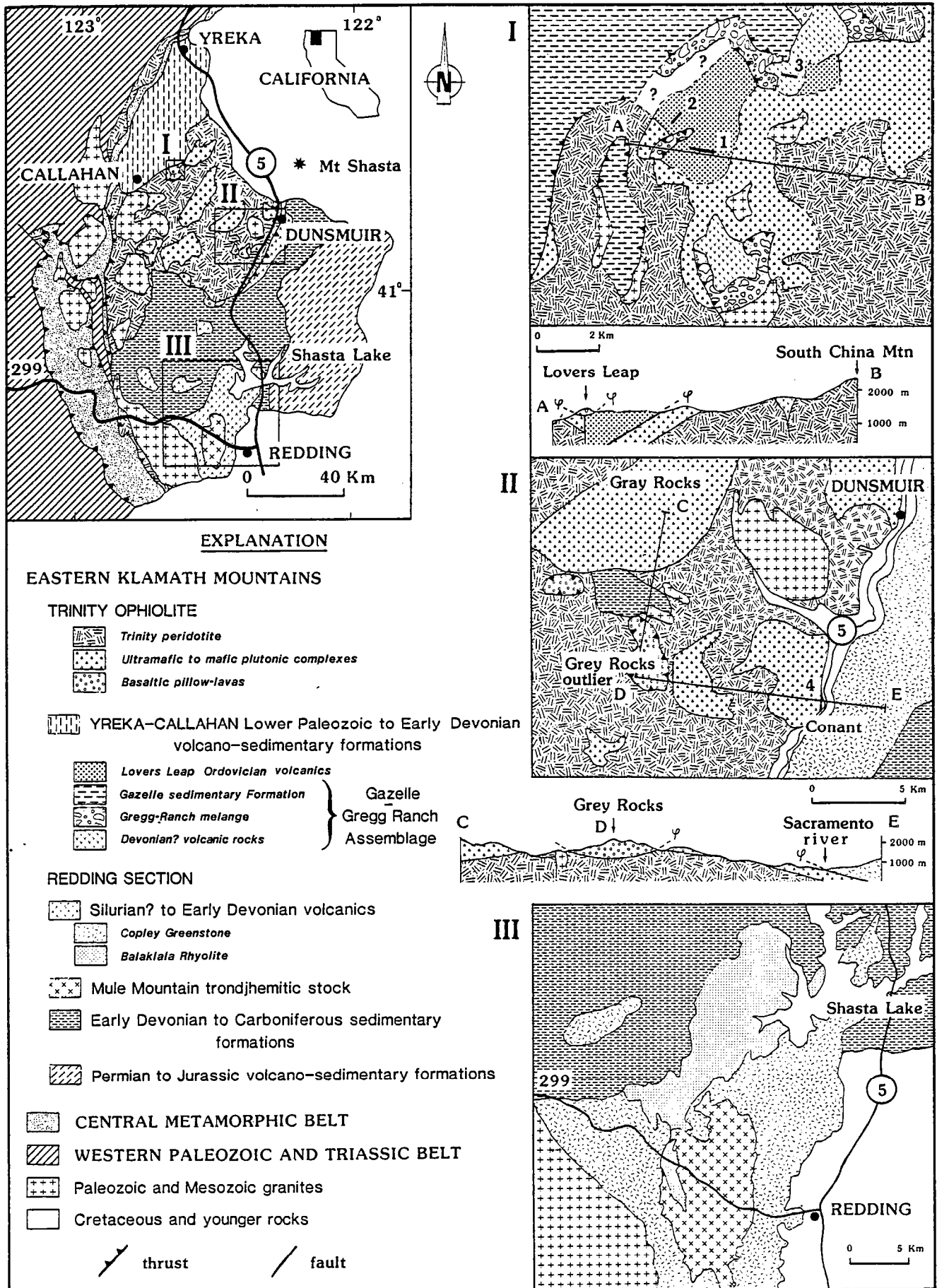


Figure 1

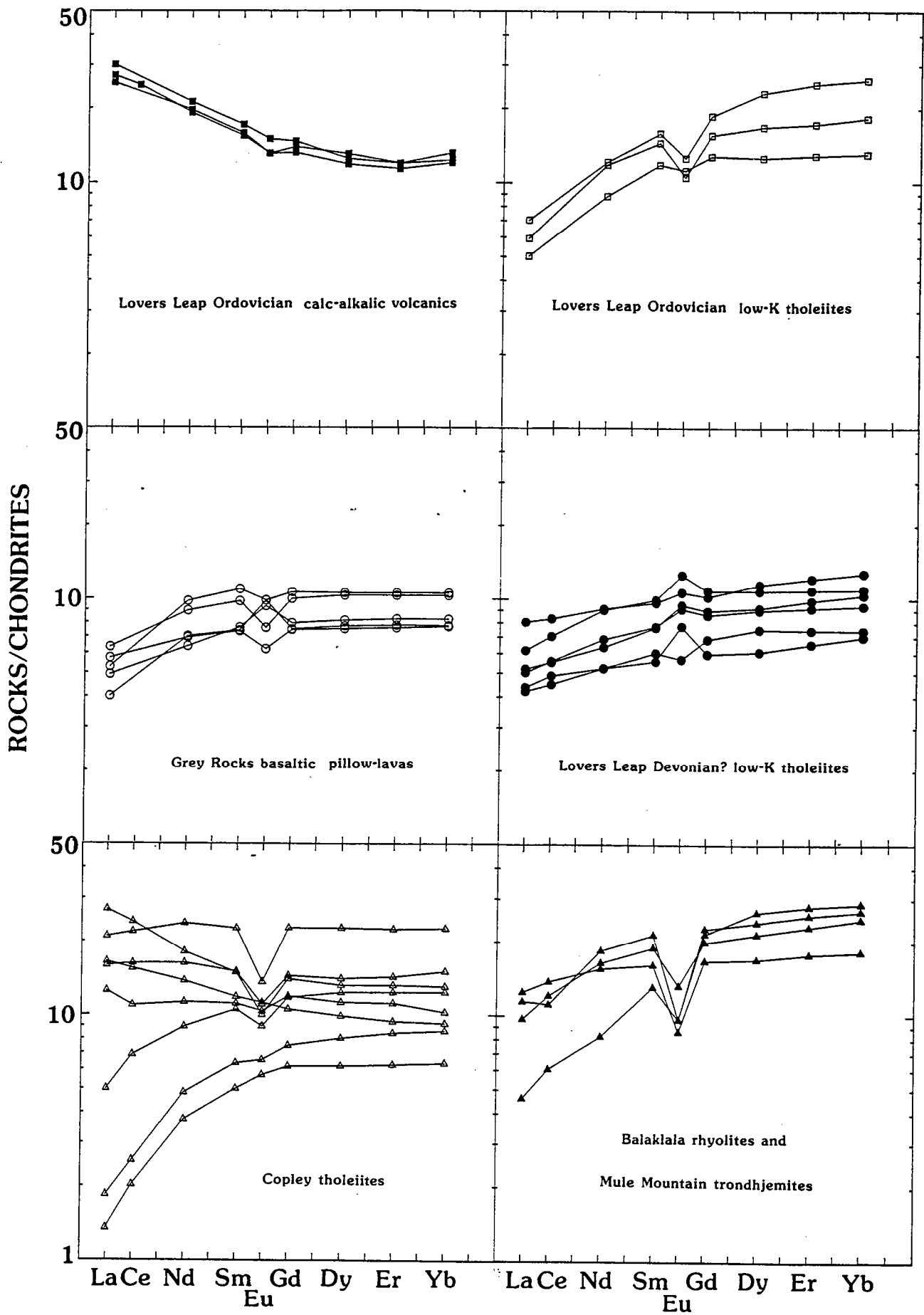


Figure 2

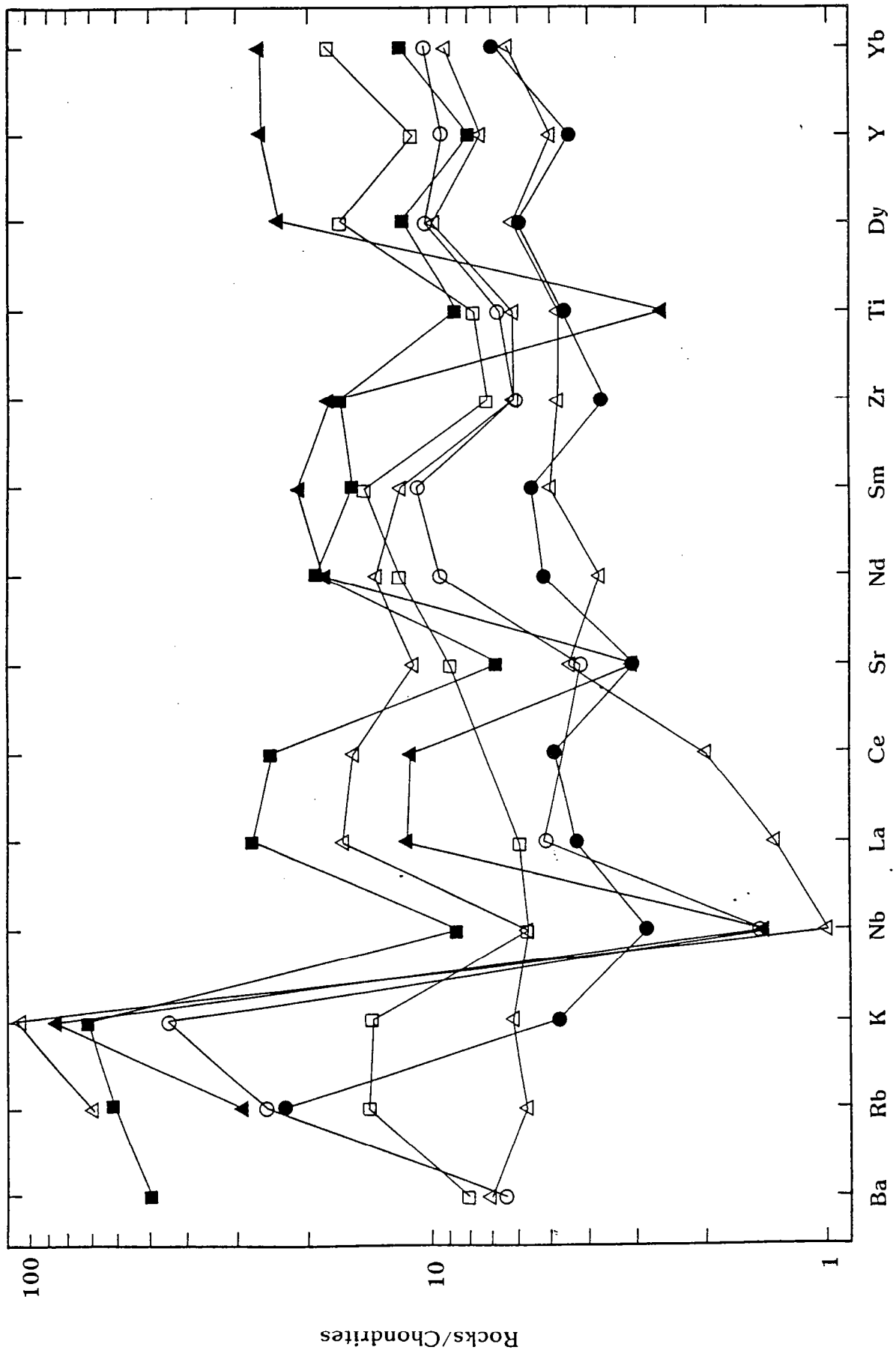


Figure 3

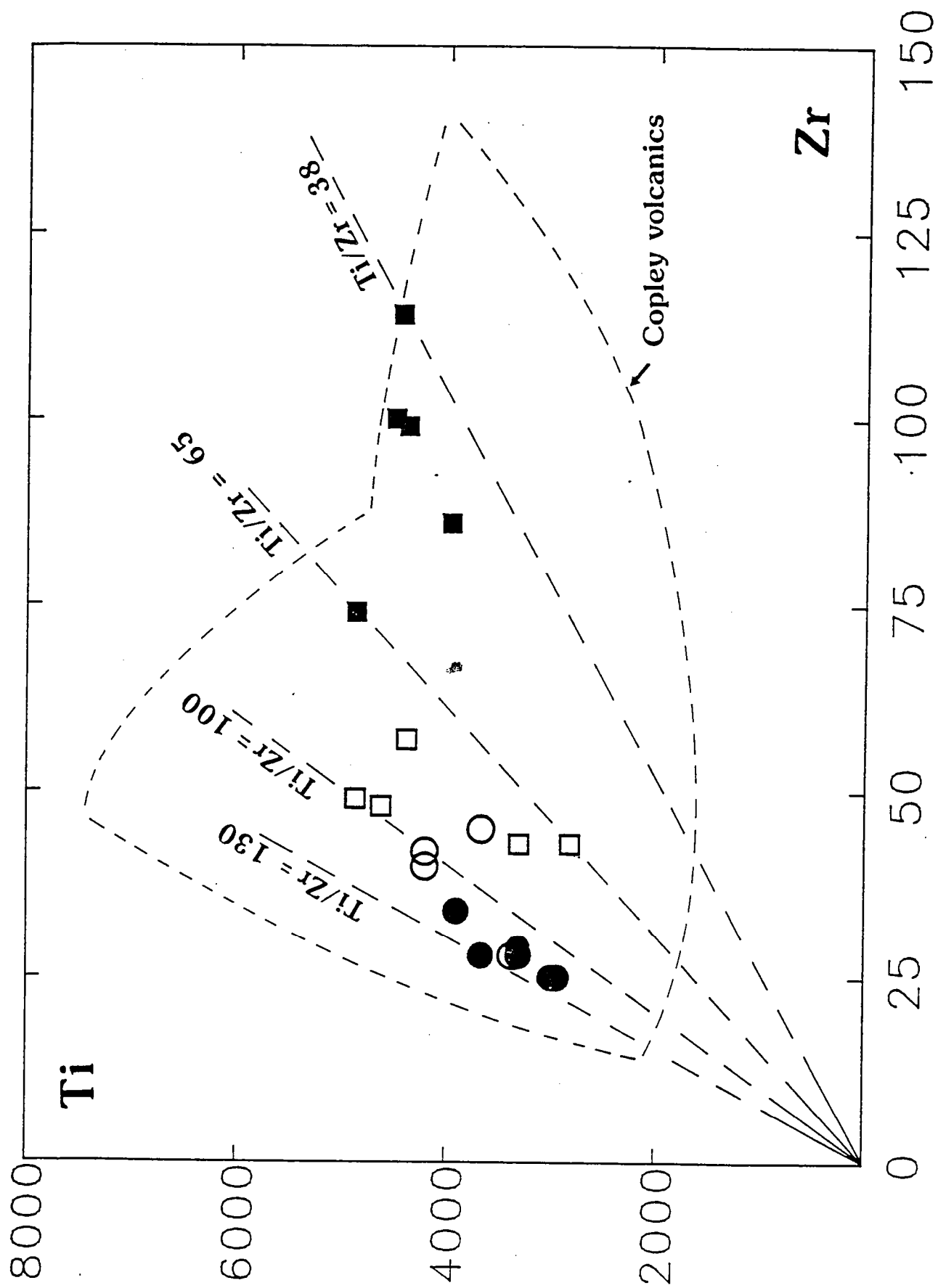


Figure 4

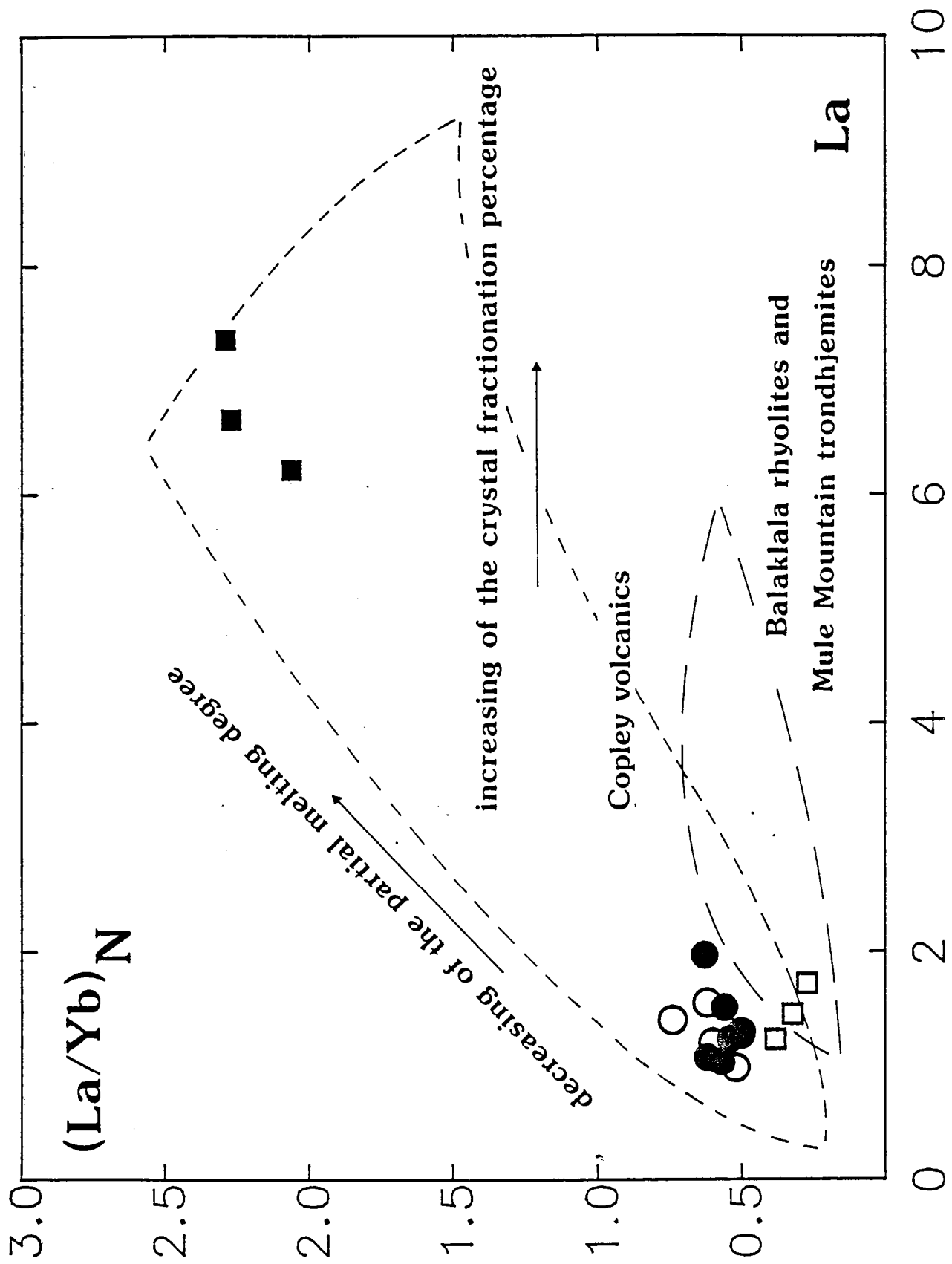


Figure 5



Tableau 1

| Samples                          | TR 467 | TR 465 | TR 462 | NG 12 | NG 8  | NG 5  |
|----------------------------------|--------|--------|--------|-------|-------|-------|
| SiO <sub>2</sub>                 | 55.39  | 59.10  | 72.43  | 43.38 | 49.23 | 48.03 |
| TiO <sub>2</sub>                 | 0.55   | 0.81   | 0.28   | 0.47  | 0.73  | 0.77  |
| Al <sub>2</sub> O <sub>3</sub>   | 16.68  | 16.02  | 13.02  | 12.56 | 15.80 | 17.87 |
| Fe <sub>2</sub> O <sub>3</sub> * | 6.36   | 6.88   | 3.86   | 8.20  | 9.54  | 9.58  |
| MgO                              | 6.04   | 4.89   | 1.14   | 6.98  | 8.74  | 5.60  |
| MnO                              | 0.11   | 0.10   | 0.07   | 0.28  | 0.19  | 0.20  |
| CaO                              | 5.06   | 2.73   | 0.37   | 11.90 | 8.58  | 11.24 |
| Na <sub>2</sub> O                | 3.65   | 5.10   | 5.64   | 0.08  | 2.41  | 2.80  |
| K <sub>2</sub> O                 | 0.95   | 0.20   | 0.09   | 1.09  | 1.64  | 0.23  |
| L.I.                             | 3.96   | 2.80   | 1.68   | 14.29 | 3.00  | 3.36  |
| Total                            | 98.75  | 98.63  | 98.58  | 99.23 | 99.86 | 99.68 |
| FeO*/MgO                         | 0.95   | 1.27   | 3.05   | 1.06  | 0.98  | 1.54  |
| Cr                               | 58     | 10     | 10     | 766   | 402   | 34    |
| Ni                               | 74     | 40     | 22     | 240   | 112   | 42    |
| Y                                | 20     | 22     | 42     | 13    | 19    | 17    |
| Zr                               | 43     | 49     | -      | 43    | 57    | 48    |
| Nb                               | 2      | 2      | -      | 1     | 3     | 1     |
| Ba                               | 94     | 55     | 28     | -     | -     | -     |
| V                                | 157    | 188    | 10     | 203   | 239   | 249   |
| Sr                               | 122    | 105    | 13     | 48    | 170   | 717   |
| Rb                               | 9      | 5      | 5      | 29    | 44    | 1     |
| La                               | 1.23   | 1.45   | 1.72   | -     | -     | -     |
| Nd                               | 4.18   | 5.60   | 5.75   | -     | -     | -     |
| Sm                               | 1.82   | 2.23   | 2.44   | -     | -     | -     |
| Eu                               | 0.65   | 0.61   | 0.73   | -     | -     | -     |
| Gd                               | 2.61   | 3.18   | 3.81   | -     | -     | -     |
| Dy                               | 3.20   | 4.27   | 5.87   | -     | -     | -     |
| Er                               | 2.14   | 2.87   | 4.17   | -     | -     | -     |
| Yb                               | 2.16   | 3.02   | 4.31   | -     | -     | -     |

Tableau 2

| Samples                          | TR 454 | TR 455 | TR 456 | NG 14 | NG 13 | NG 4  | NG 3  |
|----------------------------------|--------|--------|--------|-------|-------|-------|-------|
| SiO <sub>2</sub>                 | 51.69  | 56.04  | 57.85  | 52.14 | 51.04 | 62.21 | 66.18 |
| TiO <sub>2</sub>                 | 0.81   | 0.75   | 0.74   | 0.66  | 0.73  | 0.50  | 0.26  |
| Al <sub>2</sub> O <sub>3</sub>   | 17.46  | 18.68  | 19.27  | 15.21 | 17.25 | 17.00 | 17.02 |
| Fe <sub>2</sub> O <sub>3</sub> * | 9.43   | 7.27   | 7.17   | 7.97  | 8.79  | 5.08  | 3.11  |
| MgO                              | 5.75   | 1.31   | 3.11   | 6.61  | 7.51  | 3.08  | 1.63  |
| MnO                              | 0.12   | 0.09   | 0.18   | 0.17  | 0.18  | 0.07  | 0.05  |
| CaO                              | 4.34   | 3.83   | 1.18   | 4.98  | 3.15  | 4.45  | 2.10  |
| Na <sub>2</sub> O                | 4.69   | 4.58   | 5.54   | 1.94  | 0.97  | 4.02  | 5.61  |
| K <sub>2</sub> O                 | 0.80   | 2.56   | 1.03   | 1.55  | 2.33  | 1.09  | 1.57  |
| L.I.                             | 4.85   | 4.97   | 3.74   | 8.51  | 7.91  | 2.27  | 2.25  |
| Total                            | 99.94  | 100.08 | 99.81  | 99.74 | 99.86 | 99.77 | 99.78 |
| FeO*/MgO                         | 1.48   | 4.99   | 2.07   | 1.09  | 1.05  | 1.48  | 1.72  |
| Cr                               | 310    | 17     | 14     | 207   | 144   | 102   | 10    |
| Ni                               | 102    | 40     | 49     | 56    | 46    | 36    | 16    |
| Y                                | 20     | 18     | 16     | 15    | 18    | 13    | 8     |
| Zr                               | 74     | 100    | 114    | 86    | 99    | 102   | 102   |
| Nb                               | 3      | 3      | 3      | 2     | 4     | 4     | 3     |
| Ba                               | 358    | 758    | 336    | -     | -     | -     | -     |
| V                                | 361    | 230    | 122    | 174   | 173   | 76    | 100   |
| Sr                               | 290    | 101    | 79     | 52    | 41    | 398   | 298   |
| Rb                               | 16     | 54     | 21     | 48    | 59    | 21    | 35    |
| La                               | 7.35   | 6.21   | 6.65   | -     | -     | -     | -     |
| Ce                               | -      | -      | 15.82  | -     | -     | -     | -     |
| Nd                               | 10.01  | 9.30   | 9.06   | -     | -     | -     | -     |
| Sm                               | 2.64   | 2.44   | 2.38   | -     | -     | -     | -     |
| Eu                               | 0.87   | 0.76   | 0.76   | -     | -     | -     | -     |
| Gd                               | 3.00   | 2.85   | 2.70   | -     | -     | -     | -     |
| Dy                               | 3.17   | 3.32   | 3.01   | -     | -     | -     | -     |
| Er                               | 1.98   | 1.98   | 1.88   | -     | -     | -     | -     |
| Yb                               | 2.17   | 2.03   | 1.98   | -     | -     | -     | -     |

Tableau 3

| Samples                          | GR 16 | GR 21 | GR 19  | GR 13 | GR 10 | GR 12 |
|----------------------------------|-------|-------|--------|-------|-------|-------|
| SiO <sub>2</sub>                 | 51.85 | 53.73 | 49.02  | 56.90 | 57.51 | 55.08 |
| TiO <sub>2</sub>                 | 0.49  | 0.50  | 0.55   | 0.65  | 0.55  | 0.61  |
| Al <sub>2</sub> O <sub>3</sub>   | 15.79 | 15.84 | 16.80  | 16.11 | 15.79 | 15.76 |
| Fe <sub>2</sub> O <sub>3</sub> * | 6.64  | 6.06  | 7.71   | 6.02  | 6.68  | 7.53  |
| MgO                              | 6.86  | 6.05  | 7.61   | 5.07  | 5.24  | 5.77  |
| MnO                              | 0.16  | 0.15  | 0.15   | 0.15  | 0.16  | 0.15  |
| CaO                              | 9.80  | 7.54  | 10.04  | 4.61  | 5.00  | 5.97  |
| Na <sub>2</sub> O                | 4.34  | 6.12  | 3.94   | 7.16  | 5.72  | 5.79  |
| K <sub>2</sub> O                 | 0.07  | 0.23  | 0.06   | 0.09  | 0.26  | 0.08  |
| L.I.                             | 3.68  | 3.66  | 4.24   | 2.75  | 2.91  | 3.17  |
| Total                            | 99.68 | 99.88 | 100.12 | 99.51 | 99.82 | 99.91 |
| FeO*/MgO                         | 0.87  | 0.90  | 0.91   | 1.07  | 1.15  | 1.17  |
| Cr                               | 276   | 214   | 267    | 219   | 111   | 123   |
| Ni                               | 92    | 82    | 83     | 69    | 62    | 70    |
| Y                                | 9     | 11    | 18     | 15    | 13    | 15    |
| Zr                               | 25    | 25    | 29     | 34    | 28    | 28    |
| Nb                               | 1     | 1     | 1      | 1     | 0     | 1     |
| V                                | 222   | 267   | 267    | 235   | 210   | 236   |
| Sr                               | 36    | 31    | 27     | 37    | 93    | 27    |
| Rb                               | 8     | 6     | 7      | 5     | 5     | 5     |
| La                               | 1.07  | 1.03  | 1.97   | 1.51  | 1.23  | 1.27  |
| Ce                               | 3.11  | 2.87  | 5.31   | 4.50  | 3.56  | 3.53  |
| Nd                               | 2.48  | 2.48  | 4.33   | 4.28  | 3.25  | 3.02  |
| Sm                               | 0.86  | 0.93  | 1.49   | 1.53  | 1.19  | 1.18  |
| Eu                               | 0.45  | 0.33  | 0.62   | 0.73  | 0.53  | 0.55  |
| Gd                               | 1.22  | 1.40  | 2.09   | 2.21  | 1.76  | 1.83  |
| Dy                               | 1.55  | 1.91  | 2.92   | 2.75  | 2.29  | 2.34  |
| Er                               | 1.09  | 1.24  | 2.02   | 1.81  | 1.53  | 1.64  |
| Yb                               | 1.16  | 1.23  | 2.11   | 1.81  | 1.55  | 1.72  |

|       | TiO <sub>2</sub> | K <sub>2</sub> O | Y     | Zr     | Nb  | Sr     | Rb    | Ba      | La         | Ti/Zr   | Zr/Y     | Zr/La     | (La/Yb) <sub>N</sub> |
|-------|------------------|------------------|-------|--------|-----|--------|-------|---------|------------|---------|----------|-----------|----------------------|
| Range | 0.26-0.81        | 0.80-2.56        | 8-20  | 86-114 | 2-4 | 41-398 | 16-59 | 336-758 | 9.06-10.01 | 15- 66  | 3.7-12.8 | 10.1-17.1 | 2.06-2.29            |
| Mean  | 0.64             | 1.56             | 15    | 97     | 3   | 180    | 36    | 484     | 6.74       | 41      | 6.9      | 14.4      | 2.21                 |
| Range | 0.27-0.90        | 0.01-1.64        | 13-42 | 43- 57 | 1-3 | 10-717 | 1-44  | 19- 94  | 1.23- 1.72 | 66- 99  | 2.2- 3.3 | 33.8-35.0 | 0.27-0.38            |
| Mean  | 0.55             | 0.44             | 24    | 48     | 2   | 121    | 11    | 44      | 1.47       | 83      | 2.7      | 34.4      | 0.32                 |
| Range | 0.49-0.65        | 0.06-0.26        | 9-18  | 25- 34 | 0-1 | 27- 93 | 5- 8  | -       | 1.03- 1.97 | 114-131 | 1.6- 2.8 | 14.7-24.3 | 0.50-0.63            |
| Mean  | 0.56             | 0.13             | 14    | 28     | 1   | 42     | 6     | -       | 1.35       | 119     | 2.2      | 21.6      | 0.57                 |
| Range | 0.48-0.91        | 0.06-0.65        | 13-19 | 28- 45 | 0-1 | 38- 86 | 2- 8  | 10- 46  | 0.98- 1.55 | 81-120  | 1.7- 3.5 | 25.8-32.6 | 0.50-0.74            |
| Mean  | 0.66             | 0.21             | 16    | 39     | 0.5 | 58     | 5     | 26      | 1.28       | 102     | 2.5      | 30        | 0.59                 |
| Range | 0.30-1.23        | 0-3.49           | 7-42  | 14-141 | 0-4 | 8-666  | 0-61  | 15-1045 | 0.32- 9.34 | 27-169  | 1.3- 4.1 | 7.0-90.4  | 0.21-2.53            |
| Mean  | 0.65             | 0.42             | 21    | 48     | 1   | 110    | 9     | 129     | 2.73       | 96      | 2.3      | 22.9      | 0.97                 |
| Range | 0.15-0.52        | 0.10-1.88        | 28-60 | 70-147 | 1-2 | 19-114 | 1-33  | 79-1270 | 1.09- 5.91 | 7- 40   | 1.3- 4.9 | 13.4-96.5 | 0.16-0.72            |
| Mean  | 0.28             | 0.80             | 42    | 117    | 1   | 57     | 11    | 320     | 2.90       | 16      | 2.9      | 44.5      | 0.47                 |

Tableau 4

**SIGNIFICANCE OF THE UPPER PALEOZOIC ISLAND ARC MAGMAS FROM NORTHERN CALIFORNIA AND EASTERN OREGON IN THE GEODYNAMIC EVOLUTION OF THE CORDILLERA**

Rouer, O. (1, 2), Lecuyer, C. (2, 3), Lapierre, H. (1), Charvet, J. (1), Coulon, C. (4) and Martin, P. (2).

(1) Laboratoire de Géologie structurale, ID/CNRS 5149, Université d'Orléans, BP 6759, 45067 ORLEANS Cedex 02, France

(2) Laboratoire de Pétrologie, Université de Nancy I, BP 239, 54506 VANDOEUVRE/Nancy Cedex, France

(3) Laboratoire de Géochimie, Université de Rennes, CAESS/CNRS, 35042 RENNES, France

(4) Laboratoire de Pétrologie Magmatique, URA/CNRS 1277, Université d'Aix-Marseille III, 13397 MARSEILLE Cedex 13, France

## ABSTRACT

Island arc volcanism represents an important clue in the geodynamic evolution of the western American margin particularly for the Permian period for which it is possible to study and correlate contemporaneous volcanic activity in areas like the eastern Klamath Mountains, Blue Mountains and northern Sierra Nevada. Petrological and geochemical data show that the emitted volcanics of eastern Klamath and Blue Mountains belong to low-K tholeiitic suites, whereas in northern Sierra Nevada calc-alkaline rocks are present. The occurrence of Permian ophiolitic cumulates and volcanics in the Central Belt of Sierra Nevada and in the Havallah-Pumpnickel Formations in Nevada reveals the presence of ocean and/or back-arc basins between the different arc-segments. The tectonic constraints of these aforementioned areas are also different. The Late Permian-early Triassic Sonoma orogeny, recorded in northern Sierra Nevada, lacks in the eastern Klamath and Blue Mountains. Taking into account 1) the magmatic affinity of the island arc and ophiolitic sequences and 2) the age and geographic distribution of the tectonic phases, a geodynamic model is proposed for the Cordillera during Late Paleozoic-Early Mesozoic times, before the building-up of the American-Mexican block.

## INTRODUCTION

The American Cordillera domain consists of a mosaic of continental or oceanic fragments which are considered autochthonous by Churkin (1974) or allochthonous ("suspect terranes") by Coney and others (1980). These authors proposed that these lithospheric fragments have collided the North American craton during Mesozoic or Cenozoic times. On the contrary, for Roure and Sosson (1986), the building up of the Cordillera consists first of the collision of these lithospheric fragments during the Cimmerian orogeny (Late Triassic-Early Jurassic) to form a microcontinent called American-Mexican block; then to the accretion of this block to the passive American margin, during the Late Jurassic Nevadan orogeny.

Thus, it appears that Permian-Late Triassic time is a key period preceeding the American-Mexican block building-up because of the occurrence of various geologic events (magmatism, tectonics) in these different lithospheric fragments. The best exposures of island arc and/or ophiolitic sequences (Speed, 1979; Coney and others, 1980) are located in the eastern Klamath Mountains, the Blue Mountains (eastern Oregon), and the Central and Eastern Belts of northern Sierra Nevada.

Despite similar ages, differences exist among the volcanic terranes involving polyphased tectonic histories and/or geochemistry of the igneous rocks.

This study offers to correlate these data in the aim to propose a model of geodynamic evolution of the American Cordillera during Permian-Late Triassic time.

The four regions, in which a Permian volcanic activity occurs, are set out between California, Oregon and Idaho States. The Eastern and Central Belts of northern Sierra Nevada and eastern Klamath Mountains are in the north-east and northern parts of the California state, whereas the Blue Mountains are settled along the Snake River between the Oregon-Idaho state limit (Fig. 1).

## THE EASTERN KLAMATH ISLAND ARC VOLCANIC SUITES

The eastern Klamath Mountains (Fig. 1) can be divided into three main geologic units that are from the north to the south : 1) the Lower Paleozoic arc volcanic and sedimentary rocks of the Yreka-Callahan area, 2) the Lower Paleozoic Trinity ophiolite and 3) the Silurian to Middle Jurassic island arc volcanic and sedimentary rocks of the Redding section where has been previously defined a Permian-early Triassic island arc sequence (Albers and Roberston 1961; Martin and others, 1984; Lapierre and others, 1986-1987). The Permian-Triassic volcanics conformably rest on the Permian McCloud limestone (Albers and Robertson, 1961; Fig. 2) and are exposed along EW striking monoclinial sections tilted to the east. The island arc sequence consists at the base of the Nosoni Formation and at the top of the Dekkas Formation which is conformably overlain in the south by the Bully Hill rhyolite. The Pit shales and the Hosselkus limestone conformably overlie the volcanic sequence (Fig. 2). The eastern Klamath lavas are metamorphosed in the zeolite facies (prehnite + pumpellyite + quartz + epidote).

In the Nosoni Formation, basaltic, andesitic, dacitic and rhyolitic flows are associated with pyroclastic beds and are interlayered with fossiliferous mudstones and fusulinids bearing limestones (Permian age: Coogan, 1960; Roure, 1984). The overlying sequence (Dekkas Formation) consists of minor basalts and andesites (flows, tufs, breccias) overlain by dacitic and rhyolitic flows. The sediments are siliceous mudstones and siltstones. The Bully Hill rhyolite,

which constitutes the top of the Permian volcanic sequence (Fig. 2), occurs only in the south and is formed of acid pyroclastics and massive basaltic and rhyolitic flows (Albers and Robertson, 1961). The Nosoni and Dekkas lavas have similar petrological characteristics. The basalts are generally highly porphyritic with olivine, augite, plagioclase + orthopyroxene phenocrysts (Martin and others, 1984; Lapierre and others, 1986-1987). Andesites contain zoned plagioclase, augite + orthopyroxene phenocrysts. The rhyolites differ from the dacites by the occurrence of quartz phenocrysts (Martin and others, 1984).

The Nosoni and Dekkas basalts and andesites (Table 1) are SiO<sub>2</sub> saturated and TiO<sub>2</sub> (< 1,2%) and K<sub>2</sub>O (< 1,4%) poor. Most of the basalts and andesites are poor in Cr (10 - 100 ppm) and Ni (22 - 53 ppm) suggesting that they underwent crystal fractionation (Lapierre and others, 1987). Clinopyroxene and olivine accumulation process is responsible for the very high contents in MgO (>13 %) Cr (> 1200 ppm) and Ni (365 ppm) of some basalts (Table 1). The chondrites normalized abundance patterns (Figs. 3 A-B) show positive anomalies in Rb, K and Sr in both suites. The Nb negative anomalies present in these volcanics, in comparison with the slightly enrichment in light rare earth elements (LREE) are characteristic of orogenic arc magmas (Thompson and others, 1984). The depletion in Zr, compared to the abundance of Sm and Ti, for the Dekkas basalts (Fig. 3B) is generally observed in SiO<sub>2</sub> saturated basalts and is compatible with the Nb negative anomaly (Thompson and others, 1984). The absence of negative anomalies in Ti, linked to the absence of early iron-oxide fractionation, is related to the tholeiitic affinity of the Nosoni and Dekkas volcanics. As attested by their detritic and carbonate plate-like interlayers, which contain neritic fauna (brachiopods, fusulinids), the Permian-Triassic lavas were erupted partly subaerially in a carbonate platform environment. Thus, the Permian Nosoni, Dekkas and Bully Hill Formations which belong to low-K tholeiitic suites, characterized by 1) a predominance of andesites and dacites relative to basalts, 2) a carbonate platform environment, represent the development of a mature island arc (Martin and others, 1984; Lapierre and others, 1987).

#### THE BLUE MOUNTAINS ISLAND ARC VOLCANIC SUITES

The pre-Cenozoic rocks present in the Blue Mountains (Fig. 1) form a NE-SW belt and can be subdivided into three main units: 1) the pre-Liassic Formations on which rest 2) the unconformable Jurassic series and finally 3) the post Late-Jurassic (Nevadan) "molasses" (Roure and Sosson, 1986). The pre-Liassic Formations include the Permo-Triassic island arc volcanics and sediments, the John Day Late Triassic flysch and the Late Triassic-Early Jurassic melange deposits (Cimmerian orogeny: Roure, 1984; Roure and Sosson, 1986).

The Blue Mountains Formations were affected by a polyphased tectogenesis (Liassic Cimmerian, Late Jurassic Nevadan and Middle Cretaceous Oregonian orogenies). The lithostratigraphic succession of the Permian-Triassic island arc sequence was established by Vallier (1974) along the Snake River Canyon (Seven Devils Group). The unconformity of the Middle and Late Trias on the Permian sediments and volcanics, related to the Sonoma orogeny, suspected by Vallier (1974) and Vallier and others, (1977) was never recognized along the Snake River (Lapierre and others, 1988). According to Vallier (1974), the basement of the Permian-Triassic arc sequence is formed of amphibolites, crosscut by intensively deformed quartz-dioritic dykes and intrusions. According to our own observations (Lapierre and others, 1988), these intensively deformed metamorphic and plutonic rocks do not likely represent the basement of the Permian-Triassic island arc series because a NNE-SSW major transcurrent fault affects both these above mentioned rocks and the Permian to Late Triassic Formations.

All the Permian and Triassic rocks are affected by a low-greenschist facies metamorphism. In the lavas, mineralogical assemblages are albite + chlorite + epidote + calcite (Vallier and others, 1977). The clinopyroxene is the only primary preserved phase.

The Permian series (Fig. 2), the basement of which is unknown, may be divided into three lithostratigraphic successions (Lapierre and others, 1988). The first (Windy Ridge Formation) contains rhyolitic flows and acidic pyroclastic rocks intruded by numerous basic dykes. The second (bottom of the Hunsaker Creek Formation) consists of massive basaltic, andesitic and rhyolitic flows, interstratified within graded-bedded pyroclastic rocks, volcanoclastic and detritic sediments (sandstones, graywackes and microconglomerates). The third (top of the Hunsaker Creek Formation) is formed of coarse-grained andesitic breccias overlain by ignimbrites, well layered water-laid acidic tuffs with scarce intercalated graded-bedded sandstones. After Vallier (1974), this formation is dated by Guadalupian and Leonardian brachiopods. The rhyolites from the Windy Ridge Formation (SiO<sub>2</sub> = 75%; Table 2) contain quartz and plagioclase phenocrysts embayed in a recrystallized mesostasis. These rhyolites

have K<sub>2</sub>O contents ranging from 0.80 to 2.41%, Rb contents ranging from 14 to 37 ppm and Sr contents ranging from 25 to 74 ppm. Their rare earth elements patterns are slightly enriched in light rare earth elements with (La/Yb)<sub>N</sub> ratios comprised between 1.24 and 2.05 (Lapierre and others, 1988). The pronounced Ti negative anomalies (Fig. 4A) are typical of orogenic series and the important depletions in Nb and Sr (Fig. 4A) are common features of island arc series (Thompson and others, 1984). The basalts of the Hunsaker Creek Formation exhibit either an intersertal fluidal texture (plagioclase laths molded by fresh clinopyroxene) with olivine and scarce plagioclase phenocrysts or extremely porphyritic (more than 50% phenocrysts) with orthopyroxene and glomeroporphyritic aggregates of plagioclase phenocrysts. Their mesostasis is characterized by the presence of numerous iron-titanium oxide grains. The Hunsaker Creek basalts (Table 2) have TiO<sub>2</sub> contents comprise between 0.93% and 1.67%, their higher contents are linked to iron-titanium oxides accumulation. They have variable K<sub>2</sub>O contents (0.09% < K<sub>2</sub>O < 1.46%). They display flat rare earth elements patterns sometimes slightly enriched in LREE with (La/Yb)<sub>N</sub> ratios ranging between 1.23 to 2.07. The Nb negative anomalies relative to the enrichment in LREE (Fig. 4B) are evidence that the Hunsaker basalts belong to orogenic arc magmas (Thompson and others, 1984). The tholeiitic affinity of these basalts appears with the lack of negative Ti anomalies on the extended diagrams (Fig. 4B). Indeed, these patterns are very similar to those of the eastern Klamath Permian volcanics (Lapierre and others, 1988).

The Wallowa-Seven Devils Permian-Triassic volcanism started with low-K tholeiitic rhyolites followed by a low-K basalt-rhyolite suite, the basic terms of which display similar geochemical affinities with the underlying rhyolites. It was developed in an island arc environment.

## THE NORTHERN SIERRA NEVADA

### 1) ISLAND ARC VOLCANIC SUITES

The northern Sierra Nevada is divided into four tectonostratigraphic units : the Smartville Complex to the west, the Central Belt, the Feather River Peridotite Belt and the Eastern Belt (Day and others, 1985). The latter represents the Lower Paleozoic to Lower Mesozoic island arc sequence. The Paleozoic-Early Mesozoic sequence represents a continuous suite from Late Devonian to Early Triassic in which the Permian sequence outcrops on the east sides of the Hough and Genesee blocks (Durrell and D'Allura, 1977; D'Allura and others, 1977). The Permian sequence conformably overlies the sedimentary Carboniferous Peale Formation represented by sandstones, greywackes, conglomerates and radiolarites which contain radiolaria of Early Pennsylvanian age (Holdsworth and Jones, 1980). These data provide for the base of the Permian sequence a Late Carboniferous age or, as it was described by Durrell and D'Allura (1977), a Late Pennsylvanian or Early Permian-age for the base of the Goodhue Formation. The Permian sequence consists of three formations, the Goodhue and Reeve Formations dominated by volcanic activity (McMath, 1966; Durrell and D'Allura, 1977; D'Allura and others, 1977; Hannah and Moores, 1986; Fig. 2) and the Robinson Formation characterized by sedimentary and volcanoclastic deposits. Laterally, in the north of the Hough block, the Permian sequence is replaced by the Arlington Formation, which is formed of redeposited tuffs, tuff-breccias, slate and minor volcanic conglomerate-breccia (McMath, 1966) in which is interbedded fossiliferous oolitic limestone (D'Allura and others, 1977) interpreted as the equivalent of the Permian McCloud limestone of the eastern Klamath Mountains (Wilde in D'Allura and others, 1977). The Permian-Early Triassic volcanic pile is unconformably overlain by the Hosselkus limestone (McMath, 1966; Harwood, 1983).

The Goodhue Formation represents, in the southern and north-eastern parts of the Eastern Belt, a volcanic episode dominated by basaltic magmas (McMath, 1958-1966; Durrell and D'Allura, 1977; D'Allura and others, 1977; Hannah and Moores, 1986). Pillowed flows are common at the base of the formation, while the top is formed of massive flows (Fig. 2). The volcanics are interbedded with hyaloclastites, basaltic breccias and fine- or coarse-grained tuffs (Fig. 2). The basalts have porphyritic texture with generally more than 20% of phenocrysts (McMath, 1966; D'Allura and others, 1977; Durrell and D'Allura, 1977). These phenocrysts are largely represented by plagioclase, clinopyroxene and orthopyroxene. The matrix is rich in plagioclase microlites and also contains abundant iron oxides. The lavas of the Goodhue Formation are affected by a low grade greenschist metamorphism. The clinopyroxene phenocrysts of augitic composition are generally preserved. The plagioclase is sometimes replaced by epidote + quartz. The orthopyroxene is always replaced by chlorite or serpentine.



(McMath, 1966). The groundmass is recrystallized in an assemblage of actinolite, chlorite and quartz. The Reeve Formation shows at the base sandstones containing fragments of clinopyroxene phenocrysts and conglomerates with basaltic pebbles (Fig. 2). This thin sedimentary sequence is overlain by massive andesitic flows associated with chert, tuff, sandstone and andesitic pebbles conglomerate. Locally, some rhyodacitic extrusions appear in the sedimentary sequence. The Reeve andesites are porphyritic and often contain up to 30% of phenocrysts. These latter, sometimes pluricentimetric in size, consist always of : plagioclase (An40-50), clinopyroxene (augite, En41-Fs17-Wo42 / En42-Fs12-Wo46) + orthopyroxene which is replaced by ferriferous chlorite. The matrix of the andesites is rich in plagioclase microlites and iron oxides. The mesostasis is recrystallized in chlorite + epidote + quartz.

The Goodhue basalts ( $45\% < \text{SiO}_2 < 53\%$ ) are  $\text{TiO}_2$  ( $< 1\%$ ),  $\text{K}_2\text{O}$  (generally  $< 1\%$ ), Cr ( $< 140$  ppm) and Ni ( $< 50$  ppm) poor. Their  $\text{Fe}_2\text{O}_3$  contents range from 8 to 12,5% (Table 3). The Reeve andesites ( $\text{SiO}_2 > 53-54\%$ ) display the same contents in  $\text{TiO}_2$  ( $< 1\%$ ) but have higher  $\text{K}_2\text{O}$  contents ( $> 1.3\%$ ) and lower  $\text{Fe}_2\text{O}_3$  contents ( $< 9\%$ ; Table 3; Rouer and others, 1988) than those of the Goodhue basalts. Their lower contents in Cr (10 - 26 ppm) and Ni (10 - 25 ppm) indicate that they are more fractionated than the Goodhue basalts. Their extended Rare Earth diagrams (Fig. 5A-B) show: 1) a strong negative Nb anomalies which is characteristic of orogenic arc magmas (Thompson and others, 1984), 2) a high enrichment in the more incompatible (Y, Nb) trace elements. Their enrichment in K and Rb is probably linked to crustal contamination and is more important in the andesites and rhyolites than in the basalts (Fig. 5B). The negative Ti anomalies (Fig. 5B), as well as the lack of  $\text{Fe}_2\text{O}_3$  enrichment in the Reeve andesites relative to basalt contents (Table 3) reveal the early fractionation of the Ti-oxides and confirm the calc-alkalic affinity of the Goodhue and Reeve volcanic suite.

Thus, the Permian volcanism in northern Sierra Nevada belongs to a calc-alkaline suite and represents the last stage of magmatic activity in a continent-based island arc.

## 2) THE CENTRAL BELT VOLCANIC-PLUTONIC OCEANIC REMNANTS

The thick Chert-Argillite sedimentary Unit (Day and others, 1985) of Permian-Triassic age crops out widely in the Central Belt of Sierra Nevada (Hietanen, 1973; Schweickert and Cowan, 1975). Included within this unit, there are intercalated slate, argillaceous and quartzose sandstone, chert, minor pebbly mudstone and conglomerate, and isolated blocks of Permian-Carboniferous limestone (Day and others, 1985; Standlee and Nestell, 1985; Watkins and others, 1987).

Vaitl (1980) showed that massive volcanic rocks and volcanic breccias as well as gabbro and serpentinite occur in the Chert-Argillite unit as fault-bounded blocks or slices. On the eastern side of the Central Belt, near the Melones Fault, basaltic massive and pillowed flows (Bucks Lake Road sequence, Fig. 2) are interlayered conformably within the sedimentary pile of the Chert-Argillite Unit. Ultrabasic-basic slices are tectonically imbricated together with the Chert-Argillite Unit and serpentinized peridotites (Pilot Peak sequence; Lecuyer and others, 1988; Fig. 2).

In the Chert-Argillite Unit, Day and others (1985) have recognized, on the westside of the Central Belt, a melange containing limestone clasts in mud matrix (Watkins and others, 1987). The study of the fauna shows that the limestone clasts are of Early Permian age (Watkins and others, 1987) and similar to the McCloud limestone of the eastern Klamath Mountains. The matrix of the limestone clasts also contains a Late Permian fauna (Watkins and others, 1987). They interpret this melange (diamictite) as the result of the destruction of carbonate platform represented by the McCloud limestone during Early Permian. The same melange (Early Permian limestone clasts in the Chert-Argillite Unit) has been described by Standlee and Nestell (1985) on the east side of the Central Belt where occurs the Bucks Lake basalts and the Pilot Peak ultrabasic-basic plutonic slice.

The Bucks Lake basalts are decimetric flattened pillows generally associated to pillow breccias. These breccias are formed of sharp fragments embayed in an argillaceous matrix. These basalts show flow microlitic textures with various proportions of plagioclase phenocrysts. Their groundmass includes plagioclase and augite microlites associated to several tiny iron oxides. They ( $47\% < \text{SiO}_2 < 51\%$ ) are  $\text{Fe}_2\text{O}_3$  ( $8\% < \text{Fe}_2\text{O}_3 < 14.1\%$ ) and  $\text{TiO}_2$  rich ( $\text{TiO}_2 > 1.58\%$ ; Table 4). They display flat to strong enriched patterns (Fig. 6) without Nb, Zr or Ti anomalies which are typical features of anorogenic and transitional tholeiitic magmas (Thompson and others, 1984). Thus, the Bucks Lake basalts exhibit magmatic affinities of N or P type MORB (Lecuyer and others, 1988).

The Pilot Peak plutonic slice (dated Permian by K/Ar on whole rock), about 300m thick, is wedged in the Chert-Argillite Unit. It is bounded on the northeastern side by sheared serpentized peridotites and on the southwestern one by amphibolite-bearing metagabbros. It consists of a thin ultramafic cumulate layer (50m) which gradually passes to fine-layered metagabbros that are intruded by scarce centimetric to decimetric doleritic dikes. The cumulate sequence begins by highly serpentized ultramafic cumulates in which uncommon Cr-rich spinels are included in olivine and pyroxene relics. These ultramafic cumulates grade upwards into thin adcumulate clinopyroxenites layers which are overlain by a thick sequence of fine-layered mesocumulate gabbros. In these latter, the clinopyroxene (Augite, Wo<sub>43</sub>-Fs<sub>14</sub>-En<sub>44</sub> / Wo<sub>47</sub>-Fs<sub>17</sub>-En<sub>36</sub>) is well preserved while the plagioclase is always replaced by epidote (Ps<sub>2-6</sub>). The poecilitic brown hornblende (magnesian-hornblende and magnesian-hastingsite; Leake, 1978), that grows in contact with the ilmenites, mantles the clinopyroxenes. The Pilot Peak cumulates display ultrabasic (SiO<sub>2</sub> = 44%) to basic (SiO<sub>2</sub> = 51%) compositions with a Fe<sub>2</sub>O<sub>3</sub> (4 to 8.5%) and TiO<sub>2</sub> (0.07 < TiO<sub>2</sub> < 0.69%; Table 4) enrichment. This enrichment is related to the occurrence of ilmenite and brown hornblende. Mineralogical and geochemical data support a tholeiitic affinity for the cumulates (Lecuyer and others, 1988). The doleritic (SiO<sub>2</sub> = 49%) dikes which locally crosscut the cumulates are TiO<sub>2</sub> (1.34%) and Cr (491 ppm) rich (Table 4). Their Zr/Nb ratio are high (9 < Zr/Nb < 20). The extended REE diagram of one analyzed dike (Fig. 6) displays a concave downward curve which is typical of E-MORB (Thompson and others, 1984).

#### GEODYNAMIC ENVIRONMENTS OF THE CORDILLERA DURING EARLY PERMIAN-EARLY JURASSIC TIMES

Owing to the magmatic affinities of the emitted volcanics and the occurrence of the Late Permian-early Triassic Sonoma orogeny restricted to the Sierra Nevada Eastern Belt and the Humboldt-Sonoma Ranges (refer above section), it appears that during Permian times six domains can be discriminated from west to east (nowday disposition; Fig. 1) :

- 1) the first one is represented by the northern Sierra Nevada Late Paleozoic volcanic suite, in which the lavas exhibit calc-alkaline affinity; it is named the "Northern Sierra Nevada Block".
- 2) the second one includes the eastern Klamath and Blue Mountains Permian volcanic series, where the lavas belong to low-K tholeiitic suites and it is called the "Eastern Klamath-Blue Mountains Block".
- 3) the third one is an open oceanic domain (back-arc-basin); the remnants of which are represented now by the "Bucks Lake basalts" of the Chert-Argillite sequence and the Permian "Pilot Peak" ultrabasic-basic cumulates slice (refer above section) and perhaps the abundant undifferentiated ultramafic and mafic bodies of the Central Belt (Day and others, 1985). Some of these bodies are considered older than late Jurassic because they contain evidence for a pre-Nevadan metamorphic phase (Mazaheri, 1982).
- 4) the fourth one is an oceanic domain represented by the Havallah-Pumpnickel ophiolites located in the Humboldt-Sonoma-Tobin Ranges in Nevada (Silberling and Roberts, 1962).
- 5) the fifth one is a Permian platform block represented by the dolomitic unit that crops out at the center of the Hot Spring Range (Fig. 1; Nevada, Roure and Sosson, 1986).
- 6) the last one is represented by the North American Craton.

The geodynamic model we propose and discuss here deals with the period ranging from Early Permian to Early Jurassic times and concerns the following areas: eastern Klamath Mountains, Sierra Nevada Eastern and Central Belts, Blue Mountains and Sonoma-Humboldt-Tobin Ranges (Fig.1) where Late Paleozoic strata crop out. It is important to point out first that the Antler orogeny (early to Late Mississippian times), defined in Nevada (Roberts and others, 1958) is recorded in the eastern Klamath Mountains (Charvet and others, 1988 a-b) and in the Sierra Nevada Eastern Belt (Varga et Moores, 1981, Girty and others, 1984). It is therefore assumed that only after the Antler tectonic event, the Sierra Nevada Eastern Belt and the eastern Klamath Mountains formed two different blocks (Charvet and others, 1988 b). The Roberts Mountain allochthon was either attached or apart from the North American Craton and was not affected by the Sonoma orogenic event.

Permian limestones deposits are widespread in all the Cordillera terranes and constitute a key horizon. In the eastern Klamath Mountains, the Permian sequence started with the deposition of the McCloud limestone (Fig. 1). In the Blue Mountains, Guadalupian limestone lenses are interlayered in the volcano-sedimentary pile, Vallier, 1974-1977). In the northern Sierra Nevada Eastern belt, limestone deposits of the Arlington Formation are considered as lateral facies variation of the eastern Klamath Mc Cloud Formation; D'Allura and others, 1977). In

the Sierra Nevada Central Belt, limestone blocks containing fauna similar to those of the Mc Cloud limestone were described at the base of the Chert-Argillite sequence (Standlee and Nestell, 1985; Watkins and others, 1987). According to these authors, the presence of these limestone blocks is the result of the destruction of the arc carbonate platform which extended from the eastern Klamath to north-western Nevada. We will discuss later this interpretation. In the Sonoma-Humboldt Ranges, the limestone deposits that rests unconformably on Silurian rocks are considered as part of this carbonate platform (Silberling, 1973; Miller, 1987).

The plate-tectonics of the eastern Klamath Mountains, the Blue Mountains, the Sierra Nevada Eastern and Central Belts and the Sonoma-Humboldt-Tobin Ranges in Nevada can be narrated in the light of the tectonic, petrological and geochemical features of their island arc volcanic and ophiolitic belts (Fig. 7). We have assumed that the subductions of the Klamath-Sierra and Pumpernickel-Havallah oceanic terranes remained westwards during Permian to Late Triassic.

Permian times (Fig. 7a).

During Permian times, arc-volcanic activity occurred in the eastern Klamath, in the Blue Mountains and in northern Sierra Nevada. In the eastern Klamath, the differentiated low-K island arc volcanism began during Middle Permian (Nosoni and Dekkas Formations), and lasted until Late Permian (Bully Hill rhyolite; Watkins and Stensrud, 1983). The low-K tholeiitic Late Permian volcanics of the Blue Mountains (Windy Ridge rhyolite, Hunsaker Creek basalt-rhyolite suite) display much similarities with those of the eastern Klamath Mountains. Thus, these two tholeiitic sequences can be considered as belonging to the same island arc. In the northern Sierra Nevada, the contemporaneous volcanism (Goodhue and Reeve Formations) produced calc-alkaline submarine pillowed basalts, followed by subaerial andesitic flows and locally rhyolitic domes and flows (Hannah and Moores, 1986; Rouer and others, 1988). These latter represent the final magmatic stage of the Sierra Nevada Paleozoic continent-based island arc. This continental basement is likely represented by the Sonomia microplate defined by Speed (1979).

Two oceanic domains occurred during this same time. The first divided the tholeiitic "Eastern Klamath-Blue Mountains" and the calc-alkaline northern "Sierra Nevada" island arcs. It was either an open oceanic domain or an evolved back-arc basin, related to the northern Sierra Nevada island arc, because the Permian ophiolitic slices exposed in the Sierra Nevada Central Belt display MORB tholeiitic affinities (no influence of the subducting wedge). Moreover the N. to P.MORB tholeiitic affinities of the "Bucks Lake pillow-basalts" suggest they were developed in a spreading ridge environment. The second oceanic domain, represented by the Pumpernickel-Havallah ophiolites, divided the Sierra Nevada island arc from the continental limestone platform, located eastwards. Presently, the nature of this oceanic domain is unknown (evolved or not back-arc basin) because petrological and geochemical data on the Pumpernickel-Havallah ophiolites are lacking.

Permian-Early Triassic boundary and Early Triassic times (Fig. 7b-c).

Arc-volcanism stopped in the eastern Klamath Mountains and was followed by the deposition of the Pit Formation. During Middle Triassic, a massive disturbance occurred (related perhaps to rifting) leading to the formation of a huge olistostrome observed in the lower Pit Formation (Eastoe and others, 1987). The crystal-rich and tuffaceous turbidites present in the upper Pit Formation likely derived from the arc-volcanism that continued in the Blue Mountains with the eruption of the Wild Sheep Creek-Doyle Creek (Seven Devils Group) and Huntington low-K tholeiitic basalt-rhyolite suites. Calc-alkaline andesites of the upper Doyle Creek Formation are the last emitted products of the "Eastern Klamath-Blue Mountains" island arc (Lapierre and others, 1988).

Volcanic activity stopped in the Sierra Nevada Paleozoic island arc and erosion took place with the deposition of the Robinson Formation. A major tectonic event, Sonoma orogeny, occurred at the Permian-Triassic boundary and was caused by 1) the collage of the Sonomia microplate (Sierra Nevada continent-based island arc) with the easternmost Permian limestone platform block and 2) the closure of the Pumpernickel-Havallah oceanic domain. These ophiolitic nappes were then obducted on the easternmost Permian limestone block.

Late Triassic to Early Jurassic times (Fig. 7d).

In the eastern Klamath-Blue Mountains block, deposition of carbonate platform took place with the Hosselkus and Martin Bridge Formations. In the eastern Klamath, the Hosselkus limestone was succeeded by black shales and water-laid pyroclastic debris (erosion of the Blue Mountain arc magmatic sequence) within the Upper Triassic Modin Formation (Sanborn, 1960). In the Blue Mountains, argillaceous limestone, mudstone and volcanoclastic rocks (Hurval Formation; Vallier, 1974) rest conformably on the Martin Bridge limestone.

In the Sonoma edifice of Nevada (Sonoma-Humboldt-Tobin Ranges, Fig. 1) the calc-alkaline predominantly acid volcanism (Koipato Group; Silberling, 1973; Lapierre and others, 1989), that rests unconformably on the Permian tectonized oceanic suture indicates subduction of an oceanic domain that previously had divided the Permian carbonate platform block and the passive margin of the north American craton. In Sierra Nevada, the Late Triassic Hosselkus limestone and its basal conglomerate rests with an angular unconformity on the tectonized Paleozoic sequences (Harwood, 1983).

During Early Jurassic times, the Cimmerian orogeny took place (Roure, 1984; Roure and Sosson, 1986). This latter is evinced by : 1) the unconformity of the Middle Jurassic deposits on the older rocks, present in the eastern Klamath and Blue Mountains, 2) the occurrence of slices and/or blocks of Late Triassic blue schists in the Central Belts of eastern Klamath and Sierra Nevada and in the Blue Mountains.

This Cimmerian orogeny corresponds to the closure of the oceanic domain represented by the "Bucks Lake" basalts and the pro parte Permian and early Mesozoic cumulate ultrabasic-slices (Chert-Argillite unit) present both in the Sierra Nevada and Klamath (Rattle Snake dismembered ophiolite of early Mesozoic age; Irwin, 1981) Central Belts and the collision of the eastern Klamath-Blue Mountains microblock with the Sonoma Sonoma-Humboldt Ranges microplate. It is probably, during this collision that the Permian limestones were tectonically incorporated in the Klamath and Sierra Nevada Central Belts (Cimmerian melange of Roure and Sosson, 1986) during this collision.

This culmination of amalgamation in the western Cordillera consists of what Roure and Sosson (1986) call the American-Mexican continental block.

#### ACKNOWLEDGEMENTS

Field studies were supported by the ASP Cordillères américaines and C.N.R.S (action initiative). We would like to thank the US Geological Survey (Menlo Park, California) in providing us a vehicle. The geochemical data were supported by the Unité Associée 736 "Ophiolites et Paléosutures".

#### REFERENCES CITED

- Albers, J.P., and Robertson, J.F., 1961, Geology and ore deposits of East Shasta copper zinc district, Shasta County, California: U.S. Geological Survey Professional Paper 338, 103 p.
- Charvet, J., Lapierre, H., and Campos, C., 1988a, Mise en évidence de la phase Antler (Dévonien supérieur - Carbonifère inférieur) dans les Klamath orientales (Nord Californie), Implications géodynamiques: Comptes Rendus de l'Académie des Sciences de Paris (submitted).
- Charvet, J., Lapierre, H., and Campos C., 1988b, Extension of the Antler orogeny in the eastern Klamath Mountains (N. California), geodynamic implications: Geology (submitted).
- Churkin, M., Jr., 1974, Paleozoic marginal ocean basin-volcanic arc systems in the Cordilleran fold-belt: Society of Economic Paleontologists and Mineralogists, Special Publication 19, p. 174-192.
- Coney, P.J., Jones, D.L., and Monger, J.W.H., 1980, Cordilleran suspect terranes: Nature, v. 288, p. 329-333.
- Coogan, A.H., 1960, Stratigraphy and paleontology of the Permian Nosoni and Dekkas Formations (Bolliboka Group): University of California, Publication in Geologic Sciences, v. 36, p. 243-316.

D'Allura, J.A., Moores, E.M., and Robinson, L., 1977, Paleozoic rocks of the Northern Sierra Nevada: Their structural and paleogeographic implications, in Stewart, J.M., Stevens, C., and Fritsche A.E., eds., *Paleozoic Paleogeography of the western United States: Society of Economic Paleontologists and Mineralogists, Pacific Section, Pacific Coast Paleogeography Symposium, 1st*, p. 395-408.

Day, H.W., Moores, E.M., and Tuminas, A.C., 1985, Structure and tectonics of the northern Sierra Nevada: *Geological Society of America Bulletin*, v. 96, p. 436-450.

Durrell, C., and D'Allura, J., 1977, Upper Paleozoic section in eastern Plumas and Sierra Counties, northern Sierra Nevada: *Geological Society of America Bulletin*, v. 88, p. 844-852.

Eastoe, C.J., Gustin, M.M., and Nelson, S.E., 1987, Problems of recognition of olistostromes: an example from the Lower Pit Formation, eastern Klamath Mountains, California: *Geology*, v. 15, p. 541-544.

Girty, G.H., Wardlaw, M.S., Schweickert, R.A., Hanson, R.E., and Bowring, S.A., 1984, Timing of pre-Antler deformation in the Shoo Fly complex, Sierra Nevada, California: *Geology*, v. 12, p. 673-676.

Hannah, J.L., and Moores, E.M., 1986, Age relationships and depositional environments of Paleozoic strata, northern Sierra Nevada, California: *Geological Society of America Bulletin*, v. 97, p. 787-797.

Harwood, D.S., 1983, Stratigraphy of upper Paleozoic volcanic rocks and regional unconformities in part of the northern Sierra terrane, California: *Geological Society of America Bulletin*, v. 94, p. 413-422.

Hietanen, A., 1973, Origin of andesitic and granitic magmas in the northern Sierra Nevada, California: *Geological Society of America Bulletin*, v. 84, p. 2111-2118.

Holdsworth, B.K., and Jones, D.L., 1980, Preliminary radiolarian zonation for Late Devonian through Permian time: *Geology*, v. 8, p. 281-285.

Irwin, W.P., 1981, Age and tectonics of plutonic belts in accreted terranes of the Klamath Mountains, California and Oregon, in Ernst, W.G., ed., *The geotectonic development of California*: New York, Prentice-Hall, p. 29-49.

Lapierre, H., Brouxel, M., Martin, P., Coulon, C., Mascle, G., and Cabanis, B., 1986, The Paleozoic and Mesozoic geodynamic evolution of the eastern Klamath Mountains (N. California) inferred from its magmatism: *Bulletin de la Société Géologique de France*, (8), t. II, n° 6, p. 969-980.

Lapierre, H., Brouxel, M., Albarède, F., Coulon, C., Lecuyer, C., Martin, P., Mascle, G., and Rouer, O., 1987, Paleozoic and Lower Mesozoic magmas from the eastern Klamath Mountains (North California) and the geodynamic evolution of the northwestern America: *Tectonophysics*, v. 140, p. 155-177.

Lapierre, H., Rouer, O., Charvet, J., Lecuyer, C., Gross, E., and Coulon, C., 1988, Les magmatismes tholéitiques d'arc permo-triasiques des Blues Mountains (Oregon oriental): corrélations possibles avec les unités voisines de Californie: *Comptes Rendus de l'Académie des Sciences de Paris*, v. 306, p. 1103-1108.

Lapierre, H., Charvet, J., Coulon, C., and Bucher, H., 1989, The Triassic Koipato calc-alkaline volcanism (Nevada USA): the ultimate arc magmatism before the american-mexican building. *European Union of Geosciences V, Strasbourg, March 1989, Terra Cognita* (submitted).

Leake, B.E., 1978, Nomenclature of amphiboles, compiled for subcommittee on amphiboles, International Mineralogical Association: *Mineralogical Magazine*, v. 42, p. 533-563.

Lecuyer, C., Rouer, O., Lapierre, H., and Zimmermann J.L., 1988, Mise en évidence d'un domaine océanique au Paléozoïque dans la Central Belt de la Sierra Nevada, Californie: Comptes Rendus de l'Académie des Sciences de Paris (in press).

Martin, P., Lapierre, H., and Rocci, G., 1984, Présence d'un arc insulaire permien dans les Klamath orientales (N. Californie): Comptes Rendus de l'Académie des Sciences de Paris, v. 298, p. 223-228.

Mazaheri, S.A., 1982, The petrology and metamorphism of ultramafic and mafic rocks near Pulga, Butte County, California (M.S. thesis): Davis, University of California, 139 p.

McMath, V.E., 1958, Geology of the Taylorsville area, northern Sierra Nevada, California (Ph.D. thesis): Los Angeles, California, University of California.

McMath, V.E., 1966, Geology of the Taylorsville Area, Northern Sierra Nevada, in Bailey, E.H., ed., Geology of northern California: California Division of Mines and Geology, Bulletin 190, p. 173-183.

Miller, M.M., 1987, Dispersed remnants of a northeast Pacific fringing arc, Upper Paleozoic island arc terranes of Permian McCloud faunal affinity, western U.S.: Tectonics, v. 6, p. 807-830.

Roberts, R.J., Holtz, P.E., Gilluly, H., and Ferguson, H.G., 1958, Paleozoic rocks of north central Nevada, American Association of Petroleum Geologists, Bulletin 42, p. 2813-2857.

Rouer, O., Lapierre, H., and Coulon, C., 1988, La série calco-alkaline permienne d'arc du N. de la Sierra Nevada (Californie, USA): ultime étape dans l'évolution de la bordure de la microplaque Sonomia: Comptes Rendus de l'Académie des Sciences de Paris, v. 307, p. 57-62.

Roure, F., 1984, Une coupe géologique de Golconda au Pacifique (Orégon, Nord-Ouest du Nevada, Nord de la Californie). Evolution mésozoïque et cénozoïque de la marge ouest-américaine: Thèse de Doctorat d'Etat, Université Pierre et Marie Curie, Paris VI, 250 p.

Roure, F. and Sosson, M., 1986, Late Jurassic collision between a composite exotic block and the North American continent, a model for the Cordillera building: Bulletin de la Société géologique de France, (8), t. II, n° 6, p. 945-959.

Sanborn, A.F., 1960, Geology and paleontology of the southwest quarter of the Big Bend quadrangle, Shasta County, California: California Division of Mines and Geology, Special Report 63, 26 p.

Schweickert, R.A., and Cowan, D.S., 1975, Early Mesozoic tectonic evolution of the western Sierra Nevada, California: Geological Society of America Bulletin, v. 86, p. 1329-1336.

Silberling, N.J., and Roberts, R.J., 1962, Pre-Tertiary stratigraphy and structure of northwestern Nevada: Geological Society of America Special Paper 72, 58 p.

Silberling, N.J., 1973, Geologic events during Permian-Triassic time along the Pacific margin of the United States, in Logan, A., and Hills, L.V., eds., the Permian and Triassic systems and their mutual boundary: Canadian Society of Petroleum Geologists, v. 2, p. 345-362.

Speed, R.C., 1979, Collided Paleozoic microplate in the western United States: Journal of Geology, v. 87, p. 182-201.

Standlee, L.A., and Nestell, M.K., 1985, Age and tectonic significance of terranes adjacent to the Melones fault zone, N. Sierra Nevada, California: Geological Society of America Abstracts with Programs, v. 17, p. 410.

Thompson, R.N., Morrison, M.A., Hendry, G.L., and Parry, S.J., 1984, An assessment of the relative roles of crust and mantle in magma genesis: an elemental approach: Philosophical Transaction of the Royal Society of London, A 310, p. 549-590.

Vaitl, J., 1980, Geology of the Cherokee area, northern Sierra Nevada, California (M.S. thesis): Davis, California, University of California, 93 p.

Vallier, T.L., 1974, A preliminary report on the geology of part of the Snake River Canyon, Oregon and Idaho: Geological Map Series, GMS-6, 15 p.

Vallier, T.L., Brooks, H.C., and Thayer, T.P., 1977, Paleozoic rocks of eastern Oregon and western Idaho, in Stewart, J.H., Stevens, C.H., and Fritsche, A.E., eds., Paleozoic paleogeography of the western United States: Society of Economic Paleontologists and Mineralogists, Pacific Section, Pacific Coast Paleogeography Symposium, 1st, p. 455-466.

Varga, R.J., and Moores, E.M., 1981, Age, origin and significance of an unconformity that predate island-arc volcanism in the northern Sierra Nevada: *Geology*, v. 9, p. 512-518.

Watkins, R., and Stensrud, H.L., 1983, Age of sulfide ore in the west Shasta and east Shasta districts, Klamath Mountains, California: *Economic Geology*, v. 78, p. 340-343.

Watkins, R., Reinheimer, C.E., Wallace, J.W., and Nestell, M.K., 1987, Paleogeographic significance of a Permian sedimentary megamictite in the Central Belt of the northern Sierra Nevada: *Geological Society of America Bulletin*, 99, p. 771-778.

#### Figures captions.

Figure 1: Simplified geological map of the western Cordillera domain (After Silberling, 1973; Roure, 1984). Localisation of the Permian island-arc sequences.

Figure 2: Lithostratigraphic columns of the Permian Formations in the eastern Klamath, Blue Mountains and northern Sierra Nevada.

Figure 3: Chondrite normalized abundance patterns of the eastern Klamath rocks: a) Nosoni low-K tholeiitic basalts and andesites, b) Dekkas low-K tholeiitic basalts.

Figure 4: Chondrite normalized abundance patterns of the Blue Mountains rocks: a) Windy Ridge low-K tholeiitic rhyolites, b) Hunsaker Creek low-K tholeiitic basalts.

Figure 5: Chondrite normalized abundance patterns of the northern Sierra Nevada rocks: a) Goodhue calc-alkaline basalts, b) Reeve calc-alkaline andesites and rhyolites.

Figure 6: Chondrite normalized abundance patterns of the Bucks Lake transitional tholeiitic type basalts and Pilot Peak diabase.

Figure 7: Geodynamic evolution of the Cordillera during Permian to Early Jurassic times.

#### Tables :

Table 1: Major, trace and rare earth elements of the Permian eastern Klamath Mountains lavas.

Table 2 : Major, trace and rare earth elements of the Permian Blue Mountains lavas

Table 3 : Major, trace and rare earth elements analysis of the Permian northern Sierra Nevada lavas.

Table 4 : Major, trace and rare earth elements analysis of the Permian volcanic and plutonic ophiolitic relicts in the Central Belt of northern Sierra Nevada.

Table 1 : Major, trace and rare earth elements analysis of the Permian Klamath lavas.

| Sample                         | NOSONI FORMATION |        |        |       | DEKKAS FORMATION |         |        |        |
|--------------------------------|------------------|--------|--------|-------|------------------|---------|--------|--------|
|                                | ES 141           | ES 156 | ES 316 | ES34B | ES 223           | ES 100A | ES 106 | ES 133 |
| SiO <sub>2</sub>               | 50.69            | 55.69  | 48.47  | 48.89 | 49.37            | 48.40   | 49.60  | 50.14  |
| TiO <sub>2</sub>               | 0.94             | 0.94   | 1.16   | 0.77  | 0.60             | 1.12    | 0.88   | 0.75   |
| Al <sub>2</sub> O <sub>3</sub> | 18.16            | 16.47  | 17.00  | 16.23 | 12.02            | 15.10   | 18.72  | 17.78  |
| Fe <sub>2</sub> O <sub>3</sub> | 10.49            | 9.93   | 10.96  | 9.72  | 12.07            | 14.60   | 11.03  | 9.83   |
| MgO                            | 5.01             | 3.28   | 6.07   | 7.36  | 13.20            | 4.75    | 4.93   | 4.70   |
| MnO                            | 0.27             | 0.18   | 0.18   | 0.18  | 0.22             | 0.24    | 0.08   | 0.18   |
| CaO                            | 4.07             | 2.55   | 8.53   | 9.34  | 7.59             | 7.24    | 4.77   | 8.27   |
| Na <sub>2</sub> O              | 5.83             | 6.56   | 3.07   | 2.86  | 2.76             | 3.25    | 1.78   | 3.39   |
| K <sub>2</sub> O               | 0.64             | 1.01   | 1.31   | 0.17  | 0.51             | 0.43    | 0.55   | 0.16   |
| LOI                            | 3.77             | 3.17   | 2.98   | 4.75  | 1.66             | 3.73    | 6.94   | 4.43   |
| Total                          | 99.87            | 99.68  | 99.73  | 99.75 | 100.00           | 99.01   | 99.28  | 99.63  |
| Cr                             | 45               | 21     | 89     | 246   | 1249             | 10      | 26     | 87     |
| Ni                             | 44               | 35     | 36     | 60    | 365              | 53      | 49     | 22     |
| V                              | n.d.             | 250    | 316    | 267   | 184              | 371     | 229    | 300    |
| Sr                             | 333              | 335    | 287    | 425   | 353              | 254     | 164    | 127    |
| Rb                             | 6                | 11     | 27     | 5     | 11               | 15      | 6      | 10     |
| Zr                             | 48               | 51     | 90     | 72    | 37               | 34      | 37     | 32     |
| Y                              | 22               | 24     | 20     | 17    | 12               | 19      | 19     | 17     |
| Nb                             | 2                | 3      | 4      | 3     | 3                | 4       | 3      | 2      |
| La                             | 3.84             | 3.04   | 11.84  | 8.77  | 5.28             | 3.29    | 2.99   | 2.26   |
| Ce                             | 13.17            | 12.16  | 28.54  | 21.47 | 15.64            | 10.31   | 10.33  | 8.18   |
| Nd                             | 7.05             | 7.61   | 14.86  | 12.07 | 7.59             | 6.31    | 5.98   | 4.65   |
| Sm                             | 2.22             | 2.67   | 4.04   | 3.20  | 2.00             | 1.98    | 1.74   | 1.90   |
| Eu                             | 0.71             | 0.92   | 1.41   | 1.02  | 0.61             | 0.75    | 0.67   | 0.73   |
| Gd                             | 2.61             | 3.00   | 3.58   | 2.78  | 1.65             | 1.98    | 1.86   | 2.16   |
| Dy                             | 2.90             | 3.62   | 3.59   | 2.89  | 1.41             | 2.39    | 2.24   | 2.71   |
| Er                             | 1.72             | 2.17   | 1.98   | 1.65  | 0.81             | 1.38    | 1.26   | 1.68   |
| Yb                             | 1.79             | 2.35   | 2.11   | 1.81  | 0.82             | 1.52    | 1.33   | 1.94   |
| Lu                             | 0.29             | 0.36   | 0.29   | 0.26  | 0.15             | 0.22    | 0.19   | 0.32   |

LOI : loss on ignition

n.d. : not determined



Table 2 : Major, trace and rare earth elements analysis of the Permian Blue Mountains lavas.

| WINDY RIDGE FORMATION          |       |       |       |       |       | HUNSAKER CREEK FORMATION |       |       |       |       |
|--------------------------------|-------|-------|-------|-------|-------|--------------------------|-------|-------|-------|-------|
| Sample                         | BM 75 | BM 78 | BM 80 | BM 98 | BM 99 | BM 86                    | BM 92 | BM 94 | BM 95 | BM 96 |
| SiO <sub>2</sub>               | 78.84 | 76.41 | 74.63 | 69.75 | 73.05 | 46.51                    | 47.64 | 51.10 | 50.75 | 48.28 |
| TiO <sub>2</sub>               | 0.38  | 0.39  | 0.42  | 0.43  | 0.38  | 1.14                     | 1.67  | 1.28  | 1.19  | 0.93  |
| Al <sub>2</sub> O <sub>3</sub> | 12.93 | 11.94 | 12.65 | 12.60 | 12.99 | 19.26                    | 16.59 | 17.66 | 16.94 | 17.62 |
| Fe <sub>2</sub> O <sub>3</sub> | 2.34  | 2.13  | 2.54  | 3.07  | 2.31  | 11.29                    | 11.43 | 10.00 | 10.28 | 10.41 |
| MnO                            | 0.08  | 0.07  | 0.99  | 0.12  | 0.08  | 0.17                     | 0.23  | 0.17  | 0.18  | 0.21  |
| MgO                            | 1.03  | 1.62  | 1.91  | 1.42  | 1.26  | 6.84                     | 5.79  | 3.30  | 4.68  | 8.38  |
| CaO                            | 0.29  | 0.31  | 0.30  | 2.30  | 1.68  | 4.71                     | 4.03  | 8.73  | 9.14  | 3.50  |
| Na <sub>2</sub> O              | 4.96  | 4.04  | 4.43  | 4.19  | 2.32  | 4.94                     | 3.83  | 3.01  | 3.53  | 5.01  |
| K <sub>2</sub> O               | 0.80  | 1.03  | 1.22  | 1.03  | 2.41  | 0.09                     | 0.90  | 1.46  | 0.96  | 0.50  |
| LOI                            | 1.19  | 1.48  | 1.60  | 3.68  | 3.11  | 4.65                     | 6.41  | 1.85  | 1.70  | 4.89  |
| Total                          | 98.87 | 99.42 | 99.81 | 98.64 | 99.61 | 99.77                    | 98.92 | 98.79 | 99.54 | 99.81 |
| Cr                             | 13    | 14    | <10   | 11    | 10    | 100                      | 45    | 56    | 96    | 151   |
| Ni                             | 15    | 31    | 61    | 56    | 25    | 49                       | 32    | 33    | 49    | 37    |
| V                              | 66    | 61    | 62    | 79    | 70    | 290                      | 313   | 297   | 286   | 298   |
| Sr                             | 63    | 54    | 74    | 50    | 25    | 218                      | 241   | 135   | 157   | 236   |
| Rb                             | 14    | 20    | 18    | 15    | 37    | 6                        | 15    | 23    | 16    | 12    |
| Zr                             | 172   | 175   | n.d.  | 159   | 149   | 45                       | 117   | n.d.  | 85    | 29    |
| Y                              | 41    | 43    | n.d.  | 29    | 26    | 19                       | 38    | 35    | 31    | 14    |
| Nb                             | 5     | 6     | n.d.  | 3     | 4     | 1                        | 3     | n.d.  | 3     | 1     |
| La                             | 8.97  | 11.50 | 10.13 | 9.79  | 10.41 | n.d.                     | 10.85 | 7.09  | 5.98  | 2.44  |
| Ce                             | 24.79 | 31.48 | 28.23 | 25.90 | 26.16 | n.d.                     | 31.73 | 20.27 | 17.35 | 9.91  |
| Nd                             | 15.84 | 19.97 | 17.01 | 15.93 | 15.36 | n.d.                     | 19.55 | 12.09 | 10.33 | 4.49  |
| Sm                             | 4.87  | 5.86  | 5.29  | 4.46  | 4.15  | n.d.                     | 5.81  | 4.06  | 3.52  | 1.78  |
| Eu                             | 0.99  | 1.69  | 1.50  | 1.07  | 0.84  | n.d.                     | 1.53  | 1.50  | 1.06  | 0.71  |
| Gd                             | 4.57  | 5.57  | 5.09  | 3.90  | 3.73  | n.d.                     | 5.60  | 4.13  | 3.51  | 1.92  |
| Dy                             | 5.83  | 6.53  | 6.20  | 4.06  | 4.30  | n.d.                     | 5.53  | 4.73  | 4.26  | 1.95  |
| Er                             | 3.79  | 3.96  | 3.88  | 2.54  | 2.89  | n.d.                     | 3.07  | 2.81  | 2.54  | 1.18  |
| Yb                             | 4.85  | 4.82  | 4.94  | 3.22  | 3.91  | n.d.                     | 3.53  | 3.27  | 2.96  | 1.33  |
| Lu                             | 0.75  | 0.69  | 0.76  | 0.43  | 0.56  | n.d.                     | 0.53  | 0.51  | 0.44  | 0.22  |

LOI : loss on ignition

n.d. : not determined

Table 3 : Major, trace and rare earth elements analysis of the Permian northern Sierra Nevada lavas.

## GOODHUE FORMATION

## REEVE FORMATION

| Sample                         | MR 4  | MR 8  | MR 9  | KM 1  | KM 5  | KM 10 | SLR 2 | SLR 6 | KM 51 | HL 9  | HL 18 | HL 21 |
|--------------------------------|-------|-------|-------|-------|-------|-------|-------|-------|-------|-------|-------|-------|
| SiO <sub>2</sub>               | 49.35 | 52.61 | 52.23 | 50.86 | 51.46 | 51.74 | 46.83 | 48.29 | 72.24 | 68.92 | 53.24 | 54.01 |
| TiO <sub>2</sub>               | 0.61  | 0.62  | 0.82  | 0.58  | 0.56  | 0.55  | 0.17  | 0.70  | 0.34  | 0.52  | 0.71  | 0.80  |
| Al <sub>2</sub> O <sub>3</sub> | 10.94 | 12.01 | 16.42 | 17.24 | 14.65 | 16.51 | 12.57 | 11.98 | 13.74 | 14.75 | 17.20 | 16.78 |
| Fe <sub>2</sub> O <sub>3</sub> | 11.12 | 9.61  | 8.10  | 10.06 | 10.69 | 9.48  | 11.69 | 12.18 | 1.77  | 3.93  | 7.94  | 8.72  |
| MnO                            | 0.20  | 0.19  | 0.15  | 0.19  | 0.20  | 0.18  | 0.20  | 0.21  | 0.03  | 0.05  | 0.13  | 0.18  |
| MgO                            | 12.16 | 9.78  | 6.20  | 5.61  | 6.49  | 6.16  | 11.84 | 10.01 | n.d.  | 0.77  | 2.35  | 2.71  |
| CaO                            | 9.94  | 11.21 | 8.48  | 8.05  | 9.76  | 8.29  | 9.66  | 11.36 | 0.84  | 2.26  | 7.64  | 7.87  |
| Na <sub>2</sub> O              | 2.10  | 2.16  | 2.98  | 3.00  | 1.68  | 1.34  | 2.72  | 2.66  | 4.15  | 4.79  | 5.02  | 3.30  |
| K <sub>2</sub> O               | 0.98  | 0.36  | 3.09  | 0.86  | 0.67  | 0.87  | 1.68  | 0.87  | 4.49  | 2.32  | 1.37  | 3.11  |
| LOI                            | 1.64  | 1.22  | 1.23  | 2.98  | 3.02  | 4.51  | 1.53  | 1.21  | 1.06  | 1.48  | 2.47  | 1.05  |
| Total                          | 99.04 | 99.77 | 99.70 | 99.43 | 99.18 | 99.63 | 98.89 | 99.47 | 98.66 | 99.79 | 98.07 | 98.53 |
| Cr                             | n.d.  | n.d.  | n.d.  | 78    | 137   | 87    | n.d.  | n.d.  | <10   | <10   | 25    | 26    |
| Ni                             | n.d.  | n.d.  | n.d.  | 28    | 30    | 25    | n.d.  | n.d.  | <10   | 11    | 25    | 25    |
| V                              | n.d.  | n.d.  | n.d.  | 267   | 251   | 223   | n.d.  | n.d.  | 14    | 26    | 215   | 215   |
| Sr                             | 475   | 387   | 496   | 378   | 230   | 315   | 254   | 243   | 155   | 209   | 331   | 703   |
| Rb                             | 21    | 8     | 78    | 23    | 21    | 24    | 12    | 27    | 125   | 62    | 27    | 15    |
| Zr                             | 47    | 44    | 95    | 48    | 52    | 51    | 44    | 42    | 213   | 172   | 90    | 96    |
| Y                              | 15    | 15    | 19    | 11    | 14    | 10    | 16    | 15    | 26    | 25    | 22    | 28    |
| Nb                             | 5     | 5     | 9     | 4     | 5     | 4     | 6     | 5     | 16    | 13    | 8     | 8     |
| La                             | 12.01 | 11.63 | 19.97 | 9.98  | 9.68  | 9.40  | 6.97  | 7.45  | 33.66 | n.d.  | 18.37 | 21.46 |
| Ce                             | 27.71 | 27.16 | 44.13 | 20.42 | 21.70 | 18.03 | 19.17 | 20.28 | 77.91 | n.d.  | 53.90 | 56.68 |
| Nd                             | 15.05 | 14.86 | 21.15 | 8.51  | 8.08  | 7.70  | 11.39 | 12.47 | 33.70 | n.d.  | 23.91 | 28.08 |
| Sm                             | 3.05  | 3.45  | 4.39  | 1.98  | 2.02  | 1.69  | 2.87  | 3.12  | 7.12  | n.d.  | 5.59  | 6.40  |
| Eu                             | 0.90  | 1.14  | 1.13  | 0.75  | 0.87  | 0.45  | 0.81  | 0.86  | 1.58  | n.d.  | 1.77  | 2.06  |
| Gd                             | 2.89  | 2.95  | 3.79  | 2.03  | 2.02  | 1.57  | 2.93  | 3.12  | 6.81  | n.d.  | 5.33  | 5.73  |
| Dy                             | 2.31  | 2.31  | 3.05  | 1.67  | 1.88  | 1.58  | 2.40  | 2.53  | 4.47  | n.d.  | 3.48  | 4.33  |
| Er                             | 1.20  | 1.22  | 1.57  | 0.97  | 1.14  | 0.88  | 1.33  | 1.39  | 2.64  | n.d.  | 2.37  | 2.58  |
| Yb                             | 1.22  | 1.26  | 1.61  | 1.04  | 1.24  | 1.04  | 1.32  | 1.36  | 2.40  | n.d.  | 1.94  | 2.53  |
| Lu                             | 0.22  | 0.18  | 0.29  | 0.18  | 0.22  | 0.20  | 0.21  | 0.23  | 0.39  | n.d.  | 0.36  | 0.41  |

Table 4 : Major, trace and rare earth elements analysis of the Permian volcanic and plutonic ophiolitic relics in the Central Belt of northern Sierra Nevada.

| BUCKS LAKE                     |       |       |       |       |       |       |       | PILOT PEAK |        |       |       |       |
|--------------------------------|-------|-------|-------|-------|-------|-------|-------|------------|--------|-------|-------|-------|
| Sample                         | D 9   | D 11  | D 12  | D 13  | D 14  | D 16  | D 19  | PP 5       | PP 7   | PP 10 | PP 11 | PP 12 |
| SiO <sub>2</sub>               | 51.47 | 47.21 | 48.63 | 47.08 | 47.83 | 50.79 | 47.87 | 51.28      | 44.23  | 47.18 | 44.20 | 49.37 |
| TiO <sub>2</sub>               | 1.58  | 1.84  | 1.74  | 1.71  | 1.76  | 2.68  | 2.78  | 0.12       | 0.69   | 0.48  | 0.07  | 1.34  |
| Al <sub>2</sub> O <sub>3</sub> | 12.60 | 17.62 | 19.34 | 17.40 | 17.88 | 13.11 | 13.09 | 1.62       | 20.17  | 15.39 | 18.51 | 14.42 |
| Fe <sub>2</sub> O <sub>3</sub> | 9.89  | 11.26 | 8.00  | 9.97  | 9.80  | 14.07 | 14.62 | 4.21       | 8.44   | 7.98  | 4.97  | 10.57 |
| MnO                            | 0.18  | 0.19  | 0.17  | 0.18  | 0.18  | 0.25  | 0.23  | 0.10       | 0.16   | 0.15  | 0.10  | 0.19  |
| MgO                            | 5.64  | 4.47  | 6.23  | 4.42  | 6.39  | 4.28  | 4.54  | 18.79      | 7.93   | 10.43 | 11.56 | 8.46  |
| CaO                            | 10.21 | 9.59  | 6.34  | 9.66  | 6.51  | 6.80  | 8.53  | 21.63      | 13.23  | 12.99 | 16.12 | 8.77  |
| Na <sub>2</sub> O              | 0.09  | 1.21  | 0.98  | 1.94  | 2.10  | 1.85  | 0.69  | 0.10       | 1.85   | 1.44  | 0.80  | 3.23  |
| K <sub>2</sub> O               | 4.74  | 3.62  | 4.91  | 3.76  | 3.60  | 4.59  | 4.46  | 0.02       | 0.32   | 0.74  | 0.45  | 0.39  |
| LOI                            | 2.98  | 2.85  | 3.35  | 3.70  | 3.49  | 1.05  | 2.68  | 1.39       | 3.04   | 3.06  | 3.12  | 2.34  |
| Total                          | 99.38 | 99.86 | 99.69 | 99.82 | 99.54 | 99.47 | 99.49 | 99.26      | 100.06 | 99.84 | 99.90 | 99.08 |
| Cr                             | 240   | 163   | 178   | 170   | 178   | 111   | 115   | 2937       | 30     | 183   | 365   | 491   |
| Ni                             | 81    | 54    | 57    | 44    | 53    | 55    | 52    | 331        | 28     | 26    | 98    | 97    |
| V                              | 247   | 213   | 213   | 214   | 219   | 280   | 268   | 186        | 331    | 315   | 133   | 184   |
| Sr                             | 165   | 344   | 249   | 327   | 278   | 167   | 188   | 12         | 326    | 150   | 213   | 345   |
| Rb                             | 10    | 27    | 10    | 42    | 44    | 56    | 25    | 11         | 9      | 29    | 18    | 8     |
| Zr                             | 117   | 135   | 127   | 127   | 131   | 197   | 203   | 10         | 13     | 11    | 9     | 142   |
| Y                              | 34    | 26    | 23    | 25    | 26    | 36    | 37    | 4          | 6      | 6     | 7     | 22    |
| Nb                             | 6     | 15    | 12    | 14    | 14    | 21    | 21    | 1          | 1      | 1     | 1     | 15    |
| La                             | 4.49  | 13.96 | 13.10 | 13.41 | 12.36 | 16.49 | 17.00 | n.d.       | n.d.   | n.d.  | n.d.  | 28.35 |
| Ce                             | 22.48 | 41.48 | 38.21 | 40.07 | 37.59 | 46.34 | 54.34 | n.d.       | n.d.   | n.d.  | n.d.  | 73.13 |
| Nd                             | 12.32 | 19.76 | 18.38 | 17.94 | 18.74 | 25.54 | 26.44 | n.d.       | n.d.   | n.d.  | n.d.  | 32.27 |
| Sm                             | 4.97  | 5.77  | 5.37  | 5.13  | 5.21  | 6.99  | 7.47  | n.d.       | n.d.   | n.d.  | n.d.  | 7.91  |
| Eu                             | 1.78  | 2.02  | 1.61  | 1.62  | 1.73  | 2.13  | 2.41  | n.d.       | n.d.   | n.d.  | n.d.  | 2.14  |
| Gd                             | 5.49  | 5.80  | 5.41  | 5.28  | 5.38  | 6.79  | 7.41  | n.d.       | n.d.   | n.d.  | n.d.  | 6.94  |
| Dy                             | 5.63  | 4.67  | 4.34  | 4.24  | 4.42  | 5.96  | 6.49  | n.d.       | n.d.   | n.d.  | n.d.  | 4.58  |
| Er                             | 3.69  | 2.82  | 2.63  | 2.49  | 2.61  | 3.38  | 3.71  | n.d.       | n.d.   | n.d.  | n.d.  | 2.80  |
| Yb                             | 3.65  | 2.29  | 2.14  | 2.08  | 2.20  | 3.00  | 3.09  | n.d.       | n.d.   | n.d.  | n.d.  | 2.13  |
| Lu                             | 0.58  | 0.41  | 0.35  | 0.35  | 0.36  | 0.50  | 0.53  | n.d.       | n.d.   | n.d.  | n.d.  | 0.42  |

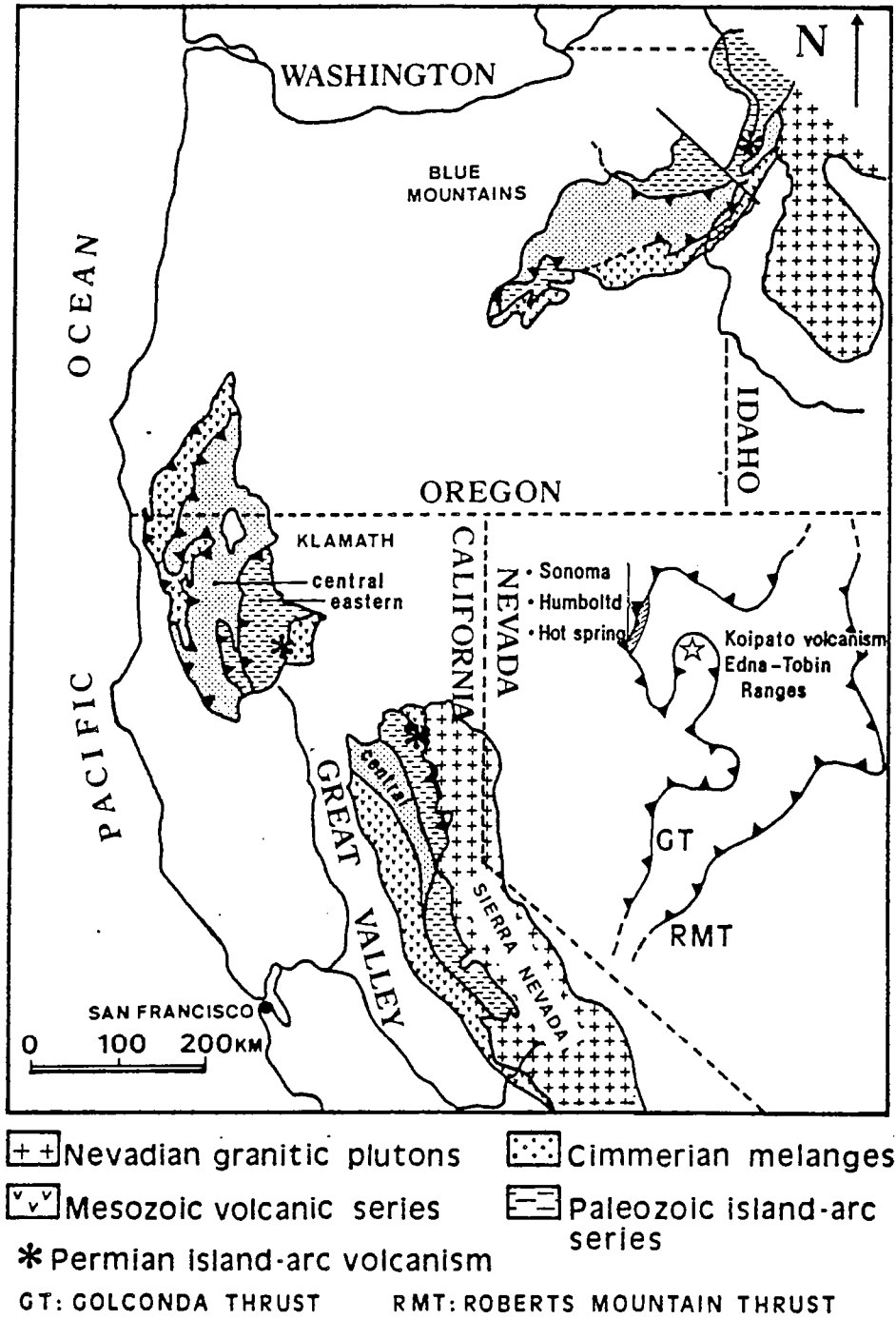
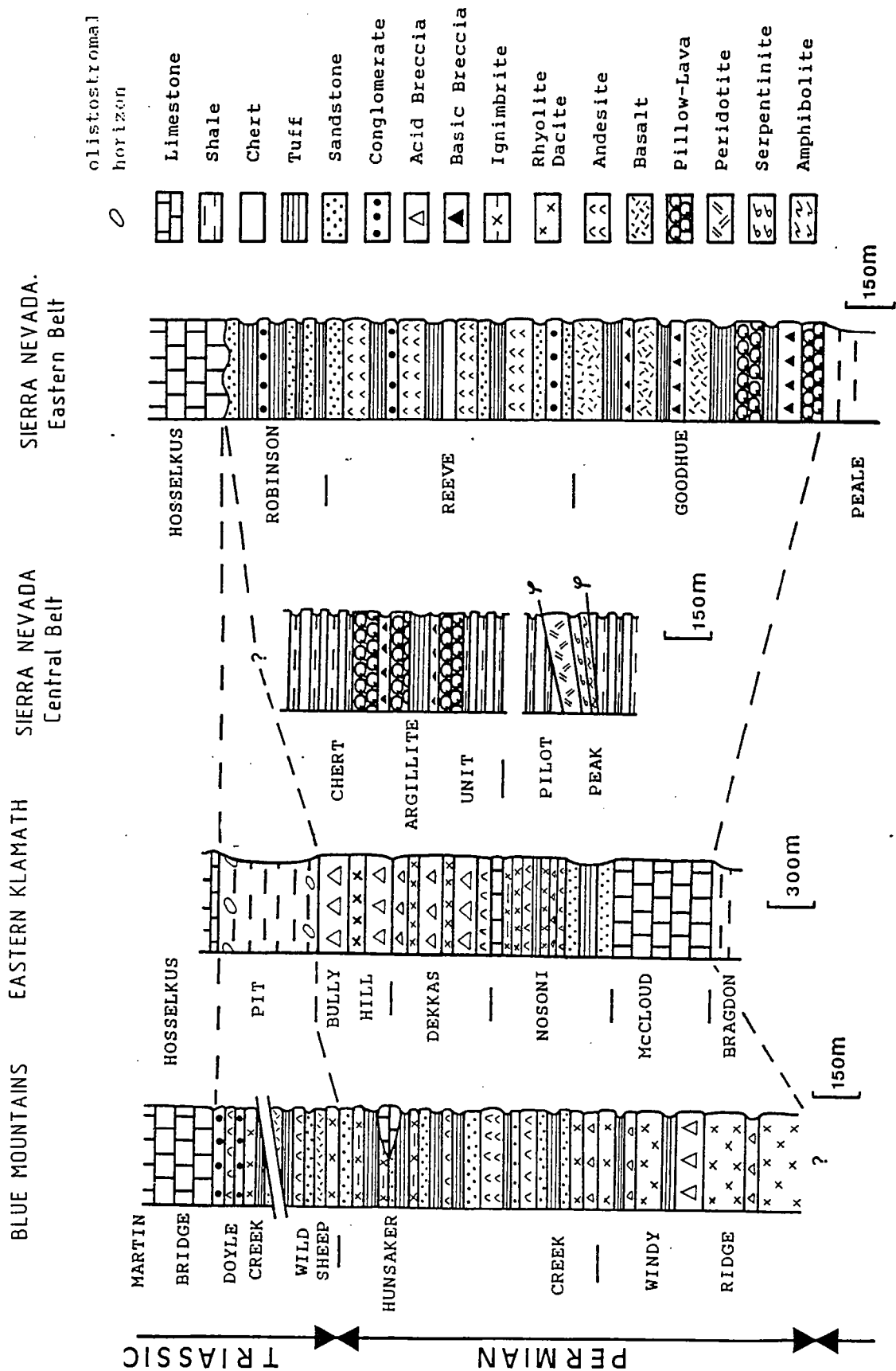


Figure 1

57  
Figure 2



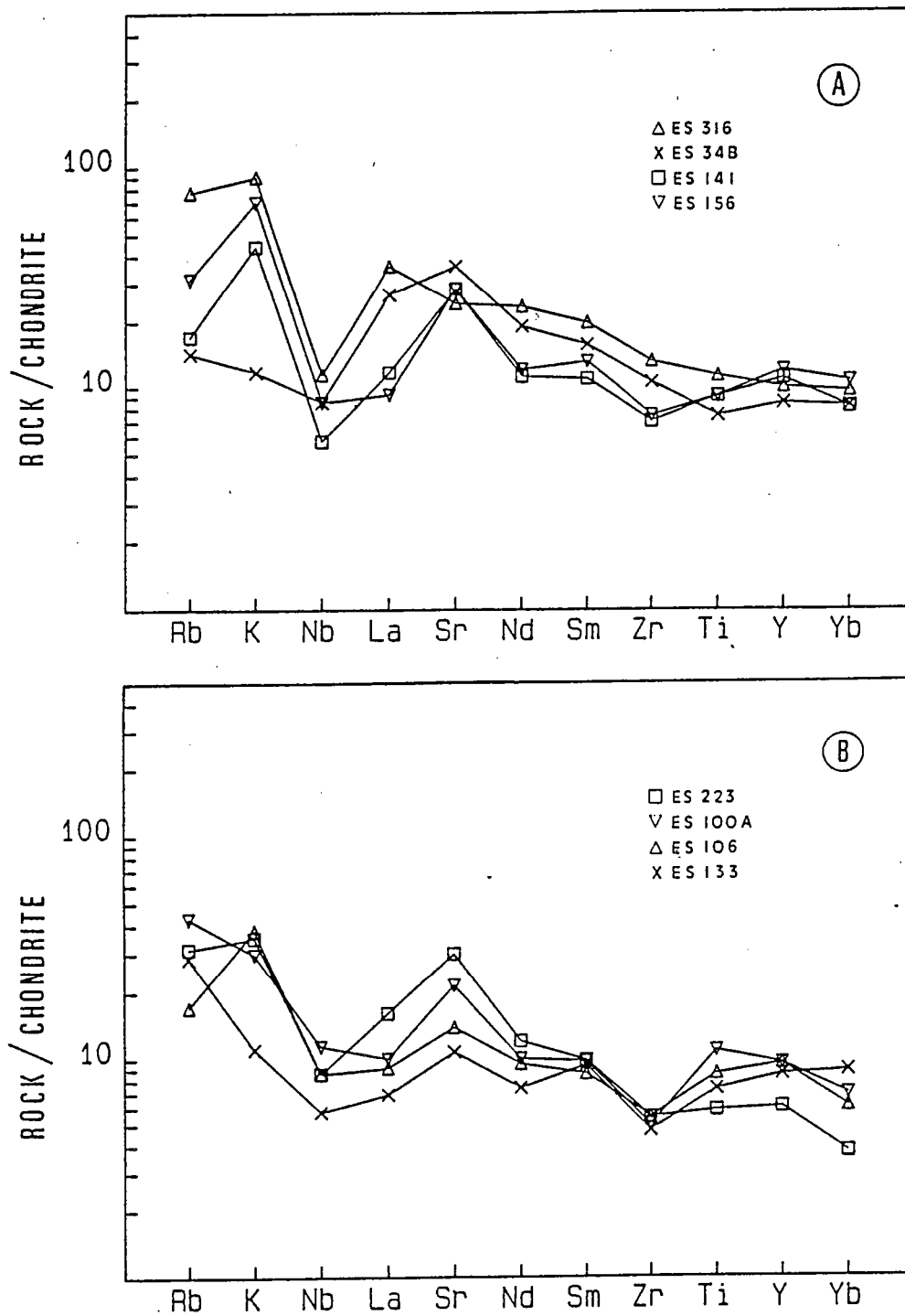


Figure 3

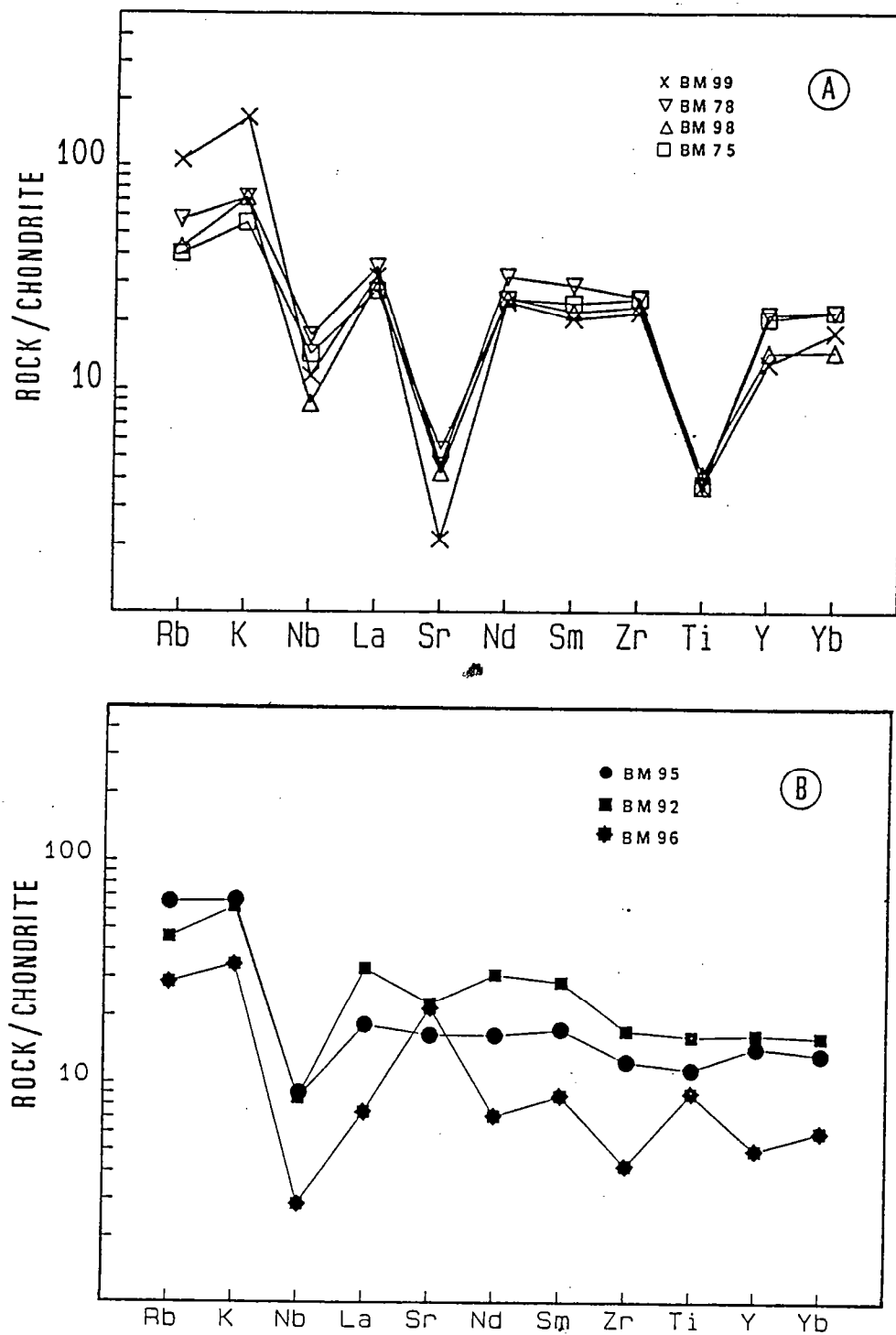


Figure 4

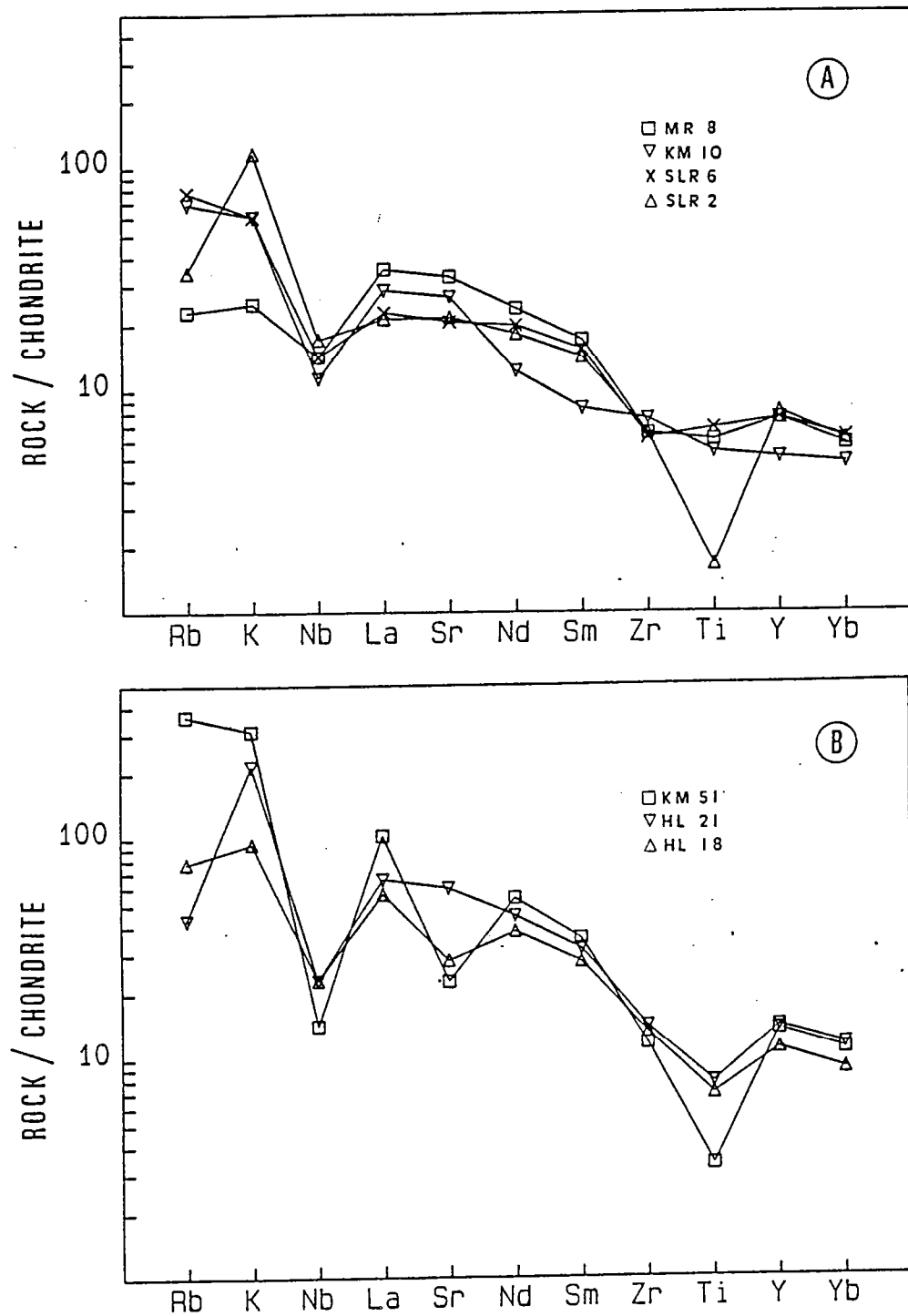
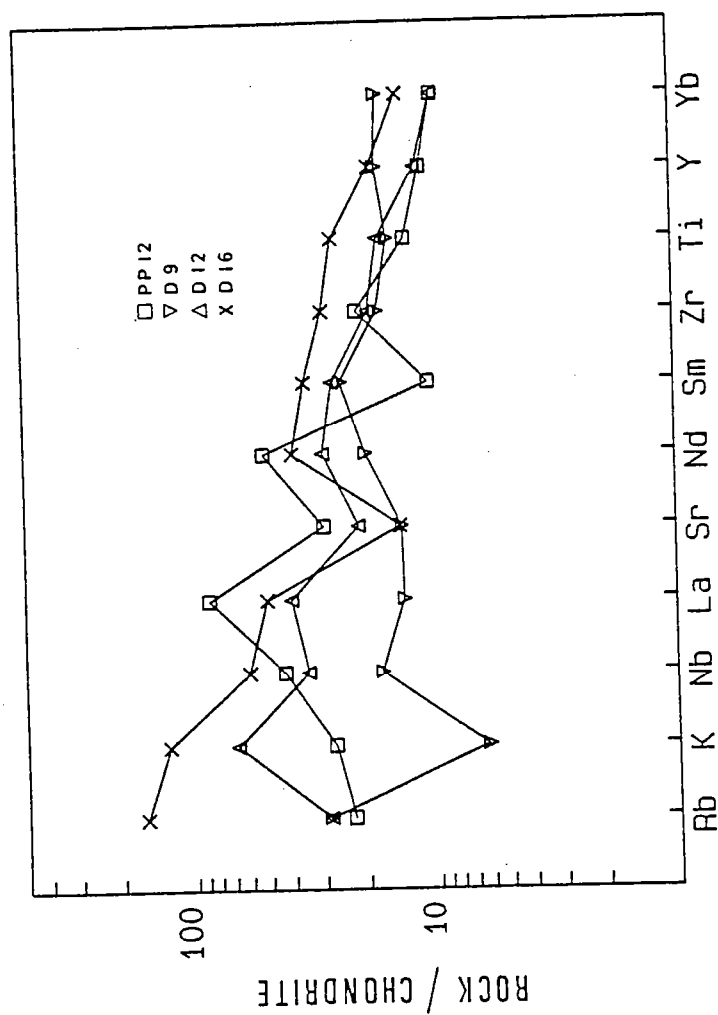


Figure 5



Figure 6



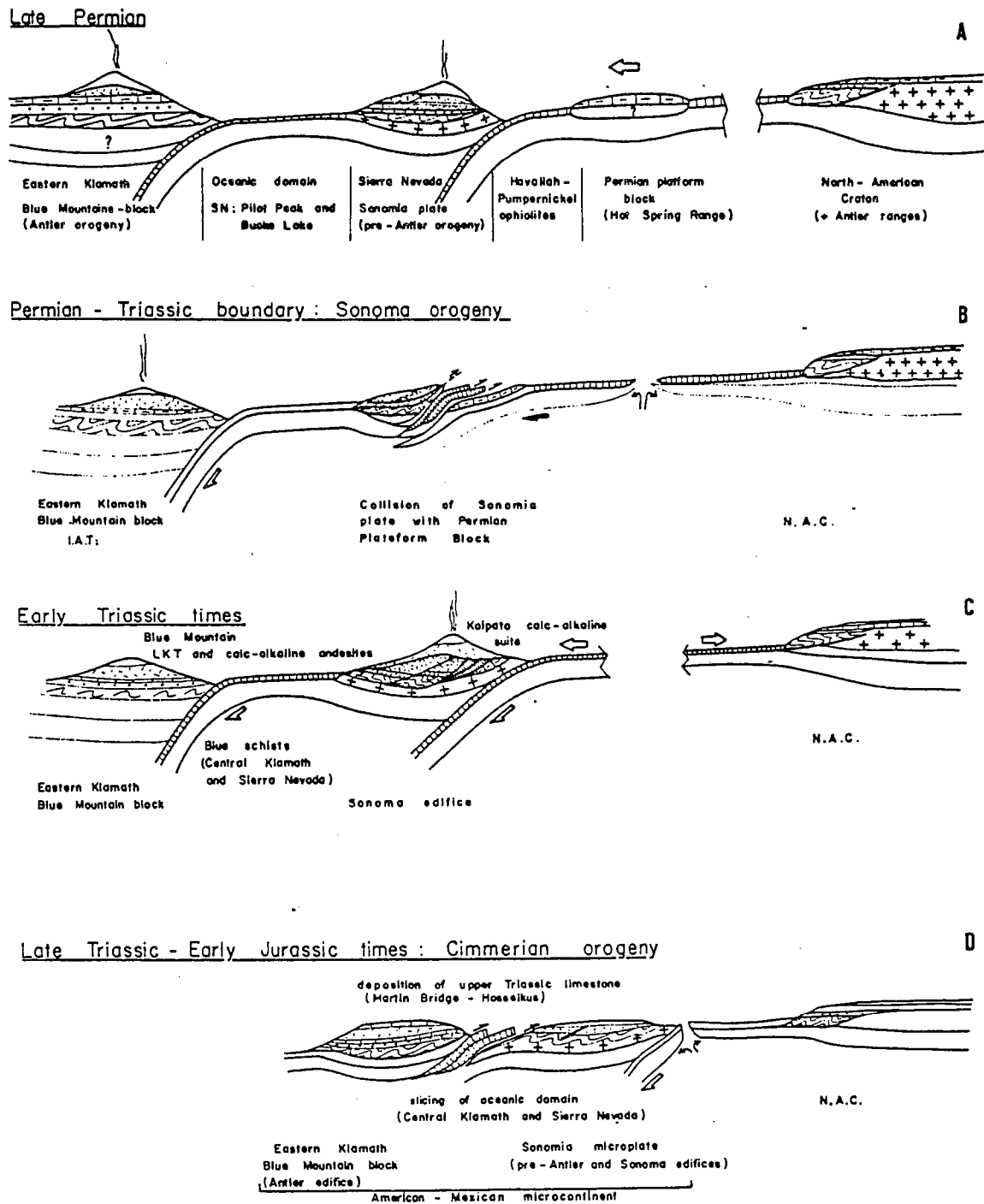


Figure 7

## Références

- Albers J.P. et Bain J.H. 1985. Regional setting and new information on some critical geologic features of the West Shasta District, California. *Econom. Geol.*, 80 : 2072-2091.
- Albers J.P. et Robertson J.F. 1961. Geology and ore deposits of East Shasta copper zinc district, Shasta County, California : U.S. Geological Survey Professional Paper, 338, 103p.
- Barker J.P., Millard H.T. et Knight R.J. 1979. Reconnaissance geochemistry of Devonian island-arc volcanic and intrusive rocks, West Shasta district, California. In: *Trondjemites, dacites and related rocks*, F. Barker (Ed.), Elsevier : 531-545.
- Boudier F. et Nicolas A. 1985-86. Harzburgite and lherzolite subtypes in ophiolite and oceanic environments. *Earth Planet. Sci. Lett.*, 76 : 84-92.
- Brouxel M. 1987. Géochimie d'un arc insulaire intra-océanique fossile et son bassin marginal : les séries paléozoïques de Copley, Balaklala et le cortège ophiolitique de Trinity (Klamath orientales, Nord Californie, U.S.A.). Thèse Doct. Univ. Nancy I, 323pp.
- Brouxel M. et Lapierre H. 1984. La série basaltique de Trinity (Klamath orientales, Nord Californie) : témoin de l'existence d'un bassin marginal au Dévonien moyen. *C. R. Acad. Sc. Paris*, t. 299, Série II, n°8 : 457-462.
- Brouxel M. et Lapierre H. 1985. Un bassin marginal dévonien dans les Klamath orientales (Californie du Nord, Etats Unis) : le cortège ophiolitique de Trinity. *Ophioliti*, 10 : 181-202.
- Brouxel M. et Lapierre H. 1988. Geochemical study of an early Paleozoic island arc - back arc basin system. Part I : The Trinity ophiolite (Northern California). *Geol. Soc. Am. Bull.*, 100 : 1111-1119.
- Brouxel M., Lecuyer C. et Lapierre H. 1989. Diversity of magma types in a Lower Paleozoic island-arc marginal basin system. *Accepté à Chem. Geol.*
- Cannat M. et Boudier F. 1986. Charriages infra-ophiolitiques et convergence océanique dans les Klamath Mountains (Californie du Nord). *Bull. Soc. géol. France*, 6 : 1001-1005.
- Cashman S.M. 1980. Devonian metamorphic in the northeastern Klamath Mountains, California. *Geol. Soc. Am. Bull.*, 91 : 453-459.
- Charvet J., Lapierre H. et Campos C. 1989. Mise en évidence de la phase Antler (Dévonien supérieur - Carbonifère inférieur) dans les Klamath orientales (Nord Californie), Implications géodynamiques : *C. R. Acad. Sci. Paris* (soumis).
- Charvet J., Lapierre H. et Campos C. 1989. Extension of the Antler orogeny in the eastern Klamath Mountains (N. California), geodynamic implications. *Soumis à Geology*.
- Clayton R.N. et Mayeda T.K. 1963. The use of bromine pentafluoride in the extraction of oxygen from oxides and silicates for isotopic analyses. *Geochim. Cosmochim. Acta*, 27 : 43-52.
- Davis G.A. 1966. Metamorphic and granitic history of the Klamath Mountains. *Calif. Div. Min. Geol. Bull.*, 80 : 1095-1108.
- Govindaraju K. et Montanari R. 1978. Routine performance of a matrix-correction free X-Ray fluorescence spectrometric method for rock analysis. *X-Ray spectrometry*, 7 : 148-151.

- Harper G.D. 1984. The Josephine Ophiolite, Northwestern California. *Geol. Soc. Am. Bull.*, 95 : 1009-1026.
- Henoc J. et Tong M. 1978. Automatisation de la microsonde. *J. Microsc. Spectros. Electron.*, 3 : 247-254.
- Irwin W.P. 1966. Geology of the Klamath Mountains Province. *Calif. Div. Min. Geol. Bull.*, 190 : 19-38.
- Irwin W.P. 1977. Ophiolitic terranes of California, Oregon and Nevada. In : R.G. Coleman and W.P. Irwin (Editors), *North American Ophiolites*, *Oreg. Dept. Geol. Miner. Ind. Bull.*, 95 : 75-92.
- Jacobsen S.B., Quick J.E. et Wasserburg G.J. 1984. A Nd and Sr isotopic study of the Trinity peridotite; implications for mantle evolution. *Earth Planet. Sci. Lett.*, 68 : 361-378.
- Kinkel A.R.J., Hall W.E. et Albers J.P. 1956. Geology and base metal deposits of West Shasta Copper - Zinc district Shasta County, California. *U.S. Geol. Surv. Prof. Pap.*, 258 : 156 p.
- Lanphere M.A., Irwin W.P. et Hotz P.E. 1968. Isotopic age of the Nevada orogeny and older plutonic and metamorphic events in the Klamath Mountains, California. *Geol. Soc. Am. Bull.*, 79 : 1027-1052.
- Lapierre H. 1983. Andésites riches en magnésium, témoins de l'existence d'un arc insulaire dévonien dans les Klamath orientales (Nord Californie, Etats Unis). *C. R. Acad. Sci. Paris*, 296 : 287-290.
- Lapierre H., Albarède F., Albers J., Cabanis B. et Coulon C. 1985a. The early Devonian volcanism in the Eastern Klamath Mountains, California : evidence for an immature island arc. *Can. J. Earth Sci.*, 22 : 214-227.
- Lapierre H., Cabanis B., Coulon C., Brouxel M. et Albarède F. 1985b. The geodynamic setting of the Early Devonian Kuroko-type sulfide deposits in the eastern Klamath Mountains (northern California) inferred by the petrological and geochemical characteristics of associated island - arc volcanic rocks. *Econom. Geol.*, 80 : 2100-2113.
- Lapierre H., Brouxel M., Albarède F., Coulon C., Lecuyer C., Martin P., Mascle G. et Rouer O. 1987. Paleozoic and Lower Mesozoic magmas from the eastern Klamath Mountains (North California) and the geodynamic evolution of northwestern America. *Tectonophysics*, 140 : 155-177.
- Lecuyer C. 1989. Chemical transfers between ultrabasic xenoliths and basic magmas : evidences for oceanic magma chambers (the Trinity ophiolite, N. California). *Soumis à Lithos*.
- Lecuyer C., Lapierre H. et Charvet J. 1989a. Un exemple d'accrétion d'îles océaniques à une marge continentale active : les séries volcano-sédimentaires d'Yreka-Callahan (Nord Californie). *Soumis aux C. R. Acad. Sci. Paris*.
- Le Sueur E. et Boudier F. 1986. Structures du complexe basique et ultrabasique de Trinity, Californie : genèse d'une ophiolite atypique. *Bull. Soc. géol. France*, 6 : 1007-1014.
- Le Sueur E., Boudier F., Cannat M., Ceuleneer G. et Nicolas A. 1984. The Trinity mafic-ultramafic complex : first results of the structural study of an untypical ophiolite. *Ophioliti*, 9 : 487-498.
- Lindsley-Griffin N. 1977. The Trinity ophiolite, Klamath Mountains, California. In: *North American ophiolites*. R.G. Coleman and W.P. Irwin (Eds.). *Oregon Department of Geology and Mineral Industries Bulletin*, 95 : 107-120.

- Martin P., Lapierre H. et Rocci G. 1984. Présence d'un arc insulaire permien dans les Klamath orientales (N. Californie). Comptes rendus de l'Académie des Sciences, Paris, 298 : 223-228.
- Mattinson J.M. et Hopson C.A. 1972. Paleozoic ophiolitic complexes in Washington and northern California. Carnegie Institution, Annual Report of the Geophysical Laboratory : 578-583.
- O'Neil J.R., Clayton R.N. et Mayeda T.K. 1969. Oxygen isotope fractionation in divalent metal carbonates. J. Chem. Phys., 51 : 5547-5558.
- Quick J.E. 1981. Petrology and petrogenesis of the Trinity peridotite, an upper mantle diapir in the eastern Klamath Mountains, northern California. J. Geophys. Res., 87 : 3831-3848.
- Roure F. 1984. Une coupe géologique de Golconda au Pacifique (Oregon, Nord-Ouest du Nevada, Nord de la Californie). Evolution mésozoïque et cénozoïque de la marge ouest américaine. Doctorat d'état, Université Pierre et Marie Curie, Paris VI : 250.
- Strand R.G. 1962. Geologic Atlas of California, Redding sheet : 1 / 250 000. Calif. Div. Min. Geol.
- Strand R.G. 1963. Geologic Atlas of California, Weed sheet : 1 / 250 000. Calif. Div. Min. Geol.
- Wagner D. et Saucedo G.J. 1986. Geological map of the Weed quadrangle, 1 / 250 000, California. Calif. Div. Min. Geol., Reg. Geol. Map Ser., 4A.

## CHAPITRE 2 - Structures et magmatisme.

### 2.1. Rappels.

Le terme ophiolite est une définition pétrographique qui rassemble au sein d'un même massif des péridotites plus ou moins serpentinisées, des roches cumulatives de nature gabbroïque litées et des gabbros isotropes dans lesquels s'enracinent des filons pouvant s'organiser en de véritables réseaux appelés "complexe filonien" et des laves en coussins. Ces dernières peuvent être associées à des sédiments qui sont dans la majeure partie des cas des radiolarites. Brunn (1960) a été le premier à voir une analogie entre le concept de cortège ophiolitique et celui de lithosphère océanique.

Lors du développement de la théorie de la tectonique des plaques, la communauté scientifique a vraiment commencé à s'intéresser à cette analogie (Dewey et Bird, 1970; Moores et Vine, 1971). Il a fallu attendre la Penrose Conference de 1972 pour reconnaître les cortèges ophiolitiques comme des fragments de lithosphère océanique échoués sur les continents à la faveur de processus d'écaillages lors du plongement de la lithosphère dans les zones de subduction. Le devenir de la lithosphère océanique étant par définition d'être engloutie dans les zones de subduction et recyclée dans le manteau terrestre, la préservation sur les continents de fragments de lithosphère océanique est apparue pour de nombreux scientifiques comme un phénomène à caractère exceptionnel. Ainsi, le problème a été posé de savoir si les complexes ophiolitiques sont réellement représentatifs de la néolithosphère engendrée à l'aplomb des zones d'accrétion océanique comme dans les grands bassins Pacifique, Atlantique et Indien (Hall, 1983; Moores, 1982).

Toutefois, même si les ophiolites ont pu être engendrées dans des environnements géotectoniques particuliers, elles présentent toutes les caractéristiques suivantes : elles ont été mises en place dans des zones d'extension sous-marines, les massifs de péridotites tectonisées et chimiquement "réfractaires" ou "appauvries" constituant la semelle du cortège représentent la source mantellique des magmas ultrabasiques et basiques dont dérivent les roches ophiolitiques. L'ensemble de ces caractères témoigne de processus d'accrétion de lithosphère dans des centres d'expansion océanique.

Il est actuellement admis (Coleman, 1984) que les ophiolites sont des fragments de lithosphère océanique formés dans des environnements géotectoniques variés 1) les rides médio-océaniques 2) les bassins arrière-arc 3) les bassins avant-arc et 4) les petits bassins (bassins marginaux et bassins océaniques naissants (de type Mer Rouge).

Les travaux de reconstruction géodynamique portant sur l'ophiolite de Trinity (LeSueur et al., 1984; LeSueur et Boudier, 1986; Boudier et Nicolas, 1985/86; Nicolas et Dupuy, 1984; Brouxel et Lapierre, 1985; Lapierre et al., 1987; Brouxel et Lapierre, 1988) ne permettent pas de trancher véritablement quant à l'environnement précis dans lequel s'est mis en place le complexe ophiolitique de Trinity. Toutefois, au vu de ces résultats, il faut considérer que le complexe ophiolitique de Trinity représente probablement un petit bassin océanique soit de type bassin marginal ou arrière-arc soit de type Mer Rouge engendré à l'aplomb d'une ride océanique à expansion lente.

### 2.2. Buts de l'étude.

Les problèmes suivants seront évoqués :

1) L'étude des relations pétrologiques et structurales entre les chambres magmatiques et les péridotites mantellaires qui a pour but de préciser la dimension, la géométrie des chambres magmatiques et les modalités de leur alimentation par fusion partielle des péridotites mantellaires adjacentes. Ce problème est développé dans la première partie de ce chapitre qui propose une étude comparative des chambres magmatiques de Toad Lake et Castle Lake (figure 2.1). L'étude de terrain a été conduite en collaboration avec M. Cannat du G.I.S. de Brest.

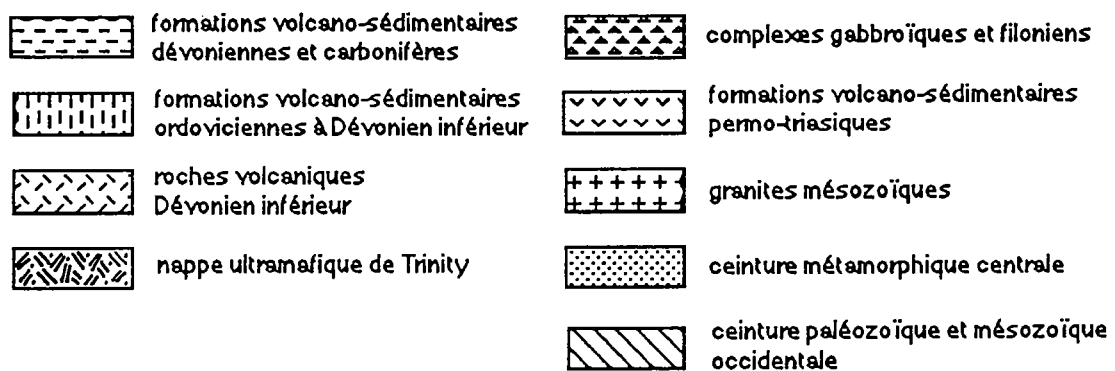
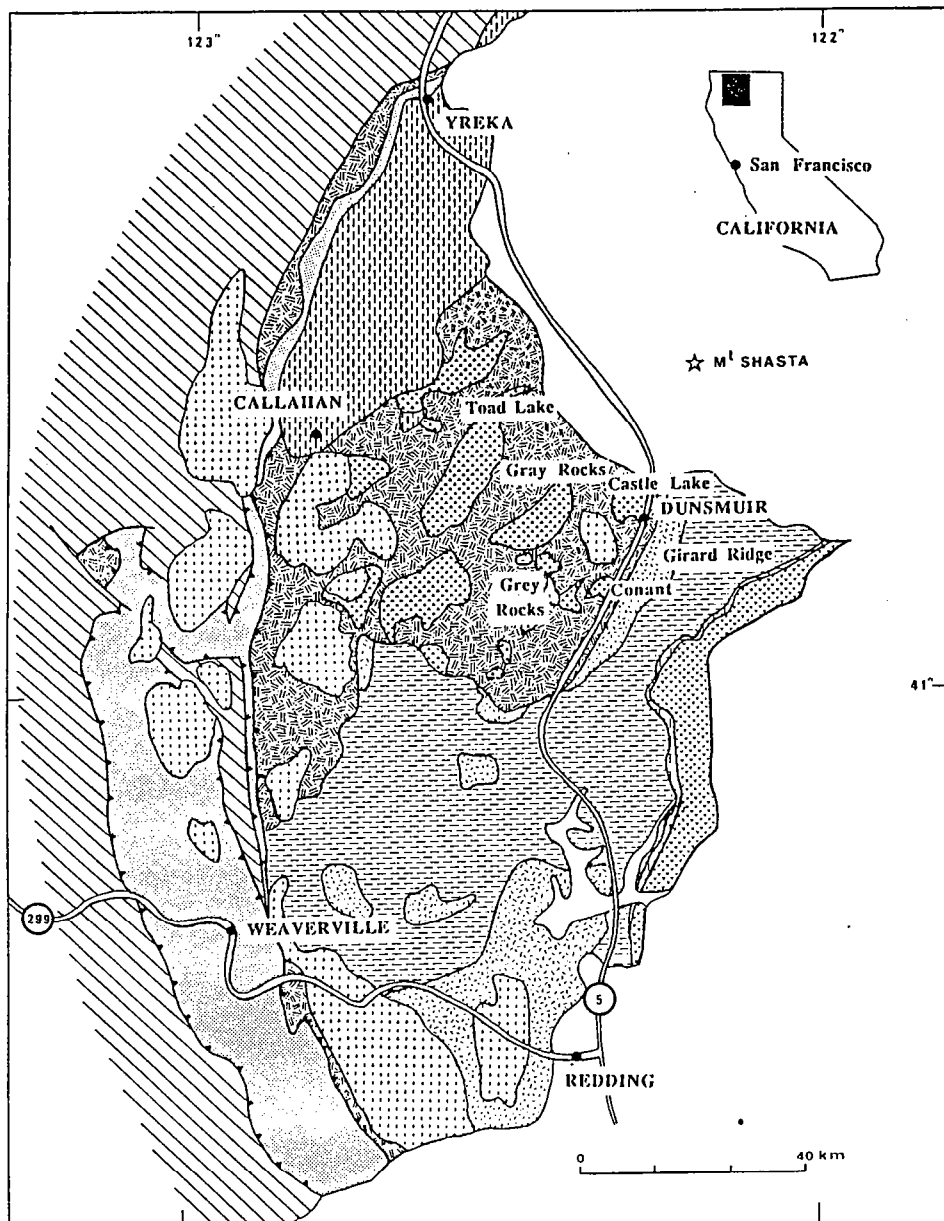
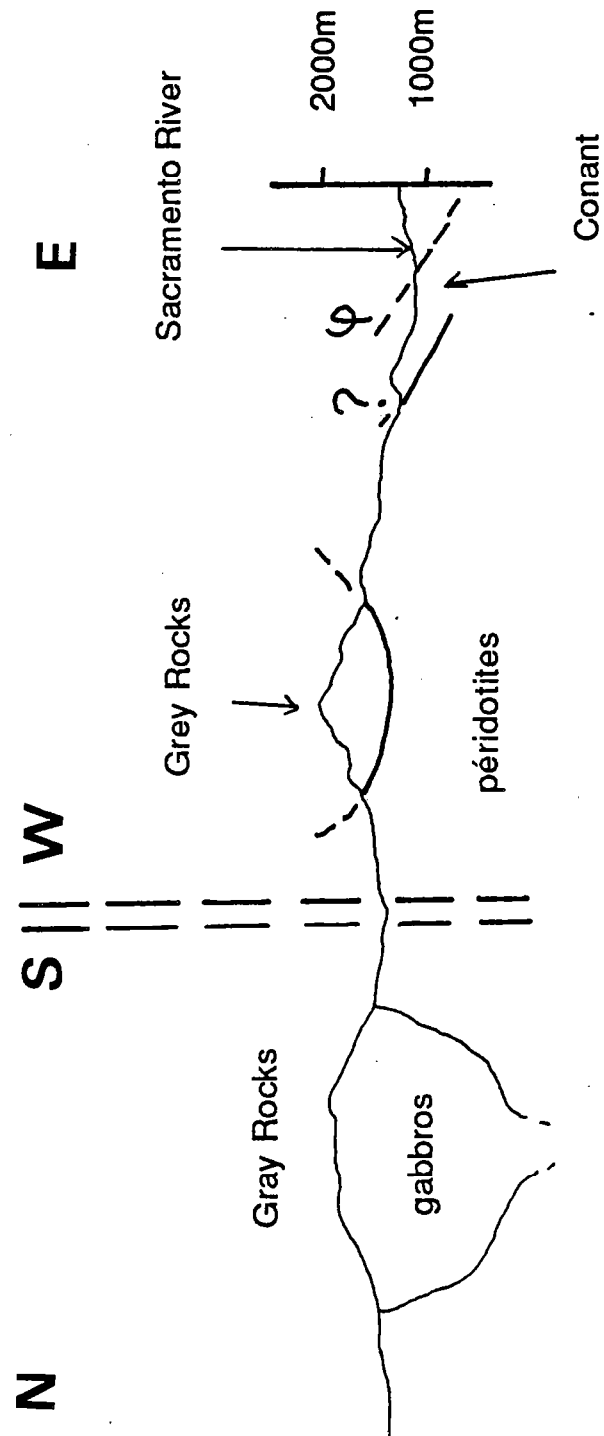


Figure 2.1 : carte géologique générale des Klamath orientales d'après Strand (1962, 1963), Irwin (1977) et Wagner et Saucedo (1986).





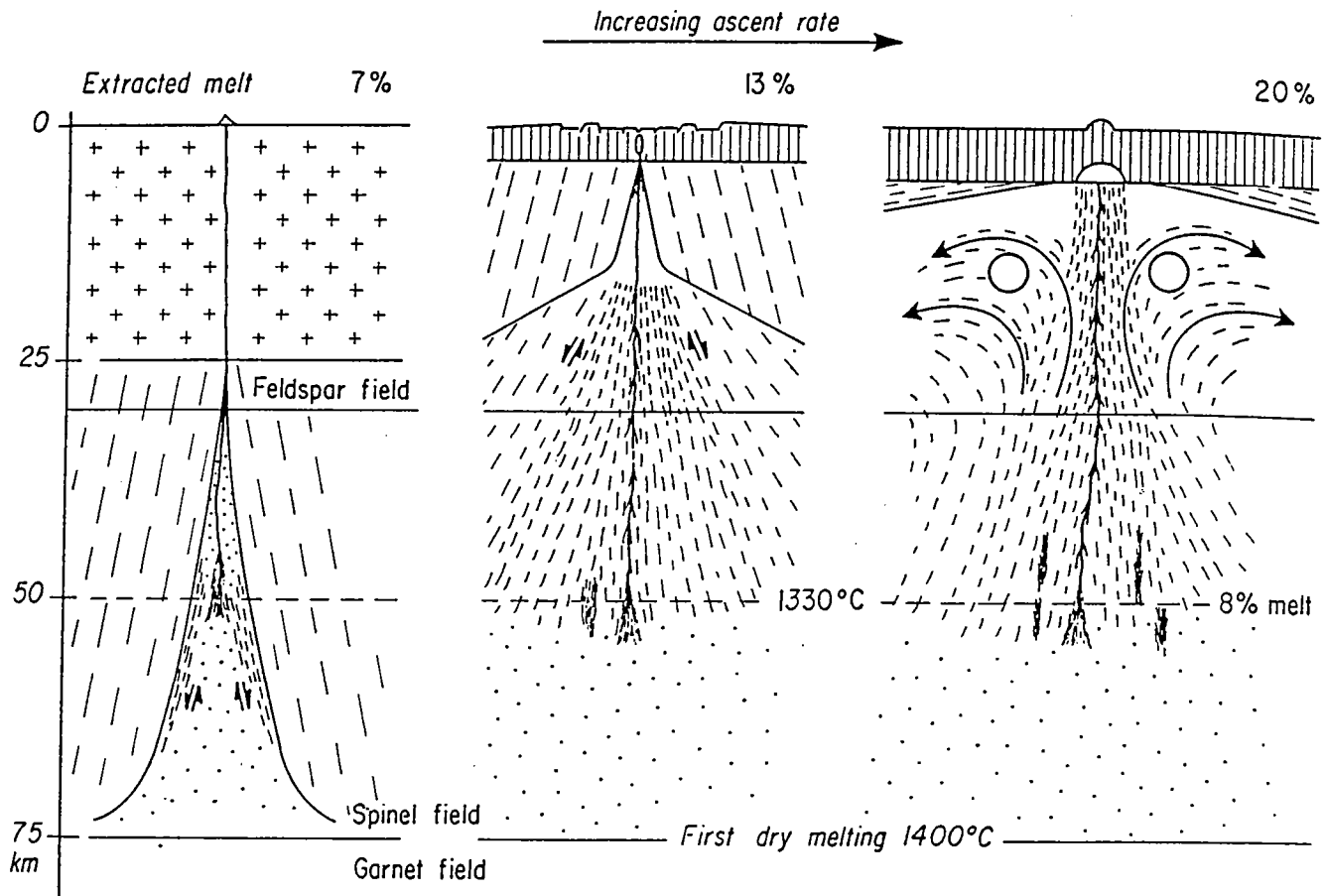


Figure 2.2 : relations manteau-croûte et conditions d'extraction des liquides magmatiques dans une situation de rift continental avec des lherzolites à spinelle (à gauche), dans une situation de type Mer Rouge avec des lherzolites à plagioclase (au centre) et dans une situation océanique avec des harzburgites (à droite). D'après Nicolas (1986).

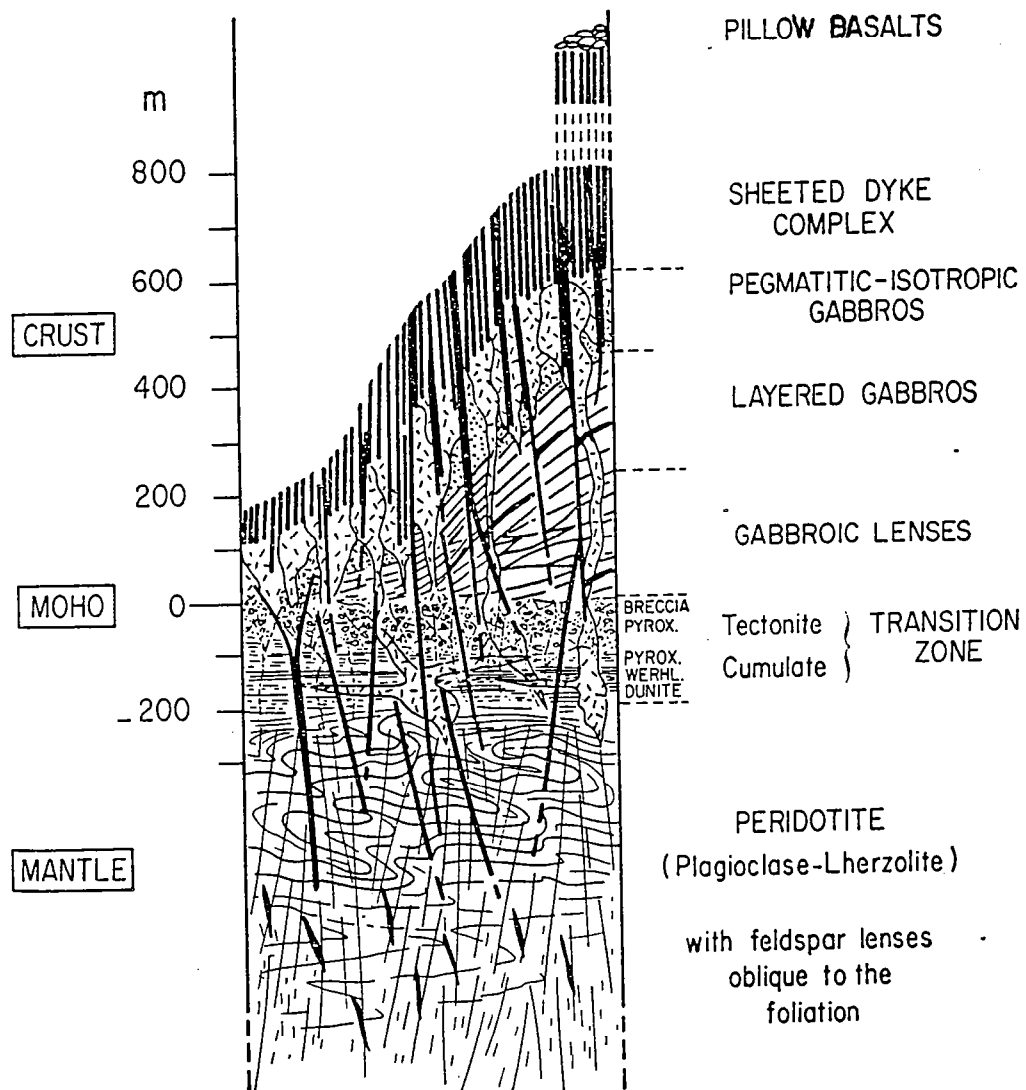


Figure 2.3 : Le log synthétique de la pile ophiolitique de Trinity d'après LeSueur et Boudier (1986).

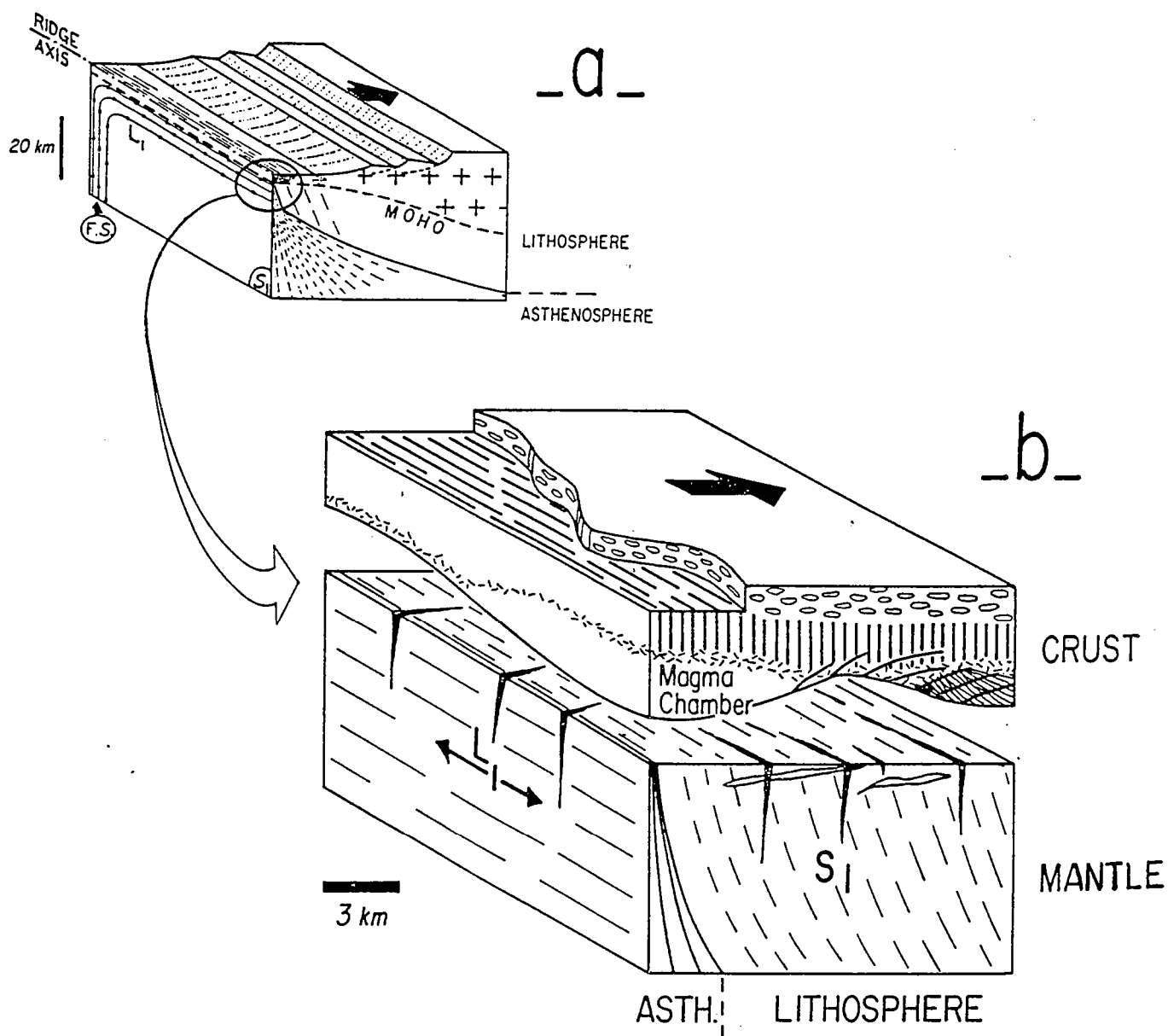


Figure 2.4 : Modèle géodynamique de la genèse de l'ophiolite atypique de Trinity proposé par LeSueur et Boudier (1986) basé sur l'analyse de ses structures internes.  
 a : dans le plan axial de la ride (plan de foliation S1 vertical), centre d'alimentation (F.S.) et trajectoires possibles (L1) du flux asthénosphérique; b : - section mantellaire = structures acquises dans les conditions asthénosphériques : S1, plans d'écoulement subverticaux; L1, directions d'écoulement subhorizontales et parallèles à l'axe de la ride; 2 générations de filons de pyroxénite et de gabbros perpendiculaires et parallèles à la ride; - section crustale = petites chambres magmatiques, non permanentes et discontinues, injectées de filons et sills de gabbro pegmatoïde de diabase; la flèche indique la direction d'extension donnée par l'orientation du complexe filonien.

Ce travail s'appuie également sur les travaux de pétrologie et géologie structurales réalisés par A. Nicolas, F. Boudier, E. LeSueur et M. Cannat sur la nappe de péridotites mantellaires du complexe ophiolitique de Trinity. Ils déduisent ainsi de leurs travaux une océanisation dans un environnement à faible vitesse d'expansion (de type Mer Rouge) avec création d'une croûte océanique mince (figures 2.2 et 2.3) et de petites chambres magmatiques non permanentes surmontant un dôme asthénosphérique dont le flux est canalisé parallèlement à l'axe de la ride (figure 2.4).

2) Un article est plus précisément consacré à l'étude détaillée d'une chambre magmatique du complexe ophiolitique de Trinity (chambre de Gray Rock; figure 2. 1). Les mécanismes de fusion partielle de la péridotite de Trinity, la nature du magma parent et son cursus de cristallisation fractionnée ont été examinés afin de contraindre la chronologie et les volumes relatifs des différents événements magmatiques qui ont marqué l'accrétion océanique. L'étude de l'évolution de la densité du magma au sein de la chambre apparaît comme paramètre fondamental contrôlant l'émission des magmas basiques sous forme de pillow lavas vers la surface. La courbe d'évolution en densité du magma de la chambre de Gray Rock a été ainsi comparée à celle des liquides de MORB proposée par Stolper et Walker (1980).

L'origine des volumes limités de filons et stocks de plagiogranites (<10%) ainsi que les intrusions ou sills métriques à plurimétriques de gabbros pegmatitiques qui recoupent à la fois les péridotites mantellaires et la séquence cumulative ont fait l'objet d'une discussion. En effet, la présence de volumes restreints de liquides magmatiques de composition trondhjémitique localisés principalement aux toits des chambres magmatiques ophiolitiques pose le problème de leur genèse. Couramment, plusieurs hypothèses sont proposées :

- magmas résiduels issus de la cristallisation fractionnée en système clos (Menzies et al., 1980; Pallister et Knight, 1981; Ashley et al., 1983; Pedersen et Malpas, 1984).
- produits de la fusion partielle de gabbros dans des conditions hydratées (Gerlach et al., 1981; Pedersen et Malpas, 1984).
- phénomènes d'immiscibilité de magmas (Ohnenstetter, 1982).

Les gabbros pegmatitiques de par leur abondance sur le terrain sont intéressants à examiner car ils signent un événement particulier peut-être d'origine diastrophique au cours de la maturation de la croûte océanique. Les conditions de leur genèse et de leur mise en place au sein de l'édifice ophiolitique peuvent apporter des éléments nouveaux sur les mécanismes magmatiques et le rôle des fluides au sein des chambres magmatiques.

3) La signification pétrologique et géochimique des péridotites mantellaires a été examinée dans l'ensemble de ce travail à la suite des travaux de Quick (1981) sur le massif de péridotites de Trinity. Le massif est constitué de lherzolites, lherzolites à plagioclase, harzburgites, harzburgites à plagioclase et de dunites dont la distribution est très hétérogène sur le terrain. L'examen des textures des péridotites à plagioclase suggèrent des phénomènes de piégeage de liquides magmatiques sous forme de lentilles de plagioclase et de pyroxènes xénomorphes lors de la percolation au sein du manteau supérieur. Ces phénomènes d'imprégnation ont été suggérés et étudiés par Nicolas et al., (1980) et Nicolas et Dupuy (1984).

Le phénomène d'imprégnation des péridotites mantellaires est particulièrement spectaculaire au sein du massif de Trinity. L'existence de réactions minéralogiques de haute température affectant les bordures des filons gabbroïques recoupant les péridotites mantellaires ou les xénolites de ces dernières le long des parois des chambres magmatiques m'a conduit à un essai de quantification de la modification de la composition chimique du magma parent qui vient alimenter les chambres magmatiques. Une approche qualitative de ces phénomènes de fractionnement géochimique au sein du manteau supérieur a été proposée précédemment par Gregory (1984) et Pallister (1984). Nous avons effectué une étude d'analyses en composantes principales pour les spinelles (figure 2. 5) et pour les clinopyroxènes (figure 2. 6) des péridotites mantellaires et de ses xénolites et met en évidence l'enrichissement de ces minéraux en Fe, Ti et Na en présence de lentilles de plagioclase.

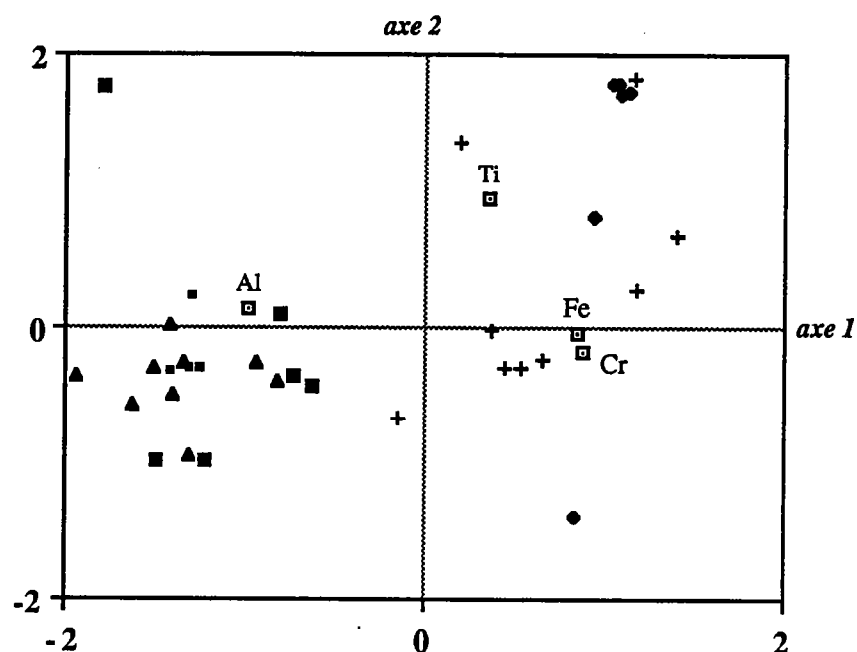


Figure 2.5 : Diagramme d'analyse factorielle pour les spinelles. Carrés pointés : pôles chimiques; carrés vides : xénolites de péridotites mantellaires en enclaves dans les chambres magmatiques; petits carrés pleins : dunites foliées; losanges pleins : lherzolites à plagioclase; triangles pleins : harzburgites; plus : harzburgites à plagioclase; gros carrés pleins : lherzolites et croix : filons de gabbros intrusifs dans les péridotites mantellaires.

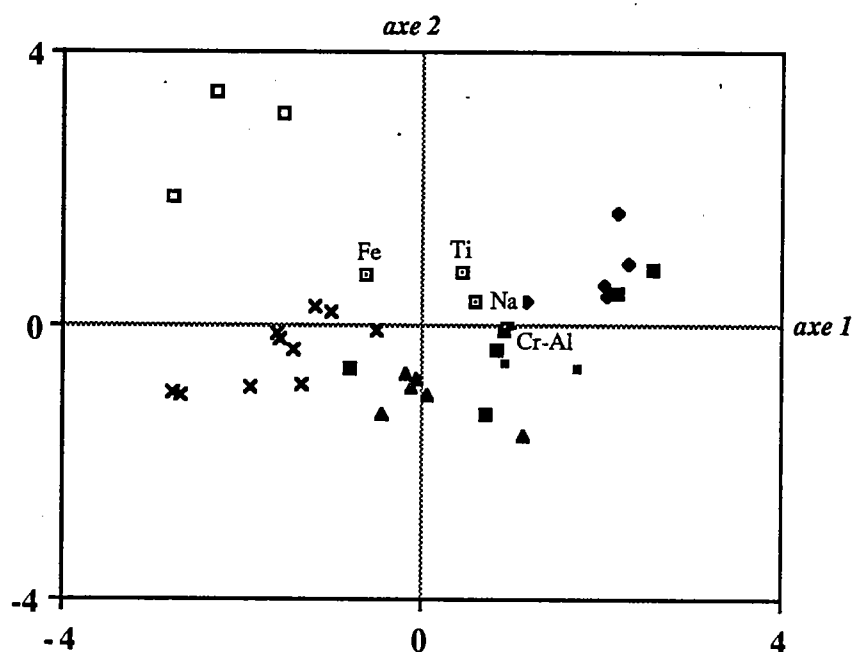


Figure 2.6 : Diagramme d'analyse factorielle pour les clinopyroxènes. Même légende.

Dans ce but, des bilans de masse ont été effectués et proposés pour la chambre magmatique de Gray Rock (Lecuyer et al., 1989b; premier article de ce chapitre). La composition chimique des péridotites mantellaires et de ses minéraux a été étudiée autour de la chambre magmatique de Toad Lake (Lecuyer et Cannat, 1989; première partie de ce chapitre). Enfin, des transferts chimiques ont été mis en évidence entre les xénolites de péridotites mantellaires et les magmas basiques tapissant le plancher et les murs des chambres magmatiques de Castle Lake et de Toad Lake afin de caractériser les processus de "magma stopping" et d'assimilation qui prennent place le long des parois des. De tels phénomènes ont été précédemment observés dans les complexes ophiolitiques de Norvège par Pedersen (1986).

## 2.3. La chambre magmatique de TOAD LAKE.

### 2.3.A Géologie.

#### 2.3.A.a Les péridotites.

Elles sont présentes depuis les dunites jusqu'aux lherzolites avec une foliation de spinelle régulière sensiblement EW à pendage Nord modéré.

Les dunites forment des poches discordantes plutôt horizontales (figure 2.7).

Ces péridotites sont recoupées 1) par des veines riches en clinopyroxène; discordantes sur la foliation mais localement plissées et 2) par des veines et des filons de gabbro à grain centimétrique d'orientation moyenne EW à pendage Sud modéré (figure 2.7).

On observe également la concentration de petites lentilles de feldspath et de clinopyroxène (interstitielles dans la lherzolite) en veines gabbroïques.

#### 2.3.A.b Les gabbros.

A la base de la chambre magmatique (figure 2.8), la péridotite est bréchifiée et partiellement assimilée, on y trouve :

- 1) les gabbros issus des filons décrits plus haut (échantillons cités plus loin et TOAD14).
- 2) des gabbros lités à ilménite. Ce litage est NS à NNE-SSW, à pendage W modéré (figure 2.7) et parallèle au contact de base de chambre (TOAD10, TOAD12, TOAD22 et TOAD23). Les gabbros lités se retrouvent sur environ 800 mètres (figure 2.8) et sont recoupés par des gabbros isotropes à passées pegmatoïdes (TOAD27). Des fragments ultrabasiques (anciennes péridotites) sont contenus dans les premiers niveaux de gabbros isotropes qui se poursuivent dans les 100m supérieurs de la coupe.

#### 2.3.A.c Les filons.

L'ensemble de la série gabbroïque est recoupé par des filons de diabase verticaux WNW-ESE (figure 2.7). La taille de ces filons croît vers le haut de la série (figure 2.8).

Sur le terrain on distingue :

##### 1) dans les péridotites:

- des veines riches en clinopyroxène localement plissées et donc déformées avec la péridotite (TOAD34; TOAD35).

- des veines riches en clinopyroxène non plissées mais recoupées par les veines gabbroïques (TOAD5).

- des veines gabbroïques à grain plurimillimétrique à centimétrique (TOAD7; TOAD9; TOAD20; TOAD17; TOAD18; TOAD38 et TOAD40).

- des veines de microgabbro à ilménite (TOAD21) qui pourraient être injectées à partir de la chambre magmatique.

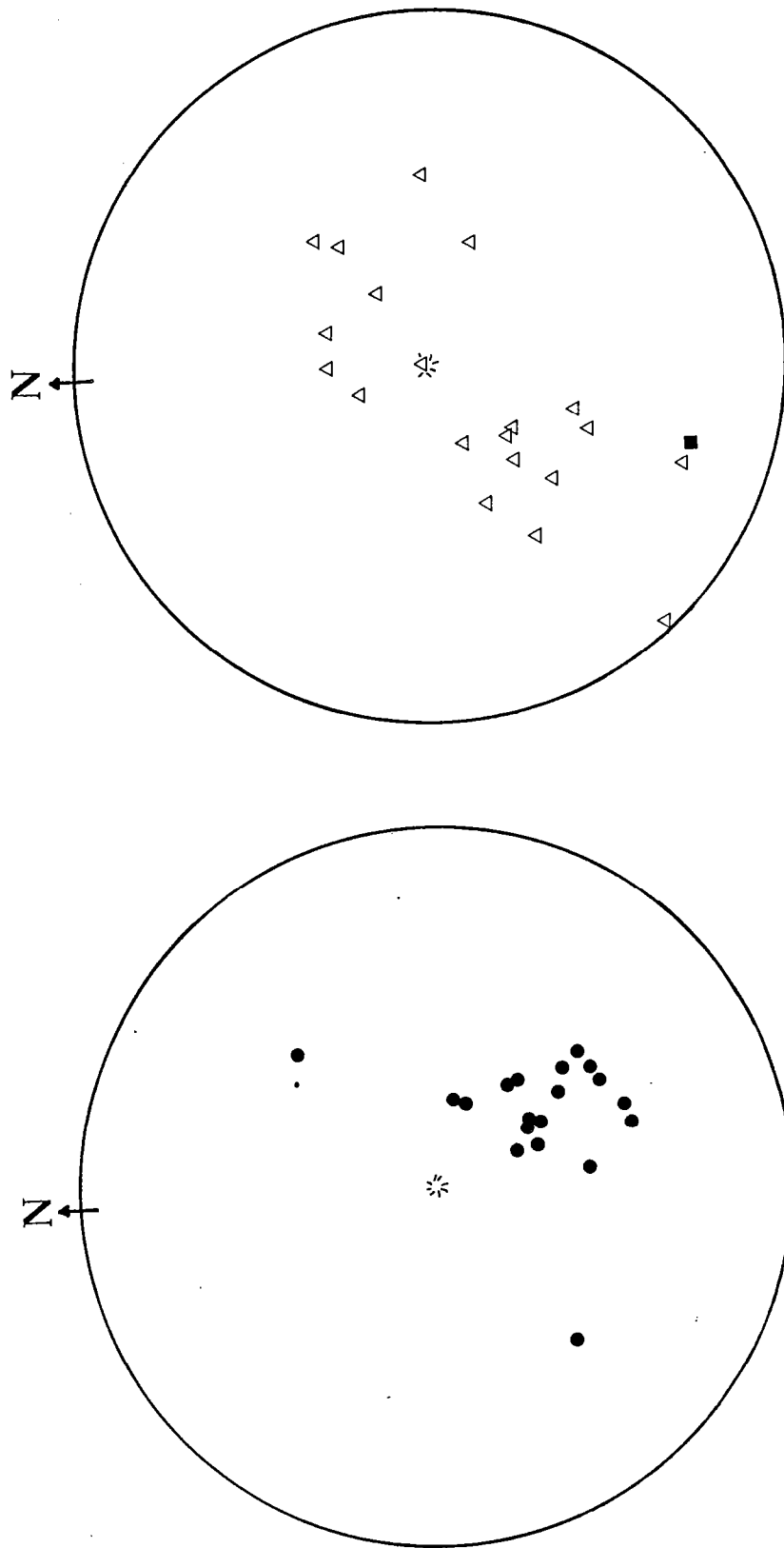
- des veines de microgabbro riches en clinopyroxène (TOAD11).

##### 2) Dans les gabbros.

- des veines de microgabbro riches en pyroxène (TOAD25).

- des microgabbros clairs légèrement déformés (TOAD24 et TOAD26). Cette déformation suggère une injection dans des cumulats encore mal consolidés.

- des microgabbros clairs non déformés formant des masses importantes dans les gabbros isotropes susjacentes (TOAD28).



**Castle Lake :**

à gauche : ronds pleins = litage dans les gabbros.

à droite : carré plein = foliation de spinelle dans une werhlite.  
triangles normaux vides = litage dans les brèches gabbroïques  
basales.

*Figure 2.33.*



- des filons acides (TOAD29).

### 2.3.A.d La chambre magmatique.

Le contact de base de la chambre magmatique n'est que localement cisailé à froid. Il est en général non déformé, redressé et parallèle au litage des cumulats. L'orientation verticale des filons de diabase dans la chambre magmatique et l'absence d'indication du basculement du massif de Trinity (ou de la région de

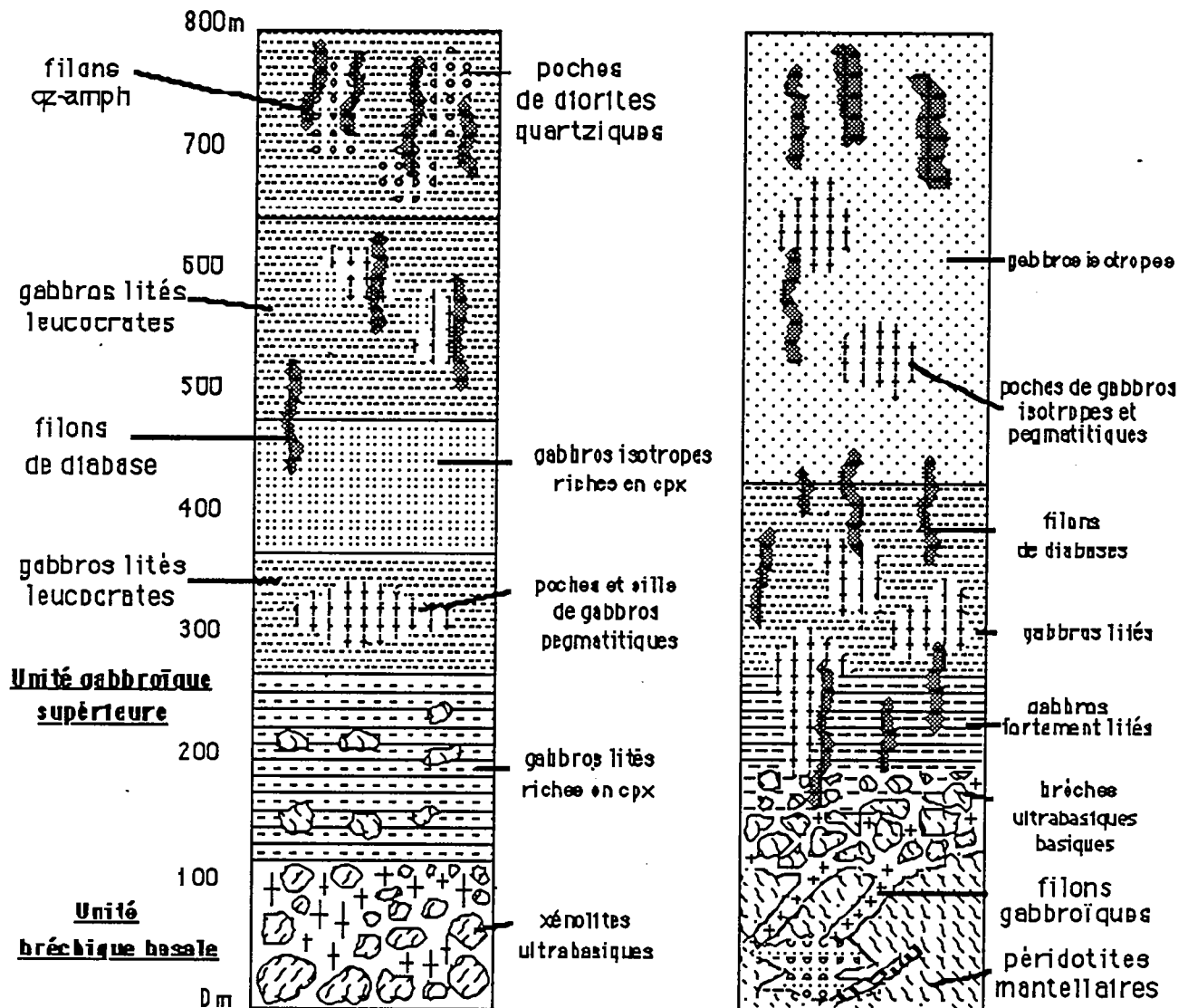
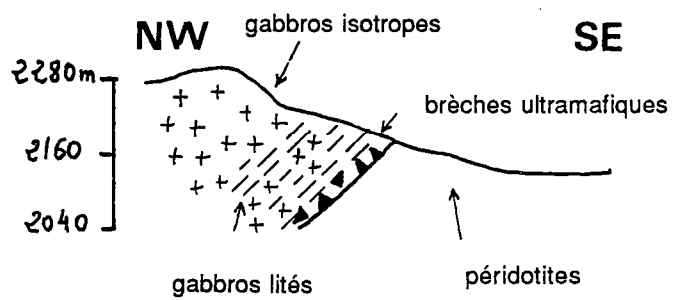
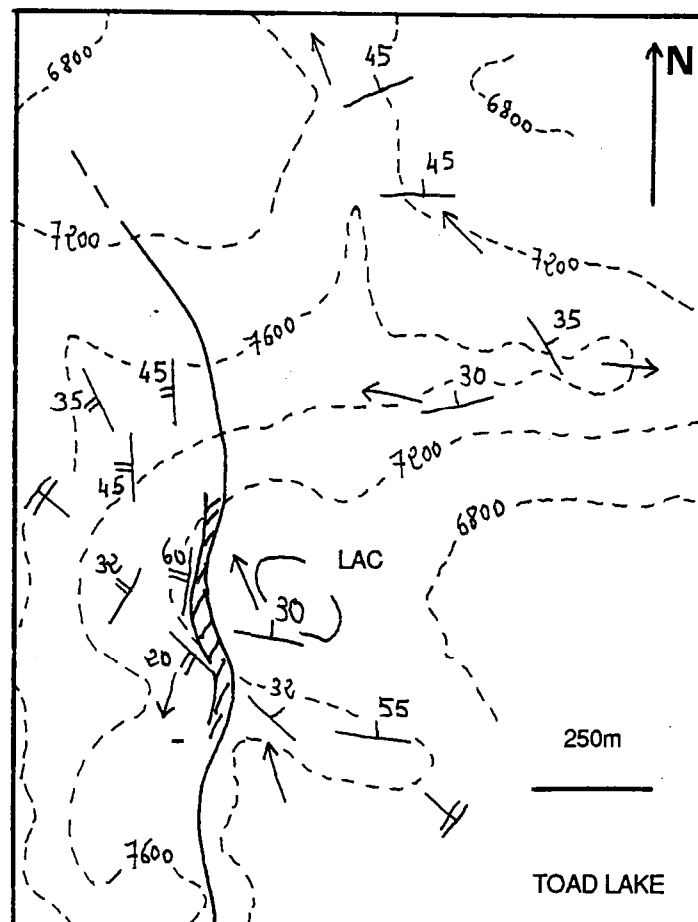


Figure 2.8 : successions lithostratigraphiques des chambres magmatiques de Castle Lake et Toad Lake.

Toad Lake par rapport au reste du massif) suggèrent que ce contact représente un niveau structural correspondant à une paroi latérale de la chambre magmatique et non à un contact de base.

Cette paroi est caractérisée par un régime magmatique assez dynamique comme en témoignent la présence de fortes laminations localement entrecroisées au sein de gabbros évolués (gabbro-norites à ilménite). Vers le centre de la chambre (figure 2.9), les gabbros isotropes largement dominants sont intrusifs dans les gabbros lités et contiennent localement des enclaves ultrabasiques. La présence des enclaves ultramafiques dans les niveaux de gabbros lités témoigne



de phénomènes de "ramonage" au sein de la péridotite lors des injections successives de magmas dans la chambre. L'ensemble est recoupé par des microgabbros localement déformés qui commencent à se mettre en place avant la consolidation complète des gabbros encaissants. L'orientation très régulière de ces gabbros indique une contrainte minimale orientée NNE-SSW et sub-horizontale (direction d'expansion océanique?). Cette direction est similaire à celle déduite d'une étude du massif de Trinity à grande échelle (LeSueur et Boudier, 1984).

### 2.3.A.e Les relations péridotites-gabbros.

Le contact de base apparaît nettement discordant sur la foliation des péridotites. Cette relation rend compte de l'achèvement de la déformation des péridotites avant la constitution de la chambre magmatique. Les corps dunitiques présents dans la lherzolite sont également discordants sur la foliation (figure 2.8, Quick, 1981; LeSueur et Boudier, 1984). Ainsi, la genèse des corps de dunites est également postérieure à la déformation des autres péridotites. Toutefois, le fait que la foliation de spinelle se poursuive dans ces corps dunitiques discordants indique que ces dunites résultent essentiellement (ou partiellement) de la fusion partielle de la lherzolite.

Au contact des filonnets gabbroïques, la péridotite foliée est souvent appauvrie en clinopyroxène et plagioclase; ces témoignages de phénomènes de fusion partielle illustrent l'enracinement génétique et géométrique des gabbros dans la péridotite.

L'injection des filons de gabbros à grain plurimillimétrique à centimétrique, qui résulte probablement de la concentration des petites lentilles à feldspath et clinopyroxène piégées dans la lherzolite, se produit après la formation des dunites (ces dernières sont recoupées par des filons de gabbros). L'orientation NNW-ESE de ces filons de gabbros correspond à une contrainte minimale dominante NNE-SSW pentée au Nord, donc de même orientation mais de pendage différent de ceux relevés dans la chambre magmatique (pendage sub-horizontale).

Il n'existe donc pas de relation entre le système de contraintes dominant la déformation des péridotites et celui dominant l'injection des filons vers la chambre magmatique. Ces résultats suggèrent donc une nette séparation entre l'épisode de déformation mantellaire et les événements magmatiques associés.

### 2.3.B. Pétrographie et minéralogie.

#### 2.3.B.a Les péridotites.

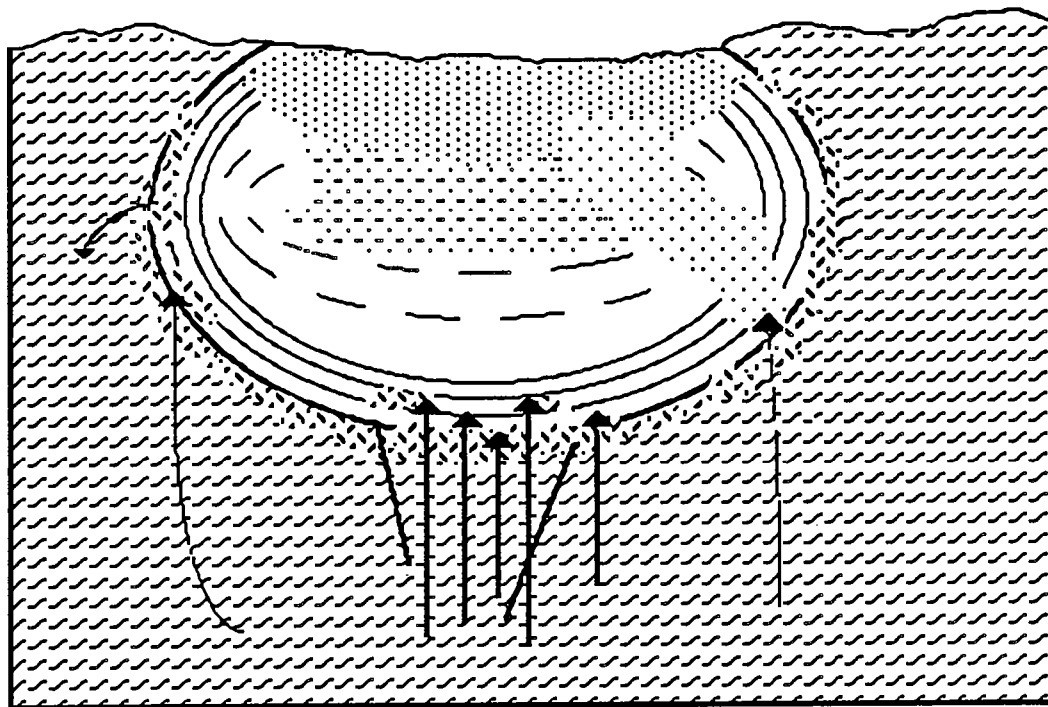
##### 1) Les dunites (TOAD15).

Ces roches à débit de dunites sont partiellement serpentinisées, elles contiennent de l'orthopyroxène frais et peuvent montrer des bandes d'imprégnation de clinopyroxène.

Les orthopyroxènes présentent de courtes et larges lamelles d'exsolution, ils ont des teneurs élevées en  $\text{SiO}_2$  (57,3%) et très faibles en Fs (9,1%). Les clinopyroxènes sont également riches en  $\text{SiO}_2$  (54,2%), pauvres en Wo (47,7%), Fs (3,4%) et  $\text{TiO}_2$  (0,07%). Les olivines sont riches en  $\text{SiO}_2$  (41,6%), Fo (91%) et NiO (0,41%; annexes).

##### 2) Les harzburgites.

Elles sont caractérisées par la présence de plagioclase interstitiel épidotitisé (TOAD19). Dans ces roches, les olivines sont moins riches en  $\text{SiO}_2$  (41,3%) et Fo (90%) que les dunites tandis que les spinelles sont riches en chromite (41,2%) et  $\text{TiO}_2$  (0,41%).



### LEGENDE :

300M

- ALIMENTATION MAGMATIQUE
- CUMULATS LITES
- GABBROS ISOTROPES
- BRECHES ULTRAMAFIQUES
- PERIDOTITES MANTELLAIRES
- GABBROS PEGMATITIQUES

Figure 2.9 : schéma interprétatif de la géométrie et des relations pétro-structurales entre les chambres magmatiques de l'ophiolite de Trinity et les péridotites mantellaires.

### 3) Les lherzolites.

L'échantillon TOAD8 montre des évidences texturales d'imprégnation du plagioclase et du clinopyroxène qui se regroupent en amas de cristaux xénomorphes. Dans d'autres échantillons (lherzolite TOAD35 et lherzolite à plagioclase TOAD40), le clinopyroxène a un habitus xénomorphe à subautomorphe tandis que le plagioclase en petites lentilles millimétriques orientées parallèlement à la foliation du spinelle peut être présent (TOAD40). Dans les échantillons TOAD35 et TOAD40, les spinelles très bruns sont davantage titanifères (0,35-0,42%) et chromifères (38,2-41,9%) et le clinopyroxène est plus riche en Fs (4-4,1%), Na<sub>2</sub>O (0,19-0,33%) et TiO<sub>2</sub> (0,21-0,37%) comparativement à ceux de la lherzolite TOAD8. L'orthopyroxène et l'olivine ne montrent pas de

différences chimiques notables entre ces divers types d'échantillons.

La comparaison des lherzolites plagifères (TOAD40) et non plagifères (TOAD35) révèle qu'en présence du plagioclase, les spinelles et accessoirement le clinopyroxène sont davantage chromifères et titanifères (annexes). En outre, le rapport  $\text{Fe}_2\text{O}_3/\text{FeO}$  dans les spinelles est plus élevé dans les lherzolites que dans les lherzolites plagifères (annexes).

Des calculs de composition modale pour les péridotites et un gabbro à ilménite de Toad Lake sont rassemblées dans le tableau 2.1.

| Echantillons  | TOAD22 | TOAD8 | TOAD15 | TOAD19 | TOAD35 | TOAD40 |
|---------------|--------|-------|--------|--------|--------|--------|
| OLIVINE       |        | 0,61  | 0,53   | 0,58   | 0,55   | 0,53   |
| SPINELLE      |        | 0,07  | 0,02   | 0,07   | 0,07   | 0,02   |
| SERPENTINE    |        |       |        |        |        |        |
| AMPHIBOLE     |        |       |        |        |        |        |
| TALC          |        |       |        |        |        |        |
| CLINOPYROXÈNE |        | 0,14  | 0,02   | 0,21   | 0,13   | 0,21   |
| ORTHOPYROXÈNE | 0,22   | 0,22  | 0,20   | 0,27   | 0,25   | 0,20   |
| PLAGIOCLASE   | 0,55   | 0,08  | 0,04   | 0,08   | 0,04   |        |
| ILMENITE      | 0,09   |       |        |        |        |        |

Tableau 2.1.

### 2.3.B.b Les cumulats.

#### 1) Les cumulats laminés.

Ce sont des gabbro à ilménite (TOAD10; TOAD12; TOAD22 et TOAD23 et composition modale de TOAD22 présentée dans le tableau 2.1) à texture de mésocumulus ou d'orthocumulus caractérisés par un net litage magmatique. Ce litage est défini par l'association d'un contact de proportions et d'un contact granulométrique (TOAD21). De manière générale, les lits les plus grossiers sont les plus riches en plagioclase. Ce dernier peut être altéré soit en albite soit en épidote. Les pyroxènes sont généralement frais, le clinopyroxène peut être transformé en actinote dans certains échantillons. Ces gabbros sont caractérisés par la cristallisation précoce du plagioclase en phase cumulus suivi par le clinopyroxène, l'orthopyroxène et l'ilménite. Les pyroxènes sont caractérisés par des teneurs élevées en Fs (Cpx : Fs13,4-13,6%; Opx : Fs29,8-31,9%) contrastant fortement avec celles des pyroxènes des péridotites (annexes).

Au contact avec les péridotites mantellaires, certains de ces gabbros laminés (TOAD12) contiennent de petites enclaves de ces péridotites aux contours diffus. Ces enclaves sont caractérisées par le développement de textures symplectitiques et coronitiques.

La texture symplectitique est constituée d'une association étroite de magnétite et d'orthopyroxène en remplacement de l'olivine. La magnétite et l'orthopyroxène peuvent se présenter soit respectivement en granules intersticielles et en grains polygonaux ayant remplacé totalement ou partiellement l'olivine soit en fins vermicules étroitement mêlés. Les compositions chimiques de l'olivine, de l'orthopyroxène et du spinelle évoluent très rapidement depuis la bordure vers le cœur des enclaves ultramafiques (figure 2.10). Les teneurs en %En et  $\text{Al}_2\text{O}_3$  pour les orthopyroxènes se répartissent linéairement entre deux pôles qui correspondent respectivement aux compositions minéralogiques des minéraux hôtes du cumulus et des péridotites (figure 2.10).

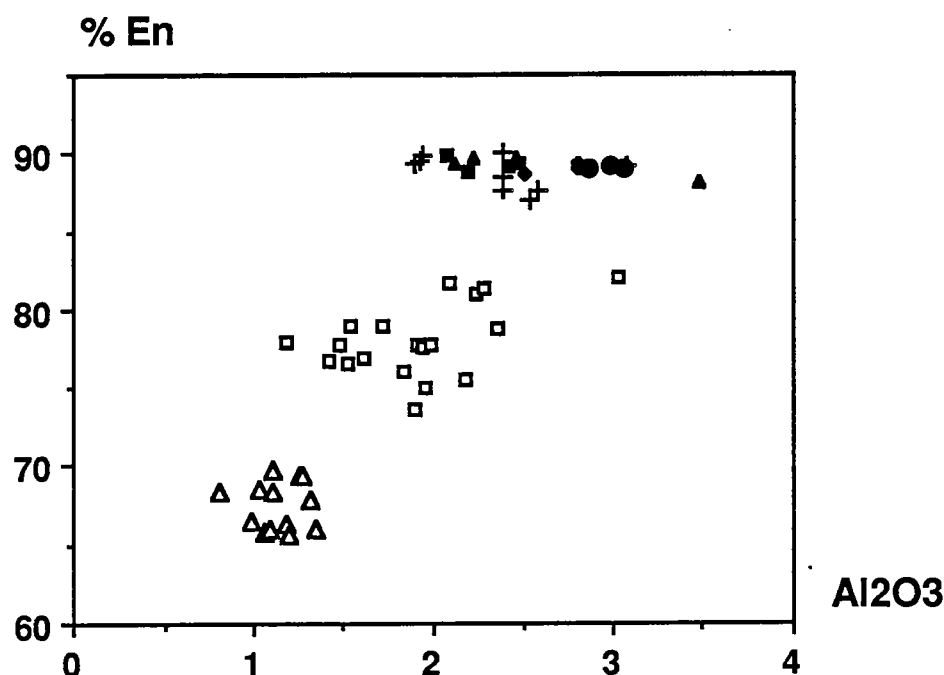


Figure 2.10 : triangle vide : cumulat gabbroïque; carré vide : xénolites de péridotites mantellaires dans les cumulats. Péridotites mantellaires : rond plein : dunites; losanges pleins : hercynites à plagioclase; triangle noir : harzburgite; symbole plus : harzburgite à plagioclase.

Le développement de la texture de type "corona" est très local et s'exprime par la présence de hornblende brune poecilitique en remplacement du plagioclase quand celui-ci est en présence de la magnétite. Cette réaction est donc postérieure et certainement liée à la transformation de l'olivine en symplectite d'orthopyroxène et magnétite.

## 2) Les gabbros pegmatoïdes.

Ces gabbros isotropes (TOAD27) montrent des différences notables avec les gabbros lités à ilménite. Ils sont plus riches en clinopyroxène et dépourvus d'orthopyroxène et d'ilménite. En outre, les larges clinopyroxènes cumulus ont cristallisé avant le plagioclase.

### 2.3.B.c Les filons dans les péridotites.

#### 1) Les veines gabbroïques (TOAD7; 9; 17; 18; 38).

Ces petits filons sont riches en clinopyroxène cumulus avec du plagioclase interstitiel épidotitisé. L'ilménite est absente et les pyroxènes sont caractérisés par des figures de pliage et des compositions chimiques identiques à ceux présents en imprégnation dans des dunites foliées (TOAD15). Parallèlement aux épontes de ces filons intrusifs dans la péridotite se développent sur quelques millimètres de fines aiguilles d'actinote.

#### 2) Les veines de microgabbros à ilménite (TOAD21).

Ce sont des veines à clinopyroxène dont les bordures sont fréquemment altérées en actinote. Le plagioclase est altéré en épidote et en albite. La composition de ces filons rappelle la nature des gabbro-norites à ilménite tapissant les parois de la chambre magmatique. Ces filons sont probablement l'expression de phénomènes d'injection magmatique depuis la chambre vers l'encaissant péridotitique.

### 3) Les veines de microgabbros riches en clinopyroxène (TOAD11).

Ces veines riches en clinopyroxène et dépourvues d'ilménite présentent des caractères pétrologiques voisins de ceux des veines gabbroïques (TOAD7; 9; 17; 18; 38). Ils sont de nature primitive comme en témoigne la présence discrète d'olivine cumulus englobée dans les clinopyroxènes poecilites du filon TOAD20. Ces filons peuvent être considérés comme les témoins de l'alimentation de la chambre magmatique par fusion des péridotites mantellaires.

#### 2.3.B.d Les filons dans les gabbros.

##### 1) Les veines de microgabbros riches en clinopyroxène (TOAD25).

Ces veines représentent la continuité du système d'alimentation magmatique déjà présent dans les péridotites mantellaires et illustré par les filons TOAD11 et TOAD20.

##### 2) Les veines de microgabbros leucocrates déformées (TOAD24; 26).

Ces petits filons sont également précoces dans l'histoire de la chambre magmatique; leurs éponges légèrement déformées témoignent de leur mise en place dans un encaissant gabbroïque encore chaud et visqueux. Le plagioclase a cristallisé en premier, le clinopyroxène et l'orthopyroxène abondants cristallisent avant les ilménites.

##### 3) Les veines de microgabbros leucocrates non déformées (TOAD28).

Ces filons plus tardifs dans la séquence magmatique se caractérisent par l'abondance d'ilménite et magnétite, la présence de magnésio-hornblende cristallisant avant le plagioclase. Ces niveaux sont marqués par la disparition de l'orthopyroxène.

##### 4) Les filons acides (TOAD29).

Ces filons sont comparables aux plagiogranites échantillonnés dans la chambre magmatique voisine de Gray Rock et sont simplement constitués de plagioclase albitisé localement séricité et de quartz.

#### 2.3.C. Géochimie.

##### 2.3.C.a Fusion partielle et phénomènes d'imprégnation magmatique dans le manteau.

La chimie des olivines et des orthopyroxènes révèle des hétérogénéités géochimiques au sein des divers types de péridotites reconnues sur le terrain. Ces variations sont similaires à celles des péridotites alpines (Beccaluva et al., 1984) et océaniques (Hamlyn et Bonatti, 1980; Dick et al., 1984; Savel'yeva, 1984; Michael et Bonatti, 1985; Shibata et Thompson, 1986) et indiquent une nature résiduelle croissante de ces roches mantellaires depuis les lherzolites jusqu'aux dunites.

L'examen de la composition chimique des spinelles et des clinopyroxènes des péridotites plagifères et non plagifères révèle l'impact géochimique des phénomènes d'imprégnation par des liquides de fusion partielle qui en percolant ont plus ou moins déstabilisé les minéraux des péridotites encaissantes.

Ainsi les spinelles des péridotites plagifères sont relativement enrichis en  $TiO_2$  par rapport à leurs analogues dépourvus de lentilles de plagioclase. Ils sont également caractérisés par une substitution Cr-Al qui correspond à un échange avec le liquide intersticiel avec apport d'Al pour former du plagioclase (figure 2.11).

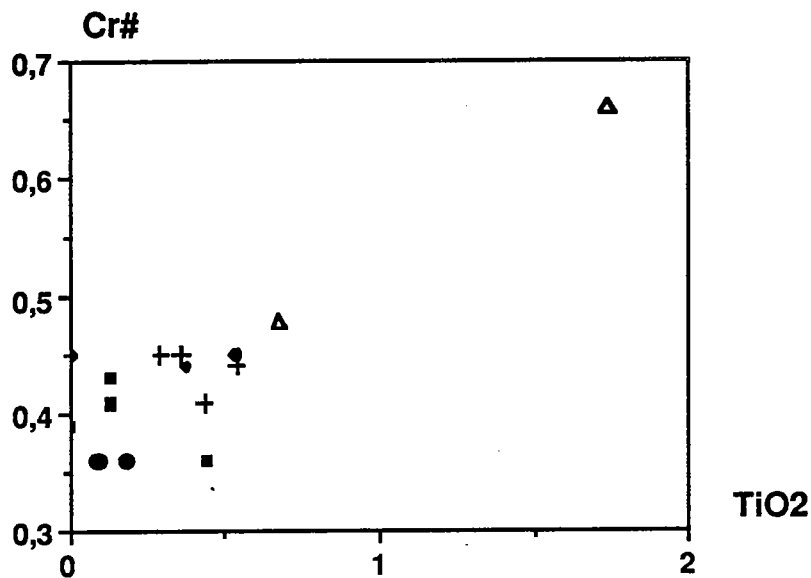
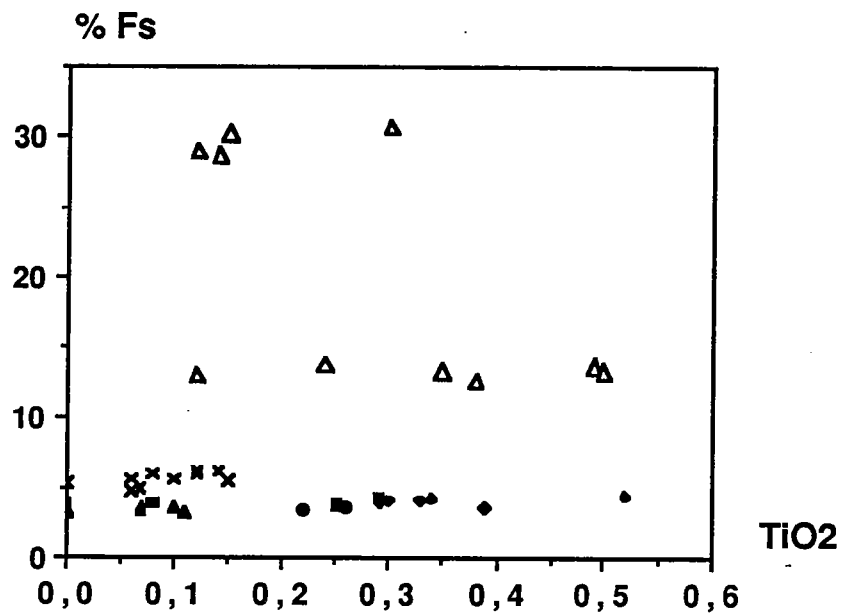


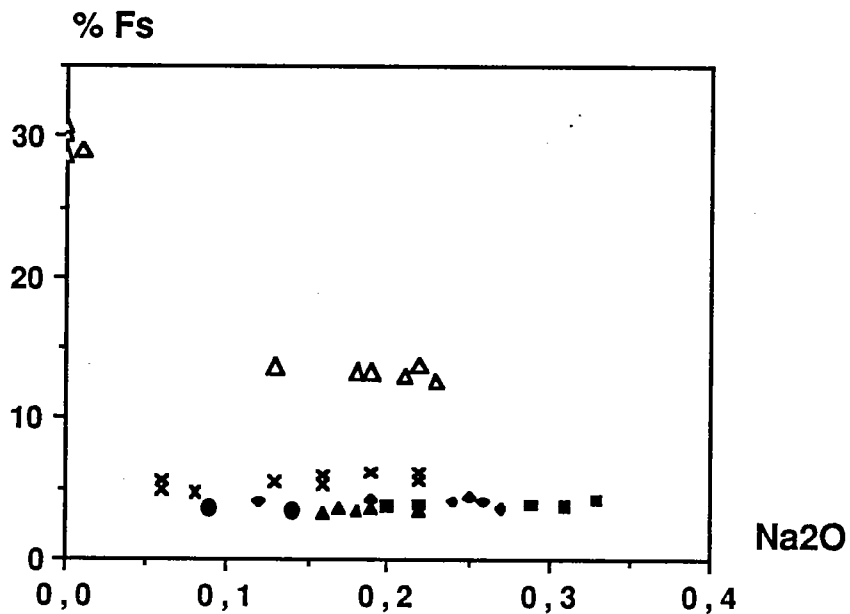
Figure 2.11 : triangle vide : cumulat gabbroïque; losange plein : lherzolite à plagioclase; carré plein : lherzolite; rond plein : dunite; plus : harzburgite à plagioclase.  $Cr\# = Cr / (Cr + Al)$ .

Les clinopyroxènes des péridotites plagifères sont enrichis en TiO<sub>2</sub> et moins nettement en Na<sub>2</sub>O par rapport aux péridotites dépourvues de plagioclase (figures 2.12 et 2.13). Les filons gabbroïques (TOAD17) qui recoupent les péridotites mantellaires sont caractérisés par des clinopyroxènes systématiquement enrichis en %Fs par rapport à leur encaissant et établissent ainsi une transition dans la lacune de composition chimique qui existe entre les péridotites mantellaires et les cumulats gabbroïques (figures 2.12 et 2.13).





Figures 2.12 et 2.13 : %Fs = % de ferrosillite. triangle vide : cumulat gabbroïque; croix : filons de gabbros recoupant les péridotites mantellaires; losange plein : lherzolite à plagioclase; carré plein : lherzolite; triangle plein : harzburgite; rond plein : dunite.



La corrélation positive (figure 2.14) entre les teneurs en  $\text{Al}_2\text{O}_3$  et  $\text{Cr}_2\text{O}_3$  des orthopyroxènes des péridotites mantellaires est tout à fait similaire à celle présente dans les cumulats et xénolites de péridotites incluses dans les cumulats. Cette corrélation peut être traduite en termes

de fractionnement "in situ" dans le manteau. En effet les phénomènes de fusion partielle conduiraient à l'observation d'une corrélation négative.

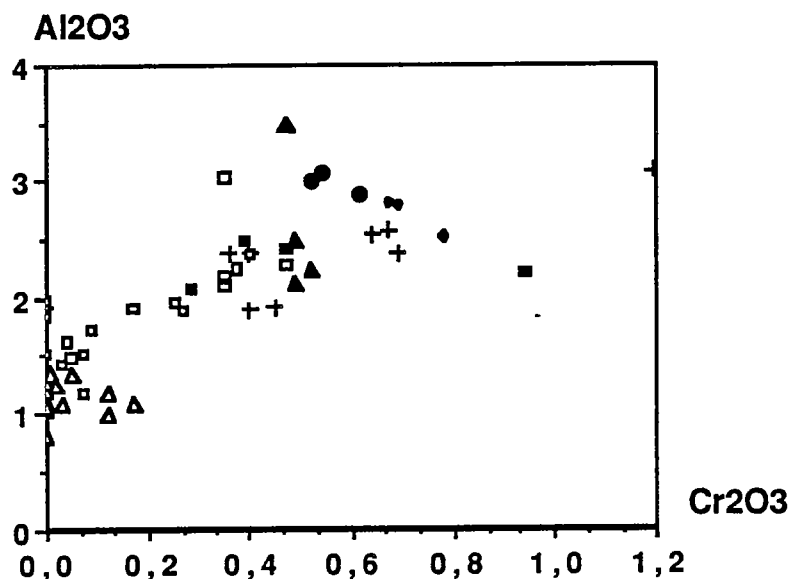


Figure 2.14 : même légende que figures précédentes.

Il s'agit donc de comprendre si l'association étroite de lherzolites à spinelle et de lherzolites à plagioclase sur le terrain est une conséquence de réactions minéralogiques solide-solide qui ont débuté lors de la remontée diapirique du manteau supérieur (Quick, 1981) ou s'il s'agit de réactions solide-fluide faisant intervenir une source externe et mobile d'éléments chimiques migrant dans le manteau supérieur lors des phénomènes de fusion partielle. Ces deux hypothèses peuvent être respectivement testées par le modèle suivant :

Soit une lherzolite source donnant une lherzolite à plagioclase (TOAD40) :

$w.Ol + x.Opx + y.Cpx + z.Sp \longrightarrow a.Ol + b.Opx + c.Cpx + d.Pl + e.Sp$  avec somme des  $w, x, y$  et  $z = 1$ ; fraction en poids de chaque minéral constituant la roche de départ et somme des  $a, b, c, d$  et  $e = 1$ ; fraction en poids de chaque minéral (connu) constituant la roche d'arrivée (TOAD40).

Pour tous les éléments chimiques  $i$  considérés (Si, Al, Fe, Mg, Ca, Na, Cr, Mn, Ti) :

Existe-il  $w, x, y$  et  $z$  qui satisfassent la relation suivante :  $w.Ol + x.Opx + y.Cpx + z.Sp =$  analyse roche totale (TOAD40)?

La relation n'est jamais vérifiée pour les péridotites de l'ophiolite de Trinity, la différence entre les compositions chimiques des deux types de péridotites n'est pas une conséquence de la variation dans le mode de la roche mais d'une réaction solide-fluide qui se produit en système ouvert. Les éléments apportés par le liquide d'imprégnation qui sont Ti, Na et Fe se retrouvent ainsi dans les minéraux (clinopyroxènes et spinelles) qui constituent les lherzolites à plagioclase.

Le piégeage de magma jusqu'à 10% en poids dans les interstices des péridotites tectonites est également illustré par les corrélations positives en roches totales entre  $Al_2O_3$ , V et Zr avec  $TiO_2$  (figures 2.15, 2.16 et 2.17) ou encore  $Na_2O$  avec  $Al_2O_3$  (figure 2.18). Compte tenu des basses teneurs pour ces roches en Zr, la figure 2.17 a juste une valeur indicative.

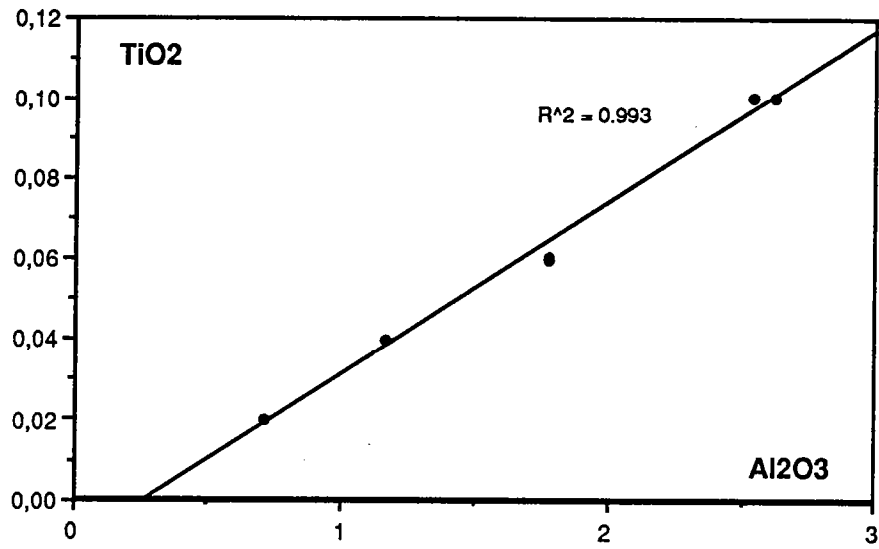


Figure 2.15.

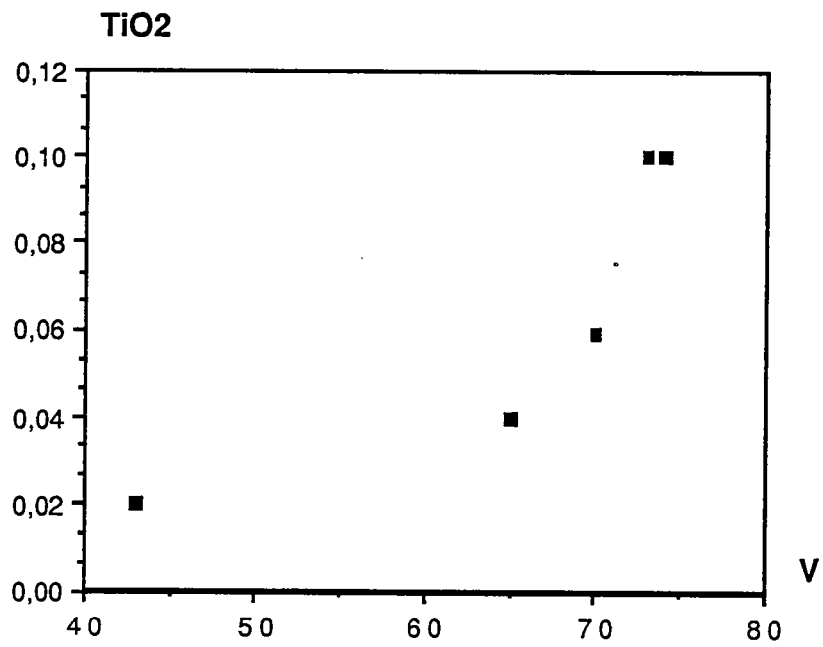


Figure 2.16.

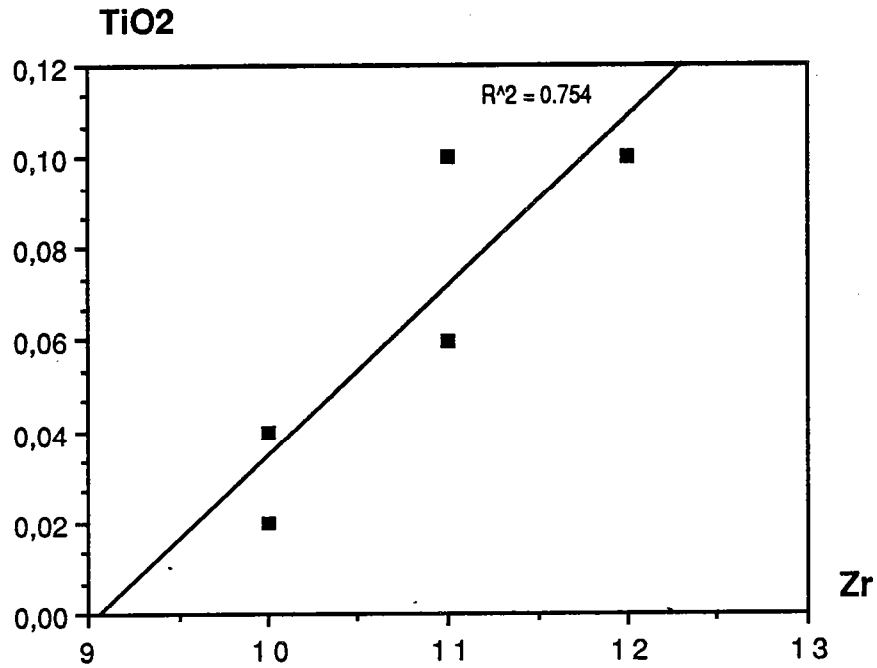


Figure 2.17.

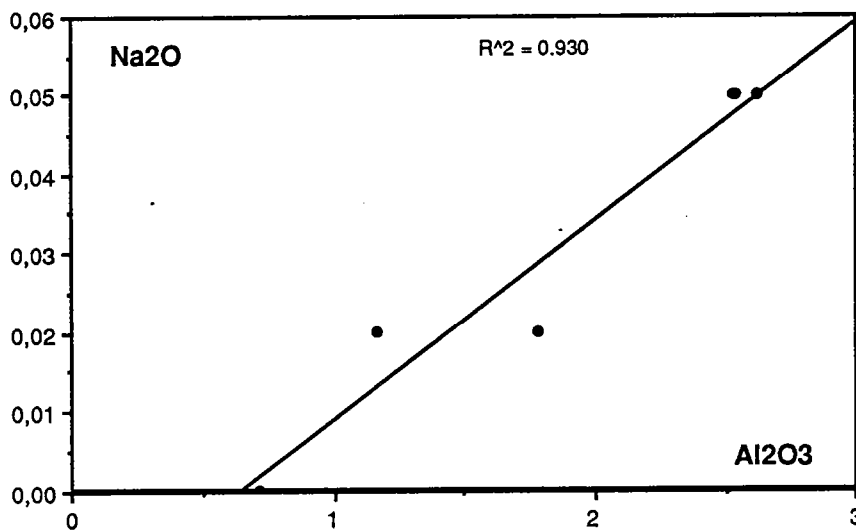


Figure 2.18.

Dans ce cas, un piégeage sélectif d'éléments chimiques au sein du manteau peut être assimilé à un phénomène de "fractionnement mantellique". L'ampleur d'un tel phénomène peut avoir des conséquences significatives sur la nature des magmas alimentant les chambres magmatiques crustales et de ceux émis à la surface.

Le transport d'éléments chimiques au sein du manteau pose donc le problème de la présence d'un liquide (magma + fluide?) et de sa nature. Les observations de terrain suggèrent la possibilité de la circulation de tels fluides pouvant être responsables du développement d'amphibole aux épontes des filons recoupant les affleurements de dunites imprégnées de clinopyroxène. La

présence de fluides a été invoquée par certains auteurs pour expliquer le développement très localisé de corps dunitiques résiduels (Malpas, 1978; Boudier et Coleman, 1981; Lago et al., 1982). Ainsi des magmas porteurs de fluides peuvent venir alimenter une chambre magmatique et être à l'origine de variations spectaculaires de granulométrie au sein des lits magmatiques ou des poches diffuses de gabbros isotropes ainsi que du développement de hornblende brune.

La présence de spinelles dans les péridotites mantellaires ou dans les xénolites de péridotites présents dans les gabbros à ilménite et magnétite peuvent être indicateurs de par leur composition chimique de la fugacité en oxygène (Maurel et Maurel; 1984; Murck et Campbell, 1986).

Les travaux expérimentaux ont mis en évidence l'interdépendance entre les teneurs en  $\text{Fe}_2\text{O}_3$  des spinelles,  $f\text{O}_2$ , température et composition en FeO total du bain silicaté ainsi qu'une loi de distribution du fer ferrique entre spinelle chromifère et bain silicaté basique en équilibre.

$$\frac{(\text{Fe}_2\text{O}_3)_{\text{spinel}} = (0.0045 \cdot 10^{4813/T} \cdot (\text{FeO})_{\text{total}}(\text{liquid}))}{1 + 562 \cdot (f\text{O}_2 - 0.2185) \cdot 10^{-5502/T}}$$

Dans les roches de Toad Lake, les teneurs en  $\text{Fe}_2\text{O}_3$  des spinelles ont été estimées à partir des analyses ponctuelles à la microsonde à partir de la formule stoechiométrique du minéral. Les résultats donnent pour les lherzolites à spinelle un  $\text{Log } f\text{O}_2$  de l'ordre de -9,5 (pour des températures comprises entre 1200°C et 1300°C) en accord avec les fugacités estimées dans les roches du manteau supérieur. Le bain silicaté en équilibre devait avoir des teneurs en  $\text{Fe}_2\text{O}_3 = 0,58\%$  et  $\text{FeO}_{\text{total}} = 11,6\%$  ( $\text{Fe}^{3+}/\text{Fe}_t = 0,048$ ). Dans les lherzolites plagifères,  $f\text{O}_2$  est légèrement supérieure ( $\text{Log } f\text{O}_2 = -8$ ) et suggère la présence d'un fluide oxydant.

Le magma en équilibre avec les spinelles de ces péridotites contiendrait 1% de  $\text{Fe}_2\text{O}_3$  et 10,6% de FeO total ( $\text{Fe}^{3+}/\text{Fe}_t = 0,08-0,09$ ). Les valeurs calculées en FeO total du magma imprégnant les péridotites sont voisines des teneurs en FeO total calculées à partir d'un magma en équilibre total avec des olivines (FO 89-91; FeO total = 10%; Roeder et Emslie; 1970) de péridotites mantellaires. Ces résultats suggèrent que les magmas imprégnant les péridotites sont en équilibre avec ces roches et sont donc susceptibles d'échanges chimiques significatifs à haute température.

Les spinelles des enclaves ultrabasiques dans les gabbro-norites lités révèlent des fugacités en oxygène élevées ( $\text{Log } f\text{O}_2 = -5$ ) et un magma à FeO total = 8% et  $\text{Fe}_2\text{O}_3 = 4\%$  ( $\text{Fe}^{3+}/\text{Fe}_t = 0,5$ ) pouvant correspondre à la composition chimique du gabbro encaissant riche en ilménite. Le développement de textures symplectitiques orthopyroxène-magnétite peut provenir de la déstabilisation progressive de l'olivine due à la présence d'un magma oxydant riche en Fe.

### 2.3.C.b Comparaison avec les péridotites modernes : rôle du site géotectonique.

Les péridotites mantellaires de Trinity présentent des phénomènes d'imprégnation par des magmas qui s'expriment par la présence de ségrégations de lentilles intersticielles de plagioclase, de cristaux xénomorphes de clinopyroxène et d'olivine. Il est peut être utile d'examiner la composition chimique des minéraux des péridotites plagifères et non plagifères qui proviennent aussi bien des sites ophiolitiques que des planchers océaniques modernes. Ainsi un début de compilation bibliographique de la composition des spinelles et des clinopyroxènes a été effectué dans le but de comparer des analyses provenant de l'océan atlantique, pacifique et indien avec les analyses des péridotites de Trinity.

Les spinelles des péridotites mantellaires plagifères de Trinity sont nettement enrichis en  $\text{TiO}_2$  (0,40%) par rapport à celles des océans modernes (0,05 à 0,15%; figure 2.19).

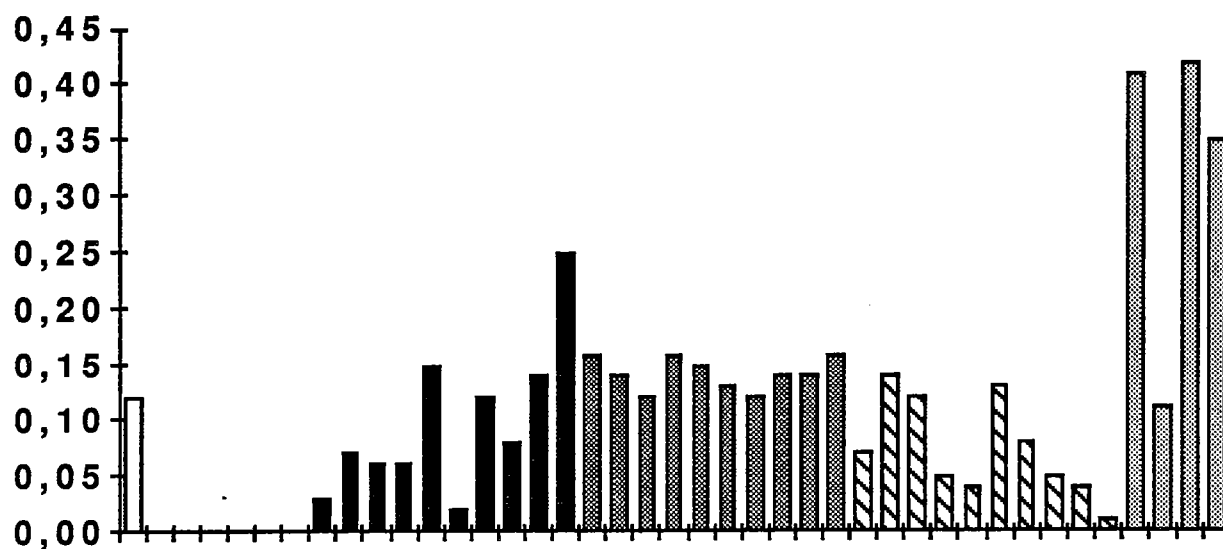
TiO<sub>2</sub>

Figure 2.19. : colonnes blanches : océan Atlantique (Hékinian, 1982); colonnes noires : océans Pacifique et Indien (Savel'Yeva, 1984); colonnes grisé foncé : site 395, Atlantique (Sinton, 1979); colonnes zébrées : site 395 Atlantique (Arai et Fujii, 1979); colonnes grisé clair : ophiolite de Trinity.

Ils sont également plus riches en Fe<sub>2</sub>O<sub>3</sub> (jusqu'à 25%) comme cela peut être le cas pour certains échantillons des océans Pacifique et Indien (figure 2.20).

## FeO\*

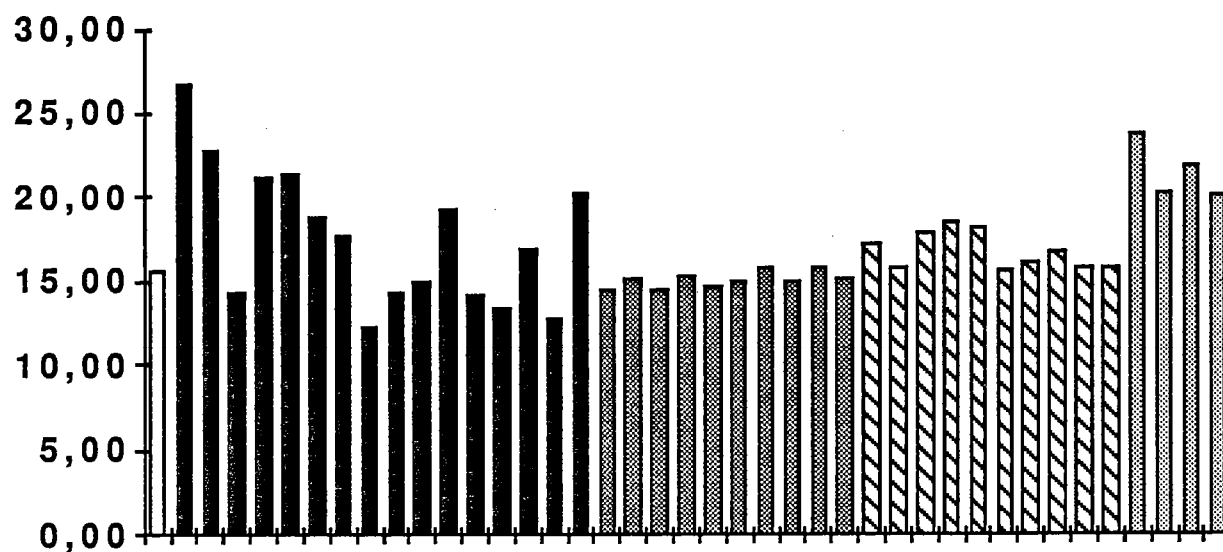


Figure 2.20.

Les clinopyroxènes sont également marqués par un enrichissement en  $\text{TiO}_2$  également reconnaissable dans certains échantillons des océans Pacifique et Indien (figure 2.21). Ceux-ci sont marqués par un enrichissement en  $\text{Na}_2\text{O}$  (jusqu'à 0,6%) qui est modéré dans les échantillons de Trinity (0,3%; figure 2.22). Il faut également remarquer les basses teneurs en  $\text{Cr}_2\text{O}_3$  ( $\leq 1\%$ ) et  $\text{Al}_2\text{O}_3$  (3%) des clinopyroxènes de Trinity (figures 2.23 et 2.24).

### $\text{TiO}_2$

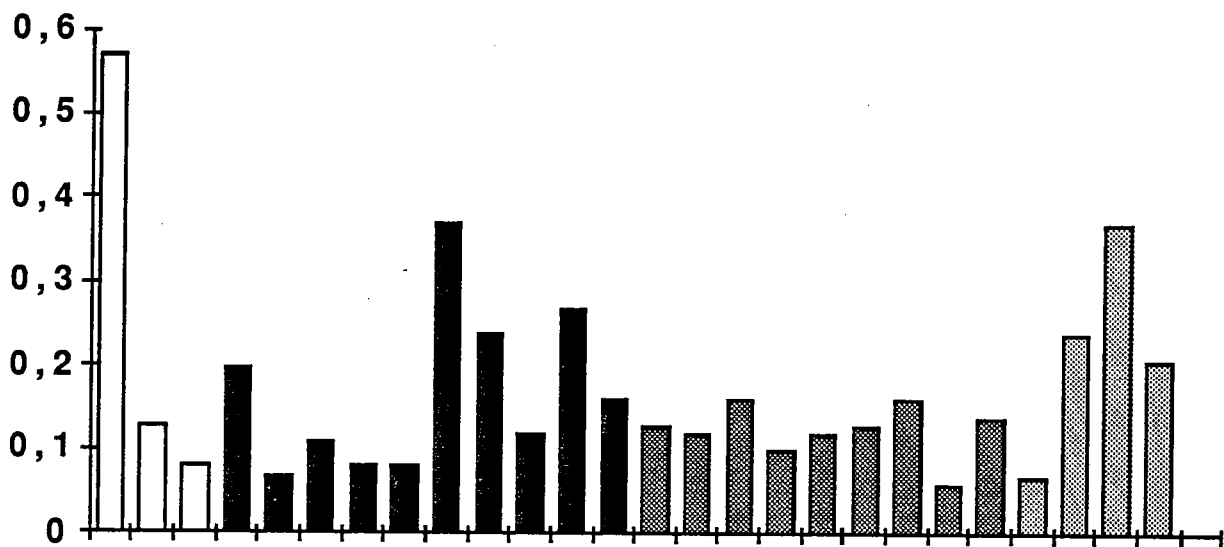


Figure 2.21.

### $\text{Na}_2\text{O}$

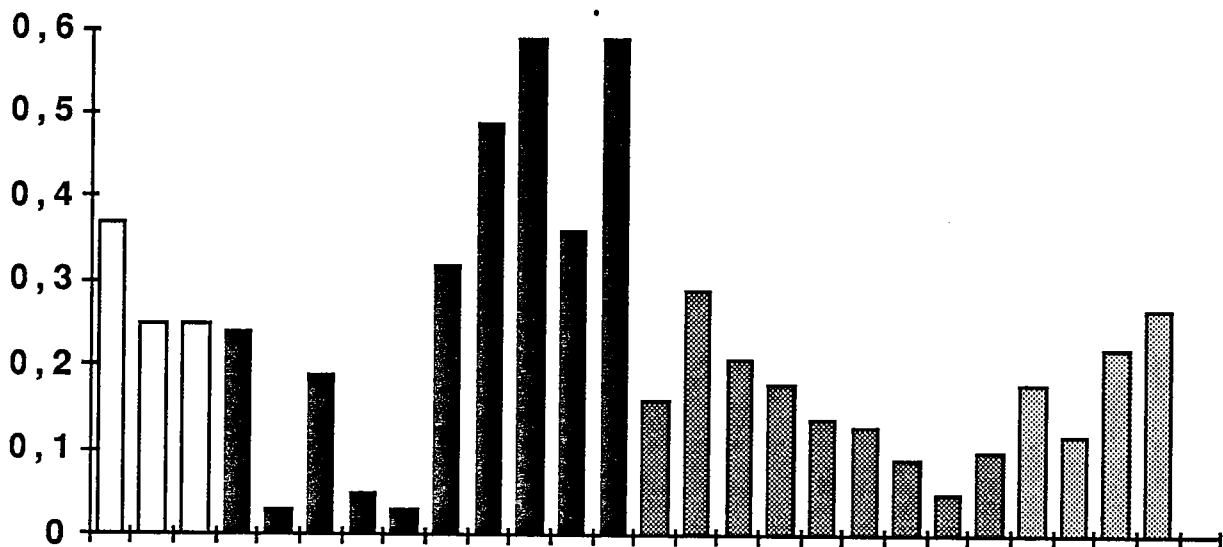


Figure 2.22.

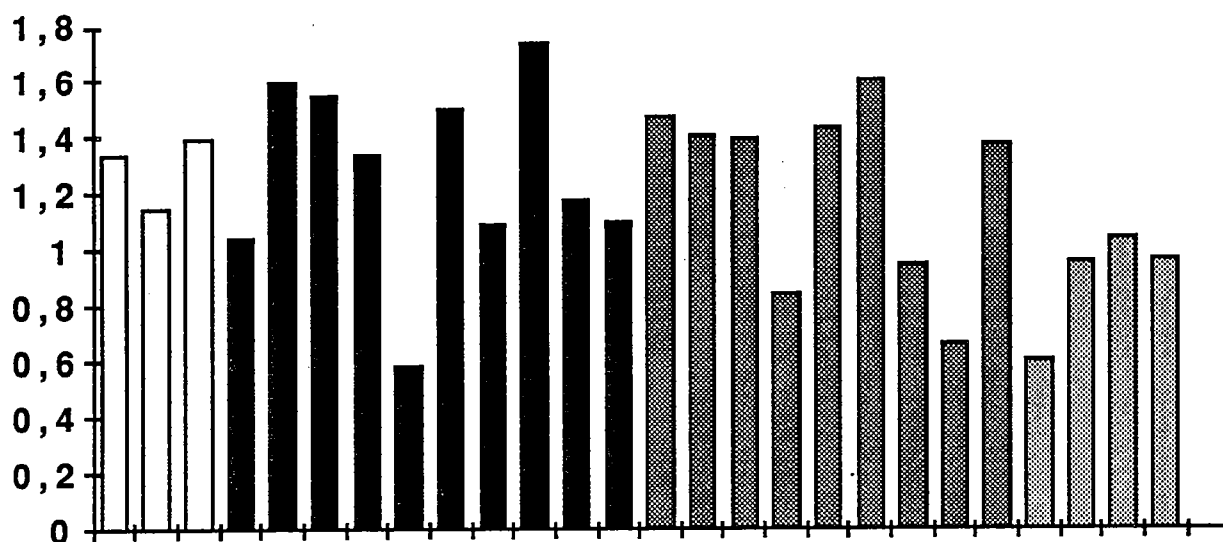
**Cr<sub>2</sub>O<sub>3</sub>**

Figure 2.23.

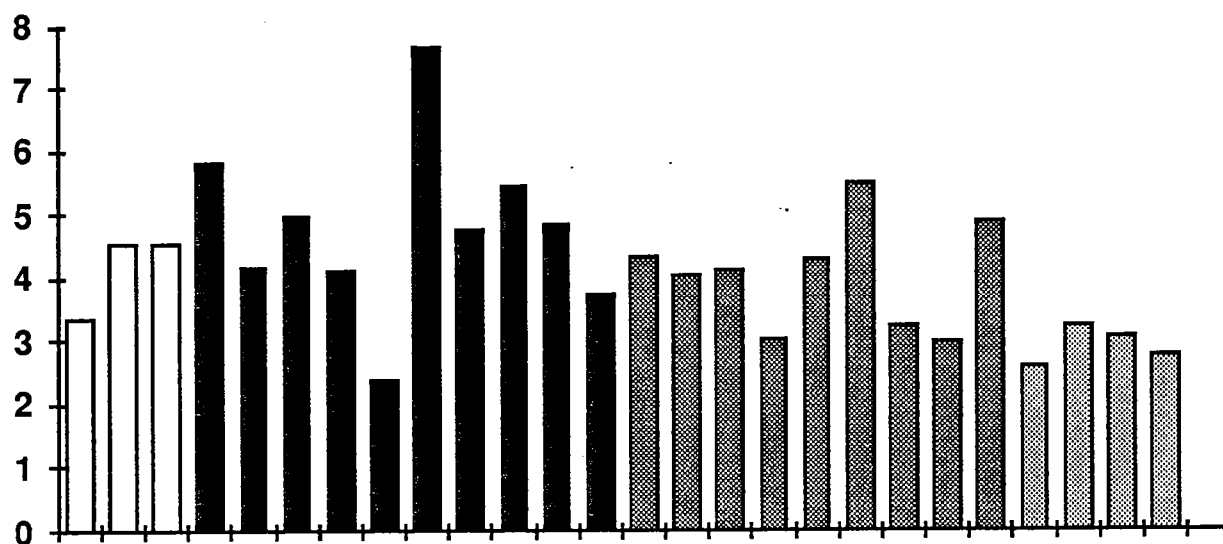
**Al<sub>2</sub>O<sub>3</sub>**

Figure 2.24.

Le premier résultat de cette étude suggère que les phénomènes de percolation et de réaction des magmas au sein du manteau supérieur peuvent être favorisés dans les domaines de zones océaniques à expansion lente dans lesquelles l'ascension des magmas est difficile. Dans ce cas des températures élevées (1000 à 1300°C) et des temps de résidence suffisamment longs peuvent permettre des transferts chimiques significatifs et susceptibles de modifier la composition du magma qui alimente les chambres crustales.



### 2.3.C.c Les filons : marqueurs de l'évolution chimique du magma dans la chambre.

#### 1) Evolution des éléments majeurs et traces.

Les filons peuvent être considérés comme échantillonnant une chambre magmatique évoluant par cristallisation fractionnée. Toutefois, il est bien connu que les magmas évoluant dans des caisses filoniennes sont susceptibles de subir des phénomènes de ségrégation d'origine mécanique (effet Bagnold; Bhattacharji et Smith, 1964; Gagny, 1978; Hammond, 1986). Dans ce cas, afin d'atténuer cet effet, les filons sélectionnés pour cette étude sont les moins porphyriques et représentatifs de l'ensemble d'une caisse filonienne (bordure + coeur). Quatre filons ont été sélectionnés (tableau 2.2) parmi ceux qui recoupent les péridotites mantellaires et alimentant la chambre magmatique jusqu'à ceux présents au toit de la chambre magmatique.

|                                 | Parent<br>Toad11 | Fils1<br>Toad24 | Fils2<br>Toad28 | Fils3<br>Toad29 | M1<br>Pl | M2<br>Cpx | M3<br>Opx | M4<br>Ilm | M5<br>Mag | M6<br>Hbl |
|---------------------------------|------------------|-----------------|-----------------|-----------------|----------|-----------|-----------|-----------|-----------|-----------|
| SiO <sub>2</sub>                | 46.01            | 48.47           | 53.45           | 77.31           | 45.29    | 52.23     | 54.47     | 0.00      | 0.00      | 51.17     |
| TiO <sub>2</sub>                | 0.24             | 0.23            | 1.19            | 0.18            | 0.00     | 0.36      | 0.18      | 51.10     | 3.22      | 0.94      |
| Al <sub>2</sub> O <sub>3</sub>  | 11.75            | 12.89           | 14.73           | 12.56           | 34.75    | 1.78      | 1.30      | 0.00      | 0.51      | 6.29      |
| Fe <sub>2</sub> O <sub>3t</sub> | 8.27             | 7.09            | 12.41           | 0.21            | 0.34     | 8.31      | 18.87     | 49.35     | 92.81     | 9.89      |
| MnO                             | 15.47            | 15.16           | 3.77            | 0.09            | 0.00     | 14.47     | 24.75     | 0.03      | 0.34      | 17.48     |
| MgO                             | 0.18             | 0.13            | 0.21            | 0.00            | 0.00     | 0.21      | 0.35      | 0.90      | 0.16      | 0.14      |
| CaO                             | 13.96            | 11.57           | 8.05            | 4.19            | 19.46    | 22.34     | 1.08      | 0.00      | 0.00      | 11.53     |
| Na <sub>2</sub> O               | 0.81             | 0.15            | 3.04            | 3.59            | 0.76     | 0.20      | 0.00      | 0.00      | 0.00      | 0.76      |
| K <sub>2</sub> O                | 0.03             | 0.00            | 0.75            | 0.24            | 0.05     | 0.00      | 0.00      | 0.00      | 0.00      | 0.02      |
| Total                           | 99.67            | 99.50           | 99.35           | 99.00           | 100.65   | 99.90     | 101.00    | 101.38    | 97.04     | 98.22     |

Tableau 2.2.

L'évolution en éléments majeurs et traces de ces liquides magmatiques permet d'estimer la composition du magma qui entre dans la chambre ainsi que l'ordre et l'amplitude des minéraux fractionnés au sein de cette même chambre. En effet, la solution du calcul implique qu'entre deux étapes considérées, la composition chimique des minéraux reste constante ce qui est faux par définition, ce type de calcul ne propose donc qu'une estimation. Cette évolution géochimique du magma va être discutée en considérant la chambre magmatique divisée en trois parties comprises respectivement entre les générations de filons présentées ci-dessus. Les quatre filons sélectionnés sont censés représenter l'évolution de la chambre magmatique. Ils sont les mieux préservés du métamorphisme, les moins porphyriques et ont été sélectionnés parmi les quatre grandes populations de filons présentes dans cette chambre magmatique.

Le premier filon (TOAD11) est caractérisé par une composition de tholéiite à olivine, des teneurs très basses en éléments incompatibles comme Zr, Y et Nb et des teneurs en Cr et Ni caractéristiques de magmas primaires peu fractionnés. L'ensemble de l'évolution dans la chambre magmatique est marquée (figure 2.25) par une diminution régulière des teneurs en CaO couplée à une augmentation des teneurs en SiO<sub>2</sub> et Al<sub>2</sub>O<sub>3</sub> (figures 2.26 et 2.27).

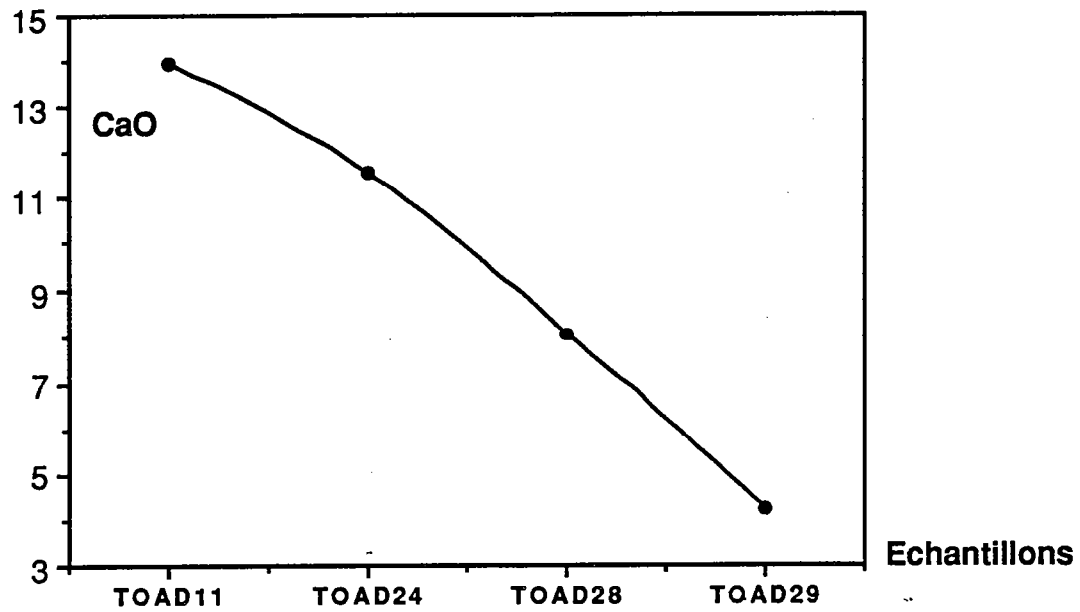


Figure 2.25.

La première partie de l'évolution de la chambre est caractérisée par une faible diminution des teneurs en  $\text{MgO}$ ,  $\text{Fe}_2\text{O}_3$  et  $\text{Na}_2\text{O}$  et une augmentation des teneurs en  $\text{SiO}_2$  et  $\text{Al}_2\text{O}_3$  (figures 2.28 et 2.29).

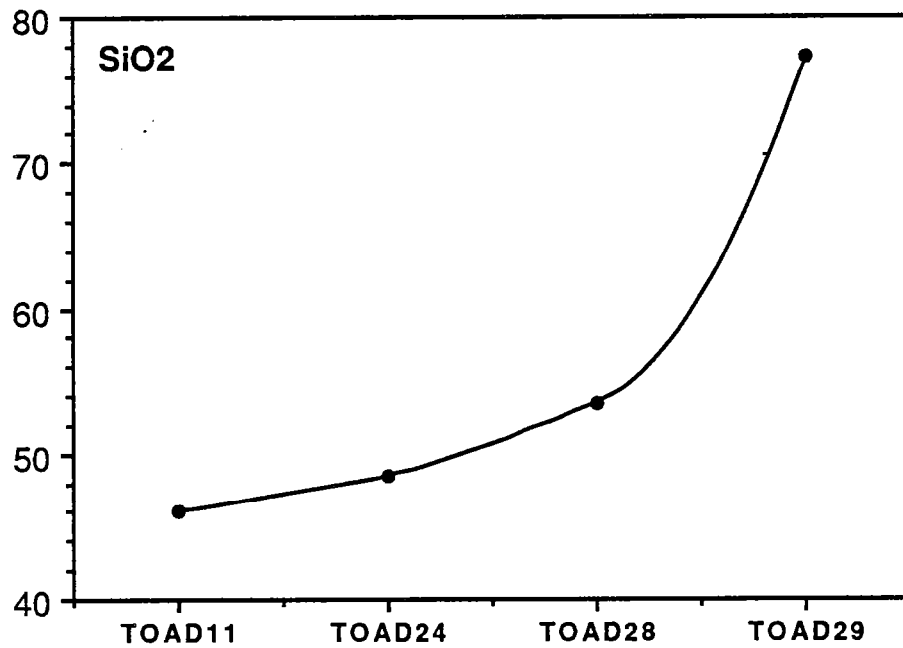


Figure 2.26.

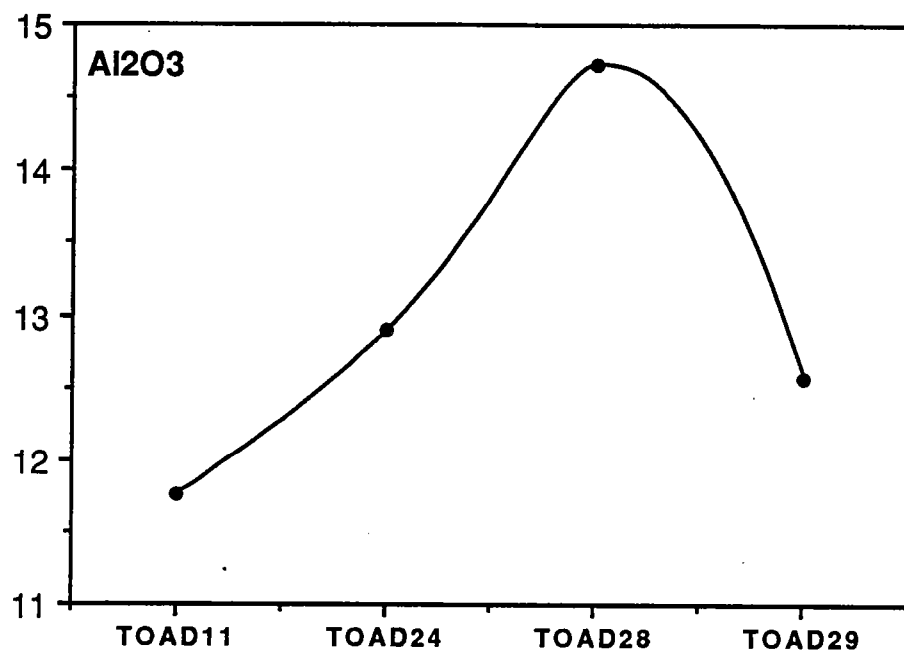


Figure 2.27.

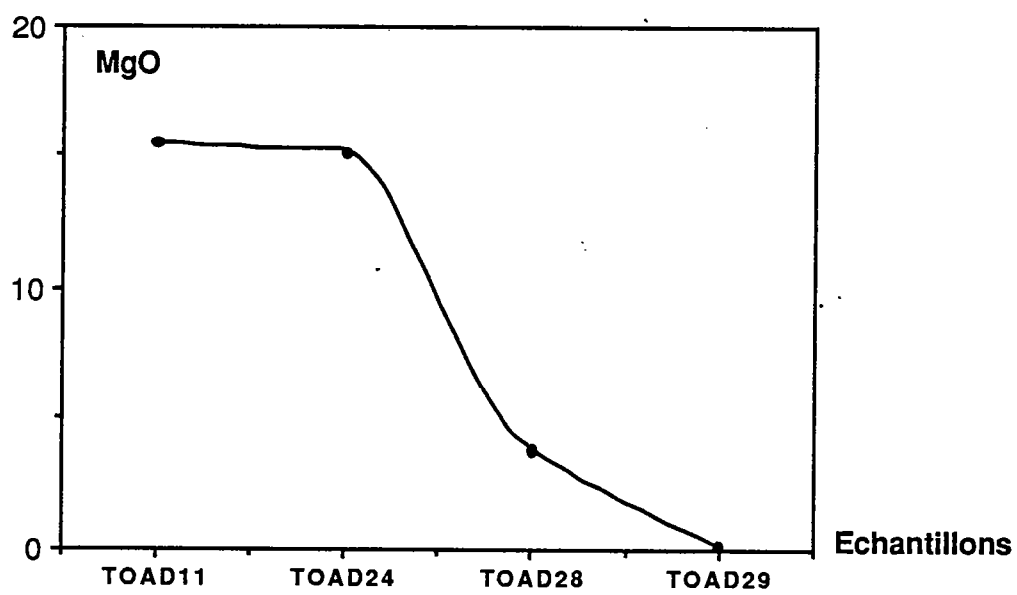


Figure 2.28.

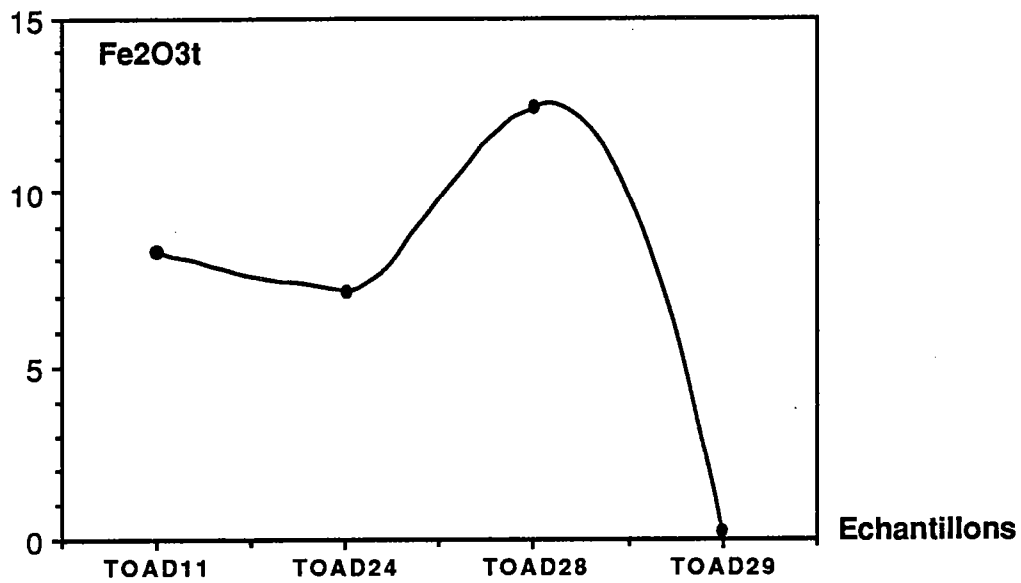


Figure 2.29.

La deuxième partie de la chambre est caractérisée par une forte diminution des teneurs en  $\text{MgO}$ , conséquence de la cristallisation de l'orthopyroxène qu'on retrouve abondamment dans les cumulats. La soustraction de plagioclase, de clinopyroxène et d'orthopyroxène du magma conduit ce dernier à s'enrichir progressivement en  $\text{SiO}_2$ ,  $\text{Na}_2\text{O}$ ,  $\text{FeO}$  et  $\text{TiO}_2$  (figures 2.30 et 2.31).

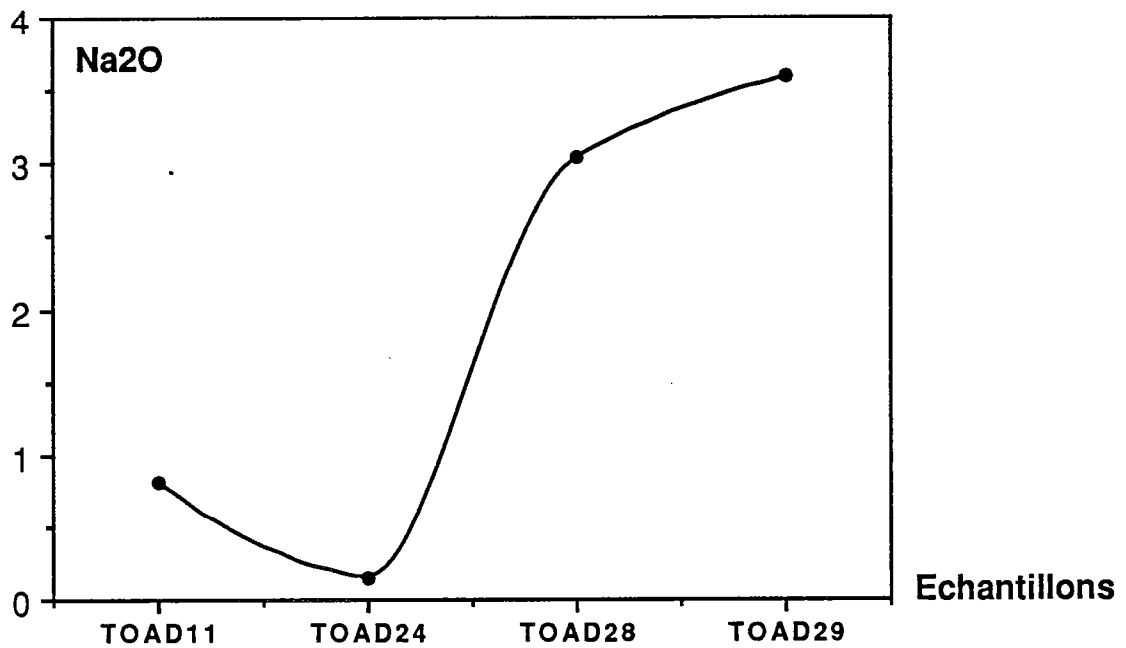


Figure 2.30.

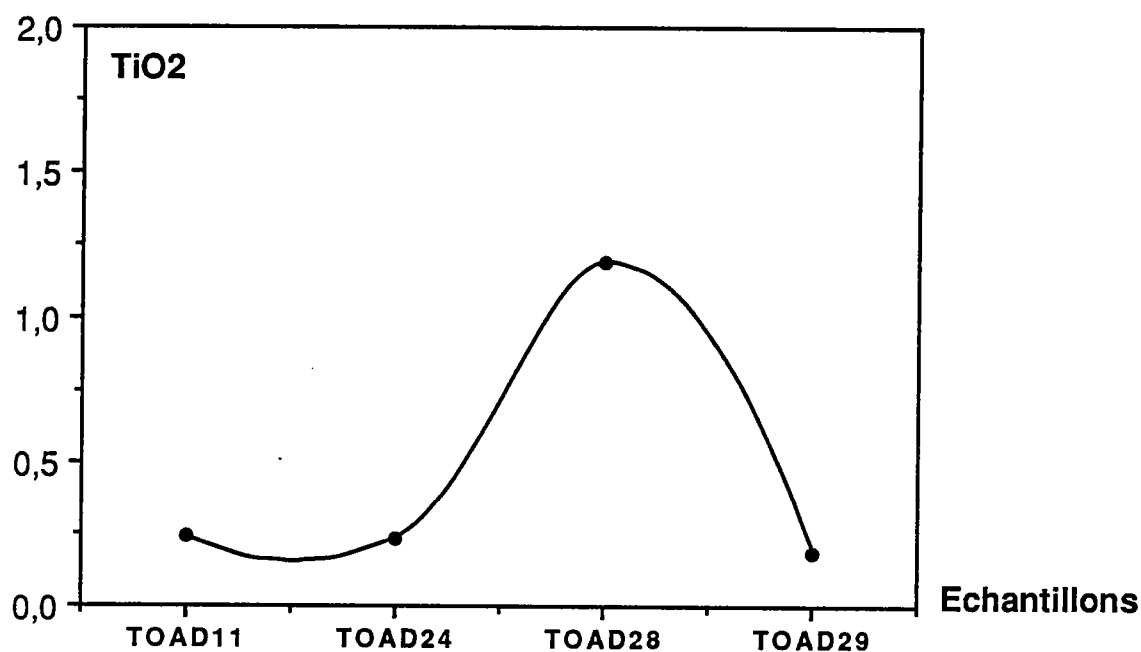


Figure 2.31.

Une telle évolution conduit le magma résiduel à cristalliser en abondance de l'ilménite et de la magnétite (présents dans les cumulats de la partie II de la chambre magmatique) puis de la hornblende, du plagioclase sodique et du quartz dans la partie III. La cristallisation de la hornblende finit d'appauvrir totalement le magma en MgO et FeO pour finalement exprimer des plagiogranites constitués exclusivement de plagioclase et de quartz. Ainsi, il est possible de reconstituer l'ordre de cristallisation des minéraux : plagioclase - clinopyroxène - orthopyroxène - ilménite et magnétite - hornblende et quartz. La course de cristallisation du magma est illustrée dans la figure 2.32 dans laquelle sont reportées en fonction de MgO et CaO les compositions des filons de la chambre de Toad lake ainsi que les compositions moyennes des minéraux soustraits du magma.

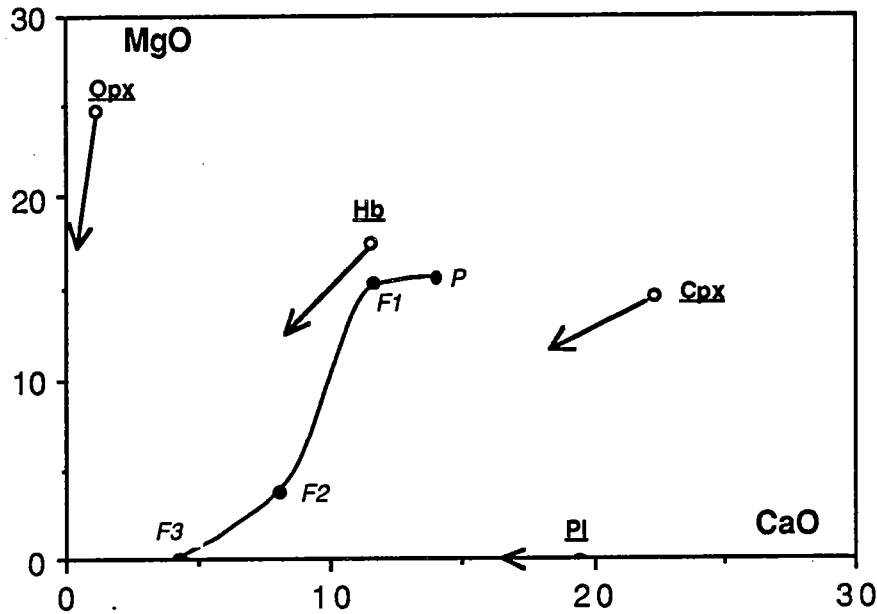


Figure 2.32.

Le problème de la quantification des processus de cristallisation dans une chambre magmatique peut maintenant être discuté.

## 2) Discussion des modèles de cristallisation des magmas.

Une première approche peut être effectuée uniquement à l'aide des compositions en éléments majeurs des filons et de chaque minéral intervenant dans le cursus de cristallisation. Il s'agit de chercher la combinaison linéaire (solution unique) de minéraux (pondérés par leurs poids respectifs et avec la somme des fractions de chaque minéral = 1) permettant de produire un magma fils à partir d'un magma parent selon le modèle suivant (Bryan et al., 1968) :

Le calcul d'approximation par la méthode des moindres carrés à l'intérêt de donner une solution unique satisfaisant l'ensemble des données :

$$XB = Y$$

$$X = \begin{bmatrix} x_{11} & x_{12} & x_{13} & \dots & x_{1k} \\ x_{21} & x_{22} & x_{23} & \dots & x_{2k} \\ x_{31} & x_{32} & x_{33} & \dots & x_{3k} \\ \vdots & \vdots & \vdots & \ddots & \vdots \\ x_{n1} & x_{n2} & x_{n3} & \dots & x_{nk} \end{bmatrix}$$

$$B' = [b_1, b_2, b_3 \dots b_k]$$

et

$$Y' = [y_1, y_2, y_3 \dots y_n]$$

B' et Y' sont respectivement les transposés des vecteurs colonnes B et Y.

$$X'XB = X'Y$$

$$\text{solution unique : } \hat{B} = [X'X]^{-1}X'Y$$

$$\text{somme des carrés des résidus : } S = \sum_{i=1}^n (y_i - \hat{y}_i)$$

Les données sont rassemblées dans le tableau 2.2 et les résultats des calculs dans les tableaux 2.3, 2.4 et 2.5. Les calculs ont été effectués 1) entre les générations de filons de type TOAD11 considérés comme représentatifs du magma parent P et la seconde génération de filons de type TOAD24 (magma fils F1), 2) entre les générations de filons de type TOAD28 (magma fils F2) et TOAD29 (magma fils F3), ce dernier étant considéré comme le magma le plus différencié et 3) un bilan entre le magma parent P et la troisième génération F3 (afin de vérifier la validité de la somme des solutions étape par étape).

a) magma P donne F1 (tableau 2.3) : l'évolution d'un tel liquide rejette la participation précoce d'un minéral sursaturé comme l'orthopyroxène, par contre le modèle nécessite la participation d'environ 14% d'olivine (par rapport à F) ce qui n'est pas incompatible avec la présence de ce minéral dans les filons du type TOAD11 en phase cumulus. Le clinopyroxène (27%) et le plagioclase (18%) sont les minéraux les plus abondants à être fractionnés lors de cette première étape.

| Parent : P                       |        | Fils : F1 |
|----------------------------------|--------|-----------|
| liquide "crystal sorting" (100%) |        |           |
| P                                | 100.00 |           |
| M0 (olivine)                     | -13.90 | 23.30     |
| M1 (plagioclase)                 | -18.00 | 30.06     |
| M2 (clinopyroxène)               | -26.90 | 44.92     |
| M4 (ilménite)                    | -1.00  | 1.72      |
| F1                               | 40.10  |           |

Somme des Carrés des Résidus=3.061

Tableau 2.3.

b) magma F2 donne F3 (tableau 2.4) : l'évolution du magma dans les derniers stades est particulièrement caractérisée par l'abondance du fractionnement de la magnétite et de l'ilménite (11%) ce qui fait l'une des originalités de la chambre magmatique de Toad Lake par rapport à celles de Castle Lake et de Gray Rock. Un fractionnement de 21% de hornblende est ainsi nécessaire pour expliquer la genèse des magmas acides représentés par les plagiogranites. Ce processus a été déjà proposé pour expliquer la présence de plagiogranites au toit de la chambre magmatique de Gray Rock par un fractionnement de 13% de hornblende utilisant le comportement des lanthanides dans les magmas (Lecuyer et al., 1989b).

| Parent : F2      |        | Fils : F3                |
|------------------|--------|--------------------------|
| liquide          |        | "crystal sorting" (100%) |
| P                | 100.00 |                          |
| M1 (plagioclase) | -23.70 | 42.00                    |
| M4 (ilménite)    | -0.13  | 2.22                     |
| M5 (magnétite)   | -10.90 | 19.30                    |
| M6 (hornblende)  | -20.60 | 36.48                    |
| F3               | 43.60  |                          |

Somme des Carrés des Résidus=1.872

Tableau 2.4.

c) magma P donne F3 (tableau 2.5) : ce calcul surestime la participation de l'orthopyroxène et du clinopyroxène due à l'obligation de retirer la hornblende du calcul (dans ce cas la matrice d'inversion A devient carrée, le système n'est plus surdéterminé). Le calcul confirme que les magmas acides de type F3 sont les termes extrêmes de la différenciation magmatique (≈0% de liquide résiduel!) laissant un cumulat de composition moyenne pauvre en olivine (11%), riche en plagioclase (34%) avec 22% d'orthopyroxène soustrait dans la partie II de la chambre magmatique.

Toutefois, un tel calcul, même s'il permet un essai de quantification des processus de

cristallisation au sein d'une chambre magmatique, est soumis aux perturbations plus ou moins aléatoires du métamorphisme (ici beaucoup moins intense que dans la chambre de Gray Rock) et ne donne pas d'indications sur la nature des processus de cristallisation magmatique.

Parent : P      Fils : F3

liquide "crystal sorting" (100%)

|                    |        |              |
|--------------------|--------|--------------|
| P                  |        | 100.00       |
| M0 (olivine)       |        | -11.30 10.77 |
| M1 (plagioclase)   | -35.50 | 33.85        |
| M2 (clinopyroxène) |        | -35.00 33.55 |
| M3 (orthopyroxène) |        | -23.60 22.46 |
| M4 (ilménite)      |        | -0.20 0.19   |
| M5 (magnétite)     | 0.07   | -0.63        |
| F3                 |        | -0.05        |

Somme des Carrés des Résidus=19.543

Tableau 2.5.

L'utilisation des éléments traces compatibles et incompatibles permet également d'approcher la quantification des processus de cristallisation magmatique. Ils permettent pour les moins mobiles (Cr, Ni, Zr et Y) de se soustraire des effets secondaires du métamorphisme. Par contre, ce type d'approche fait intervenir les coefficients de partage minéral/liquide connus des travaux expérimentaux qui dépendent de paramètres thermodynamiques comme la température ou les fugacités de fluides qui sont encore mal connues dans les chambres magmatiques, l'effet de la pression pouvant être négligé au sein de la croûte océanique.

Deux modèles classiques sont généralement proposés :

- le **modèle de cristallisation à l'équilibre** où une fraction donnée de solide se forme globalement à l'équilibre au contact du liquide magmatique (1).

$$(1) \quad C_{if} = \frac{F(C_{ii}, D_i + F(1 - D_i))}{1}$$

avec :  $C_{if}$  = concentration de l'élément i considéré dans le liquide final.  
 $C_{ii}$  = concentration de l'élément i considéré dans le liquide initial.  
 $F$  = fraction de liquide résiduel.  
 $D_i$  = coefficient de partage global minéral/liquide.  
 $D_i = \sum X.K$        $X$  = fraction en poids de chaque minéral.  
 $K$  = coefficient de partage minéral/liquide.

Ce modèle peut être appliqué dans le cas d'une chambre magmatique fonctionnant en système ouvert; les textures des cumulats (solides formés) sont généralement de type adcumulat ou hétéradcumulat avec de gros cristaux pouvant être pluricentimétriques. Ce modèle ne semble pas convenir au cas de la chambre magmatique de Toad Lake. En effet, le faible nombre d'injections de magma et le volume restreint de cette chambre (1Km de diamètre) ont favorisé un refroidissement rapide du réservoir magmatique. L'application de ce modèle dans le but de faire dériver le magma fils acide F3 du magma parent P pour Cr conduit à un non-sens (taux de cristallisation  $\gg 1$ ). En effet, la forte diminution des éléments de transition (depuis P jusqu'à F3) comme le Cr et le Ni (coefficients de partage  $> 1$  pour les pyroxènes et l'olivine) dans un volume de magma aussi limité ne semble pas compatible avec ce type de processus de cristallisation magmatique.

- en revanche, le modèle de cristallisation fractionnée qui est l'une des applications de la loi de Rayleigh (2) semble mieux convenir à ce cas particulier.

$$(2) \quad C_{if} = C_{ii} \cdot F^{(D_i - 1)}$$

Le calcul (indépendant de la composition du magma en éléments majeurs) donne une estimation du taux de cristallisation fractionnée qui est de 90% si l'on considère le Ni et le Zr pour



l'évolution du magma depuis ses termes les plus basiques (tholéiite à olivine TOAD 11) aux plus acides (plagiogranite TOAD 29).

## 2.4. La chambre magmatique de CASTLE LAKE.

### 2.4.A. Géologie.

#### 2.4.A.a Les péridotites déformées.

Elles affleurent sur la crête entre Castle Lake et Mont Bradley juste sous l'unité bréchique basale (figure 2.8). Ce sont des dunites, des harzburgites et des werhlites localement litées avec une foliation de spinelle EW à pendage Nord modéré à fort (figure 2.33). Il est à noter l'absence de lherzolites et lherzolites à feldspath.

Le contact avec l'unité bréchique basale est progressif mais rapide : les péridotites deviennent riches en filons gabbroïques et laissent place à des brèches de péridotites à éléments de gabbros.

#### 2.4.A.b L'unité bréchique de base.

Elle est bien développée à Castle Lake (>100m de puissance) avec un litage discontinu de l'encaissant gabbroïque : NW-SE à pendage faible à modéré NE ou SW. Cette unité se retrouve le long de la coupe en direction de Mont Bradley et définit donc un niveau sensiblement horizontal.

Cette unité de base est constituée de gabbros riches en pyroxènes - voire des pyroxénites - à enclaves ultrabasiques. Les enclaves sont plus ou moins métamorphisées. Leur composition d'origine varie depuis des dunites et harzburgites à des werhlites et pyroxénites. Les gabbros riches en pyroxènes sont recoupés par des veines, sills et passées diffuses de gabbros leucocrates et pegmatoïdes. Les petits sills soulignent le litage.

La coupe effectuée le long du "Castle Lake trail" permet d'interpréter cette unité bréchique basale (figure 2.8) comme une ancienne série litée ultramafique constituée de dunites occasionnellement transformées en talc, des pyroxénites trémolitisées et des gabbros qui peuvent être également en enclaves dans les pyroxénites. La plupart des dunites sont très peu altérées, il est donc improbable de faire provenir l'eau de serpentines préexistantes dans le modèle de refusion d'une partie de la base de la chambre pour donner les diorites et les diorites quartziques. Des niveaux de pyroxénites à passées progressives de gabbros apparaissent concordants avec la foliation des dunites et peuvent donc être considérés comme des sills. L'observation d'une transition entre harzburgites-dunites et werhlites-pyroxénites progressive et concordante permet d'interpréter cette unité bréchique basale comme la transition pétrologique entre le manteau supérieur et la croûte océanique.

#### 2.4.A.c L'unité gabbroïque supérieure.

Les gabbros lités atteignent 600 à 900m d'épaisseur et sont caractérisés par un litage très net, NE-SW à pendage NW modéré. Ce litage (acquis sans déformation plastique) est discordant sur le litage des gabbros de l'unité basale.

Cependant les premiers niveaux lités semblent similaires à certains gabbros lités encaissants de la brèche basale. Les premiers 100m de cette unité supérieure sont constitués de gabbros à lits leucocrates et à lits plus riches en pyroxènes et à enclaves ultrabasiques métamorphisées identiques à celles de l'unité basale (figure 2.8).

Ces premiers niveaux sont surmontés par environ 150m de gabbros lités davantage leucocrates, dépourvus d'enclaves et à passées pegmatoïdes diffuses. Puis ces derniers laissent place à environ 100m de gabbros isotropes (un litage discontinu peut être présent localement) riches en pyroxènes, dépourvus d'enclaves ultrabasiques et parsemés de gabbros pegmatoïdes. Enfin affleurent sur environ 300m des gabbros lités localement isotropes (à quartz et amphibole) recoupés par des petits filonnets d'orientations diverses et par des passées diffuses de diorites quartziques (figure 2.8).

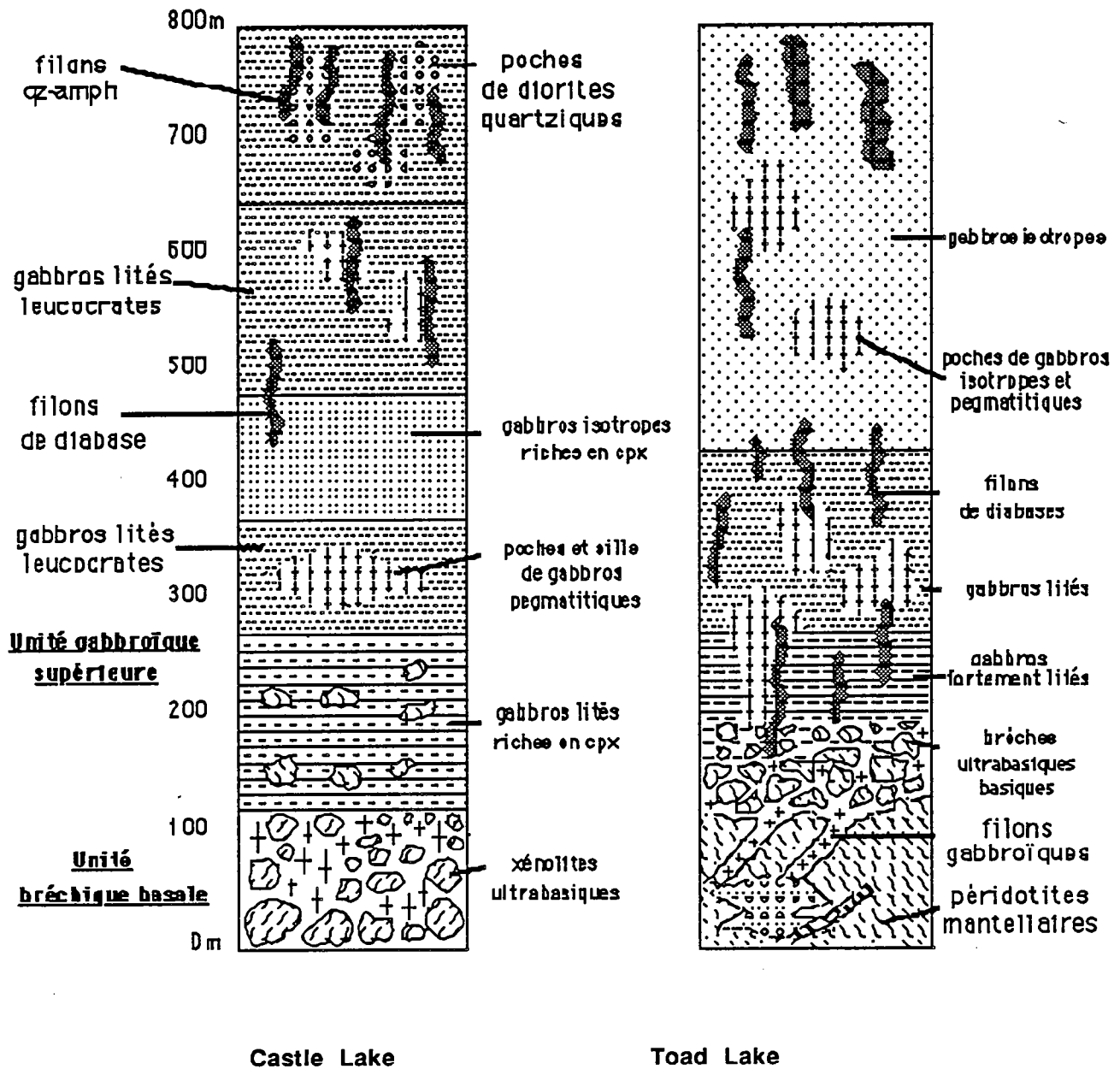


Figure 2.8.

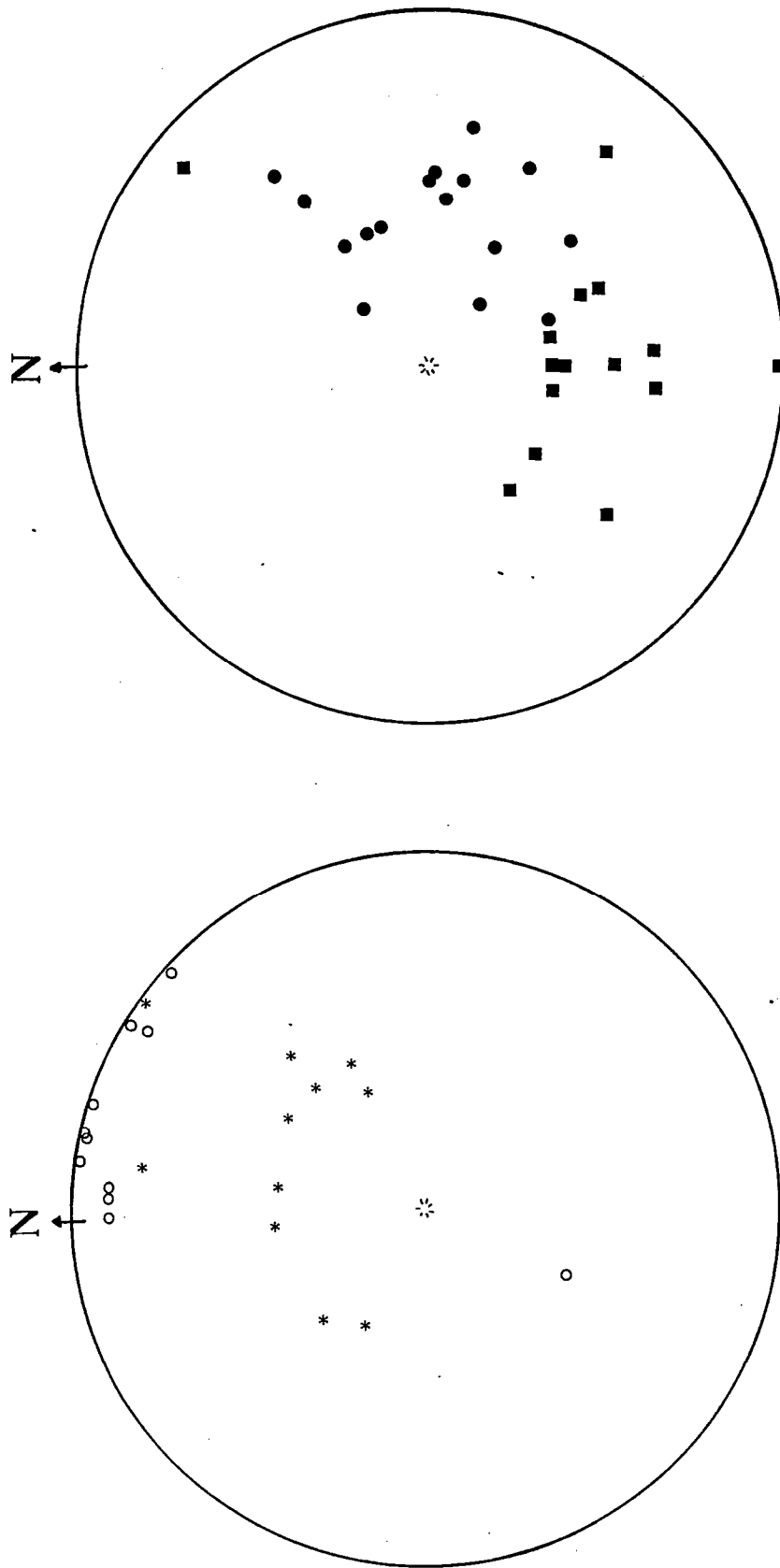
2.4.B. Pétrographie et Minéralogie.2.4.B.a L'unité bréchique basale.

## 1) Les brèches ultrabasiques.

## a) les fragments :

Ces fragments sont d'anciennes péridotites caractérisées par la présence d'olivine serpentinisée en proportions variables, d'orthopyroxène transformé en serpentine (bastite) et en talc, de spinelle chromifère et de hornblende brune.

L'olivine (0,15-0,8mm; Fo86-89) est caractérisée par des teneurs élevées en NiO (0,2-0,42%). Toutefois, localement, une olivine moins magnésienne (Fo80) peut se rencontrer étroitement associée à l'orthopyroxène et au talc (annexes). La serpentine en remplacement de l'olivine est caractérisée par des teneurs élevées en NiO (0,14-0,37%).



**Toad Lake :**

à gauche :

étoiles = filons de gabbros intrusifs  
dans les péridotites mantellaires.

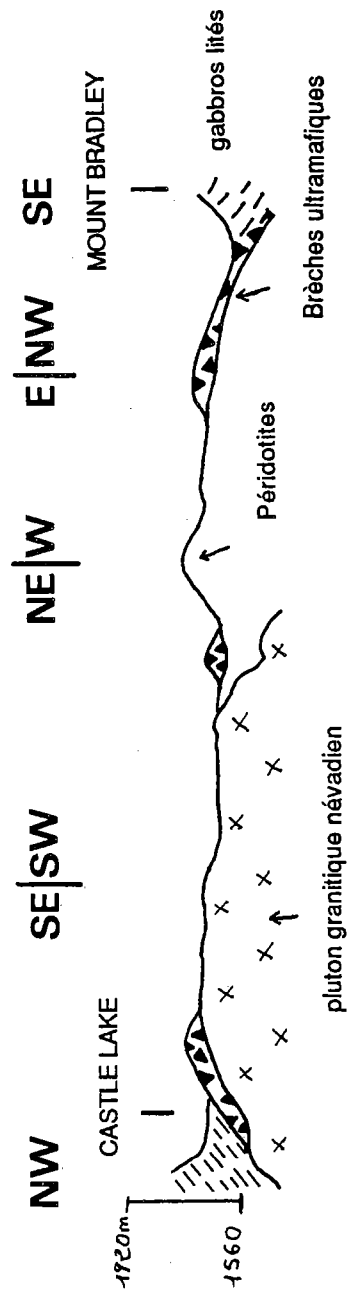
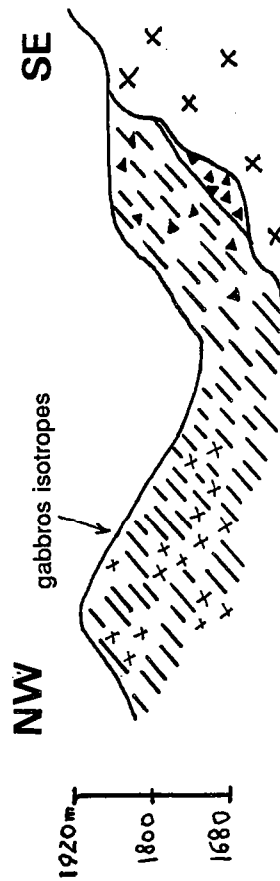
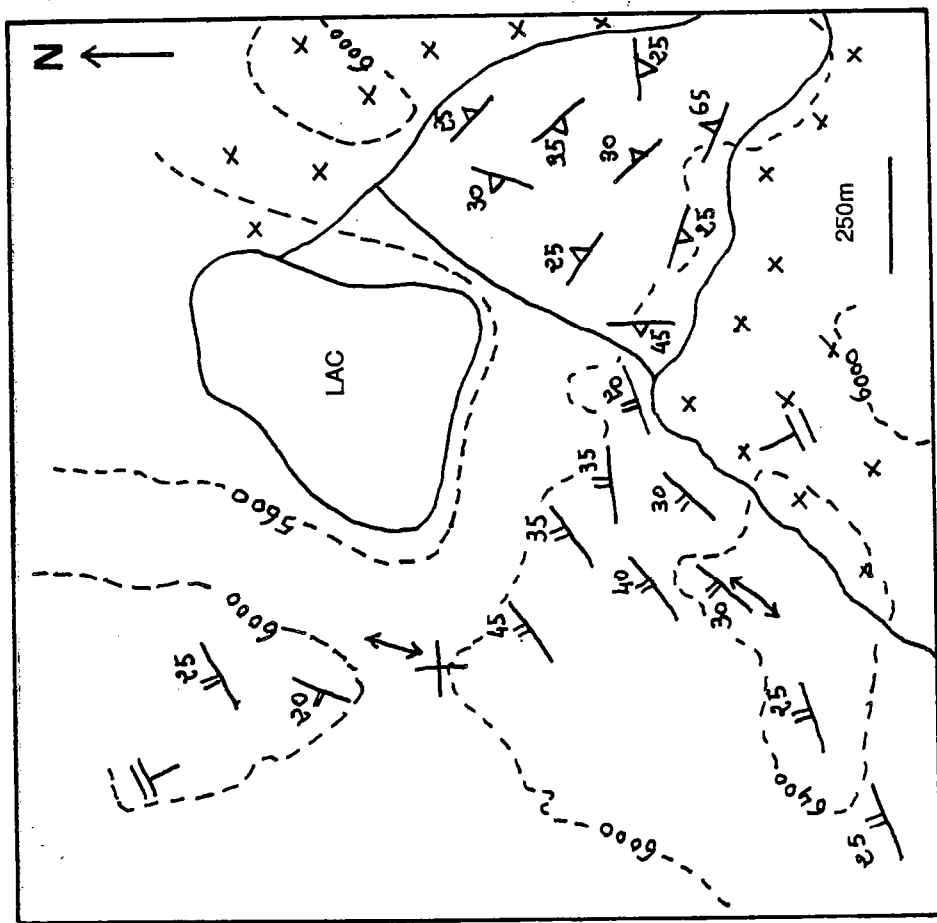
ronds vides = filons de gabbros intrusifs  
dans la chambre magmatique.

à droite :

carrés pleins : foliation de spinelle dans les péridotites.

ronds pleins : litage des gabbros dans la chambre.

*Figure 2.7.*



L'orthopyroxène (1,25mm sur 0,6mm) est pseudomorphosé par une serpentine riche en  $\text{Cr}_2\text{O}_3$  (0,52-0,59%) de type bastite (variété d'antigorite) selon un phénomène d'épitaxie. Du talc très magnésien ( $\text{MgO} = 29,7-31,8\%$ ) et chromifère ( $\text{Cr}_2\text{O}_3 = 0,29-0,53\%$ ) est également présent en remplacement de l'orthopyroxène et se présente en plages situées au coeur du minéral d'origine (annexes).

Le spinelle chromifère (0,3mm) présente de fortes variations de sa composition chimique principalement dans les composants hercynite et spinelle (annexes). Quand il est étroitement associé à la hornblende, il est caractérisé par ses plus faibles teneurs en  $\text{Al}_2\text{O}_3$  (10,5%) et  $\text{MgO}$  (1,9%) contrastant avec les plus fortes en  $\text{FeO}$  (48,4%),  $\text{TiO}_2$  (1,15%) (annexes).

La hornblende brune (0,6 sur 0,3mm) est poecilitique et contient fréquemment de petites olivines automorphes. Selon la classification de Leake (1978), c'est une hornblende pargasitique ( $\text{TiO}_2 = 0,82-1,48\%$ ;  $\text{Cr}_2\text{O}_3 = 0,83-1,7\%$ ;  $\text{Na}_2\text{O} = 1,68-2,21\%$ ; annexes).

#### b) la matrice :

Elle est constituée localement de clinopyroxénites très transformées et caractérisées par deux générations d'amphibole : des magnésio-hornblendes poecilitiques et des hornblendes actinolitiques à actinotes. D'autre part la matrice peut être également de nature gabbroïque avec des amphiboles poecilitiques et de rares reliques de plagioclase en phase cumulus (An91,4-95,1).

Les clinopyroxénites sont également caractérisées par la présence d'enclaves centimétriques d'ultrabasites qui pourraient être d'anciennes dunites mantellaires avec du spinelle chromifère et de l'olivine très magnésienne ( $\text{MgO} = 46,9-49,8\%$ ) et nickelifère ( $\text{NiO} = 0,35-0,48\%$ ; annexes).

#### 2) Les gabbros pegmatoïdes.

Ce sont des gabbros constitués de minéraux pluricentimétriques et identiques à ceux constituant le ciment de la brèche, toutefois ils peuvent contenir quelques % d'ilménite.

### 2.4.B.b L'unité gabbroïque supérieure.

#### 1) Les gabbros lités.

Ces gabbros abondants dans l'unité supérieure ont un litage bien marqué par l'orientation préférentielle des amphiboles. Ils contiennent du plagioclase cumulus très riche en anorthite (An91,4-95,1) et de l'amphibole en remplacement du clinopyroxène. La première génération d'amphibole est une magnésio-hornblende assez riche en  $\text{TiO}_2$  (2%) qui est couramment rétrotransformée en hornblende actinolitique ( $\text{TiO}_2 = 0,5-1\%$ ) et actinote ( $\text{TiO}_2 = 0,1-0,3\%$ ; annexes).

#### 2) Les gabbros isotropes.

Aucun litage n'est observable sur le terrain, la minéralogie, le cursus de cristallisation et le métamorphisme de ces roches sont similaires à ceux des gabbros lités sous-jacents. Les derniers niveaux de gabbros isotropes sont par contre caractérisés par l'apparition soudaine d'un plagioclase beaucoup plus riche en albite (An46,6-37,7), de grands prismes de magnésio-hornblende automorphe (0,9-1,87%) et de quartz intersticiel.

### 2.4.C. Géochimie.

#### 2.4.C.a L'unité bréchique de base.

##### Origine de la matrice et des enclaves et signification pétrologique.

L'unité bréchique basale de la chambre de Castle Lake constitue une zone magmatique de transition entre les cumulats lités et les péridotites mantellaires. L'examen de la composition pétrographique et géochimique des enclaves révèle qu'il s'agit soit d'anciens fragments de péridotites mantellaires (CL6 et CL16) qui ont subi des réactions minéralogiques de haute-température (Lecuyer et Cannat, 1989) au contact de magmas basiques soit de fragments de gabbroïtes à ilménite. La matrice est constituée de gabbros de nature différente : un premier type

de gabbros (CL5) correspond à un magma primitif de composition similaire à celle des filons de gabbros qui recoupent les péridotites et alimentent la chambre magmatique. Le second type correspond à des liquides riches en FeO et TiO<sub>2</sub> dont la composition rappelle celle des gabbroïtes cumulats des parois de la chambre (présents également dans la chambre de Toad Lake).

L'ensemble de ces données permet d'interpréter cette unité bréchique basale comme une zone d'instabilité magmatique où le processus de bréchification de l'encaissant de la chambre magmatique résulte à la fois de l'alimentation de la chambre par un réseau dense de veines et filons gabbroïques provenant de la fusion du manteau supérieur et aussi de la réinjection depuis la chambre magmatique de liquides magmatiques différenciés.

Ainsi cette unité bréchique basale peut être interprétée comme une paléodiscontinuité de type Moho qui marque la transition entre la croûte océanique et le manteau supérieur.

#### 2.4.C.b Comparaison des compositions chimiques des cumulats et liquides constituant les différentes chambres magmatiques (Gray Rock, Castle et Toad Lake) du complexe ophiolitique de Trinity (tableau 2.6).

Les cumulats constituant en partie les petites chambres magmatiques du complexe ophiolitique de Trinity sont caractérisés par la présence de types pétrographiques variables. En effet, si les gabbros à orthopyroxène et ilménite sont fréquents dans le site de Toad Lake, ils n'ont jamais été reconnus dans la chambre magmatique de Gray Rock. De telles différences dans la nature des roches constituant les chambres ophiolitiques peuvent être à relier avec le taux de fusion partielle qui affecte la source, avec la composition des magmas parents et leur cursus de cristallisation fractionnée au sein de la chambre magmatique.

| Ech.                             | GR   | Toad11 | Toad24 | Toad28 | TR127  | TR125 | TR111 | TR510 | Toad29 | TR109 | TR74  | TR368 |
|----------------------------------|------|--------|--------|--------|--------|-------|-------|-------|--------|-------|-------|-------|
| SiO <sub>2</sub>                 | 48   | 46.01  | 48.47  | 53.45  | 53.44  | 50.61 | 52.02 | 50.21 | 77.31  | 60.47 | 79.67 | 78.15 |
| Al <sub>2</sub> O <sub>3</sub>   | 12   | 11.75  | 12.89  | 14.73  | 16.56  | 13.93 | 16.49 | 15.04 | 12.56  | 19.43 | 11.05 | 12.61 |
| Fe <sub>2</sub> O <sub>3</sub> t | 10   | 8.27   | 7.09   | 12.41  | 8.6    | 8.36  | 7.27  | 7.56  | 0.21   | 1.3   | 0.5   | 0.45  |
| MnO                              | 0.2  | 0.18   | 0.13   | 0.21   | 0.13   | 0.15  | 0.17  | 0.14  | 0      | 0.03  | 0.02  | 0     |
| MgO                              | 14   | 15.47  | 15.16  | 3.77   | 5.84   | 10.07 | 7.34  | 10.83 | 0.09   | 1.2   | 0     | 0.13  |
| CaO                              | 10   | 13.96  | 11.57  | 8.05   | 9.89   | 11.34 | 10.79 | 10.89 | 4.19   | 3.63  | 2.24  | 0.28  |
| Na <sub>2</sub> O                | 2    | 0.81   | 0.15   | 3.04   | 2.21   | 2.8   | 2.23  | 1.65  | 3.59   | 11.54 | 4.57  | 7.21  |
| K <sub>2</sub> O                 | -    | 0.03   | 0      | 0.75   | 0.04   | 0.3   | 0.02  | 0.04  | 0.24   | 0.08  | 0.03  | 0.08  |
| TiO <sub>2</sub>                 | 0.27 | 0.24   | 0.23   | 1.19   | 0.82   | 0.55  | 0.67  | 0.48  | 0.18   | 0.29  | 0.13  | 0.08  |
| P <sub>2</sub> O <sub>5</sub>    | -    | 0      | 0      | 0.21   | -      | -     | -     | -     | 0      | 0     | 0     | 0     |
| P.F.                             | -    | 2.95   | 3.81   | 1.54   | 2.95   | 2.16  | 2.88  | 3.15  | 0.6    | 0.8   | 0.52  | 0.31  |
| Total                            |      | 99.67  | 99.5   | 99.35  | 100.48 | 100   | 99.88 | 99.99 | 99     | 97.57 | 97.53 | 97.98 |
| Zr                               | 27   | 17     | 13     | 85     | 48     | -     | -     | 24    | 130    | 176   | 112   | 55    |
| Nb                               | -    | 2      | 3      | 6      | 1      | -     | -     | 0.5   | 4      | 0     | 3     | 4     |
| Y                                | 10   | 6      | 5      | 27     | 16     | -     | -     | 12    | 18     | 36    | 15    | 23    |
| Sr                               | -    | 102    | 16     | 311    | 131    | 81    | -     | 37    | 65     | 56    | 81    | 19    |
| Rb                               | -    | 3      | 3      | 23     | 6      | 10    | -     | 6     | 4      | <5    | 0     | 1     |
| Cr                               | 600  | 825    | 980    | 30     | 108    | 620   | 185   | 431   | 15     | <10   | <10   | <10   |
| Ni                               | 250  | 380    | 411    | 10     | 91     | 244   | 113   | 248   | 0      | 17    | 31    | 30    |

Tableau 2.6.

Ces deux exemples de chambres magmatiques ophiolitiques sont caractérisés par la présence de magmas parents saturés en silice dont la composition est nettement différente de celle des MORB (tableau 2.7).

|  | magma parent<br>(Gray Rock) | magma parent<br>ophiolite de Semail | échantillon DSDP<br>3-18-7-1 | picrite |
|--|-----------------------------|-------------------------------------|------------------------------|---------|
| SiO <sub>2</sub>                                 | 49,80                       | 51,10                               | 49,70                        | 46,40   |
| TiO <sub>2</sub>                                 | 0,32                        | 0,60                                | 0,72                         | 2,00    |
| Al <sub>2</sub> O <sub>3</sub>                   | 13,40                       | 16,60                               | 16,40                        | 8,50    |
| FeO  | 6,30                        | 7,20                                | 7,90                         | 12,30   |
| MgO  | 13,40                       | 9,20                                | 10,10                        | 20,80   |
| MnO  | 0,12                        | 0,12                                | 0,12                         | n.d.    |
| CaO  | 12,50                       | 12,80                               | 13,10                        | 7,40    |
| Na <sub>2</sub> O                                | 1,50                        | 2,30                                | 1,98                         | 1,60    |
| Mg'  | 0,79                        | 0,72                                | 0,72                         | 0,77    |
| CaO/Al <sub>2</sub> O <sub>3</sub>               | 0,93                        | 0,77                                | 0,80                         | 0,87    |
| SiO <sub>2</sub> /Al <sub>2</sub> O <sub>3</sub> | 3,72                        | 3,08                                | 3,03                         | 5,46    |

Tableau 2.7

La présence dans ces chambres de plagiogranites qui représentent vraisemblablement les termes les plus évolués de la différenciation magmatique (Lecuyer et al., 1989b) est l'expression directe de la composition des magmas parents particulière au domaine océanique illustré par l'ophiolite de Trinity. Ainsi un environnement de ride à expansion lente ou très lente peut provoquer lors de la percolation des magmas au sein du manteau supérieur des transferts chimiques considérables susceptibles de modifier la composition chimique du magma parent venant alimenter la chambre magmatique. Le fractionnement in situ dans le manteau supérieur d'olivine, de clinopyroxène et de plagioclase affecte considérablement la composition en éléments majeurs du magma. Le magma produit est ainsi davantage saturé en SiO<sub>2</sub> par réaction-dissolution de l'orthopyroxène des harzburgites laissant des corps dunitiques imprégnés de clinopyroxène et de plagioclase. Un taux d'imprégnation de 50% de la masse des péridotites par les magmas de fusion partielle a pour effet de soustraire 0,2% de TiO<sub>2</sub> du magma parent au cours de l'interaction du liquide avec la péridotite.

Un tel magma dont la composition chimique est modifiée va cristalliser l'orthopyroxène et non le plagioclase juste après l'olivine (figures 2.34 et 2.35).

| TYPE                 | OL | CPX | OPX | PL | OX | AM | index<br>mafique | TEXTURES                            |
|----------------------|----|-----|-----|----|----|----|------------------|-------------------------------------|
| GABBRO<br>ISOTROPE   |    |     |     |    |    |    | 0,6              | ORTHOCUMULAT<br>SUBDOLERITIQUE      |
| LEUCO-<br>GABBRO     |    |     |     |    |    |    | 0,5              | MESO-<br>AND<br>HETERAD-<br>CUMULAT |
| MELA-<br>GABBRO      |    |     |     |    |    |    | 0,4              |                                     |
| CLINO-<br>PYROXENITE |    |     |     |    |    |    | 0,3              | HETERAD-<br>ET<br>ADCUMULAT         |
| WEBSTERITE           |    |     |     |    |    |    | 0,25             |                                     |
| WERHLITE             |    |     |     |    |    |    | 0,25             |                                     |
| LHERZOLITE           |    |     |     |    |    |    | 0,23             |                                     |
| DUNITE               |    |     |     |    |    |    | 0,2              |                                     |

Figure 2.34 : nomenclature, textures des roches et ordres d'apparition des minéraux dans la séquence plutonique de Gray Rock.



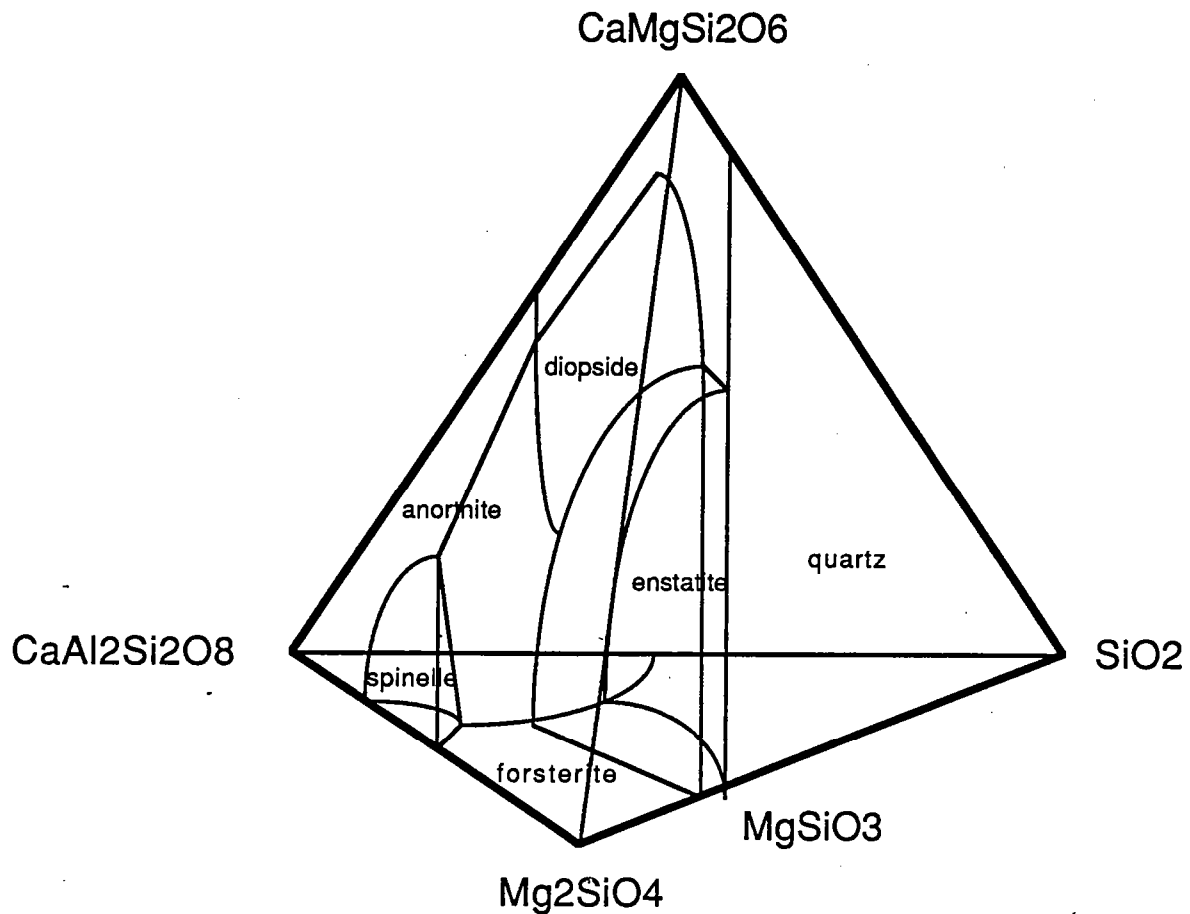


Figure 2.35 : course de cristallisation du magma parent de la chambre magmatique de Gray Rock dans le tétraèdre de phases d'après Presnall et al. (1978;1979).

C'est une caractéristique de l'ophiolite de Trinity dans laquelle les ordres de cristallisation fractionnée ou la proportion des minéraux sont variables d'une chambre magmatique à l'autre.

Ainsi, il est délicat d'utiliser les ordres de cristallisation fractionnée dans les chambres magmatiques ophiolitiques pour établir une classification en relation avec le site géotectonique. Si bien entendu la nature de la source et le taux de fusion partielle sont des paramètres décisifs de la composition des magmas produits à l'aplomb de la croûte océanique, il est important également de considérer la possibilité de la modification de la composition chimique du magma au cours de sa percolation et de son ascension vers les chambres magmatiques. Ainsi de tels processus de fractionnement chimique in situ dans le manteau supérieur en relation avec la dynamique de l'environnement (vitesse d'expansion du domaine océanique) peuvent expliquer des variations régionales de la composition des magmas.

Petrogenesis of magmas  
at a fossil slow-spreading center: The Trinity ophiolite  
(Northern California, U.S.A. ).

**C. Lécuyer**

Laboratoire de Géochimie, CAESS, Campus de Beaulieu, Avenue du Général Leclerc, 35042  
Rennes, France.

**M. Brouxel**

Centre de Recherches Pétrographiques et Géochimiques, B.P. 20,  
54501 Vandœuvre-les-Nancy, France.  
*Present address* : U.S. Geological Survey, Branch of isotope Geology,  
MS 963, P.O. Box 25046, Denver CO 80225, U.S.A.

**H. Lapierre**

Laboratoire de Géologie Structurale, Université d'Orléans, B.P. 6557,  
45067 Orléans Cedex 2, France.

*Abstract :*

The Trinity ophiolite complex exposes a widespread mantle unit (Trinity ultramafic sheet) and a thin crustal sequence in discontinuous outcrops constituting small magma chambers (Gray Rocks Lake outcrop, Dunsmuir area). The crustal sequence (about 2 km thick) consists of a layered succession of ultramafic-mafic cumulates grading upwards to isotropic gabbros. The isotropic gabbros uppermost levels are intruded by isolated or swarms of diabasic dikes and minor plagiogranites. An homogeneous pillow lava sequence crops out in the Grey Rock klippe, thrust over the Trinity ultramafic sheet. Plagiogranites crosscut all the cumulate sequence and huge masses of pegmatitic gabbros intrude both the cumulates and the mantle unit. The pillow lavas have oceanic tholeiitic island-arc affinities with transitional aspects with respect to MORB.

Mass balances and trace element modelling suggest that the Gray Rock ophiolitic magma chamber has been produced by about 20% partial melting of a depleted lherzolitic source. This magma has fractionated 42% clinopyroxene, 31% plagioclase, 20% olivine, 6% orthopyroxene and 1% spinel in two distinct steps. An open system has erupted pillow lavas as a result of decreasing melt density. The rapid evolution towards a closed system produced the more differentiated high-level gabbros. The Trinity ophiolite likely took place in a back-arc basin environment and a slow-spreading rate has been deduced from structural studies in the mantle body. The restricted development of the oceanic basin is certainly related to its geotectonic environment. In such a context, the primary magma has experienced an early mantle stage of fractionation as it slowly ascended through the upper mantle and reacted with the surrounding peridotites. The resulting shift of its chemical composition from classical MORB-type is revealed by the olivine - orthopyroxene - clinopyroxene - plagioclase crystallization sequence. This magma produced differentiated liquids (plagiogranites) by protracted fractional crystallization in a small magma chamber. The break in the oceanic basin development was characterized by a late extensive melting of lherzolitic mantle layers, producing huge masses of gabbroic pegmatitic intrusives.

## 1. Introduction

Well preserved ophiolitic complexes directly provide the products of oceanic crustal genesis and are thus powerful tools in the knowledge of the petrological and geochemical differences between the plutonic - volcanic suites of many ophiolitic associations and those of typical ocean ridges (Leitch, 1984).

The Ordovician Trinity ophiolite, likely formed in a marginal basin (Lapierre et al., 1987; Brouxel and Lapierre, 1988), as many other ophiolites of Paleozoic to Mesozoic age in the northwestern American margin (Del Puerto (Evarts, 1977), Point Sal (Menzies et al., 1977), Canyon Mountain (Thayer, 1977), Josephine (Harper, 1984)), is a good example to illustrate the first development stages of an oceanic basin in a slow spreading-ridge environment (Le Sueur et al., 1984; Boudier and Nicolas, 1985-86; Boudier et al., 1989).

$\epsilon\text{Nd}$  isotopes have been obtained by Jacobsen et al. (1984) and Brouxel and Lapierre (1988) on basalts, dikes and gabbros belonging to the ophiolite with values ranging from +6.6 to +7.5. These data suggest that these rocks are derived from a depleted mantle source. However, a value of  $+9.6 \pm 1.2$  has been obtained for a mantle plagioclase-lherzolite. Jacobsen et al. (1984) deduced from these data that the peridotite and the crustal rocks are not genetically related but the Trinity massif has recorded a multiple stage history with the preservation of ancient Nd isotopic values.

Structural studies (Boudier and Nicolas, 1984/85; LeSueur et al., 1984) and geochemical modelling (Brouxel and Lapierre, 1988) for the Trinity ophiolite suggest that the crustal rocks have been produced by a moderate partial melting rates (18%). Consequently, only a restricted part of the Trinity peridotite has been may affected by the melting event.

This paper attempts to explain the possible relationships between the geotectonic environment and the magmatic processes occurring within magma chambers beneath a slow spreading center. The three main objectives of this study were to determine:

- if some present-day ultramafic rocks could represent the residual solid of a fertile upper mantle section, following the partial melting event which led to the formation of the Trinity crustal sequence.
- the composition of the melts that fed the crustal magma chambers.
- the geochemical relationships between the plutonic rocks of the layered sequence, the late-stage gabbroic intrusives, and the effusive sequence composed of basaltic pillow lavas.

## 2. Geological setting

The Trinity ophiolite consists of a widespread mantle unit (Trinity ultramafic sheet) and a thin crustal sequence in discontinuous outcrops (< 3 km; Lindsley-Griffin, 1977; Fig. 1). The Trinity peridotite is a 2-4 km thick east-dipping ultramafic sheet which covers about 2750 km<sup>2</sup> through all the eastern Klamath Mountains (Irwin, 1960; Irwin and Bath, 1962; Lafehr, 1966; Blakely, 1985). A Sm/Nd mineral isochron age of  $472 \pm 27$  Ma has been obtained on a plagioclase lherzolite [ $\epsilon_{\text{Nd}} = 9.6$ ; (Jacobsen et al., 1984)]. However, they obtain an age of  $435 \pm 21$  Ma and a much lower  $\epsilon_{\text{Nd}}$  value ( $\epsilon_{\text{Nd}} = 6.6$ ) on a gabbroic dike intruding the Trinity peridotite. A reconstruction of the Trinity ophiolite in the Dunsuir area is proposed in Fig. 2. Gradational contacts between the ultramafic tectonites and the lower ultramafic cumulates have been recognized in several areas (Le Sueur et al., 1984). However, in the studied area such contacts have not been observed.

At Gray Rocks (Fig. 1), a continuous succession of ultramafic and mafic cumulates grading upwards to isotropic gabbros constitute a small magma chamber (about 800 meters thick). The lower cumulate layers are polycyclic dunites, lherzolites and werhlites overlain by clinopyroxenites with gabbroic interlayers. Clinopyroxenites and gabbros become more abundant towards the top of the cumulate sequence. The uppermost isotropic gabbros contain decimetric plagiogranite pockets and are intruded by diabasic dikes which can reach up to 30% of the total volume. However, no contact with the sheeted dike complex exposed at Conant (Fig. 1) has been observed. Homogeneous basaltic pillow lavas crop out in the Grey Rock klippe (Fig. 1).

Pegmatitic gabbros may occur as huge masses on the field. They occur as metric to plurimetric dikes crosscutting both the peridotite and the cumulus gabbros. Locally, these coarse-grained rocks (with a crystal size up to 20 centimeters) occur as metric sills or diffuse pockets which gradually pass to fine-layered gabbros. Plagiogranites crosscut both the cumulate rocks and the associated diabasic dikes.

## 3. Results

### 3.1. Analytical techniques

Major elements, Cr, Ni, Sr, V, and REE for plagiogranites have been analyzed by ICP spectroscopy at the Centre de Recherches Pétrographiques et Géochimiques (C.R.P.G., Vandœuvre-les-Nancy) or by X-Ray fluorescence and atomic absorption at the Service Commun d'Analyses of the University of Nancy. REE for pegmatitic gabbros have been analyzed by isotope dilution at the C.R.P.G. following techniques described by (Michard et al., 1986). Zr, Nb, and Y have been analyzed by X-Ray fluorescence at the Service Commun d'Analyses of the University of Nancy I and mineral analyses have been carried out by electron microprobe at the University of Nancy. The modal compositions shown in Table 1 result from least-square calculations based on bulk-rock chemistry and average mineral compositions. This method is certainly more accurate than the determination by point counting because it directly provides weight modal fractions on a whole-rock (Bryan et al., 1969).

### 3.2. Petrography

#### 3.2.1. The Trinity Peridotite

Dominantly lherzolites and plagioclase lherzolites have been recognized by Quick (1981) and Le Sueur et al. (1984) along the western border of the eastern Klamath Mountains leading them to interpret the Trinity peridotite as a fragment of fertile upper mantle. Nevertheless, in the Dunsuir area, collected samples are dominantly clinopyroxene-poor harzburgites and harzburgites (Table 1). Numerous samples present scarce interstitial plagioclase.

The Trinity peridotites are plastically deformed under high temperature and low stress conditions similar as those of the upper mantle (Quick, 1981). Observed textures are porphyroclastic in the terminology of Mercier and Nicolas (Mercier and Nicolas, 1975). The size and shape of olivine grains are highly variable (0.6-1mm). Larger grains are commonly elongated and contain regular kink-bands. Recrystallized olivines are fine-grained (0.1 - 0.3mm), strain-free, and constitute an equant mosaic texture.

Orthopyroxene porphyroclasts (1.5-2.5mm) often contain clinopyroxene exsolution lamellae. The elongated grains are kink-banded with slightly irregular grain boundaries. Most of the clinopyroxenes are small (<1mm), undeformed with xenomorphic grain boundaries.

Reddish-brown spinel (0.4-0.6mm) are anhedral, elongated, and mark a lineation interpreted as flow direction during the peridotite deformation (Le Sueur et al., 1984).

### 3.2.2. The plutonic sequence

While most of the rocks were metamorphosed to the greenschist facies, the degree of preservation of primary minerals is highly variable and the primary textures are not destroyed (Lécuyer et al., 1989). A transitional greenschist-amphibolite facies metamorphism affects the lower cumulates. In any case, the primary minerals, partially or completely replaced, can usually be inferred.

In the **lower cumulates**, dunites are serpentinized to various degrees, ranging from 10% to 100%. The primary mineralogy is only olivine plus euhedral spinel. Lherzolites have heteradcumulate textures and are made of 70% cumulus olivine, 18% clinopyroxene, 8% orthopyroxene (large poikilitic minerals), and 4% euhedral spinel. Clinopyroxene is completely replaced by a pargasitic hornblende. These rocks are associated with heteradcumulate and adcumulate werhlites, containing 50% clinopyroxene and 50% olivine.

**Adcumulate clinopyroxenites** are coarse-grained (2-4mm) and characterized by irregularly intergrown grains, resulting from postcumulus overgrowth.

The transition between these ultramafic cumulates and the overlying dominant layered gabbros is made by either plagioclase- or olivine-bearing clinopyroxenites interlayered with heteradcumulate and mesocumulate gabbros (average modal composition : 65% clinopyroxene and 45% plagioclase).

**Fine-grained layered gabbros** which overly this transition zone are plagioclase - clinopyroxene mesocumulates. The layering is defined by variations in the proportions of cumulus phases or by variations in the grain size. The layer thicknesses vary from several centimeters to a few meters and discontinuous layering is common throughout the cumulate sequence. Although many gabbros at the top of the cumulate sequence are not layered, they possess a slight igneous lamination defined by a preferred orientation of tabular plagioclase.

The change in the nature of cumulus phases from the base to the top of the cumulate sequence suggests the following crystallization order : spinel - olivine - orthopyroxene - clinopyroxene - plagioclase (Fig. 3).

**High level gabbros** have orthocumulate to doleritic textures consisting of euhedral plagioclase, greenish-brown hornblende and a few percent ilmenite. Grain sizes are very variable within hand specimens.

At the top of the cumulate sequence, **Plagiogranites** are quartz diorites following the Coleman and Peterman terminology (Coleman and Peterman, 1975). They consist of euhedral green hornblende, plagioclase (albite to oligoclase), ilmenite and variable amounts of xenomorphic quartz. When crosscutting the cumulate sequence, they correspond to medium-grained albitite and trondhjemite dikes, predominantly consisting of hypidiomorphic albite and quartz. Ferromagnesian minerals, less than 5% in modal proportions, are hornblendes. They also present common accessory minerals, magnetite, sphene, apatite, and zircon particularly in the more acidic rocks. Intergrowths of plagioclase and quartz which are a typical textural feature of plagiogranites (Coleman and Donato, 1979) has been locally observed.

**Pegmatitic gabbros** are characterized by cumulate and coarse-grained textures with grain sizes reaching 20 centimeters locally. They consist of clinopyroxene or primary hornblende and plagioclase.

### 3.3. Mineral chemistry

**Olivine:** In the ultramafic tectonites, the forsterite contents range from Fo<sub>90</sub> to Fo<sub>92</sub> and NiO from 0.2% to 0.45%. Olivine in the cumulate sequence rapidly disappears in the course of crystallization, exhibiting a slight variation of chemical composition: from the dunites to the clinopyroxenites the forsterite content ranges from Fo<sub>99</sub> to Fo<sub>81</sub> and the NiO contents from 0.16 to 0.08% (Table 2).

**Pyroxenes:** In the ultramafic tectonites, clinopyroxenes as well as exsolution lamellae are Mg-rich diopsides (Wo<sub>47</sub> En<sub>50</sub> Fs<sub>3</sub>) and TiO<sub>2</sub>-poor (TiO<sub>2</sub> ≤ 0.25%). The Al<sub>2</sub>O<sub>3</sub> and Cr<sub>2</sub>O<sub>3</sub> contents of the Ca-rich pyroxene exsolution lamellae in orthopyroxenes (respectively 4.5% and 1.25%) are higher to smaller xenomorphic clinopyroxene grains lacking exsolution (Al<sub>2</sub>O<sub>3</sub> = 2.3% and Cr<sub>2</sub>O<sub>3</sub> = 1%). In contrast, the cumulate clinopyroxene composition is Fe- (Wo<sub>45</sub> En<sub>49</sub> Fs<sub>6</sub>)

and Ti- ( $\text{TiO}_2$  up to 0.25%) enriched, but Al-poor ( $\text{Al}_2\text{O}_3$  ranges from 1.5 to 2.5%).

Orthopyroxenes present a similar chemical evolution: enstatites in ultramafic tectonites ( $\text{Wo}_{1-2}$  En<sub>89-90</sub> Fs<sub>8-9</sub>) are typically poor in  $\text{TiO}_2$ ,  $\text{FeO}^*$  and CaO compared with those from cumulate lherzolites ( $\text{Wo}_{2.5}$  En<sub>84.9</sub> Fs<sub>12.6</sub>; Table 3).

Our data show that within mantle orthopyroxene porphyroclasts,  $\text{Al}_2\text{O}_3$  content decreases from the core (up to 4%) to the rim (1.8%) and that the average  $\text{Al}_2\text{O}_3$  content of orthopyroxene in each sample of mantle peridotite is not dependent on the composition of both coexisting chromian spinel and bulk rock abundances.

**Spinel:** Cr-rich brown spinels (Magnetite<sub>2-6</sub> Hercynite<sub>52-60</sub> Chromite<sub>35-44</sub>) are well preserved in the Trinity ultramafic tectonites with  $\text{Cr}/(\text{Cr}+\text{Al})$  and  $\text{Mg}/(\text{Mg}+\text{Fe})$  ratios similar to those from abyssal peridotites (Dick and Bullen, 1984; Hamlyn and Bonatti, 1980; Fig. 4). Spinel from plagioclase-bearing peridotites have significantly higher  $\text{TiO}_2$  and  $\text{Cr}/(\text{Cr}+\text{Al})$  contents than those present in the plagioclase-free peridotites.

In the cumulates, the chromite component decreases from dunites (Chromite 54-57%) to lherzolites (Chromite 49%), whereas the magnetite component increases from 7-8 to 10% (Table 4).

### 3.4. Bulk rock chemistry

Because of the greenschist metamorphism which affects the Trinity rocks, mainly the less mobile major elements (Ti and Fe/Mg ratios), immobile compatible elements (Cr and Ni), and incompatible trace elements (Zr and the rare earth elements, REE) will be further considered.

The harzburgite tectonites are highly depleted in fusible elements with low  $\text{FeO}^*/\text{MgO}$  ratios,  $\text{TiO}_2$ ,  $\text{Al}_2\text{O}_3$  and CaO contents (Table 5) similar to non-cumulus peridotites of other ophiolites or mid-ocean ridges (Hamlyn and Bonatti, 1980; Menzies and Allen, 1974; Michael and Bonatti, 1985; Shibata and Thompson, 1986). The presence of an interstitial epidote in replacement of primary plagioclase explains the higher  $\text{Al}_2\text{O}_3$  and CaO contents of the harzburgite sample TR 79 (Table 5). This plagioclase-harzburgite has been analyzed for rare earth elements and is characterized by lower REE contents (0.046ppm Nd) than the ultramafic cumulates and a more severe light REE (LREE) depletion ( $(\text{Ce}/\text{Yb})_N = 0.04$ ; Brouxel and Lapierre, 1988).

The lower part of the cumulate sequence composed of polycyclic ultramafic-mafic cumulate layers is characterized by large variations of the Cr and Ni contents, and very low and constant Ti and Zr contents and  $\text{FeO}^*/\text{MgO}$  ratios (Fig. 2; Table 5). In the upper, fine-grained, layered gabbros, the Cr and Ni contents moderately decrease towards the top of the sequence. Contrasting with the lower part of the sequence, the upper-layered cumulates and isotropic gabbros and quartz diorites show a regular increase in incompatible trace element and  $\text{FeO}^*/\text{MgO}$  ratio (Fig. 2; Table 5).

The cumulate gabbros show LREE-depleted patterns with positive Eu anomalies ( $(\text{Eu}/\text{Eu}^*)_N = 1.2-2.2$ ). LREE-depleted patterns and negative Eu anomalies have been recorded in the ultramafic cumulates ( $(\text{Eu}/\text{Eu}^*)_N = 0.83$ ; Brouxel and Lapierre, 1988; Fig. 5). They have strong similarities with those recognized in other ophiolitic complexes such as Troodos (Kay and Senechal, 1976), Bay of Islands (Suen et al., 1979), Semail (Pallister and Knight, 1981) and Papua (Jaques and Chappell, 1980).

Pegmatitic rocks have gabbroic or pyroxenitic compositions similar to those of layered cumulates (Table 6). They present LREE-depleted patterns with negative Eu anomalies (Fig. 5).

Plagiogranites evolve from quartz diorites ( $\text{SiO}_2=60\%$ ) to albitites and trondhjemites ( $\text{SiO}_2$  ranging from 65 to 80%). They are characterized by low  $\text{K}_2\text{O}$ , high  $\text{Na}_2\text{O}$  contents, and very low Rb/Sr ratios (Table 7). With increasing  $\text{SiO}_2$ , there is a consistent decrease of FeO, MgO, Cr, and Ni. They present variable incompatible trace element contents ( $\text{Y}=15-40\text{ppm}$ ,  $\text{Zr}=50-170\text{ppm}$ ), LREE-enriched patterns ( $(\text{La}/\text{Sm})_N = 1.38 - 2.62$ ) with large negative Eu anomalies ( $(\text{Eu}/\text{Eu}^*)_N = 0.08-0.53$ ), and a slight heavy-REE enrichment ( $(\text{Yb}/\text{Dy})_N = 1.27 - 1.32$ ; Fig. 5).

The sheeted dikes and pillow lavas are of basaltic composition. The basalts have constant compatible and incompatible trace element contents and LREE-depleted patterns (Fig. 5; Brouxel and Lapierre, 1988). Nd isotopic ratios are similar in pillow lavas, plagiogranites, and cumulate, isotropic and pegmatitic gabbros ( $\epsilon_{\text{Nd}} = 6.6 - 7.6$ , Brouxel and Lapierre, 1988).

## 4. Discussion

### 4.1. Mineralogical variability.

#### 4.1.a. Cumulate rocks.

The presence of orthopyroxene in ultramafic cumulates of the Trinity ophiolite may be explained either 1) by crystallization of olivine tholeiite at a pressure  $\geq 10$ Kb (Fujii and Kushiro, 1977; Fujii and Bougault, 1983; Elthon and Scarfe, 1984) in agreement with experimental data on crystallization of mid-ocean ridge basaltic magmas or 2) by crystallization at low pressures of magmas with chemical characteristics significantly different than those produced along mid-ocean ridges.

In the first case, such rocks could represent cumulates settled at island-arc roots as it was proposed by several authors (Quick, 1981; Burns, 1985). However, numerous investigations at modern oceanic crust have indicated that cumulate rocks produced by the crystal fractionation of basaltic liquids contain orthopyroxene (Mid-Cayman Rise: (Elthon, 1987); DSDP Site 334: (Hodges and Papike, 1976)). (Elthon et al., 1982) proposed a formation at moderate pressure (5-10Kb) for the gabbroic rocks will ascend along with the upwelling mantle until they reach shallow levels underneath a slow-spreading center in spite of their deep-seated origin.

(Elthon, 1987) examined the mineral chemistry of gabbroic rocks from the Mid-Cayman Rise and deduced an origin by crystal fractionation of basaltic liquids at moderate pressures because of the high and covariant  $\text{Al}_2\text{O}_3$ ,  $\text{TiO}_2$  and  $\text{Mg}'$  contents in clinopyroxene. The clinopyroxenes from the Trinity cumulate rocks have high  $\text{Mg}'$  contents (Table 3) similar to those studied by (Elthon, 1987) but have opposite low  $\text{Al}_2\text{O}_3$  and  $\text{TiO}_2$  contents (Table 3). Mineralogical data from the Trinity cumulates give no evidence for the basaltic magma to crystallize clinopyroxenes at moderate or high pressure. The chemical parameters previously cited certainly reflect more a variability in liquid compositions and temperature of crystallization than pressure conditions.

In the second case, the modification of primary melts has been proposed by (Gregory, 1984) who considered that melts passed through and reacted with the mantle peridotites at low pressures in a slow-spreading environment.

The mantle peridotites have likely record the effects of melt impregnation. The mantle mineral chemistry can be now examined.

#### 4.2.b. Mantle peridotites.

The mineral chemistry of both harzburgites and lherzolites which constitute the Trinity Peridotite has been previously studied by Quick (Quick, 1981), demonstrating a mantle origin. These ultramafic rocks preserve an excellent record of a complex mantle history involving plastic deformation and partial melting.

Fo and NiO contents in olivine discriminate mantle peridotites from crustal ultramafic cumulates. NiO-rich olivines are present in the harzburgites and dunites which are the most depleted mantle rocks. These olivines with Fo $>$ 90 and high Ni contents were in equilibrium with a high-Mg parent magma ( $\text{Mg}'=0.75$ ; Roeder and Emslie, 1970). They contrast with the Ni-poor olivine from plagioclase-harzburgites and plagioclase-lherzolites (Fig. 6). In cumulate rocks, a strong and coupled decrease of Fo and NiO contents suggests the rapid subtraction of olivine by crystal settling in the magma chamber.

Spinel from plagioclase-peridotites have higher Cr/Cr+Al ratios,  $\text{Fe}_2\text{O}_3$  (as stoichiometric ferric iron), and  $\text{TiO}_2$  contents than in plagioclase-free peridotites (Fig. 7). This feature has been also recognized in other ophiolites and abyssal peridotites (Dick and Bullen, 1984; Dick et al., 1984; Hamlyn and Bonatti, 1980), and may be explained by a reaction between ascending and percolating trapped melts with the host peridotites. The scattering of plagioclase-bearing samples in the field suggests an irregular distribution of the trapped melt within the upper mantle, according to the modal data of Dick et al. (1984) along mid-ocean ridges. Consequently, only the mineral chemistry of plagioclase-free peridotites may reflect rates and variations of partial melting. Very low  $\text{TiO}_2$ , low  $\text{Al}_2\text{O}_3$ , and  $\text{FeO}^*$  contents in both pyroxenes and spinels indicate the highly residual character of the Trinity harzburgites (Tables 3 and 4). In the plagioclase-free harzburgites, spinel and pyroxene compositions are constant, suggesting similar melting rates for all samples. An evidence for partial melting is suggested by the decrease of  $\text{Al}_2\text{O}_3$  content in orthopyroxene from the core to the rim whereas most of the clinopyroxenes are unzoned. Our data on the pyroxenes from the Trinity peridotites clearly indicate difficulties in estimating equilibration temperatures from coexisting pyroxenes because of the presence of clinopyroxenes likely crystallized from the

percolating melt within the host rock. Plagioclase-free lherzolites recognized by Quick (1981) contain spinels with higher  $\text{TiO}_2$  contents and pyroxenes with higher  $\text{Al}_2\text{O}_3$  contents than in harzburgites. These lherzolites may have, however, experienced a low percentage of partial melting, but do not represent preserved fertile upper mantle rocks when they are compared to the less refractory chemical compositions of abyssal peridotites (Michael and Bonatti, 1985).

The Trinity peridotites in the vicinity of the Gray Rocks offer strongly depleted mantle rocks impregnated by percolating melts with minor "lherzolitic screens" which have less refractory compositions.

#### 4.2. Crystallization paths in the magma chamber.

Variations in major and trace element contents along the lithostratigraphic succession lead to discriminate two distinct parts in this magma chamber.

In the lower part of the cumulate sequence (part I, Fig. 2), the absence of zoning and the nearly constant mineral compositions on the one hand, and the low and constant incompatible trace element contents in the numerous cyclic layers in the other hand, are consistent with equilibrium crystallization in an open system. These cumulates, free of significant amounts of trapped liquid, show slight variations of Ti and Zr contents, well correlated with the clinopyroxene proportion ( $D_{\text{Zr}} = 0.3$  and  $D_{\text{Ti}} = 0.2$  in clinopyroxene (Ray et al., 1983; Watson and Ryerson, 1986); and  $= 0$  in plagioclase and olivine). Cr and Ni contents strongly decrease as a consequence of extensive fractionation of olivine and two pyroxenes.

Contrasting with this feature, the strong increase of the  $\text{FeO}^*/\text{MgO}$  ratio and incompatible trace element contents in part II reflects an efficient process of mineral fractionation in a closed system which was not fed any longer by new batches of magma (Fig. 2). The stacking of gabbroic cumulate layers, evolving from mesocumulate to orthocumulate textures, suggests a trapping of residual melts in the pores of the cumulates. This trapped melt strongly contributes to the increase of incompatible trace element contents in these cumulates (Fig. 2).

In summary, the evolution of the Gray Rocks magma chamber may correspond to an open system in the first stages, evolving towards a closed system. This drastic change must be related to the restricted volume of the magma chamber inferred from field observations (less than 1 km in thickness).

The trace element contents of the magma co-existing with the Trinity cumulates has been estimated assuming a total equilibrium between solid and melt, and taking into account the lack of interstitial melt in the lower part of the sequence as well as the absence of mineral zonation. Modal proportions of the cumulates were determined by least-squares calculations using mineral chemistry and whole-rock analyses.

The Ni, Cr, Zr and Ti abundances of the magma, assumed in equilibrium with the more primitive ultramafic cumulate (lherzolite TR 113; Table 5), have been estimated using modal calculations and partition coefficients taken from the literature (Pearce and Norry, 1979; Suen et al., 1979).

The calculated magma in equilibrium with the ultramafic cumulates (Ni = 220 ppm; Cr = 600 ppm; Zr = 13 ppm and  $\text{TiO}_2 = 0.27\%$ ) has fractionated abundant olivine and clinopyroxene before producing the basaltic pillow lavas (Ni = 136 ppm; Cr = 266 ppm; Zr = 39 ppm;  $\text{TiO}_2 = 0.67\%$ ; Fig. 2). At the top of the magma chamber, orthocumulate and isotropic gabbros with the lowest Ni and Cr contents (Cr = 66 ppm and Ni = 77 ppm) are the products of magmatic differentiation. They show contents in incompatible trace elements which grade progressively to the level observed in effusive rocks because of the increasing trapped intercumulus melt (Fig. 2). They correspond to the last products of magmatic differentiation in a closed system.

Sparks and Huppert (Sparks and Huppert, 1984) have emphasized the role of olivine and clinopyroxene extraction in a basaltic melt which produces a decrease of density in the residual liquid. Such a decrease of the melt density may have favoured the eruption of the basaltic liquids (Stolper and Walker, 1980). Estimated densities of the Trinity cumulates, calculated following the method of Bottinga et al. (Bottinga et al., 1983), suggest that the production of pillow lavas principally occurred when the magma had reached its minimum density (Fig. 8). The "window" of eruptibility corresponds to MgO values of cumulates ranging from 11 to 18% with a corresponding minimum density ranging from 2.68 to 2.70. The liquidus temperature of the magma within the chamber was assumed to evolve from 1300°C at the base to 1100°C at the top. When ilmenite and hornblende joined the crystallization sequence, the cumulates had reached their maximum density of 2.77. The density of high-level rocks (isotropic gabbros and diorites) began to decrease when ilmenite, hornblende and clinopyroxene were subtracted from the magma until the lowest density value of 2.41 was reached in the more differentiated plagiogranites. The rapid evolution to a closed



system may explain the limited volumes of pillow lavas observed on the field. In typical MORB tholeiitic series, abundant subtraction of plagioclase commonly increases Fe and Ti contents simultaneously in the melt (Stolper and Walker, 1980). In the Trinity rocks, the absence of ferrogabbros and the scarcity of ilmenites in the high-level rocks does not suggest an increased density of the melt.

#### 4.3. Partial melting.

An estimate of melting rates is possible using a geochemical mass balance on the basis of major element chemistry. The method requires least-squares approximations in which data are compiled in a matrix form: each column is represented by the chemical composition of the mantle restites, cumulates, and effusives, respectively. The dependent vector is the bulk-rock composition of the mantle source. The calculations, which give the weight fractions of respective residual mantle, cumulate sequence, and effusive rocks, require two hypotheses. The first one is the global composition of the cumulate sequence calculated by a linear combination between the various proportions of minerals and their chemistry. The second one is the chemical composition of the mantle source. The strong depletion in incompatible elements of the Trinity crustal rocks suggest that they have been produced by partial melting of a previously depleted mantle source (Brouxel and Lapierre, 1988). A plagioclase-free lherzolite (reference is Tinaquillo spinel lherzolite (Green, 1963) has therefore been retained for the mantle source instead of a plagioclase lherzolite. A 20% partial melting leaving a residual harzburgite (TR 423) may explain the geochemical features of the Trinity ophiolitic rocks. The produced liquids yield 60% cumulates and 40% hypabyssal and effusive rocks.

Partial melting calculations based on REE show that 19% of partial melting of the same mantle source could produce a basaltic liquid with a composition similar to that of the Trinity basalts (continuous partial melting with 10% irremovable melt (Langmuir et al., 1977); mineral/liquid partition coefficient data from (Hanson, 1980). The calculated residue presents REE contents similar to those of the TR79 harzburgite ((Ce/Yb)<sub>N</sub>=0.044; Brouxel and Lapierre, 1988).

The two methods give similar rates of partial melting. Thus, it is possible to calculate an average parental magma composition for the Trinity crust, to be compared to compositions calculated on the Semail ophiolite (Pallister, 1984), MORB, and picritic magma data (Table 8; Fig. 9). A comparison between the Trinity parental magma and a MORB picritic magma ( $Mg' = 0.72$ ; Elthon, 1979) reveals that the Trinity parent is more silicic and more depleted in Mg and Fe, but possesses a higher  $Mg'$  value ( $Mg' = 0.79$ ). Such results may be explained by fractionation of the primary melt while it was ascending through the upper mantle and reacted with wall-rock peridotite. The  $Mg'$  increase during mantle fractionation suggests the fractionation of a Fe-rich phase. Mg-olivine, Fe-spinel and orthopyroxene have been used in a mass balance calculation involving a picritic composition for the primary magma and the above calculated Trinity parent magma as the secondary magma (mineral compositions taken as dunite olivine and lherzolite, tables 2; 3 and 4). The calculation yields a fractionation of 14% olivine and 6% spinel combined with a 10% orthopyroxene addition. These results agree with the common occurrence of dunitic bodies in the mantle suite (Boudier and Nicolas, 1985-86; Quick, 1981). These dunitic bodies could be produced through a reaction of the host harzburgite with the primary melt which would be undersaturated with orthopyroxene (Gregory and Coleman, 1981).

In the thin Trinity cumulate sequence (<2 km), orthopyroxene is the first mineral to crystallize after olivine and spinel (Fig. 3). The richness of SiO<sub>2</sub> in the parent magma and its depletion in Mg and Fe result from a reaction of the primary melt with the surrounding mantle rocks. From such a modified magma, orthopyroxene is able to crystallize before plagioclase at low pressure. Consequently, the Trinity parent magma is not of MORB-type according to experimental studies which have shown that orthopyroxene cannot be a liquidus phase in MORB-type magmas at pressures less than 10 kb (Stolper, 1980; Gerlach et al., 1981).

#### 4.4. Origin of the intrusives

##### 4.4.1. Plagiogranites

The large variation of the Sr isotopic ratios, compared to constant Nd isotopic ratios, suggest a strong interaction of these acidic rocks with hot seawater (Lecuyer et al., 1989). This extensive hydrothermal alteration is responsible for the low K<sub>2</sub>O, high Na<sub>2</sub>O contents, and the very low

Rb/Sr ratios related to albitization of calcic plagioclase (Table 7).

Classically, three distinct petrogenetic models may be proposed to explain the origin of ophiolitic acidic rocks.

1) Partial melting of basic rocks under hydrous conditions has been argued for the Canyon Mountain plagiogranites (Gerlach et al., 1981).

2) Liquid immiscibility has been proposed by (Ohnenstetter, 1982) to explain the gap of composition between plagiogranites and other basic rocks in the Corsican ophiolite.

3) An origin by fractional crystallization of a basic magma was proposed for the Smartville and Semail ophiolite plagiogranites (Menzies et al., 1980; Pallister and Knight, 1981).

The restricted volume of plagiogranites in the field, compared to the volume of rocks of basic composition (layered gabbros) permit us to retain the fractional crystallization model. A test, computed with REE contents on the basis of least - square approximations, gives calculated REE patterns similar to those observed in plagiogranites through fractionation of hornblende, clinopyroxene, and plagioclase from a basaltic source (see results of computation and explanations in the Table 9). The fractionation of clinopyroxene and hornblende explain the enrichment in LREE and Yb for these plagiogranites, whereas the strong negative Eu anomaly is the consequence of plagioclase fractionation (Fig. 5).

The Trinity plagiogranites probably represent late-stage leucocratic differentiates of the magma that produced the basic sequence. Their original REE patterns, which result from a significant fractionation of hornblende, are untypical of plagiogranites produced at modern mid-ocean ridges and ophiolitic plagiogranites (Troodos (Kay and Senechal, 1976); Semail (Coleman and Donato, 1979); (Pallister and Knight, 1981); Smartville (Menzies, et al., 1980).

Their location in the upper mafic section, at the top of the magma chamber, argues for a protracted fractionation process which took place during the rapid cooling of the small magma chamber.

#### 4.4.2. Pegmatitic gabbroic rocks

The presence of enormous masses of pegmatitic gabbros, intruding both the mantle peridotites and the plutonic sequence, is a typical but intriguing feature of the Trinity ophiolite. Such a huge volume of pegmatites is rarely observed in ophiolites and it would be interesting to study their origin in an oceanic environment.

Pegmatitic gabbros contain abundant cumulus calcic plagioclase, but nevertheless display negative Eu anomalies (Fig. 5). These rocks may be derived from a magma in which abundant plagioclase has been previously subtracted or from a source previously depleted by earlier melting events.

Field observations and petrographic data support a model in which the huge intrusions of pegmatitic gabbros belong to the oceanic basin story, and mark the last stages of magma activity. In addition, Nd isotopic data attest to the cogenetism of these pegmatitic gabbros with the cumulates and pillow lavas (Brouxel and Lapierre, 1988). The large size of crystals (up to 20 cm) with large variations over several meters and the frequent occurrence of primary hornblende (Schwindinger and Anderson, 1987) suggest the presence of fluids in the magma. The gabbroic pegmatitic rocks may have been generated by partial melting of lherzolitic mantle layers. This process may have been favoured by addition of fluids coming from a subducted oceanic lithospheric plate. Hydration processes in a mantle wedge above a subducting slab have already been proposed by (Peacock, 1987) in order to explain alteration features in the Trinity peridotite. Such a model agrees with the geotectonic environment proposed by (Lapierre et al., 1987) in which the Trinity ophiolite, interpreted as a marginal basin, took place in an island-arc environment.

## 5. Conclusion

The Trinity ophiolite represents a segment of thin oceanic crust, generated by partial melting of a mantle body. Geochemical mass balance calculations suggest that the melts were produced by about 20% partial melting of depleted mantle lherzolites. Preserved lherzolitic layers support the idea of an incomplete stage of partial melting of the upper mantle.

A low spreading rate has been proposed for the Trinity ophiolite, deduced from structural studies in the mantle body (Le Sueur et al., 1984). In such a context, the primary magma has experienced an early mantle stage of fractionation as it slowly ascended through the upper mantle and reacted with the surrounding peridotites. The resulting shift of its chemical composition from classical MORB-type is revealed by the olivine - orthopyroxene - clinopyroxene - plagioclase

crystallization sequence observed in the cumulates, which indicates higher  $\text{CaO}/\text{Al}_2\text{O}_3$  and  $\text{SiO}_2/\text{Al}_2\text{O}_3$  ratios in the Trinity parent magma than primary MORB magmas. This magma produced differentiated liquids (plagiogranites) by a protracted fractional crystallization in a small magma chamber.

The restricted development of the oceanic basin is certainly related to its geotectonic environment. (Lapierre et al., 1987) proposed that the Trinity ophiolite took place in a back-arc basin while (Le Sueur et al., 1984) and (Boudier and Nicolas, 1985-86; Boudier et al., 1989) precise a slow-spreading environment. The break in the oceanic basin development was characterized by a late extensive melting of lherzolitic mantle layers producing huge masses of gabbroic pegmatitic intrusives. This partial melting stage may have been favoured by the addition of fluids from a subducted lithospheric plate.

## REFERENCES

- Arth JG (1976) Behavior of trace elements during magmatic processes. A summary of theoretical models and their applications. *J Res U S Geol Surv* 4 : 41-47
- Blakely RJ, Jachens RC, Simpson RW and Couch RW (1985) Tectonic setting of the southern Cascade Range as interpreted from its magnetic and gravity fields. *Geol Soc Am Bull* 96 : 43-48
- Bottinga Y, Richet P and Weill DF (1983) Calculation of the density and thermal expansion coefficient of silicate liquids. *Bull Minéral* 106 : 129-138
- Boudier F and Nicolas A (1985-86) Harzburgite and lherzolite subtypes in ophiolite and oceanic environments. *Earth Planet Sci Lett* 76 : 84-92
- Boudier F, Le Sueur E and Nicolas A (1989) Structure of an atypical ophiolite: The Trinity complex, eastern Klamath Mountains, California. *Geol Soc Am Bull* 101 : 820-833
- Brouxel M and Lapierre H (1988) Geochemical study of an early Paleozoic island arc - back arc basin system. Part I : The Trinity ophiolite (Northern California). *Geol Soc Am Bull* 100 : 1111-1119
- Bryan WB, Finger LW and Chayes F (1969) Estimating Proportions in Petrographic Mixing Equations by Least-Squares Approximation. *Science* 163 : 926-927
- Burns LE (1985) The Border Ranges ultramafic and mafic complex, south-central Alaska: cumulate fractionates of island-arc volcanics. *Can J Earth Sci* 22 : 1020-1038
- Coleman RG and Donato MM (1979) Oceanic plagiogranite revisited. In: Barker F (eds) *Trondjhemites, dacites and related rocks*. Elsevier, pp 149-168
- Coleman RG and Peterman ZE (1975) Oceanic plagiogranite. *J Geophys Res* 80 : 1099-1108
- Dick HJB and Bullen T (1984) Chromian spinel as a petrogenetic indicator in abyssal and alpine-type Peridotites and spatially associated lavas. *Contrib Mineral Petrol* 86 : 54-76
- Dick HJB, Fisher RL and Bryan WB (1984) Mineralogic variability of the uppermost mantle along mid-ocean ridges. *Earth Planet Sci Lett* 69 : 88-106
- Elthon D (1979) High magnesia liquids as the parental magma for ocean floor basalts. *Nature* 278 : 514-518
- Elthon D (1987) Petrology of gabbroic rocks from the Mid-Cayman Rise spreading center. *J Geophys Res* 92 : 658-682
- Elthon D, Casey JF and Komor S (1982) Mineral chemistry of ultramafic cumulates from the North Arm Mountain massif of the Bay of Islands ophiolite: evidence for high-pressure crystal fractionation of oceanic basalts. *J Geophys Res* 87 : 8717-8734
- Elthon D and Scarfe CM (1984) High-pressure phase equilibria of a high-magnesia basalt and the genesis of primary oceanic basalts. *Am Mineral* 69 : 1-15

- Evarts RC (1977) The Geology and petrology of the Del Puerto ophiolite, Diablo Range, Central California Coast Ranges. In: Coleman RG, Irwin WP (eds) North American Ophiolites. State of Oregon, Dep of Geol Min Ind Bull, 95, pp 121-139
- Fujii T and Bougault H (1983) Melting relations of a magnesian abyssal tholeiite and the origin of MORBs. *Earth Planet Sci Lett* 62 : 283-295
- Fujii T and Kushiro I (1977) Melting relations and viscosity of abyssal tholeiite. *Year Book Carnegie Inst Washington* 76 : 461-465
- Gerlach DC, Leeman WP and Ave Lallemand HG (1981) Petrology and geochemistry of plagiogranite in the Canyon Mountain ophiolite, Oregon. *Contrib Mineral Petrol* 77 : 82-92
- Green DH (1963) Alumina content of enstatite in a Venezuelan high-temperature peridotite. *Geol Soc Am Bull* 74 : 1397-1402
- Gregory RT (1984) Melt percolation beneath a spreading ridge : evidence from the Semail Peridotite, Oman. In: Gass IG, Lippard SJ, Shelton AW (eds) Ophiolites and Oceanic Lithosphere, Blackwell Scientific Publications, pp 55-62
- Gregory RT and Coleman RG (1981) Evidence for melt migration through the uppermost mantle beneath a spreading ridge (abs.). Chapman Conference, The Generation of the Oceanic Lithosphere. Amer Geophys Union, Washington, USA
- Grützeck M, Kridelbaugh S and Weill D (1974) The distribution of Sr and REE between diopside and silicate liquid. *Geophys Res Lett* 1 : 273-275
- Hamlyn PR and Bonatti E (1980) Petrology of mantle-derived ultramafics from the Owen fracture zone, northwest Indian Ocean : implications for the nature of the oceanic upper mantle. *Earth Planet Sci Lett* 48 : 65-79
- Hanson GN (1980) Rare earth elements in petrogenetic studies of igneous systems. *Ann Rev Earth Planet Sci* 8 : 371-406
- Harper GD (1984) The Josephine Ophiolite, Northwestern California. *Geol Soc Am Bull* 95 : 1009-1026
- Hodges FN and Papike JJ (1976) DSDP Site 334 : magmatic cumulates from oceanic layer 3. *J Geophys Res* 81 : 4135-4151
- Irwin WP (1960) Geological reconnaissance of the northern Coast Ranges and Klamath Mountains, California, with a summary of the mineral resources. *Calif Div Min Geol Bull* 179 : 180
- Irwin WP (1977) Ophiolitic terranes of California, Oregon and Nevada. In: Coleman RG, Irwin WP (eds) North American Ophiolites. *Oreg Dept Geol Miner Ind Bull*, 95, pp 75-92
- Irwin WP and Bath GD (1962) Magnetic anomalies and ultramafic rock in northern California. *U S Geol Surv Prof Pap* 450-B : 65-67
- Jacobsen SB, Quick JE and Wasserburg GJ (1984) A Nd and Sr isotopic study of the Trinity peridotite; implications for mantle evolution. *Earth Planet Sci Lett* 68 : 361-378
- Jaques AL and Chappell BW (1980) Petrology and trace element geochemistry of the Papuan Ultramafic Belt. *Contrib Mineral Petrol* 75 : 55-70
- Kay RW and Senechal RG (1976) The rare earth geochemistry of the Troodos ophiolite complex. *J Geophys Res* 81 : 964-970
- Lafehr TR (1966) Gravity in the eastern Klamath Mountains, California. *Geol Soc Am Bull* 77 : 1177-1190

- Langmuir CH, Bender JB, Bence AE, Hanson GN and Taylor SR (1977) Petrogenesis of basalts from the FAMOUS area: Mid-Atlantic Ridge. *Earth Planet Sci Lett* 36 : 133-156
- Lapierre H, Brouxel M, Albarède F, Coulon C, Lecuyer C, Martin P, Mascle G and Rouer O (1987) Paleozoic and Lower Mesozoic magmas from the eastern Klamath Mountains (North California) and the geodynamic evolution of northwestern America. *Tectonophysics* 140 : 155-177
- Le Sueur E, Boudier F, Cannat M, Ceuleneer G and Nicolas A (1984) The Trinity mafic-ultramafic complex : first results of the structural study of an untypical ophiolite. *Ophioliti* 9 : 487-498
- Lécuyer C, Brouxel M and Albarède F (1989) Elemental fluxes during the hydrothermal alteration of the Trinity ophiolite (California) by seawater. *Soumis à Chem Geol*
- Leitch EC (1984) Island-Arc Elements and Arc-Related Ophiolites. *Tectonophysics* 106 : 177-203
- Lindsley-Griffin N (1977) The Trinity ophiolite, Klamath Mountains, California. In: Coleman RG, Irwin WP (eds) *North American ophiolites. State of Oregon, Dep of Geol Min Ind Bull*, 95, pp 107-120
- Menzies M and Allen C (1974) Plagioclase lherzolite - residual mantle relationships within two Eastern Mediterranean ophiolites. *Contrib Mineral Petrol* 45 : 197-213
- Menzies M, Blanchard D and Jacobs J (1977) Rare earth and trace element geochemistry of metabasalts from the Point Sal ophiolite, California. *Earth Planet Sci Lett* 37 : 203-215
- Menzies M, Blanchard D and Xenophontos C (1980) Genesis of the Smartville Arc - ophiolite, Sierra Nevada foothills, California. *Am J Sci* 280A : 329-344
- Mercier JC and Nicolas A (1975) Textures and fabrics of upper mantle peridotites as illustrated by basalt xenoliths. *J Petrol* 16 : 454-487
- Michael PJ and Bonatti E (1985) Peridotite composition from the North Atlantic : regional and tectonic variations and implications for partial melting. *Earth Planet Sci Lett* 73 : 91-104
- Michard A, Montigny R and Schlich R (1986) Geochemistry of the mantle beneath the Rodrigues Triple Junction and the South-East Indian Ridge. *Earth Planet Sci Lett* 78 : 104-114
- Ohnenstetter M (1982) Importance de la nature et du rôle des discontinuités au sein des ophiolites lors du développement d'un orogène. Thèse d'état Université de Nancy I : 590
- Pallister JS (1984) Parent magmas of the Semail ophiolite, Oman. In: Gass IG, Lippard SJ, AW (eds) *Ophiolites and Oceanic Lithosphere*. Blackwell Scientific Publications : 63-70
- Pallister JS and Knight RJ (1981) Rare-earth element geochemistry of the Semail ophiolite near Ibra, Oman. *J Geophys Res* 86 : 2673-2697
- Peacock SM (1987) Serpentinization and infiltration metasomatism in the Trinity peridotite, Klamath province, northern California : implications for subduction zones. *Contrib Mineral Petrol* 95 : 55-70
- Pearce JA and Norry MJ (1979) Petrogenetic implications of Ti, Zr, Y and Nb variations in volcanic rocks. *Contrib Mineral Petrol* 69 : 33-47
- Quick JE (1981) Petrology and petrogenesis of the Trinity peridotite, an upper mantle diapir in the eastern Klamath Mountains, northern California. *J Geophys Res* 86 : 11837-11863
- Ray GL, Shimizu N and Hart SR (1983) An ion microprobe study of the partitioning of trace elements between clinopyroxene and liquid in the system diopside - albite - anorthite. *Geochim Cosmochim Acta* 47 : 2131-2140
- Roeder PL and Emslie RF (1970) Olivine-liquid equilibrium. *Contrib Mineral Petrol* 29 : 275-289
- Schwindinger K.R. and Anderson JAT (1987) Probable low - pressure intrusion of gabbro into

- serpentinized peridotite, northern California. *Geol Soc Am Bull* 98 : 364-372
- Shibata T and Thompson G (1986) Peridotites from the Mid-Atlantic Ridge at 43°N and their petrogenetic relation to abyssal tholeiites. *Contrib Mineral Petrol* 93 : 144-159
- Sparks RSJ and Huppert HE (1984) Density changes during the fractional crystallization of basaltic magmas: fluid dynamic implications. *Contrib Mineral Petrol* 85 : 300-309
- Stolper E (1980) A phase diagram for mid-ocean ridge basalts : preliminary results and implications for petrogenesis. *Contrib Mineral Petrol* 74 : 13-27
- Stolper E and Walker D (1980) Melt density and the average composition of basalt. *Contrib Mineral Petrol* 74 : 7-12
- Strand RG (1963) *Geologic Atlas of California, Weed sheet : 1 / 250 000*. Calif. Div. Min Geol
- Suen CJ, Frey FA and Malpas J (1979) Bay of Islands ophiolite suite, Newfoundland : Petrologic and geochemical characteristics with emphasis on rare-earth element geochemistry. *Earth Planet Sci Lett* 45 : 337-348
- Thayer TP (1977) The Canyon Mountain complex, Oregon, and some problems of ophiolites In: Coleman RG, Irwin WP (eds) *North American Ophiolites, State of Oregon*, pp 93-105
- Wagner D and Saucedo GJ (1986) Geological map of the Weed quadrangle, 1 / 250 000, California. *Calif Div Min Geol Reg Geol Map Ser, 4A*
- Watson EB and Ryerson FJ (1986) Partitioning of zirconium between clinopyroxene and magmatic liquids of intermediate composition. *Geochim Cosmochim Acta* 50 : 2523-2526

### FIGURE CAPTIONS

- Fig. 1: General map of the eastern Klamath Mountains after (Strand, 1963), (Irwin, 1977) and (Wagner and Saucedo, 1986), with locations of samples.
- Fig. 2: Synthetic lithologic column of the Trinity ophiolite with the position of studied samples and their variations of bulk-rock major and trace element contents. Filled diamonds: mantle peridotites, filled squares: ultramafic cumulates, open squares: mafic cumulates, filled circles: isotropic gabbros, filled triangles: pegmatitic gabbros, open triangles: dikes, open circles: pillow basalts.
- Fig. 3: Mineral proportions and crystallization sequence in the Trinity ophiolite. M.I. = Mafic Index.
- Fig. 4:  $Cr/Cr+Al$  versus  $Mg/Mg+Fe^{2+}$  in spinels from the Trinity Peridotite (open squares). open square with dot: mantle spinels; open square: mantle dunite; filled diamonds: cumulate dunite. Dashed field for abyssal peridotites; hachured field: stratiform intrusions.
- Fig. 5: Chondrite-normalized ( $C_1$  of Evensen et al., 1978) rare earth element patterns of plagiogranites (TR368, TR109, TR74), isotropic (TR64) and pegmatitic gabbros (PEGMB), and the field of Trinity basalts. dotted square : plagiogranites, open circles : pillow basalts, filled triangles : pegmatitic gabbros.
- Fig. 6: NiO versus Fo contents of olivines from the Trinity ophiolite.  
Trinity peridotite: harzburgite (inverse filled triangles), lherzolite (normal filled triangles) and dunite (filled circles).  
Plutonic sequence: dunite (open circles), lherzolite (normal open triangles), werhlite (open diamonds) and pyroxenite (open squares).
- Fig. 7:  $100Cr/(Cr+Al)$  versus  $TiO_2$  from spinels in the Trinity peridotites and cumulates. Open circle: peridotite dunite; filled circle: cumulate dunite; filled square: plagioclase-harzburgite; filled triangle: plagioclase-lherzolite; open square: harzburgite; open triangle: lherzolite.

**Fig. 8:** Estimated densities of silicate liquids corresponding to the Trinity cumulates, high-level gabbros and plagiogranites versus MgO with the input and output of crystallizing mineralogical phases. Plagiogranite: filled diamonds; ultramafic cumulates: filled squares; mafic cumulates: open squares; high-level gabbros: filled circles.

**Fig. 9:** Calculated proportions of Trinity crustal and upper mantle units based on major and trace element data and comparison with results on the Oman ophiolite (data from Pallister, 1984).

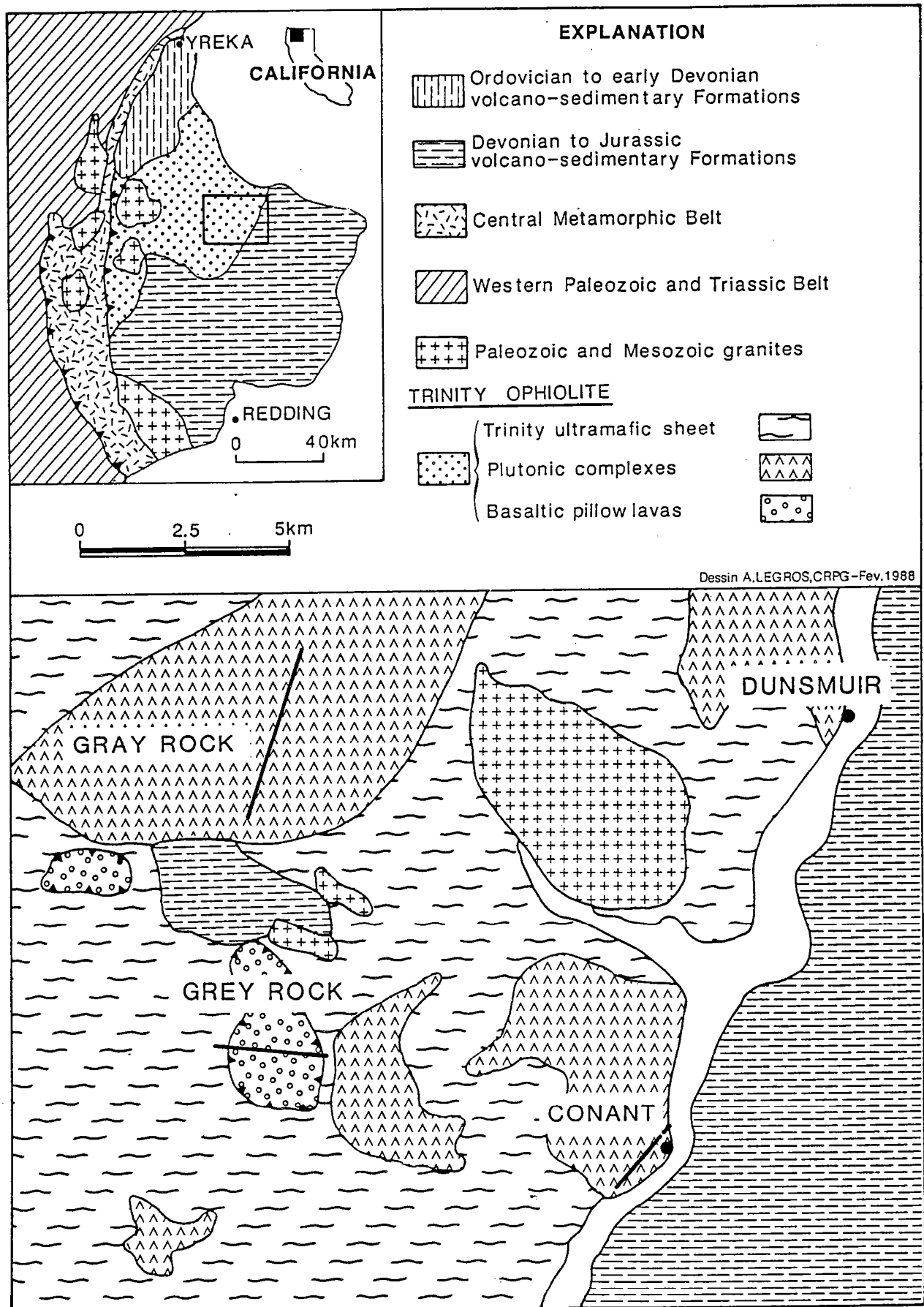


Figure 1



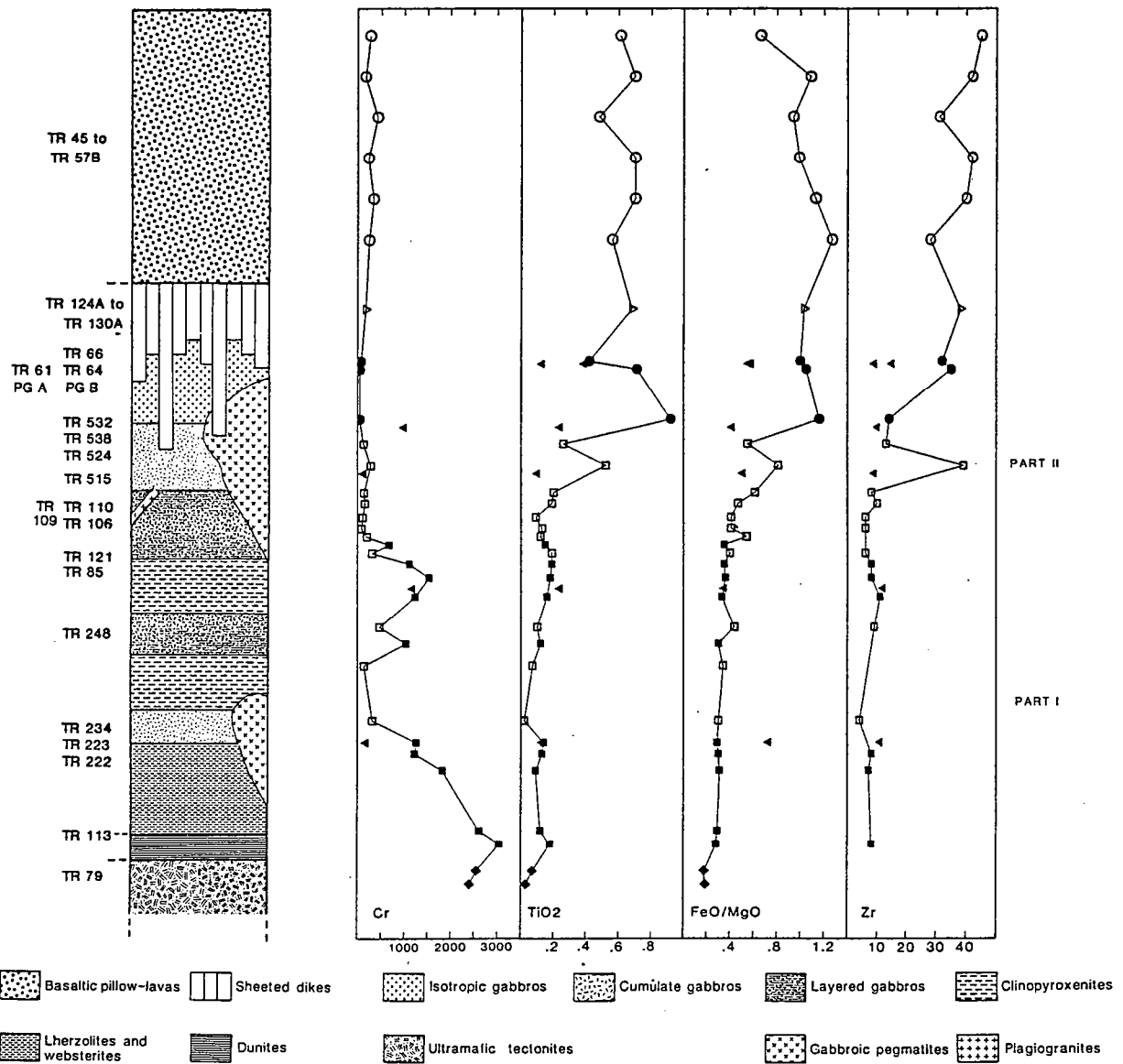


Figure 2

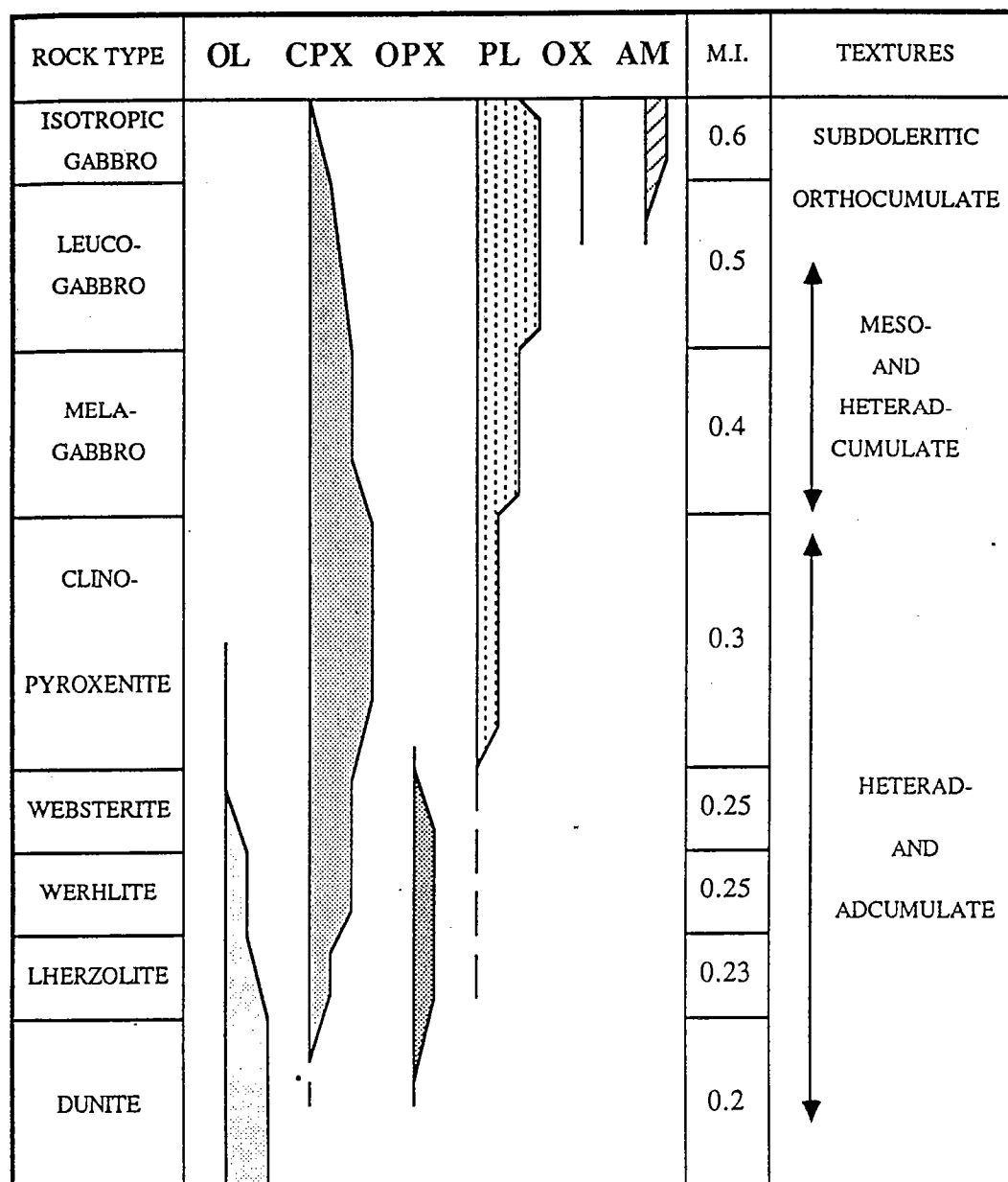


Figure 3

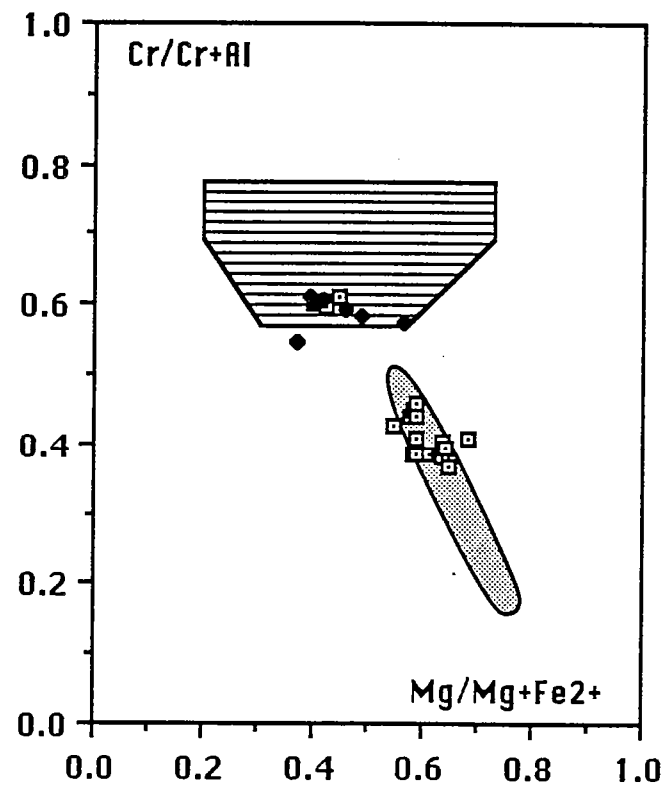


Figure 4

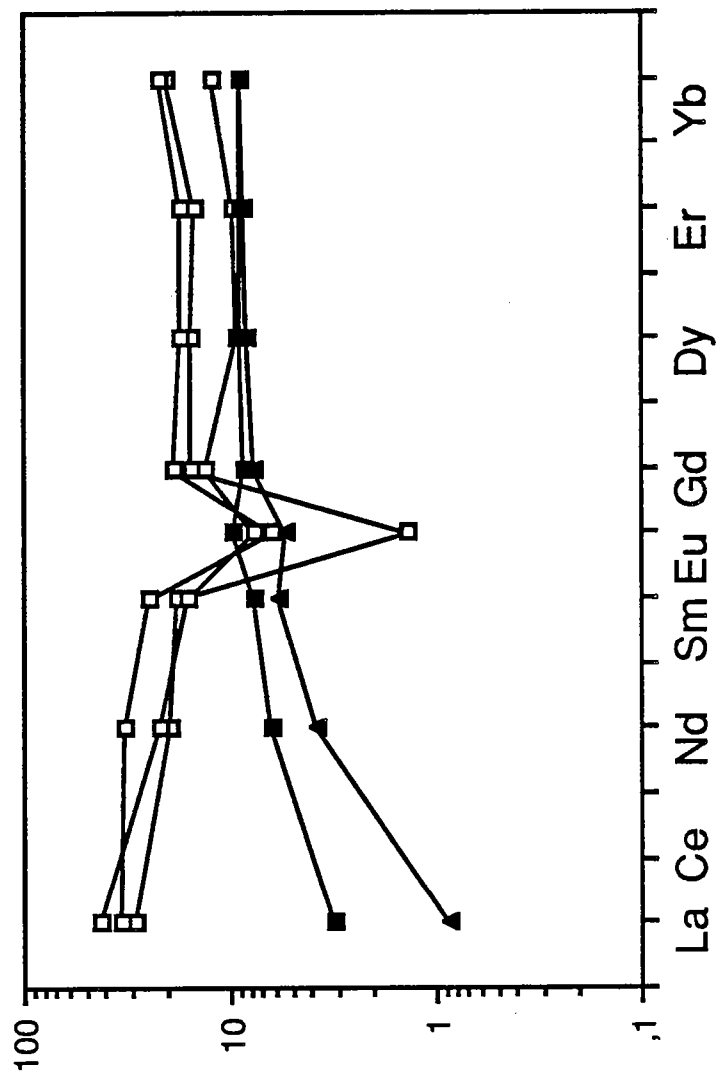
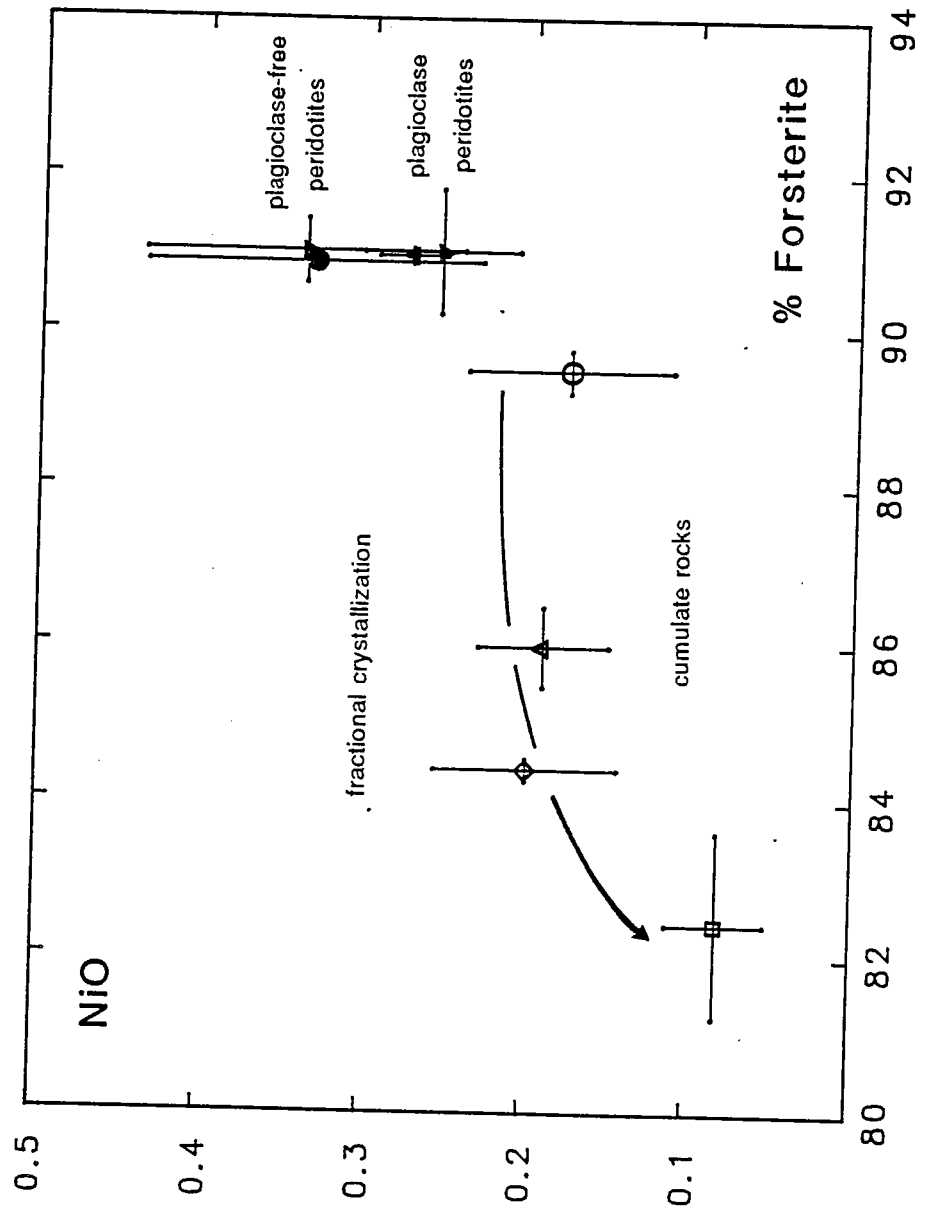


Figure 5



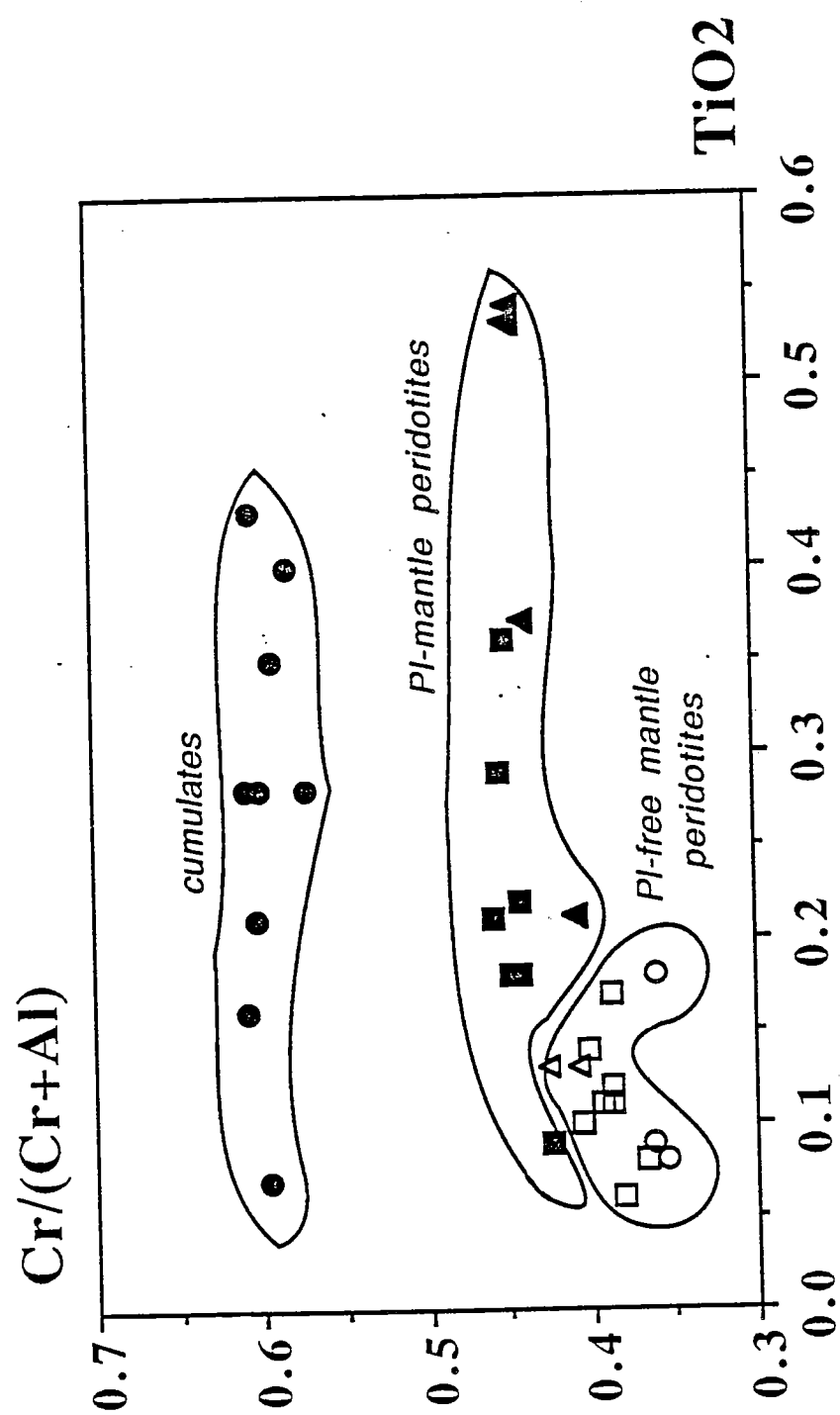
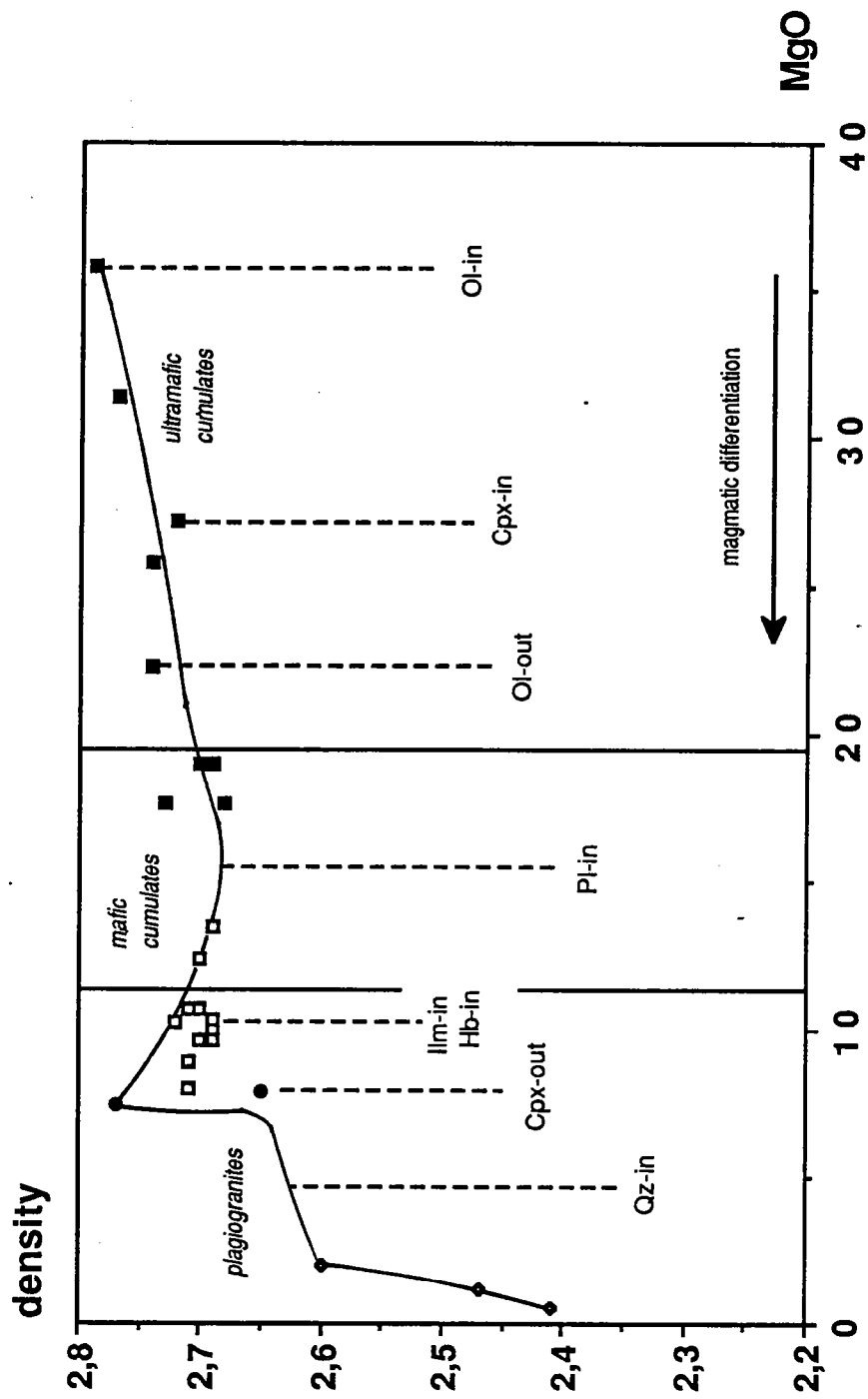


Figure 7



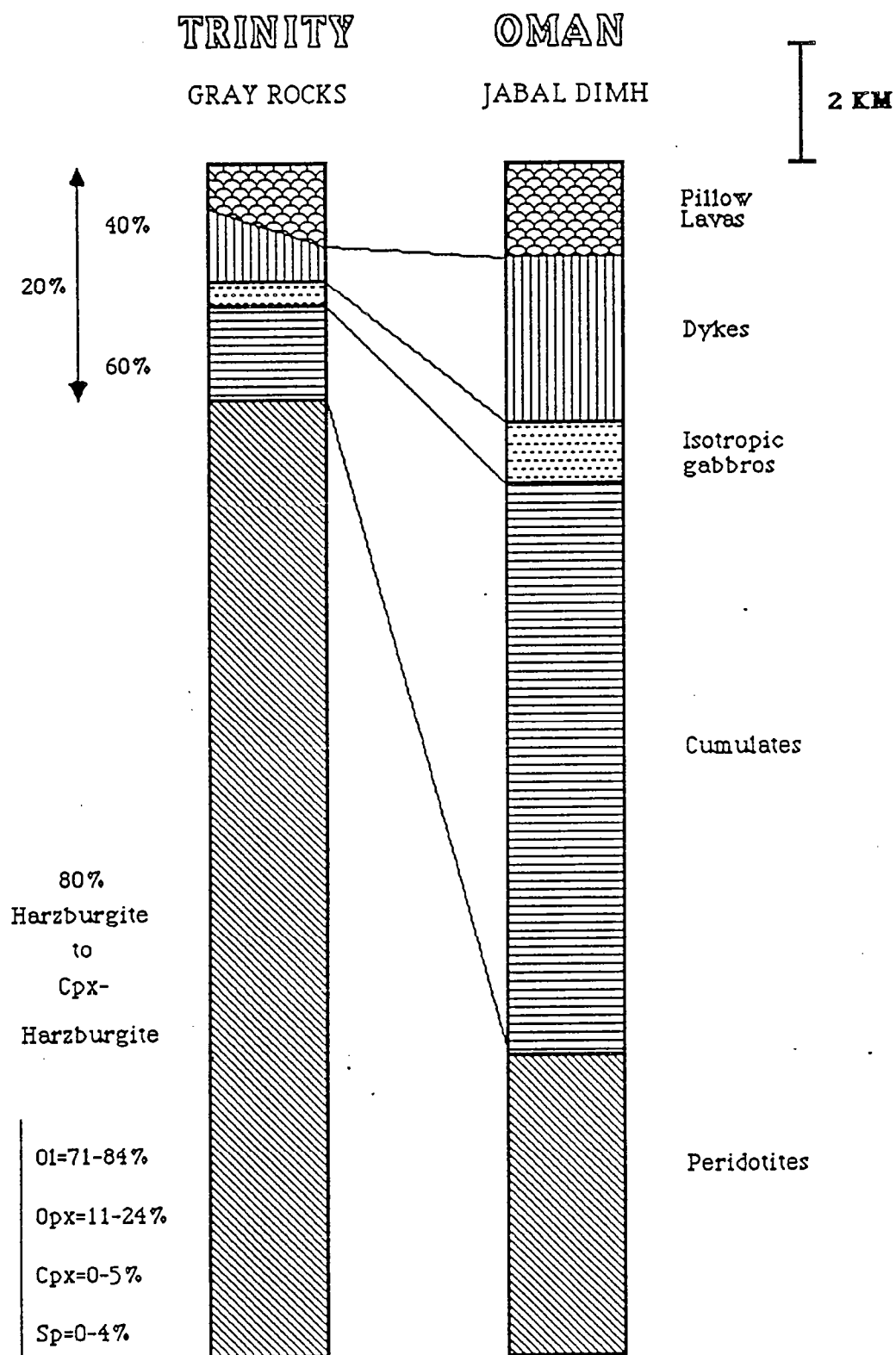


Figure 8



## TRINITY PERIDOTITE

| Samples | Nature          | Olivine | Orthopyroxene | Clinopyroxene | Spinel | Plagioclase | M S W D |
|---------|-----------------|---------|---------------|---------------|--------|-------------|---------|
| TR423   | Harzburgite     | 70.7    | 22.0          | 3.5           | 3.8    | 0.0         | 0.600   |
| TR2     | Cpx-Harzburgite | 81.5    | 14.3          | 3.8           | 0.3    | 0.0         | 0.080   |
| TR1     | Pl-Harzburgite  | 76.0    | 16.0          | 4.1           | 0.0    | 3.9         | 0.320   |
| TR13    | Cpx-Harzburgite | 83.3    | 13.7          | 2.0           | 1.0    | 0.0         | 0.087   |
| TR14    | Cpx-Harzburgite | 74.0    | 23.9          | 1.6           | 0.5    | 0.0         | 0.163   |
| TR17    | Pl-Harzburgite  | 72.1    | 20.8          | 1.2           | 0.0    | 6.4         | 0.197   |
| TR3     | Cpx-Harzburgite | 83.4    | 11.3          | 4.7           | 0.6    | 0.0         | 0.052   |
| TR6     | Pl-Harzburgite  | 76.0    | 16.0          | 4.0           | 0.0    | 4.0         | 0.330   |
| TR7     | Pl-Harzburgite  | 73.6    | 19.3          | 2.1           | 0.7    | 4.3         | 0.018   |
| TR8     | Cpx-Harzburgite | 81.1    | 15.6          | 2.3           | 1.0    | 0.0         | 0.195   |
| TR9     | Cpx-Harzburgite | 79.7    | 16.2          | 3.2           | 0.9    | 0.0         | 0.161   |
| TR12    | Harzburgite     | 76.9    | 20.1          | 0.0           | 0.5    | 2.5         | 0.089   |

Tableau 1

| SAMPLES | TR 252 | TR 222<br>cumulates | TR 113 | TR 413 | TR 83  | TR 79<br>mantle peridotites | TR 423 |
|---------|--------|---------------------|--------|--------|--------|-----------------------------|--------|
| SiO2    | 39.93  | 39.35               | 41.22  | 41.46  | 39.79  | 40.10                       | 40.74  |
| TiO2    | 0      | 0                   | 0      | 0      | 0.06   | 0                           | 0      |
| Al2O3   | 0.05   | 0.03                | 0.03   | 0      | 0.02   | 0.03                        | 0.01   |
| FeO     | 15.52  | 14.65               | 12.72  | 10.29  | 9.00   | 9.63                        | 8.38   |
| MgO     | 43.77  | 45.36               | 45.52  | 50.83  | 51.32  | 50.49                       | 49.46  |
| MnO     | 0.09   | 0.26                | 0.17   | 0.12   | 0.02   | 0.04                        | 0.15   |
| CaO     | 0.01   | 0.03                | 0.02   | 0.03   | 0      | 0.03                        | 0      |
| Na2O    | 0.03   | 0                   | 0.01   | 0.01   | 0      | 0                           | 0      |
| Cr2O3   | 0      | 0.02                | 0.08   | 0      | 0.19   | 0                           | 0      |
| NiO     | 0.12   | 0.16                | 0.22   | 0.11   | 0.35   | 0.27                        | 0.51   |
| Sum     | 99.52  | 99.85               | 99.99  | 102.85 | 100.75 | 100.60                      | 99.25  |
| Ni      | 0.0025 | 0.0032              | 0.0044 | 0.0021 | 0.0068 | 0.0052                      | 0.0100 |
| Na      | 0.0016 | 0                   | 0.0006 | 0.0004 | 0      | 0                           | 0      |
| Ca      | 0.0003 | 0.0008              | 0.0006 | 0.0007 | 0      | 0.0009                      | 0      |
| Fe      | 0.3278 | 0.3081              | 0.2637 | 0.2055 | 0.1833 | 0.1967                      | 0.1722 |
| Si      | 1.0082 | 0.9898              | 1.0213 | 0.9899 | 0.9690 | 0.9788                      | 1.0012 |
| Ti      | 0      | 0                   | 0      | 0      | 0.0012 | 0                           | 0      |
| Mn      | 0.0019 | 0.0056              | 0.0035 | 0.0025 | 0.0005 | 0.0009                      | 0.0031 |
| Mg      | 1.6475 | 1.7006              | 1.6811 | 1.8090 | 1.8626 | 1.8372                      | 1.8115 |
| Cr      | 0      | 0.0003              | 0.0016 | 0      | 0.0036 | 0                           | 0      |
| Al      | 0.0015 | 0.0008              | 0.0009 | 0      | 0.0006 | 0.0009                      | 0.0002 |
| Fo      | 83.22  | 84.29               | 86.09  | 89.6   | 90.72  | 90.06                       | 90.72  |

Tableau 2

| SAMPLES                        | TR 252 | TR 248<br>cumulates | TR 113 | TR 79<br>mantle peridotites | TR 81<br>mantle peridotites | TR 423 |
|--------------------------------|--------|---------------------|--------|-----------------------------|-----------------------------|--------|
| SiO <sub>2</sub>               | 54.20  | 53.33               | 56.01  | 55.71                       | 54.06                       | 55.62  |
| Al <sub>2</sub> O <sub>3</sub> | 1.27   | 1.47                | 2.24   | 2.34                        | 3.95                        | 2.63   |
| TiO <sub>2</sub>               | 0.05   | 0.15                | 0.11   | 0.09                        | 0.05                        | 0.07   |
| FeO                            | 3.46   | 3.97                | 7.97   | 5.77                        | 6.07                        | 5.74   |
| MgO                            | 16.84  | 16.85               | 31.23  | 34.64                       | 32.34                       | 34.07  |
| CaO                            | 24.02  | 23.92               | 1.26   | 0.80                        | 0.63                        | 1.11   |
| MnO                            | 0.16   | 0.20                | 0.31   | 0.38                        | 0.10                        | 0.03   |
| Cr <sub>2</sub> O <sub>3</sub> | 0.02   | 0.37                | 0.59   | 0.66                        | 0.58                        | 0.61   |
| NiO                            | 0      | 0.01                | 0      | 0.08                        | 0                           | 0.03   |
| Na <sub>2</sub> O              | 0.05   | 0.10                | 0      | 0.01                        | 0.02                        | 0.02   |
| Sum                            | 100.07 | 100.7               | 99.72  | 100.48                      | 97.8                        | 99.93  |
| Si                             | 1.975  | 1.948               | 1.958  | 1.919                       | 1.909                       | 1.923  |
| Al                             | 0.055  | 0.063               | 0.092  | 0.095                       | 0.164                       | 0.107  |
| Ti                             | 0.001  | 0.004               | 0.003  | 0.002                       | 0.001                       | 0.002  |
| Fe                             | 0.105  | 0.121               | 0.233  | 0.166                       | 0.179                       | 0.166  |
| Mg                             | 0.915  | 0.917               | 1.627  | 1.779                       | 1.702                       | 1.756  |
| Ca                             | 0.938  | 0.936               | 0.047  | 0.030                       | 0.024                       | 0.041  |
| Mn                             | 0.005  | 0.006               | 0.009  | 0.011                       | 0.003                       | 0.001  |
| Cr                             | 0.001  | 0.011               | 0.016  | 0.018                       | 0.016                       | 0.017  |
| Ni                             | 0      | 0                   | 0      | 0.002                       | 0                           | 0.001  |
| Na                             | 0.004  | 0.007               | 0      | 0.001                       | 0.001                       | 0.001  |
| %En                            | 46.6   | 46.3                | 84.9   | 89.6                        | 89.2                        | 89.4   |
| %Fs                            | 5.6    | 6.4                 | 12.6   | 8.9                         | 9.5                         | 8.5    |
| %Wo                            | 47.8   | 47.3                | 2.5    | 1.5                         | 1.3                         | 2.1    |

Tableau 3

| SAMPLES                        | TR 113 | TR 413<br>cumulates | TR 81 | TR 79<br>mantle peridotites | TR 423 |
|--------------------------------|--------|---------------------|-------|-----------------------------|--------|
| TiO <sub>2</sub>               | 0.68   | 0.40                | 0.21  | 0.18                        | 0.14   |
| Al <sub>2</sub> O <sub>3</sub> | 20.79  | 20.54               | 33.10 | 29.65                       | 33.46  |
| Cr <sub>2</sub> O <sub>3</sub> | 37.67  | 42.56               | 34.23 | 34.96                       | 33.50  |
| FeO*                           | 30.54  | 25.05               | 15.56 | 21.40                       | 17.93  |
| MnO                            | 0.24   | 0.66                | 0.20  | 0.28                        | 0.19   |
| MgO                            | 7.65   | 10.24               | 15.67 | 12.82                       | 14.49  |
| Sum                            | 97.57  | 99.45               | 98.97 | 99.29                       | 99.71  |
| Ti                             | 0.134  | 0.076               | 0.037 | 0.033                       | 0.025  |
| Al                             | 6.397  | 6.121               | 9.111 | 8.391                       | 9.210  |
| Cr                             | 7.772  | 8.505               | 6.318 | 6.634                       | 6.183  |
| Fe <sub>3</sub> +              | 1.564  | 1.222               | 0.497 | 0.910                       | 0.559  |
| Fe <sub>2</sub> +              | 5.030  | 4.075               | 2.542 | 3.387                       | 2.943  |
| Mn                             | 0.053  | 0.141               | 0.040 | 0.057                       | 0.038  |
| Mg                             | 2.977  | 3.860               | 5.455 | 4.588                       | 5.044  |
| Fe <sub>2</sub> O <sub>3</sub> | 7.96   | 6.42                | 2.83  | 5.04                        | 3.18   |
| FeO                            | 23.38  | 19.27               | 13.02 | 16.87                       | 15.07  |
| %Magnetite                     | 9.9    | 7.7                 | 3.1   | 5.7                         | 3.5    |
| %Hercynite                     | 40.7   | 38.6                | 57.2  | 52.7                        | 57.7   |
| %Chromite                      | 49.4   | 53.7                | 39.7  | 41.6                        | 38.8   |
| Cr"                            | 0.548  | 0.582               | 0.410 | 0.442                       | 0.402  |
| Mg"                            | 0.371  | 0.489               | 0.684 | 0.578                       | 0.634  |

Tableau 4

| SAMPLES                        | TR 79<br>mantle peridotites | TR 423 | TR 222 | TR 252 | TR 523<br>cumulates | TR 532 |
|--------------------------------|-----------------------------|--------|--------|--------|---------------------|--------|
| SiO <sub>2</sub>               | 41.59                       | 43.05  | 44.72  | 48.13  | 53.32               | 46.48  |
| TiO <sub>2</sub>               | 0.07                        | 0.03   | 0.09   | 0.16   | 0.52                | 0.92   |
| Al <sub>2</sub> O <sub>3</sub> | 2.16                        | 0.93   | 1.68   | 2.57   | 15.84               | 18.41  |
| Fe <sub>2</sub> O <sub>3</sub> | 8.10                        | 8.91   | 8.88   | 8.24   | 7.12                | 9.60   |
| MgO                            | 39.83                       | 43.29  | 25.75  | 22.30  | 7.90                | 7.42   |
| MnO                            | 0.13                        | 0.13   | 0.14   | 0.15   | 0.12                | 0.16   |
| CaO                            | 2.20                        | 0.60   | 11.93  | 15.14  | 9.90                | 13.06  |
| Na <sub>2</sub> O              | 0.05                        | 0.03   | 0.01   | 0.06   | 1.63                | 0.40   |
| K <sub>2</sub> O               | 0.06                        | 0.02   | 0.03   | 0.04   | 0.09                | 0.03   |
| I.L.                           | 4.44                        | 2.22   | 5.31   | 2.94   | 2.27                | 2.17   |
| Sum                            | 98.63                       | 99.21  | 98.54  | 99.73  | 98.73               | 98.65  |
| FeO*/MgO                       | 0.18                        | 0.19   | 0.31   | 0.33   | 0.81                | 1.16   |
| Cr                             | 2548                        | 2402   | 1819   | 1225   | 283                 | 51     |
| Ni                             | 2128                        | 1696   | 790    | 617    | 182                 | 75     |
| Y                              | n.d.                        | n.d.   | 12     | 10     | 18                  | 14     |
| Zr                             | n.d.                        | n.d.   | 7      | 11     | 39                  | 14     |
| Nb                             | n.d.                        | n.d.   | 3      | 2      | 3                   | 5      |
| Sr                             | 0.654                       | n.d.   | 2      | 13     | 48                  | 73     |
| Rb                             | 0.117                       | n.d.   | 16     | 11     | 4                   | 24     |
| V                              | 73                          | n.d.   | 204    | n.d.   | 173                 | 425    |

Tableau 5

| SAMPLES                        | PEGMA  | PEGMB  | TR 223 | TR 515 | TR 273 | TR 538 |
|--------------------------------|--------|--------|--------|--------|--------|--------|
| SiO <sub>2</sub>               | 48.09  | 47.74  | 43.81  | 51.77  | 51.98  | 49.79  |
| TiO <sub>2</sub>               | 0.13   | 0.39   | 0.13   | 0.10   | 0.24   | 0.24   |
| Al <sub>2</sub> O <sub>3</sub> | 18.24  | 19.91  | 19.64  | 16.48  | 4.26   | 11.38  |
| Fe <sub>2</sub> O <sub>3</sub> | 5.87   | 4.97   | 5.79   | 4.46   | 6.83   | 6.27   |
| MgO                            | 9.03   | 7.94   | 7.08   | 7.78   | 17.36  | 13.49  |
| MnO                            | 0.10   | 0.09   | 0.10   | 0.09   | 0.12   | 0.13   |
| CaO                            | 14.69  | 14.12  | 19.68  | 15.93  | 16.25  | 14.19  |
| Na <sub>2</sub> O              | 0.69   | 1.86   | 0.18   | 0.89   | 0.55   | 0.61   |
| K <sub>2</sub> O               | 0.02   | 0.03   | 0.05   | 0.05   | 0.06   | 0.06   |
| l.L.                           | 3.15   | 2.99   | 3.24   | 2.08   | 1.80   | 3.47   |
| Sum                            | 100.01 | 100.04 | 99.70  | 99.63  | 99.45  | 99.63  |
| FeO*/MgO                       | 0.59   | 0.56   | 0.74   | 0.52   | 0.35   | 0.42   |
| Cr                             | 84     | 47     | 181    | 138    | 1175   | 990    |
| Ni                             | 102    | 85     | 68     | 97     | 232    | 176    |
| Y                              | 5      | 11     | 6      | 4      | 8      | 9      |
| Zr                             | 9      | 15     | 11     | 9      | 12     | 10     |
| Nb                             | 0.5    | traces | 2      | 1      | 2      | 1      |
| Sr                             | 45     | 50.6   | 81     | 52     | 13     | 31     |
| Rb                             | 7      | 0.088  | 9      | 6      | 9      | 8      |
| V                              | n.d.   | n.d.   | 166    | 187    | 277    | 240    |
| La                             | 0.67   | 0.21   | n.d.   | n.d.   | n.d.   | n.d.   |
| Ce                             | 1.45   | 0.92   | n.d.   | n.d.   | n.d.   | n.d.   |
| Nd                             | 0.66   | 1.80   | n.d.   | n.d.   | n.d.   | n.d.   |
| Sm                             | 0.33   | 0.90   | n.d.   | n.d.   | n.d.   | n.d.   |
| Eu                             | 0.14   | 0.31   | n.d.   | n.d.   | n.d.   | n.d.   |
| Gd                             | 0.56   | 1.55   | n.d.   | n.d.   | n.d.   | n.d.   |
| Dy                             | 0.63   | 2.11   | n.d.   | n.d.   | n.d.   | n.d.   |
| Er                             | 0.41   | 1.43   | n.d.   | n.d.   | n.d.   | n.d.   |
| Yb                             | 0.35   | 1.47   | n.d.   | n.d.   | n.d.   | n.d.   |

Tableau 6

| SAMPLES                        | TR 109 | TR 70 | TR 74  | TR 368 |
|--------------------------------|--------|-------|--------|--------|
| SiO <sub>2</sub>               | 60.47  | 74.54 | 79.67  | 78.16  |
| TiO <sub>2</sub>               | 0.29   | 0.37  | 0.13   | 0.08   |
| Al <sub>2</sub> O <sub>3</sub> | 19.43  | 12.70 | 11.05  | 12.61  |
| Fe <sub>2</sub> O <sub>3</sub> | 1.30   | 2.70  | 0.50   | 0.45   |
| MgO                            | 1.20   | 0.56  | traces | 0.13   |
| MnO                            | 0.03   | 0.04  | 0.02   | traces |
| CaO                            | 3.63   | 3.78  | 2.24   | 0.28   |
| Na <sub>2</sub> O              | 11.54  | 3.15  | 4.57   | 7.21   |
| K <sub>2</sub> O               | 0.08   | 0.22  | 0.03   | 0.08   |
| I.L.                           | 0.80   | 0.98  | 0.52   | 0.31   |
| Sum                            | 98.77  | 99.04 | 98.73  | 99.31  |
| FeO*/MgO                       | 0.98   | 4.34  |        | 3.12   |
| Cr                             | <10    | <10   | <10    | 8      |
| Ni                             | 17     | 31    | 31     | 30     |
| Y                              | 36     | n.d.  | 15     | 23     |
| Zr                             | 176    | n.d.  | 112    | 55     |
| Nb                             | traces | n.d.  | 3      | 4      |
| Sr                             | 56     | 74    | 81     | 19     |
| Rb                             | <5     | <10   | traces | 1      |
| V                              | n.d.   | 39    | <10    | n.d.   |
| La                             | 8.22   | n.d.  | 10.19  | 6.98   |
| Ce                             | 23.85  | n.d.  | 24.21  | 18.85  |
| Nd                             | 15.18  | n.d.  | 10.26  | 9.14   |
| Sm                             | 3.74   | n.d.  | 2.45   | 2.81   |
| Eu                             | 0.36   | n.d.  | 0.45   | 0.08   |
| Gd                             | 3.83   | n.d.  | 2.66   | 3.16   |
| Dy                             | 4.44   | n.d.  | 2.34   | 3.84   |
| Er                             | 2.89   | n.d.  | 1.60   | 2.41   |
| Yb                             | 3.67   | n.d.  | 2.01   | 3.27   |

Tableau 7

|  | Parent magma<br>for the<br>Trinity ophiolite | Parent magma<br>for the<br>Semail ophiolite | DSDP sample<br>3-18-7-1 | Picritic<br>magma |
|--|--|---|-------------------------|-------------------|
| SiO <sub>2</sub>                                 | 49.80  | 51.10                                       | 49.70                   | 46.40             |
| TiO <sub>2</sub>                                 | 0.32   | 0.60  | 0.72                    | 2.00              |
| Al <sub>2</sub> O <sub>3</sub>                   | 13.40  | 16.60                                       | 16.40                   | 8.50              |
| FeO  | 6.30   | 7.20  | 7.90                    | 12.30             |
| MgO  | 13.40  | 9.20  | 10.10                   | 20.80             |
| MnO  | 0.12   | 0.12  | 0.12                    | n.d.              |
| CaO  | 12.50  | 12.80                                       | 13.10                   | 7.40              |
| Na <sub>2</sub> O                                | 1.50   | 2.30  | 1.98                    | 1.60              |
|  |  |   |                         |                   |
| Mg'  | 0.79   | 0.72  | 0.72                    | 0.77              |
| CaO/Al <sub>2</sub> O <sub>3</sub>               | 0.93   | 0.77  | 0.8                     | 0.87              |
| SiO <sub>2</sub> /Al <sub>2</sub> O <sub>3</sub> | 3.72   | 3.08  | 3.03                    | 5.46              |

Tableau 8



|                             | TR 368 | TR 109 | TR 74 |
|-----------------------------|--------|--------|-------|
|                             |        |        |       |
| Residual fraction of liquid | 19.3   | 12.7   | 13.5  |
| Composition of cumulate :   |        |        |       |
| Clinopyroxene %             | 4      | 35.5   | 64.8  |
| Amphibole %                 | 11.7   | 8.7    | 13.1  |
| Plagioclase %               | 84.2   | 55.8   | 22.1  |

Tableau 9

**CHEMICAL TRANSFER  
BETWEEN MANTLE XENOLITHS AND BASIC MAGMAS:  
EVIDENCE FROM OCEANIC MAGMA CHAMBERS.  
*THE TRINITY OPHIOLITE (NORTHERN CALIFORNIA).***

Christophe Lécuyer. Laboratoire de Géochimie isotopique. CAESS-CNRS, 35042 Rennes, France.

**Abstract:**

The Trinity ophiolite consists of small magma chambers intrusive into a large mantle body. Xenoliths of mantle peridotite occur both in gabbroic cumulates along the walls and in the matrices of ultrabasic breccias on the floors of the magma chambers. Field relationships and petrographic data suggest that fragments of original mantle peridotite were modified at the contact with basic magmas by modal metasomatism. Mineralogical assemblages were examined and quantitative elemental mass transfers were established on density and volume variations of reacting minerals. The chemical budget has revealed both closed and open system conditions for the major (Si, Al, Ti, Na, Ca, Fe and Mg) and trace elements (Cr, Ni). In the open system, material gains and losses provide information on the composition of the metasomatic fluid taking part in the reaction.

In a first stage, high - temperature reactions (925-600°C), 1) orthopyroxene - magnetite symplectite, 2) plagioclase - magnetite corona and 3) clinopyroxene + spinel I → pargasitic hornblende + spinel II) affect the mantle xenoliths and result from the interaction between mantle lherzolites in the solid state and basic magmas. Chemical interactions between the upper mantle and oceanic magma chambers occur as soon as the basic magmas ascend through the upper mantle. The chemically modified magmas, depleted in Ti, Fe and Na, within oceanic magma chambers could partly explain regional variations in the chemical composition of primary magmas produced beneath a slow-spreading ridge. The breakdown of olivine to orthopyroxene and magnetite participates to control the partition of magnetic Fe-Ti oxides between the oceanic crust and mantle.

In a second stage, the serpentinization of olivine and the production of talc which requires large amounts of H<sub>2</sub>O was superimposed on the first stage. The hydrothermal fluid, probably seawater, circulated in the brecciated area along the walls and the floors of magma chambers located at shallow depths. These structural discontinuities have thus played the role of channels favouring seawater circulation in the oceanic crust.

All the mineralogical reactions examined suggest significant elemental transfer by circulating fluids or infiltrating melts in open systems. The results of this study suggest that care must be exercised in the interpretation of mineralogical and chemical information provided by mantle xenoliths brought up to the surface by magmas.

**1) INTRODUCTION.**

Mantle xenoliths have been extensively studied in different eruptive rocks of various volcanic provinces (reviewed in Nixon, 1987). These xenoliths contribute to our understanding of the petrological and chemical interactions between crust and mantle. Metasomatism is widely documented in mantle xenoliths and is considered as a process responsible for generating particular geochemical characteristics in related magmas. In the context of metasomatism, many of the phenomena (such as modal metasomatism) described in mantle nodules appear to involve melt (or fluid derived from melt) infiltration.

Quantitative information, however, on the metasomatic "fluid" in the mantle or lower crust is poorly assessed from mantle xenoliths since:

- field relationships such as small-scale contact and intrusive features are not observed.
- the mineralogy and chemistry of a xenolith prior to a metasomatic event are generally difficult to establish and the contributions of original rock and metasomatic fluid to the chemical components of neofomed minerals are hard to define precisely.

The nature of mantle precursors to metasomatised mantle xenoliths may be inferred from the study of peculiar ophiolitic complexes in which the mantle-oceanic crust boundary is well documented. The Trinity ophiolite is a good example of a mantle diapir (The Trinity Peridotite; Quick, 1981) associated with small intrusive magma chambers (Cannat and Lécuyer, 1989). The geodynamical environment of the Trinity ophiolite has already been discussed by Lapierre et al. (1987) and Brouxel and Lapierre (1988) who suggest its formation in a marginal basin while Le Sueur et al. (1984), Boudier and Nicolas (1985/86) and Boudier et al. (1989) precise a slow-spreading environment. Previous work (Brouxel and Lapierre, 1988; Lécuyer et al., 1989) attests to a strong rock alteration by oceanic hydrothermal activity.

Xenoliths of mantle peridotite occur in the gabbroic cumulates along the walls in the matrices of ultrabasic breccias on the floors of the magma chambers. A direct comparison of bulk elemental abundances between mantle precursors and metasomatised rocks cannot be achieved because of the extreme variation within primary modal compositions (Hamlyn and Bonatti, 1980; Michael and Bonatti, 1985). The understanding of metasomatism is dependent on the knowledge of quantitative interaction between melts or fluids and their host rocks.

Mineralogical assemblages were examined and quantitative elemental mass transfers have been established on density and volume variations of reacting minerals. In summary, the aim of this paper is to examine the successive mineralogical reactions recorded by mantle xenoliths and to discuss:

- 1) the importance of metasomatism (interaction between rocks and basic melts) as a process responsible for generating geochemical variations in MOR magmas.
- 2) possible subsequent interaction between rock and circulating hydrothermal water (modified seawater) in the deep levels of the oceanic crust.

## **II) FIELD OBSERVATIONS.**

Two areas were selected for this study; the Toad Lake and Castle Lake magma chambers (Fig. 1). These magma chambers occur as pockets of gabbro intrusive into the surrounding mantle peridotites. The gabbro/peridotite contact is not significantly deformed and the internal succession of the gabbro section is not disrupted. A schematic view of these magma chambers is shown in Fig. 2 with the localization and description of their stratigraphic columns.

### **THE CASTLE LAKE MAGMA CHAMBER.**

The ultramafic tectonites are mostly represented by foliated harzburgites with discordant meter-sized dunite bodies. The contact with the basal breccia unit, roughly horizontal, is gradual and marked over a few meters by an increase in the density of gabbro dykes in the underlying mantle peridotite (Fig. 2).

The basal breccia unit of the Castle Lake magma chamber is >100m thick and consists of banded werhlites and pyroxene-rich gabbros (Fig. 2) containing ultrabasic xenoliths (lherzolites and plagioclase-lherzolites). The xenoliths vary in composition from dunites and harzburgites to werhlites and pyroxenites. The pyroxene-rich gabbros and werhlites are crosscut by dykelets, sills and leucocratic gabbros with pegmatitic patches.

The upper gabbroic unit consists of layered gabbros which range from 600 to 900m in thickness and are characterized by a strong layering. This layering is free of plastic deformation and is discordant to the gabbro layering of the basal unit (Fig. 2).

At the base of this unit, the layered gabbros are petrographically similar to those surrounding the ultrabasic fragments of the basal breccia unit. The lowermost 100m of this upper unit are composed of an alternation of leucocratic gabbros and pyroxene-rich gabbros including metamorphosed ultrabasic xenoliths similar to those present in the basal unit (Fig. 2). These previous levels are overlain by about 150m of layered leucocratic gabbros devoid of ultrabasic breccias and 100m of pyroxene-rich isotropic gabbros characterized by numerous pegmatitic patches. The top of the lithologic succession consists of layered gabbros containing dykelets and irregular masses of quartz diorites (Fig. 2).

### **THE TOAD LAKE MAGMA CHAMBER**

The ultramafic tectonites range in composition from dunites to lherzolites. The dunites constitute discordant horizontal pockets with respect to the spinel foliation (Fig. 2). These peridotites are crosscut by locally folded clinopyroxene-rich veinlets discordant to the spinel foliation, and by coarse gabbroic dykes.

Locally, the peridotites are impregnated by feldspathic lenses evolving towards veinlets, with anastomosing and cross-cutting patterns, and then by gabbroic dykes which fed the magma chamber.

The contact between the mantle unit and cumulate gabbros is generally undeformed, straight and parallel to the cumulate layering and is continuously underlined by a layer of several meters thickness of ultrabasic-basic breccias (Fig. 2). The vertical strike of diabase dykes crosscutting the magma chamber and the absence of tilting of the Trinity massif, especially in the Toad Lake area, suggest that this contact is a primary structural feature corresponding to one of the walls of the magma chamber.

This wall was characterized by active dynamic flows as illustrated by strong interbedded layers within these cumulate gabbros which usually contain ultrabasic xenoliths. Towards the center of the chamber, dominantly isotropic gabbros are intrusive into the layered gabbros and also contain ultrabasic xenoliths. All of the cumulate sequence is crosscut by subvertical microgabbros and diabase dykes with local, weakly deformed margins. This latter feature suggests that these dykes intruded the gabbros before they were totally consolidated (Fig. 2).

### III) PETROGRAPHY AND MINERALOGY

The chemical compositions of minerals have been carried out by electron microprobe analysis at the Service Commun d'Analyses of the University of Nancy I. Representative microprobe analysis of minerals from Castle Lake and Toad Lake areas are presented in Table 1 and Table 2. The amphibole names are following the classification of Leake (1978).

#### A) The mantle peridotites:

The mineral chemistry of the PI-harzburgites - harzburgites and the PI-lherzolites - lherzolites which constitute the Trinity Peridotite has been previously studied by Quick (1981) demonstrating a mantle origin. These ultramafic rocks preserve an excellent record of a complex mantle history that involved plastic deformation and partial melting.

Observed textures are porphyroclastic following the terminology of Mercier and Nicolas (1975). The size and shape of olivine grains (Fo<sub>90</sub> to Fo<sub>92</sub>; NiO from 0.2 to 0.45%) are highly variable (0.6-1mm). Larger grains are commonly elongated and contain regular kink-bands. Recrystallized olivines are fine-grained (0.1-0.3mm), strain-free, and constitute an equant mosaic texture.

Orthopyroxene porphyroclasts (Wo<sub>1-2</sub> En<sub>89-90</sub> Fs<sub>8-9</sub>; 1.5-2.5mm) often contain clinopyroxene exsolution lamellae. The elongated grains are kink-banded with slightly irregular grain boundaries. Most of the clinopyroxenes (Wo<sub>47</sub> En<sub>50</sub> Fs<sub>3</sub>) are small (<1mm), undeformed with xenomorphic grain boundaries.

Reddish-brown spinel (Magnetite<sub>2-6</sub> Hercynite<sub>52-60</sub> Chromite<sub>35-44</sub>; 0.4-0.6mm) are anhedral, elongated, and mark a lineation interpreted as flow direction during the peridotite deformation (Le Sueur et al., 1984).

#### B) Castle Lake: the ultrabasic breccias of the basal unit.

The xenoliths are metamorphosed mantle lherzolites characterized by various degrees of olivine serpentinization, chromian spinel, brown hornblende and the replacement of orthopyroxene by bastite and talc.

Olivine (0.15-0.8mm) is characterized by high NiO (up to 0.42%) and Fo (Fo<sub>86-89</sub>) contents (Table 1). A less magnesian olivine (Fo<sub>80</sub>) may be intimately associated with orthopyroxene and talc (Fig. 3a; Table 1). The serpentine which replaces olivine is characterized by high NiO contents (0.14-0.37%; Table 1).

Orthopyroxene (1.25mm length by 0.6mm width) is pseudomorphed by a Cr<sub>2</sub>O<sub>3</sub> rich-bastite (0.52-0.59%; Table 1). Some magnesian (MgO=29.7-31.8%) and chromiferous (Cr<sub>2</sub>O<sub>3</sub>=0.29-0.53%; Table 1) talc is also present as a replacement of orthopyroxene and occurs as patches within the crystal.

The Cr-spinels (0.3mm) show strong chemical variations within a given sample, particularly in hercynite and spinel components (Table 1). Cr-spinels intimately associated with hornblende (Fig.3b) are characterized by the lowest Al<sub>2</sub>O<sub>3</sub> (10.5%) and MgO (1.9%) contents which contrast with their rather high FeO (48.4%) and TiO<sub>2</sub> (1.15%) contents.

The poikilitic brown hornblende in replacement of clinopyroxene (0.6mm length by 0.3mm width), which usually contains little euhedral olivine inclusions, is a pargasitic hornblende (Table 1).

The matrix is heterogeneous in composition and is made up of metamorphosed clinopyroxenites with two generations of amphibole which, respectively, are poikilitic magnesio-hornblendes and actinolitic hornblendes. These clinopyroxenites contain centimetric ultrabasic xenoliths which are ancient tectonite dunites with high-magnesian olivine (MgO=46.9-49.8%) and high NiO contents (NiO=0.35-0.48%).

The matrix may be also gabbroic with poikilitic amphiboles and scarce cumulus plagioclase relicts (An<sub>91.4-95.1</sub>).

#### C) Toad Lake: the layered cumulates and their xenoliths.

The layered cumulates of the Toad Lake magma chamber are ilmenite-rich gabbronorites with mesocumulate to orthocumulate textures. The well developed magmatic layering is defined by mineralogical changes and granulometric contacts. Generally, the coarse-grained layers have plagioclase (altered into epidote or albite) dominant proportions. The pyroxenes are generally fresh, although orthopyroxene may be altered to chlorite and clinopyroxene to actinolite. These gabbronorites are characterized by early plagioclase cumulus followed by clinopyroxene, orthopyroxene and finally interstitial ilmenite. The pyroxenes have high Fs contents (Cpx=Fs<sub>13.4-13.6</sub>; Opx=Fs<sub>29.8-31.9</sub>; Table 2) rather contrasting with those from fresh mantle peridotites. The gabbronorites located near the walls of the magma chamber are rich in millimetric to centimetric xenoliths of mantle peridotite (Fig. 4a). The cores of the largest

xenoliths often show textural and mineralogical features characteristic of mantle lherzolites: they contain Cr-spinel (0.3-0.4mm), kink-banded grains (0.5-1mm) and unstrained neoblasts (0.2-0.5mm) of olivine, kink-banded orthopyroxene porphyroclasts (2-3mm in length; Fig. 4b) with exsolution lamellae of clinopyroxene (up to 15µm), aggregates of subhedral clinopyroxene and plagioclase lenses altered to epidote (50µm). The small xenoliths (mm-sized) and the rims of the largest xenoliths develop orthopyroxene-magnetite symplectites and magnetite-plagioclase coronas.

The symplectite consists of an association of magnetite and orthopyroxene as a replacement of olivine (Fo76-78; Table 2). Two textural varieties are present with the first one consisting of numerous fine platelets and vermicules of magnetite (3 to 30µm) in subparallel sets enclosed in orthopyroxene (Fig. 4c). The second one consists of polygonal orthopyroxene grains (0.1-0.3mm) and interstitial granular magnetite (30µm to 0.25mm) in partial or complete replacement of olivine (Fig. 4d).

Orthopyroxene is characterized by high Fs (Fs19.9-23.5) and low Cr<sub>2</sub>O<sub>3</sub> contents (0-0.1%) while the magnetite has TiO<sub>2</sub> contents ranging from 0.3 to 2% and Cr<sub>2</sub>O<sub>3</sub> from 1.79 to 2.76% (Table 2). The chemical compositions of olivine, orthopyroxene and spinel show wide variations from the rim to the core of the centimetric mantle xenoliths. The TiO<sub>2</sub>, Fe<sub>2</sub>O<sub>3</sub> and Al<sub>2</sub>O<sub>3</sub> contents lie between two poles corresponding to host cumulate and peridotite mineral compositions (Fig. 5).

The local development of a plagioclase-magnetite reaction corresponds with the presence of a brown hornblende zone (coronas=25-40µm in width; Table 2) including micrometric spinels in replacement of an An-rich plagioclase (An<sub>89.6-94.4</sub>; Table 2) when this latter is rimmed by magnetite (Fig. 4e). This magnesio-hornblende shows high TiO<sub>2</sub> (1-1.4%) and Na<sub>2</sub>O (1.5-1.7%) contents. This mineralogical reaction succeeds to the orthopyroxene-magnetite symplectite.

#### IV) Mineralogical reactions - elemental mass transfers.

Field relationships and petrographic data suggest that fragments of original mantle peridotites were modified by contact with basic magmas by a process called "modal metasomatism" (Harte, 1983). In modal metasomatism, changes in bulk chemistry are associated with the modification in modal mineralogy. Many cases of this type of metasomatism seen in mantle xenoliths appear to result from the presence of melt or fluid (Harte, 1987). In an attempt to characterize these fluids and their participation in the neoformed minerals, amounts of material lost or gained during the mineralogical reactions were calculated by the following method.

##### A) Method.

The gains and losses of chemical elements by weight related to mineralogical reactions require the knowledge of the chemical compositions and densities of reactants and the global volume change (Gresens, 1967).

For a mineralogical reaction in which the amount a of mineral source A gives an amount b of produced mineral B with a total amount X of material subtracted from or added to A, Gresens (1967) has formulated a set of equations characteristic of composition-volume relationships involving mineral chemistry, specific gravities and volume factors {1}.

$$\{1\} 100(fv.(gB/gA).cnB-cnA) = xn.$$

*fv* is defined as the volume factor, when *fv*=1, replacement is volume for volume. The specific gravities of minerals A and B are designated by *gA* and *gB*.

*cnA* and *cnB* are the weight fractions of component *n* for each mineral and *xn* is the amount of material lost or gained.

Generally, if *N* minerals participate in the reaction, *N*-1 assumptions or additional data are necessary to solve the problem (Gresens, 1967). For equation {1}, it is necessary to assume that either the reaction is isovolumetric (*fv*=1) or that one component is immobile (more exactly dispatched between the two reacting minerals in a closed system). The choice of one of these assumptions may be inferred from the textural relationships in thin sections (for example, *fv*=1 when the replacement is pseudomorphic) or by the knowledge of the chemical behavior of a component (for example, Al is considered to be relatively immobile during most alteration processes).

In the following discussion, the amount of primary minerals is fixed at 100g by the use of weight mineral analyses. The specific gravities of minerals are those given by Deer et al. (1966).

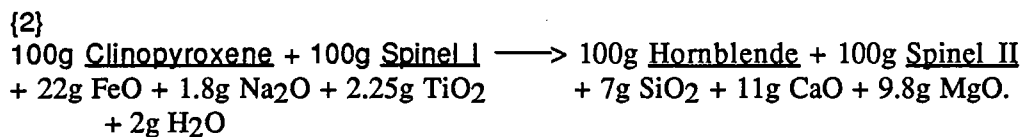
## B) Results and discussion.

### CASTLE LAKE

#### 1) Origin of the pargasitic hornblende.

The low Si and high (AlIV + Na + K)<sub>A</sub> contents of the pargasitic hornblende (Table 1) are consistent with crystallization at magmatic temperatures (Spear, 1981). The high Cr<sub>2</sub>O<sub>3</sub> contents and close association with Cr-spinel also corresponds to a high temperature reaction (T=925°C; Spear, 1981; Fig. 6) involving clinopyroxene and spinel in the presence of a fluid phase.

The pseudomorphic replacement of clinopyroxene by the pargasitic hornblende and the negligible differences between the densities of these two minerals allows the following reaction to be written:

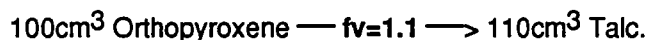


In such a reaction, Al<sub>2</sub>O<sub>3</sub>, Cr<sub>2</sub>O<sub>3</sub> and NiO are redistributed between the minerals in a closed system while a low hydration accompanies gains of Na<sub>2</sub>O, TiO<sub>2</sub> and FeO and losses of MgO, SiO<sub>2</sub> and CaO.

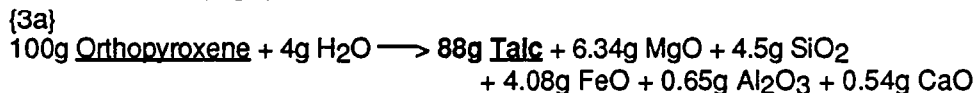
#### 2) Mineralogical reactions destroying orthopyroxene: production of talc and secondary olivine.

##### a) talc production:

Considering this reaction, Cr (high and constant values; Table 1) may be considered as an immobile component:

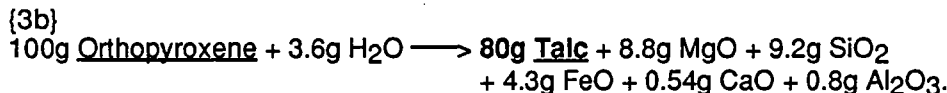


Then:



T=800°C (Hemley et al., 1977a; Fig. 6).

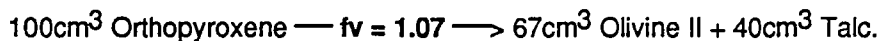
The formation of talc involves hydration of orthopyroxene with a volume increase and significant losses in MgO, FeO and SiO<sub>2</sub>. We can compare the results of this reaction {3a} with those of the same reaction considered as isovolumetric:



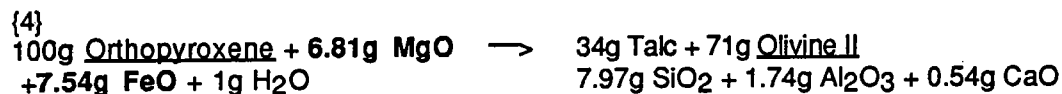
The isovolumetric assumption implies a reduced proportion of talc which is balanced by a more important release of SiO<sub>2</sub> and MgO. Taking into account the volume change {3a}, the final proportions of secondary minerals and elemental mass transfers are obviously different and must be considered in the aim to quantify more realistic elemental transfers for mineralogical reactions involving high hydration rates.

##### b) Production of secondary olivine.

Reaction {3a}, involving orthopyroxene at T = 725°C (Hemley et al., 1977a; Fig. 6) leads to the formation of talc and a secondary magnesian olivine.



Then:



This reaction is able to balance the FeO and MgO productions of the previous reaction {3a} to form secondary Fe-enriched olivine at lower temperatures. Both of these reactions are characterized by large losses in SiO<sub>2</sub>.

### 3) Serpentinization of olivine.

#### a) the example of Mg-olivine.

The chemical transition between olivine and its alteration product, serpentine, shows the progressive leaching of FeO, MgO and NiO with increasing serpentinization of olivine while SiO<sub>2</sub> remains constant (Fig. 7):

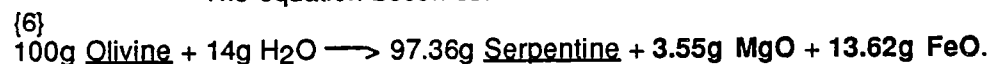


At T = 450°C (Hemley et al., 1977b; Fig. 6).

The serpentinization of olivine is characterized by a strong volume increase and important losses of MgO and FeO.

#### b) The example of a ferriferous olivine: serpentinization of secondary olivine.

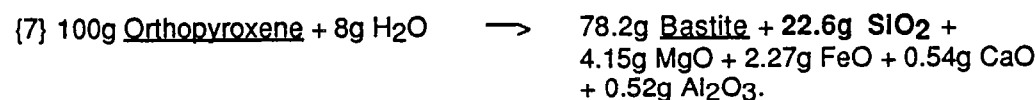
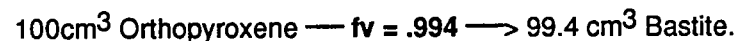
The equation becomes:



The serpentinization of either Mg- or Fe-olivine is characterized by a common rate of hydration and by the strong increase of the FeO / MgO weight ratio ranging from 0.55 to 3.84 which rather contrasts with the primary FeO / MgO weight ratio of olivine which only varies from 0.21 to 0.44. During the serpentinization of olivine, FeO is more mobile than MgO and forms magnetite.

### 4) Serpentinization of orthopyroxene.

Cr may again be considered as an immobile component during the replacement of orthopyroxene by bastite. The equation is reduced to:



The serpentinization of olivine and orthopyroxene is thus correlated with different levels of hydration. In contrast to the volume increase of 26% during olivine alteration, the production of bastite corresponds to an isovolumetric reaction which agrees with the petrographic evidence for pseudomorphic replacement. Furthermore, the serpentinization of orthopyroxene induces an important SiO<sub>2</sub> loss which is a typical feature of pyroxene or pyroxenite alteration (Gresens, 1967).

These mineralogical reactions are restricted to the ultrabasic breccia zone while the surrounding mantle peridotites are relatively fresh. They have also been recognized in the abyssal peridotites of the Islas Orcadas Fracture Zone (Dick, 1979; Kimball et al., 1985) and of the Mid-Atlantic Ridge near 45°N (Aumento



and Loubat, 1971). It was suggested by the above authors that these high-temperature alteration processes may reflect seawater circulation into the upper mantle.

Sr isotopic data from a continuous section of gabbroic cumulates within a magma chamber adjacent to Castle Lake has revealed that seawater has reached the deep cumulate layers (Lécuyer et al., 1989). If the contributions of magmatic water and/or meteoric water are not to exclude in the development of serpentine, the presence of dominantly modified seawater is more possible. Oxygen and hydrogen isotope studies on serpentinized ultramafic rocks are currently in progress to test the possible sources of water. Modified seawater probably circulated in the brecciated area along the walls and the floor of magma chambers located at shallow levels (Cannat and Lécuyer, 1989). These structural discontinuities have played the role of channels favouring seawater circulation in the oceanic crust. These data confirm the results of Brikowski and Norton (1989) who highlight the role of magma chamber geometry on the control of seawater circulation through the oceanic crust.

The high-temperature reaction which produces pargasitic hornblende is probably the result of the addition of  $\text{Na}_2\text{O}$ ,  $\text{TiO}_2$  and  $\text{FeO}$  to the mantle xenoliths from an infiltrating melt. This mineralogical reaction represents the interaction of mantle lherzolites in the solid state with basic magmas which fed the magma chambers. Such kinds of interaction are best documented in the Toad Lake example.

## TOAD LAKE

Cr-spinels are typical of oceanic mantle xenoliths and are recognized as good indicators of  $f\text{O}_2$  (Maurel and Maurel, 1984; Murck and Campbell, 1986).

Experimental studies have emphasized the relationships between the  $\text{Fe}_2\text{O}_3$  contents of spinels,  $f\text{O}_2$ , temperature and the  $\text{FeO}$  content of silicate melts (Maurel and Maurel, 1984):

$$\{8\} \frac{(\text{Fe}_2\text{O}_3)_{\text{spinel}} = (0.0045 \cdot 10^{4813/T} \cdot (\text{FeO})_{\text{total(liquid)}})}{1 + 562 \cdot (f\text{O}_2 - 0.2185) \cdot 10^{-5502/T}}$$

For the mantle xenoliths of the Toad Lake complex, the  $\text{Fe}_2\text{O}_3$  contents of spinels have been calculated from electron microprobe analyses assuming stoichiometric formulae. The spinels reveal a high  $f\text{O}_2$  ( $\log f\text{O}_2 = -5$ ) with about  $\text{FeO} = 8\%$  and  $\text{Fe}_2\text{O}_3 = 4\%$  in the silicate melt ( $\text{Fe}^{3+}/\text{Fe}_{\text{total}} = 0.5$ ). The development of orthopyroxene-magnetite symplectites may result from the progressive breakdown of olivine at high  $f\text{O}_2$  and  $\text{Fe}_2\text{O}_3$  contents in the magma.

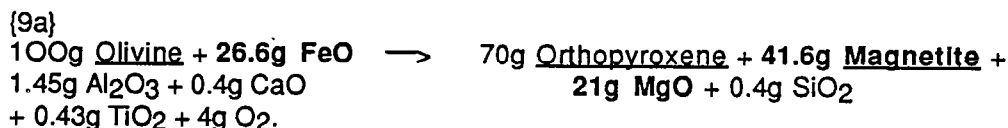
### 5) Orthopyroxene-magnetite symplectite .

a) first assumption: isovolumetric reaction.

The volume proportions of orthopyroxene and magnetite have been measured by point counting (1400 points) on a xenolith in which the reaction may be considered as complete (no relicts of olivine). The selected counting area was devoid of primary orthopyroxene porphyroclasts and amphibole corona.



Then:



The chemical balance confirms the presence of an iron-rich fluid which also contained  $\text{Al}_2\text{O}_3$ ,  $\text{TiO}_2$  and  $\text{CaO}$ . It also reveals an important release of  $\text{MgO}$  whereas  $\text{SiO}_2$  remains relatively immobile which is in agreement with the previous work of Lamoen (1979). However, some authors (Goode, 1974; Lamoen, 1979) consider that the  $\text{FeO}$  released in the breakdown of olivine contributes to the ferrosilite component of orthopyroxene and results in the formation of magnetite. It is thus necessary to compare these results with those obtained from an equation constrained by the mass-balance conservation of  $\text{SiO}_2$  and  $\text{FeO}$ .

b) second assumption: conservation of Fe and Si.

In this case, the volume factor of the reaction becomes different:



Then:

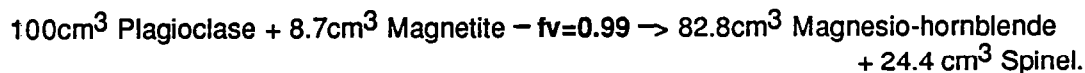


This new reaction requires a lower  $f\text{O}_2$  than the previous one to produce similar amounts of orthopyroxene and MgO. In contrast, lesser amount of magnetite is produced which is at variance with the modal proportion measured by point counting after corrections of mineral specific gravities. In addition, a volume change during the reaction disagrees with the microscopic observation that primary polygonal structures of olivine are mimicked by orthopyroxene.

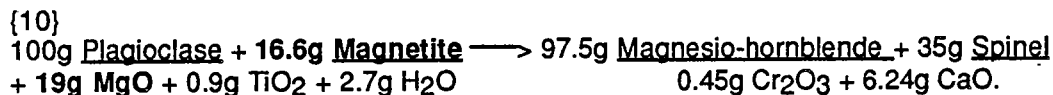
Thus, the orthopyroxene-magnetite symplectite association may result from an isovolumetric reaction controlled by high  $f\text{O}_2$  and the presence of an iron-rich magmatic fluid (Johnson and Stout, 1984) according to the chemistry of the Cr-spinels. The formation of the symplectite is not only the result of the oxidization of olivine in a closed system but rather is an open-system reaction (Ambler and Ashley, 1977) taking place in an iron-rich basic magma.

#### 6) The Plagioclase-Magnetite corona.

Plagioclase (An<sub>99.6-94.4</sub>) has reacted with magnetite to produce fine coronas of magnesio-hornblende containing inclusions of spinel. The restricted mobility of Si and Al deduced from the diffusion models for corona formation (Grant, 1988) lead us to assume that the total amounts of Si and Al are provided by the plagioclase and Fe by the magnetite to form both the magnesio-hornblende and the spinel.



equivalent to:



The plagioclase-magnetite corona reaction is characterized by a negligible volume variation, a gain of  $\text{TiO}_2$ , a loss of  $\text{CaO}$  and the destruction of the magnetite produced by the previous breakdown of olivine {9a}. The total amount of MgO released by reaction {9a} is used to form the magnesio-hornblende.

The presence of scarce Ilmenite-Magnetite pairs in equilibrium yields the temperatures of last chemical equilibrium (Buddington and Lindsley, 1964); they range from 600°C to 400°C which corresponds to the stability field of the magnesio-hornblende produced by the previous reaction involving magnetite and plagioclase. The early cumulus plagioclase has crystallized at a temperature of around 1000°C (Kudo and Weill, 1971).

The breakdown of olivine to form orthopyroxene and magnetite participates to control the partition of magnetic Fe-Ti oxides between the crust and mantle. Mantle peridotites contain primary Cr-Al spinels which are non-magnetic at mantle pressures and temperatures (Wasilewski et al., 1979; Wasilewski and Mayhew, 1982). However, field relationships show a transition zone of ultrabasic breccias at the oceanic crust-mantle boundary where mantle xenoliths react at high temperature with basic magmas to form magnetite-orthopyroxene symplectites. The magnetic character across the oceanic crust-mantle boundary may be considered as a complex transition zone most likely resulting from the mixture of mantle rocks and cumulate layers (Wasilewski, 1987).

According to numerous works (Wilshire and Trask, 1971; Lloyd and Bailey, 1975; Harte et al., 1975; Francis, 1976; Wass et al., 1980; Wilshire et al., 1980) concerning the modal metasomatism which affects the mantle nodules and demonstrate an origin by replacement of pre-existing rock, the development of

pargasitic hornblende and oxides rich in Fe-Ti is commonly observed. Similarly, Ti, Na, Fe and H<sub>2</sub>O are added to the modal metasomatised rocks. Gurney and Harte (1980) have shown that the chemical composition of many mantle nodules have been affected by metasomatism at the contact of intrusions. Consequently, the data and results collected from this study provide evidences for a metasomatic signature overprinted on depleted compositions. They suggest that the interpretation of chemistry given by mantle xenoliths is difficult knowing that they have studied intensively for clues to the evolution of the mantle.

The orthopyroxene-magnetite symplectite has also been observed along gabbroic dyke margins crosscutting the Trinity mantle peridotites. These dykes have been interpreted as the magma conduits to the overlying chamber (Cannat and Lécuyer, 1989). These mineralogical reactions which take place in chemically open system conditions reveal that chemical interactions between mantle rocks and basic melts occur as soon as they ascend through the upper mantle. The chemically modified magmas within oceanic magma chambers could partly explain regional variations in the chemical composition of primary magmas.

## V) CONCLUSION.

The presence of mantle xenoliths in oceanic magma chambers of the Trinity ophiolite yields to distinguish two stages of mineralogical reactions.

In a first stage, high - temperature reactions (T from 925 to 600°C) 1) *orthopyroxene - magnetite symplectite* 2) *plagioclase - magnetite corona* and 3) *clinopyroxene + spinel I -> pargasitic hornblende + spinel II*) affect the mantle xenoliths from both the Toad Lake and Castle Lake chambers and result from the interaction between mantle lherzolites in the solid state and basic magmas. These magmas are characterized by high Fe<sub>2</sub>O<sub>3</sub> contents and fO<sub>2</sub> as revealed by the chemistry of spinels. Chemical interactions between the upper mantle and oceanic magma chambers occur as basaltic melts ascend through the upper mantle and feed the magma chambers. These primary melts are thus depleted in Ti, Fe and Na. Such chemical modifications of magmas within the oceanic crust could partly explain regional variations in the chemical composition of primary magmas related to a peculiar geotectonic environment (slow-spreading ridge).

In a second stage, serpentinization of olivine and production of talc which require high amounts of H<sub>2</sub>O was superimposed on the first stage. Seawater has probably circulated in the brecciated area along the walls and the floors of chambers located at shallow depths. These structural discontinuities have played the role of channels favouring seawater circulation in the oceanic crust. It appears thus that the geometry of magma chambers partly control seawater circulation in the oceanic crust. The contributions of meteoric water and/or magmatic water are not to exclude in the development serpentine during the genesis and after the obduction of the ophiolitic complex.

All the mineralogical reactions reviewed in this paper suggest significant elemental transfers in open system supported by infiltrating melts or circulating fluids. Consequently, these results suggest that care must be exercised in the interpretation of mineralogical and chemical informations provided by mantle xenoliths brought up towards the surface by magmas.

## REFERENCES

- Ambler, E.P. and Ashley, P.M., 1977. Vermicular orthopyroxene-magnetite symplectites from the Wateranga layered mafic intrusion, Queensland, Australia. *Lithos*, 10 : 163-172.
- Aumento, F. and Loubat, H., 1971. The Mid-Atlantic Ridge near 45°N XVI. Serpentinized ultramafic intrusions. *Can. J. Earth Sci.*, 8 : 631-663.
- Boudier, F. and Nicolas, A., 1985/86. Harzburgite and lherzolite subtypes in ophiolite and oceanic environments. *Earth Planet. Sci. Lett.*, 76 : 84-92.
- Boudier, F., Le Sueur, F. and Nicolas, A., 1989. Structure of an atypical ophiolite: The Trinity complex, eastern Klamath Mountains, California. *Geol. Soc. Am. Bull.*, 101 : 820-833.
- Brikowski, T. and Norton, D., 1989. Influence of magma chamber geometry on hydrothermal activity at mid-ocean ridges. *Earth Planet. Sci. Lett.*, 93 : 241-255.
- Brouxel, M. and Lapierre, H., 1988. Geochemical study of an early Paleozoic island arc - back arc basin system. Part I : The Trinity ophiolite (Northern California). *Geol. Soc. Am. Bull.*, 100 : 1111-1119.

- Buddington, A. F. and Lindsley, D. H., 1964. Iron-titanium oxide minerals and synthetic equivalents. *J. Petrol.*, 5 : 310-357.
- Cannat, M. and Lécuyer, C., 1989. Ephemeral magma chambers in the Trinity peridotite, Northern California. Submitted to *Tectonophysics*.
- Deer, W.A., Howie, R.A. and Zussman, J., 1966. An introduction to the rock forming minerals. Longman, London, 528 pp.
- Dick, H.J.B., 1979. Alteration and metamorphism of peridotite at Islas Orcadas Fracture Zone (abstract). *EOS Trans. Am. Geophys. Un.*, 60 : 973.
- Francis, D. M., 1976. Amphibole pyroxenite xenoliths: cumulate or replacement phenomena from the upper mantle, Nunivak Island, Alaska. *Contrib. Mineral. Petrol.*, 58 : 51-61.
- Goode, A.D.T., 1974. Oxidation of natural olivines. *Nature*, 248 : 500-501.
- Grant, S.M., 1988. Diffusion models for corona formation in metagabbros from the Western Grenville Province, Canada. *Contrib. Mineral. Petrol.*, 98 : 49-63.
- Gresens, R.L., 1967. Composition-volume relationships of metasomatism. *Chem. Geol.*, 2 : 47-65.
- Gurney, J. J. and Harte, B., 1980. Chemical variations in upper mantle nodules from southern African Kimberlites. *Phil. Trans. Roy. Soc. Lond.*, A297 : 273-293.
- Hamlyn, P. R. and Bonatti, E., 1980. Petrology of mantle-derived ultramafics from the Owen fracture zone, northwest Indian Ocean : implications for the nature of the oceanic upper mantle. *Earth Planet. Sci. Lett.*, 48 : 65-79.
- Harte, B., 1983. Mantle peridotites and processes<sup>2</sup> the kimberlite sample. In: Hawkesworth and Norry (Editors), pp. 46-91.
- Harte, B., 1987. Metasomatic events recorded in mantle xenoliths: an overview. In: P.H. Nixon (Editor), *Mantle xenoliths*. John Wiley & Sons Ltd, pp. 836.
- Harte, B., Cox, K. G. and Gurney, J. J., 1975. Petrography and geological history of upper mantle xenoliths from the Matsoku kimberlite pipe. *Phys. Chem. Earth*, 9 : 447-506.
- Hemley, J.J., Montoya, J.W., Christ, C.L. and Hostetler, P.B., 1977a. Mineral equilibria in the MgO-SiO<sub>2</sub>-H<sub>2</sub>O system : I. Talc-chrysotile-forsterite-brucite stability relations. *Am. J. Sci.*, 277 : 322-335.
- Hemley, J.J., Montoya, J.W., Shaw, D.R. and Luce, R.W., 1977b. Mineral equilibria in the MgO-SiO<sub>2</sub>-H<sub>2</sub>O system : II. Talc-antigorite-forsterite-anthophyllite-enstatite stability relations and some geologic implications in the system. *Am. J. Sci.*, 277 : 353-383.
- Johnston, A.D. and Stout, J.H., 1984. Development of orthopyroxene-Fe/Mg ferrite symplectites by continuous olivine oxidation. *Contrib. Mineral. Petrol.*, 88 : 196-202.
- Kimball, K.L., Spear, F.S. and Dick, H.J.B., 1985. High temperature alteration of abyssal ultramafics from the Islas Orcadas Fracture Zone, South Atlantic. *Contrib. Mineral. Petrol.*, 91 : 307-320.
- Kudo, A. M. and Weill, D.F., 1970. An igneous plagioclase thermometer. *Contrib. Mineral. Petrol.*, 25 : 52-65.
- Lamoén van, H., 1979. Coronas in olivine gabbros and iron ores from Susimäki and Riuttamaa, Finland. *Contrib. Mineral. Petrol.*, 68 : 259-268.
- Lapierre, H., Brouxel, M., Albarède, F., Coulon, C., Lécuyer, C., Martin, P., Mascié, G. and Rouer, O., 1987. Paleozoic and Lower Mesozoic magmas from the eastern Klamath Mountains (North California) and the geodynamic evolution of northwestern America. *Tectonophysics*, 140 : 155-177.

- Leake, B.E., 1978. Nomenclature of amphiboles. *Am. Mineral.*, 63 : 1023-1059.
- Lécuyer, C., Brouxel, M. and Albarède, F., 1989. Elemental fluxes during the hydrothermal alteration of the Trinity ophiolite (California) by seawater. Submitted to *Chem. Geol.*
- Le Sueur, E., Boudier, F., Cannat, M., Ceuleneer, G. and Nicolas, A., 1984. The Trinity mafic-ultramafic complex : first results of the structural study of an untypical ophiolite. *Ophioliti*, 9 : 487-498.
- Lloyd, F. E. and Bailey, D. K., 1975. Light element metasomatism of the continental mantle: the evidence and the consequences. *Phys. Chem. Earth*, 9 : 389-416.
- Maurel, C. and Maurel, P., 1984. Etude expérimentale de la distribution du fer ferrique entre spinelle chromifère et bain silicaté basique. *Bull. Minéral.*, 107 : 25-33.
- Mercier, J.C. and Nicolas, A., 1975. Textures and fabrics of upper mantle peridotites as illustrated by basalt xenoliths. *J. Petrol.*, 16 : 454-487
- Michael, P. J. and Bonatti, E., 1985. Peridotite composition from the North Atlantic : regional and tectonic variations and implications for partial melting. *Earth Planet. Sci. Lett.*, 73 : 91-104.
- Murck, B.W. and Campbell, I.H., 1986. The effects of temperature, oxygen fugacity and melt composition on the behaviour of chromium in basic and ultrabasic melts. *Geochim. Cosmochim. Acta*, 50 : 1871-1887.
- Nixon, P. H., 1987. Mantle xenoliths. In: P.H. Nixon (Editor), John Wiley & Sons Ltd, pp. 836.
- Quick, J.E., 1981. Petrology and petrogenesis of the Trinity peridotite, an upper mantle diapir in the eastern Klamath Mountains, northern California. *J. Geophys. Res.*, 87 : 3831-3848.
- Spear, F.S., 1981. An experimental study of hornblende stability and compositional variability in amphibolite. *Am. J. Sci.*, 281 : 697-734.
- Wass, S. Y., Henderson, P. and Elliott, C. J., 1980. Chemical heterogeneity and metasomatism in the upper mantle: evidence from rare earth and other elements in apatite-rich xenoliths in basaltic rocks from eastern Australia. *Phil. Trans. Roy. Soc. Lond.*, A297 : 333-346.
- Wasilewski, P. J., 1987. Magnetic properties of mantle xenoliths and the magnetic character of the crust-mantle boundary. In: P.H. Nixon (Editor), *Mantle xenoliths*. John Wiley & Sons Ltd, pp. 836.
- Wasilewski, P. J., Thomas, H. H. and Mayhew, M. A., 1979. The Moho as a magnetic boundary. *Geophys. Res. Lett.*, 6 : 541-544.
- Wasilewski, P. and Mayhew, M. A., 1982. Crustal xenolith magnetic properties and long wavelength anomaly source requirements. *Geophys. Res. Lett.*, 9 : 329-332.
- Wilshire, H. G. and Trask, N. J., 1971. Structural and textural relationships of amphibole and phlogopite in peridotite inclusions, Dish Hill, California. *Am. Mineral.*, 56 : 240-255.
- Wilshire, H. G., Pike, J. E. N., Meyer, C. E. and Schwarzmann, E. C., 1980. Amphibole-rich veins in ilherzolite xenoliths, Dish Hill and Deadman Lake, California. *Am. J. Sci.*, 280A : 576-593.

#### FIGURE CAPTIONS

- Figure 1: Simplified geological map of the eastern Klamath Mountains, modified after Strand (1962,1963), Irwin (1977) and Wagner and Saucedo (1986).  
 1: sheeted dykes, gabbros and pillow lavas of the Trinity ophiolite; 2: mesozoic granites; 3: Trinity Peridotite; 4: Paleozoic volcano-sedimentary formations; 5: central metamorphic belt; CMBT: central metamorphic belt thrust; 6: occidental Paleozoic and Mesozoic belt.

Figure 2: Schematic diagram showing the Trinity magma chambers intrusive in the mantle peridotites with the localization and description of the stratigraphic columns of the Castle Lake and Toad Lake areas.

Figure 3: Transmitted light microphotographs of mantle xenoliths from Castle Lake (100X).

3a: talc (1) and secondary olivine (2) replacing orthopyroxene (3).

3b: secondary spinel (1) associated with pargasitic hornblende (2). (3) is a primary cumulus olivine.

Figure 4: Transmitted light microphotographs of mantle xenoliths from Toad Lake (100X).

4a: lherzolitic mantle xenoliths (1) within a layered gabbro-norite cumulate (2).

4b: (1) kink-banded orthopyroxene in the mantle xenolith core.

4c: olivine (1) and orthopyroxene (2) enclosing subparallel sets of numerous fine platelets and vermicules of magnetite.

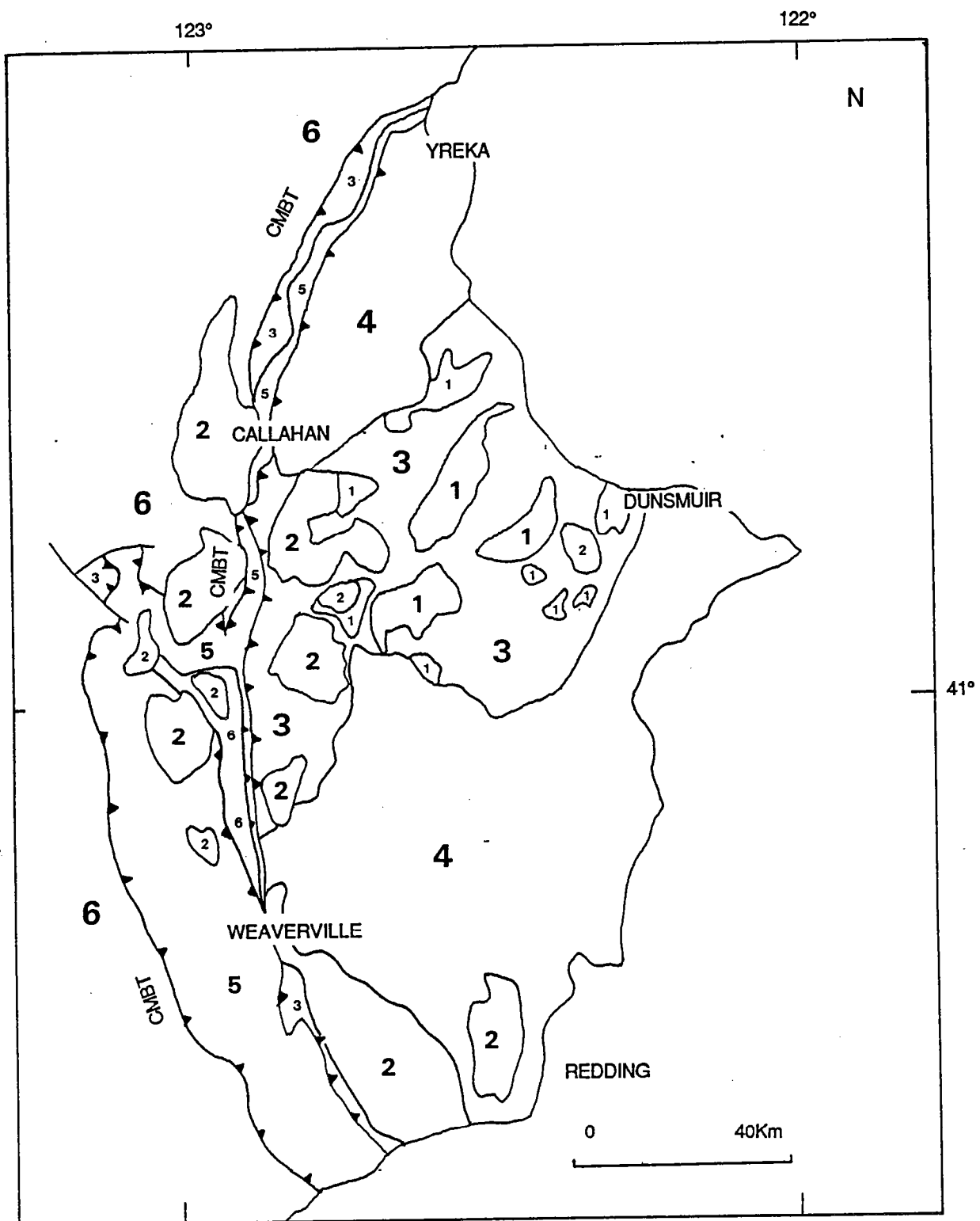
4d: intergranular magnetite (1) and polygonal orthopyroxene grains (2) in partial or complete replacement of olivine (3).

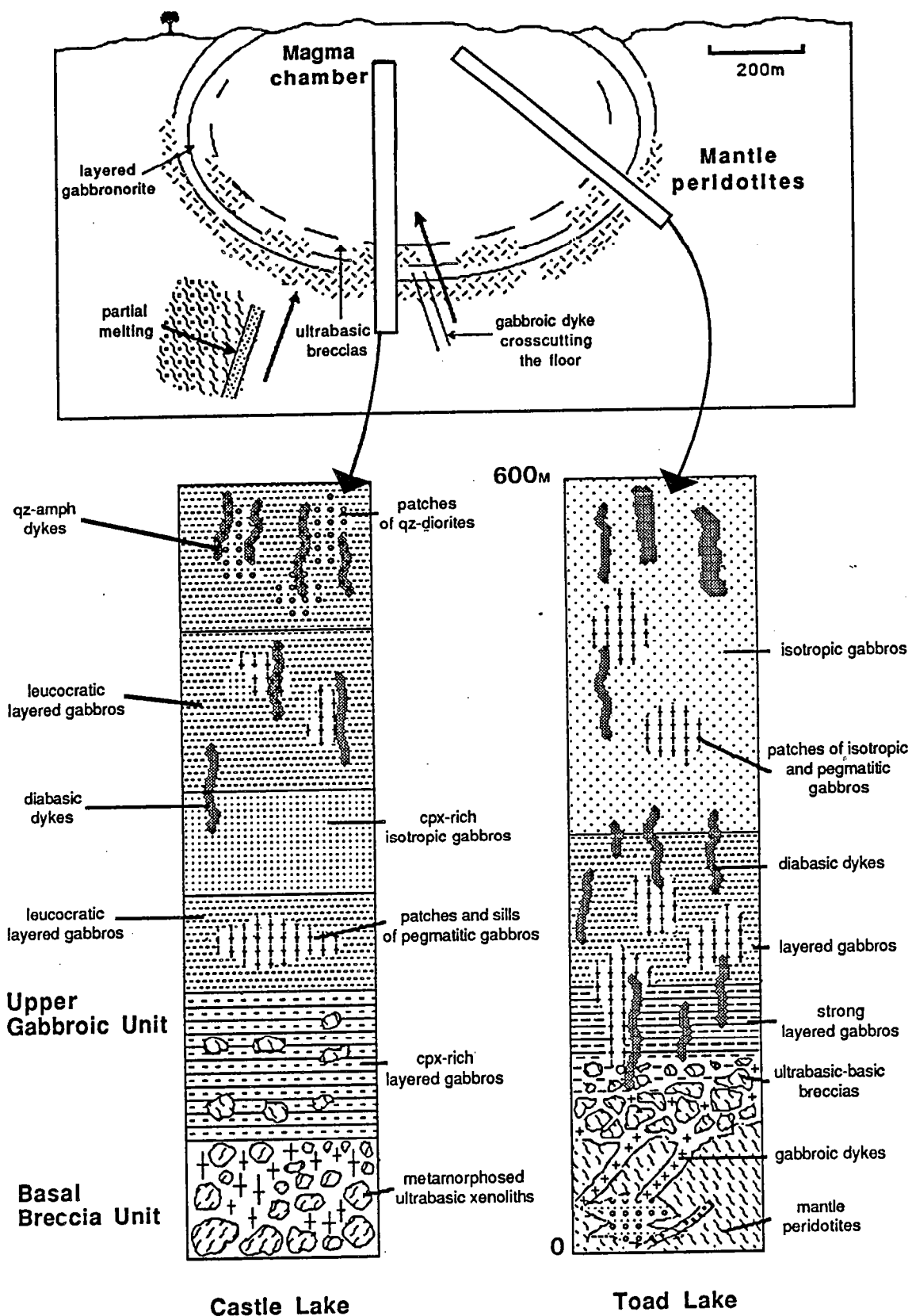
4e: magnetite grains (1) replaced by magnesio-hornblende (2) adjacent to plagioclase (3) altered to epidote.

Figure 5: Enstatite component versus  $\text{Al}_2\text{O}_3$  content of orthopyroxene from mantle peridotites (filled squares), mantle xenoliths (open squares) and layered cumulate gabbros (filled circles). See text for explanations.

Figure 6: Pressure - temperature diagram showing experimental curves for the reactions discussed in the text.

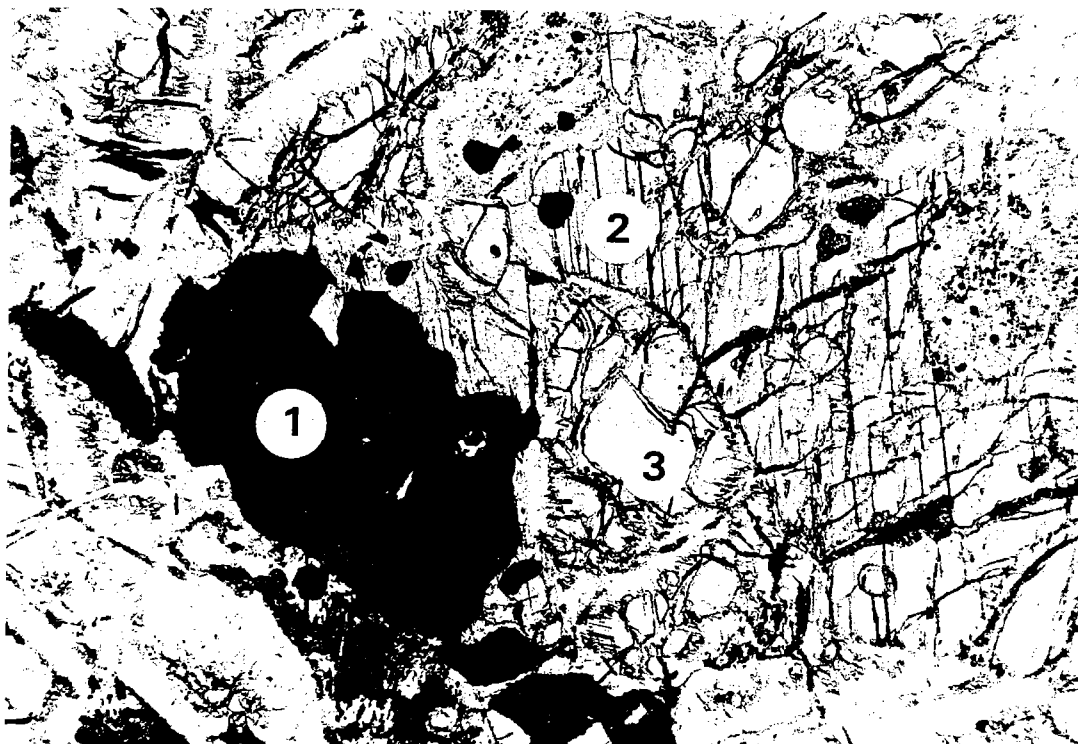
Figure 7: Variation of MgO, FeO and NiO versus  $\text{H}_2\text{O}^+$  content of olivine with increasing serpentinization. Interval between microprobe analysis is  $10\mu\text{m}$ .





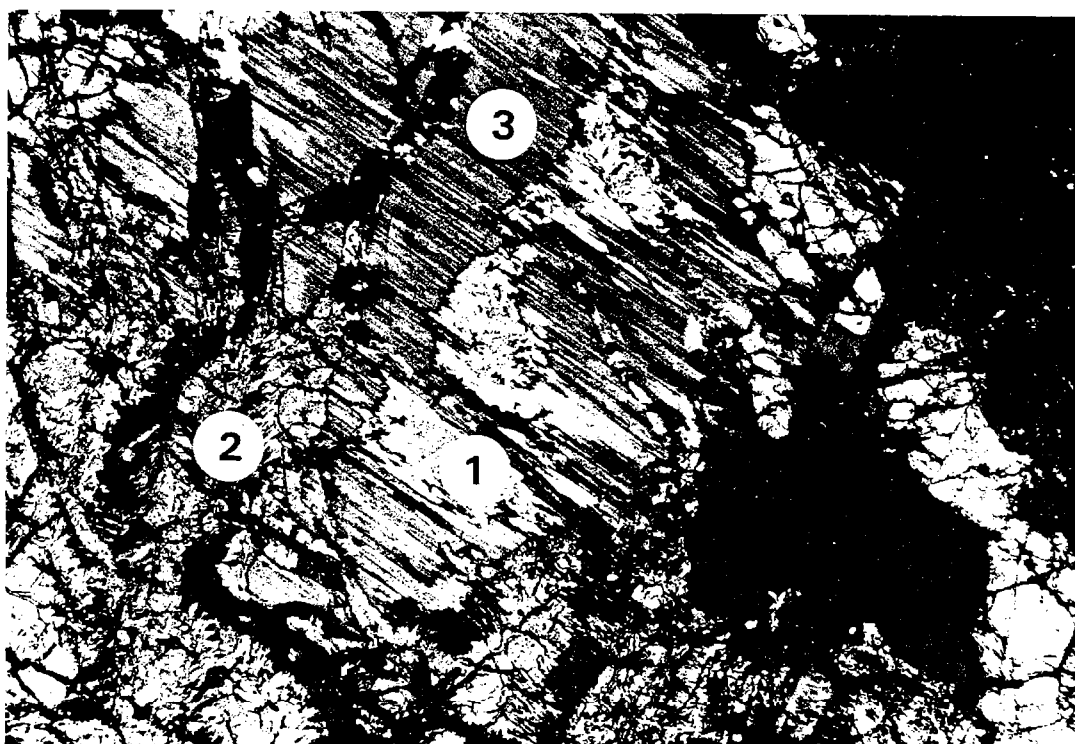


3b



0.1mm

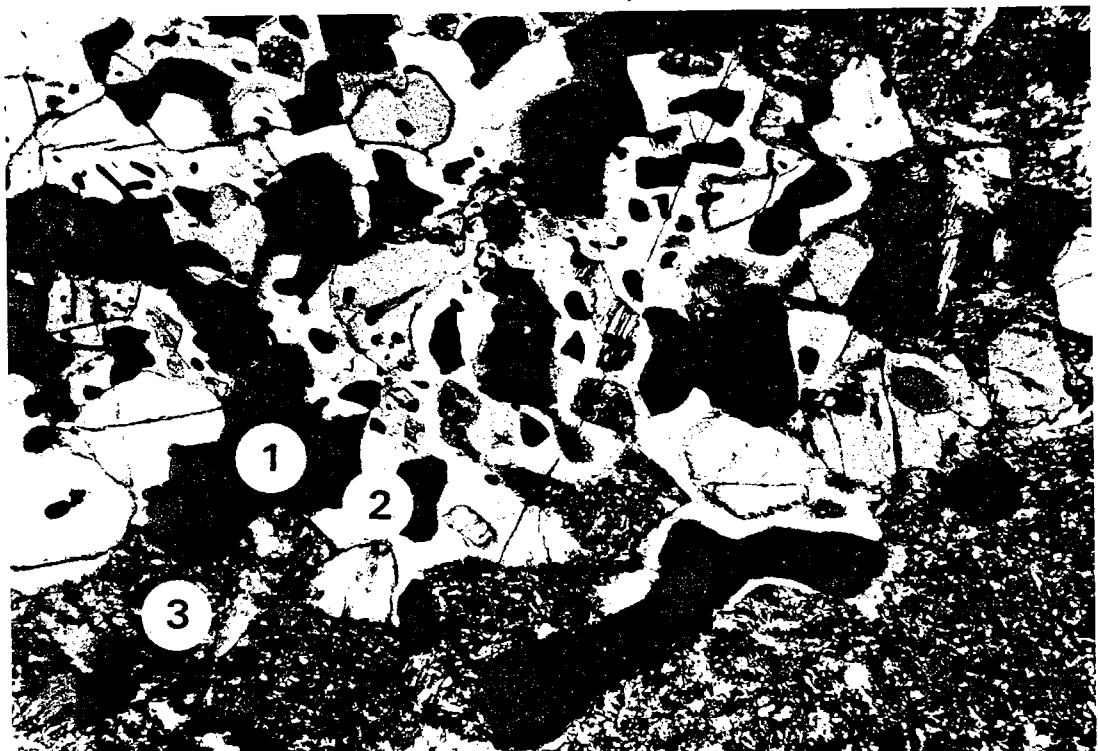
3a



50µm



4d



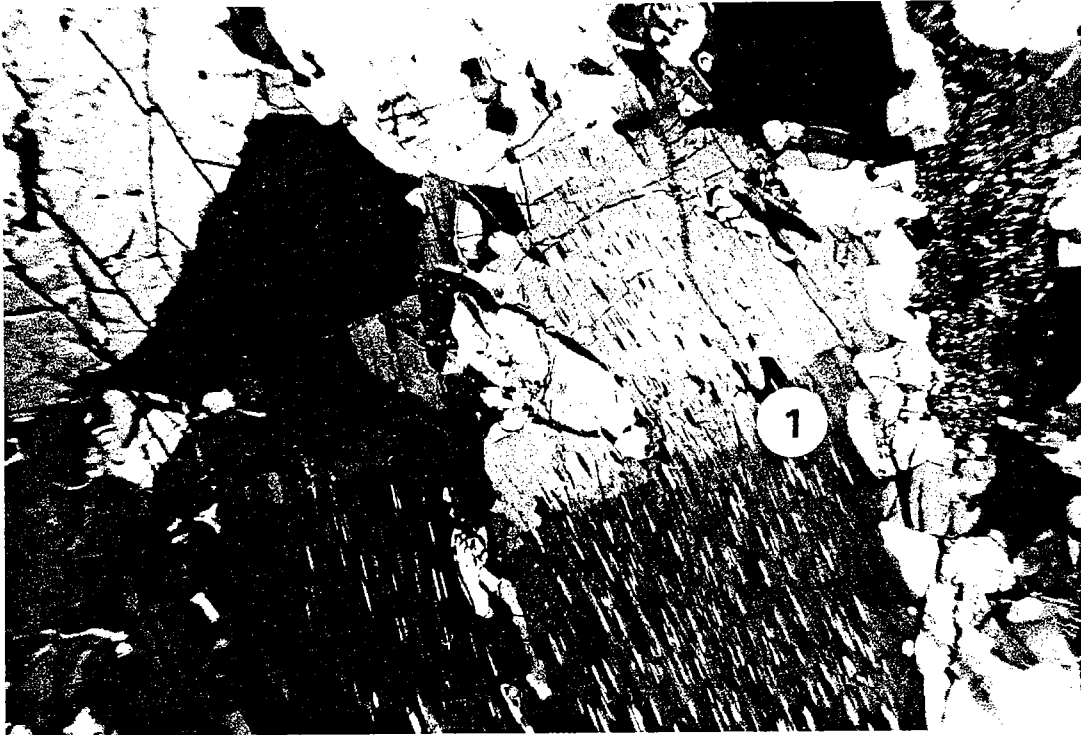
4e

0,1mm



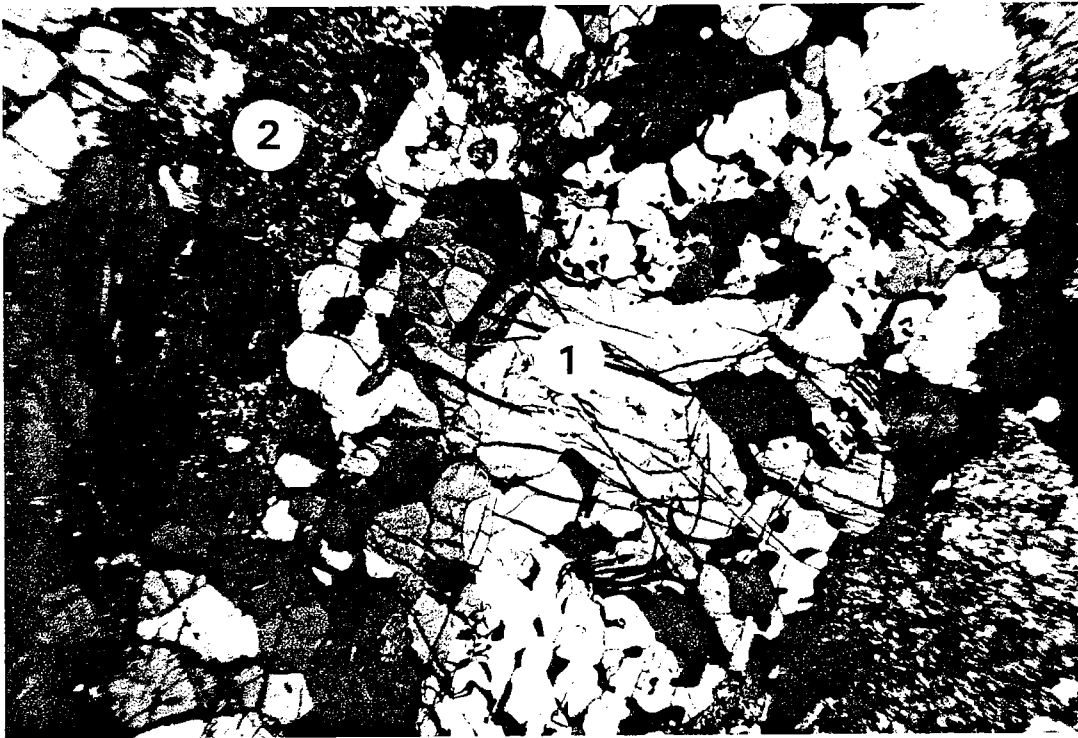
Fig. 4c

4b

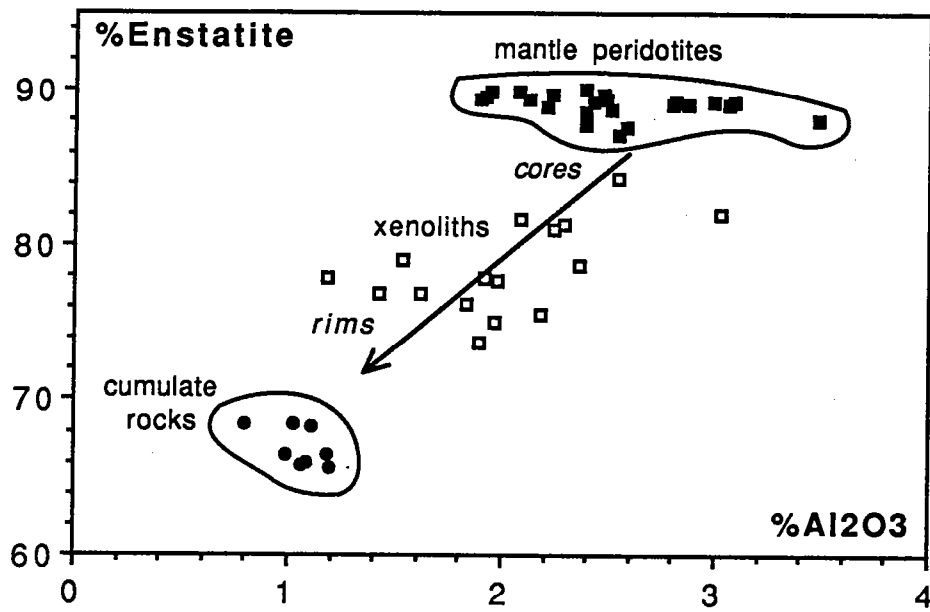


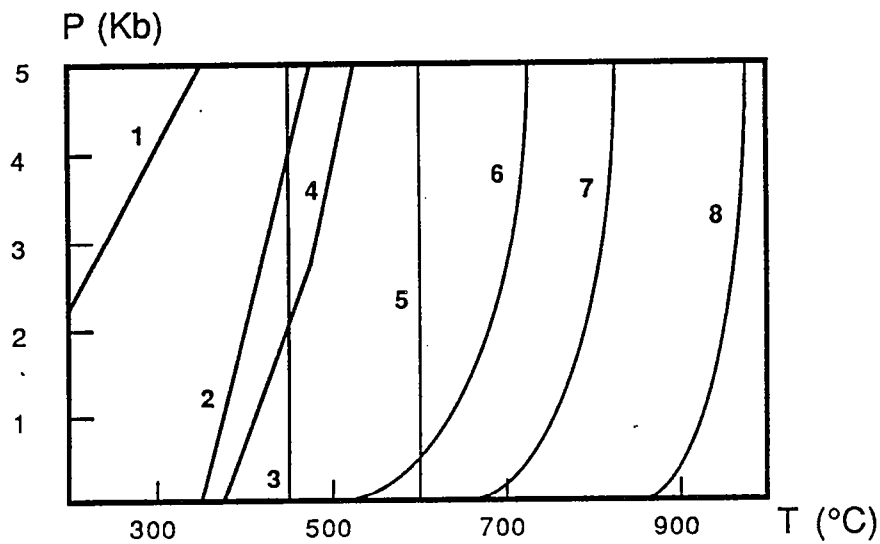
0,25mm

4a



0,25mm





1 : TALC = SERPENTINE +  $\text{SiO}_2$ .

2 : OLIVINE +  $\text{H}_2\text{O}$  = SERPENTINE.

3 : LOWER LIMIT OF HORNBLENDE + TREMOLITE STABILITY.

4 : OLIVINE + TALC +  $\text{H}_2\text{O}$  = SERPENTINE.

5 : LOWER LIMIT OF SUPERSOLVUS HORNBLENDE STABILITY.

6 : ORTHOPYROXENE +  $\text{H}_2\text{O}$  = TALC + OLIVINE.

7 : ORTHOPYROXENE +  $\text{H}_2\text{O}$  = TALC

8 : HORNBLENDE = CLINOPYROXENE + PLAGIOCLASE + OLIVINE  
+ ILMENITE +  $\text{H}_2\text{O}$ .

163

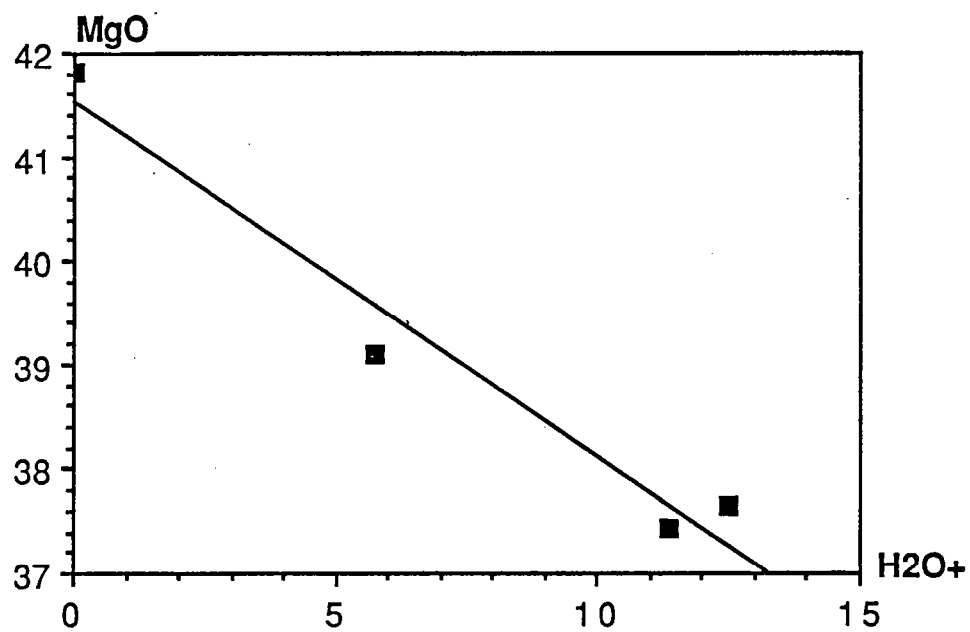
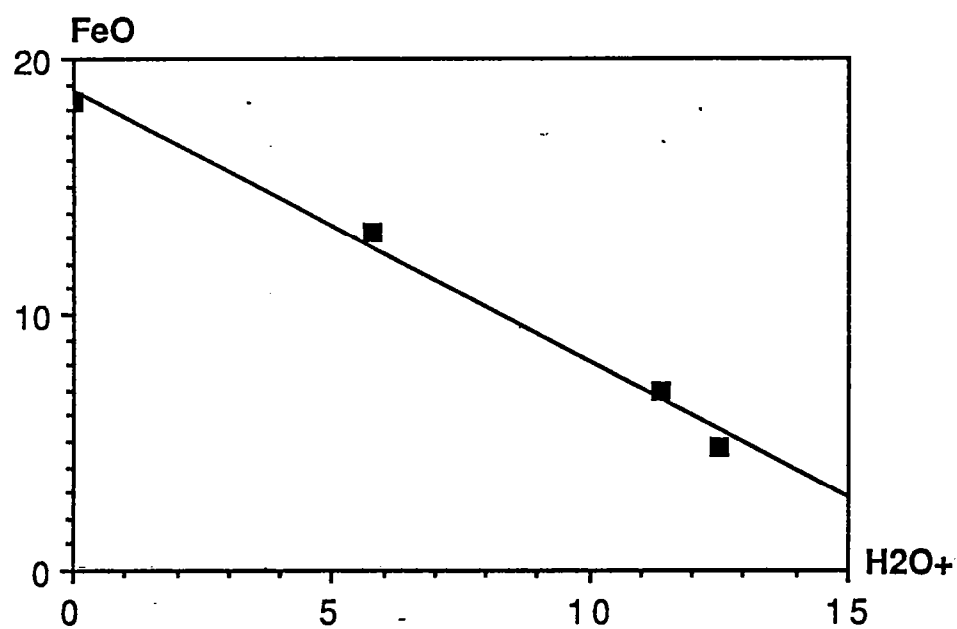
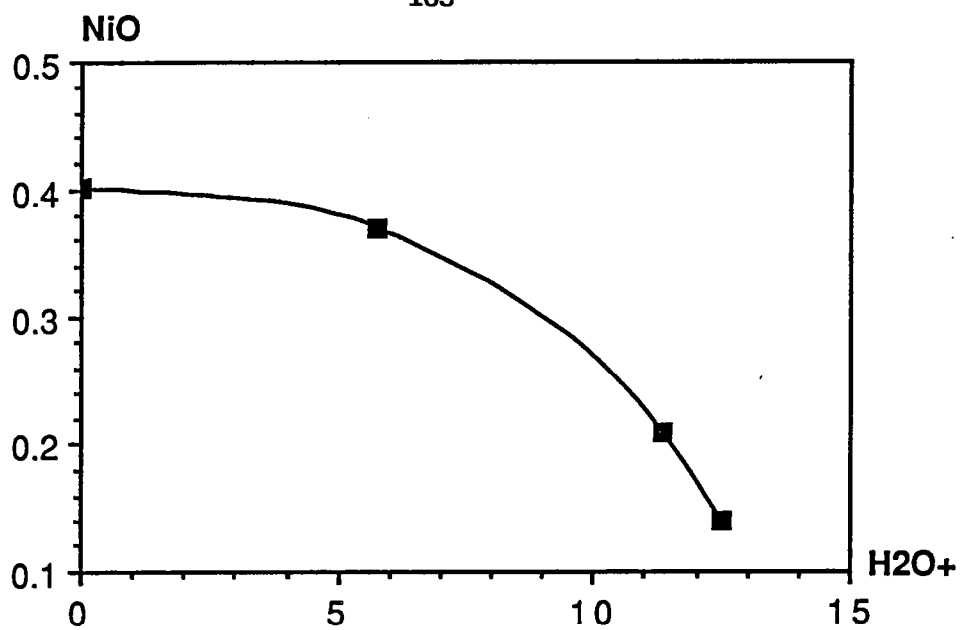


Table 1: Representative microprobe analyses of minerals from Castle Lake xenoliths and mantle peridotites.

| Sample Type Mineral Reference*   | CL mantle peridotite Clinopyroxene {2} | CL6 mantle xenolith Spinel {2} | CL6 mantle xenolith Spinel II {2} | CL6 mantle xenolith Pargasitic-Hb {2} | CL6 mantle xenolith Talc {3a-b} | CL6 mantle xenolith Olivine II {4}, {6} | CL6 mantle xenolith Serpentine I {6} | CL6 mantle xenolith Serpentine II {6} | CL6 mantle xenolith Serpentine III {6} |
|----------------------------------|--|--------------------------------|-----------------------------------|---------------------------------------|---------------------------------|---|--------------------------------------|---------------------------------------|--|
| SiO <sub>2</sub>                 | 52.36                                  | 0                              | 0.01                              | 45.58                                 | 59.01                           | 39.99                                   | 40.14                                | 40.83                                 | 44.23                                  |
| TiO <sub>2</sub>                 | 0.25                                   | 0.58                           | 1.15                              | 1.48                                  | 0                               | 0                                       | 0.04                                 | 0                                     | 0                                      |
| Al <sub>2</sub> O <sub>3</sub>   | 2.84                                   | 21.70                          | 10.52                             | 11.59                                 | 2.01                            | 0                                       | 1.02                                 | 3.06                                  | 0.65                                   |
| Fe <sub>2</sub> O <sub>3</sub> t | 2.33                                   | 30.05                          | 48.40                             | 4.36                                  | 2.52                            | 18.30                                   | 13.28                                | 7.01                                  | 4.81                                   |
| MgO                              | 16.64                                  | 8.71                           | 1.86                              | 18.26                                 | 30.60                           | 41.81                                   | 39.10                                | 37.44                                 | 37.65                                  |
| MnO                              | 0.07                                   | 0.31                           | 0.65                              | 0                                     | 0.06                            | 0.35                                    | 0.26                                 | 0.03                                  | 0                                      |
| CaO                              | 24.03                                  | 0                              | 0.02                              | 12.35                                 | 0                               | 0                                       | 0.01                                 | 0.04                                  | 0.02                                   |
| Na <sub>2</sub> O                | 0.51                                   | 0                              | 0                                 | 2.04                                  | 0.14                            | 0                                       | 0.03                                 | 0.03                                  | 0                                      |
| K <sub>2</sub> O                 | 0.00                                   | 0.01                           | 0                                 | 0.08                                  | 0                               | 0                                       | 0                                    | 0                                     | 0                                      |
| NiO                              | 0.19                                   | 0.19                           | 0.28                              | 0.12                                  | 0.12                            | 0.40                                    | 0.37                                 | 0.21                                  | 0.14                                   |
| Cr <sub>2</sub> O <sub>3</sub>   | 1.10                                   | 38.50                          | 30.67                             | 1.59                                  | 0.45                            | 0                                       | 0                                    | 0                                     | 0.01                                   |
| Sum                              | 100.12                                 | 100.05                         | 93.57                             | 97.45                                 | 94.91                           | 100.13                                  | 100.85                               | 94.25                                 | 88.65                                  |

| Sample Type Mineral Reference*   | CL6 mantle xenolith Olivine {5} | CL6 mantle xenolith Serpentine {5} | CL6 Orthopyroxene {7} | CL6 Bastite {7} |
|----------------------------------|---------------------------------|------------------------------------|-----------------------|-----------------|
| SiO <sub>2</sub>                 | 40.64                           | 43.23                              | 56.42                 | 43.23           |
| TiO <sub>2</sub>                 | 0                               | 0                                  | 0                     | 0               |
| Al <sub>2</sub> O <sub>3</sub>   | 0.04                            | 0.06                               | 2.42                  | 2.43            |
| Fe <sub>2</sub> O <sub>3</sub> t | 10.44                           | 4.77                               | 6.30                  | 5.16            |
| MgO                              | 48.36                           | 38.85                              | 33.27                 | 37.24           |
| MnO                              | 0.21                            | 0                                  | 0.19                  | 0.04            |
| CaO                              | 0.04                            | 0                                  | 0.54                  | 0               |
| Na <sub>2</sub> O                | 0                               | 0                                  | 0                     | 0               |
| K <sub>2</sub> O                 | 0.04                            | 0.01                               | 0                     | 0               |
| NiO                              | 0.36                            | 0.17                               | 0.05                  | 0               |
| Cr <sub>2</sub> O <sub>3</sub>   | 0                               | 0                                  | 0.43                  | 0.55            |
| Sum                              | 87.50                           | 87.10                              | 99.66                 | 88.65           |

\* the number refers to mineralogical reactions discussed in the text.



Table 2: representative microprobe analyses of minerals from Toad Lake mantle xenoliths and cumulate gabbronorites.

| Samples<br>Type<br>Mineral<br>Reference* | TOAD12<br>gabbronorite<br>Clinopyroxene | TOAD12<br>gabbronorite<br>Orthopyroxene | TOAD12<br>mantle xenolith<br>Olivine<br>{9a-b} | TOAD12<br>mantle xenolith<br>Orthopyroxene<br>{9a-b} | TOAD12<br>mantle xenolith<br>Orthopyroxene<br>{9a-b} | TOAD12<br>mantle xenolith<br>Orthopyroxene<br>{9a-b} | TOAD12<br>mantle xenolith<br>Magnetite<br>{9a-b}, {10} | TOAD12<br>mantle xenolith<br>Plagioclase<br>{10} | TOAD12<br>mantle xenolith<br>Mg-hornblende<br>{10} | TOAD12<br>mantle xenolith<br>Mg-hornblende<br>{10} |
|--|---|---|--|--|--|--|--|--|--|--|
| SiO <sub>2</sub>                         | 52.77                                   | 53.71                                   | 39.17  | 55.00  | 55.34  | 0  | 0  | 45.93  | 46.24  | 44.79  |
| TiO <sub>2</sub>                         | 0.49                                    | 0.10                                    | 0  | 0.18   | 0.21   | 0.67   | 0.67   | 0  | 1.41   | 1.06   |
| Al <sub>2</sub> O <sub>3</sub>           | 1.71                                    | 1.09                                    | 0  | 1.94   | 1.72   | 0.62   | 0.62   | 34.91  | 11.92  | 13.29  |
| Fe <sub>2</sub> O <sub>3t</sub>          | 8.18                                    | 19.89                                   | 19.07  | 13.80  | 12.71  | 88.36  | 88.36  | 0.29   | 6.71   | 7.67   |
| MgO                                      | 14.02                                   | 23.86                                   | 41.48  | 28.96  | 29.24  | 0.20   | 0.20   | 0  | 17.13  | 15.96  |
| MnO                                      | 0.18                                    | 0.44                                    | 0.39   | 0.37   | 0.39   | 0.08   | 0.08   | 0  | 0.07   | 0.10   |
| CaO                                      | 21.9                                    | 1.21                                    | 0  | 0.55   | 0.58   | 0  | 0  | 17.64  | 11.41  | 11.69  |
| Na <sub>2</sub> O                        | 0.13                                    | 0                                       | 0  | 0.01   | 0.01   | 0.07   | 0.07   | 1.03   | 1.51   | 1.65   |
| K <sub>2</sub> O                         | 0.00                                    | 0                                       | 0.01   | 0  | 0.01   | 0  | 0  | 0.16   | 0  | 0.02   |
| NiO                                      | 0.02                                    | 0.07                                    | 0.32   | 0.06   | 0.09   | 0.18   | 0.18   | 0  | 0  | 0.11   |
| Cr <sub>2</sub> O <sub>3</sub>           | 0                                       | 0.17                                    | 0  | 0  | 0.09   | 2.73   | 2.73   | 0  | 0  | 0.02   |
| Sum                                      | 99.40                                   | 100.54                                  | 100.44   | 100.87   | 100.38   | 92.93  | 92.93  | 99.96  | 96.40  | 96.36  |

\* the number refers to mineralogical reactions discussed in the text.

## Références

- Arai S. et Fujii T. 1979. Petrology of ultramafic rocks from site 395. Site 395, DSDP, 45 : 587-594.
- Ashley P.M., Franklin B.J. et Ray A.S. 1983. Plagiogranites in the Coolac ophiolite suite, New South Wales, Australia. *Geol. Mag.*, 120 : 1-19.
- Beccaluva L., Macciotta G., Piccardo G.B. et Zeda O. 1984. Petrology of lherzolitic rocks from the Northern Apennine ophiolites. *Lithos*, 17 : 299-316.
- Bhattacharji S. et Smith C.H. 1964. Flowage differentiation. *Science* : 145-153.
- Boudier F. et Coleman R.G. 1981. Cross section through the peridotite in the Semail ophiolite, southeastern Oman mountains. *J. Geophys. Res.*, 86 : 2573-2593.
- Boudier F. et Nicolas A. 1985-86. Harzburgite and lherzolite subtypes in ophiolite and oceanic environments. *Earth Planet. Sci. Lett.*, 76 : 84-92.
- Brouxel M. et Lapierre H. 1985. Un bassin marginal dévonien dans les Klamath orientales (Californie du Nord, Etats Unis) : le cortège ophiolitique de Trinity. *Ophioliti*, 10 : 181-202.
- Brouxel M. et Lapierre H. 1988. Geochemical study of an early Paleozoic island arc - back arc basin system. Part I : The Trinity ophiolite (Northern California). *Geol. Soc. Am. Bull.*, 100 : 1111-1119.
- Brunn J. H. 1960. Mise en place et différenciation de l'association pluto-volcanique du cortège ophiolitique. *Revue géogr. phys. géol. dyn.*, 3 : 115-132.
- Bryan W.B., Finger L.W. et Chayes F. 1969. Estimating Proportions in Petrographic Mixing Equations by Least-Squares Approximation. *Science*, 163 : 926-927.
- Coleman R.G. 1984. Preaccretion tectonics and metamorphism of ophiolites. *Ophioliti*, 9 : 205-222.
- Dewey J.J. et Bird J.M. 1970. Mountain belts and the new global tectonics. *J. Geophys. Res.*, 75 : 2625-2647.
- Dick H.J.B., Fisher R.L. et Bryan W.B. 1984. Mineralogic variability of the uppermost mantle along mid-ocean ridges. *Earth Planet. Sci. Lett.*, 69 : 88-106.
- Gagny C. 1978. Quelques réflexions sur la pétrologie structurale appliquée à l'étude des filons. 103 Cong. Nat. Soc. Sav., Nancy, 4 : 9-20.
- Gerlach D.C., Leeman W.P. et Avé Lallemant H.G. 1981. Petrology and geochemistry of plagiogranite in the Canyon mountain ophiolite, Oregon. *Contrib. Mineral. Petrol.*, 77 : 82-92.
- Gregory R.T. 1984. Melt percolation beneath a spreading ridge : evidence from the Semail Peridotite, Oman. In : *Ophiolites and Oceanic Lithosphere*, I.G. Gass, S.J. Lippard and A.W. Shelton (Ed). Blackwell Scientific Publications, pp. 55-62.
- Hamlyn P.R. et Bonatti E. 1980. Petrology of mantle-derived ultramafics from the Owen fracture zone, northwest Indian Ocean : implications for the nature of the oceanic upper mantle. *Earth Planet. Sci. Lett.*, 48 : 65-79.
- Hammond J.G. 1986. Geochemistry and petrogenesis of Proterozoic diabase in the southern Death Valley region of California. *Contrib. Mineral. Petrol.*, 93 : 312-321.
- Hall R. 1983. Ophiolites and passive continental margins. *Ophioliti*, 7 : 279-298.

- Hékinian R. 1982. Petrology of the ocean floor. Elsevier Oceanography series 33, 393pp.
- Lago B.L., Rabinowicz M. et Nicolas A. 1982. Podiform chromite ore bodies : a genetic model. *J. Petrol.*, 23 : 103-125.
- Lapierre H., Brouxel M., Albarède F., Coulon C., Lecuyer C., Martin P., Mascle G. et Rouer O. 1987. Paleozoic and Lower Mesozoic magmas from the eastern Klamath Mountains (North California) and the geodynamic evolution of northwestern America. *Tectonophysics*, 140 : 155-177.
- Lecuyer C. 1989. Chemical transfers between ultrabasic xenoliths and basic magmas : evidences for oceanic magma chambers (the Trinity ophiolite, N. California). *Soumis à Lithos*.
- Lecuyer C., Brouxel M. et Lapierre H. 1989b. Petrogenesis of magmas at a slow-spreading center: The Lower Paleozoic Trinity ophiolite. *Soumis à Contrib. Mineral. Petrol.*
- Le Sueur E. et Boudier F. 1986. Structures du complexe basique et ultrabasique de Trinity, Californie : genèse d'une ophiolite atypique. *Bull. Soc. géol. France*, 6 : 1007-1014.
- Le Sueur E., Boudier F., Cannat M., Ceuleneer G. et Nicolas A. 1984. The Trinity mafic-ultramafic complex : first results of the structural study of an untypical ophiolite. *Ophioliti*, 9 : 487-498.
- Malpas J. 1978. Magma generation in the upper mantle, field evidence from ophiolitic suites, and application to the generation of oceanic lithosphere. *Phil. Trans. R. Soc. Lond.*, a288 : 527-546.
- Maurel C. et Maurel P. 1984. Etude expérimentale de la distribution du fer ferrique entre spinelle chromifère et bain silicaté basique. *Bull. Minéral.*, 107 : 25-33.
- Menzies M., Blanchard D. et Xenophontos C. 1980. Genesis of the Smartville Arc - ophiolite, Sierra Nevada foothills, California. *Am. J. Sci.*, 280A : 329-344.
- Michael P.J. et Bonatti E. 1985. Peridotite composition from the North Atlantic : regional and tectonic variations and implications for partial melting. *Earth Planet. Sci. Lett.*, 73 : 91-104.
- Moore E.M. 1982. Origin and emplacement of ophiolites. *Rev. Geophys. Space Phys.*, 20 : 735-760.
- Moore E.M. et Vine F.J. 1971. The Troodos massif, Cyprus and other ophiolites as oceanic crust : evaluation and implications. *Phil. Trans. Roy. Soc. Lond.*, 268 : 443-466.
- Murck B.W. et Campbell I.H. 1986. The effects of temperature, oxygen fugacity and melt composition on the behaviour of chromium in basic and ultrabasic melts. *Geochim. Cosmochim. Acta*, 50 : 1871-1887.
- Nicolas A. 1986. A Melt Extraction Model Based on Structural Studies in Mantle Peridotites. *J. Petrol.*, 27 : 999-1022.
- Nicolas A. et Dupuy C. 1984. Origin of ophiolitic and oceanic lherzolites. *Tectonophysics*, 110 : 177-187.
- Nicolas A., Boudier F. et Bouchez J.L. 1980. Interpretation of peridotite structures from ophiolitic and oceanic environments. *Am. J. Sci. E.D. Jackson Mem.*, 280A : 192-210.
- Ohnenstetter M. 1982. Importance de la nature et du rôle des discontinuités au sein des ophiolites lors du développement d'un orogène. Thèse d'état, Université de Nancy I : 590.

- Pallister J.S. 1984. Parent magmas of the Semail ophiolite, Oman. In : *Ophiolites and Oceanic Lithosphere*, (Ed) I.G. Gass, S.J. Lippard and A.W. Shelton. Blackwell Scientific Publications, pp. 63-70.
- Pallister J.S. et Knight R.J. 1981. Rare-earth element geochemistry of the Semail ophiolite near Ibra, Oman. *J. Geophys. Res.*, 86 : 2673-2697.
- Pedersen R.B. 1986. The nature and significance of magma chamber margins in ophiolites : examples from the Norwegian Caledonides. *Earth Planet. Sci. Lett.*, 77 : 100-112.
- Pedersen R.B. et Malpas J. 1984. The origin of oceanic plagiogranites from the Karmoy ophiolite, Western Norway. *Contrib. Mineral. Petrol.*, 88 : 36-52.
- Presnall D.C. et Hoover J.D. 1987. High pressure phase equilibrium constraints on the origin of mid-ocean ridge basalts. In : *magmatic processes : physicochemical principles*, Ed. B.O. Mysen. The Geochemical Society, Special Publication, N°. 1, pp. 75-89.
- Presnall D.C., Dixon J.R., O'Donnell T.H., Brenner N.L., Schrock R.L. et Dycus D.W. 1978. Liquidus phase relations on the join diopside-forsterite-anorthite from 1 atm to 20 kbar : their bearing on the generation and crystallization of basaltic magma. *Contrib. Mineral. Petrol.*, 66 : 203-220.
- Quick J.E. 1981. Petrology and petrogenesis of the Trinity peridotite, an upper mantle diapir in the eastern Klamath Mountains, northern California. *J. Geophys. Res.*, 87 : 3831-3848.
- Roeder P.L. et Emslie R.F. 1970. Olivine-liquid equilibrium. *Contrib. Mineral. Petrol.*, 29 : 275-289.
- Savel'yeva G.N. 1984. Mineral assemblage evolution in ocean-floor ultrabasites. *Geokhimiya*, 5 : 691-704.
- Shibata, T. Thompson G. et Frey F.A. 1979. Tholeiitic and alkali basalts from the Mid-Atlantic Ridge at 43° N. *Contrib. Mineral. Petrol.*, 70 : 127-141.
- Sinton J.M. 1979. Petrology of (alpine-type) peridotites from site 395, DSDP Leg 45. Site 395, DSDP, 45 : 595-601.
- Stolper E. et Walker D. 1980. Melt density and the average composition of basalt. *Contrib. Mineral. Petrol.*, 74 : 7-12.

## CHAPITRE 3 - Hydrothermalisme océanique.

### 3.A. L'hydrothermalisme océanique.

#### 3.A.1 Généralités.

Avec l'avènement de la théorie de la tectonique des plaques, l'étude des dorsales associées à l'expansion océanique a permis de mettre en évidence l'existence d'une circulation d'eau de mer au sein de la croûte océanique dans des régions très localisées où la perméabilité de la croûte océanique et la présence de sources de chaleur (les chambres magmatiques) peuvent induire une circulation convective de l'eau de mer dans les fissures de la croûte océanique.

L'eau de mer froide et dense descend dans les fissures, se réchauffe au contact de la source de chaleur et remonte vers la surface. La circulation par convection de solutions aqueuses chaudes favorise les échanges thermiques et chimiques entre l'océan et la croûte.

Ainsi l'existence de ces sources chaudes est à l'origine de dépôts métallifères considérables. L'eau de mer en traversant la croûte océanique par convection participe à des échanges chimiques : l'eau de mer alcaline, oxydante et pauvre en métaux pénètre profondément dans les zones perméables de la croûte. A haute température, le magnésium est capté par les roches basiques, la réaction chimique invoquée s'accompagne d'une libération d'ions  $H^+$  qui acidifient la solution.

D'autre part, les composés ferreux des roches volcaniques réduisent les sulfates dissous en soufre et produisent de l'hydrogène sulfuré. L'eau devenue très acide dissout les métaux présents en très faible concentration dans les roches (de l'ordre du ppm au ppb). Les fluides d'origine magmatique et les éléments volatils provenant du manteau (Sb, As, Hg et Se) constituent d'autres sources de métaux.

Les solutions hydrothermales se mélangent à l'eau de mer pure quand la pression hydrostatique empêche leur ébullition; c'est le cas pour les solutions dont la température est de  $350^{\circ}C$  libérées à des profondeurs supérieures à 2000m. Lors du mélange des solutions hydrothermales avec de l'eau de mer froide, la température de la solution est abaissée et sa composition chimique modifiée : initialement acide, la solution devient alcaline et les sels minéraux métalliques peuvent précipiter. Si le milieu est réducteur, les métaux réagissent avec le soufre de l'eau de mer ou le soufre mantellique et ils se déposent sous la forme de sulfures polymétalliques; si le milieu est oxydant, les métaux réagissent avec l'oxygène, les hydroxydes, le sulfate, le carbonate de silice et forment des dépôts d'oxydes métalliques, d'hydroxydes, de silicates, de sulfates ou de carbonates.

Les différences entre les centres d'expansion océanique résultent des différentes vitesses d'expansion. Plus la vitesse d'expansion est importante, plus la différence d'altitude entre la zone axiale et les zones marginales est faible et plus les chambres magmatiques sous-jacentes sont larges (20Km au lieu d'1Km).

***Ainsi les caractéristiques des centres d'expansion océanique peuvent déterminer la nature des systèmes hydrothermaux et permettre de préciser dans chaque cas les échanges thermiques et chimiques entre l'eau de mer et la croûte océanique.***

En 1979, des chercheurs américains, français et mexicains ont découvert sur la dorsale Pacifique Est ( $21^{\circ}N$ , Sud de la Californie), au voisinage des amas de sulfures massifs, des volutes de fluide noir émis par des événements baptisés depuis "fumeurs noirs". Le fluide est une solution réductrice riche en métaux, acide et dont la température est égale environ à  $350^{\circ}C$ , lorsqu'il se mélange à l'eau de mer, des sulfures de zinc, de fer et de cuivre précipitent en formant de fines particules noires en suspension dans le panache qui s'élève au-dessus de la cheminée. Les datations radiométriques ont révélé que l'activité des fumeurs noirs ne dure que quelques années, ces structures pouvant atteindre jusqu'à dix mètres de haut.

#### 3.A.2 Bilans géochimiques entre la croûte océanique et l'hydrosphère : les flux élémentaires.

Les flux de matière entre le manteau et le système exogénique sont particulièrement complexes et invoquent la connaissance de nombreux domaines en géologie. Ainsi des valeurs globales de flux chimiques sont difficiles à établir. La synthèse proposée par Wolery et Sleep (1988) offre des estimations de ces flux chimiques (tableau 3. 1). En effet, le volume, la

## Revue des estimations des flux endogéniques-exogéniques

| Elément          | Altération<br>basse-température | Altération<br>off-axis | activité hydrothermale<br>axiale | Total         | Flux net      | References              |
|------------------|---------------------------------|------------------------|----------------------------------|---------------|---------------|-------------------------|
| Na               | -0,35 à -0,04                   | 0,48                   | ?                                | ?             | 0,13-0,44     | Gregor et al. (1988)    |
|                  | 0,009                           | -                      | -                                | -1,96         | -             | Maynard (1976)          |
|                  | 1,39                            | -                      | -                                | -10,39        | -             | R. Hart (1973)          |
|                  | -                               | -                      | -                                | 0 à -3,83     | -             | Mottl (1976)            |
|                  | -                               | -                      | -8,6 à 1,9                       | -             | -             | Von Damm (1983)         |
|                  | -0,47                           | 0,17                   | -                                | -             | -             | Thompson (1983a,b)      |
| K                | -0,51 à -0,1                    | 0,33                   | 0,21                             | 0,54          | 0,03 à 0,44   | Gregor et al. (1988)    |
|                  | -0,31                           | -                      | -                                | 0,61          | -             | Maynard (1976)          |
|                  | -1,54                           | -                      | -                                | 0             | -             | R. Hart (1973)          |
|                  | -                               | -                      | -                                | < 0,26        | -             | Mottl (1976)            |
|                  | 0 à -0,17                       | -                      | -                                | -             | -             | Seyfried (1976)         |
|                  | -                               | -                      | -                                | 1,28          | -             | Edmond et al. (1979b)   |
|                  | -                               | -                      | 1,9 à -2,3                       | -             | -             | Von Damm (1983)         |
|                  | -0,26                           | -0,56                  | 0,13 à 1,26                      | -0,43 à 0,69  | -0,69 à 0,44  | Thompson (1983a,b)      |
| Ca               | 0,25 à 1,25                     | 1,20                   | 0,60                             | 1,80          | 2,05 à 3,05   | Gregor et al. (1988)    |
|                  | 0,06                            | -                      | -                                | 0,38          | -             | Maynard (1976)          |
|                  | 4,68                            | -                      | -                                | 15,58         | -             | R. Hart (1973)          |
|                  | -                               | -                      | -                                | 2,58 à 7,05   | -             | Mottl (1976)            |
|                  | 0,15 à 0,70                     | -                      | -                                | 3,80          | -             | Seyfried (1976)         |
|                  | -                               | -                      | 2,05 à 4,30                      | -             | -             | Edmond et al. (1979b)   |
|                  | 0,20 à 1,25                     | -                      | -                                | 1,63 à 3,38   | -             | Wolery and Sleep (1976) |
|                  | -                               | -                      | 0,24 à 1,5                       | -             | -             | Von Damm (1983)         |
| Mg               | 0,32                            | 1,18                   | 0,32 à 3,25                      | 1,50 à 4,43   | 1,83 à 4,75   | Thompson (1983a,b)      |
|                  | 0,29 à 1,89                     | -1,23                  | 1,27                             | -1,50         | -2,21 à -0,61 | Gregor et al. (1988)    |
|                  | 0,05                            | -                      | -                                | -1,73         | -             | Maynard (1976)          |
|                  | 4,98                            | -                      | -                                | -8,39         | -             | R. Hart (1973)          |
|                  | 0,41 à 0,58                     | -                      | -                                | -4,52         | -             | Seyfried (1976)         |
|                  | 0,04 à 0,45                     | -                      | -                                | -2,71         | -             | Wolery and Sleep (1976) |
|                  | -                               | -                      | -7,5                             | -             | -             | Von Damm (1983)         |
|                  | 1,21                            | 0,46                   | -7,79 à -4,17                    | -7,33 à -3,71 | -6,13 à -2,5  | Thompson (1983a,b)      |
| SiO <sub>2</sub> | 0,08 à 0,47                     | 0,37                   | 0,52                             | 0,89          | 0,97 à 1,36   | Gregor et al. (1988)    |
|                  | 0,87                            | -                      | -                                | 3,27          | -             | Maynard (1976)          |
|                  | 4,83                            | -                      | -                                | 6,67          | -             | R. Hart (1973)          |
|                  | 0 à 0,63                        | -                      | -                                | -             | -             | Seyfried (1976)         |
|                  | -                               | -                      | 3,10                             | -             | -             | Edmond et al. (1979b)   |
|                  | 0,50 à 1,33                     | -                      | -                                | -             | 0,50 à 1,50   | Wolery and Sleep (1976) |
|                  | -                               | -                      | 2,2 à 2,8                        | -             | -             | Von Damm (1983)         |
|                  | 1,88                            | 0,71                   | 0,31 à 3,10                      | 1,02 à 3,81   | 2,96 à 5,71   | Thompson (1983a,b)      |

Tableau 3.1

nature et le degré d'altération dans la croûte océanique sont extrapolés des forages dans la croûte océanique et des complexes ophiolitiques encore suffisamment préservés. Seules quelques sources hydrothermales axiales et "off-axis" ont été échantillonnées et les flux potentiels déduits d'extrapolations des précédentes données doivent être considérées comme des valeurs limites en comparaison avec la connaissance du système exogénique (tableau 3.1).

### 3.A.3 L'altération basse-température des basaltes du plancher océanique.

L'altération de basse-température (0 à 100°C) affecte les quelques centaines de mètres de la partie supérieure de la croûte océanique. Ce processus est souvent appelé par les anglosaxons "oceanic weathering". Les basaltes altérés à basse température peuvent être considérés comme un "mélange" de matériel frais et de produits d'altération (Muehlenbachs, 1977). Le degré d'altération est ainsi caractérisé par la composition isotopique en oxygène de la roche totale. Les teneurs en  $\text{H}_2\text{O}^+$  des roches totales peuvent être utilisées comme un index de l'altération du basalte. Ainsi, quand un composant chimique du basalte est reporté dans un diagramme contre  $\text{H}_2\text{O}^+$ , une relation linéaire est couramment observée. Cette relation est valable pour  $\delta^{18}\text{O}-\text{H}_2\text{O}^+$  (Muehlenbachs, 1977; Muehlenbachs, 1980) et pour certains éléments majeurs sous forme d'oxydes (Hart, 1973). Dans le but d'estimer les flux chimiques résultant de l'altération de basse température, les tendances ou "trends" d'altération de Hart (1973) ont été utilisés ainsi que l'estimation d'un degré moyen d'altération équivalent à 2-2,5%  $\text{H}_2\text{O}^+$  pour les roches totales. Assumant une profondeur moyenne d'altération de 200-800m, la masse de basalte altéré est de 1,8-7,0.  $10^{15}$  g/année.

### 3.A.4 Deux cas typiques de problème de bilan : le potassium et le magnésium.

#### 3.A.4.a Le potassium.

La quantité de potassium dans les basaltes frais est d'environ 0,06% (Langmuir et al., 1977) et l'enrichissement en potassium dans le fluide hydrothermal à 350°C des Galapagos est d'environ 0,035% (Corliss et al., 1979a et b). Un rapport roche-eau minimum de 0,58 est ainsi requis dans le fluide hydrothermal de la zone axiale pour extraire dans sa totalité le potassium de la croûte océanique. Considérant cette valeur, le flux d'eau de mer de 1,4.  $10^{17}$  g/année des vents axiaux utilisé par Edmond et al. (1979) nécessite la réaction d'eau de mer avec au moins 9Km de croûte océanique! Les contraintes thermiques (chaleur latente + flux de chaleur) dans le premier kilomètre de la zone axiale ont été utilisées par Wolery et Sleep (1988) pour estimer le flux présenté dans le tableau 3.2. qui nécessite seulement 1,5Km de croûte, une valeur élevée, mais qui reste possible. Cette valeur peut-être considérée comme une valeur limite supérieure (Wolery et Sleep, 1988) et susceptible d'être corrigée en fonction des teneurs primitives des basaltes en  $\text{K}_2\text{O}$  qui peut être sujette à caution.

• A des températures d'interaction de 350°C, le potassium peut être extrait des basaltes (Mottl et Holland, 1978). Cependant, en dessous de cette valeur, il peut être inversement soustrait de l'eau de mer pour être inclus dans des phases minérales comme la smectite, la céladonite et la philipsite. Le flux de potassium du basalte vers l'eau de mer qui se produit à hautes températures est probablement faible en comparaison avec celui de signe opposé à basses températures. La croûte océanique se comporte ainsi comme un piège pour le potassium au cours des processus hydrothermaux.

#### 3.A.4.b Le magnésium.

La concentration de magnésium dans les fluides hydrothermaux des Galapagos est fortement appauvrie par rapport à l'eau de mer environnante (Corliss et al., 1979a,b); les travaux expérimentaux sur les fluides hydrothermaux montrent les mêmes effets. Après réaction de 0,06g de roche avec 1g d'eau, le magnésium est entièrement soustrait de l'eau de mer suggérant que les rides médio-océaniques peuvent être potentiellement des pièges efficaces pour le magnésium. Wolery et Sleep (1988) utilisent leur estimation selon laquelle un sixième de la perte de chaleur hydrothermale se produit depuis les événements axiaux; 1,27.  $10^{12}$  moles de magnésium sont ainsi extraites. La valeur exacte de l'anomalie en magnésium dans le système exogénique reste incertaine, Wolery et Sleep (1988) prennent une valeur de 2,5.  $10^{12}$  moles/an. Le résultat de leur calcul est un rapport roche-eau d'environ 0,005 pour expliquer la balance du magnésium dans les océans. Les flux de quelques éléments pour ce rapport eau-

**Comparaison des échanges chimiques basalte-eau de mer**  
**avec les flux du système exogénique**  
**(1E12 moles / an)**

|                        | Flux<br>Basalte - eau de mer | Flux<br>des rivières | Flux<br>vers le réservoir des<br>sédiments pélagiques | Total<br>du réservoir exogénique<br>( 4E09 années) |
|------------------------|------------------------------|----------------------|---|--|
| <b>Na</b>              | 0,28±0,16                    | 5,91                 | 0,35  | 0,52   |
| <b>K</b>               | 0,24±0,20                    | 1,17                 | 0,44  | 0,41   |
| <b>Ca</b>              | 2,55±0,50                    | 12,36                | 3,03  | 1,58   |
| <b>Mg</b>              | -1,41±0,80                   | 4,85                 | 0,78  | 0,66   |
| <b>SiO<sub>2</sub></b> | 1,17±0,19                    | 6,47                 | 6,87  | 7,17   |

Tableau 3.2

**Flux chimiques globaux produits par l'activité hydrothermale off-axis**  
**pour des températures variables et un rapport roche-eau de 0,005 (g / g)**  
**(flux en 1E12 moles / an)**

| Temperature (°C) | Na   | K     | Ca   | Mg    | SiO <sub>2</sub> | Mn    |
|------------------|------|-------|------|-------|------------------|-------|
| 80               | 0,62 | -0,81 | 1,75 | -2,22 | 0,75             | 0,015 |
| 120              | 0,41 | -0,58 | 1,18 | -0,95 | 1,07             | 0,010 |
| 160              | 0,31 | -0,24 | 0,88 | -0,78 | 0,57             | 0,008 |
| 200              | 0,25 | -0,01 | 0,45 | -0,62 | 0,45             | 0,006 |
| 240              | 0,73 | 0,04  | 1,70 | -1,56 | 1,14             | 0,022 |
| Moyenne          | 0,48 | 0,33  | 1,20 | -1,23 | 0,79             | 0,012 |

Tableau 3.3



roche sont donnés pour une fourchette de températures de 80-240°C dans le tableau 3.3. Ce rapport roche-eau est équivalent à la réaction d'une portion de croûte océanique d'une épaisseur moyenne de 170m durant l'activité hydrothermale off-axis.

Il est difficile d'estimer avec précision le flux hydrothermal actuel de magnésium ou de tout autre élément chimique. Cependant, un point critique doit être souligné. Une quantité non négligeable de magnésium apparaît être soustraite de la croûte océanique lors de l'altération palagonitique de basse température. Ce phénomène représente une source de magnésium endogénique qui n'est pas pris en compte dans le cycle total (Wolery et Sleep, 1988). Le problème de la balance du magnésium n'est donc pas encore réellement résolu. Pour de nombreux éléments chimiques (comme le sodium également), un examen attentif des processus hydrothermaux et des transformations minéralogiques associées apparaît nécessaire pour mieux comprendre leur cycle.

### 3.A.5 Buts de l'étude.

L'approche des bilans chimiques dans la croûte océanique lors de son interaction avec l'hydrosphère peut être également réalisée par l'intermédiaire des complexes ophiolitiques considérés comme des fragments de lithosphère océanique échoués sur les continents.

L'étude de l'activité hydrothermale fossile enregistrée par le complexe ophiolitique de Trinity fait le sujet de ce chapitre.

Cette ophiolite apparaît à plusieurs titres comme un objet adéquat pour réaliser une telle étude :

- l'ophiolite de Trinity présente une succession lithologique complète depuis les cumulats ultramafiques et mafiques et des gabbros isotropes fossilisant le toit de la chambre magmatique dans lequel s'enracine un complexe filonien alimentant le complexe de laves basaltiques en coussins. La présence dans ces basaltes intensément hydrothermalisés de céladonite et d'adulaire témoigne de l'absence de tout événement métamorphique postérieur. Ce dernier aurait pu effacer une partie de la "mémoire" des processus hydrothermaux océaniques enregistrés par le cortège ophiolitique dans les temps siluro-ordoviciens.

- La mise en évidence des modalités de l'activité hydrothermale dans une paléoride océanique à expansion lente fournit l'occasion de connaître la nature des événements hydrothermaux dans de tels sites qui sont encore mal définis dans les rides actuelles (ride Médio-Atlantique). Les bilans géochimiques pour les flux élémentaires et les rapports eau-roche dans une ride lente sont-ils identiques à ceux d'une ride océanique à expansion rapide?

- L'estimation du bilan des flux élémentaires entre la croûte océanique représentée par l'ophiolite de Trinity et le réservoir océanique est une occasion de comparer les bilans entre l'actuel et le Paléozoïque inférieur.

Les problèmes posés sont abordés dans le premier article constituant ce chapitre :

- 1) Le bilan des flux élémentaires entre le complexe ophiolitique de Trinity et son réservoir océanique contemporain.

- 2) Quelles sont les caractéristiques principales de l'activité hydrothermale dans une ride lente?

- 3) La dimension du système hydrothermal et les paléocirculations de fluides au sein de la croûte océanique.

- 4) Les relations entre rapports massiques eau-roche et l'amplitude des flux élémentaires ainsi que l'oxydation de la croûte océanique et son contrôle minéralogique.

Dans cette première partie, la méthodologie repose sur la caractérisation des associations métamorphiques, la connaissance des réactions minéralogiques, des compositions modales des roches métamorphiques ainsi qu'une étude des isotopes du Sr afin de quantifier la variation des rapports eau-roche au travers de la séquence crustale.

Les effets géochimiques de l'altération hydrothermale (développement de paragenèses métamorphiques) sur la composition chimique des roches totales est bien illustrée par les corrélations entre la composition chimique des épidotes (figure 3.1) et des amphiboles (figure 3.2) et celle des roches totales.

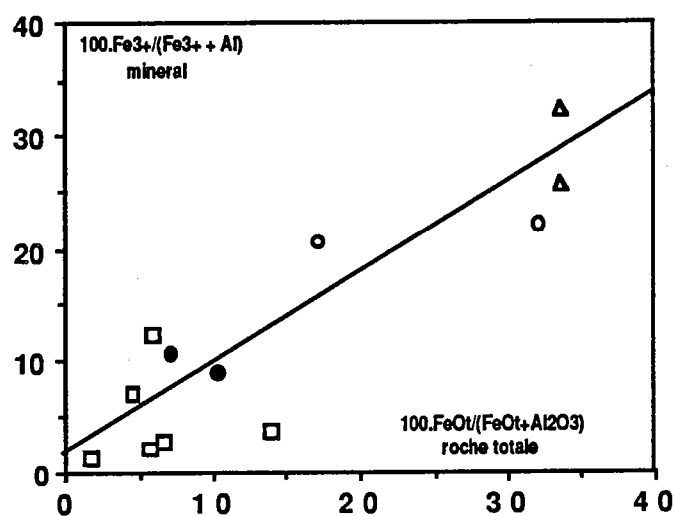


Figure 3.1 : corrélation chimique entre le rapport Fe/Al des épidotes et celui des roches hôtes. Carrés blancs : cumulats; ronds noirs : gabbros isotropes; ronds vides : basaltes et triangles vides : filons.

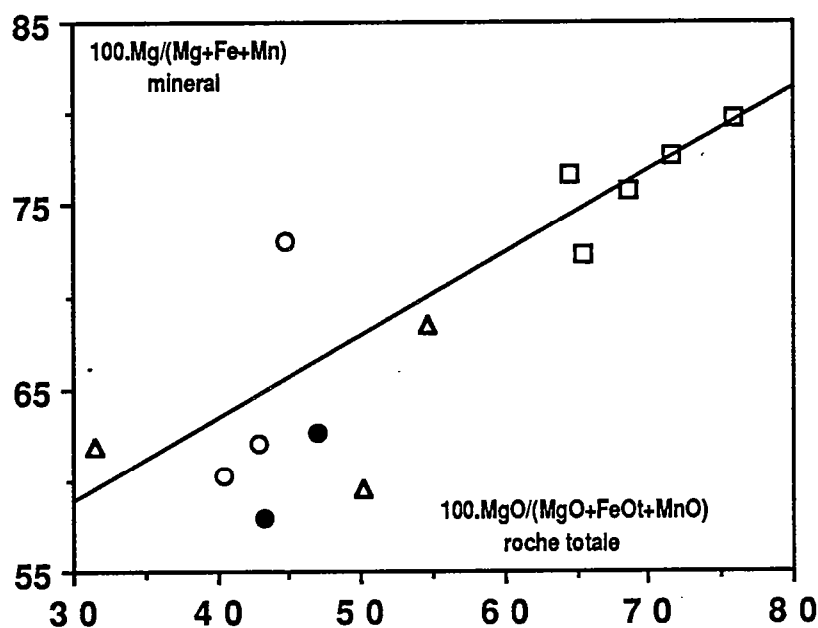


Figure 3.2 : corrélation chimique entre le rapport Mg/Fe+Mn des amphiboles et celui des roches hôtes. Carrés blancs : cumulats; ronds noirs : gabbros isotropes; ronds vides : basaltes et triangles vides : filons.

Le calcul des flux élémentaires est développé dans le premier article de ce chapitre (Lecuyer et al., 1989c). Il repose sur la connaissance des modes des échantillons qui ont été calculés à partir de la composition chimique de la roche totale (voir annexes) et de la composition chimique de chacun des minéraux constituant la roche (analyses microsonde, voir annexes). L'approche des moindres carrés (Bryan et al., 1968) offre l'avantage de fournir une

## Associations métamorphiques des basaltes de Trinity

|                      | TR45     | TR47A    | TR48  | TR49  | TR51B | TR52B    | TR55A | TR57B    | TR53B |
|----------------------|----------|----------|-------|-------|-------|----------|-------|----------|-------|
| ALBITE               | 15       | 18       | 30    | 32    | 44    | 13       | 40    | 44       | 43    |
| EPIDOTE              | 42       | 38       | 28    | 24    | 12    | 36       | 4     | 15       | 19    |
| ACTINOTE             | 25       | 29       | 20    | 36    | 30    | 39       | 28    | 34       | 21    |
| CHLORITE             | 0        | 0        | 22    | 0     | 11    | 0        | 28    | 4        | 15    |
| QUARTZ               | 16       | 12       | 0     | 3     | 0     | 9        | 0     | 0        | 0     |
| OXYDES <sub>Fe</sub> | 2        | 3        | 2     | 5     | 3     | 2        | 0     | 3        | 2     |
| MSWD                 | 4.40E-04 | 9.50E-03 | 0.038 | 0.031 | 0.01  | 6.20E-03 | 0.019 | 6.84E-04 | 0.039 |

Tableau 3.4

## Associations métamorphiques des cumulats de Trinity

|               | TR113 | TR222 | TR234 | TR248 | TR85 | TR121 | TR106 | TR110 | TR532 | TR64 |
|---------------|-------|-------|-------|-------|------|-------|-------|-------|-------|------|
| Clinopyroxène |       | 53    |       |       |      |       |       |       |       |      |
| Orthopyroxène | 13    |       |       |       |      |       |       |       |       |      |
| Olivine       | 47    | 5     |       |       |      |       |       |       |       |      |
| Serpentine    | 15    | 36    |       |       |      |       |       |       |       |      |
| Magnetite     |       | 6     |       |       |      |       |       |       |       |      |
| Ilm-Sph-Sp    | 8     |       |       |       |      |       |       |       | 0.7   | 1    |
| Actinote      |       |       | 47    | 56    | 85   | 50    | 52    | 49    |       | 16   |
| Chlorite      |       |       |       |       |      |       |       |       | 18.5  | 12   |
| Quartz        |       |       |       |       |      |       |       |       | 14.5  | 3    |
| Epidote       |       |       | 53    | 44    | 15   | 50    | 48    | 51    | 41.5  | 28   |
| Albite        |       |       |       |       |      |       |       |       |       | 40   |
| Hornblende    | 17    |       |       |       |      |       |       |       | 24.8  |      |

Tableau 3.5

## bilan bibliographique de la mobilité des éléments majeurs

système de référence = roche

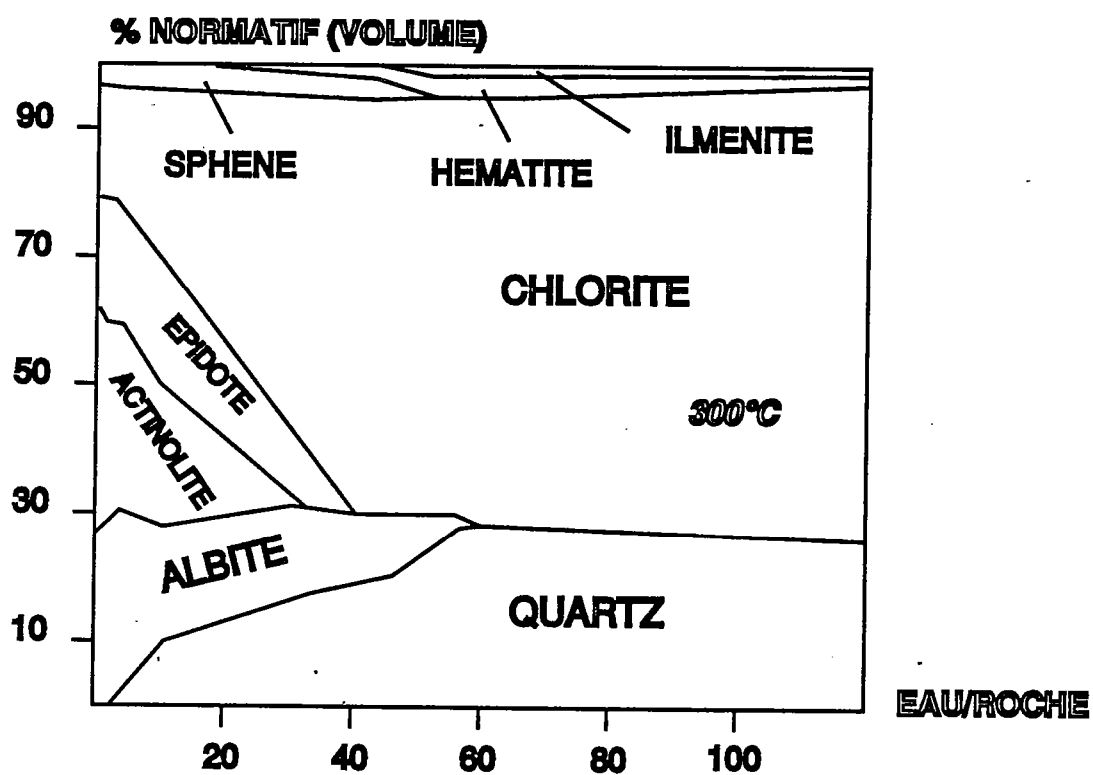
| Élément                        | Cette étude<br>1989 | Edmond et al.<br>1979 | Hékinian<br>1968 | Paster<br>1968 | Shido et al.<br>1974 | Hart<br>1973 | Thompson<br>1973 | Alt et Emmermann<br>1985 |
|--------------------------------|---------------------|-----------------------|------------------|----------------|----------------------|--------------|------------------|--------------------------|
| SiO <sub>2</sub>               | ±                   | - -                   | - -              | - -            | ±                    | - -          | -                | - -                      |
| TiO <sub>2</sub>               | -                   | n.d.                  | -                | ±              | ++                   | ++           | ±                | -                        |
| Al <sub>2</sub> O <sub>3</sub> | - -                 | n.d.                  | - -              | - -            | ++                   | ±            | ±                | -                        |
| Fe <sub>2</sub> O <sub>3</sub> | ++                  |                       | ++               | ++             | ++                   | ++           | ++               | ++                       |
| FeO                            | - -                 |                       | - -              | - -            | - -                  | - -          | - -              | -                        |
| FeO total                      | ++                  |                       | ++               | +              | ++                   | +            | ±                | ±                        |
| MnO                            | n.d.                |                       | +                | +              | ++                   | +            | ±                | ±                        |
| MgO                            | ++                  | ++                    | ±                | - -            | +                    | -            | - -              | +                        |
| CaO                            | - -                 | - -                   | - -              | - -            | - -                  | - -          | -                | - -                      |
| Na <sub>2</sub> O              | ±                   | +                     | -                | -              | ±                    | +            | ±                | ±                        |
| K <sub>2</sub> O               | +                   | ±                     | ++               | ++             | ++                   | ++           | ++               | +                        |

Tableau 3.8

### Compositions modales des filons de Trinity

| Echantillon | Actinote | Albite | Epidote | Chlorite | Quartz | Oxyde Fe | MSWD     |
|-------------|----------|--------|---------|----------|--------|----------|----------|
| TR128A      | 12       | 46     | 16      | 12       | 12     | 2        | 0.0118   |
| TR128B      | 8        | 36     | 21      | 15       | 18     | 2        | 1.35E-03 |
| TR128C      | 17       | 35     | 17      | 13       | 16     | 2        | 0.012    |
| TR128D      | 19       | 36     | 16      | 12       | 15     | 2        | 7.03E-03 |
| TR128E      | 18       | 34     | 17      | 14       | 15     | 2        | 8.72E-03 |
| TR128F      | 8        | 33     | 25      | 13       | 19     | 2        | 0.0298   |
| TR128G      | 17       | 33     | 21      | 12       | 15     | 2        | 7.24E-04 |
| TR128H      | 20       | 30     | 21      | 14       | 14     | 1        | 4.94E-05 |
| TR128I      | 23       | 27     | 22      | 16       | 11     | 1        | 6.43E-03 |
| TR128J      | 24       | 29     | 21      | 16       | 10     | 0        | 6.83E-03 |
| TR128K      | 21       | 32     | 21      | 12       | 13     | 1        | 3.93E-03 |
| TR128L      | 21       | 30     | 22      | 13       | 13     | 1        | 8.58E-03 |
| TR128M      | 21       | 27     | 23      | 16       | 12     | 1        | 0.0117   |
| TR128N      | 23       | 28     | 22      | 15       | 11     | 1        | 6.35E-03 |
| TR128O      | 22       | 26     | 24      | 16       | 12     | 0        | 0.0177   |
| TR128P      | 20       | 23     | 26      | 18       | 13     | 0        | 0.0146   |
| TR128Q      | 21       | 22     | 26      | 18       | 13     | 0        | 0.0151   |
| TR128R      | 24       | 27     | 23      | 14       | 11     | 1        | 8.25E-04 |
| TR128S      | 24       | 26     | 24      | 15       | 11     | 0        | 9.21E-03 |
| TR128T      | 27       | 27     | 23      | 13       | 9      | 1        | 1.71E-03 |
| TR134       | 11       | 24     | 27      | 15       | 21     | 2        | 0.029    |
| TR130A      | 49       | 24     | 14      | 13       | 0      | 0        | 0.349    |
| TR130B      | 7        | 14     | 38      | 15       | 26     | 0        | 0.911    |
| TR124A      | 23       | 44     | 13      | 9        | 8      | 3        | 0.0273   |
| TR124BC     | 31       | 33     | 20      | 12       | 4      | 0        | 0.184    |
| TR124D      | 36       | 39     | 9       | 15       | 0      | 1        | 0.136    |
| TR125AB     | 52       | 26     | 13      | 9        | 0      | 0        | 0.246    |
| TR127       | 19       | 26     | 26      | 15       | 13     | 1        | 0.0173   |

Tableau 3.6

*figure 3.3*

solution unique sur l'ensemble des données (système surdéterminé). Les compositions modales des basaltes, cumulats et filons ont été groupées respectivement dans les tableaux 3.4 et 3.5. Les modes minéralogiques des basaltes altérés hydrothermalement permettent d'après les travaux expérimentaux de Mottl (1983) de faire une première approximation du rapport eau-roche (figure 3.3). Ainsi, ces rapports eau-roche ont du être inférieurs à 30.

Le calcul des flux élémentaires nécessite l'acquisition de compositions chimiques de minéraux reliques dans l'ensemble de la séquence (voir annexes) afin de pouvoir reconstituer une composition chimique théorique de la roche totale de départ. Cette démarche repose sur la connaissance des réactions minéralogiques qui ont affecté les roches. L'estimation des changements de volume lors des réactions minéralogiques a été faite à partir de l'application des équations de Gresens (1967). La densité des minéraux invoqués dans chaque réaction provient du tableau 3.7 qui rassemble des densités de minéraux courants provenant de l'ouvrage de Deer et al. (1966). Les basaltes et filons étant intensément hydrothermalisés, ils ne présentent pas de reliques et des hypothèses ont été faites pour la composition du plagioclase (An75) et du clinopyroxène (diopside magnésien).

Les directions des flux élémentaires calculés pour l'ophiolite de Trinity ont été reportées dans le tableau 3. 8 à titre de comparaison avec les estimations issues des travaux des auteurs précédents. Les flux élémentaires ont été reportés pour chacun des échantillons le long de la séquence lithostratigraphique. Des courbes ont ainsi été déduites pour chacun des éléments considérés (Si, Al, Ca, Na, Mg et Fe; Lecuyer et al., 1989c) et intégrées sur l'axe vertical des échanges nuls afin d'obtenir un flux moyen entre la séquence crustale et le réservoir océanique. Ces valeurs ont été reportées dans le tableau 3.9 et comparées à celles déduites de l'étude de Alt et al. (1986) sur le trou 504B et aux apports des rivières (Thompson, 1983).

Enfin la figure 3.4 propose un modèle de boîtes qui synthétise qualitativement la balance chimique entre l'ophiolite de Trinity et son réservoir océanique contemporain.

### 3.A.6 Résultats.

Deux résultats principaux se dégagent de cette étude :

1) L'altération des roches océaniques induite par l'activité hydrothermale au sein des rides océaniques à expansion lente apparaît davantage pervasive que celle qui affecte les rides océaniques dans les environnements à expansion rapide. Le régime de fracturation (failles normales; Choukroune et al., 1984) plus développé latéralement et en profondeur dans les centres d'expansion océanique lents est certainement à l'origine de flux chimiques considérables résultant d'interactions eau-roche en système ouvert.

2) Les flux élémentaires révèlent ainsi la grande mobilité des éléments majeurs au sein de la croûte océanique hydrothermalisée.

#### flux élémentaires ( $10^{14}$ g/an)

|    | TROU 504B TRINITY |       | RIVIERES |
|----|-------------------|-------|----------|
| Si | -1,4              | -0,7  | -1,99    |
| Al | n.d.              | ≈0    | n.d.     |
| Fe | n.d.              | ≈0    | -0,02    |
| Mg | 0,43              | 1,15  | -1,33    |
| Ca | -1,04             | -11,9 | -4,88    |
| Na | n.d.              | 0,79  | -1,31    |
| K  | 0,05              | 0,04  | -0,74    |

Tableau 3.9

| MINERAUX         | DENSITE   | MINERAUX         | DENSITE   |
|------------------|-----------|------------------|-----------|
| ALBITE           | 2,6       | BRUCITE          | 2,39      |
| ANORTHITE        | 2,76      | CHRYSTILE        | 2,55      |
| ORTHOSE          | 2,59      | LIZARDITE        | 2,55      |
| SANIDINE         | 2,59      | ANTIGORITE       | 2,6       |
| ANORTHOSE        | 2,59      |                  |           |
| NEPHILINE        | 2,61      | QUARTZ           | 2,65      |
| LEUCITE          | 2,47      | TRIDYMIT         | 2,26      |
| SODALITE         | 2,3       | CRISTOBALITE     | 2,33      |
| ANALCITE         | 2,27      |                  |           |
|                  |           | ZIRCON           | 4.6-4.7   |
| ENSTATITE        | 3,21      | SPHENE           | 3.45-3.55 |
| HYPERSTHENE      | 3,4       |                  |           |
| FE-HYPERSTHENE   | 3,8       | PYROPE           | 3,58      |
| FERROSILITE      | 3,96      | ALMANDIN         | 4,32      |
|                  |           | SPESSARTINE      | 4,19      |
| AUGITE           | 3.23-3.52 | GROSSULAIRE      | 3,59      |
| PIGEONITE        | 3.3-3.46  | ANDRADITE        | 3,86      |
| DIOPSIDE         | 3,3       | OUVAROVITE       | 3,9       |
| HEDENBERGITE     | 3,56      | HYDROGROSSULAIRE | 3,6       |
| JADEITE          | 3,42      |                  |           |
| AEGYRINE         | 3,58      |                  |           |
|                  |           | SILLIMANITE      | 3.23-3.27 |
| WOLLASTONITE     | 2.87-3.09 | ANDALOUSITE      | 3.13-3.16 |
|                  |           | STAUROLITE       | 3.74-3.83 |
| FORSTERITE       | 3,22      | CORDIERITE       | 2.53-2.78 |
| FAYALITE         | 4,39      |                  |           |
|                  |           | ZOISITE          | 3.15-3.27 |
| HORNBLende       | 3-3.4     | CLINOZOISITE     | 3.12-3.38 |
| H.BASALTIQUE     | 3.2-3.3   | EPIDOTE          | 3.38-3.49 |
| PARGASITE        | 3,05      | PIEMONTITE       | 3.45-3.52 |
| FERROHASTINGSITE | 3,5       |                  |           |
| KAERSUTITE       | 3,3       | HEMATITE         | 5,25      |
| BARKEVICITE      | 3.35-3.44 | ILMENITE         | 4.7-4.78  |
| GLAUCOPHANE      | 3,08      | SPINELLE         | 3,55      |
| RIEBECKITE       | 3-3.4     | HERCYNITE        | 4,4       |
| ARFVEDSONITE     | 3,5       | MAGNETITE        | 5,2       |
|                  |           | ULVOSPINELLE     | 4,78      |
| ANTHOPHYLLITE    | 3,01      | CHROMITE         | 5,09      |
| GEDRITE          | 3,15      | MG-CHROMITE      | 4,43      |
| GRUNERITE        | 3,6       |                  |           |
| CUMMINGTONITE    | 3,36      | APATITE          | 3.1-3.35  |
|                  |           |                  |           |
| MUSCOVITE        | 2.8-2.9   | SHERIDANITE      | 2,8       |
| PHLOGOPITE       | 2.8-2.9   | CORUNDONPHILITE  | 2,85      |
| BIOTITE          | 2.7-3.3   | RIPIDOLITE       | 2,96      |
|                  |           | CLINOCHLORE      | 3,02      |
|                  |           | PYCHNOCHLORITE   | 2,82      |
|                  |           | BRUNSVIGITE      | 2,98      |
|                  |           | THURINGITE       | 3,31      |
|                  |           | CHAMOSITE        | 3,03      |

tableau 3.7.

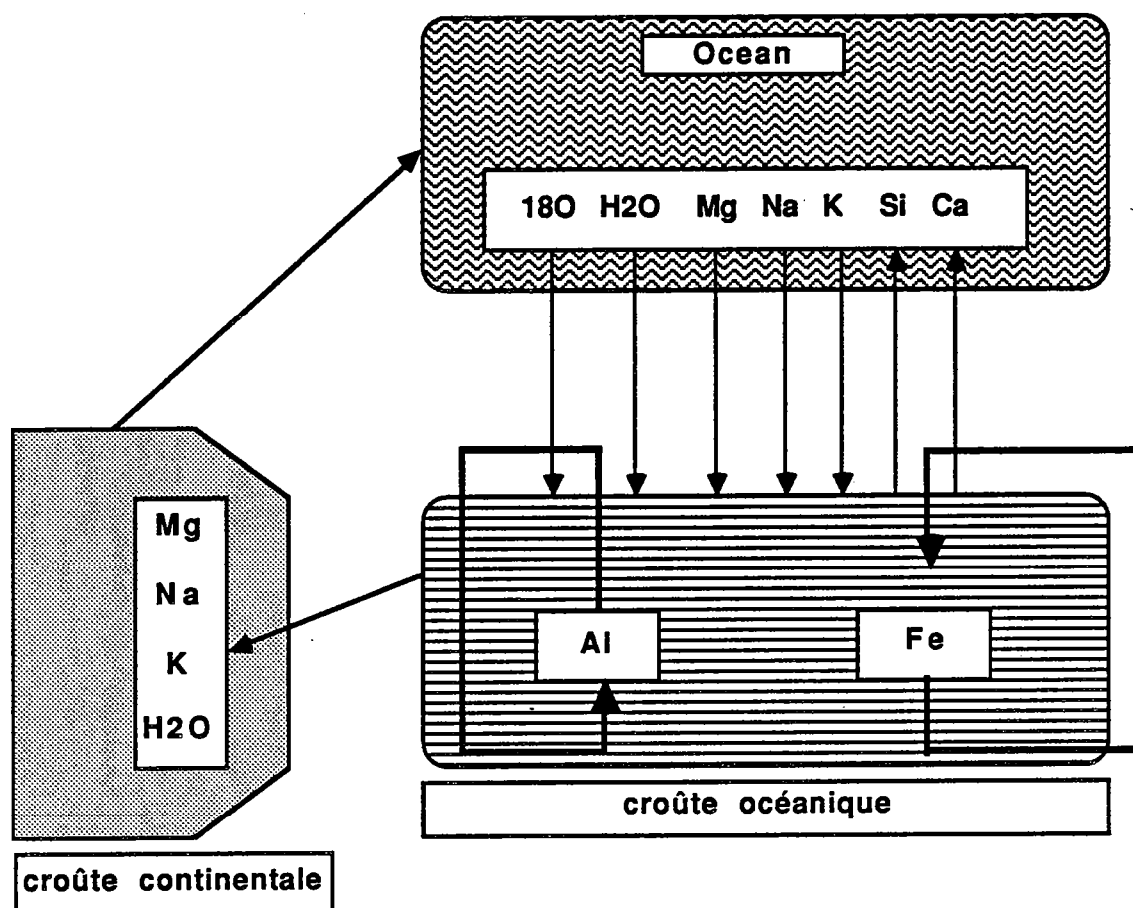


Figure 3.4

Ces flux se développent aussi bien dans des conditions de basse température et de rapports eau-roche élevés que sous des conditions de haute température et rapports eau-roche faibles. Si ces résultats confirment la grande mobilité des éléments calco-alcalins et alcalins au cours de l'hydrothermalisme; ils mettent également en évidence la mobilité d'éléments métalliques comme l'aluminium. Cet élément est ainsi très mobile au sein de la croûte océanique sans toutefois échanger avec le réservoir océanique. Il apparaît ainsi opportun de rappeler qu'une grande prudence doit être adoptée au cours de l'utilisation des éléments majeurs comme critères géochimiques discriminants des séries volcaniques métamorphisées.

Une possible mobilité du titane n'a pu être quantifiée à cause de ses faibles concentrations dans les roches de l'ophiolite de Trinity, ses difficultés analytiques de dosage et celles concernant la composition des phases minérales primaires les contrôlant (oxydes ferrotitanés). Toutefois, une analyse qualitative a été envisagée à partir du report des concentrations en titane des basaltes de Trinity et de ceux du trou 504B (ride Est Pacifique) en fonction des teneurs en  $H_2O^+$  (figure 3.5).



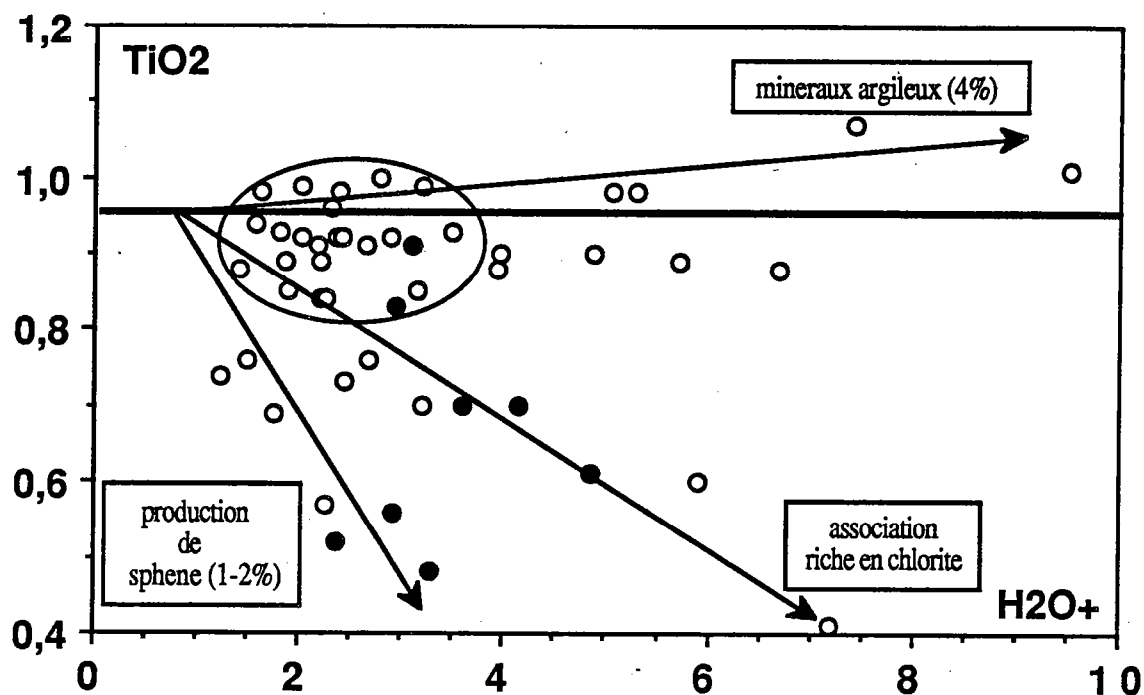


Figure 3.5 : ronds pleins = basaltes de l'ophiolite de Trinity; ronds vides = basaltes du trou 504B (Alt et Emmermann, 1985).

Alt et Emmermann (1985) ont ainsi observé une corrélation positive pour les basaltes du trou 504B et évoquent des départs significatifs de titane lors de l'hydrothermalisme des basaltes de la croûte océanique. et la figure 3.5 suggère également un enrichissement en Fe au cours de la cristallisation des minéraux phylliteux lors de l'altération de basse température.

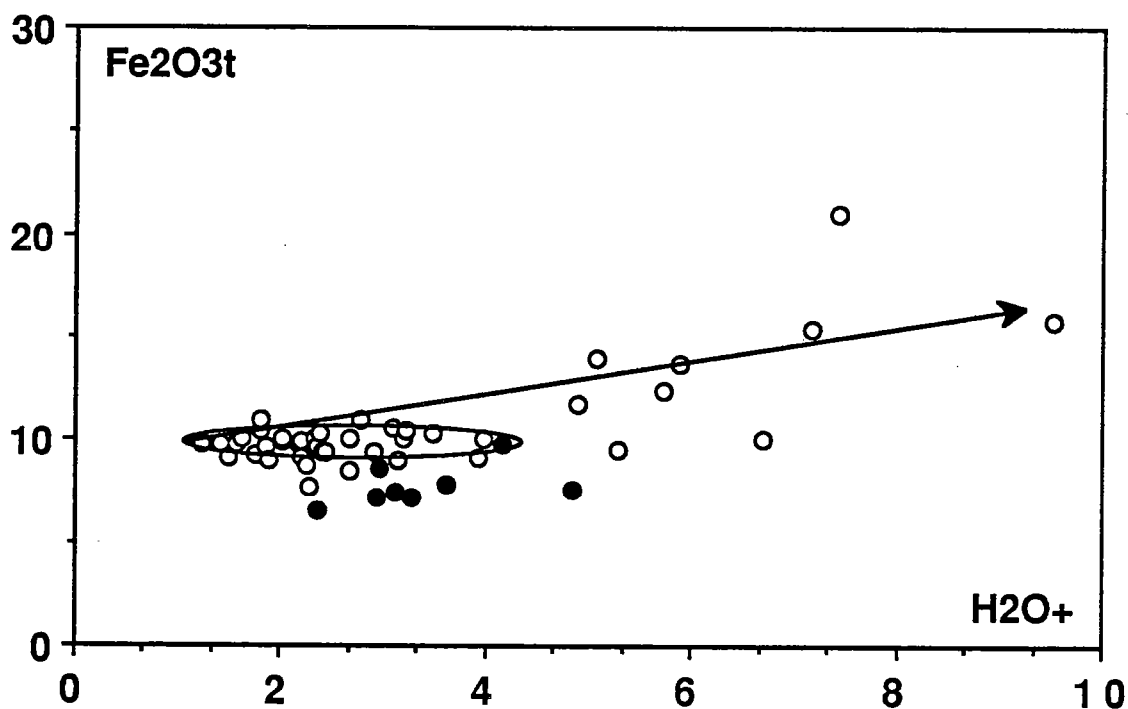


Figure 3.6 : même légende que figure 3.5.

La variation des concentrations en titane dans les basaltes de Trinity peut être ainsi expliquée dans une certaine mesure par la transformation des oxydes ferro-titanés en sphène qui se produit en système ouvert. La production de 2% de sphène est susceptible d'appauvrir la roche initiale de 0.4% en Ti. Le Ti ainsi libéré se retrouve dans les palagonites (jusqu'à 5% de Ti) en remplacement du verre basaltique lors de l'altération de basse température. La présence de telles argiles explique également certaines anomalies positives en Ti dans des basaltes hydrothermalisés indépendamment des processus magmatiques. En effet l'altération de 10% de verre basaltique en palagonite permet de récupérer le Ti fourni par la transformation de 2% d'ilménite en sphène.

Le Ti est un élément généralement admis comme immobile au cours des phénomènes d'altération (Pearce et Cann, 1973; Floyd et Winchester, 1975; Sivell et Rankin, 1982). La classification des complexes ophiolitiques dans des sites géotectoniques variés (océan ouvert, bassin marginal et arcs) repose principalement sur la concentration en Ti des laves (Miyashiro et Shido, 1975; Bébien, 1980; Serri, 1981; Ohnenstetter, 1982; Ohnenstetter, 1985). L'étude des concentrations en Ti dans les basaltes hydrothermalisés suggère la plus grande prudence quant à l'utilisation des teneurs en Ti comme marqueurs pétrogénétiques décisifs.

### 3. B. L'hydrothermalisme océanique fossile dans l'ophiolite de Trinity : étude isotopique de l'oxygène et du carbone.

#### 3.B.1 Rappels.

Un domaine d'application de prédilection de la géochimie des isotopes stables est celui de l'étude de l'altération hydrothermale de la croûte océanique (ex : Muehlenbachs, 1986). Au fur et à mesure de la création de nouvelle lithosphère océanique, cette dernière encore chaude est rapidement mise en contact avec d'énormes quantités d'eau de mer dont la circulation convective est guidée par la porosité de la croûte océanique et son réseau de fractures. L'acquisition de données isotopiques en oxygène sur des roches océaniques actuelles ou fossiles peut permettre d'élucider les grands caractères du régime hydrothermal. De tels modèles peuvent être contraints grâce en particulier à la remarquable constance des signatures isotopiques de l'eau de mer ( $\delta^{18}\text{O} = 0 \pm 0,2$ ; Epstein et Mayeda, 1953) et des roches dérivées du manteau ( $\delta^{18}\text{O} = +5,7 \pm 0,2$ ; Taylor, 1968; Muehlenbachs et Clayton, 1972; Pineau et al., 1976; Ito et al., 1982). En outre, les équations de fractionnement à l'équilibre entre minéraux secondaires et eau sont relativement bien connues dans le domaine des températures de l'hydrothermalisme sous-marin sauf pour les basses températures.

De nombreuses difficultés sont toutefois présentes telles le caractère hétérogène de l'altération hydrothermale à l'échelle de la croûte océanique (Böhlke et al., 1981) et la méconnaissance de l'évolution isotopique du fluide hydrothermal au fur et à mesure qu'il pénètre dans la croûte océanique et réagit avec les roches encaissantes. Enfin, les valeurs isotopiques en oxygène enregistrées par les roches à l'axe de la ride peuvent être couramment modifiées par les processus hydrothermaux tardifs de basse température (altération "off-axis" ou encore "oceanic weathering").

***Le temps de vie moyen de la croûte océanique, autour de 200Ma, implique la nécessité d'étudier les complexes ophiolitiques si l'on veut acquérir des informations globales sur les modalités de l'hydrothermalisme au cours des temps géologiques.***

Un certain nombre de complexes ophiolitiques ont été analysés en oxygène tels les complexes de Xigaze, Grèce, Italie, Chypre, Chili, Macquarie, Oman, Californie (Del Puerto et Josephine), Terre-Neuve et l'Afrique du Sud (Agrinier et al., 1988; Montigny et al., 1970; Wenner et Taylor, 1973; Spooner et al., 1974 et Schiffman et Smith, 1988; Stern et al., 1976; Heaton et Sheppard, 1977; Cocker et al., 1982; Gregory et Taylor, 1981; Schiffman et al., 1984 et Harper et al., 1988; Hoffman et al., 1986) respectivement. A priori, l'ensemble de ces données est cohérent avec celles acquises au cours des études du plancher océanique :

- la croûte océanique est extensivement altérée.
- certaines parties de la croûte sont enrichies en  $^{18}\text{O}$ , d'autres sont nettement appauvries.

Un examen détaillé de la distribution des valeurs de  $\delta^{18}\text{O}$  dans les séquences ophiolitiques révèle des différences d'un complexe à l'autre si l'on compare les unités lithostratigraphiques constituant le cortège :

- les ophiolites "californiennes" situées typiquement dans un domaine de "terrane" (Howell, 1985) se distinguent par un enrichissement global en oxygène  $^{18}\text{O}$ .
- les autres complexes montrent généralement une séquence de pillow lavas ou coulées massives enrichies en  $^{18}\text{O}$  (+5 à +14) et une séquence plutonique appauvrie ( $\delta^{18}\text{O} = +3,4$  à +5,7). Par contre les complexes filoniens en position intermédiaire dans la séquence peuvent présenter systématiquement des valeurs élevées comme à Oman (+5,8 à +10) ou des

valeurs basses comme à Macquarie ( $\delta^{18}\text{O} = +4$  à  $+5,9$ ) ou encore un mélange des deux comme dans les ophiolites chiliennes ( $\delta^{18}\text{O} = +3,4$  à  $+9,6$ ).

***Au constat de la disparité de la distribution des valeurs de  $\delta^{18}\text{O}$  au sein des croûtes océaniques fossiles, il est important d'essayer de relier la variabilité de ces signatures géochimiques à l'environnement géotectonique.***

### 3.B.2 Buts de l'étude.

A la suite de l'approche de l'hydrothermalisme effectuée à partir du calcul des flux élémentaires et des isotopes du Sr. Une étude isotopique de l'oxygène sur les mêmes échantillons (roches totales et quartz séparés; chambre de Gray Rock) et du carbone sur les calcites en remplissage des vésicules des basaltes ou contenues dans les interstices des filons et gabbros isotropes pouvait donner des informations complémentaires sur les modalités de l'activité hydrothermale qui a affecté l'ophiolite de Trinity. Cette étude effectuée dans le laboratoire de géochimie du CAESS (Rennes) sous la direction de S. Fourcade a été accompagnée de données microthermométriques sur des inclusions fluides primaires des quartz contenus dans les basaltes et gabbros isotropes (P. Nehlig, Université de Brest). Les résultats de cette étude sont présentés dans un article (Lecuyer et Fourcade, 1989) qui fait suite à cette introduction.

Les problèmes posés sont les suivants :

1) Mise en évidence de phases hydrothermales successives au cours du temps et de leur régime thermique.

2) La réalisation d'un bilan en oxygène sur l'ensemble de la séquence crustale afin de comparer le profil déduit de celui connu dans les rides à expansion rapide illustré par l'ophiolite de Semail (Oman; Gregory et Taylor, 1981) et de celui connu dans les rides à expansion lente (Xigaze; Agrinier et al., 1988).

3) La confrontation des données de **méthodologies diverses et complémentaires** (bilans de masse, isotopes du strontium, de l'oxygène, du carbone et données microthermométriques sur inclusions fluides) afin de contraindre la composition isotopique initiale de l'eau de mer qui a réagi avec les roches du cortège ophiolitique de Trinity. L'intérêt de l'utilisation de méthodes complémentaires est illustrée par la corrélation qui est obtenue au sein de la séquence lithologique de Trinity (chambre de Gray Rock) entre les valeurs de  $\delta^{18}\text{O}$  et les rapports eau-roche (figure 3.7) calculés à partir des concentrations et des valeurs isotopiques du Sr d'après la méthode d'Albarède et al. (1981). Cette corrélation révèle que la précision sur les valeurs de rapports eau-roche dépend directement du rapport des concentrations des éléments dans chacun des réservoirs. Ainsi les faibles concentrations en Sr de l'eau de mer (8ppm en moyenne) par rapport à celle des basaltes de Trinity (entre 39 et 86ppm; facteur 0,09 à 0,2) permettent une quantification de grande résolution dans le domaine des rapports eau-roche élevés à l'inverse des valeurs isotopiques de l'oxygène qui sont tamponnées par l'eau de mer (facteur 0,5 entre la concentration en oxygène d'une roche silicatée et de l'eau de mer). Par contre, les isotopes de l'oxygène fournissent des informations plus précises sur les rapports eau-roche dans le domaine des rapports eau-roche faibles (roche en excès).

L'analyse isotopique de l'oxygène sur les carbonates permet de connaître leurs paléotempératures de précipitation (ou de rééquilibrage!) et ainsi de quantifier les conditions thermiques de l'altération de basse température. Les valeurs de  $\delta^{13}\text{C}$  permettent de connaître la nature et la source du carbone (carbone juvénile, organique et marin; figure 3.8).

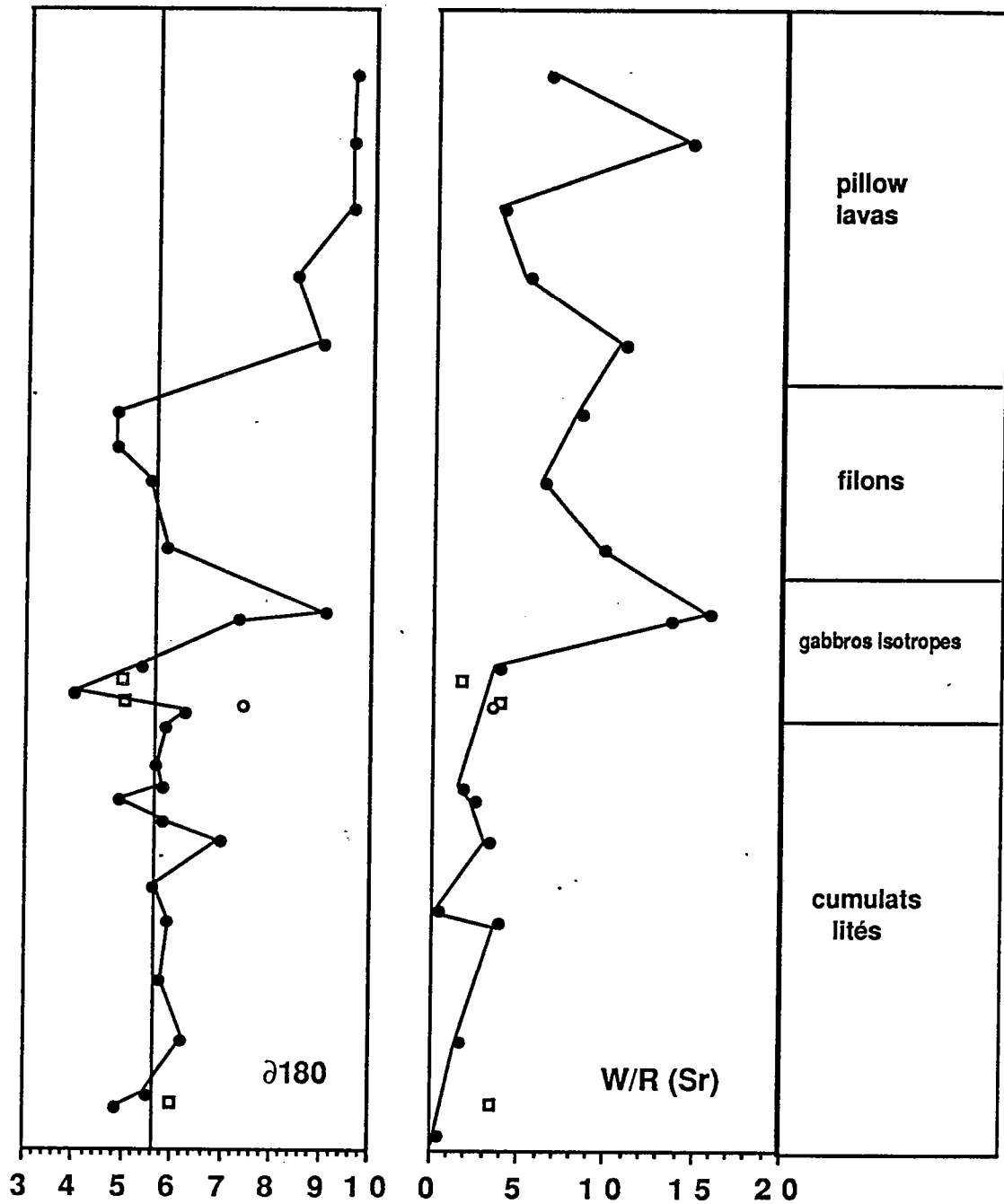


figure 3.7 : corrélation entre les profils en  $\delta^{18}O$  et rapports eau-roche (Sr) sur roches totales en fonction de la séquence lithostratigraphique de l'ophiolite de Trinity (chambre de Gray Rock).

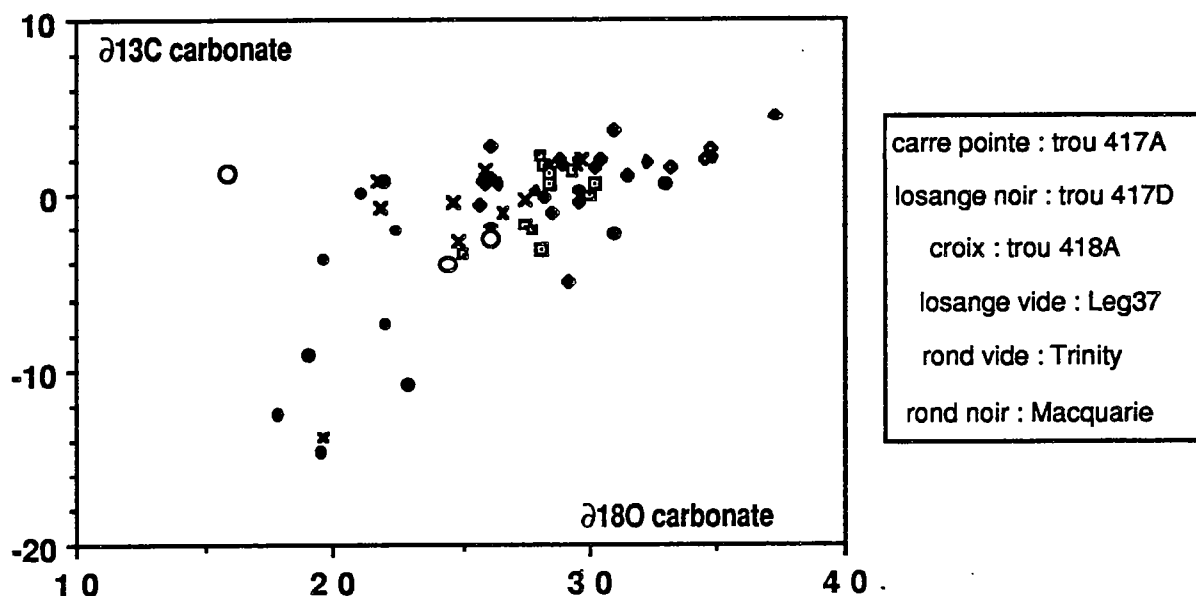


Figure 3.X :  $\delta^{18}\text{O}$  des carbonates du plancher océanique (Javoy et Fouillac, 1979), des ophiolites de Macquarie (Cocker et al., 1982) et de Trinity en fonction de  $\delta^{13}\text{C}$ .

Les mesures isotopiques effectuées sur des échantillons de fluides hydrothermaux non mélangés à de l'eau de mer pure ("end-member" ou pôle pur) par Craig et al. (1980) indiquent l'existence de fluides profonds dont les signatures isotopiques peuvent être considérablement modifiées ( $\delta^{18}\text{O}$  variant entre +1 et +2). L'existence de tels fluides émis à l'axe des rides (fumeurs noirs) a été aussi prise en compte et expliquée par les modèles thermodynamiques et géochimiques de Bowers et Taylor (1985; figure 3.9). Il est important de savoir si de tels fluides modifiés isotopiquement existent dans les environnements de rides lentes dans lesquelles l'activité des fumeurs noirs est extrêmement réduite.

Une telle approche a pour but également de connaître la composition isotopique en oxygène de l'océan siluro-ordovicien (océan actuel :  $\delta^{18}\text{O} = 0$ ) afin de confirmer ou infirmer la possibilité d'une évolution séculaire de la composition isotopique en oxygène de l'océan mondial depuis les temps paléozoïques.

La connaissance simultanée des flux chimiques, des rapports eau-roche, des températures d'altération hydrothermale et de la composition isotopique en oxygène des fluides qui ont réagi avec les roches a permis de proposer un modèle spatio-temporel encore qualitatif de l'activité hydrothermale qui a siégé dans une paléoride océanique à expansion lente (figure 3.10).

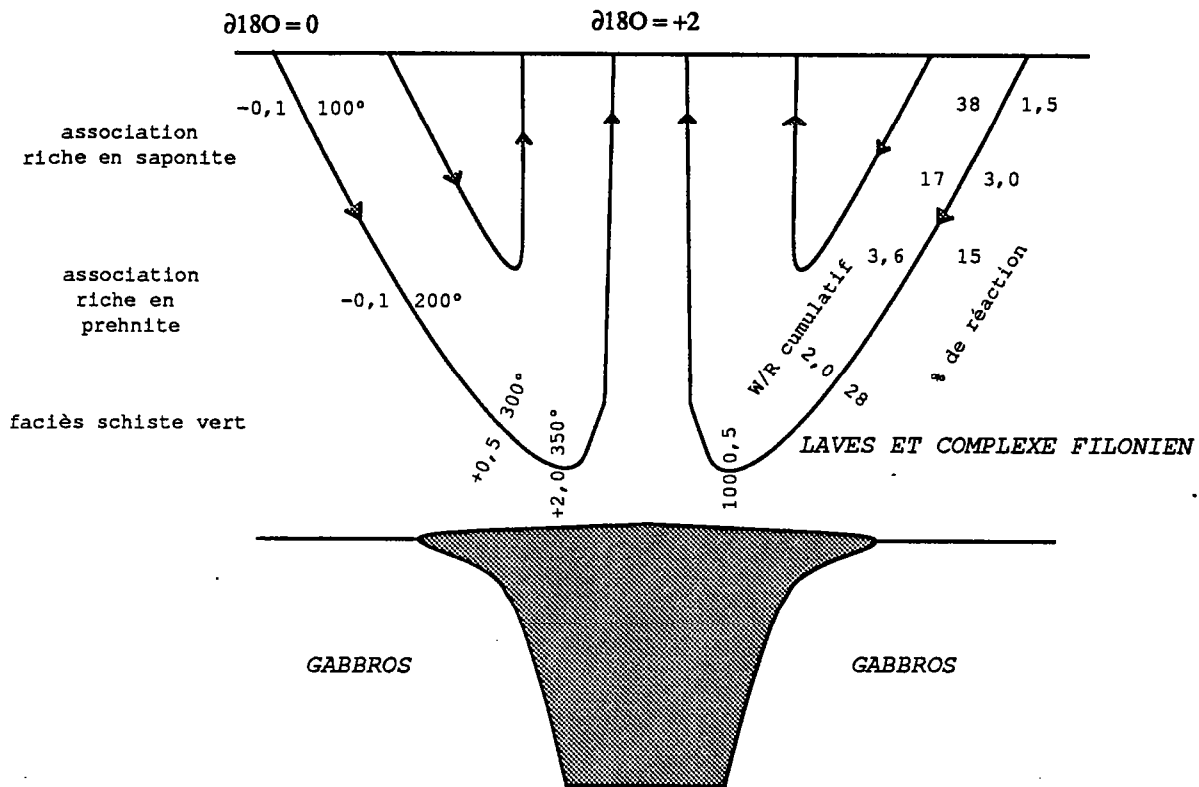


figure 3.9

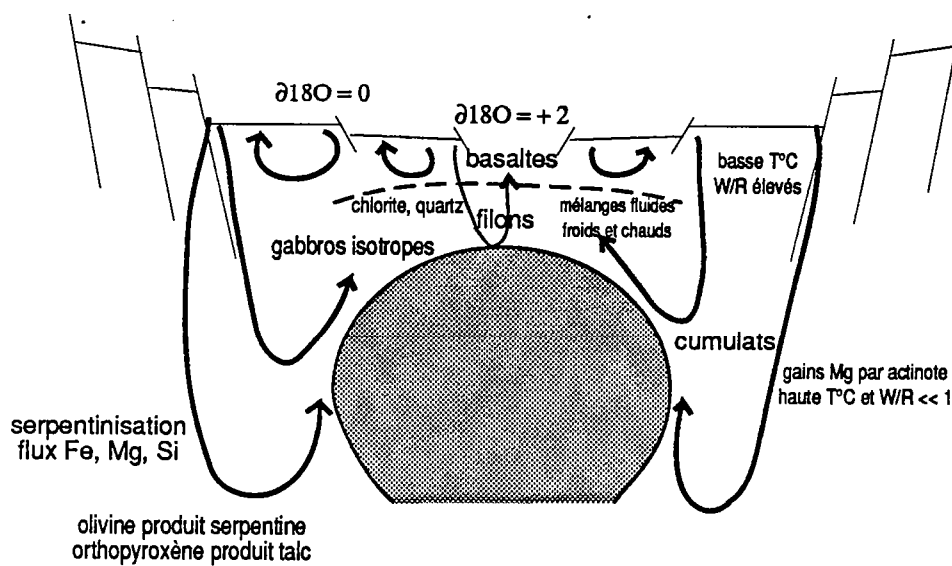


figure 3.10

### 3.B.3 Comparaison de l'activité hydrothermale fossile entre un arc insulaire et un bassin océanique.

L'activité hydrothermale bien mise en évidence à l'aplomb des rides océaniques et même dans les bassins marginaux apparaît comme un phénomène majeur de grande amplitude qui affecte la quasi totalité de la croûte océanique. Les arcs insulaires semblent moins affectés par l'hydrothermalisme océanique. Leurs rapports isotopiques  $^{87}\text{Sr}/^{86}\text{Sr}$  légèrement plus élevés par comparaison avec ceux des basaltes de MORB sont interprétés comme le résultat de l'addition au cours des phénomènes de subduction de sédiments et de basaltes précédemment hydrothermalisés plutôt que par interaction avec de grandes masses d'eaux hydrothermales. Toutefois, il faut remarquer que la plupart des échantillons étudiés représentent les niveaux subaériens des arcs volcaniques et non leurs niveaux profonds.

Les séries volcaniques siluro-dévonniennes de Copley-Balaklala ont été disséquées par la tectonique et mettent à jour ainsi des niveaux volcaniques profonds (figure 3.11). Ces séries sont interprétées comme spatialement et temporellement associées à un bassin marginal de type arrière-arc représenté par le complexe ophiolitique de Trinity (Brouxel et al., 1988) qui est encore interprété comme un petit bassin océanique formé à l'aplomb d'une ride océanique à expansion lente (LeSueur et al., 1984; LeSueur et Boudier, 1986). L'ensemble de ces massifs volcaniques a été affecté par un hydrothermalisme sous-marin qui offre la possibilité de comparer son activité au sein de structures géologiques différentes.

### 3.B.4 Les volcanites d'arcs insulaires et les roches ophiolitiques de Trinity.

Les 1800m de puissance de roches vertes du Copley sont représentées par des basaltes porphyriques, andésites et andésites riches en Mg qui sont surmontés en discordance par les rhyolites porphyriques de la formation de Balaklala (1000m de puissance). Ces deux formations sont recoupées par le stock trondhjémite de Mule Mountain âgé de 400Ma (Albers et al., 1981) considéré comme cogénétique avec les rhyolites de Balaklala (Barker et al., 1979; Lapierre et al., 1985a et b; Brouxel et al., 1988).

Les roches volcaniques de Copley et de Balaklala ont subi un métamorphisme schiste vert et plus localement zéolite et amphibolite (Barker et al., 1979). La présence du faciès amphibolite est à lier au métamorphisme de contact au voisinage de l'intrusion de Shasta Bally (Kinkel et al., 1956; Barker et al., 1979) tandis que les faciès schiste vert et zéolite sont les témoins de l'activité hydrothermale qui a conduit à la formation de dépôts massifs de sulfures au sein de la Rhyolite de Balaklala. Dans les "roches vertes" du Copley, les feldspaths sont albitisés ou séricitisés tandis que l'olivine et l'orthopyroxène sont remplacés par des smectites, chlorites et serpentines. Les phénocristaux de clinopyroxène et les spinelles chromifères sont les seuls minéraux préservés. Quelquefois altéré, le clinopyroxène est transformé en actinote ou en hornblende actinolitique. Au sein de la Rhyolite de Balaklala et du stock de Mule Mountain, aucun minéral primaire à l'exception de phénocristaux de quartz n'a été observé. Les feldspaths sont systématiquement albitisés, de rares biotites chloritisées et quelques amphiboles ont été identifiées par Lapierre et al. (1985b). Les amphiboles métamorphiques des roches volcaniques du Copley sont principalement des actinotes avec des teneurs faibles en Ti ( $<0,05$  atomes/formule), AlIV ( $<1,2$ ) et alcalins ( $<0,3$ ). Les amphiboles des volcanites de Balaklala sont plus riches en Ti, AlIV et alcalins mais aucune relation entre la composition des minéraux et leur position stratigraphique n'a pu être détectée. La composition des épidotes des roches volcaniques du Copley présente une grande plage de variations ( $100\text{Fe}^{3+} / (\text{Fe}^{3+} + \text{Al})$  compris entre 6 et 28) avec une distribution bimodale (figure 3.12). La composition de ces épidotes est comparée à celle des roches ophiolitiques de Trinity (figure 3.13).



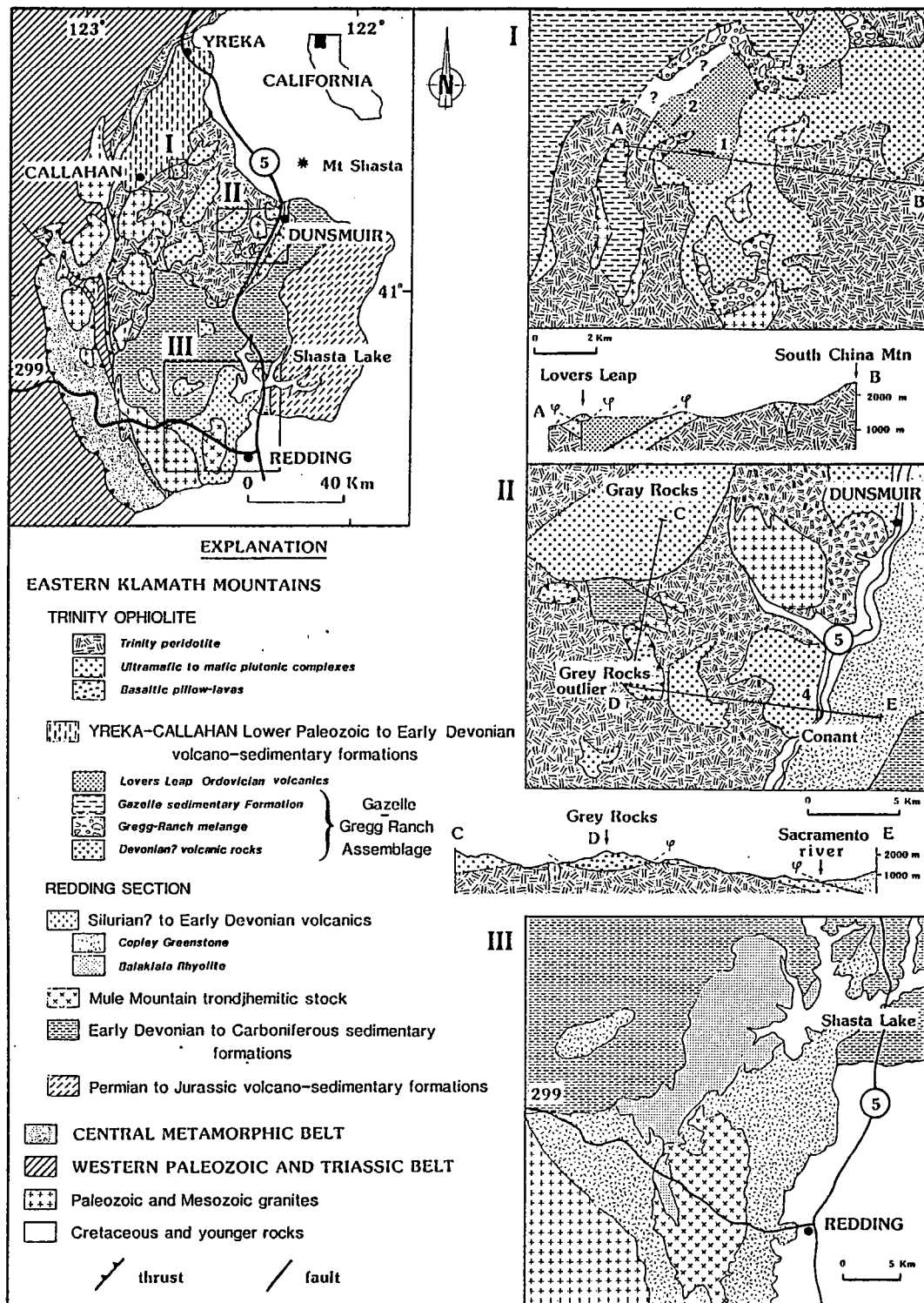


figure 3.11 : carte géologique des Klamath orientales avec la localisation des séries volcaniques de Copley-Balaklala et de Mule Mountain.

**Histogramme de fréquence des teneurs en Ps  
des epidotes de Copley et Balaklala-Mule Mountain**

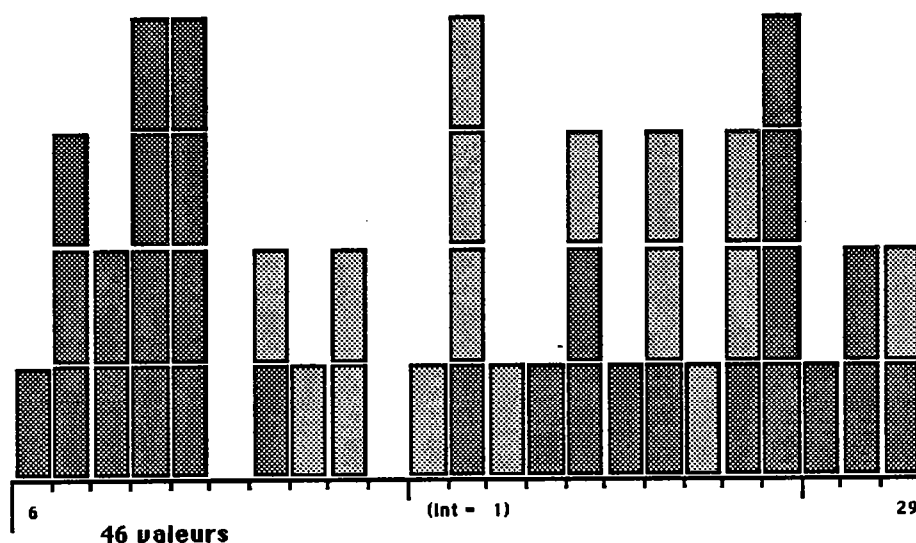


Figure 3.12 : grisé foncé : Copley et grisé clair : Balaklala et Mule Mountain.

**Histogramme de fréquence des teneurs en Ps  
du complexe ophiolitique de Trinity**

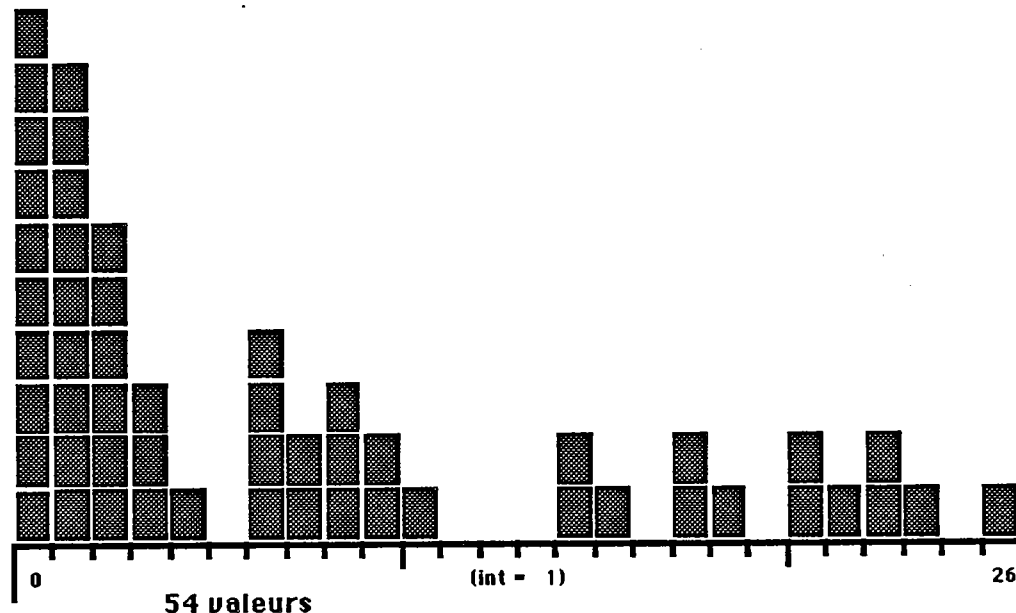


Figure 3.13.

Les épidotes des rhyolites de Balaklala et des trondhjémites de Mule Mountain présentent une variation de composition plus restreinte (%Pistachite compris entre 12 et 28).

Les caractères géochimiques des volcanites du Copley et de Balaklala et des roches ophiolitiques de Trinity ont été étudiées par M. Brouxel dans sa thèse. Toutes ces roches sont des tholéiites pauvres en Ti et K et très appauvries en éléments traces incompatibles. L'ensemble de ces roches présente des rapports isotopiques initiaux  $^{143}\text{Nd} / ^{144}\text{Nd}$  suggérant une origine commune à partir d'une même source mantellique (Brouxel, 1987). Au

contraire, leurs rapports isotopiques initiaux  $^{87}\text{Sr} / ^{86}\text{Sr}$  varient largement entre -21,4 et +21,6 pour le complexe ophiolitique de Trinity, entre -9 et +34 pour les roches du Copley, entre +7 et +39 pour les rhyolites de Balaklala et entre +2 et +28 pour Mule Mountain.

Dans le complexe ophiolitique de Trinity, il a été montré (Lecuyer et al., 1989c) que les rapports eau / roche sont compris entre 0 (référence mantellique) et 16, qu'ils augmentent depuis les basaltes jusqu'aux gabbros isotropes et diminuent régulièrement vers la base de la séquence ophiolitique. De fortes variations du rapport eau / roche ont été également enregistrées dans les laves de l'arc insulaire Copley-Balaklala dans lequel les plus fortes valeurs peuvent atteindre 33. De façon similaire, aucune corrélation n'est possible entre l'amplitude des rapports eau / roche et la position stratigraphique des échantillons.

Taylor et South (1985) ont réalisé une étude régionale systématique en  $\delta^{18}\text{O}$  et  $\delta\text{D}$  des formations constituant l'arc volcanique de Copley-Balaklala. Les données sont rappelées dans le tableau 3.10 ci-dessous.

| Ech.   | $\delta^{18}\text{O}$ | $\text{H}_2\text{O}+$ |
|--------|-----------------------|-----------------------|
| IM-6   | 8,50                  | 3,77                  |
| IM-8   | 4,90                  | 3,35                  |
| IM-20  | 4,90                  | 4,81                  |
| IM-22  | 4,70                  | 6,01                  |
| IM-38  | 6,40                  | 3,16                  |
| IM-41  | 3,50                  | 8,34                  |
| IM-43  | 5,40                  | 4,94                  |
| S-8    | 8,50                  | -                     |
| S-10   | 7,20                  | -                     |
| S-13   | 9,30                  | -                     |
| S-13c  | 8,00                  | -                     |
| S-14   | 8,00                  | -                     |
| S-15   | 9,50                  | 4,19                  |
| S-17-2 | 10,60                 | 1,95                  |
| S-18   | 9,60                  | 2,97                  |
| S-20   | 8,50                  | 3,50                  |
| S-23   | 8,30                  | 1,78                  |
| S-25   | 10,60                 | 2,36                  |
| S-26d  | 11,30                 | 0,73                  |
| S-27b  | 10,50                 | 2,30                  |
| S-30   | 10,70                 | -                     |
| S-32   | 8,90                  | 2,96                  |
| S-38   | 9,10                  | 2,61                  |
| S-60A  | 8,30                  | 3,69                  |
| S-61   | 8,40                  | 3,48                  |
| S-67   | 5,70                  | 3,21                  |
| S-68A  | 6,60                  | 3,59                  |
| S-69A  | 7,30                  | 4,99                  |
| S-70   | 8,60                  | 4,06                  |
| S-71   | 9,00                  | 2,96                  |
| S-77d  | 9,30                  | 3,39                  |
| S-81   | 7,00                  | 4,00                  |
| S-111  | 7,20                  | 3,27                  |
| S-113c | 7,80                  | 2,33                  |
| S-113e | 7,40                  | 3,32                  |
| S-117  | 9,80                  | 3,11                  |
| S-126A | 11,60                 | 3,48                  |
| S-45   | 12,00                 | 2,44                  |
| IM-46  | 8,90                  | -                     |
| IM-54  | 12,50                 | -                     |
| IM-57b | 7,60                  | 0,95                  |
| S-28   | 12,70                 | 0,33                  |
| S-33   | 10,80                 | 0,87                  |
| S-59A  | 11,20                 | 1,35                  |
| S-35   | 10,90                 | 0,99                  |
| S-56A  | 12,20                 | 0,99                  |
| S-57   | 12,00                 | 0,81                  |

|        |       |      |
|--------|-------|------|
| S-36-2 | 13,30 | 0,61 |
| IM-7   | 8,50  | 1,89 |
| IM-45  | 7,50  | 0,84 |
| S-120A | 10,40 | -    |
| S-125  | 9,10  | 1,01 |

Ainsi les roches volcaniques du Copley présentent les valeurs les plus basses en  $\delta^{18}\text{O}$  à l'encontre des rhyolites de Balaklala qui présentent les plus élevées. Taylor et South (1985) interprètent ces résultats comme l'effet de la chlorite à la fois sur la composition isotopique en oxygène et les teneurs en  $\text{H}_2\text{O}^+$  des roches totales. Ainsi les roches riches en chlorite ont été hydrothermalisées à haute température ( $T = 400^\circ\text{C}$ ) produisant des  $\delta^{18}\text{O}$  diminuant jusqu'à +3 (figure 3. 14).

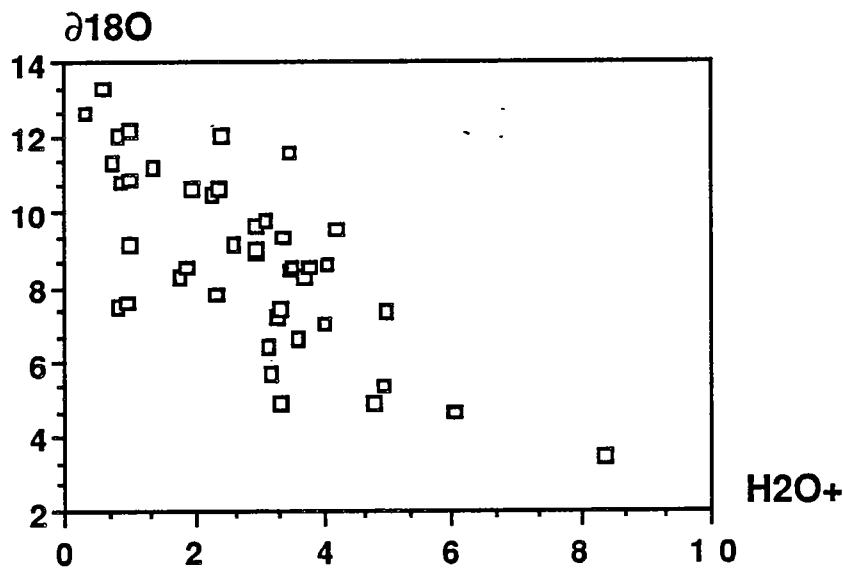


Figure 3.14.

Si cette relation a été précédemment mise évidence par Casey et Taylor (1982) et Larson (1984), elle contraste avec les effets de l'altération de basse-température des basaltes du plancher océanique dans lesquels une augmentation du  $\delta^{18}\text{O}$  avec le pourcentage de perte au feu est une conséquence de la formation de minéraux argileux et carbonatés (Muehlenbachs et Clayton, 1972; Pineau et al., 1976; Hoernes et al., 1978). Un tel schéma d'évolution hydrothermale n'est pas reconnaissable dans le complexe ophiolitique de Trinity (figure 3.15).

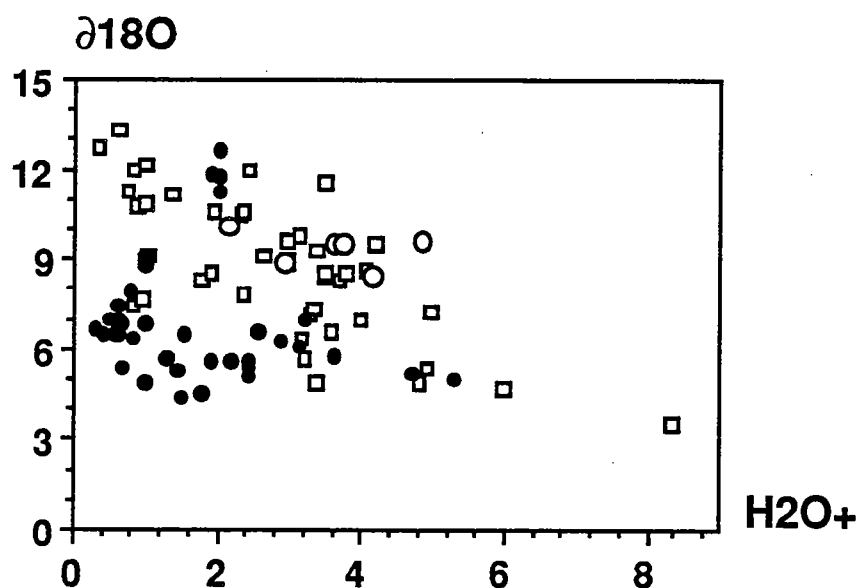


Figure 3.15 : carrés vides : Copley; ronds pleins : MORB; ronds vides : basaltes de Trinity.

Dans l'association volcanique de Copley-Balaklala, les roches sont progressivement appauvries en  $^{18}\text{O}$  à l'approche des dépôts métallifères. La zonation isotopique est ainsi parfaitement corrélée à la zonation minéralogique depuis les roches à zéolites, à montmorillonite et finalement à chlorite avant d'atteindre les dépôts sulfurés.

Dans le complexe ophiolitique de Trinity, les basaltes ont des valeurs de  $\delta^{18}\text{O}$  comprises entre +9 et +10 quelque soit le type d'association métamorphique (albite et chlorite pour le premier type d'association, épidote et quartz pour le second type). Ces valeurs élevées et constantes sont interprétées comme le résultat du vieillissement isotopique de la couche basaltique supérieure au fur et à mesure que la croûte altérée s'éloigne de la zone d'expansion axiale (Muehlenbachs, 1980; figure 3.16).

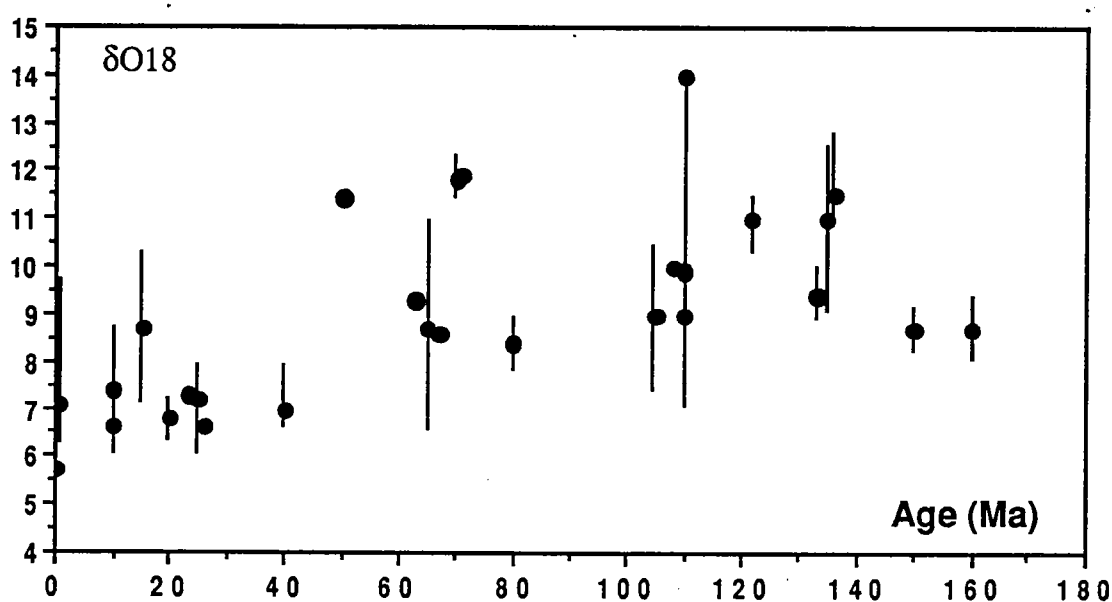


Figure 3. 16.

Ce type de processus ne semble pas affecter les arcs insulaires, ainsi l'histoire d'altération hydrothermale et la signature isotopique finale d'une portion de la croûte océanique dépend de l'environnement géotectonique.

### **3.B.5 Conclusion.**

La comparaison minéralogique et isotopique entre les histoires hydrothermales qui ont affecté respectivement les séries volcaniques de Copley-Balaklala et l'ophiolite de Trinity suggère pour cette dernière un modèle d'activité hydrothermale conditionné par une circulation d'eau de mer au sein d'un édifice structuré, rapidement constitué et se déplaçant au cours du temps en direction d'un environnement plus froid. Tandis que l'arc insulaire de Copley-Balaklala est caractérisé par une altération hydrothermale, dont l'intensité fut très variable au sein d'un édifice volcanique stable, produisant dans la zone hydrothermale de haute température des dépôts métallifères sulfurés exploitables. Si de nombreux complexes ophiolitiques appartenant actuellement à la marge nord-ouest américaine sont interprétés comme des sections plus ou moins complètes d'arcs insulaires, la caractérisation du système hydrothermal fossile de l'ophiolite de Trinity permet d'exclure ce type de genèse.

**ELEMENTAL FLUXES DURING THE HYDROTHERMAL ALTERATION OF  
THE TRINITY OPHIOLITE (CALIFORNIA) BY SEAWATER.**

C. Lécuyer (1), M. Brouxel (2) and F. Albarède (2,3)

(1) Laboratoire de Géochimie, CAESS-CNRS, Université  
de Rennes, Campus de Beaulieu, 35042 Rennes, France.

(2) Centre de Recherches Pétrographiques et Géochimiques, B.P. 20, 54501 Vandœuvre-lès-Nancy,  
France.

*Present address* : U.S.G.S., Federal Center, M.S. 963, Box 25046,  
Denver CO 80225, U.S.A.

(3) Ecole Nationale Supérieure de Géologie, 54501 Vandoeuvre Cedex, France.

## Abstract

The Trinity ophiolite has undergone hydrothermal alteration in greenschist to transitional amphibolite facies conditions. The mineralogical assemblages and Sr isotopic results reveal a widespread seawater circulation which has principally affected the upper part of the oceanic crust. The interface between sheeted dikes and isotropic gabbros has experienced the largest supply of heated seawater with water/rock ratios (W/R) up to 16.

W/R ratios and temperature are the most important parameters in determining the direction and amplitude of chemical changes during seawater-rock interaction. In addition, calculation of elemental fluxes by mass balance on a crustal section reveals the important role of magma chemistry and related variations of primary modal compositions. The large chemical fluxes calculated in Trinity rocks agree with their strong degree of alteration. The W/R of about 8 in the Trinity basalts are larger than those from Hole 504B and East Pacific Rise (about 1.5). This is a possible consequence of a longer life time convective hydrothermal system in relation with a slow spreading center generating a thin crust. Contrasting with hole 504B, this hydrothermal pattern is likely able to equilibrate the chemical budget for Mg, Na and partly for K between seawater and oceanic crust.

The strong degree of alteration recorded by ophiolites correspond to the time-integrated effects of both initial and off-axis hydrothermal activity. Ophiolites certainly represent valuable probes in tracking the chemical budget of the oceanic reservoir.

## 1. Introduction

New crust generated at spreading centers is rapidly submitted to interactions with a large mass of seawater. Hydrothermal activity well-known in mid-ocean ridges (Edmond et al., 1979) has also been recently discovered in the Mariana Trough (Poreda, 1985; Horibe et al., 1986). Submarine hydrothermal systems play an important role in both the geochemical mass balance of the oceans and the composition of the lithosphere subducted into the mantle. However, current estimates of elemental fluxes are mostly based on recent hydrothermal systems inferred from what is known from the uppermost oceanic crust such as the upper basaltic and sheeted dike levels sampled at the DSDP Hole 504B (Staudigel and Hart, 1983; Alt et al., 1986). Unfortunately, such a procedure of mass balance calculation depends entirely on the distribution of the alteration in the crust and essentially in the deepest parts.

Ophiolites are commonly interpreted as remnants of oceanic crust whether formed at mid-ocean ridges or in marginal basins (Dewey and Bird, 1971; Miyashiro, 1973; Crawford et al., 1981), they provide potential information on the deep layers of the hydrothermally-altered oceanic crust (Gregory and Taylor, 1981; Alt et al., 1986). The 472-435 Ma old Trinity ophiolite (Lanphere et al., 1968; Jacobsen et al., 1984) has been suggested by Lapierre et al. (1987) and Brouxel et al. (1988) to represent the floor of a marginal basin in a slow-spreading environment. The Dunsmuir area (Fig. 1) offers a particularly fresh cross-section of the Trinity ophiolite being distant from any Mesozoic dioritic plutons and from the underthrust of the Central Metamorphic Belt. In contrast with the peridotites studied by Peacock (1987), which have recorded at least three stages of metamorphic events, the tectonite harzburgites located in the Dunsmuir area are surprisingly fresh while the degree of metamorphic recrystallization within the crustal sequence generally decreases from the extrusive sequence and sheeted dikes to the lowermost ultramafic cumulates. Field observations suggest that the ophiolitic sequence has been substantially modified neither during its accretion to the North-American continent nor during later events. Preliminary results (Brouxel and Lapierre, 1988) suggest that the Trinity ophiolite has experienced an extensive hydrothermal activity leading to important mineralogical and geochemical variations. The presence of very-low temperature minerals, such as celadonite, in the uppermost pillow lavas is a persuasive argument to consider that Trinity ophiolite offers a good picture of oceanic hydrothermal activity, virtually free of overprinting processes. A thick section of ultramafic-mafic cumulates and isotropic gabbros has been observed without any apparent disruption, giving informations on a whole magmatic chamber. The detailed sampling of continuous and well-exposed outcrops enables a complete crustal sequence with both identifiable magmatic minerals and structures and well-preserved primary metamorphic assemblages to be reconstituted.

The present study had different objectives. Associations of secondary minerals and Sr isotopic characteristics of the Trinity ophiolitic rocks were determined in order to estimate the physical conditions of hydrothermal activity: pressure, temperature and water / rock ratios. The mass balance of major elements during interaction of the whole crustal sequence with seawater was calculated using simple mineralogical arguments and the Gresens (1967) method complemented by least-square modelling. The results were compared with previous estimates made on the Hole 504B



and the Troodos ophiolite in order to assess the reliability of the method and the role of a different geotectonic environment. Finally, the effect of rock alteration by seawater on the geochemical budget of the oceans has been compared with that of runoff.

## 2 Geological setting

The Trinity ophiolite lower unit consists of the 2-4 km-thick Trinity ultramafic sheet (Irwin, 1981; Quick, 1981), mainly comprised in the Dunsmuir area of tectonized harzburgites associated with a few clinopyroxenite dike and tabular dunites and a thin crustal sequence comprising small magma chambers (about 1Km, Fig. 1). The plutonic complex at Gray Rocks (Fig. 1) consists of a base of ultramafic cumulates (dunites, lherzolites, werhlites) overlain first by cumulate clinopyroxene gabbros interlayered with cumulate clinopyroxenites and then by layered and cumulate gabbros. This cumulate sequence (800m) is itself overlain by isotropic gabbros. Huge masses of pegmatitic gabbros (decametric dikes) and abundant plagiogranites crosscut the entire plutonic sequence. The pegmatitic gabbros occur as metric to plurimetric dikes with chilled margins when cross-cutting the Trinity ultramafic sheet but not in the gabbros. Diabasic dikes (up to 30percent), are rooted in the top of this magma chamber but the contact with the sheeted dike complex (located at Conant; Fig. 1) has not been observed. The extrusive member of the Trinity ophiolite is represented by the 500 meter-thick Grey Rocks basaltic pillowed succession which is thrust on the Trinity ultramafic sheet (Brouxel and Lapierre, 1988). The studied samples are located on the geological map (Fig. 1) and reported in the synthetic lithologic column (Fig. 2).

## 3. Analytical techniques

Major elements have been analyzed by ICP spectroscopy at the Centre de Recherches Pétrographiques et Géochimiques of Vandoeuvre-lès-Nancy (C. R. P. G.) or by X-Ray fluorescence and atomic absorption at the Service Commun d'Analyses of the University of Nancy I.

$\text{Fe}^{2+}/\text{Fe}^{3+}$  ratios on whole rock were measured at the C. R. P. G. and at the Service Commun d'Analyses of the University of Nancy I: the sample is decomposed by HF and  $\text{H}_2\text{SO}_4$  in a non-oxidizing environment then the  $\text{Fe}^{2+}$  is determined by titration with a standard potassium-dichromate solution (Blanchet and Malaprad, 1967).

Mineral analyses were carried out by electron microprobe at the University of Nancy I.

Strontium isotopes were analyzed using techniques described by Alibert et al. (1983) and Michard et al. (1985).

## 4 Petrography and Mineralogy

None of the Trinity *basalts* exhibits its magmatic mineralogy but the absence of intensive shearing or brecciation permits the primary textural features to be identified. Metamorphic zones were defined by the sequential appearance of critical mineral associations with depth. The basalts and the dikes present a retromorphic association developed at the expense of a previous metamorphic paragenesis of higher grade.

Replacement of clinopyroxene and plagioclase phenocrysts by greenish fibrous actinolite and coarse-grained epidote respectively is observed. Actinolite itself is often partially replaced by a ripidolitic chlorite (Table 1). Groundmass is systematically recrystallized and made of albite, epidote, actinolite and occasionally quartz. Hematite is often present and, in sample TR 51B, celadonite, K-feldspath and K-chlorite have been identified. Scarce crystals of calcite are present in vesicle fillings in most of the samples. Proportions of albite and epidote vary widely and the development of interstitial granular quartz is common when epidote is more abundant than albite. Modal data discriminate basalts in two groups: the Albite-Chlorite-rich associations and the Quartz-Epidote-rich associations (Fig. 3).

Similar metamorphic parageneses are found in the *dikes*. In the high-level gabbros, large and well-developed euhedral magnesio-hornblende crystals characterized by a strong brown to green pleochroism are present. Clinopyroxene relicts were not observed.

In the *upper mafic cumulates*, clinopyroxene is commonly replaced by fibrous actinolite, whereas plagioclase is replaced by epidote. Commonly, low-birefringence epidote is well-developed as short prismatic minerals. Abundance of albite and chlorite decreases rapidly towards the base of the cumulate sequence while hematite disappears and occasional sphene is observed (Fig. 2).

The *lower cumulate gabbros* are less altered and relicts of clinopyroxene and plagioclase are frequent. Clinopyroxene is often replaced by tremolite. Olivine from the *ultramafic cumulates*

(lherzolite and werhlite) is partially replaced by serpentine and magnetite. Pargasitic hornblende, scarce sheridanite and talc replace clinopyroxene and orthopyroxene respectively.

Pegmatitic gabbros, characterized by cumulate and coarse-grained textures (minerals locally reach a size of 20 centimeters) contain metamorphic associations similar to those found in the surrounding rocks. Albite, epidote and fibrous crystals of actinolite to actinolitic hornblende develop in the isotropic gabbros. Plagiogranites are medium-grained hypidiomorphic - granular rocks predominantly consisting of albite and quartz. Hornblende, which represented less than 5 percent of the mode, was replaced by chlorite. These plagiogranites contain also common accessory minerals (magnetite, sphene and apatite), particularly in the more acidic types. They are also characterized by intergrowths of plagioclase and quartz, a feature which is typical of oceanic plagiogranites (Coleman and Donato, 1979).

In summary, the volcanics and sheeted dikes have been strongly affected whereas the extent of the metamorphic recrystallization of the plutonic rocks decreases with depth. The petrographic data indicate 1) the existence of retrograde polymetamorphic associations across the section reflecting a temperature decreasing with time for the circulating seawater 2) the extent of alteration spatially decreases with depth for increasing temperatures.

Representative microprobe analyses of metamorphic *amphiboles* from the Trinity ophiolite are listed in table 2 together with their structural formulae calculated according the procedure of Mevel (1984). Among the Trinity amphiboles, the Ti - Al<sup>IV</sup> substitution defines three groups (Fig. 4a):

- actinolites with very low to low Ti (less than 0.06 atoms Ti per formula unit) and Al<sup>IV</sup> values.
- magnesio-hornblendes from the high-level gabbros exhibit high Ti (0.12 to 0.22 atoms per formula unit) and Al<sup>IV</sup> values (0.8 to 1.4 atoms per formula unit). Textural relationships and mineral chemistry show evidence for magnesio-hornblende being replaced by actinolite with an important gap of composition (Fig. 2).
- pargasitic hornblendes from the ultramafic cumulates show a different trend with low Ti (0.05 to 0.1 atoms per formula unit) and high Al<sup>IV</sup> values (about 1.5 atoms per formula unit).

Al<sup>IV</sup> contents in the Trinity amphiboles are plotted along the lithostratigraphic succession in Fig. 2. Amphiboles with high Al<sup>IV</sup> contents have been observed in the high-level gabbros and in the bottom ultramafic cumulates just above the Trinity peridotite. In contrast, the actinolite Al<sup>VI</sup> contents increases steadily from the basalts towards the base of the cumulate sequence (Table 2).

Na and K in the actinolite A-site are minute components (< 0.25 atomic Na+K) in comparison with the high contents in the magnesio-hornblendes from the high - level gabbros (0.3 - 0.4 atomic Na+K). A plot of alkalis substituted in the A-site versus Al<sup>IV</sup> (Fig. 4b) shows an enrichment of the pargasite component in the actinolite and the tremolite from mafic cumulates, and in the tremolites and the pargasitic hornblendes from the lower ultramafic cumulates. Contrasting with this general trend, magnesio-hornblendes from the high-level gabbros are enriched in tschermakitic component (Fig. 4b).

*Epidotes* show a negative correlation in the cationic substitution of Fe<sup>3+</sup> for Al<sup>VI</sup> (Table 3 and Fig. 5). The pistacite component 100 Fe/(Fe+Al) increases from the basalts to the sheeted dikes, then decreases downwards (Fig. 2). The analyzed epidote crystals from the hypabyssal and effusive rocks contain small amounts of minor elements such as MgO and MnO. Individual grains are not zoned.

A high potassium content detected in some basalts corresponds to the presence of celadonite, secondary alkali-feldspath with 7 percent K<sub>2</sub>O and scarce K-rich chlorite containing up to 2 percent of K<sub>2</sub>O which are typical hydrothermal clay minerals. Celadonite, restricted to the uppermost part of the pillowed succession, exhibit very low paragonitic contents from 2 to 5 percent and a substitution of Si by Fe and Mg (Table 4).

#### 4 Geochemistry

The bulk chemical composition of representative Trinity samples is listed in Table 5. Major elements contents in the basalts vary widely: SiO<sub>2</sub> contents range from 46 to 56 percent, CaO from 5 to 13 percent, Na<sub>2</sub>O from below detection level to 5 percent, Fe<sub>2</sub>O<sub>3</sub> from 6 to 10 percent and MgO from 4 to 10 percent. In contrast, Al<sub>2</sub>O<sub>3</sub> content is more constant (15 to 18 percent). Cr vary from 143 to 428 ppm, Ni from 90 to 188 ppm and incompatible trace element contents are more

uniform with Zr = 40 - 45 ppm, La = 0.98 - 1.55 ppm and Yb = 1.27 - 1.74 ppm (Table 5, and Brouxel and Lapierre, 1988)

The negative correlations between CaO and Na<sub>2</sub>O on one hand and MgO and CaO on the other strongly suggest two dominant metamorphic trends: (1) quartz-epidote-rich rocks with higher CaO contents and (2) albite-chlorite-rich rocks with high MgO and Fe<sub>2</sub>O<sub>3</sub> contents, which is consistent with the ripidolitic composition of the chlorites.

In the Trinity basalts the Fe<sup>3+</sup>/Fe<sup>t</sup> ratios, ranging from 0.16 to 0.52 (Table 6), encompass the range reported for Hole 504B about 0.25 by Alt et al. (1986) and is higher than those of fresh MORB glasses (0.05 ± 0.03, Christie et al., 1986). The Fe<sup>3+</sup>/Fe<sup>t</sup> ratio reaches its minimum value of 0.11 in the cumulate rocks.

Rocks have been analyzed for Sr isotopes at different levels in the ophiolitic succession. We have retained the emplacement age of 450 My suggested by the Sm-Nd isochron on microgabbros and pyroxenites (Jacobsen et al., 1984) and consistent with the Sm-Nd data on the whole suite (Brouxel and Lapierre, 1988). The initial <sup>87</sup>Sr/<sup>86</sup>Sr ratios vary from 0.70247 to 0.70568 (Table 6) hence contrasting with the nearly constant Nd isotopic ratios ( $\epsilon_{Nd}$  values range between 6.6 and 7.5; Jacobsen et al., 1984; Brouxel and Lapierre, 1988).

When  $\epsilon_{Sr}$  is plotted against the stratigraphic position (Fig. 6), a decreasing trend is observed towards the base of the sequence except in the isotropic gabbros and in the cumulate lherzolite where higher  $\epsilon_{Sr}$  values are found. Most variations are within 15  $\epsilon_{Sr}$  units except in the ultramafic cumulates where a 40  $\epsilon_{Sr}$  units variation is observed.

Intrusives such as pegmatitic gabbros and plagiogranites have nearly the same Sr concentrations and isotope compositions as their host rocks (Table 6 and Fig. 6). Exceptions are the gabbroic pegmatites which have less radiogenic Sr than the uppermost layers of the plutonic complex they intrude and a plagiogranite with a higher  $\epsilon_{Sr}$  value than their host layered gabbros.

## 7 Metamorphic Conditions

Using the calibration of mineral equilibria by Liou et al. (1974), Maruyama et al. (1983) and Moody et al. (1983), the temperature associated with metamorphic parageneses in the Trinity ophiolitic complex can be estimated at ca. 350°C for the low-grade greenschist facies at the top of the sequence (albite + epidote + actinolite ± ripidolite ± quartz ± hematite) and ca. 500°C for the transitional amphibolite facies prevailing in the deepest part of the cumulate sequence (pargasitic hornblende + epidote ± sheridanite ± talc ± magnetite: T ≈ 550°C). Mineralogy and evolution of these metamorphic associations are summarized in Fig. 2. These observations agree with studies on other ophiolites such as in Taiwan (Liou and Ernst, 1979), Dun Mountain (Sivell and Waterhouse, 1984) and the Xigaze ophiolite (Girardeau et al., 1985), where parageneses and secondary mineral chemistry suggest a prograde metamorphism towards the base of the cumulate sequence.

We speculate that the distribution of metamorphic associations is related to the stratigraphy upon magma emplacement at spreading centers. A preservation of the original features acquired during the hydrothermal alteration of the Trinity sequence is supported by the presence of easily-destroyed hydrothermal clay minerals such as celadonites in the Trinity basalts. Celadonite is indeed frequently observed in modern oceanic hydrothermal systems such as in Hole 504B in replacement of basaltic glass (Alt et al., 1986). Its presence is restricted to the uppermost part of the pillowed succession in keeping with its low temperature and pressure of formation. The paragonitic substitution in celadonites (paragonite ranging from 2 to 5 percent) is a reliable geothermometric parameter and gives a temperature of formation lower than 50°C in the Trinity basalts (Lambert, 1959). Oxygen isotopic data on celadonites from seafloor basalts indicate formation at temperatures less than 40°C (Kastner and Gieskes, 1976; Seyfried et al., 1978; Stakes and O'Neil, 1982; Bohlke et al., 1984). The Fe and Mg cation excess in the structural formula reflects that this mineral has crystallized in equilibrium with a K-Fe-Mg-rich fluid upon waning of the hydrothermal circulation.

Experimental data have shown that the Al, Na, K and Ti contents of metamorphic amphiboles are pressure and temperature dependent (Leake, 1965; Deer et al., 1966; Liou et al., 1974; Spear, 1981; Moody et al., 1983). The increase of Al and Ti in amphibole from basalts to ultramafic cumulates and the sympathetic enrichment of the pargasite component mark the increasing metamorphic grade towards the base of the ophiolitic sequence (Fig. 2). As suggested by the above authors, the abundance of octahedral-Al in actinolite correlates with pressure. Its regular increase with

depth in the Trinity ophiolite suggests that the main features of the magmatic stratigraphy have been preserved in their original position.

Miyashiro et al. (1971) attributed the relative scarcity of epidote in oceanic gabbros to low pressure. However, epidote has been widely reported from hydrothermally-altered oceanic basalts (Humphris and Thompson, 1978) and in active geothermal areas where hydrothermal alteration occurs at pressures probably less than 500 bars and temperature lower than 350°C (Steiner, 1968; Keith et al., 1968; Liou and Ernst, 1979). The pistacite (Ps) content of epidote decreases from a value of 15 in the basalts to 0 in the cumulates (Fig. 2) suggesting a maximum oxygen fugacity in the sheeted dike complex (Ps = 20; Cooper, 1972; Holdaway, 1972; Liou, 1973).

Decreasing oxygen fugacity with depth is also supported by the whole rock  $\text{Fe}^{3+}/\text{Fe}_{\text{total}}$  ratio. This ratio increases from 0.11 to 0.29 in ultramafic and mafic cumulates to 0.34 in the sheeted dikes and 0.28 in the basaltic pillow lavas (Fig. 6 and Table 6). A high  $f\text{O}_2$  activity in dikes and basalts is also expressed by a few percent of hematite (2 - 5 percent), likely in replacement of a primary iron - rich oxide.

The important shift of the  $^{87}\text{Sr}/^{86}\text{Sr}$  initial ratios relative to mantle values at nearly constant  $\epsilon_{\text{Nd}}$  values is commonly observed in ophiolites (Jacobsen and Wasserburg, 1979; Lanphere et al., 1981; McCulloch et al., 1981; Edwards and Wasserburg, 1985) and is interpreted as the result of important seawater addition at the hydrothermal stage.

The water/rock (W/R) ratios prevailing during the hydrothermal alteration of the ophiolitic rocks have been calculated from the Sr concentrations and isotopic ratios using the method of Albarède et al. (1981) which assumes isotopic equilibrium between the interacting rocks and hydrothermal solution. The rock with the lowest  $^{87}\text{Sr}/^{86}\text{Sr}$  isotopic ratio (0.7025) is considered to represent the unaltered mantle value, while a value of 0.7085 is used for the Silurian seawater (Burke et al., 1982). The calculated W/R ratios ranging between 0 and 16 are similar to those calculated for other ophiolitic series (McCulloch et al., 1981). When plotted against the stratigraphic succession, the calculated W/R ratio increases from the basalts to the isotropic gabbros and decreases towards the base of the sequence. Intrusive rocks are off the main trend: calculated values of the W/R ratio are lower in the pegmatitic gabbros PegA and PegB than in their host rocks while the contrary is observed for the plagiogranite TR 109.

## Elemental fluxes

The oceanic crust represented by the Trinity ophiolite has clearly undergone an extensive alteration by significant volumes of seawater which must result in material exchange at different extents over the whole magmatic sequence. The elemental fluxes in bulk rock have been calculated by the Gresens's method and, since fine grain size does not permit point counting, least-square estimates of modal mineral abundances. The steps taken for these calculations are represented in flow-chart form (Fig. 7) and developed in Appendix.

The fluxes of Si, Al, Fe, Ca, Mg and Na calculated in grams per 100g and per 100 cm<sup>3</sup> of rock are respectively shown in Fig. 8 and 10. In the basalts, material fluxes are a function of the metamorphic associations. In the Albite-Chlorite- rich association, albitization is responsible for large Ca and Al loss and Na gain. When chlorite becomes the dominant mineral phase, Mg and Fe gain and Si loss are observed. Extensive chloritization of clinopyroxene induces Mg and Fe gain and significant Ca loss. In contrast, in Quartz-Epidote- rich associations, large Si gain seems associated with the presence of quartz in crack fillings within the matrix while slight Fe gain and moderate Ca, Na and Al loss mark the development of epidote.

In the cumulate sequence, alteration is characterized by a considerable loss of Si and Ca and a significant gain of Fe, Mg and Al, while Na varies little and randomly along the sequence (Fig. 8). Little K exchange is observed, which is not unexpected since both seawater and tholeiitic magmas are K-poor. As shown by the occurrence of the highest Ca loss and the highest Mg and Fe gain in the cumulate clinopyroxenites, the relative abundance of plagioclase and clinopyroxene seems to be the major factor controlling the magnitude of chemical transfers.

In the ultramafic rocks, serpentinization is the dominant transformation of the olivine-bearing rocks (werhlite and lherzolite). Calculated losses exceed gains by far and agree with the measured loss on ignition which range from 5 to 12 percent. Serpentinization takes place with significant losses in Si, Ca, Fe and Mg. Al is relative immobile and Na is randomly affected.

Figure 8 presents the calculated elemental fluxes and W/R ratios versus depth. The largest fluxes correspond to the highest W/R ratios and correspond to the lower part of the sheeted complex

and the top of the isotropic gabbros, where conventional model locates the top of the magma chamber. This is consistent with previous findings on the Cayman Rise, which is an atypical oceanic crust (Ito and Clayton, 1983), or in the Semail ophiolite, Oman (McCulloch et al., 1981). From the silica content of the hydrothermal fluids from the East Pacific Rise at 13 degrees N, Michard et al. (1984) have also suggested that water-rock interaction takes place on the thermal boundary layer of the magma chamber, an interpretation supported by the present analysis. The calculated W/R ratio is smaller for ultramafic than for mafic cumulates. Again, the contact between mafic and ultramafic cumulates has previously been shown to be associated with a sharp decrease of the water/rock interaction in Oman (Gregory and Taylor, 1981) and in the Cayman Rise, although this contact is significantly shallower in Trinity (2 km instead of 5 and 4 km respectively).

The correlation between the curve of W/R ratios and that of Mg and Na fluxes (Fig. 8) suggests that the larger the influx of seawater, the larger the chemical transfers. In contrast, when WR ratios becomes  $\ll 1$ , all the curves converge towards the no gain- no loss line and define the geometric limit of the hydrothermal system (Fig. 8). As documented with oxygen and strontium isotopes by Gregory and Taylor (1981) and McCulloch et al. (1981) for the Semail ophiolite, the present W/R ratio profile indicates that seawater has reached the deep plutonic layers of the Trinity ophiolite, but its penetration strongly diminished at the transition between mafic and ultramafic cumulates. In the ultramafic cumulates seawater interaction seems to be limited (low W/R ratios) but is still able to change their  $^{87}\text{Sr}/^{86}\text{Sr}$  isotopic ratios likely because of their very low Sr concentrations ( $\leq 5$  ppm). Leaching experiments conducted on some Sr-poor rocks (HCl 5N in ultrasonic bath for 10 minutes) show that isotopic differences between the unleached and leached sample increase with the decreasing Sr concentration (Table 6).

Flux direction and amplitude change abruptly at the contact between isotropic and cumulate gabbros for most elements. A cross-over of the Si and Al fluxes is also observed at this level. The observed Al pattern suggests that Al is transported from the lower layers to the top of the crustal sequence. Sizable Al concentrations have indeed been observed in the hydrothermal solutions from the East Pacific Rise: those solutions, which have a pH in the range 3.3 to 3.8, show increasing Al concentrations above 250°C (Edmond et al., 1982; Bowers and Taylor, 1985; Von Damm et al., 1985). Our results suggest however that the net Al flux from or into the oceanic crust is very small.

Small amounts of Fe are added to the rock column over the entire depth. This excess is intriguing since hydrothermal solutions at ridge crest are known to be strongly enriched in iron relative whereas seawater is virtually iron free. This may indicate that the section as a whole cannot be considered as a closed system and iron is added from the inaccessible lowermost peridotite (serpentinization), or, a more worrisome possibility, a lateral component of the flux. Mg is certainly removed from seawater over a wide temperature range. Different mineral phase responsible for Mg uptake have been suggested: Mg-hydroxi- sulfate precipitated at low temperature quantitatively removes Mg from the reacting solution (Janecky and Seyfried, 1983) will redissolve upon cooling or further react to produce other Mg-rich phases. Actinolite may form at 300-500°C and Magnesiohornblende at temperature of about 500-700°C. These reactions lower the pH of the solution favouring the silicate hydrolysis reactions consuming  $\text{H}^+$  (Bischoff and Dickson, 1975; Mottl and Seyfried, 1977, 1978). At high temperatures, hydrothermal reaction rates are certainly high (Wood and Walther, 1983) and can produce large chemical changes in a short time.

At the contact between the sheeted complex and the isotropic gabbros, the content of dissolved silica in discharged water is calculated with a rather good precision and can tentatively be used to estimate the temperature of reacting seawater for the last equilibrium with quartz (Kennedy, 1950; Fournier and Rowe, 1966). In the isotropic gabbros, a value of 0.22 g of  $\text{SiO}_2$  per 100 g of  $\text{H}_2\text{O}$  is calculated by diluting the calculated Si loss (3.47 g per 100 g of rock) into the solution volume estimated by the W/R ratio of 16). Pressure is taken at 80 - 90 MPa has been estimated assuming an average specific gravity for basic rocks of 3 g/cm<sup>3</sup> and a overlying water column of 4000 m. This calculation gives a temperature of about 500 - 600°C at the top of the magma chamber, in agreement with the mineral equilibrium data discussed above.

### Mineralogical control of the iron oxidation state

As epidote is the main repository of ferric iron in the Trinity basalts, the  $\text{Fe}^{3+}/\text{Fe}^{\text{t}}$  ratio changes smoothly with the calculated epidote proportions. Hosting  $\text{Fe}^{3+}$  in epidote instead of hematite is consistent with the W/R ratios lower than about 20 (Mottl, 1983).  $\text{Fe}^{3+}/\text{Fe}^{\text{t}}$  ratios in Epidote-Quartz-rich basalts and dikes are correlated with the W/R ratio (Fig. 9) and hint to The least-square straight line obtained for the Epidote-Quartz rocks gives a  $\text{Fe}^{3+}/\text{Fe}^{\text{t}}$  ratio of about 0.1 at water/rock = 0. At least for this assemblage, the reasonably smooth variation of  $\text{Fe}^{3+}/\text{Fe}^{\text{t}}$  with the

W/R ratio and the intercept value reasonably close to the fresh rock oxidation state of basalts (Christie et al., 1986) suggest that oxidation affected the magmatic rock in a one-step process. Moreover, the mass balance of oxygen requires that the hydrothermal fluid must have contained oxidized species: sulfate is an ubiquitous species abundant enough in natural water and is easily reduced upon water-rock interaction at temperatures in excess of 200 degrees C (Bischoff and Dickson, 1975). The pattern of  $\text{Fe}^{3+}/\text{Fe}^{\text{t}}$  variations thereby lends support to the assumption that the metamorphic transformation took place at the hydrothermal stage at the spreading center and that seawater is the interacting fluid.

However, the present data show evidence of some water/rock disequilibrium, since a simple mass balance calculation would indicate that a seawater/rock ratio of about 6 would be sufficient to oxidize the bulk of the iron contained in the rock. Since kinetics of iron oxidation is known to be fast, some iron must therefore be locked in minerals (amphibole) which do not participate into the hydrothermal reactions. In Albite-Chlorite-rich basalts and gabbros, the smaller increase of  $\text{Fe}^{3+}/\text{Fe}^{\text{t}}$  ratios with water/rock ratios may be interpreted by a progressive oxidation of amphibole during water/rock interaction.

### Comparison with the Troodos ophiolite and Hole 504 B.

The Trinity major element fluxes were compared to those from Hole 504B basalts (Figure 10; DSDP hole 504B which is located in 5.9My old crust about 200Km south of the Costa Rica Rift). Alt and Emmermann (1985) have estimated chemical fluxes in Hole 504B crust from the comparison of average composition of fresh glass with altered whole rock. They assumed that 1Km of crust is altered as the site 504 lithologic transition zone and dike section. In the case of the Troodos ophiolite, the chemical budgets of elemental changes were quantified by calibration of drill whole rock analyses via systematic stable element variations of fresh glasses found throughout the extrusive section (Bednarz and Schmincke, 1989).

Both Troodos and Trinity extrusive sections are a major sink for  $\text{MgO}$ ,  $\text{K}_2\text{O}$  and  $\text{Na}_2\text{O}$  and a source for  $\text{CaO}$  while  $\text{SiO}_2$  is randomly affected. The large chemical fluxes computed in both cases correspond to high W/R ratios in the range 10-15 (W/R ratios in the Troodos basalts were calculated from the Sr data given by Peterman and Hedge, 1971 and Rautenschlein et al., 1983). Generally, calculated W/R ratios in the ophiolitic basalts (see also the Semail ophiolite; McCulloch et al., 1981) are larger than those estimated in modern oceanic crust: Albarède et al. (1981) and Kawahata et al. (1987) calculated W/R ratios about 1.5 in the East Pacific Rise (21°N) and Hole 504B.

Like the Albite-Chlorite rich Trinity basalts, Hole 504B samples show loss of Si, Al and Ca and gain of Mg and Na, although amplitudes are smaller. A major difference is a substantial Fe loss which contrasts with Fe uptake deduced from the Trinity section. Hole 504B basalts is significantly less altered than in the Trinity ophiolite. Clinopyroxene is barely altered and the extent of albitization remains small, which may reflect smaller Ca loss and Na gain. Alteration of olivine into serpentine, chlorite, talc and clay minerals (Alt and Emmermann, 1985) represents a net loss of iron and magnesium. Epidote is only present in veins and cracks whereas, in the Trinity ophiolite, Fe is hosted by abundant iron-rich epidote, and accessory hematite in the matrix. Such a difference suggests that solutions at Trinity were quite rich in Fe relative to those from Hole 504B.

The different fluxes observed in the Trinity ophiolite and Hole 504B can also result from differences in primary bulk chemistry and related modal proportions (Table 7). In the Trinity basalts, the higher Ca and Al and lower Fe and Mg contents compared to typical pyroxene- and olivine-rich MORB (FAMOUS basalts, Table 7) are related to the presence of high modal plagioclase/clinopyroxene ratios and to the systematic absence of olivine. Nevertheless, reconstituted primary major element compositions of Trinity basalts are comparable to the low-Ti plagioclase-rich MORB known at the North Atlantic Ridge (Table 7).

### Large-Scale Material Fluxes

Total fluxes have been calculated by integrating the curves of Fig. 8 about the no gain-no loss line over the whole Trinity section. This result provides a good opportunity to compare material balance from different geotectonic environments and with different extent of alteration: the Trinity ophiolite has been suggested to have been emplaced in a back-arc basin (Brouxel and Lapierre, 1988) generated in a slow-spreading environment (LeSueur et al., 1984; Cannat and Lécuyer, 1989), whereas Hole 504B represents a section of oceanic crust generated in a large open basin (6.2 cm/y, Ballard et al., 1981). The fluxes have also been compared with those computed for the Troodos ophiolite by Bednarz and Schmincke (1989). The Troodos ophiolite is thought to represent oceanic crust associated to either an island-arc (Miyashiro, 1973) or a complex active ridge/transform intersection above a subduction zone (Moores et al., 1984; Varga and Moores, 1985) (Bednarz and Schmincke, 1989).

Figure 11 displays both elemental fluxes in  $10^{14}$  g/year for Trinity, Troodos (Bednarz and Schmincke, 1989) and Hole 504B (Alt et al., 1986) basalts in comparison to river inputs (Thompson, 1983). Elemental fluxes per year are calculated for the Trinity ophiolite assuming a production of  $2.94 \text{ km}^2$  of oceanic crust per year (Williams and Von Herzen, 1974) and a crustal column of 3Km (Lindsley-Griffin, 1977; Gregory, 1984).

The data indicate that the Trinity ophiolite is a net sink for Mg, Na and K and a very important source for Ca and Si. The average *magnesium* flux of  $1.15 \cdot 10^{14}$  g/year calculated for the Trinity ophiolite is indistinguishable from the figure of  $1.1 \cdot 10^{14}$  g/year given by Bednarz and Schmincke (1989) for the Troodos ophiolite. These fluxes are similar to those estimated from the hydrothermal fluxes (Edmond et al., 1979) and balance the river input of about  $1.3 \cdot 10^{14}$  g/year (Drever, 1974; Thompson, 1983). The behavior of Mg during rock-seawater interaction remains a controversial problem in the understanding of its global cycle within the Earth. Wolery and Sleep (1988) state that the leaching of Mg from the oceanic crust by low-temperature palagonitic alteration is at least of the same magnitude as hydrothermal uptake. They conclude that basalt-seawater interaction is not a major net sink of Mg.

The similar chemical fluxes of Mg and W/R ratios calculated in Trinity and Troodos basalts reveal that the time-integrated W/R parameter is meaningful in determining the amplitude of chemical changes during seawater interaction. At W/R ratios in the range 10-15, the hydrothermal activity is able to equilibrate the chemical budget for Mg between seawater and oceanic crust. Estimates on ophiolitic bodies support the uptake of Mg by the oceanic crust during hydrothermal alteration in amounts commensurate to the river input.

Net positive fluxes of *sodium* ( $0.79 \cdot 10^{14}$  g/year) and *potassium* ( $0.04 \cdot 10^{14}$  g/year) for the Trinity ophiolite are observed in spite of small-scale heterogeneities in K and Na uptake by the crust. Na flux is about one fourth of the river input while K flux is about one fifteenth. Contrasting with this pattern, the alteration of a Troodos-type crust would balance the K input into the oceans (Bednarz and Schmincke, 1989) (Fig. 11). We suggest that these variations are of regional nature further studies of altered oceanic crust generated in various geotectonic environment is needed to understand the K and Na oceanic budget.

The Trinity oceanic crust is equally an important source for *calcium* ( $-12 \cdot 10^{14}$  g/year) and *Si* ( $-0.7 \cdot 10^{14}$  g/year). These elements are respectively released in calcite deposits and quartz and epidote filling of cracks and veins. The strong Ca flux calculated for the Trinity ophiolite is related to the plagioclase-rich basalts representative of magmas erupted at slow-spreading ridges (Flower, 1980; 1981; 1984).

The evaluation of Si fluxes into altered crust appears only suitable when taking account the Si-leaching of the deep mafic and ultramafic cumulate layers. The estimation of Si fluxes emphasizes the interest of studying complete crust sections. This partly may explain the difficulty for Bednarz and Schmincke (1989) to estimate Si fluxes in Troodos ophiolite from the study of extrusive series and sheeted dike complex.

The comparison of elemental fluxes obtained between ophiolites and young drilled oceanic crust point out that ophiolites are useful objects to constrain the whole chemical budget of seawater-crust interaction. Bednarz and Schmincke (1989) propose that steeper geothermal gradients in thin crusts may have intensified convection and consequently facilitate a higher seawater flux through the crust. If very thin oceanic crust may be produced generally by slow-spreading ridges (Orcutt et al., 1984) or in the vicinity of transform faults (Karson and Elthon, 1987); we can speculate that the geodynamic environment plays an important role in geochemical mass balances of the oceans. The influence of magma chamber geometry on hydrothermal activity has been recently modeled by Brikowski and Norton (1989) and the development of large normal faults through oceanic crust generated in slow-spreading environments has been recognized both in modern oceanic crust (Choukroune et al., 1984) and ophiolite sections (Harper et al., 1988). Such structural features may have been responsible for a more pervasive circulation of seawater through the crust.

One may also consider that the strong degree of alteration recorded by ophiolites correspond to the effects of both initial and off-axis hydrothermal activity until oceanic crust is either obducted or reinjected into the mantle. The strong degree of alteration depicted by most of the ophiolites has been considered as not representative of processes now observed within the oceanic crust (Coleman, 1984). Gregory and Taylor (1981) and Brikowski and Norton (1989) focused that hydrothermal activity at the ridge is sufficient to produce the chemical changes through the whole thickness of crust in the same magnitude that those observed in ophiolites. Thus the record of elemental fluxes in ophiolites is relevant to the time-integrated hydrothermal history. Ophiolites certainly represent valuable probes in tracking the chemical budget of the oceanic reservoir.

## 6. Conclusion

In this study, the mineralogical data, the Sr isotopic study and the calculation of elemental fluxes on the basis of major element chemistry have emphasized the extensive hydrothermal activity which has affected the Trinity ophiolite. The main results will be summarized:

1) The presence of andesine and magnesio-hornblende in the high-level gabbros suggest a high-temperature of water-rock interaction located at the top of the magma chamber. The evolution of the metamorphic parageneses from high (amphibolite and primary greenschist facies) to low temperature (retrograde greenschist facies and sea floor weathering) represents the progressive aging of the crust.

2) The Sr isotopic results reveal that the "interface" sheeted dike complex - isotropic gabbros, defining the top of the magma chamber, has experienced the largest supply of heated seawater. According to the decrease of W/R ratios (calculated from Sr isotopic data) towards the bottom of the cumulate sequence, the curves of chemical fluxes converge to the gain-loss zero line and define the geometric limit of the hydrothermal system. The seawater has reached the deep plutonic layers but its penetration was strongly diminished.

3) The large chemical fluxes calculated in the Trinity ophiolite are consistent with the strong degree of rock alteration. According to elemental fluxes, the calculated water/rock ratios of about 8 in the basalts are larger than those calculated in the Eastern Pacific Rise (21°N) which are of about 1.5 in both cases. This could be a possible consequence of a very active hydrothermal system generated within a slow spreading center (Le Sueur et al., 1984). This type of geodynamic environment can favours a widespread and protracted interaction between rocks and seawater. The alteration of a whole crustal sequence appears to control the equilibrium of the chemical exchanges between the seawater "box" and the oceanic crust "box".

4) When comparing the seawater-crustal budgets, the present results reveal that Trinity and Troodos ophiolites are more appropriate sites to subtract Mg and Na from seawater than Hole 504B. Ophiolites are certainly useful objects to establish the chemical budget of the oceanic reservoir: calculated elemental fluxes and W/R ratios are relevant to the time-integrated hydrothermal history.

It also appears that the geodynamic environment plays an important role in geochemical mass balances of the oceans. The site of seawater crust interactions may partly control the thermal energy, the life time of the hydrothermal system and the fault development. Crust generated under slow spreading rates such as Trinity (2 cm/y, LeSueur et al., 1984; Boudier and Nicolas, 85/86) may be extensively altered on a depth of several kilometers. In these conditions, the seawater-crust chemical exchanges are more buffered than in fast spreading ridges located in a widespread basin such as Hole 504B.

## References

- Albarède, F., Michard, A., Minster, J.F. and Michard, G., 1981.  $^{87}\text{Sr}/^{86}\text{Sr}$  ratios in hydrothermal waters and deposits from the East Pacific Rise at 21°N. *Earth Planet. Sci. Lett.*, 55: 229-236.
- Alibert, C., Michard, A. and Albarède, F., 1983. The transition from alkali basalts to kimberlites: isotope and trace element evidence from Melittites. *Contrib. Mineral. Petrol.*, 82: 176-186.
- Alt, J.C. and Emmermann, R., 1985. Geochemistry of hydrothermally altered basalts: Deep Sea Drilling Project Hole 504B, Leg 83. *Init. Rept. Deep Sea Drill. Proj.*, 83: 249-262.
- Alt, J.C., Honnorez, J., Laverne, C. and Emmermann, R., 1986. Hydrothermal alteration of a 1Km section through the upper oceanic crust, deep sea drilling project Hole 504B: mineralogy, chemistry and evolution of seawater-basalt interactions. *J. Geophys. Res.*, 91: 309-335.
- Ballard, R.D., Francheteau, J., Juteau, T., Rangan, C. and Normark, W., 1981. East Pacific Rise at 21°N: the volcanic, tectonic and hydrothermal processes of the central axis. *Earth Planet. Sci. Lett.*, 55: 1-10.
- Bednarz, U. and Schmincke, H. U., 1989. Mass transfer during sub-seafloor alteration of the upper Troodos crust (Cyprus). *Contrib. Mineral. Petrol.*, 102: 93-101.
- Bischoff, J.L. and Dickson, F.W., 1975. Seawater-basalt interaction at 200°C and 500 bars: implications for origin of sea-floor heavy-metal deposits and regulation of seawater chemistry. *Earth Planet. Sci. Lett.*, 25: 385-397.
- Blanchet, M.L. and Malaprad, L., 1967. Méthode rapide de dosage des principaux éléments d'une roche silicatée. *Chim. Anal.*, 49: 11-27.
- Bohlke, J.K., Alt, J.C. and Muehlenbachs, K., 1984. Oxygen isotope-water relationships in altered deep sea basalts: Low temperature mineralogical controls. *Can. J. Earth Sci.*, 21: 67-77.
- Boudier, F. and Nicolas, A., 1985/86. Harzburgite and lherzolite subtypes in ophiolite and oceanic environments. *Earth Planet. Sci. Lett.* 76: 84-92.



- Bowers, T.S. and Taylor, H.P., 1985. An integrated chemical and stable-isotope model of the origin of Midocean Ridge hot spring systems. *J. Geophys. Res.*, 90: 12583-12606.
- Brikowski, T. and Norton, D., 1989. Influence of magma chamber geometry on hydrothermal activity at mid-ocean ridges. *Earth Planet. Sci. Lett.*, 93: 241-255.
- Brouxel, M. and Lapierre, H., 1988. Geochemical study of an early Paleozoic island-arc - back-arc basin system. Part 1: The Trinity ophiolite (northern California). *Geol. Soc. Am. Bull.*, 100: 1111-1119.
- Brouxel, M., Lapierre, H., Michard, A. and Albarède, F., 1988. Geochemical study of an early Paleozoic island-arc - back-arc basin system. Part 2: Eastern Klamath, early to middle Paleozoic island-arc volcanic rocks (northern California). *Geol. Soc. Am. Bull.*, 100: 1120-1130.
- Bryan, W.B., Finger, L.W. and Chayes, F., 1968. Estimating proportions in petrographic mixing equations by least-squares approximation. *Science*, 163: 926-927.
- Burke, W.M., Denison, R.E., Hetherington, E.A., Koepnick, R.B., Nelson, M.F. and Otto, J.B., 1982. Variation of seawater  $^{87}\text{Sr}/^{86}\text{Sr}$  throughout Phanerozoic time. *Geology*, 10: 516-519.
- Cannat, M. and Lécuyer, C., 1989. Ephemeral magma chambers in the Trinity ophiolite (California). Submitted to *Tectonophysics*.
- Choukroune, P., Francheteau, J. and Hékinian, R., 1984. Tectonics of the East Pacific Rise near  $12^{\circ}50'\text{N}$ : a submersible study. *Earth Planet. Sci. Lett.*, 68: 115-127.
- Christie, D.M., Carmichael, I.S.E. and Langmuir, C.H., 1986. Oxidation states of mid-ocean ridge basalt glasses. *Earth Planet. Sci. Lett.*, 79: 397-411.
- Coleman, R.G., 1984. Preaccretion tectonics and metamorphism of ophiolites. *Ophioliti*, 9: 205-222.
- Coleman, R.G. and Donato, M.M., 1979. Oceanic plagiogranite revisited. In: F. Barker (Editor), *Trondhjemites, dacites, and related rocks*. Amsterdam-Oxford-New-York, Elsevier Publ. Co., pp. 149-167.
- Cooper, A.F., 1972. Progressive metamorphism of metabasic rocks from the Haast Schist Group of southern New Zealand. *J. Petrol.*, 13: 457-492.
- Crawford, A.J., Beccaluva, L. and Serri, G., 1981. Tectono-magmatic evolution of the West Philippine-Mariana region and the origin of boninites. *Earth Planet. Sci. Lett.*, 54: 346-356.
- Deer, W.A., Howie, R.A. and Zussman, I., 1966. An introduction to Rock - forming Minerals, Longmans, Wiley & Sons, New York, 528 pp.
- Dewey, J.F. and Bird, J.M., 1971. Origin and emplacement of the ophiolitic suite: Appalachians ophiolites in Newfoundland. *J. Geophys. Res.*, 76: 3179-3206.
- Drever, J.I., 1974. The magnesium problem. In: E.D. Goldberg (Editor), *Ideas and observations on progress in the study of the seas*. Vol 5 Marine Chemistry. Wiley, New York, pp 337-358.
- Edmond, J.M., Measures, C., McDuff, R.E., Chan, L.H., Collier, R., Grant, B., Gordon, L.I. and Corliss, J.B., 1979. Ridge crest hydrothermal activity and the balances of the major and minor elements in the ocean: the Galapagos data. *Earth Planet. Sci. Lett.*, 46: 1-18.
- Edmond, J.M., Von Damm, K.L., McDuff, R.E. and Measures, C.I., 1982. Chemistry of hot springs on the East pacific rise and their effluent dispersal. *Nature*, 297: 187-191.
- Edwards, R.L. and Wasserburg, G.J., 1985. The age and emplacement of obducted oceanic crust in the Urals from Sm-Nd and Rb-Sr systematics. *Earth Planet. Sci. Lett.*, 72: 389-404.
- Flower, M.F.J., 1980. Accumulation of calcic plagioclase in ocean-ridge tholeiite: an indication of spreading rate? *Nature*, 287: 530-532.
- Flower, M.F.J., 1981. Thermal and kinematic control on ocean-ridge magma fractionation: contrasts between Atlantic and Pacific spreading axes. *J. Geol. Soc. London*, 138: 695-712.
- Flower, M.F.J., 1984. Spreading-rate parameters in oceanic crust: analogue for ophiolite? In: I.G. Gass, S.J. Lippard and A.W. Shelton (Editors), *Ophiolites and Oceanic Lithosphere*. Blackwell Scientific Publications, pp. 25-40.
- Fournier, R.O. and Rowe, J.J., 1966. Estimation of underground temperatures from the silica content of water from hot springs and wet-steam wells. *Am. J. Sci.*, 264: 685-697.
- Girardeau, J., Mercier, J.C. and Xibin, W., 1985. Petrology of the mafic rocks of the Xigaze ophiolite, Tibet. *Contrib. Mineral. Petrol.*, 90: 309-321.
- Gregory, R.T., 1984. Melt percolation beneath a spreading ridge: evidence from the Semail peridotite, Oman. In: I. G. Gass, S. J. Lippard and A. W. Shelton (Editors), *Ophiolites and Oceanic Lithosphere*. Geological Society Special Publication N° 13, Blackwell Scientific Publications, pp. 55-62.
- Gregory, R.T. and Taylor, H.P., 1981. An oxygen isotopic profile in a section of Cretaceous oceanic crust, Semail ophiolite, Oman: evidence for  $^{18}\text{O}$  buffering of the oceans by deep (> 5 km) seawater-hydrothermal circulation at mid-ocean ridges. *J. Geophys. Res.*, 86: 2737-2756.
- Gresens, R.L., 1967. Composition-Volume relationships of metasomatism. *Chem. Geol.*, 2: 47-65.

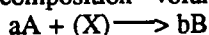
- Harper, G.D., Bowman, J.R. and Kuhns, R., 1988. A field, chemical, and stable isotope study of subseafloor metamorphism of the Josephine ophiolite, California-Oregon. *J. Geophys. Res.*, 93: 4625-4656.
- Hékinian, R., 1982. Petrology of the ocean floor. Elsevier Oceanography series 33, pp. 393.
- Holdaway, M.J., 1972. Thermal stability of Al-Fe epidote as a function of fO<sub>2</sub> and Fe content. *Contrib. Mineral. Petrol.*, 37: 307-340.
- Horibe, Y., Kim, K.R. and Craig, H., 1986. Hydrothermal methane plumes in the Mariana back-arc spreading centre. *Nature*, 324: 131-133.
- Humphris, S.E. and Thompson, G., 1978. Hydrothermal alteration of oceanic basalts by seawater. *Geochim. Cosmochim. Acta*, 42: 107-125.
- Irwin, W.P., 1981. Tectonic accretion of the Klamath Mountains. In: W.G. Ernst (Editor), *The geotectonic development of California*. Englewood Cliffs, New Jersey, Prentice-Hall, pp. 29-49.
- Ito, E. and Clayton, Jr.N., 1983. Submarine Metamorphism of Gabbros from the Mid - Cayman Rise: an oxygen isotopic study. *Geochim. Cosmochim. Acta*, 47: 535-546.
- Jacobsen, S.B. and Wasserburg, G.J., 1979. Nd and Sr isotopic study of the Bay of Islands ophiolite complex and the evolution of the source of mid-ocean ridge basalts. *J. Geophys. Res.*, 84: 7429-7445.
- Jacobsen, S.B., Quick, J.E. and Wasserburg, G.J., 1984. A Nd and Sr isotopic study of the Trinity peridotite; implications for mantle evolution. *Earth Planet. Sci. Lett.*, 68: 361-378.
- Janecky, D.R. and Seyfried W.E. 1983. The solubility of magnesium-hydroxyde-sulfate-hydrate in seawater at elevated temperatures and pressures. *AM. J. Sci.*, 283 : 831-860.
- Karson, J.A. and Elthon, D., 1987. Evidence for variations in magma production along oceanic spreading centers: A critical appraisal. *Geology*, 15: 127-131.
- Kastner, M. and Gieskes, J.M., 1976. Interstitial water profiles and sites of diagenetic reactions: Leg 35, DSDP, Bellingshausen abyssal plain. *Earth Planet. Sci. Lett.*, 33: 11-20.
- Kawahata, H., Kusakabe, M. and Kikuchi, Y., 1987. Strontium, oxygen and hydrogen isotope geochemistry of hydrothermally altered and weathered rocks in DSDP Hole 504B, Costa Rica Rift. *Earth Planet. Sci. Lett.*, 85: 343-355.
- Keith, T.E.C., Muffler, L.J.P. and Cremer, M., 1968. Hydrothermal epidote formed in the Salton Sea geothermal system, California. *Am. Mineral.*, 53: 1635-1644.
- Kennedy, G.C., 1950. A portion of the system silica-water. *Econ. Geol.*, 45: 629-653.
- Lambert, R.St J., 1959. The mineralogy and metamorphism of the Moine schists of the Morar and Knoydart district of Inverness-shire. *Trans. Roy. Soc. Edin.*, 63: 553.
- Lanphere, M.A., Coleman, R.G. and Hopson, C.A., 1981. Sr isotopic tracer study of the Samail Ophiolite, Oman. *J. Geophys. Res.*, 86: 2709-2720.
- Lanphere, M.A., Irwin, W.P. and Hotz, P.E., 1968. Isotopic age of the Nevada orogeny and older plutonic and metamorphic events in the Klamath Mountains, California. *Geol. Soc. Am. Bull.*, 79: 1027-1052.
- Lapierre, H., Brouxel, M., Albarède, F., Coulon, C., Lécuyer, C., Martin, P., Mascle, G. and Rouer, O., 1987. Paleozoic and Lower Mesozoic magmas from the eastern Klamath Mountains (N. California) and the geodynamic evolution of the north - western America. *Tectonophysics*, 140: 155-177.
- Leake, B.E., 1965. The relationship between tetrahedral aluminium and the maximum possible octahedral aluminium in natural calciferous and subcalciferous amphiboles. *Am. Mineral.*, 50: 843-851.
- LeSueur, E., Boudier, F., Cannat, M., Ceuleneer, G. and Nicolas, A., 1984. The Trinity mafic - ultramafic complex: first results of the structural study of an untypical ophiolite. *Ophioliti*, 9: 487-498.
- Lindsley-Griffin, N., 1977. The Trinity ophiolite, Klamath Mountains, California. *Bull. Oreg. Dept. Geol. Mineral. Ind.*, 95: 107-120.
- Liou, J.G., 1973. Synthesis and stability relations of epidote, Ca<sub>2</sub>Al<sub>2</sub>FeSi<sub>3</sub>O<sub>12</sub>(OH). *J. Petrol.*, 14: 381-413.
- Liou, J.G. and Ernst, W.G., 1979. Oceanic Ridge Metamorphism of the East Taiwan Ophiolite. *Contrib. Mineral. Petrol.*, 68: 335-348.
- Liou, J.G., Kuniyoshi, S. and Ito, K., 1974. Experimental studies of the phase relations between greenschist and amphibolite in a basaltic system. *Am. J. Sci.*, 274: 613-632.
- McCulloch, M.T., Gregory, R.T., Wasserburg, G.J. and Taylor, H.P.Jr., 1981. Sm-Nd, Rb-Sr, and <sup>18</sup>O/<sup>16</sup>O isotopic systematics in an oceanic crustal section: evidence from the Samail ophiolite. *J. Geophys. Res.*, 86: 2721-2735.
- Maruyama, S., Suzuki, K. and Liou, J.G., 1983. Greenschist - Amphibolite Transition Equilibria at Low Pressures. *J. Petrol.*, 24: 583-604.

- Mevel, C., 1984. Le métamorphisme dans la croûte océanique. Apport de la pétrologie à la compréhension des phénomènes de circulation hydrothermale (exemples dans l'Atlantique). Thèse doctorat ès-Sciences, Univ. Pierre et Marie Curie, pp. 434.
- Michard, A., Gurriet, P., Soudant, M. and Albarède, F., 1985. Nd isotopes in French Phanerozoic shales: external vs. internal aspects of crustal evolution. *Geochim. Cosmochim. Acta*, 78: 104-114.
- Michard, G., Albarède, F., Michard, A., Minster, J.F., Charlou, J.L. and Tan, N., 1984. Chemistry of solutions from the 13°N East Pacific Rise hydrothermal site. *Earth Planet. Sci. Lett.*, 67: 297-307.
- Miyashiro, A., 1973. The Troodos ophiolitic complex was probably formed in an island arc. *Earth Planet. Sci. Lett.*, 19: 218-224.
- Miyashiro, A., Shido, F. and Ewing, M., 1971. Metamorphism in the mid - Atlantic ridge near 24° and 30°N. *Philos. Trans. R. Soc. London, A* 268: 589-603.
- Moody, J.B., Meyer, D. and Jenkins, J.E., 1983. Experimental characterization of the greenschist / amphibolite boundary in mafic systems. *Am. J. Sci.*, 283: 48-92.
- Moores, E. M., Robinson, P. T., Malpas, J. and Xenophontos, C., 1984. Model for the origin of the Troodos massif, Cyprus, and other mideast ophiolites. *Geology*, 12: 500-503.
- Mottl, M.J., 1983. Metabasalts, axial hot springs, and the structure of hydrothermal systems at mid-ocean ridges. *Geol. Soc. Am. Bull.*, 94: 161-180.
- Mottl, M.J. and Seyfried, W.E., 1977. Experimental basalt/seawater interaction: rock- vs. seawater-dominated systems and the origin of submarine hydrothermal deposits. *Geol. Soc. Am.*, 9: 1104 (abstract).
- Mottl, M.J. and Seyfried, W.E., 1978. Sub-sea floor hydrothermal systems: rock- vs. seawater-dominated systems. In: P.A. Rona (Editor), *Hydrothermal Systems at Oceanic Spreading Centers*. Academic Press, 643 pp.
- Orcutt, J.A., McClain, J.S. and Burnett, M., 1984. Evolution of the ocean crust: results from recent seismic experiments. In: I.G. Gass, S.J. Lippard and A.W. Shelton (Editors), *Ophiolites and Oceanic Lithosphere*, Blackwell Scientific Publications, 7-16.
- Peacock, S.M., 1987. Serpentinization and infiltration metasomatism in the Trinity peridotite, Klamath province, northern California: implications for subduction zones. *Contrib. Mineral. Petrol.*, 95: 55-70.
- Peterman, Z.E. and Hedge, C.E., 1971. Related strontium isotopic and chemical variations in oceanic basalts. *Geol. Soc. Am. Bull.*, 82: 493-500.
- Poreda, R., 1985. Helium-3 and deuterium in back-arc basalts: Lau Basin and the Mariana Trough. *Earth Planet. Sci. Lett.*, 73: 244-254.
- Quick, J.E., 1981. Petrology and petrogenesis of the Trinity peridotite, an upper mantle diapir in the eastern Klamath Mountains, northern California. *J. Geophys. Res.*, 87: 3831-3848.
- Rautenschlein, M., Jenner, G.A., Hertogen, J., Hofmann, A.W., Kenich, R., Schmincke, H.-U. and White, W.M., 1985. *Earth Planet. Sci. Lett.*, 75: 369-383.
- Seyfried, W.E., Shanks, W.C. and Dibble, W.E., 1978. Clay mineral formation in DSDP leg 34 basalts. *Earth Planet. Sci. Lett.*, 41: 265-276.
- Sivell, W.J. and Waterhouse, J.B., 1984. Oceanic ridge metamorphism of the Patuki Volcanics, D'Urville Island, New Zealand. *Lithos*, 17: 19-36.
- Spear, F.S., 1981. An experimental study of hornblende stability and compositional variability in amphibolite. *Am. J. Sci.*, 281: 697-734.
- Stakes, D.S. and O'Neil, J.R., 1982. Mineralogy and stable isotope geochemistry of hydrothermally altered oceanic rocks. *Earth Planet. Sci. Lett.*, 57: 285-304.
- Staudigel, H. and Hart, S. R., 1983. Alteration of basaltic glass: Mechanisms and significance for the oceanic crust-seawater budget. *Geochim. Cosmochim. Acta*, 47: 337-350.
- Steiner, A., 1968. Clay minerals in hydrothermal altered rocks at Wairakei, New Zealand, *Clays, Clay Mineral.*, 16: 193-213.
- Thompson, G., 1983. Basalt-seawater interaction. In: P.A. Rona, K. Bostrom and K.L. Smith (Editors), *Hydrothermal Processes at Seafloor Spreading Centers*. Plenum, New York, pp. 225-278.
- Varga, R. J. and Moores, E. M., 1985. Spreading structure of the Troodos ophiolite, Cyprus. *Geology*, 13: 846-850.
- Von Damm, K.L., Edmond, J.M., Grant, B., Measures, C.I., Walden, B. and Weiss, R.F., 1985. Chemistry of submarine hydrothermal solutions at 21°N, East Pacific Rise. *Geochim. Cosmochim. Acta*, 49: 2197-2220.
- Williams, D.L. and Von Herzen, R.P., 1974. Heat loss from the Earth: New estimate. *Geology*, 2: 227-238.

- Wolery, T.J. and Sleep, N.H., 1988. Interactions of geochemical cycles with the mantle. In: C.B. Gregor, R.M. Garrels, F.T. Mackenzie and J.B. Maynard (Editors), *Chemical cycles in the evolution of the Earth*, John Wiley and sons, New York, 276pp.
- Wood, B.J. and Walther, J.V., 1983. Rates of Hydrothermal Reactions. *Science*, 222: 413-415.

#### APPENDIX: Elemental fluxes calculation

The method first involves the calculation of the modal compositions of altered rocks from the mineral chemistry (electron microprobe) and bulk rock compositions (X-ray fluorescence) by a standard least-square method (e.g. Bryan et al., 1968). Then, the magmatic modal proportions are calculated by correcting the metamorphic modal proportions calculated by least-squares from the change of density estimated by the Gresens's method (1967). This requires that the chemical composition of both primary and secondary phases is known. Let us assume that the source mineral source (A) breaks down into the mineral product (B), a and b being the amounts in grams of each mineral and X the total amount of material lost or gained in grams, then the two minerals/two components composition - volume equation reads:



The problem may be expanded to a n components equation in which  $c_{nA}$  and  $c_{nB}$  are the weight fractions of component n in mineral A and B (chemical analysis),  $x_n$  the amount of component n lost or gained,  $g_A$  and  $g_B$  the specific gravities of minerals A and B and  $F_v$  the volume factor.

$$100[F_v \cdot (g_B/g_A) \cdot c_{nB} - c_{nA}] = x_n A$$

In order to solve the problem, we need to assume that either one component is immobile or  $F_v = 1$  (isovolumic replacement). The first assumption is generally done by considering Al to be immobile but is not valid in the case of albitization of anorthite-rich plagioclase as previously demonstrated by Gresens (1967). In contrast, textural relationships indicate that the shape of the primary minerals is fairly well preserved, hinting therefore to small volume changes, hence  $F_v$  is probably not much different from unity. Hence,  $F_v = 1$  has been assumed for the replacement of plagioclase by albite ( $g_B/g_A = 0.95 - 0.97$ ) has been considered because no swelling is observed. For other mineral reactions, this estimate can be refined in the composition - volume diagram of Gresens (1967). When plotting gains and losses against  $F_v$ , the actual  $F_v$  value corresponds to the intersection of the straight lines defined by each mineral reaction. The graphic solution gives  $F_v = 0.9$  for the replacement of plagioclase by epidote ( $g_B/g_A = 1.18 - 1.26$ ),  $F_v = 1.07$  for that clinopyroxene by actinolite ( $g_B/g_A = 0.91 - 0.94$ ),  $F_v = 1.1$  for chloritization of actinolite ( $g_B/g_A = 0.91 - 0.97$ ), and  $F_v = 1.15$  for replacement of olivine by serpentine ( $g_B/g_A = 0.73$ ).

Then, the chemical composition of the magmatic rock is estimated from the composition of fresh mineral relicts and their weight fraction calculated as above. The difference between ideal and measured bulk rock composition gives the mass elemental fluxes in grams of oxide per of whole rock.

The method is not valid when glass is present. However, the small fraction of glass observed in the Trinity basalts suggests that it does not introduce a significant error into the calculation.

An average error of 3 percent on the calculated fluxes has been estimated from the cumulated effects of the propagated errors through the different steps of calculations. Source of errors is associated with mineral (electron microprobe) and whole rock analyses (XRF), modal calculations, mineral density and estimates of volume changes.

#### Figure captions

Fig.1: Geological map of the studied area with the position of the samples.

Fig. 2: Synthetic lithologic column of the Trinity ophiolite with the position of the studied samples and the observed mineralogical parageneses. The variations of the epidotes Ps contents and of the amphibole Al<sup>IV</sup> contents are shown together with the position of the sample in the lithologic column. Filled circles: basalts, open circles: dikes, filled triangles: isotropic gabbros, open triangles: gabbroic pegmatites, open squares: cumulate gabbros, filled circles: ultramafic cumulates.

Abbreviations: Ab: albite; Ep: epidote; Ac: actinolite; Chl: chlorite; Ox: oxides; Qz: quartz; Spt: serpentine; Hbl: hornblende; Px: pyroxene; Ol: olivine. Ta: talc; Tr: tremolite; Ce: celadonite; F: K-feldspar; Ca: calcite.

Fig. 3: chemical compositions of Trinity basalts plotted in a ACF diagram.

Fig. 4: Ti versus  $Al^{IV}$  and Na+K (atoms/formula unit) versus  $Al^{IV}$  in the Trinity ophiolite amphiboles. Same symbols as in figure 2.

Fig. 5:  $Fe^{3+}$  versus  $Al^{VI}$  (atoms/formula unit) in the Trinity ophiolite epidotes (average values for basalts and dikes,  $n = 10$ ). Same symbols as in figure 2.

Fig. 6: Variation of Sr and Rb contents, Sr initial isotopic ratios, calculated water/rock ratios (see text for details) and  $Fe^{3+}/Fe^t$  ratios in the Trinity ophiolite. Same symbols as in figure 2. Filled stars: plagiogranite dikes.

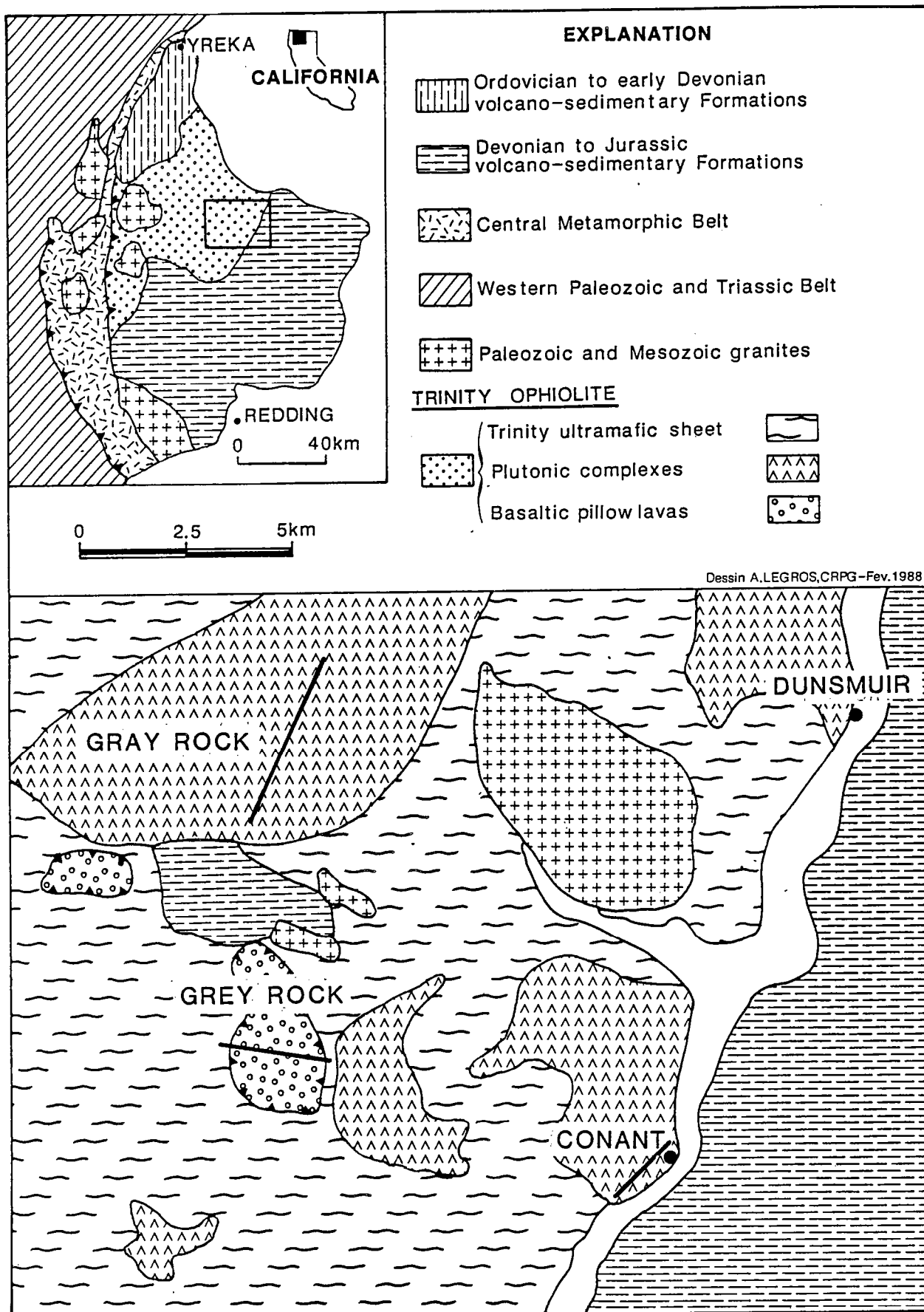
Fig. 7: Flow chart representation of the method used for the calculations of elemental fluxes. See text and Appendix for explanations.

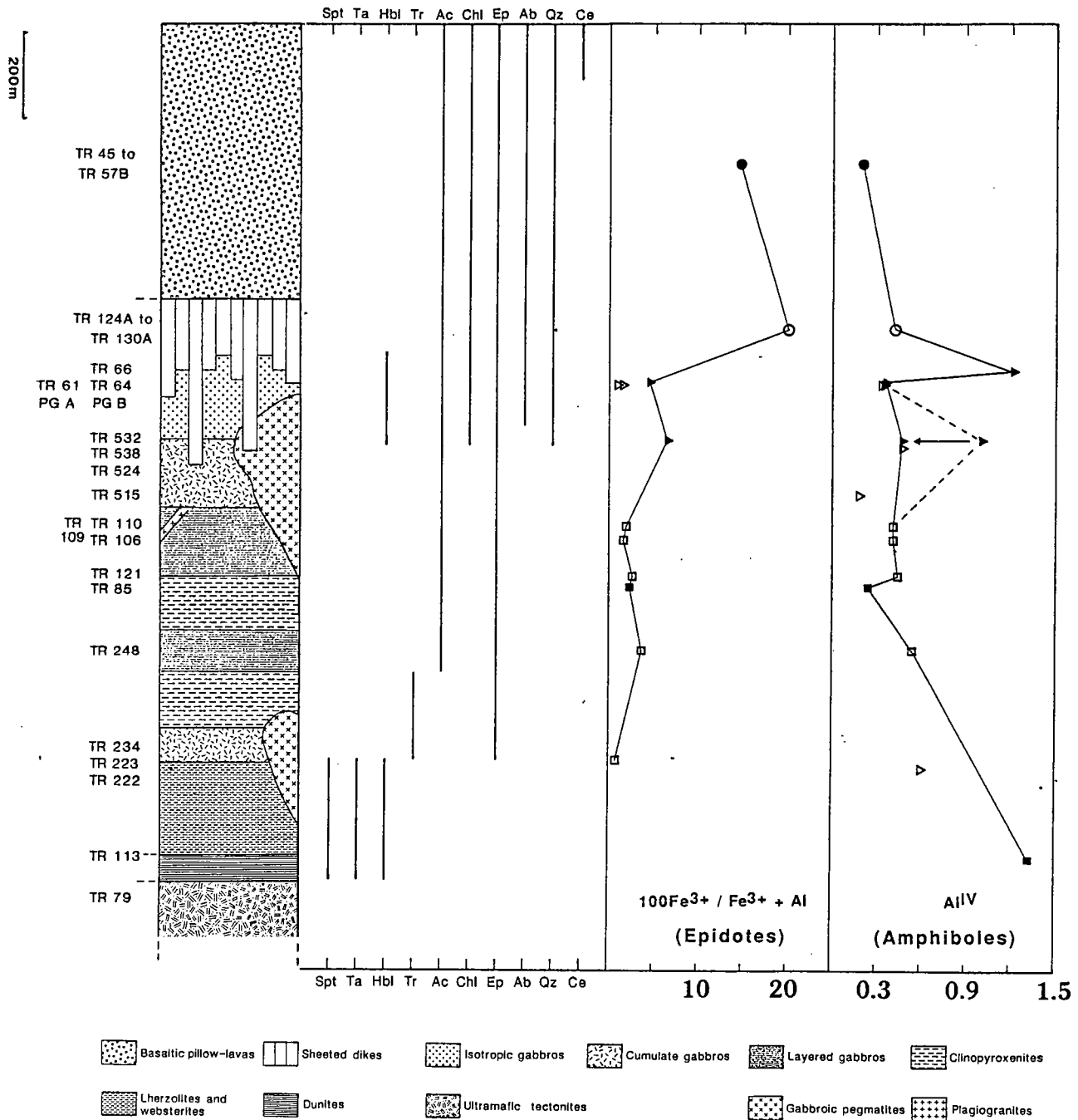
Fig. 8: Variation of the calculated fluxes in the Trinity ophiolite. The calculated secondary parageneses are represented for the samples used in the calculation. Same symbols as in figure 2. Curves for W/R ratios represent the field of data. Ab: albite; Ep: epidote; Ac: actinolite; Chl: chlorite; Ox: oxides; Qz: quartz; Spt: serpentine; Hbl: hornblende; Px: pyroxene; Ol: olivine.

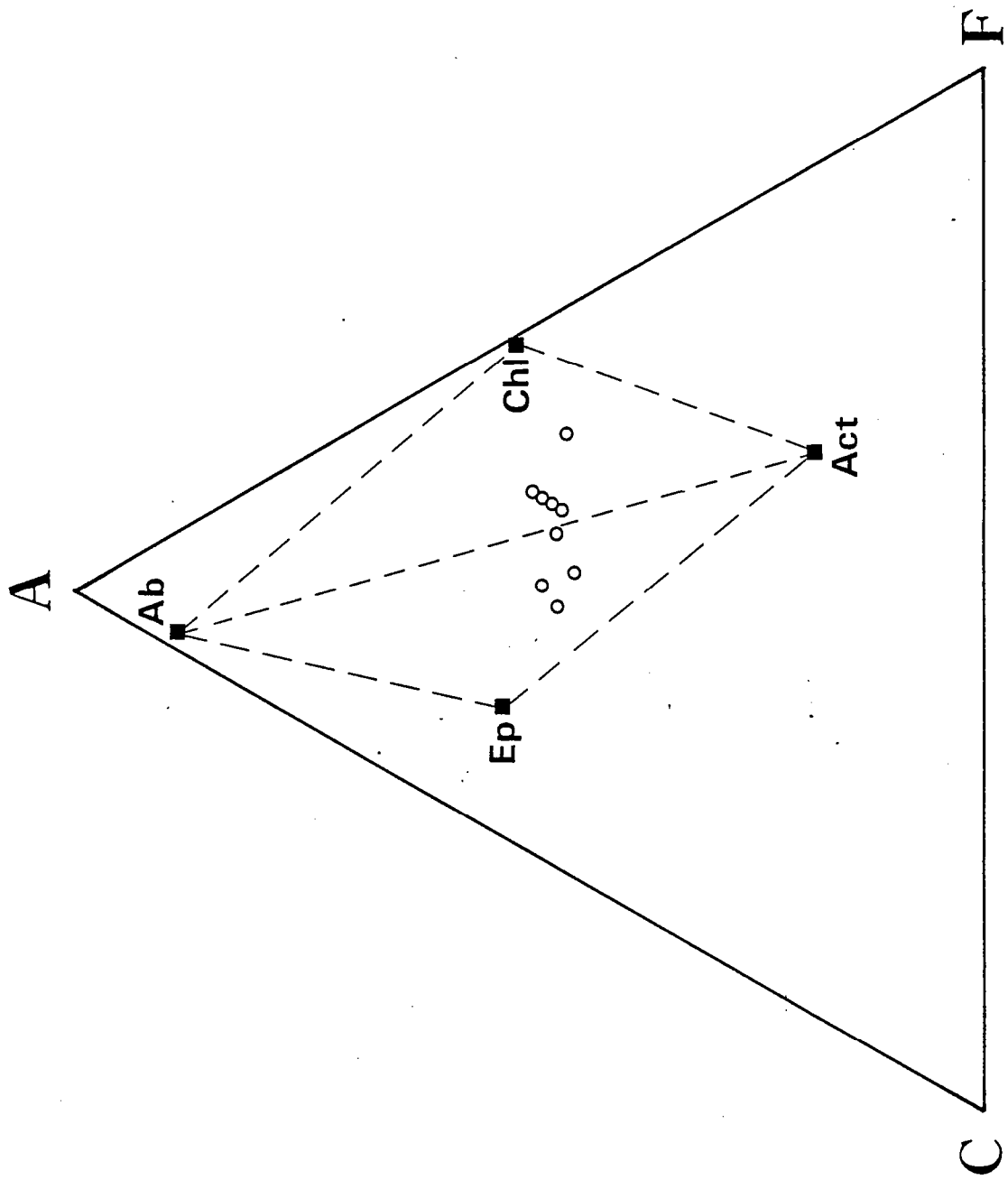
Fig. 9:  $Fe^{3+}/Fe^t$  ratio versus calculated water/rock ratio in the Trinity ophiolitic rocks. Same symbols as in figure 2.

Fig. 10: Calculated elemental fluxes in the Trinity ophiolitic basalts. Comparison with the calculated fluxes in the Hole 504B.

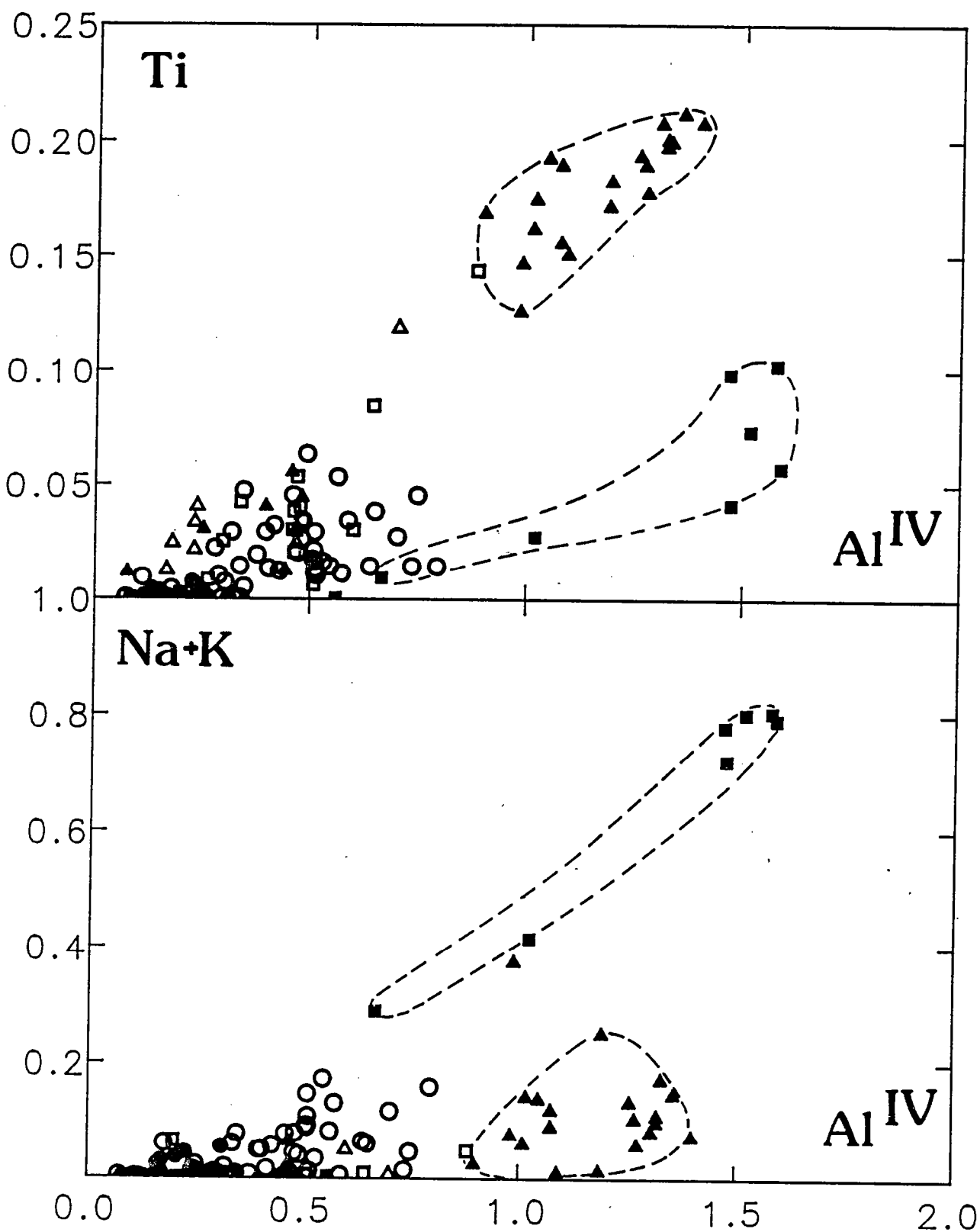
Fig. 11: comparison of elemental fluxes in  $10^{14}$  g/year for Trinity, Troodos (Bednarz and Schmincke, 1989) and Hole 504B (Alt et al., 1986) basalts in comparison to river inputs (Thompson, 1983). Positive flux into oceanic crust. See text for explanations.



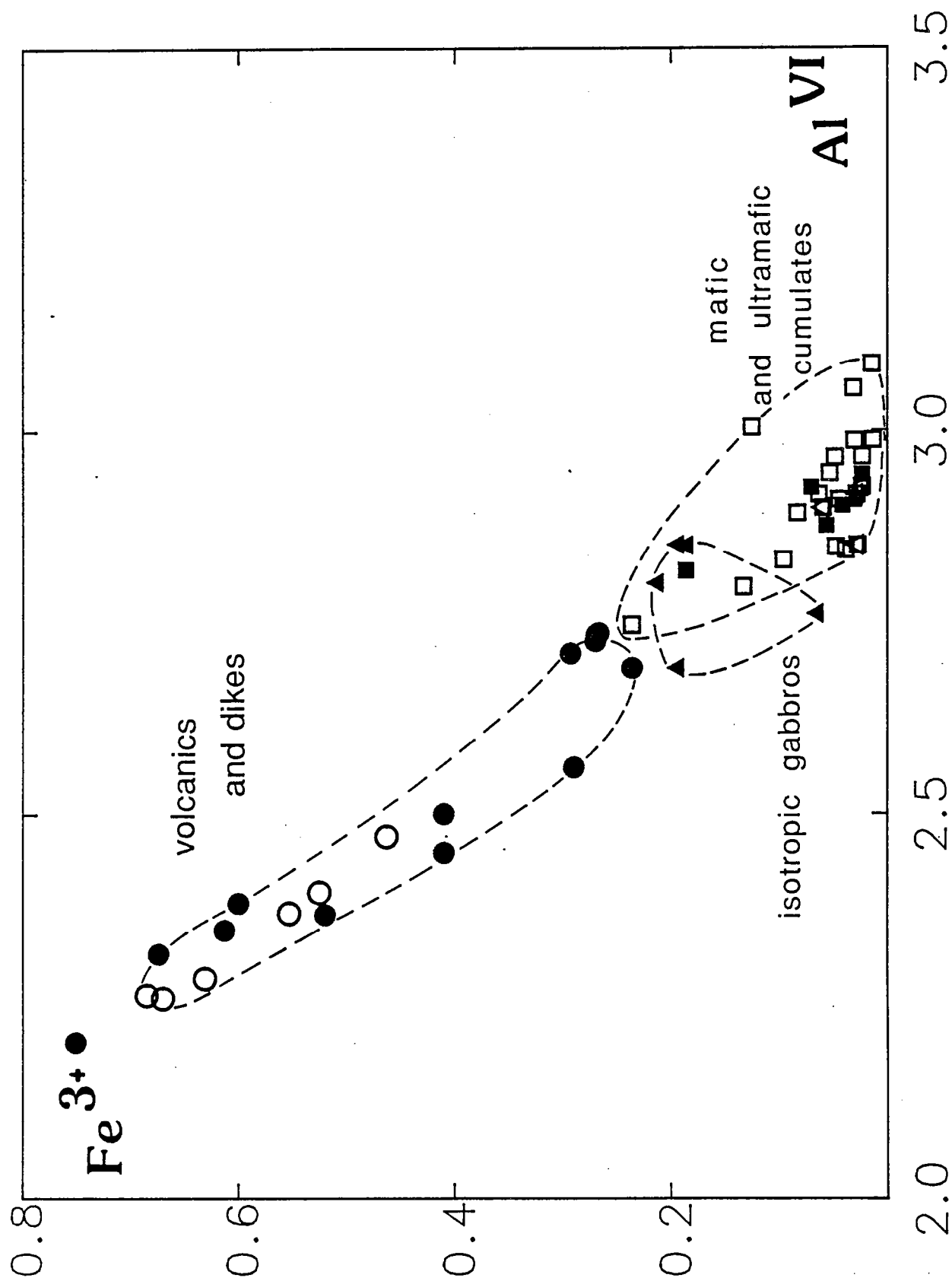


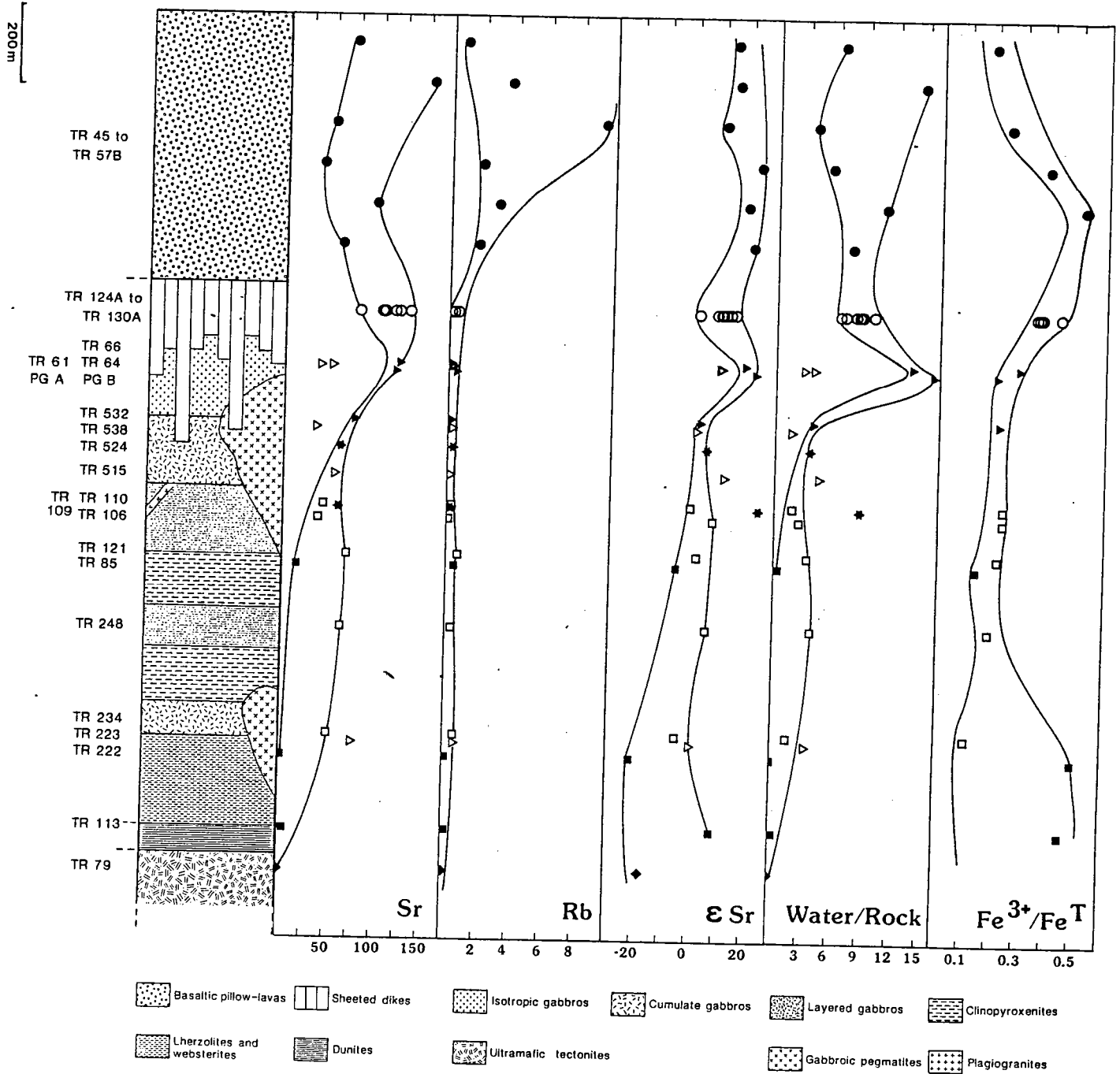


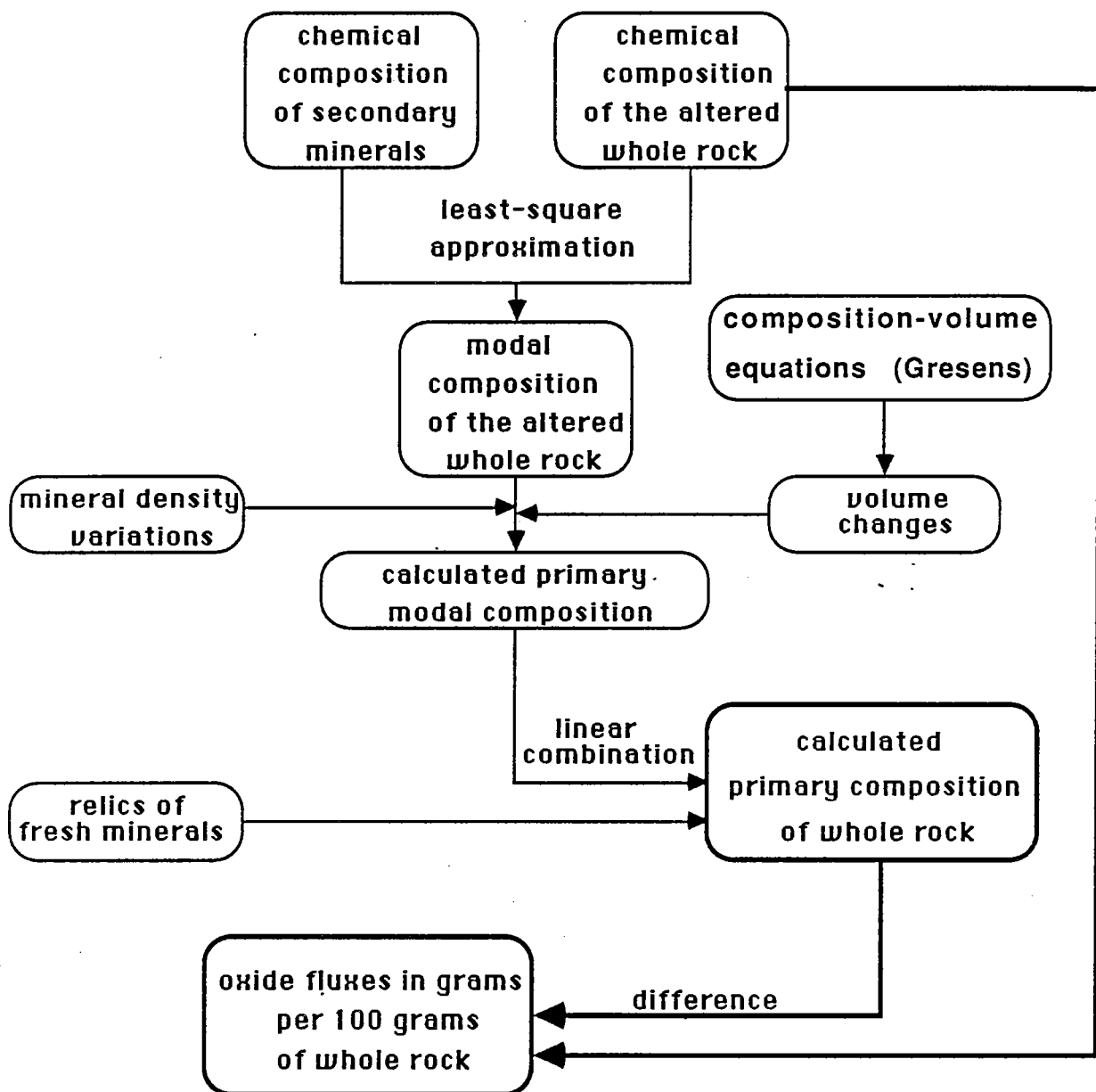


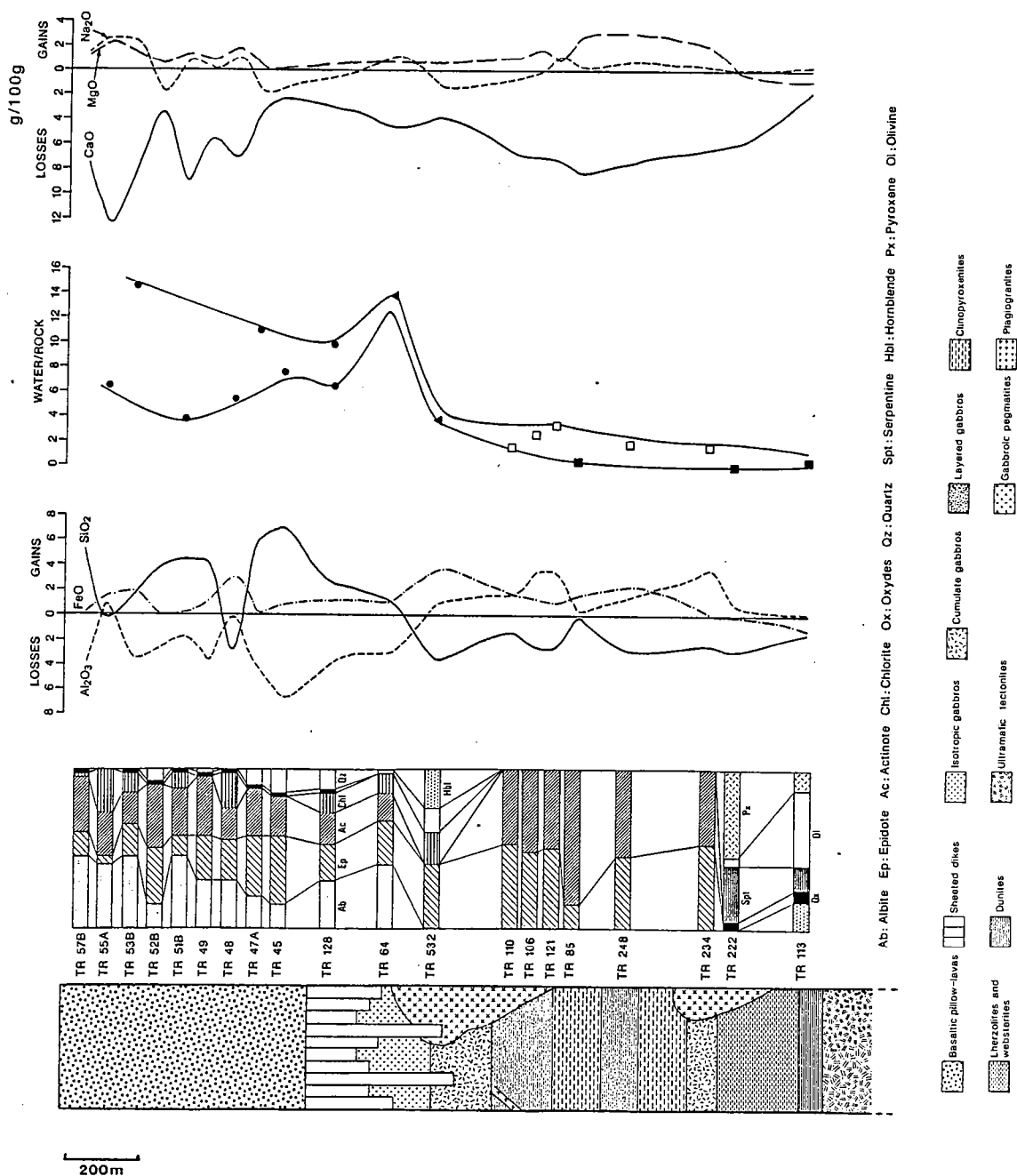


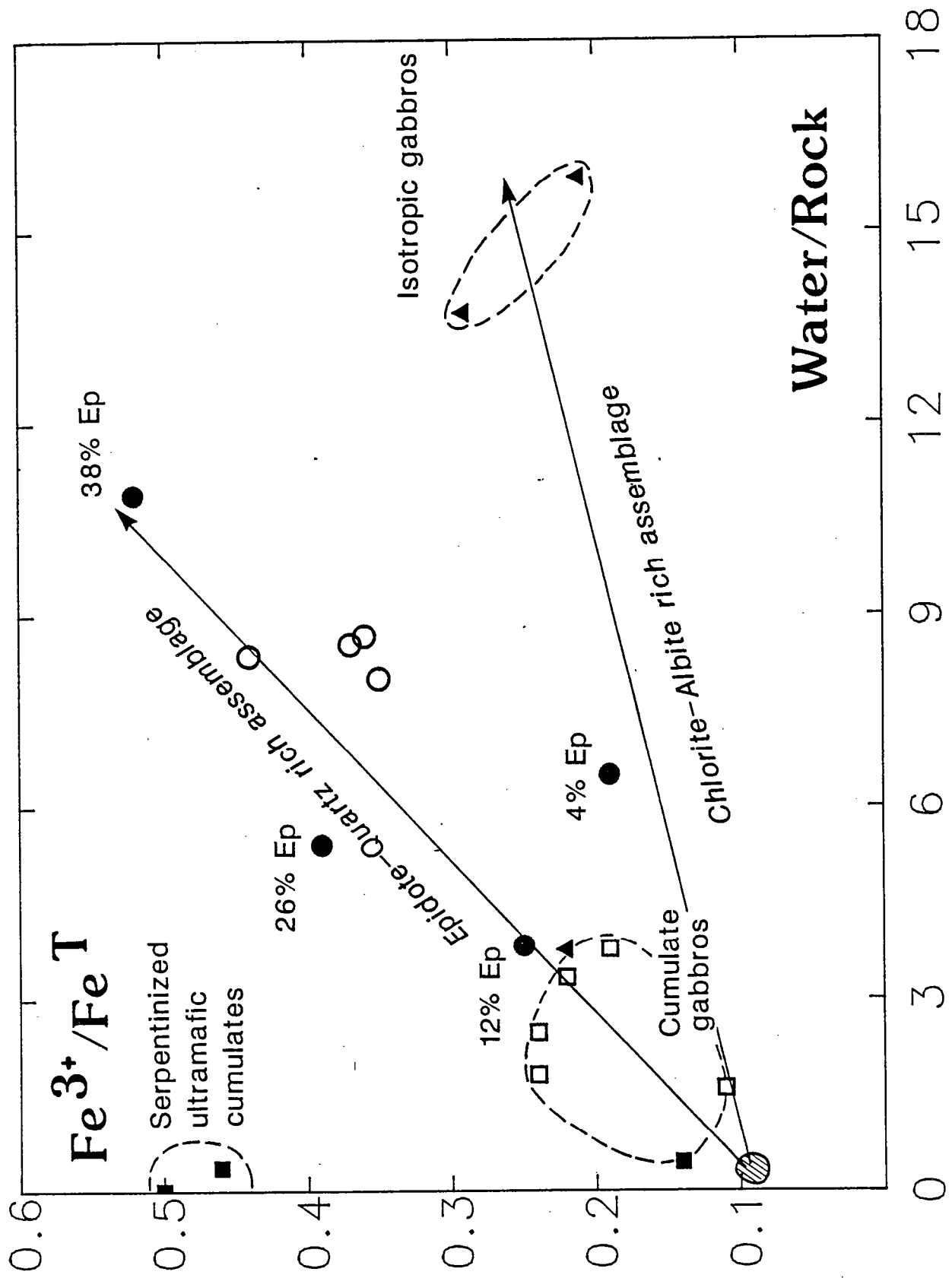
- ▲ Isotropic gabbros magnesio-hornblende
- Cumulate lherzolite pargasitic hornblende

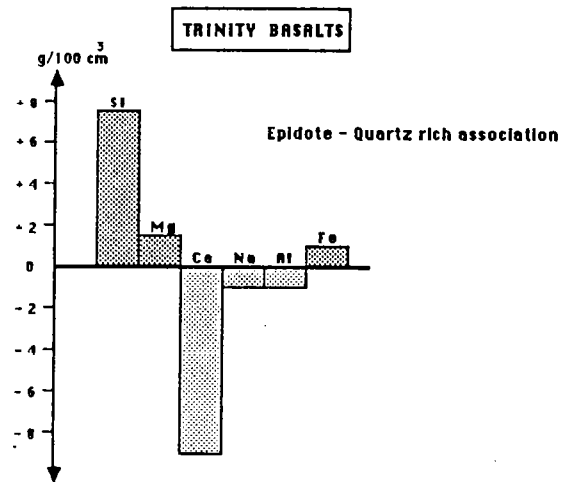
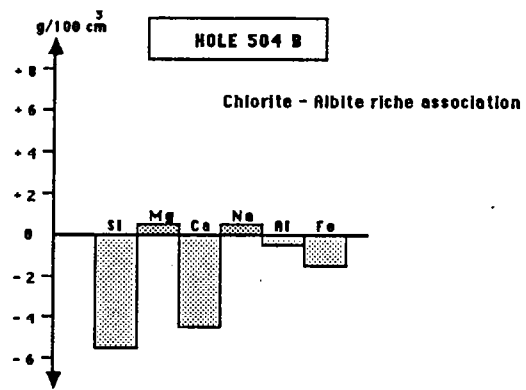
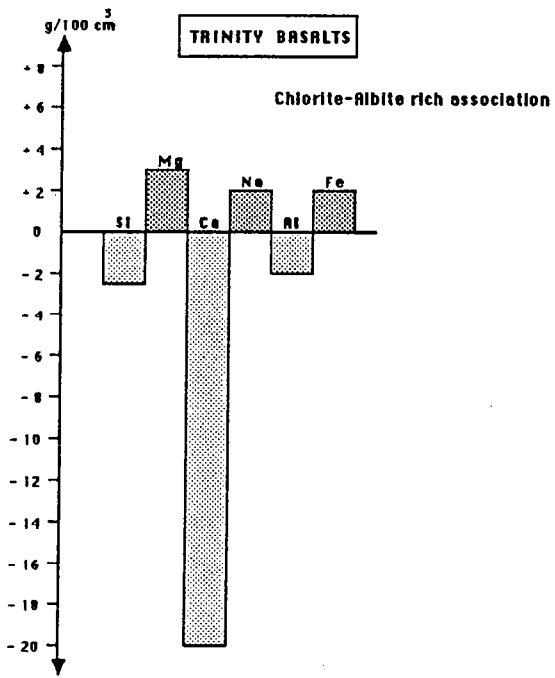












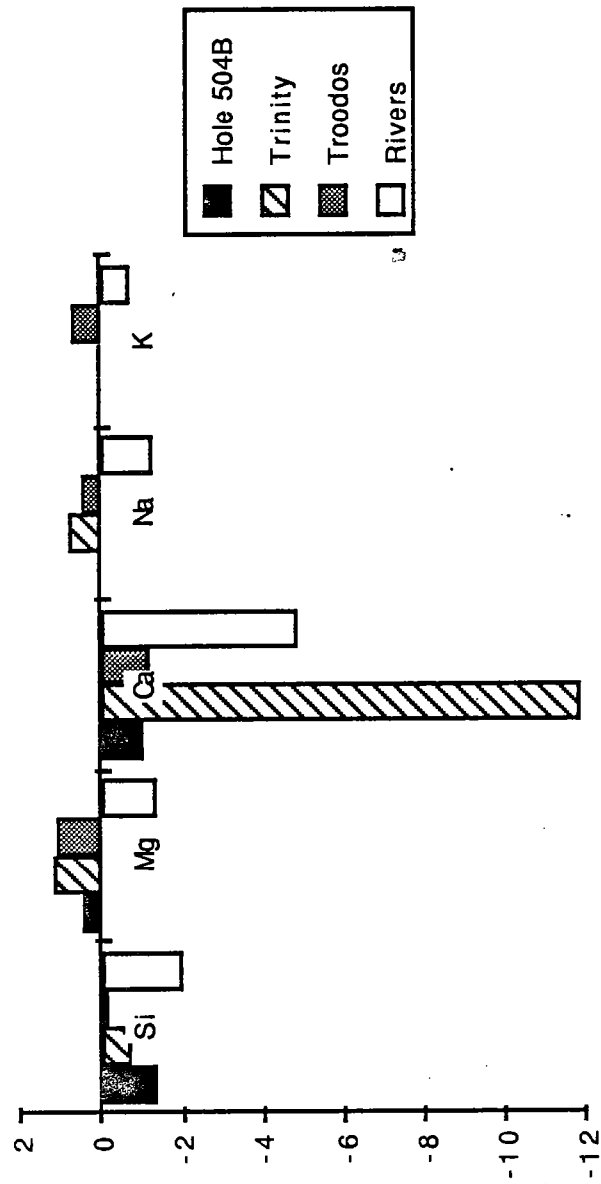




Table 1: Chlorite microprobe analyses of the Trinity ophiolitic rocks.

|       | TR 532    | TR 234   | TR 128J | TR 128J | TR 128R       | TR 128R | TR 128R | TR 128R | TR 128R       | TR 128R | TR 128T | TR 128T | TR 128T |
|-------|-----------|----------|---------|---------|---------------|---------|---------|---------|---------------|---------|---------|---------|---------|
|       | isotropic | cumulate |         |         | sheeted dikes |         |         |         | sheeted dikes |         |         |         |         |
|       | gabbro    | gabbro   |         |         |               |         |         |         |               |         |         |         |         |
| SiO2  | 27,15     | 27,85    | 26,96   | 26,07   | 26,95         | 27,54   | 27,39   | 26,63   | 27,45         | 26,86   | 26,65   | 26,11   |         |
| Al2O3 | 21,28     | 22,96    | 21,61   | 21,59   | 22,24         | 22,05   | 22,12   | 22,27   | 22,08         | 20,57   | 21,65   | 21,52   |         |
| TiO2  | 0,00      | 0,00     | 0,00    | 0,00    | 0,00          | 0,10    | 0,08    | 0,08    | 0,00          | 0,01    | 0,05    | 0,03    |         |
| FeO   | 18,72     | 9,11     | 17,69   | 19,55   | 17,35         | 15,89   | 16,15   | 16,98   | 15,71         | 17,15   | 17,16   | 17,62   |         |
| MgO   | 18,67     | 25,99    | 19,59   | 19,20   | 20,29         | 20,24   | 20,45   | 20,11   | 20,49         | 20,72   | 20,39   | 19,91   |         |
| MnO   | 0,18      | 0,01     | 0,37    | 0,42    | 0,41          | 0,25    | 0,17    | 0,21    | 0,31          | 0,32    | 0,29    | 0,24    |         |
| CaO   | 0,08      | 0,10     | 0,01    | 0,03    | 0,06          | 0,01    | 0,00    | 0,00    | 0,21          | 0,08    | 0,03    | 0,00    |         |
| Na2O  | 0,00      | 0,00     | 0,01    | 0,00    | 0,00          | 0,00    | 0,06    | 0,04    | 0,00          | 0,00    | 0,00    | 0,11    |         |
| K2O   | 0,00      | 0,00     | 0,00    | 0,00    | 0,06          | 0,01    | 0,03    | 0,00    | 0,04          | 0,00    | 0,00    | 0,03    |         |
| Cr2O3 | 0,00      | 0,00     | 0,27    | 0,20    | 0,19          | 0,37    | 0,33    | 0,26    | 0,25          | 0,34    | 0,03    | 0,24    |         |
| Sum   | 86,08     | 86,02    | 86,51   | 87,06   | 87,55         | 86,46   | 86,78   | 86,58   | 86,54         | 86,05   | 86,25   | 85,81   |         |
| Si    | 5,604     | 5,462    | 5,519   | 5,371   | 5,442         | 5,574   | 5,533   | 5,424   | 5,552         | 5,526   | 5,458   | 5,402   |         |
| Al    | 5,177     | 5,307    | 5,214   | 5,243   | 5,294         | 5,260   | 5,267   | 5,347   | 5,264         | 4,988   | 5,226   | 5,248   |         |
| Ti    | 0         | 0        | 0       | 0       | 0             | 0,015   | 0,012   | 0,012   | 0             | 0,002   | 0,008   | 0,005   |         |
| Fe    | 3,232     | 1,494    | 3,029   | 3,368   | 2,930         | 2,690   | 2,728   | 2,893   | 2,658         | 2,951   | 2,939   | 3,049   |         |
| Mg    | 5,745     | 7,598    | 5,978   | 5,897   | 6,108         | 6,107   | 6,158   | 6,106   | 6,178         | 6,355   | 6,225   | 6,140   |         |
| Mn    | 0,031     | 0,002    | 0,064   | 0,073   | 0,070         | 0,043   | 0,029   | 0,036   | 0,053         | 0,056   | 0,050   | 0,042   |         |
| Ca    | 0,018     | 0,021    | 0,002   | 0,007   | 0,013         | 0,002   | 0       | 0       | 0,046         | 0,018   | 0,007   | 0       |         |
| Na    | 0         | 0        | 0,004   | 0       | 0             | 0       | 0,024   | 0,016   | 0             | 0       | 0       | 0,044   |         |
| K     | 0         | 0        | 0       | 0       | 0,015         | 0,003   | 0,008   | 0       | 0,010         | 0       | 0       | 0,008   |         |
| Cr    | 0         | 0        | 0,044   | 0,033   | 0,030         | 0,059   | 0,053   | 0,042   | 0,040         | 0,055   | 0,005   | 0,039   |         |
| Sum   | 19,807    | 19,884   | 19,854  | 19,992  | 19,902        | 19,753  | 19,812  | 19,876  | 19,801        | 19,951  | 19,918  | 19,977  |         |

Table 2: Amphibole microprobe analyses of the Trinity ophiolitic rocks.

|       | TR 113<br>hercynite | TR 85<br>clinopyroxenite | TR 106<br>cumulate gabbro | TR 532<br>isotropic gabbros | TR 64<br>pegmatitic gabbros | TR 66<br>pegmatitic gabbros | TR 128F<br>sheeted dikes | TR 124D<br>sheeted dikes | TR 53B<br>pillow lavas | TR 53B<br>pillow lavas |
|-------|---------------------|--------------------------|---------------------------|-----------------------------|-----------------------------|-----------------------------|--------------------------|--------------------------|------------------------|------------------------|
| SiO2  | 45.33               | 56.53                    | 55.76                     | 52.54                       | 54.19                       | 55.97                       | 53.03                    | 53.02                    | 55.37                  | 53.41                  |
| Al2O3 | 11.58               | 1.62                     | 2.79                      | 4.71                        | 2.64                        | 1.47                        | 4.00                     | 3.70                     | 1.51                   | 1.82                   |
| FeO   | 5.27                | 6.67                     | 5.85                      | 11.16                       | 9.28                        | 6.66                        | 9.58                     | 10.38                    | 7.20                   | 10.23                  |
| MgO   | 18.33               | 20.36                    | 21.37                     | 15.56                       | 17.18                       | 19.97                       | 16.26                    | 16.21                    | 18.61                  | 16.36                  |
| MnO   | 0.05                | 0.29                     | 0.11                      | 0.20                        | 0.24                        | 0.18                        | 0.25                     | 0.24                     | 0.19                   | 0.43                   |
| TiO2  | 0.68                | 0                        | 0.25                      | 0.41                        | 0.28                        | 0.12                        | 0.18                     | 0.27                     | 0.03                   | 0                      |
| Cr2O3 | 0                   | 0.26                     | 0.03                      | 0                           | 0.36                        | 0                           | 0.28                     | 0                        | 0                      | 0.10                   |
| NiO   | 1.00                | 0                        | 0.09                      | 0                           | 0                           | 0.09                        | 0.18                     | 0                        | 0                      | 0.07                   |
| CaO   | 11.91               | 12.64                    | 12.65                     | 11.19                       | 11.89                       | 12.44                       | 11.68                    | 12.44                    | 13.57                  | 12.85                  |
| Na2O  | 2.77                | 0.22                     | 0.46                      | 0.88                        | 0.40                        | 0.28                        | 0.57                     | 0.46                     | 0.08                   | 0.10                   |
| K2O   | 0.18                | 0                        | 0                         | 0.05                        | 0.03                        | 0.02                        | 0.04                     | 0.06                     | 0                      | 0.05                   |
| Sum   | 97.10               | 98.59                    | 97.95                     | 96.7                        | 96.49                       | 97.11                       | 96.05                    | 96.78                    | 96.56                  | 95.42                  |
| Si    | 6.49                | 7.794                    | 7.702                     | 7.52                        | 7.749                       | 7.834                       | 7.624                    | 7.584                    | 7.850                  | 7.780                  |
| AlIV  | 1.52                | 0.205                    | 0.297                     | 0.479                       | 0.250                       | 0.165                       | 0.375                    | 0.415                    | 0.149                  | 0.219                  |
| AlVI  | 0.44                | 0.057                    | 0.108                     | 0.315                       | 0.194                       | 0.077                       | 0.302                    | 0.208                    | 0.103                  | 0.093                  |
| Ti    | 0.07                | 0                        | 0.025                     | 0.044                       | 0.030                       | 0.012                       | 0.019                    | 0.029                    | 0.003                  | 0                      |
| Cr    | 0                   | 0.028                    | 0.003                     | 0                           | 0.040                       | 0                           | 0.031                    | 0                        | 0                      | 0.011                  |
| Fe3+  | 0.126               | 0.178                    | 0.207                     | 0.311                       | 0.060                       | 0.135                       | 0.154                    | 0.265                    | 0.061                  | 0.132                  |
| Fe2+  | 0.503               | 0.227                    | 0.468                     | 1.024                       | 1.049                       | 0.644                       | 0.997                    | 0.976                    | 0.792                  | 1.113                  |
| Mn    | 0.006               | 0.015                    | 0.008                     | 0.024                       | 0.029                       | 0.021                       | 0.030                    | 0.029                    | 0.022                  | 0.053                  |
| Mg    | 3.909               | 3.928                    | 4.128                     | 3.319                       | 3.662                       | 4.166                       | 3.484                    | 3.456                    | 3.933                  | 3.552                  |
| Ni    | 0.115               | 0.156                    | 0                         | 0                           | 0                           | 0.010                       | 0.020                    | 0                        | 0                      | 0.008                  |
| Ca    | 1.826               | 1.867                    | 1.872                     | 1.716                       | 1.822                       | 1.866                       | 1.799                    | 1.906                    | 2.061                  | 2.005                  |
| NaA   | 0                   | 0.058                    | 0.123                     | 0.244                       | 0.110                       | 0.076                       | 0.158                    | 0.127                    | 0.021                  | 0.028                  |
| NaB   | 0.768               | 0                        | 0                         | 0                           | 0                           | 0                           | 0                        | 0                        | 0                      | 0                      |
| K     | 0.032               | 0                        | 0                         | 0                           | 0.005                       | 0.003                       | 0.007                    | 0.010                    | 0                      | 0.009                  |
| Sum   | 15.796              | 14.994                   | 14.995                    | 15.005                      | 15.000                      | 14.999                      | 15.000                   | 15.005                   | 14.995                 | 15.003                 |

Table 3: Epidote microprobe analyses of the Trinity ophiolitic rocks.

|       | TR85         | TR85  | TR121            | TR121 | TR110 | TR110 | TR110 | PEGMA            | PEGMB | TRI28J        | TRI28J | TR47         | TR47  | TR48  | TR48  |
|-------|--------------|-------|------------------|-------|-------|-------|-------|------------------|-------|---------------|--------|--------------|-------|-------|-------|
|       | clinoxeneite |       | cumulate gabbros |       |       |       |       | pegmatic gabbros |       | sheeted dikes |        | pillow lavas |       |       |       |
| SiO2  | 39.94        | 40.06 | 38.06            | 40.09 | 38.12 | 40.17 | 40.11 | 40.11            | 40.17 | 39.11         | 39.22  | 39.88        | 39.79 | 39.51 | 39.29 |
| Al2O3 | 32.94        | 32.42 | 31.81            | 32.62 | 31.91 | 32.71 | 32.50 | 32.50            | 32.71 | 25.66         | 26.51  | 30.24        | 30.25 | 27.35 | 26.85 |
| Fe2O3 | 0.42         | 0.75  | 0.93             | 0.81  | 0.41  | 0.52  | 1.07  | 1.07             | 0.52  | 9.17          | 8.10   | 4.86         | 4.85  | 7.80  | 8.89  |
| MgO   | 0.00         | 0.00  | 0.01             | 0.00  | 0.03  | 0.02  | 0.00  | 0.00             | 0.02  | 0.02          | 0.04   | 0.00         | 0.00  | 0.00  | 0.00  |
| MnO   | 0.00         | 0.02  | 0.00             | 0.03  | 0.11  | 0.13  | 0.09  | 0.09             | 0.13  | 0.31          | 0.19   | 0.10         | 0.15  | 0.08  | 0.08  |
| TiO2  | 0.01         | 0.01  | 0.00             | 0.00  | 0.06  | 0.00  | 0.00  | 0.00             | 0.00  | 0.15          | 0.10   | 0.00         | 0.00  | 0.00  | 0.00  |
| CaO   | 24.46        | 24.64 | 23.98            | 24.67 | 23.42 | 24.39 | 24.58 | 24.58            | 24.39 | 23.64         | 23.64  | 23.84        | 23.90 | 23.86 | 23.65 |
| Na2O  | 0.07         | 0.01  | 0.00             | 0.05  | 0.00  | 0.19  | 0.09  | 0.09             | 0.19  | 0.01          | 0.02   | 0.00         | 0.00  | 0.00  | 0.00  |
| K2O   | 0.00         | 0.00  | 0.00             | 0.00  | 0.01  | 0.00  | 0.02  | 0.02             | 0.00  | 0.00          | 0.00   | 0.00         | 0.00  | 0.00  | 0.00  |
| Sum   | 97.84        | 97.91 | 94.79            | 98.27 | 94.07 | 98.13 | 98.46 | 98.46            | 98.13 | 98.07         | 97.82  | 98.92        | 98.94 | 98.60 | 98.76 |
|       |              |       |                  |       |       |       |       |                  |       |               |        |              |       |       |       |
| Si    | 3.031        | 3.045 | 2.997            | 3.038 | 3.011 | 3.043 | 3.039 | 3.039            | 3.043 | 3.109         | 3.108  | 3.062        | 3.056 | 3.050 | 3.050 |
| AlVI  | 2.941        | 2.900 | 2.943            | 2.908 | 2.965 | 2.915 | 2.897 | 2.897            | 2.915 | 2.399         | 2.471  | 2.731        | 2.733 | 2.500 | 2.450 |
| Ti    | 0            | 0     | 0                | 0     | 0.003 | 0     | 0     | 0                | 0     | 0.008         | 0.005  | 0            | 0     | 0     | 0     |
| Fe3+  | 0.023        | 0.041 | 0.053            | 0.044 | 0.023 | 0.028 | 0.059 | 0.059            | 0.028 | 0.525         | 0.463  | 0.269        | 0.267 | 0.410 | 0.410 |
| Fe2+  | 0            | 0     | 0                | 0     | 0     | 0     | 0     | 0                | 0     | 0             | 0      | 0.002        | 0.006 | 0.050 | 0.120 |
| Mg    | 0            | 0     | 0.001            | 0     | 0.003 | 0.002 | 0     | 0                | 0.002 | 0.002         | 0.004  | 0            | 0     | 0     | 0     |
| Mn    | 0            | 0.001 | 0                | 0.001 | 0.007 | 0.008 | 0.005 | 0.005            | 0.008 | 0.020         | 0.012  | 0.006        | 0.009 | 0     | 0     |
| Ca    | 1.989        | 2.007 | 2.023            | 2.003 | 1.982 | 1.980 | 1.995 | 1.995            | 1.980 | 2.013         | 2.007  | 1.961        | 1.966 | 1.980 | 1.970 |
| Na    | 0.010        | 0.001 | 0                | 0.007 | 0     | 0.027 | 0.013 | 0.013            | 0.027 | 0.001         | 0.003  | 0            | 0     | 0     | 0     |
| K     | 0            | 0     | 0                | 0     | 0.001 | 0     | 0.001 | 0.001            | 0     | 0             | 0      | 0            | 0     | 0     | 0     |
| Sum   | 7.994        | 7.995 | 8.017            | 8.001 | 7.995 | 8.003 | 8.009 | 8.009            | 8.003 | 8.077         | 8.073  | 8.031        | 8.037 | 8.000 | 8.000 |
| Ps    | 0.78         | 1.39  | 1.77             | 1.49  | 0.77  | 0.95  | 2.00  | 2.00             | 0.95  | 17.95         | 15.78  | 8.97         | 8.90  | 14.09 | 14.34 |

Table 4: Celadonite microprobe analyses of the Trinity ophiolitic rocks.

|                                | CEL68 | CEL69 | CEL71 | CEL72 | CEL73 |
|--------------------------------|-------|-------|-------|-------|-------|
| SiO <sub>2</sub>               | 45,13 | 49,46 | 50,70 | 50,27 | 47,82 |
| Al <sub>2</sub> O <sub>3</sub> | 29,78 | 33,56 | 31,15 | 31,13 | 29,79 |
| FeO                            | 1,53  | 1,52  | 1,79  | 1,91  | 3,51  |
| MgO                            | 2,80  | 3,16  | 3,05  | 2,90  | 4,06  |
| MnO                            | 0,07  | 0     | 0     | 0,09  | 0,09  |
| CaO                            | 0     | 0     | 0,01  | 0,02  | 0,03  |
| Na <sub>2</sub> O              | 0,19  | 0,19  | 0,31  | 0,26  | 0,86  |
| K <sub>2</sub> O               | 10,93 | 10,35 | 10,41 | 10,19 | 8,89  |
| %Paragonite                    | 2,60  | 2,70  | 4,30  | 3,70  | 13,00 |
| %Celadonite                    | 19,00 | 18,00 | 29,00 | 28,00 | 21,00 |

Table 5 : Major and trace elements of the Trinity ophiolitic rocks.

| Samples                          | TR 113* | TR 222 | TR 85* | TR 110* | TR 532 | TR 64* | TR 128A* | TR 128R | TR 130A* | TR 47B | TR 48* | TR 55A* |
|----------------------------------|---------|--------|--------|---------|--------|--------|----------|---------|----------|--------|--------|---------|
| SiO <sub>2</sub>                 | 39.58   | 44.72  | 51.42  | 48.09   | 46.48  | 50.63  | 56.17    | 52.57   | 49.56    | 61.61  | 46.34  | 50.43   |
| TiO <sub>2</sub>                 | 0.18    | 0.09   | 0.19   | 0.19    | 0.92   | 0.42   | 1.06     | 0.65    | 0.48     | 0.64   | 0.70   | 0.61    |
| Al <sub>2</sub> O <sub>3</sub>   | 2.15    | 1.68   | 6.04   | 18.51   | 18.41  | 20.53  | 17.73    | 16.25   | 14.60    | 12.75  | 18.66  | 16.27   |
| Fe <sub>2</sub> O <sub>3</sub> * | 11.13   | 8.88   | 6.86   | 4.97    | 9.60   | 5.49   | 6.84     | 8.49    | 8.54     | 6.03   | 9.81   | 7.53    |
| Fe <sub>2</sub> O <sub>3</sub>   | 5.15    | 4.44   | 0.99   | 1.17    | 2.12   | 1.61   | 2.46     | 3.16    | -        | -      | 3.85   | 1.45    |
| FeO                              | 5.39    | 4.00   | 5.29   | 3.43    | 6.74   | 3.50   | 3.94     | 4.80    | -        | -      | 5.37   | 5.48    |
| MgO                              | 35.82   | 25.75  | 17.66  | 9.59    | 7.42   | 4.96   | 3.94     | 6.50    | 10.48    | 4.18   | 7.84   | 10.28   |
| MnO                              | 0.20    | 0.14   | 0.12   | 0.11    | 0.16   | 0.09   | 0.12     | 0.16    | 0.17     | 0.11   | 0.17   | 0.14    |
| CaO                              | 2.56    | 11.93  | 14.70  | 13.77   | 13.06  | 10.70  | 7.90     | 10.01   | 10.94    | 10.91  | 9.08   | 5.34    |
| Na <sub>2</sub> O                | 0.20    | 0.01   | 0.35   | 0.03    | 0.40   | 3.64   | 3.66     | 2.31    | 1.82     | 0      | 3.07   | 4.18    |
| K <sub>2</sub> O                 | 0.02    | 0.03   | 0.10   | 0.04    | 0.03   | 0      | 0.06     | 0.03    | 0.02     | 0.10   | 0.14   | 0.06    |
| L.I.                             | 6.82    | 5.31   | 2.09   | 3.25    | 2.17   | 2.27   | 2.38     | 2.13    | 3.07     | 2.14   | 4.16   | 4.85    |
| Total                            | 98.66   | 98.54  | 99.53  | 98.55   | 97.14  | 98.73  | 99.86    | 99.10   | 99.63    | 98.47  | 99.97  | 99.69   |
| FeO*/MgO                         | 0.28    | 0.31   | 0.35   | 0.47    | 1.16   | 1.00   | 1.56     | 1.18    | 0.73     | 1.30   | 1.13   | 0.66    |
| Cr                               | 3036    | 1819   | 1105   | 160     | 51     | 77     | 6        | 131     | 458      | 254    | 342    | 275     |
| Ni                               | 1939    | 790    | 317    | 131     | 75     | 76     | 40       | 95      | 152      | 134    | 175    | 157     |
| Zr                               | 8       | 7      | 8      | 10      | 14     | 32     | 61       | 40      | 46       | 31     | 40     | 45      |

Fe<sub>2</sub>O<sub>3</sub>\* : total iron as Fe<sub>2</sub>O<sub>3</sub> (\*) data published in Brouxel and Lapierre (1988)

Table 6 : Rb/Sr isotopic analysis, water/rock ratios and Fe<sup>3+</sup>/Fe<sup>T</sup> ratios of the Trinity ophiolitic rocks.

|           | <sup>87</sup> Sr/ <sup>86</sup> Sr | Sr    | Rb    | <sup>87</sup> Rb/ <sup>86</sup> Sr | <sup>87</sup> Sr/ <sup>86</sup> Sr (i) | ESr (T) | Water/rock | Fe <sup>3+</sup> /Fe <sup>T</sup> |
|-----------|------------------------------------|-------|-------|------------------------------------|--|---------|------------|-----------------------------------|
| TR 55 A   | basalt                             | 71.3  | 0.829 | 0.0336                             | 0.70497                                | + 14.1  | 6.5        | 0.19                              |
| TR 53 B   | basalt                             | 154   | 3.60  | 0.0676                             | 0.70503                                | + 15.1  | 14.6       |                                   |
| TR 51 B*  | basalt                             | 50.1  | 9.36  | 0.5399                             | 0.70472                                | + 10.6  | 3.8        | 0.25                              |
| TR 48*    | basalt                             | 38.5  | 1.90  | 0.1425                             | 0.70563                                | + 23.6  | 5.4        | 0.39                              |
| TR 47 A   | basalt                             | 95.5  | 2.92  | 0.0884                             | 0.70531                                | + 19.0  | 10.9       | 0.52                              |
| TR 47 B   | basalt                             | 60.0  | 1.73  | 0.0833                             | 0.70546                                | + 21.2  | 7.6        |                                   |
| TR 124 D  | diabase                            | 103   | 0.535 | 0.01508                            | 0.70504                                | + 15.1  | 9.8        |                                   |
| TR 127    | diabase                            | 133   | 0.127 | 0.00277                            | 0.70410                                | + 1.8   | 6.4        |                                   |
| TR 128 A  | diabase                            | 117   | 0.283 | 0.00701                            | 0.70467                                | + 9.9   | 8.7        | 0.36                              |
| TR 128 E  | diabase                            | 105   | 0.440 | 0.01216                            | 0.70471                                | + 10.4  | 8          | 0.35                              |
| TR 128 F  | diabase                            | 122   | 0.408 | 0.00970                            | 0.70456                                | + 8.4   | 8.4        | 0.44                              |
| TR 128 T* | diabase                            | 106   | 0.259 | 0.00704                            | 0.70479                                | + 11.6  | 8.5        | 0.37                              |
| TR 130 A  | diabase                            | 79.5  | 0.103 | 0.00374                            | 0.70491                                | + 13.3  | 7          |                                   |
| TR 64*    | isotropic gabbro                   | 122   | 0.136 | 0.00323                            | 0.70529                                | + 18.7  | 13.7       | 0.29                              |
| TR 61     | isotropic gabbro                   | 118   | 0.445 | 0.01090                            | 0.70556                                | + 22.5  | 15.9       | 0.21                              |
| PG A      | gabbroic pegmat.                   | 37.9  | 0.281 | 0.02143                            | 0.70464                                | + 9.5   | 2.8        |                                   |
| PG B*     | gabbroic pegmat.                   | 50.6  | 0.088 | 0.00507                            | 0.70467                                | + 10.0  | 3.8        |                                   |
| TR 532    | isotropic gabbro                   | 75.1  | 0.178 | 0.00685                            | 0.70415                                | + 2.5   | 3.8        | 0.22                              |
| TR 524    | plagiogranite                      | 60.8  | 0.328 | 0.01559                            | 0.70433                                | + 5.1   | 3.5        |                                   |
| TR 538    | gabbroic pegmat.                   | 34.0  | 0.251 | 0.02135                            | 0.70405                                | + 1.1   | 1.6        |                                   |
| TR 515    | gabbroic pegmat.                   | 54.4  | 0.146 | 0.00775                            | 0.70478                                | + 11.5  | 4.4        |                                   |
| TR 110*   | cumulate gabbro                    | 42.9  | 0.294 | 0.01980                            | 0.70394                                | - 0.5   | 1.8        | 0.24                              |
| TR 109*   | plagiogranite                      | 58.9  | 0.222 | 0.01089                            | 0.70568                                | + 24.3  | 8.6        |                                   |
| TR 106*   | cumulate gabbro<br><i>leached</i>  | 37.7  | 0.105 | 0.00805                            | 0.70450                                | + 7.6   | 2.5        | 0.24                              |
| TR 121    | cumulate gabbro                    | 68.5  | 0.706 | 0.02979                            | 0.70411                                | + 1.9   | 3.3        | 0.22                              |
| TR 85*    | clinopyroxenite<br><i>leached</i>  | 14.8  | 0.502 | 0.09822                            | 0.70358                                | - 5.6   | 0.4        | 0.14                              |
| TR 248    | cumulate gabbro                    | 63.1  | 0.380 | 0.01740                            | 0.70438                                | + 5.7   | 3.8        | 0.19                              |
| TR 234    | cumulate gabbro                    | 50.6  | 0.634 | 0.03621                            | 0.70363                                | - 4.8   | 1.6        | 0.11                              |
| TR 223    | gabbroic pegmat.                   | 76.6  | 0.635 | 0.02396                            | 0.70400                                | + 0.4   | 3.4        |                                   |
| TR 222    | websterite                         | 1.53  | 0.157 | 0.29656                            | 0.70247                                | - 21.4  | 0          | 0.5                               |
| TR 113*   | herzolite<br><i>leached</i>        | 5.21  | 0.234 | 0.1303                             | 0.70457                                | + 8.5   | 0.4        | 0.46                              |
| TR 79*    | harzburgite<br><i>leached</i>      | 0.654 | 0.117 | 0.51613                            | 0.70276                                | - 17.3  | 0          |                                   |

(\*) data published in Brouxel and Lapierre (1988)

Table 7 : Comparison of major element analysis between Trinity, mid-atlantic ridge (Hekinian, 1982) and Hole 504B basalts (Alt et al., 1986). HPPB : highly-phyric plagioclase basalts; POPB : plagioclase-olivine-pyroxene basalts.

|                                | Trinity ophiolite<br>average composition<br>of analyzed<br>basalts | FAMOUS basalts<br>HPPB | POPb  | Hole 504 B<br>average composition<br>of the least<br>altered basalts | of the more<br>altered basalts |
|--------------------------------|--|------------------------|-------|--|--------------------------------|
| SiO <sub>2</sub>               | 52.10  | 49.07                  | 50.21 | 50.06  | 48.40                          |
| MgO                            | 6.64   | 5.77                   | 7.99  | 8.44   | 8.57                           |
| Na <sub>2</sub> O              | 2.55   | 2.11                   | 2.20  | 2.19   | 2.36                           |
| CaO                            | 9.67   | 16.05                  | 11.78 | 12.94  | 10.96                          |
| Fe <sub>2</sub> O <sub>3</sub> | 7.56   | 6.58                   | 10.54 | 10.37  | 10.56                          |
| Al <sub>2</sub> O <sub>3</sub> | 16.90  | 19.40                  | 14.49 | 15.43  | 15.20                          |
| TiO <sub>2</sub>               | 0.66   | 0.66                   | 1.36  | 0.94   | 0.87                           |
| Total                          | 96.08  | 99.64                  | 98.57 | 100.37   | 96.92                          |

**A COMPLEX HISTORY OF HYDROTHERMAL ALTERATION  
RECORDED BY AN OPHIOLITIC SEQUENCE :  
THE TRINITY OPHIOLITE.  
EVIDENCE FROM OXYGEN ISOTOPES AND MAJOR ELEMENTAL FLUXES.**

C. Lecuyer and S. Fourcade. Laboratoire de Géochimie isotopique, CAESS, 35042 Rennes.



## Abstract

The Trinity ophiolite consists of a widespread mantle unit (the Trinity Peridotite) and a thin crustal sequence (<2Km) outcropping discontinuously. The well-exposed massifs of plutonics, diabasic dikes and pillow lavas define a complete oceanic crustal sequence. The basalts, dikes and gabbros are characterized by retrograde metamorphic associations. The petrographic study reveals that the intensity of alteration is directly correlated to the amount of circulating seawater and decreases downwards for increasing temperatures.

The water-rock ratios prevailing during the hydrothermal alteration of ophiolitic rocks have been calculated from the Sr concentrations and isotopic ratios. Across the stratigraphic succession water-rock ratios increase from the basalts ( $W/R = 7-10$ ) to the isotropic gabbros ( $W/R$  up to 16) then decrease towards the base of the sequence ( $W/R < 1$ ). Pillow lavas have  $\delta^{18}O$  values ranging from +8.45 to +10.10‰. The sheeted dikes have constant  $\delta^{18}O$  values close to those of fresh MORBS and one sample has a low  $\delta^{18}O$  value of +4.80‰. In the isotropic gabbros,  $\delta^{18}O$  values show wide variations from +4 to +9‰. The layered succession displays  $\delta^{18}O$  values more homogeneous than isotropic gabbros, with most samples around the mantle reference value, but as in the previous unit, some layered gabbros display anomalous low (+4.9‰) as well as high (+6.95‰)  $\delta^{18}O$  values. The unique fresh sample of werhlite has a  $\delta^{18}O$  value of +5.6‰ typical of the range of mantle-derived rocks while a lower ultramafic cumulate with serpentinized olivine has a low  $\delta^{18}O$  value of 4.9‰.

Pegmatitic gabbros emplaced within the isotropic gabbros have low  $\delta^{18}O$  values around +5‰ like surrounding rocks. On the contrary, one sample of pegmatitic gabbro intruded at lower levels within ultramafic layers has a  $\delta^{18}O$  value of +6‰. The plagiogranite dike has a  $\delta^{18}O$  value of +7.43‰, higher than the values of the surrounding cumulate gabbros.

Microthermometry was carried out on primary fluid inclusions from hydrothermally crystallized quartz. The trapping temperatures recorded in the pillow lavas range from 110 to 170°C and from low (130 to 160°C) to high temperatures (290 to 390°C) in the isotropic gabbros.

The correlation between the  $\delta^{18}O$  values of whole rock samples and the content in  $AlIV + (Na + K)A$  of amphiboles confirms the strong relationship between the thermal evolution of reacting fluids and the appearance of the retrograde mineral parageneses.

The complex pattern of  $\delta^{18}O$  distribution in the Trinity ophiolitic sequence likely results from the obliteration of a first high-temperature hydrothermal history by later events of low-temperature circulation in all the ophiolitic sequence. As a whole the hydrothermal alteration has produced a  $^{18}O$  enrichment of the Trinity ophiolitic sequence.

Hydrothermal activity in the oceanic crust is certainly more pervasive when associated to slow-spreading centers and the presence of channelized downflows into the deep gabbroic layers produces a pattern of heterogeneously-distributed hydrothermal recrystallization. The balance between low and high  $^{18}O$  altered rocks observed in the case of the Oman ophiolite section is apparently not realized in ophiolites generated in a slow-spreading environment on the basis of the two examples known so far (Trinity and Xigaze). Ageing of the crust and extensive low-temperature stages of alteration could be related to the fracturation pattern affecting the slow-spreading ridge environments. Thus the total budget of hydrothermal interaction in such kind of ophiolites implies a release of  $^{18}O$ -depleted fluids.

The  $^{18}O / ^{16}O$  isotope composition calculated for Siluro-ordovician seawater was close to the present-day oceanic value. As already suggested by Agrinier et al. (1988) a constancy of seawater  $\delta^{18}O$  since the early paleozoic would indicate that slowly-generated oceanic crust was not the predominant geodynamic environment controlling the oxygen isotopic composition of the oceanic reservoir.

The budget of Fe in the oceanic crust strongly depends on the seawater ability to reach and alter the olivine-rich cumulate layers of the bottom of the oceanic crust. Serpentinization of these ultramafic cumulates by seawater seems to play an important role in the chemical budget of the oceans.

## INTRODUCTION.

Strontium and oxygen isotope studies of ancient oceanic crust preserved in ophiolites are powerful tools for studying the integrated effects of seawater circulation in fossil hydrothermal systems. Many ophiolite complexes are now recognized to represent fragments of lithosphere produced in various geotectonic environments as well as in slow or fast spreading ridges.

The studies of present-day seafloor hot springs have provided the chemical and stable isotope compositions of both the starting solution and endmember of discharged thermal waters (Edmond et al., 1979; Craig et al., 1980; Edmond, 1980; Craig, 1981; Albarède et al., 1981; Michard et al., 1984; Von Damm et al., 1985). These data must be considered as boundary conditions for the development of models deduced from the study of ophiolites.

The Siluro-Ordovician Trinity ophiolite appears to be a good example of a complete oceanic crustal sequence generated in a slow-spreading ridge environment. Previous works (Brouxel and Lapierre, 1988; Lecuyer et al., 1989) have shown that this ophiolite has experienced an extensive hydrothermal activity leading to important mineralogical and geochemical variations virtually free of superimposed post-oceanic processes. The knowledge of chemical changes related to metamorphic reactions and the distribution of strontium and oxygen isotopic compositions along a vertical sequence 2Km thick can be used to constrain the whole story of seawater alteration in a slow-spreading ridge environment. A comparison of this pattern with that known respectively in the Oman ophiolite considered as generated in a fast-spreading environment (Pallister and Hopson, 1981; Boudier and Nicolas, 1985; Ceuleneer, 1986; Nicolas, 1986) and in the Xigaze ophiolite considered as generated in a slow-spreading ridge (Nicolas et al., 1981; Girardeau, 1986) may enlight some modalities of hydrothermal circulation along modern spreading ridges.

The purposes of the study are :

- to unravel the history of hydrothermal alteration in the Trinity ophiolite by associating the data of oxygen and strontium isotopes, of microthermometry on primary fluid inclusions, of chemical fluxes calculated from metamorphic reactions, all these data being obtained on the same rock samples.
- to compare the model of hydrothermal alteration to those established in ophiolites generated in fast-spreading environments in order to build a qualitative model of seawater penetration in relation with the regime of fracturation.
- to estimate the oxygen isotopic composition of seawater during the siluro-ordovician time. The isotopic composition of seawater in the past is indeed the matter of a great debate. Some authors (Knauth and Epstein, 1976; Muehlenbachs and Clayton, 1976; Holland, 1984; Muehlenbachs, 1986; Muehlenbachs, 1987) estimate it was similar to the present-day composition at least during the paleozoic period while other authors argue for an evolution of this composition since the Archean (Perry, 1967; Perry and Tan, 1972; Veizer et al., 1982) and even during the Paleozoic (Veizer et al., 1986). O'Shea et al. (1988) have reported very exotic isotopic signatures for Siluro-ordovician seawater which could be confirmed or infirmed by the study of the Trinity ophiolite.

### 1) Geologic setting and metamorphic zonation.

The Trinity ophiolite consists of a widespread mantle unit (the Trinity Peridotite) and a thin crustal sequence (< 2Km) outcropping discontinuously. The well exposed massifs of plutonics, diabasic dikes and pillow lavas build a complete crustal sequence supported by a detailed sampling. Stocks of plagiogranites are located within the isotropic gabbros (figure 1). They also appear as centimetric to decimetric dikes crosscutting the upper parts of the cumulate sequence. An original feature of this ophiolite consists in the presence of huge masses of pegmatitic gabbros crosscutting both the Trinity Peridotite and the cumulate sequence.

The metamorphic associations in the Trinity ophiolite correspond to the greenschist facies grade in pillow lavas and dikes and evolve towards a transitional amphibolite facies grade in the deepest part of the cumulate sequence (figure 1; Lecuyer et al., 1989). Metamorphic zones may be defined by the sequential appearance of distinct mineral parageneses with depth. The basalts and the dikes are characterized by a retrograde metamorphic association developed at the expense of a previous metamorphic paragenesis of higher grade : chlorite partially replaces actinolite, albite and quartz replace the basaltic glass. Celadonites and

secondary K-feldspar are present in the uppermost pillow lavas, scarce crystals of calcite are present in vesicle fillings. The persistence of celadonite rules out the possibility of metamorphic events related to the emplacement and evolution of the ophiolitic sequence during the obduction process. The isotropic gabbros located at the top of the magma chamber (figure 1) present albite, epidote, quartz, and actinolite replaces magnesio-hornblende. The associated intrusive pegmatitic gabbros have the same metamorphic associations. The upper cumulate gabbros (figure 1) present a simple association of actinolite, tremolite and epidote. Scarce chlorite replaces actinolite in some samples. The plagiogranite dikes crosscutting this area predominantly consist of albite and quartz with small amounts of pistacite. Hornblende (<5% in weight) is altered into chlorite. These acidic rocks locally show intergrowths of plagioclase and quartz, a feature which is typical of oceanic plagiogranites (Coleman and Donato, 1979). The lower cumulate gabbros (figure 1) are less altered and overlay ultramafic cumulates in which olivine is commonly serpentinized in various proportions (10 to 100%). Clinopyroxene is replaced by pargasitic hornblende and orthopyroxene is sometimes altered into talc.

The degree of metamorphic recrystallization within the Trinity ophiolitic sequence generally decreases downwards. The volcanics and sheeted dikes have been strongly affected whereas recrystallization of the plutonic rocks decreases with depth. The petrographic data indicate 1) that the intensity of alteration is directly correlated to the amount of circulating seawater and decreases downwards for increasing temperatures and 2) the existence of retrograde polymetamorphic associations across the section indicates a temperature decreasing with time for the circulating seawater.

## 2) Analytical methods.

Chemical compositions of metamorphic minerals (microprobe analysis) and Sr isotope data come from Lecuyer et al. (1989).

The whole rock  $\delta^{18}\text{O}$  composition of 20 hydrothermally-altered samples across the ophiolitic sequence and 1 fresh werhlite of the cumulate sequence are listed in table 1. In addition, 3 samples of pegmatitic gabbros and 1 sample of plagiogranite (trondhjemite composition) crosscutting the cumulates have been analyzed. A few mineral separates were also analyzed: the three quartz samples on which thermometric data on fluid inclusions have been obtained and two hornblende samples extracted from pegmatitic gabbros. Oxygen was extracted from powders of whole rocks and minerals using the  $\text{BrF}_5$  method of Clayton and Mayeda (1963) at high temperatures ( $\approx 650^\circ\text{C}$ ) because of the presence of much epidote in the rocks. This mineral proved to be rather resistant to react quantitatively with  $\text{BrF}_5$ . The value obtained for the NBS28 quartz standard is  $+9.39\text{‰} \pm 0.22$ . An internal standard (tholeiitic basaltic glass Circe 93) repeatedly analyzed by F. Pineau in Craig's Laboratory (La Jolla) and in Paris at  $+5.68\text{‰} \pm 0.14$  gives a value of  $+5.52\text{‰} \pm 0.18$ .  $\text{CO}_2$  was extracted from carbonates (5 samples) at  $25^\circ\text{C}$  by reaction with 100%  $\text{H}_3\text{PO}_4$ . Oxygen and carbon isotope compositions are noted in the standard  $\delta$  notation with respect to the SMOW. Isotopic analyses were performed with a VG SIRA 10 triple collector mass spectrometer. The reproducibility and number of replicate analyses of the samples are presented in table 1.

Microthermometry was kindly carried out by P. Nehlig on fluid inclusions from quartz using a Chaix Meca heating and freezing stage at the Brest University following the experimental procedure of Poty et al. (1976). The freezing temperature of the liquid phase yields an estimate of the bulk salinity, which is usually described as the NaCl weight percent equivalent. The homogenization temperature of the two-phase (liquid plus vapour) inclusions corresponds to a minimum trapping temperature. Only three rock samples were found to contain fluid inclusions enough large for such a purpose. The homogenization temperatures and estimated salinities are presented in the histogram of figure 2.

## 3) Isotopic results.

The  $\delta^{18}\text{O}$  values of the 25 samples are reported with respect to a synthetic lithologic column of the Trinity ophiolite in figure 3.

Pillow lavas have rather constant and high  $\delta^{18}\text{O}$  values ranging from  $+8.45$  to  $+10.10\text{‰}$ . The sheeted dikes have constant  $\delta^{18}\text{O}$  values close to those of fresh MORBS ( $+5.7\text{‰} \pm 0.2$ ; e.g. Pineau et al. 1976; Muehlenbachs and Clayton, 1972) for most of the samples. Nevertheless, one sample has a low  $\delta^{18}\text{O}$  value of  $+4.80\text{‰}$ . In the isotropic gabbros,  $\delta^{18}\text{O}$  values show wide variations from  $+4$  to  $+9\text{‰}$ . These strong variations occur on a

plurimetric scale at the top of the magma chamber. Two pegmatitic gabbros have low  $\delta^{18}\text{O}$  values of  $\approx +5\text{‰}$ , like most of the surrounding isotropic gabbros (table 1; figure 3), whereas the third one which crosscuts the ultramafic layers at the base of the crustal sequence has a  $\delta^{18}\text{O}$  value of  $+6\text{‰}$ , slightly higher than the "mantle reference". The layered succession displays  $\delta^{18}\text{O}$  values more homogeneous than isotropic gabbros, with most samples around the mantle reference, but as in the previous unit, some rocks display anomalous low  $\delta^{18}\text{O}$  values ( $+4.9$  in layered gabbro TR106) as well as high  $\delta^{18}\text{O}$  values ( $+6.95\text{‰}$  in layered gabbro TR121). The plagiogranite dike has a  $\delta^{18}\text{O}$  value of  $+7.43\text{‰}$ , higher than the values of the surrounding cumulate gabbros. The fresh sample (werhlite TR252) has a  $\delta^{18}\text{O}$  value of  $+5.6\text{‰}$ , typical of the range of mantle-derived rocks and will be considered as the reference value in the further discussion. The selected lower ultramafic cumulates (TR222) with serpentinized olivine has a low  $\delta^{18}\text{O}$  value of  $+4.9\text{‰}$ .

Analyses of  $\delta^{18}\text{O}$  and  $\delta^{13}\text{C}$  have been performed on disseminated carbonates of vesicles fillings from 3 pillow lavas, 1 dike and 1 isotropic gabbro. Calcite has  $\delta^{18}\text{O}$  values in the range of  $+15.8\text{‰}$  to  $27.61\text{‰}$  / SMOW and  $\delta^{13}\text{C}$  values in the range  $-5.42\text{‰}$  to  $-1.39\text{‰}$  / PDB (Table 1).

The trapping temperatures recorded by quartz from the pillow lavas (figure 2) range from  $110$  to  $150^\circ\text{C}$  for the core (TR47A) and from  $130$  to  $170^\circ\text{C}$  for the rim (TR47B) of the pillow. In both cases, the salinity of the fluid inclusions is close to that of seawater (equivalent to  $3.5\%$  NaCl). In contrast, the isotropic gabbros are characterized by large range of variations in salinity and homogenization temperatures ranging from low ( $130$  to  $170^\circ\text{C}$ ) to high temperatures ( $290$  to  $390^\circ\text{C}$ ).

#### 4) Discussion.

Recent studies performed on DSDP sites have emphasized the process of ageing in the upper basaltic layer of the crust, ageing which involves the cumulative effects of hydrothermal activity as the crust moves away from the spreading center and cools down. Thus, a general increase of  $0.25$   $\delta$  units per million year in basalt has been proposed (Muehlenbachs, 1980). Consequently, the effect of off-axis alteration may overprint the isotopic signatures recorded at the ridge (Alt et al., 1986). We have compiled the  $\delta^{18}\text{O}$  values of altered MOR basalts (figure 4) and of ophiolitic basalts (figure 5). Ophiolitic basalts are systematically  $^{18}\text{O}$ -enriched relative to the mantle value and have not preserved remnants of high-temperature alteration in contrast with altered MOR basalts (see legend for the source of data).

The complex pattern of  $\delta^{18}\text{O}$  distribution in the Trinity ophiolitic sequence (figure 3) likely results from the obliteration of a first high-temperature hydrothermal history by later events of low-temperature circulation in all the ophiolitic sequence. This interpretation is supported by the presence of polymetamorphic mineral associations in the pillow lavas, dikes and most of the gabbros which all correspond to a retrograde evolution of the temperature of alteration.

However, as a whole, the low-temperature alteration has not totally erased the memory of previous hydrothermal events and there is a general feature emerging from the data : the initial stages of hydrothermal recrystallization occurred at higher temperatures in the lower part of the sequence (i.e. the magmatic chamber comprising both isotropic gabbros and the layered complex) than in the higher part of the sequence (mostly pillow lavas) : relicts of the initial parageneses are pargasitic hornblende and Mg-hornblende in the lower part while only actinolite is formed in the upper part. This is confirmed in figure 6 in which whole rock  $\delta^{18}\text{O}$  is plotted against the  $\text{AlIV} + (\text{Na} + \text{K})_{\text{A}}$  content (Graham and Navrotsky, 1986) of corresponding amphiboles. The covariation of both parameters indicates the downwards increase of temperature conditions for the whole hydrothermal process although this kind of diagram would have been more significant by plotting the  $\delta^{18}\text{O}$  composition of the amphiboles themselves.

#### A) Multi-stages hydrothermal alteration :

To unravel the isotopic effects of hydrothermal alteration in the ophiolite sequence it is necessary to make an hypothesis about the primary isotopic composition of siluro-ordovician seawater. In a first stage we will admit it had the present-day  $\delta^{18}\text{O}$  value  $= 0\text{‰}$ , and we will justify this assumption in the next chapter.

Hydrothermal alteration in open system generally introduces isotopic disequilibrium among coexisting primary and secondary mineral phases (Gregory and Criss, 1986). So it is impossible to evaluate carefully  $\Delta$  rock/water unless analyzing all the phases contained in the hydrothermally-altered rock, which is not possible owing to the fine-grained and heterogeneous texture of the rocks. As done previously by Taylor (1977); we will use the plagioclase (An<sub>80</sub>)/water fractionation of O'Neil and Taylor (1967) as an estimate of the  $\Delta$  rock/water.

With these assumptions, it is clear from oxygen isotope ratios that the ophiolite sequence has experienced several stages of hydrothermal alteration. Indeed the isotopic composition of basaltic rocks which have exchanged with seawater could be lowered with respect to the starting composition (+5.6‰) for a temperature above 250°C, increased at temperatures lower than 250°C and would not be significantly modified by isotopic exchange at a temperature close to 250°C. This is exactly what we observe in the Trinity crust in which  $\delta^{18}\text{O}$  higher, equal, or lower than the starting composition are measured.

The water-rock ratios are independent parameters introduced in the calculation. They are deduced from the Sr isotope study following the method of Albarède et al. (1981; [1]).

$$[1] \quad \frac{(87\text{Sr}/86\text{Sr})_i R_f - (87\text{Sr}/86\text{Sr})_i R_i}{(87\text{Sr}/86\text{Sr})_i W_i - (87\text{Sr}/86\text{Sr})_i W_f} \times \frac{[\text{Sr}]_R}{[\text{Sr}]_W}$$

A profile of temperatures corresponding to the isotopic composition of each sample is calculated and compared to the secondary mineral associations in figure 7.

We stress the fact that these temperatures do not represent the real temperatures of alteration. Low and high temperature events in a given rock sample produce opposite isotopic variations and the magnitude of the final isotopic shift (and consequently the calculated temperature) will be result of the balance between the different stages of hydrothermal alteration.

Thus it is possible to distinguish at least three stages of hydrothermal alteration of decreasing temperature.

1) The remnants of the first **high-temperature** alteration history are present both in sheeted dikes, isotropic gabbros and layered cumulates with temperatures ranging from 250 to 330°C (figure 7). These calculated temperatures are somewhat lower than the homogenization temperatures up to 390°C recorded by primary fluid inclusions in quartz from isotropic gabbros (figure 2). It is worth noting here that the intrusive pegmatitic gabbros located at the top of the magma chamber record the high-temperature hydrothermal event. This fact implies that these coarse-grained rocks were emplaced early within the ophiolite section, before the vanishing of the axial hydrothermal system. Thus, pegmatitic gabbros make up a significant part of the magmatism associated with the Trinity spreading center and any genetic model dealing with the origin of such rocks must take into account this constraint.

2) High water/rock ratios have been calculated for basalts by using Sr isotope ratios (Lecuyer et al., 1989) and are thus consistent with a strong alteration under high-water-rock ratios and **low-temperature** conditions ranging from 130 to 150°C. Under such high water-rock ratios, the isotopic composition of altered basalts is buffered by the fluid in great excess and the main parameter controlling the final isotopic composition of the rocks is the exchange temperature. Minerals which have typically crystallized at low to very low temperatures are celadonite and calcite. Oxygen isotopic data on celadonites from other seafloor basalts indicate celadonite formation at temperatures about 50°C (Kastner and Gieskes, 1976; Seyfried et al., 1978; Stakes and O'Neil, 1982; Bohlke et al., 1984). The noteworthy preservation of carbonates in the Trinity ophiolitic rocks provides complementary informations. Three of the analyzed rocks give  $\delta^{13}\text{C}$  typical of modern marine carbonates ( $\delta^{13}\text{C}$  about 0; Muehlenbachs, 1986). The correlation between  $\delta^{13}\text{C}$  of carbonates and carbonate content of the rock likely corresponds to a mixing line between juvenile carbon and low-temperature precipitated marine carbonates. Such a correlation is similar to that observed by Javoy and Fouillac (1979) in the deep sea drilling project Leg 51 basalts. Using the calcite-water fractionation equation of O'Neil et al. (1969), and assuming the carbonate was precipitated in equilibrium with fresh seawater ( $\delta^{18}\text{O} = 0$ ), for the three samples TR55A, TR52B and TR124D, the carbonates have precipitated or reequilibrated at temperatures of 26 to 107°C. These temperatures suggest a progressive transition between the late stage of low-temperature alteration and the stage of seafloor weathering which has affected basalts, dikes (TR124D) and isotropic gabbros (TR61).

3) An **intermediate stage** of hydrothermal alteration has possibly affected the sheeted dikes and most of the plutonic sequence leading to apparent temperatures of interaction ranging from 200 to 250°C (figure 7).

Rocks which display a  $\delta^{18}\text{O}$  composition close to the mantle value could be interpreted in three ways. A very few rocks which do not present any evidence of hydrothermal recrystallization and for which very low W/R ratios have been calculated from Sr isotope data can be considered as representative of the initial magmatic isotope composition. This is the case of rocks such as werhlite TR252 found in the deep part of the layered gabbros. The convergence of  $\delta^{18}\text{O}$  values, the strong decrease of W/R ratios inferred from Sr isotopes and the mineralogy of the rocks clearly show that pervasive circulation of  $\text{H}_2\text{O}$  did not reach the lowest portion of the oceanic crust.

Very different is the case of rocks which still display isotopic compositions close to the mantle value and for which Sr isotopes and mineralogical parageneses indicate a very intense recrystallization history under high water-rock ratios. Such rocks are located mainly in the dikes complex and at the top of the magmatic chamber (upper part of layered gabbros and isotropic gabbros). These  $\delta^{18}\text{O}$  values could have been produced in two different ways :

a - by exchange with seawater at a temperature of about  $250^\circ\text{C}$ . As these rock samples are located within the crustal portion where the stage of high-temperature interaction is recorded (low  $\delta^{18}\text{O}$  values), it implies an intermediate stage of hydrothermal alteration, which has operated between the stages of high and low temperature hydrothermal activity.

In such a situation the  $\delta^{18}\text{O}$  pattern observed in the Trinity ophiolite could well represent a continuum of hydrothermal activity starting at high temperatures ( $\approx 390^\circ\text{C}$  after fluid inclusion data) and decreasing in temperature with time.

b - the other interpretation of the  $\delta^{18}\text{O}$  values around  $+5.6\%$  in these intensely-altered rocks calls for a superimposition of a high and a low temperature event ( $300\text{--}390^\circ\text{C}$  and  $110\text{--}170^\circ\text{C}$  respectively). In such a way the  $^{18}\text{O}$  depletion produced by the first event could be cancelled by a further  $^{18}\text{O}$  enrichment produced during the late event. This explanation is also consistent with the whole data : indeed some parts of the isotropic gabbros and upper layered complex unambiguously record the effect of a low temperature event since they present  $\delta^{18}\text{O}$  values around or above  $+7\%$  (e.g. samples TR64, TR524, TR121). It is likely that a channelized circulation of water has produced an heterogeneous pattern of low-temperature alteration which is preponderant (high  $\delta^{18}\text{O}$  values) when W/R ratios are high and moderate ( $\delta^{18}\text{O}$  values around  $+5.6\%$ ) when W/R ratios are lower. This is illustrated in figure 3 where the increase of  $\delta^{18}\text{O}$  is well correlated to high water-rock ratios deduced from Sr isotopes.

We do not have any reliable constraints to choose between these two possibilities which are not exclusive. However the oxygen isotope record in the Trinity ophiolite complex bring several important conclusions :

1) A high-temperature hydrothermal event is present around the top of the magma chamber : dikes, isotropic gabbros and upper part of the layered complex.

2) A low-temperature hydrothermal event is widespread in the basalts but is also present in other parts of the sequence, especially within isotropic gabbros. At these levels, it is heterogeneously distributed and likely corresponds to a channelized fluid flow. This later stage of alteration must be related to the off-axis hydrothermal circulation affecting the upper levels of the crust and which overprints the effects of previous temperatures events.

3) The existence of an hydrothermal event of intermediate temperature is possible in the dikes complex, isotropic gabbros, and upper part of the layered cumulates.

The relative high  $\delta^{18}\text{O}$  value and water-rock ratio (table 1) recorded by the plagiogranite dike (assuming a negligible  $^{18}\text{O}$  enrichment in the differentiated magma during crystal fractionation owing to the very low amounts of magnetite observed in the ophiolitic suite) likely indicates that the dike margins may favour the late circulation of channelized fluidflows through the crust.

## **B) Slow-spreading centers and pattern of hydrothermal activity :**

As a whole, the hydrothermal alteration of the Trinity ophiolitic sequence has produced a  $^{18}\text{O}$  enrichment of the rocks (figure 3). Such a pattern has been also recognized in the Xigaze ophiolite (figure 8) by Agrinier et al. (1988). In both cases, these ophiolites have been

generated in ancient slow-spreading ridge environments. Such a model must be opposed to the model of the fast-spreading ridges which is illustrated by the Oman ophiolite in which the  $^{18}\text{O}$  enrichment of the upper part balances the  $^{18}\text{O}$  depletion of the lower part (figure 9). From this feature, Gregory and Taylor (1981) have deduced that the  $\delta^{18}\text{O}$  of the ocean is buffered by the isotope exchange between the seawater and the oceanic crust, in agreement with the predictive model of Muehlenbachs and Clayton (1976) valid as long as the seafloor spreading rates are greater than half of the present rate.

Thermal models about oceanic ridges have in common the temperature distribution under the ridge crest, temperature which is to a first approximation independent of the spreading rate (Bottinga, 1974; Bottinga and Allègre, 1973). Nevertheless the permeability of oceanic crust in a slow-spreading ridge is controlled by fracturation (Ito and Anderson, 1983). The active fracture zone in slow-spreading ridges is wider and deeper than in the fast-spreading ones according to Choukroune et al. (1984). Consequently, the normal faulting accompanying the formation of flanking rift mountains develops pathways for the penetration of seawater into the deep gabbroic layers. Thus the metamorphism of the crust in slow-spreading ridges is certainly more pervasive than in fast-spreading ones and the presence of channelized downflows into the deep gabbroic layers produces a pattern of heterogeneous hydrothermal alteration.

Isotopically, such a process may be responsible for the modification of the  $^{18}\text{O}$  balance acquired during the first stage of high-temperature alteration close to the ridge axis. Large circulation of seawater along the faults at temperatures about 200-250°C and even lower has randomly affected numerous sections of the whole crust and provides a  $\delta^{18}\text{O}$  profile resulting from the superimposition of various alteration periods at decreasing temperatures (figure 10). The  $\delta^{18}\text{O}$  balance is apparently not established in all the ophiolites on account of the two examples corresponding to slow-spreading environments known so far (Trinity and Xigaze). Extensive low-temperature stages of alteration and ageing of the crust could be related to the fracturation pattern affecting the slow-spreading ridge environments. Thus the total budget of hydrothermal interaction in such kind of ophiolites implies a release of  $^{18}\text{O}$ -depleted fluids which could have a bearing on the evolution of the  $^{18}\text{O}/^{16}\text{O}$  of seawater with time as previously suggested by Agrinier et al. (1988). This conclusion sets the problem of the seawater composition at Siluro-ordovician time.

### **c) $^{18}\text{O}/^{16}\text{O}$ composition of the siluro-ordovician oceanic reservoir :**

Veizer et al. (1986) observed a 3 per mil increase in the  $\delta^{18}\text{O}$  of the Paleozoic carbonates and concluded that the  $\delta^{18}\text{O}$  of the Paleozoic seawater jumped because of global tectonic processes. More recently, O'Shea et al. (1988) deduced from the study of evaporites in the Michigan basin (Ontario) that the Siluro-ordovician seawater had a  $\delta^{18}\text{O} = -6\text{‰}$ . However, Knauth and Beeunas (1986) have brought evidences for a  $\delta^{18}\text{O} = 0$  inferred from the study of fluid inclusions in Silurian evaporites. Ancient ophiolites are valuable clues for testing the evolution of seawater  $\delta^{18}\text{O}$  during time because they contain the memory of the intense oceanic hydrothermal activity. The present data on the Trinity ophiolite can be used to evaluate the isotopic composition of seawater at the epoch it was generated on the corresponding ridge segment :

The isotope composition of initial seawater which has reacted 1) with the layered gabbros (rock-dominated system) may be estimated using the closed-system mass balance relation [2] and 2) with the pillow lavas (seawater-dominated system) may be estimated using the open-system mass balance relation [3] :

$$[2] \quad \text{W/R closed system (mass units)} = \sqrt{F(\delta_R - \delta_{\text{R}} \cdot [\text{O}]_R, \delta_{\text{H}_2\text{O}} - (\delta_R - \Delta R - \text{H}_2\text{O}) \cdot [\text{O}]_W) = \text{WRC}}$$

$$[3] \quad \text{W/R open system (mass units)} = \frac{[\text{O}]_R}{[\text{O}]_W} \times \text{Log} \left\{ \left( \frac{[\text{O}]_W}{[\text{O}]_R} \times \text{WRC} \right) + 1 \right\}$$

with :  $\Delta R - \text{H}_2\text{O} = \delta_{\text{rock}} - \delta_{\text{H}_2\text{O}}$ .

$\delta R$  = final isotopic rock composition.

$\delta_o R$  = initial isotopic rock composition.

$\delta_o H_2O$  = initial isotopic water composition.

$[O]R$  = concentration of oxygen in the rock.

$[O]W$  = concentration of oxygen in the water.

In order to determine the value for  $\delta_o H_2O$ ,  $\Delta R-H_2O$  was approximated using the plagioclase-water fractionation (An80) calibration of O'Neil and Taylor (1967). Two independent parameters are injected into the equation: the integrated water-rock ratios are taken from the Sr isotope study of Lecuyer et al. (1989) and the temperature of water interaction are estimated from fluid inclusions data of hydrothermally-crystallized quartz. Isothermal curves for temperatures of 100, 110, 130, 140, 150, 160 and 200°C depict the variations of initial seawater composition versus integrated closed-system water-rock ratios (figure 11). The  $\delta^{18}O$  composition of the final rock ( $\delta R$ ) was fixed to +10.1 according to our measurements on the sample TR47B. The calculated water-rock ratio of 7.6 intersects the 130 to 160°C isothermal curves (range of temperatures given by fluid inclusions) for an initial  $\delta^{18}O$  ranging from -1.5 to +0.5‰ (figure 11).

There is no evidence in the ophiolites and ore deposits that Paleozoic seawater was depleted in  $^{18}O$  (Muehlenbachs, 1986). A similar conclusion was proposed by Agrinier et al. (1988) for Cretaceous time and the present data expand this conclusion back to Siluro-Ordovician time. Since the hydrothermal alteration in the Xigaze and Trinity ridge types globally releases  $\delta^{18}O$ -depleted fluids into the ocean, the strong evidences presented by Muehlenbachs (1986) for a constancy of seawater  $\delta^{18}O$  during time imply that the contribution of this type of oceanic crust to the ocean - oceanic crust exchange budget was probably not dominant in the past.

#### D) Fluxes of major element during hydrothermal alteration :

The knowledge of chemical and isotopic changes accompanying seawater-crust interaction can be used to constrain the development of hydrothermal models associated with slow-spreading ridge as exemplified by the Trinity ophiolite. The study of metamorphic associations in the Trinity ophiolite has been used to quantify the amplitude and direction of elemental fluxes for major elements (Lecuyer et al., 1989). In the Trinity basalts two kinds of metamorphic associations are observed :

In the chlorite-albite -rich association; albitization of plagioclase is responsible for large Ca and Al losses and Na gains. When chlorite becomes preponderant, Mg and Fe gains and a Si loss are observed. On the opposite, in the epidote-quartz -rich association, the presence of quartz in matrix is the result of huge Si gains while the development of epidote explains a slight Fe gain, moderate Ca, Na and Al losses, and controls the iron oxidation ratio ( $Fe^{3+} / Fe_T$ ) of the whole rock. These two major metamorphic types have been previously recognized by Humphris and Thompson (1978) and Mottl (1983) who relate them to a process of alteration by recharge and discharge of seawater under water-rock ratios less than 10.

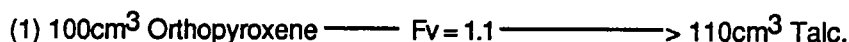
In the cumulate sequence, alteration is characterized by significant losses of Si and Ca and gains of Fe, Mg and Al while the behaviour of Na appears erratic across the sequence. Fe gains are balanced by a strong Fe depletion of the lowermost ultramafic cumulates during serpentinization. Thus the balance of Fe within the oceanic crust strongly depends on the ability of seawater to penetrate into deep levels of the oceanic crust and to alter the olivine-rich cumulate layers.

In the Trinity ophiolite, metric layers of undeformed partially (at least 10%) to totally serpentinized cumulate werhlites and lherzolites are located at the bottom of the crustal sequence. Serpentine minerals have not been separated because they are mixed with talc. The whole rock sample TR222 (table 1) is made of 40% serpentine (minor amounts of talc) and 60% fresh clinopyroxene (modal analysis taking into account the specific gravity of each mineral). Assuming clinopyroxene did not exchange oxygen isotopes, the mass balance calculation provides an estimate of the serpentine  $\delta^{18}O$  composition which ranges from 3.8 to 4.2‰.

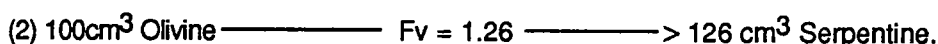
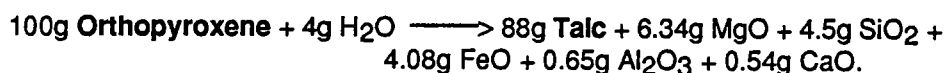
Such a low  $\delta^{18}O$  serpentine relative to the mantle value could result from a  $^{18}O$  depletion by high-temperature exchange with seawater (Cocker et al., 1982). Ultramafic cumulates serpentinized by interaction with seawater were assimilated to the oceanic layer 3 by Hess (1962), Bottinga and Allègre (1973), Girardeau and Mével (1982). Serpentinization of such deep layers of the oceanic crust could play an important role in the Fe budget in the oceans.



Indeed, the mineralogical reactions involving the production of both talc (1) and serpentine (2) by the destabilisation of orthopyroxene and olivine respectively are responsible for losses in MgO, FeO and SiO<sub>2</sub> :



equivalent to :



equivalent to :



(see Lecuyer and Cannat, 1989).

The redistribution of major elements (Si, Al, Fe, Mg, Ca, Na and K) within the Trinity ophiolite necessarily implies the existence of both downward and upward fluid circulation through the lithologic sequence (Lecuyer et al., 1989). The record of elemental fluxes and  $\delta^{18}\text{O}$  isotopic variations relevant to the time-integrated hydrothermal history leads us to propose the following scenario :

1) Hydrothermal activity at the ridge : During the recharge, seawater flows downward, water-rock ratios begin to decrease at the transition pillow lavas - sheeted dikes and temperatures increase because of the geothermal gradient. The oxidizing fluids react with rocks as clearly shown by the decrease of oxidation ratio with depth which begins at the transition pillow lavas - sheeted dikes and corresponds to a drastic permeability decrease (Becker, 1985; figure 12). Na is taken up in the development of albite and Mg in the formation of actinolite, PH of the solution dropped from a value of about 8 for seawater to about 3.5 and Al contents is increasing in the solution above 250°C (Edmond et al., 1982; Von Damm et al., 1985a et b). Bowers and Taylor (1985) proposed a model in which the isotopic composition of the reacting seawater evolves as it circulates through the hot crust. Their recharge model illustrates the interaction of fresh seawater ( $\delta^{18}\text{O} = 0$ ) reacting with the rocks located at the top of the magma chamber as it moves down under decreasing water-rock ratios (rock-dominated system). This process can produce  $^{18}\text{O}$ -enriched fluids ( $\delta^{18}\text{O} = +2-3$ ) similar to those measured by Craig et al. (1980) and Craig (1981) in the vents of East Pacific Rise.

The deep seawater penetration and high temperatures occur predominantly within the layered gabbros (low  $\delta^{18}\text{O}$  values), along the sides and beneath the axis magma chamber in agreement with the studies of Elders et al. (1984) who have demonstrated a significant component of lateral fluid flow in active hydrothermal systems. Assuming temperatures of interaction of about 350 - 400°C (maximum of temperatures given by fluid inclusions) in the Trinity isotropic and layered gabbros, a plot of  $\delta^{18}\text{O}$  of initial water as a function of water-rock ratios (figure 13) implies an isotopic composition of initial water in the range +2 to +3‰ to produce an altered rock with a final  $\delta^{18}\text{O}$  similar to the value obtained in the layered gabbro sample TR106 ( $\delta^{18}\text{O} = 4.93\text{‰}$ ). This result is in agreement with the model proposed by Bowers and Taylor (1985). For such a high temperature interaction, a 100% exchange between rock and water is a reasonable estimate (closed system behavior). Temperatures of interaction calculated in this zone when assuming a  $\delta^{18}\text{O}$  of initial water = 0 are thus underestimated.

The isotopic composition of separated quartz (table 2) can be used to determine the temperature of hydrothermal deposition. The temperatures for three curves described in the literature were calculated assuming a  $\delta^{18}\text{O}$  of initial water = 0 (table 2). The calculated temperatures are in agreement with those given by the study of the fluid inclusions. For the basalt TR47B, temperatures determined using both the Clayton et al; (1972) and Matsuhisa et al. (1978; 1979) curves are slightly higher than those proposed by the fluid inclusions. This curve was established for a temperature field of between 250 and 500°C, the extrapolation for low temperatures ( $\approx 150^\circ\text{C}$ ) could explain the differences observed. Using the same curve for the quartz included in the isotropic gabbro which has recorded high temperatures of

homogenization from fluid inclusions (figure 2), calculated temperatures are lower, it emerges that the isotopic composition of initial water was likely shifted to positive values ranging from +2 to +3.

Now the problem is to get an estimate of the  $\delta^{18}\text{O}$  composition of the fluid which could have reacted with the overlying rocks during the return flow, since the high-temperature modified discharged fluids have been more or less  $^{18}\text{O}$ -buffered by exchange with rocks under low water-rock ratios. We suggest that this discharged water is largely diluted by fresh seawater as it moves upward owing to the wide fracturation pattern associated to slow-spreading ridges. Consequently, most of the basalts have been altered by unmodified or only slightly modified seawater. The process producing ridge-crest hot springs which is responsible for the positive  $\delta^{18}\text{H}_2\text{O}$  anomaly is apparently a minor process which cannot cancel the effects of  $^{18}\text{O}$  depletion of plutonic rocks due to high-temperature alteration.

The low-temperature and likely intermediate stage of hydrothermal alteration is characterized by a strong tectonic control directly dependent on the geotectonic environment. It affects randomly the whole oceanic crust and destroys the  $\delta^{18}\text{O}$  balance previously depicted by Muehlenbachs and Clayton (1976). The alteration of the deep cumulative olivine-bearing layers produced Si, Fe and Mg-rich discharged flows which contribute to precipitate quartz and chlorite within the hypabyssal and volcanic layers of the crust.

During the late stage of hydrothermal alteration followed by seafloor weathering, Si-saturated hydrothermal solutions produced in the deep layers of the oceanic crust precipitate quartz when they come into contact with the cold fresh seawater at temperatures about 100-150°C and the crystallization of low-temperature minerals such as adularia, celadonites and calcites is responsible for K and Ca gains restricted to the uppermost layers of pillow lavas.

## CONCLUSION

Chemical changes related to metamorphic recrystallization, microthermometric, strontium and oxygen isotope data have been associated to constrain the history of seawater alteration within an ancient well-preserved oceanic crust : This study suggests that ophiolitic sequences are useful objects to constrain the whole chemical budget of seawater crust interaction because they record the effects of both initial and off-axis hydrothermal activity. They represent valuable probes in tracking the chemical secular evolution of the oceanic reservoir.

- Initial high-temperature hydrothermal events (300-400°C) are recorded in the isotropic gabbros at the top of the magma chamber and are followed by alteration at decreasing temperatures down to the stage of seafloor weathering.

- The low-temperatures hydrothermal interaction is irregularly distributed and corresponds to a channelized penetration of seawater. These intense late hydrothermal events are apparently associated to environments of slow-spreading centers and could be related to the fracturation regime (well-developed and deep normal faulting) which characterize these environments. As a whole, contrarily to the case of crust generated on fast-spreading centers, the balance of  $\delta^{18}\text{O}$  during alteration is not established in slowly generated oceanic crust. In such geodynamic situations interaction between oceanic crust and seawater is able to modify the isotopic composition of the ocean.

- The  $^{18}\text{O} / ^{16}\text{O}$  isotope composition calculated for Siluro-ordovician seawater was close to the present-day oceanic value. As already suggested by Agrinier et al. (1988) a constancy of seawater  $\delta^{18}\text{O}$  since the early paleozoic would indicate that slowly-generated oceanic crust was not the predominant geodynamic environment controlling the oxygen isotopic composition of the oceanic reservoir.

## REFERENCES

- Agrinier, P., M. Javoy, and J. Girardeau, Hydrothermal activity in a peculiar oceanic ridge : oxygen and hydrogen isotope evidence in the Xigaze ophiolite, (Tibet, China), *Chem. Geol.*, 71, 313-335, 1988.
- Albarède, F., A. Michard, J.F. Minster, and G. Michard,  $^{87}\text{Sr}/^{86}\text{Sr}$  ratios in hydrothermal waters and deposits from the East Pacific Rise at 21°N, *Earth Planet. Sci. Lett.*, 55, 229-236, 1981.
- Alt, J.C., K. Muehlenbachs, and J. Honnorez, An oxygen isotopic profile through the upper kilometer of the oceanic crust, DSDP Hole 504B. *Earth Planet. Sci. Lett.*, 80, 217-229, 1986.
- Becker, K., Large-scale electrical resistivity and bulk porosity of the oceanic crust, DSDP Hole 504B, Costa Rica Rift, Initial Rep. Deep Sea Drill. Proj., 83, 419-427, 1985.
- Bottinga, Y., Thermal aspects of sea-floor spreading, and the nature of the suboceanic lithosphere, *Tectonophysics*, 21, 15-38, 1974.
- Bottinga, Y., and C.J. Allègre, Thermal aspects of sea-floor spreading and the nature of the oceanic crust, *Tectonophysics*, 18, 1-17, 1973.
- Boudier, F., and A. Nicolas, Harzburgite and lherzolite subtypes in ophiolite and oceanic environments, *Earth Planet. Sci. Lett.*, 76, 84-92, 1985-86.
- Brouxel, M., and H. Lapierre, Un bassin marginal dévonien dans les Klamath orientales (Californie du Nord, Etats Unis) : le cortège ophiolitique de Trinity, *Ophioliti*, 10, 181-202, 1985.
- Brouxel, M., and H. Lapierre, Geochemical study of an early Paleozoic island arc - back arc basin system. Part I : The Trinity ophiolite (Northern California), *Geol. Soc. Am. Bull.*, 100, 1111-1119, 1988.
- Ceuleneer, G., Structure des ophiolites d'Oman : flux mantellaire sous un centre d'expansion océanique et charriage à la dorsale, Thèse de doctorat, Université de Nantes, pp. 350, 1986.
- Choukroune, P., J. Francheteau, and R. Hékinian, Tectonics of the East Pacific Rise near 12°50'N : a submersible study, *Earth Planet. Sci. Lett.*, 68, 115-127, 1984.
- Clayton, R.N., and T.K. Mayeda, The use of bromine pentafluoride in the extraction of oxygen from oxides and silicates for isotopic analyses, *Geochim. Cosmochim. Acta*, 27, 43-52, 1963.
- Cocker, J.D., B.J. Griffin, and K. Muehlenbachs, Oxygen and carbon isotope evidence for seawater-hydrothermal alteration of the Macquarie Island ophiolite, *Earth Planet. Sci. Lett.*, 61, 112-122, 1982.
- Coleman, R.G., and M.M. Donato, Oceanic plagiogranite revisited, in *Trondjhemites, dacites and related rocks*, edited by F. Barker, pp. 149-168, Elsevier, 1979.
- Craig, H., Hydrothermal plumes and tracer circulation along the East Pacific Rise : 20°N to 20°S (abstract), *Eos Trans. AGU*, 62, 893, 1981.
- Craig, H., J.A. Welhan, K. Kim, R. Poreda, and J.E. Lupton, Geochemical studies of the 21°N EPR hydrothermal fluids (abstract), *Eos Trans. AGU*, 61, 992, 1980.

- Edmond, J.M., The chemistry of the 350°C hot springs at 21°N on the East Pacific Rise (abstract), *Eos Trans. AGU*, 61, 992, 1980.
- Edmond, J.M., C. Measures, R.E. McDuff, L.H. Chan, R. Collier, B. Grant, L.I. Gordon, and J.B. Corliss, Ridge crest hydrothermal activity and the balances of the major and minor elements in the ocean : the Galapagos data, *Earth Planet. Sci. Lett.*, 46, 1-18, 1979.
- Edmond, J.M., K.L. Von Damm, R.E. McDuff, and C.I. Measures, Chemistry of hot springs on the East Pacific Rise and their effluent dispersal, *Nature*, 297, 187-191, 1982.
- Elders, W.A., D.K. Bird, A.E. Williams, and P. Schiffman P., Hydrothermal flow regime and magmatic heat source of the Cerro Prieto Geothermal System, Baja California, Mexico, *Geothermics*, 13, 27-47, 1984.
- Elthon, D., J.R. Lawrence, R.E. Hanson, and C. Stern, Modelling of oxygen-isotope data from the Sarmiento ophiolite complex, Chile, in *Ophiolites and Oceanic Lithosphere*, edited by I.G. Gass, S.J. Lippard and A.W. Shelton, pp. 185-197, Blackwell Scientific Publications, 1984.
- Girardeau, J., Ophiolites et chaînes de collision : exemples des chaînes Himalaya - Tibet et Hercynienne, étude pétro-structurale des ophiolites et de leurs encaissants : interprétations géodynamiques, Thèse d'état, I.P.G.P. et Université Paris VII, pp. 404, 1986.
- Girardeau, J. and, C. Mével, Amphibolitized sheared gabbros from ophiolite as indicators of the evolution of the oceanic crust : Bay of Islands, Newfoundland, *Earth Planet. Sci. Lett.*, 61, 152-165, 1982.
- Girardeau, J., J.C. Mercier, and W. Xibin, Petrology of the mafic rocks of the Xigaze ophiolite, Tibet, *Contrib. Mineral. Petrol.*, 90, 309-321, 1985.
- Graham, C.M., and A. Navrotsky, Thermochemistry of the tremolite-edenite amphiboles using fluorine analogues, and applications to amphibole-plagioclase-quartz equilibria, *Contrib. Mineral. Petrol.*, 93, 18-32, 1986.
- Gregory, R.T., and R.E. Criss R.E., Isotopic exchange in open and closed systems, in *stable isotopes in high temperature geological processes*, edited by J.W. Valley et al., pp. 570, *Rev. Mineral.*, 16, 1986.
- Gregory, R.T., and H.P. Taylor, Jr., An oxygen isotope profile in a section of Cretaceous Oceanic Crust, Samail ophiolite, Oman : evidence for  $\delta^{18}\text{O}$  buffering of the oceans by deep (>5Km) seawater-hydrothermal circulation at Mid-Ocean Ridges, *J. Geophys. Res.*, 86, 2737-2755, 1981.
- Holland, H.D., The chemical evolution of the atmosphere and oceans, *Princ. Ser. Geochim.*, Princeton Univ. Press, 1984.
- Humphris, S.E., and G. Thompson, Hydrothermal alteration of oceanic basalts by seawater, *Geochim. Cosmochim. Acta*, 42, 107-125, 1978.
- Ito, E., and A.T. Anderson, Submarine metamorphism of gabbros from the Mid-Cayman Rise : petrographic and mineralogic constraints on hydrothermal processes at slow-spreading ridges, *Contrib. Mineral. Petrol.*, 82, 371-388, 1983.
- Ito, E., and R.N. Clayton, Submarine metamorphism of gabbros from the Mid-Cayman Rise : an oxygen isotopic study, *Geochim. Cosmochim. Acta*, 47, 535-546, 1983.
- Javoy, M., and A.M. Fouillac, Stable isotope ratios in Deep Sea Drilling Project Leg 51 basalts, *Init. Rept. DSDP*, 51, 52, 53, 1153-1157, 1979.
- Kawahata, H., M. Kusakabe, and Y. Kikuchi, Strontium, oxygen and hydrogen isotope geochemistry of hydrothermally altered and weathered rocks in DSDP Hole 504B, Costa Rica Rift, *Earth Planet. Sci. Lett.*, 85, 343-355, 1987.

- Knauth, L.P., and M.A. Beeunas, Isotope geochemistry in fluid inclusions in Permian halite with implications for the isotopic history of ocean water and the origin of saline formation waters. *Geochim. Cosmochim. Acta*, 50, 419-433, 1986.
- Knauth, L.P., and S. Epstein, Hydrogen and oxygen isotope ratios in nodular and bedded cherts, *Geochim. Cosmochim. Acta*, 40, 1095-1108, 1976.
- Lapierre, H., M. Brouxel, F. Albarède, C. Coulon, C. Lecuyer, P. Martin, G. Mascle, and O. Rouer, Paleozoic and Lower Mesozoic magmas from the eastern Klamath Mountains (North California) and the geodynamic evolution of northwestern America, *Tectonophysics*, 140, 155-177, 1987.
- Lecuyer, C., M. Brouxel, and F. Albarède, Elemental fluxes during the hydrothermal alteration of the Trinity ophiolite (California) by seawater, *Soumis à Geochim. Cosmochim. Acta*, 1989.
- Lecuyer, C., and M. Cannat, Chemical transfers between mantle xenoliths and basic magmas : evidences for oceanic magma chambers (The Trinity ophiolite, North California), *Soumis à Chem. Geol.*, 1989.
- Lister, C.R.B., On the penetration of water into hot rock, *Geophys. J.R. Astron. Soc.*, 39, 465-509, 1974.
- Michard, G., F. Albarède, A. Michard, J.F. Minster, J.L. Charlou, and N. Tan, Chemistry of solutions from the 13°N East Pacific Rise hydrothermal site, *Earth Planet. Sci. Lett.*, 67, 297-307, 1984.
- Mottl, M.J., Metabasalts, axial hot springs, and the structure of hydrothermal systems at mid-ocean ridges, *Geol. Soc. Am. Bull.*, 94, 161-180, 1983.
- Muehlenbachs, K., Oxygen isotope geochemistry of rocks from DSDP Leg37, *Can. J. Earth Sci.*, 14, 771-776, 1977.
- Muehlenbachs, K., The alteration and aging of the basaltic layer of the seafloor : oxygen isotope evidence from DSDP/IPOD Legs 51, 53 and 53, *Initial Rep. Deep Sea Drill. Proj.*, 51,52, 53, 1159-1167, 1980.
- Muehlenbachs, K., Alteration of the oceanic crust and the  $^{18}\text{O}$  history of seawater. in *stable isotopes in high temperature geological processes*, edited by J.W. Valley et al., pp. 570, *Rev. Mineral.*, 16, 1986.
- Muehlenbachs, K., Oxygen isotope exchange during weathering and low temperature alteration, in *Short course in stable isotope geochemistry of low temperature fluids*, edited by T.K. Kyser, pp. 452, *Mineralogical Association of Canada*, 13, 1987.
- Muehlenbachs, K., and R.N. Clayton, Oxygen isotope studies of fresh and weathered submarine basalts, *Can. J. Earth Sci.*, 9, 172-184, 1972.
- Muehlenbachs, K., and R.N. Clayton, Oxygen isotope composition of the oceanic crust and its bearing on seawater, *J. Geophys. Res.*, 81, 4365-4369, 1976.
- Nehlig, P., and T. Juteau, Flow porosities, permeabilities and preliminary data on fluid inclusions and fossil thermal gradients in the crustal sequence of the Samail ophiolite (Oman), in *The ophiolites of Oman*, edited by F. Boudier and A. Nicolas, *Tectonophysics*, 1-4, 199-221, 1988.
- Nicolas, A., Structure and petrology of peridotites : clues to their geodynamic environment, *Rev. Geophys.*, 24, 875-895, 1986.
- Nicolas, A., J. Girardeau, J. Marcoux, B. Dupré, Wang Xibing, Zao Yougong, Zheng Haixiang and Xiao Xuchang, The Xigaze ophiolite (Tibet) : a peculiar oceanic lithosphere, *Nature*, 294, 414-417, 1981.

- O'Neil, J.R., and H.P. Taylor, Jr, The oxygen isotope and cation exchange chemistry of feldspars, *Am. mineral.*, 52, 1414-1437, 1967.
- O'Shea, K.J., M.C. Miles, P. Fritz, S.K. Frape, and D.E. Lawson, Oxygen-18 and carbon-13 in the carbonates of the Salina formation of southwestern Ontario, *Can. J. Earth Sci.*, 25, 182-194, 1988.
- Pallister, J.S., and C.A. Hopson, Samail ophiolite plutonic suite : field relations, phase variation, cryptic variation and layering, and a model of a spreading ridge magma chamber, *J. Geophys. Res.*, 86, 2593-2644, 1981.
- Perry, E.C., The oxygen isotope chemistry of ancient cherts, *Earth Planet. Sci. Lett.*, 3, 62-66, 1967.
- Perry, E.C., and F.C. Tan, Significance of oxygen and carbon isotope variations in early Precambrian cherts and carbonate rocks of S. Africa, *Geol. Soc. Am. Bull.*, 83, 647-664, 1972.
- Pineau, F., M. Javoy, J.W. Hawkins, and H. Craig, Oxygen isotope variations in marginal basin and ocean-ridge basalts, *Earth Planet. Sci. Lett.*, 28, 299-307, 1976.
- Poty, B., J. Leroy, and L. Jachimowicz, Un nouvel appareil pour la mesure des températures sous le microscope : l'installation de microthermométrie Chaix Meca, *Bull. Soc. Fr. Mineral. Cristallogr.*, 99, 182-186, 1976.
- Schiffman, P., A.E. Williams, and R.C. Evarts, Oxygen isotope evidence for submarine hydrothermal alteration of the Del Puerto ophiolite, California, *Earth Planet. Sci. Lett.*, 70, 207-220, 1984.
- Spooner, E.T.C., R.D. Beckinsale, P.C. England, and A. Senior, Hydration,  $^{18}\text{O}$  enrichment and oxidation during ocean floor metamorphism of ophiolitic metabasic rocks from E. Liguria, Italy, *Geochim. Cosmochim. Acta*, 41, 857-871, 1977.
- Spooner, E.T.C., R.D. Beckinsale, W.S. Fyfe, and J.D. Smewing,  $\text{O}^{18}$  enriched ophiolitic metabasic rocks from E. Liguria (Italy), Pindos (Greece) and Troodos (Cyprus), *Contrib. Mineral. Petrol.*, 47, 41-62, 1974.
- Veizer, J., W. Compston, J. Hoefs, and H. Nielsen, Mantle buffering of the early oceans, *Naturwissenschaften*, 69, 173-180, 1982.
- Veizer, J., P. Fritz, and B. Jones, Geochemistry of brachiopods : oxygen and carbon isotopic records of Paleozoic oceans, *Geochim. Cosmochim. Acta*, 50, 1679-1696, 1986.
- Von Damm, K.L., J.M. Edmond, B. Grant, C.I. Measures, B. Walden, and R.F. Weiss, Chemistry of submarine hydrothermal solutions at 21°N, East Pacific Rise, *Geochim. Cosmochim. Acta*, 49, 2197-2220, 1985a.
- Von Damm, K.L., J.M. Edmond, C.I. Measures, and B. Grant, Chemistry of submarine hydrothermal solutions at Guaymas Basin, Gulf of California, *Geochim. Cosmochim. Acta*, 49, 2221-2237, 1985b.
- Welhan, J.A., and H. Craig, Methane and hydrogen in the East Pacific Rise hydrothermal fluids, *Geophys. Res. Lett.*, 6, 829-831, 1979.

#### FIGURE CAPTIONS

Figure 1 : Synthetic lithologic column of the Trinity ophiolite (2Km in thickness) and associated metamorphic associations. Spt : serpentine; Ta : talc; Hbl : hornblende; Tr : tremolite; Ac : actinolite; Chl : chlorite; Ep : epidote; Ab : albite; Qz : quartz; Ce : celadonite; Cal : calcite.

Figure 2 : Histograms of homogenization temperatures measured on fluid inclusions in quartz from a pillow lava core (TR47A), rim (TR47B) and an isotropic gabbro (TR69).

Figure 3 : Distribution of  $\delta^{18}\text{O}$  values in the Trinity ophiolite versus the position of samples in the lithologic succession. Filled circles : ophiolitic sequence; open circles : plagiogranites; open squares : pegmatitic gabbros.

Figure 4 : Histogram of  $\delta^{18}\text{O}$  compositions in altered MOR basalts.

|                  |                      |  |                                   |
|------------------|----------------------|--|-----------------------------------|
| source of data : | hole 417A            |  |                                   |
|                  | hole 417D            |  | (Muehlenbachs, 1980)              |
|                  | hole 418A            |  |                                   |
|                  | Leg 37               |  | (Muehlenbachs, 1977)              |
|                  | hole 504B            |  | (Kawahata et al., 1987)           |
|                  | Atlantic greenstones |  | (Muehlenbachs and Clayton, 1972). |

Figure 5 : Histogram of  $\delta^{18}\text{O}$  compositions in altered ophiolitic basalts.

|                  |                  |                            |
|------------------|------------------|----------------------------|
| source of data : | Macquarie Island | (Cocker et al., 1982)      |
|                  | Sarmiento        | (Elthon et al., 1984)      |
|                  | Oman             | (Gregory and Taylor, 1981) |
|                  | Del Puerto       | (Schiffman et al., 1984)   |
|                  | Troodos          |                            |
|                  | Pindos           |                            |
|                  | Xigaze           | (Agrinier et al., 1988)    |
|                  | Liguria          | (Spooner et al., 1977)     |

Figure 6 : whole rock  $\delta^{18}\text{O}$  versus  $\text{Al}_V + (\text{Na} + \text{K})_A$  in amphiboles from the Trinity ophiolite.

Figure 7 : profile of apparent temperatures of alteration in the Trinity ophiolite deduced from strontium and oxygen isotope studies (see text for explanations).

Figure 8 : Comparison of  $\delta^{18}\text{O}$  profiles in two ophiolite sequences related to a slow-spreading environment : Trinity and Xigaze complexes. In both cases, the  $^{18}\text{O}$  enrichment in the upper levels does not balance the  $^{18}\text{O}$  depletion in the lower levels.

Figure 9 : Synthetic  $\delta^{18}\text{O}$  profile between enriched and depleted levels showing the balance in the Oman ophiolite.

Figure 10 : Hydrothermal model in a slow-spreading ridge, the example of the Trinity ophiolite and evidences of ageing of the crust controlled by fracturing systems.

Figure 11 : Isothermal curves showing the variation of the initial isotopic composition calculated for seawater as a function of W/R ratios during hydrothermal interaction and the estimated  $\delta^{18}\text{O}$  of the siluro-ordovician ocean. (see text for explanations).

Figure 12 : Variations of whole rock oxidation ratio ( $\text{Fe}^{3+} / \text{Fe}_T$ ) with the stratigraphic position of samples in the Trinity ophiolitic sequence.

Figure 13 : Isothermal curves showing the variation of the initial isotopic composition calculated for seawater as a function of W/R ratios during hydrothermal interaction and the estimated  $\delta^{18}\text{O}$  for deep discharged water. (see text for explanations).

| Samples           | Type        | $\delta^{18}\text{O}$ | $\sigma$    | n | $t^\circ\text{C}$ | $\delta^{13}\text{C}$ | $^{87}\text{Sr}/^{86}\text{Sr}(\text{I})$ | W/R   |
|-------------------|-------------|-----------------------|-------------|---|-------------------|-----------------------|---|-------|
| <b>Carbonates</b> |             |                       |             |   |                   |                       |   |       |
| TR55A             | <i>B</i>    | 15.83                 |             | 1 | 107               | 1.39                  | 0.70497                                   | 6.50  |
| TR52B             | <i>B</i>    | 26.14                 |             | 1 | 34                | -2.49                 |   |       |
| TR47B (rim)       | <i>B</i>    | 21.68                 |             | 1 | 43                | -3.91                 | 0.70546                                   | 7.60  |
| TR61              | <i>I.g.</i> | 24.50                 |             | 1 | 60                | -5.42                 | 0.70556                                   | 15.90 |
| TR124D            | <i>d</i>    | 27.61                 |             | 1 | 26                | -2.19                 | 0.70504                                   | 9.80  |
| <b>Silicates</b>  |             |                       |             |   |                   |                       |   |       |
| TR55A             | <i>B</i>    | 9.60                  | $\pm 0.01$  | 4 | 133               |                       | 0.70497                                   | 6.50  |
| TR53B             | <i>B</i>    | 9.55                  | $\pm 0.01$  | 2 | 139               |                       | 0.70503                                   | 14.60 |
| TR51B             | <i>B</i>    | 9.55                  | $\pm 0.2$   | 5 | 128               |                       | 0.70472                                   | 3.80  |
| TR48              | <i>B</i>    | 8.45                  | $\pm 0.1$   | 2 | 153               |                       | 0.70563                                   | 5.40  |
| TR47B (rim)       | <i>B</i>    | 10.10                 | $\pm 0.2$   | 2 | 126               |                       | 0.70546                                   | 7.60  |
| TR47A (core)      | <i>B</i>    | 8.95                  | $\pm 0.05$  | 2 | 148               |                       | 0.70531                                   | 10.90 |
| TR128F            | <i>d</i>    | 4.80                  | $\pm 0.1$   | 2 | 211               |                       | 0.70456                                   | 8.40  |
| TR128H            | <i>d</i>    | 4.80                  | $\pm 0.1$   | 3 |                   |                       |   |       |
| TR127             | <i>d</i>    | 5.50                  | $\pm 0.1$   | 3 | 227               |                       | 0.7041                                    | 6.40  |
| TR124D            | <i>d</i>    | 5.85                  | $\pm 0.15$  | 4 | 216               |                       | 0.70504                                   | 9.80  |
| TR130A            | <i>d</i>    | 5.50                  | $\pm 0.2$   | 5 |                   |                       |   |       |
| TR61              | <i>I.g.</i> | 9.05                  | $\pm 0.15$  | 5 | 148               |                       | 0.70556                                   | 15.90 |
| TR64              | <i>I.g.</i> | 7.30                  | $\pm 0.2$   | 6 | 181               |                       | 0.70529                                   | 13.70 |
| TR532             | <i>I.g.</i> | 5.36                  | $\pm 0.2$   | 2 | 288               |                       | 0.70415                                   | 3.80  |
| TR538             | <i>p.g.</i> | 4.95                  | $\pm 0.03$  | 2 | 335               |                       | 0.70405                                   | 1.60  |
| TR526             | <i>I.g.</i> | 4.00                  | $\pm 0.05$  | 5 |                   |                       |   |       |
| PEGMB             | <i>p.g.</i> | 5.00                  |             | 1 | 319               |                       | 0.70467                                   | 3.80  |
| TR524             | <i>tdj</i>  | 7.43                  | $\pm 0.2$   | 4 | 174               |                       | 0.70433                                   | 3.50  |
| TR523             | <i>I.g.</i> | 6.25                  | $\pm 0.02$  | 3 |                   |                       |   |       |
| TR510A            | <i>d</i>    | 5.85                  | $\pm 0.1$   | 3 |                   |                       |   |       |
| TR112             | <i>lg</i>   | 5.65                  | $\pm 0.1$   | 3 |                   |                       |   |       |
| TR110             | <i>lg</i>   | 5.78                  | $\pm 0.1$   | 4 | 278               |                       | 0.70394                                   | 1.80  |
| TR121             | <i>lg</i>   | 6.95                  | $\pm 0.2$   | 3 | 231               |                       | 0.70411                                   | 3.30  |
| TR106             | <i>lg</i>   | 4.93                  |             | 1 | 327               |                       | 0.7045                                    | 2.50  |
| TR105             | <i>lg</i>   | 5.80                  | $\pm 0.1$   | 2 |                   |                       |   |       |
| TR252             | <i>wrh</i>  | 5.45                  | $\pm 0.15$  | 2 |                   |                       |   |       |
| TR248             | <i>lg</i>   | 5.90                  | $\pm 0.15$  | 2 | 274               |                       | 0.70438                                   | 3.80  |
| TR241             | <i>lg</i>   | 5.75                  | $\pm 0.15$  | 2 |                   |                       |   |       |
| TR234             | <i>lg</i>   | 6.20                  | $\pm 0.2$   | 5 | 255               |                       | 0.70363                                   | 1.60  |
| TR224             | <i>wbs</i>  | 5.48                  | $\pm 0.005$ | 2 |                   |                       |   |       |
| TR223             | <i>p.g.</i> | 6.00                  | $\pm 0.2$   | 2 | 269               |                       | 0.70400                                   | 3.40  |
| TR222             | <i>wrh</i>  | 4.87                  | $\pm 0.03$  | 2 |                   |                       | 0.70276                                   | 0.00  |
| <b>Quartz</b>     |             |                       |             |   |                   |                       |   |       |
| TR47B (rim)       | <i>b</i>    | 12.73                 | $\pm 0.03$  | 2 |                   |                       |   |       |
| TR532             | <i>I.g.</i> | 11.00                 | $\pm 0.02$  | 2 |                   |                       |   |       |
| TR68              | <i>I.g.</i> | 7.96                  | $\pm 0.05$  | 2 |                   |                       |   |       |
| <b>Amphiboles</b> |             |                       |             |   |                   |                       |   |       |
| TR538             | <i>p.g.</i> | 4.54                  |             | 1 |                   |                       |   |       |
| TR223             | <i>p.g.</i> | 5.71                  |             | 1 |                   |                       |   |       |

*B* = basalt  
*d* = dyke  
*I.g.* = isotropic gabbro  
*p.g.* = pegmatitic gabbro  
*tdj* = trondhjornite  
*lg* = layered gabbro  
*wrh* = werhlite  
*wbs* = websterite

Tableau 1



| Samples | Clayton et al.<br>(1972) | Kawabe<br>(1978) | Matsuhisa et al.<br>(1978; 1979) | Microthermometric<br>data | $\delta^{18}\text{O}$ quartz<br>(n = 2) |
|---------|--------------------------|------------------|----------------------------------|---------------------------|---|
|         | (200 - 500°C)            | (0 - 100°C)      | (250 - 500°C)                    |                           |   |
| TR47B   | 185°C                    | 151°C            | 183°C                            | 130 - 150°C               | 12.73±0.03                              |
| TR68    | 272°C                    | 220°C            | 271°C                            | 290 - 390°C               | 7.96±0.05                               |
| TR532   | 211°C                    | 198°C            | 210°C                            | n. d.                     | 11.00±0.02                              |

Table 2

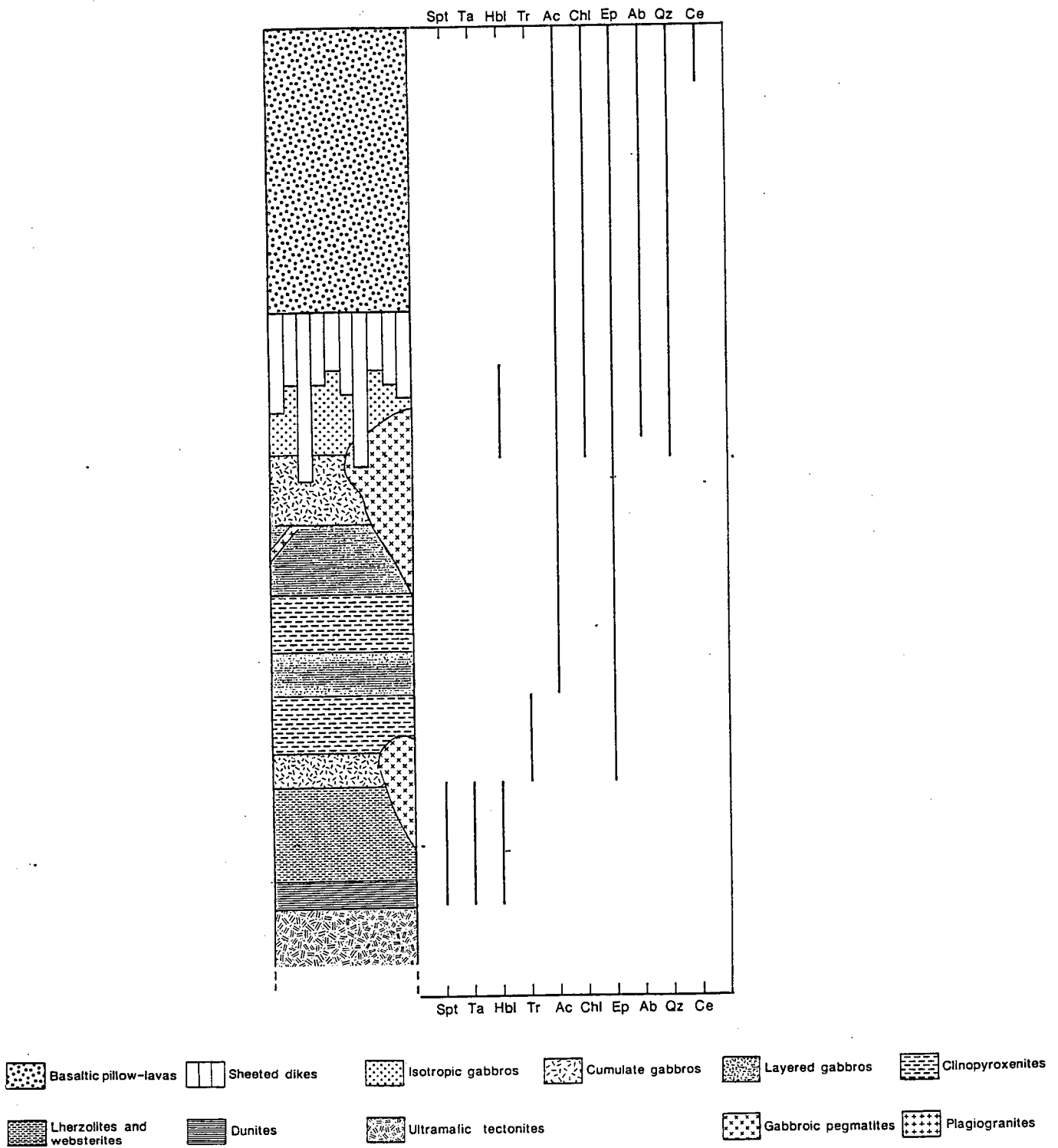


Figure 1

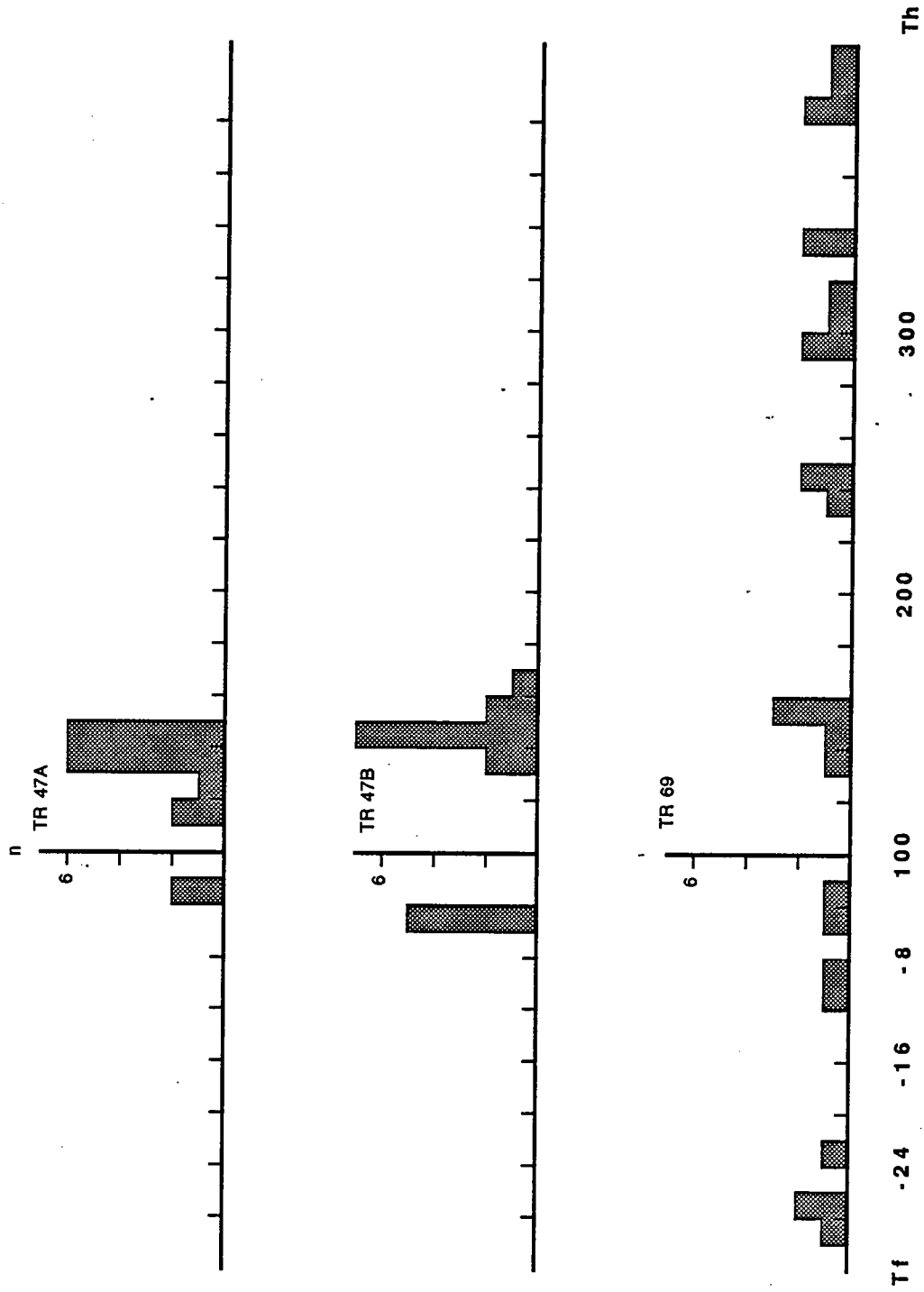


Figure 2

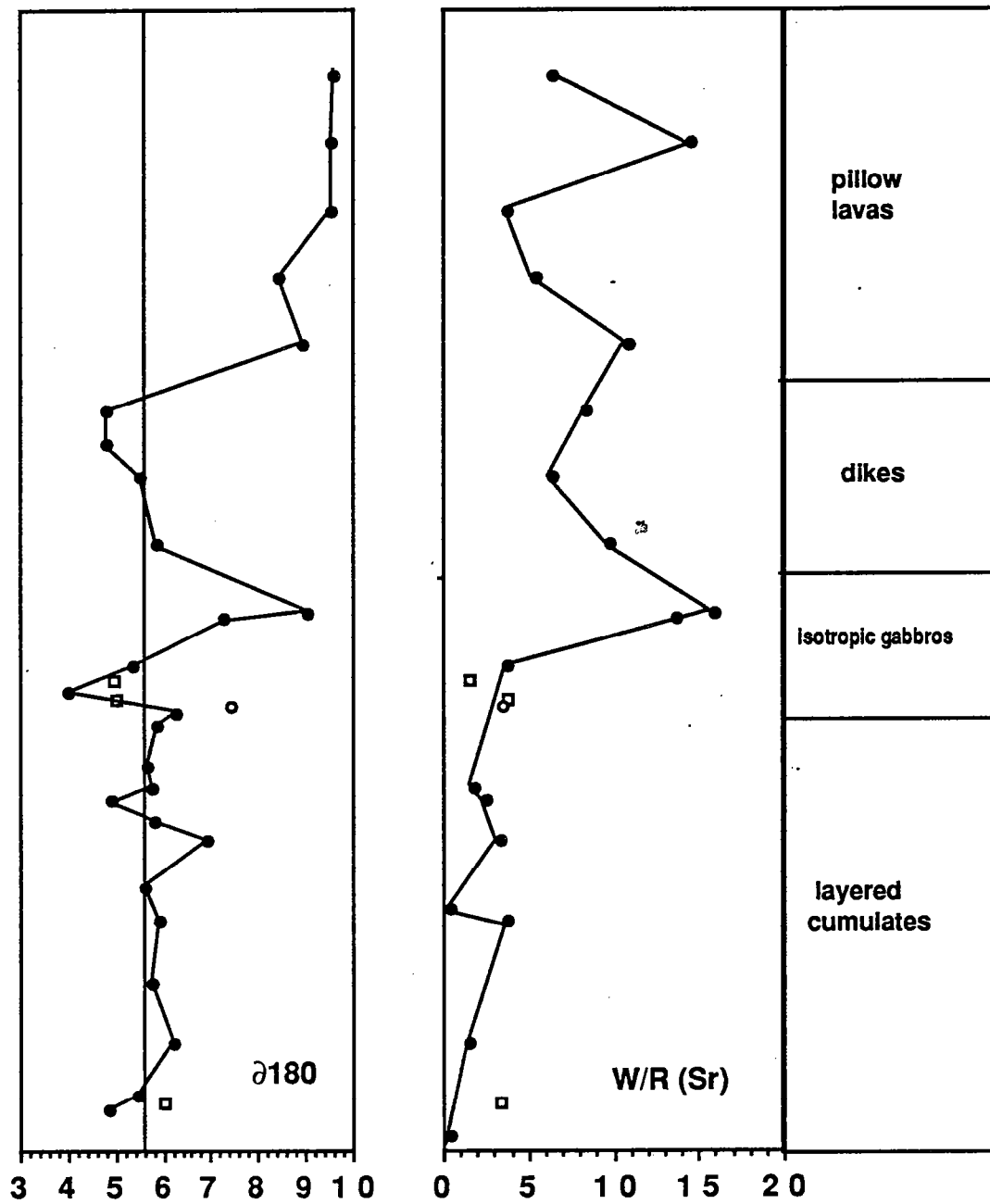


Figure 3

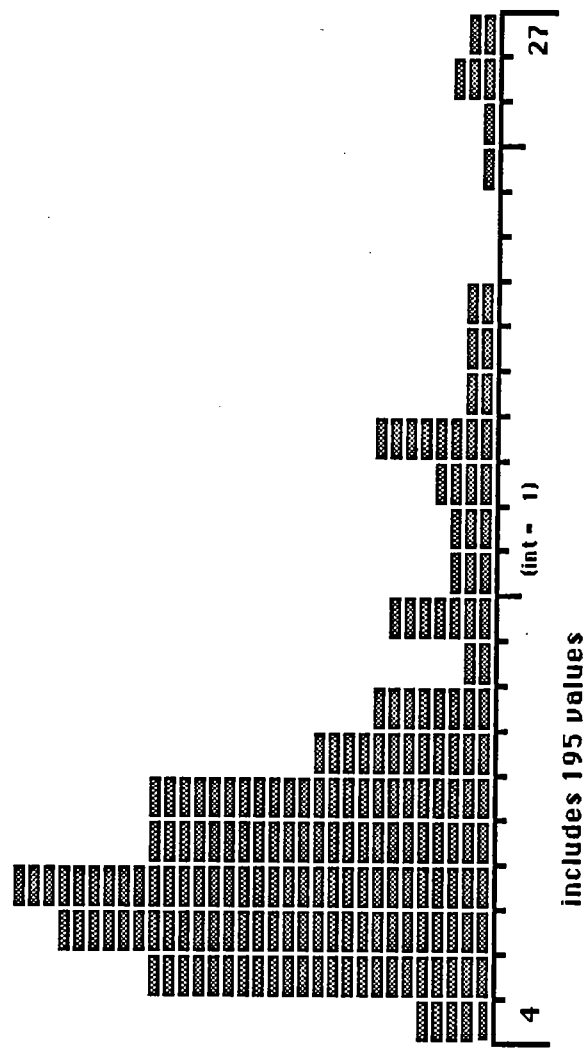


Figure 4

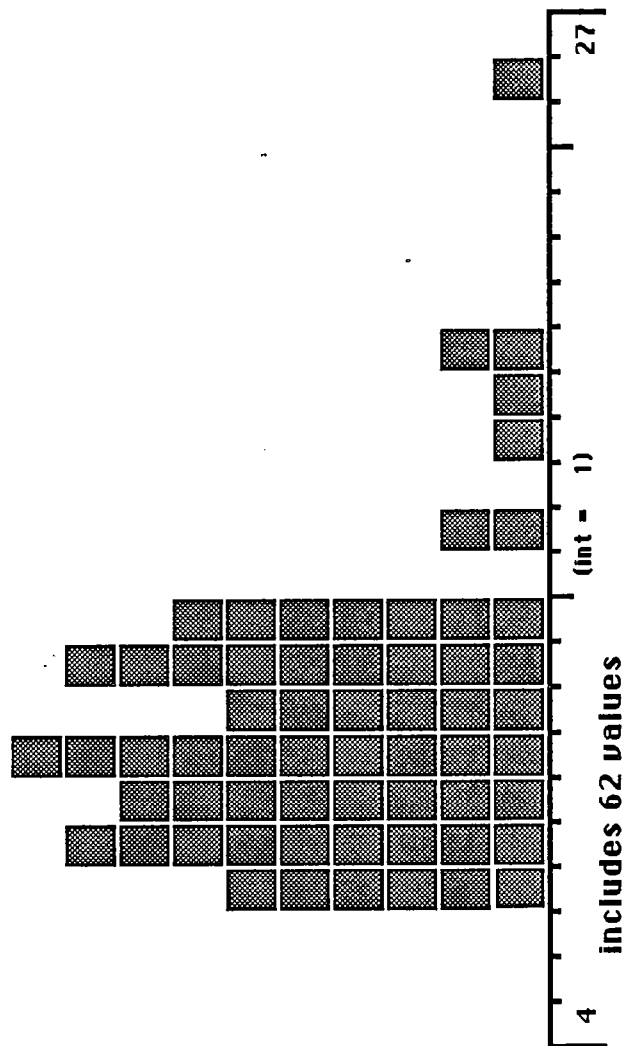


Figure 5

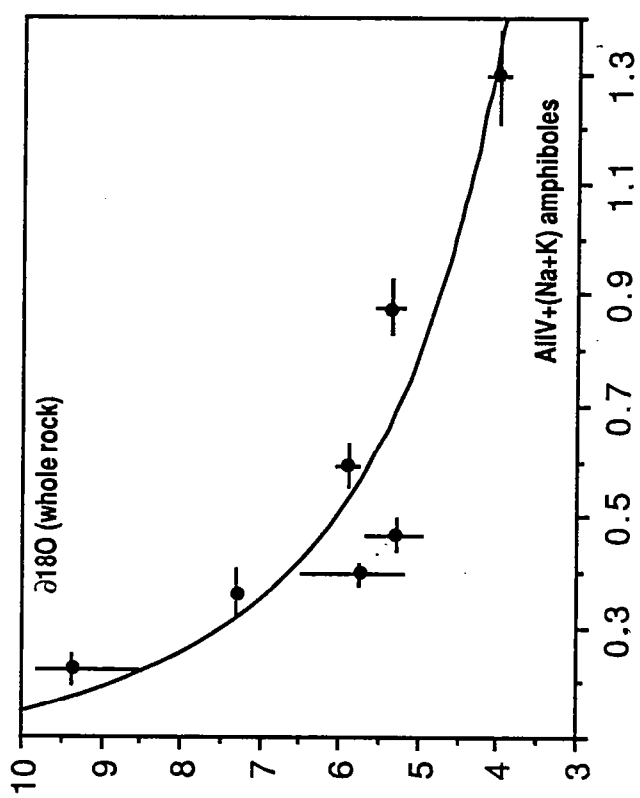


Figure 6

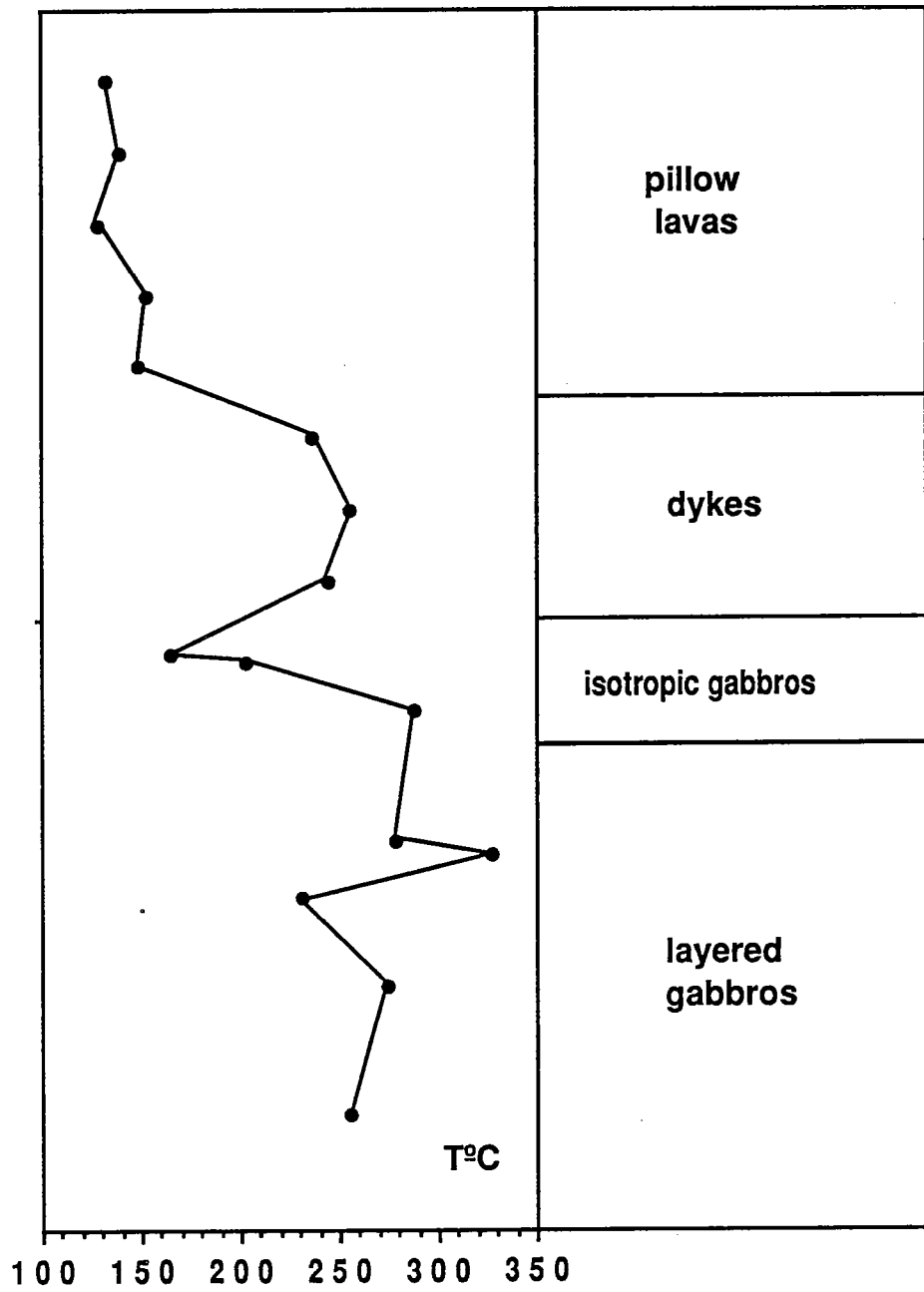


Figure 7



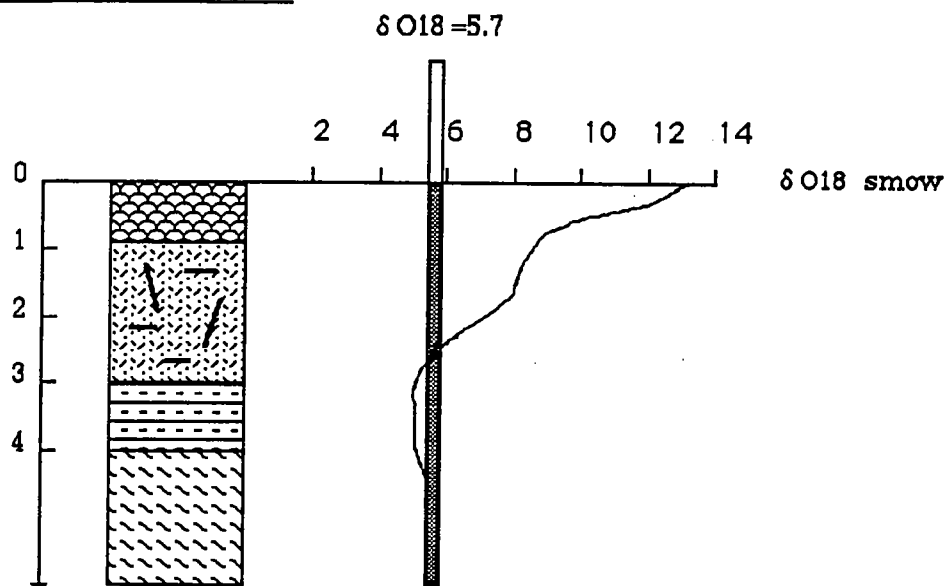
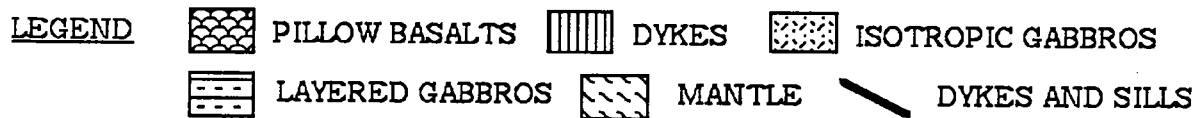
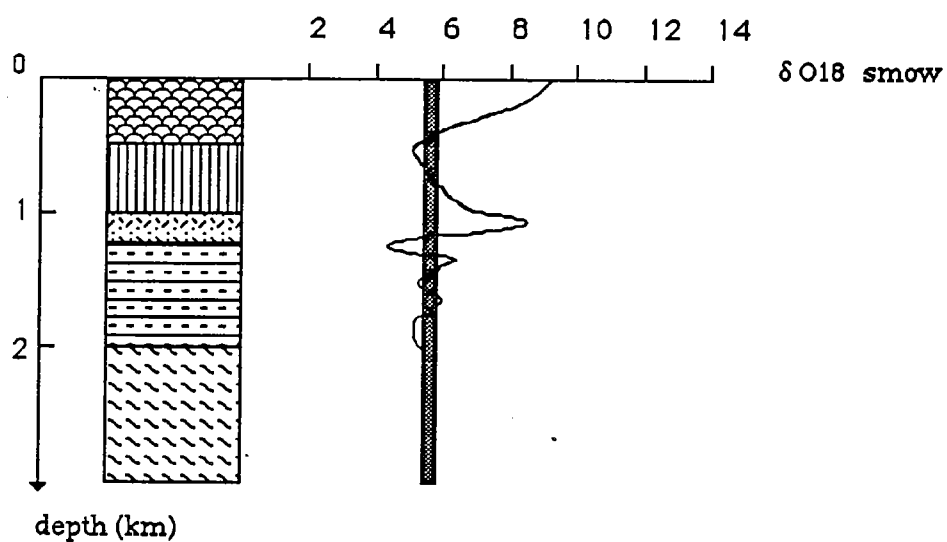
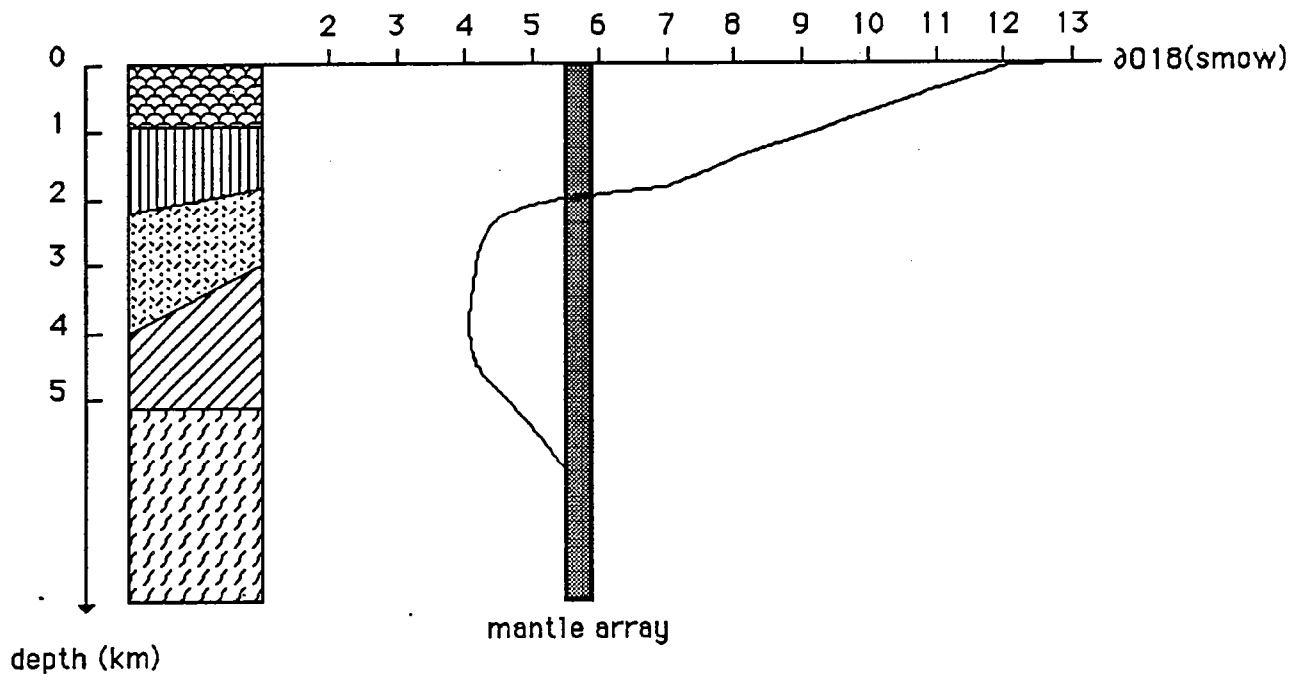





**XIGAZE OPHIOLITE****TRINITY OPHIOLITE**

Figure 8

**OMAN OPHIOLITE****LEGEND**

-  PILLOW BASALTS
-  DYKES
-  ISOTROPIC GABBROS
-  LAYERED GABBROS
-  MANTLE

HYDROTHERMAL MODEL IN A SLOW-SPREADING RIDGE  
THE EXAMPLE OF THE TRINITY OPHIOLITE  
O18 AGEING OF THE OCEANIC CRUST

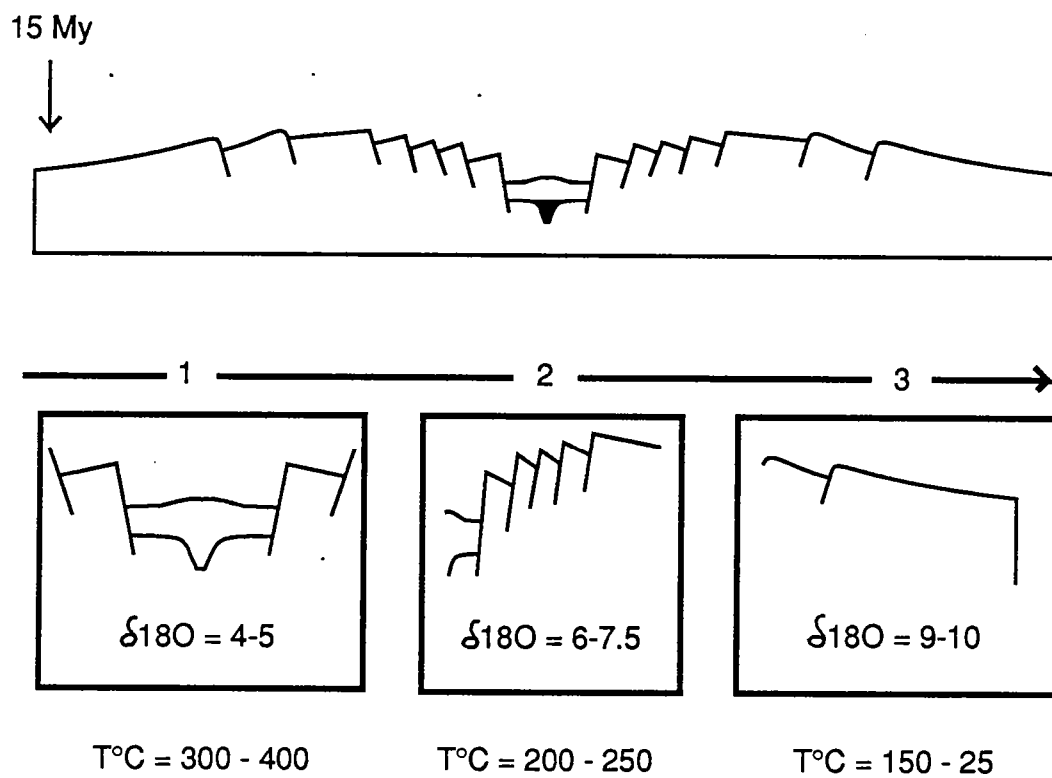


Figure 10

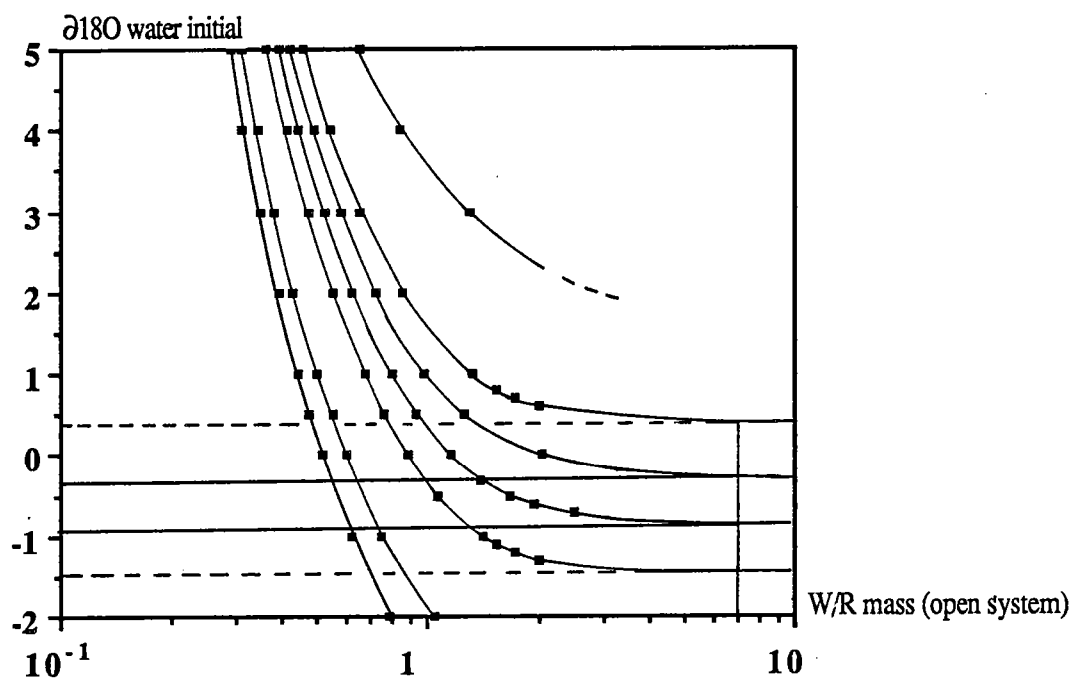


Figure 11

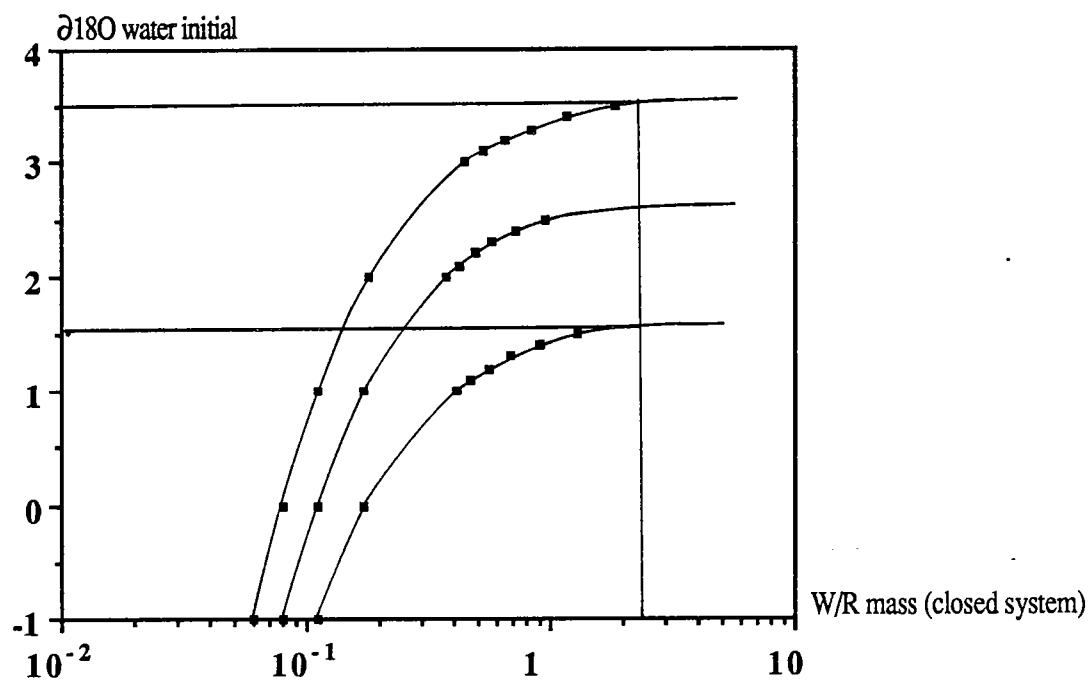


Figure 13

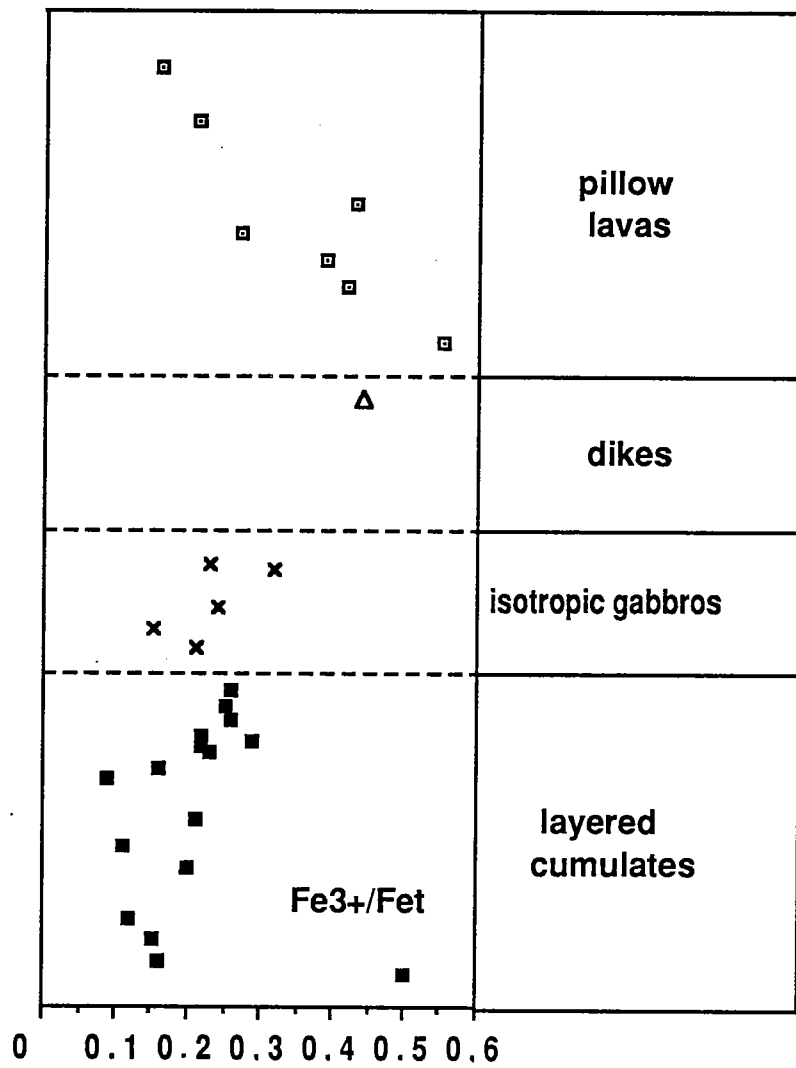


Figure 12

## Références

- Agrinier P., Javoy M. et Girardeau J. 1988. Hydrothermal activity in a peculiar oceanic ridge : oxygen and hydrogen isotope evidence in the Xigaze ophiolite, (Tibet, China). *Chem. Geol.*, 71 : 313-335.
- Albarède F., Michard A., Minster J.F. et Michard G. 1981.  $^{87}\text{Sr}/^{86}\text{Sr}$  ratios in hydrothermal waters and deposits from the East Pacific Rise at 21°N. *Earth Planet. Sci. Lett.*, 55 : 229-236.
- Albers J.P., Kistler R.W. et Kwak K.L. 1981. The Mule Mountain stock, an Early Middle Devonian pluton in northern California. *Isochron West*, 31 : 17.
- Alt J.C. et Emmermann R. 1985. Geochemistry of hydrothermally altered basalts : Deep Sea Drilling Project Hole 504B, Leg 83. *Init. Rept. Deep Sea Drill. Proj.*, 83 : 249-262.
- Alt J.C., Honnorez J., Laverne C. et Emmermann R. 1986. Hydrothermal alteration of a 1 Km section through the upper oceanic crust, deep sea drilling project hole 504B : mineralogy, chemistry and evolution of seawater-basalt interactions. *J. Geophys. Res.*, 91 : 309-335.
- Barker J.P., Millard H.T. et Knight R.J. 1979. Reconnaissance geochemistry of Devonian island-arc volcanic and intrusive rocks, West Shasta district, California. In: *Trondjemites, dacites and related rocks*, F. Barker (Ed.), Elsevier : 531-545.
- Bébian J. 1980. Magmatismes basiques dits "orogéniques" et "anorogéniques" et teneurs en  $\text{TiO}_2$  : les associations "isotitanées" et "anisotitanées". *J. Volcanol. Geotherm. Res.*, 8 : 337-342.
- Böhlke J.K., Honnorez J., Honnorez-Guerstein B.M., Muehlenbachs K. et Petersen N. 1981. Heterogeneous alteration of the upper oceanic crust : correlation of rock chemistry, magnetic properties and O isotope ratios with alteration patterns in basalts from site 396B, DSDP. *J. Geophys. Res.*, 86 : 7935-7950.
- Bowers T.S. et Taylor H.P. 1985. An integrated chemical and stable-isotope model of the origin of Mid-ocean Ridge hot spring systems. *J. Geophys. Res.*, 90 : 12583-12606.
- Brouxel M. 1987. Géochimie d'un arc insulaire intra-océanique fossile et son bassin marginal : les séries paléozoïques de Copley, Balaklala et le cortège ophiolitique de Trinity (Klamath orientales, Nord Californie, U.S.A.). Thèse Doct. Univ. Nancy I, 323pp.
- Brouxel M., Lapierre H., Michard A. et Albarède F. 1988. Geochemical study of an early Paleozoic island arc - back arc basin system. Part II : Eastern Klamath, early to middle Paleozoic island-arc volcanic rocks (northern California). *Geol. Soc. Am. Bull.*, 100 : 1120-1130.
- Bryan W.B., Finger L.W. et Chayes F. 1969. Estimating Proportions in Petrographic Mixing Equations by Least-Squares Approximation. *Science*, 163 : 926-927.
- Casey W.H. et Taylor B.E. 1982. Oxygen, hydrogen, and sulfur isotope geochemistry of a portion of the West Shasta Cu-Zn district, Shasta County, California. *Econom. Geol.*, 77 : 38-49.
- Choukroune P., Francheteau J. et Hékinian R. 1984. Tectonics of the East Pacific Rise near 12°50'N : a submersible study. *Earth Planet. Sci. Lett.*, 68 : 115-127.
- Cocker J.D., Griffin B.J. et Muehlenbachs K. 1982. Oxygen and carbon isotope evidence for seawater-hydrothermal alteration of the Macquarie Island ophiolite. *Earth Planet. Sci. Lett.*, 61 : 112-122.

- Corliss J.B., Dymond J., Gordon L.I., Edmund J.M., von Herzen R.P., Ballard R.D., Green K.L., Williams D., Brainbridge A.L., Crane K. et van Andel T.H. 1979a. Submarine thermal springs on the Galapagos rift. *Science*, 203 : 1073-1083.
- Corliss J.B., Gordon L.E. et Edmond J.M. 1979b. Some implications of heat/mass ratios in Galapagos rift hydrothermal fluids for models of seawater rock interaction and the formation of oceanic crust. In : *Deep Drilling Results in the Atlantic Ocean Crust*, (Editors) M. Talwani, C.G. Harrison and D.E. Hayes. Am. Geophys., Union, Washington, DC : 391-402.
- Craig H., Welhan J.A., Kim K., Poreda R. et Lupton J.E. 1980. Geochemical studies of the 21°N EPR hydrothermal fluids (abstract), *Eos Trans. AGU*, 61, 992.
- Deer W.A., Howie R.A. et Zussman J. 1966. *An introduction to the rock forming minerals*. Longman, London.
- Edmond J.M., Measures C., McDuff R.E., Chan L.H., Collier R., Grant B., Gordon L.I. et Corliss J.B. 1979. Ridge crest hydrothermal activity and the balances of the major and minor elements in the ocean : the Galapagos data. *Earth Planet. Sci. Lett.*, 46 : 1-18.
- Epstein S. et Mayeda T.K. 1953. Variation of  $^{18}\text{O}$  content of waters from natural sources. *Geochim. Cosmochim. Acta*, 4 : 213-224.
- Gresens R.L. 1967. Composition-Volume relationships of metasomatism. *Chem. Geol.*, 2 : 47-65.
- Floyd P.A. et Winchester J.A. 1975. Magma type and tectonic setting discrimination using immobile elements. *Earth Planet. Sci. Lett.*, 27 : 211-218.
- Gregory R.T. et Taylor H.P.Jr. 1981. An oxygen isotope profile in a section of Cretaceous Oceanic Crust, Samail ophiolite, Oman : evidence for  $\delta^{18}\text{O}$  buffering of the oceans by deep (>5Km) seawater-hydrothermal circulation at Mid-Ocean Ridges. *J. Geophys. Res.*, 86 : 2737-2755.
- Harper G. D., Bowman J. R. et Kuhns R. 1988. A field, chemical, and stable isotope study of subseafloor metamorphism of the Josephine ophiolite, California-Oregon. *J. Geophys. Res.*, 93 : 4625-4656.
- Hart R.A. 1973. A model for chemical exchange in the basalt-seawater system of oceanic layer II. *Can. J. Earth Sci.*, 10 : 799-816.
- Heaton T.H.E. et Sheppard S.M.F. 1977. Hydrogen and oxygen isotope evidence for seawater-hydrothermal alteration and ore deposition, Troodos complex, Cyprus. In : *Volcanic processes in ore genesis*. Inst. of Min. and Metal. and Geol. Soc. London.
- Hékinian R. 1968. Rocks from the mid-oceanic ridge in the Indian Ocean. *Deep-Sea Res.*, 15 : 195-213.
- Hoernes S., Friedrichsen H. et Schock H.H. 1978. Oxygen and hydrogen- isotope and trace element investigations on rocks of DSDP hole 395A, leg45. *Init. Rept. Deep Sea Drill. Proj.*, 29 : 541-550.
- Hoffman S.E., Wilson M. et Stakes D.S. 1986. Inferred oxygen isotope profile of Archean oceanic crust, Onverwacht Group, South Africa. *Nature*, 321 : 55-58.
- Howell D.G. 1985. Terranes. *Scientific American*, 253 : 90-103.
- Ito E., Göpel C., White W.M., Jochum K.P., Seufert H.W., Voshage H. et Hofmann A.W. 1982. Inferences on the composition and evolution of the source of MORB. Fifth Int'l Conf. on Geochronology, Cosmochronology Isotope Geology (Abstract).
- Javoy M. et Fouillac A. M. 1979. Stable isotope ratios in Deep Sea Drilling Project Leg 51 basalts. *Init. Rept. DSDP*, 51, 52, 53 : 1153-1157.

- Kinkel A.R.J., Hall W.E. et Albers J.P. 1956. Geology and base metal deposits of West Shasta Copper - Zinc district Shasta County, California. U.S. Geol. Surv. Prof. Pap., 258 : 156 p.
- Kyser T.K., O'Neil J.R. et Carmichael I.S.E. 1981. Oxygen isotope thermometry of basic lavas and mantle nodules. *Contrib. Mineral. Petrol.*, 77 : 11-23.
- Langmuir C.H., Bender J.B., Bence A.E., Hanson G.N. et Taylor S.R. 1977. Petrogenesis of basalts from the Famous area : Mid-Atlantic Ridge. *Earth Planet. Sci. Lett.*, 36 : 133-156.
- Lapierre H., Albarède F., Albers J., Cabanis B. et Coulon C. 1985a. The early Devonian volcanism in the Eastern Klamath Mountains, California : evidence for an immature island arc. *Can. J. Earth Sci.*, 22 : 214-227.
- Lapierre H., Cabanis B., Coulon C., Brouxel M. et Albarède F. 1985b. The geodynamic setting of the Early Devonian Kuroko-type sulfide deposits in the eastern Klamath Mountains (northern California) inferred by the petrological and geochemical characteristics of associated island - arc volcanic rocks. *Econom. Geol.*, 80 : 2100-2113.
- Larson P.B. 1984. Geochemistry of the alteration pipe at the Bruce Cu-Zn volcanogenic massive sulfide deposit, Arizona. *Econom. Geol.*, 79 : 1880-1896.
- Lecuyer C. et Fourcade S. 1989. A complex history of hydrothermal alteration recorded by an ophiolitic sequence : the Trinity ophiolite. Evidence from oxygen isotopes and major elemental fluxes. *Soumis à Contrib. Mineral. Petrol.*
- Lecuyer C., Brouxel M. et Albarède F. 1989c. Elemental fluxes during the hydrothermal alteration of the Trinity ophiolite (California) by seawater. *Soumis à Chem. Geol.*
- Le Sueur E. et Boudier F. 1986. Structures du complexe basique et ultrabasique de Trinity, Californie : genèse d'une ophiolite atypique. *Bull. Soc. géol. France*, 6 : 1007-1014.
- Le Sueur E., Boudier F., Cannat M., Ceuleneer G. et Nicolas A. 1984. The Trinity mafic-ultramafic complex : first results of the structural study of an untypical ophiolite. *Ophioliti*, 9 : 487-498.
- Miyashiro A. et Shido F. 1975. Tholeiitic and calc-alkalic series in the relation to the behaviors of titanium, vanadium, chromium, and nickel. *Am. J. Sci.*, 275 : 265-277.
- Montigny R., Javoy M. et Allègre C.J. 1970.  $^{87}\text{Sr}/^{86}\text{Sr}$ , K/Rb and  $^{18}\text{O}/^{16}\text{O}$  ratios in the Pinde ophiolitic complex, Greece. *Geol. Soc. Am. Abstr.*, 2 : 627-628.
- Mottl M.J. 1983. Metabasalts, axial hot springs, and the structure of hydrothermal systems at mid-ocean ridges. *Geol. Soc. Am. Bull.*, 94 : 161-180.
- Mottl M.J. et Holland H.D. 1978. Chemical exchange during hydrothermal alteration of basalt by seawater. I- Experimental results for major and minor components of seawater. *Geochim. Cosmochim. Acta*, 42 : 1103-1115.
- Muehlenbachs K. 1977. Oxygen isotope geochemistry of rocks from DSDP Leg37. *Can. J. Earth Sci.*, 14 : 771-776.
- Muehlenbachs K. 1980. The alteration and aging of the basaltic layer of the seafloor : oxygen isotope evidence from DSDP/IPOD Legs 51, 53 and 53. *Init. Rept. Deep Sea Drill. Proj.*, 51,52, 53 : 570pp.
- Muehlenbachs K. 1986. Alteration of the oceanic crust and the  $^{18}\text{O}$  history of seawater. In : stable isotopes in high temperature geological processes, Valley J.W. et al. (editors). *Rev. Mineral.* 16, pp. 570.
- Muehlenbachs K. et Clayton R.N. 1972. Oxygen isotope studies of fresh and weathered submarine basalts. *Can. J. Earth Sci.*, 9 : 172-184.



- Ohnenstetter M. 1982. Importance de la nature et du rôle des discontinuités au sein des ophiolites lors du développement d'un orogène. Thèse d'état, Université de Nancy I : 590.
- Ohnenstetter M. 1985. Classification pétrographique et structurale des ophiolites, écho de la dynamique des zones de transition croûte-manteau. Incidence sur la nature et la disposition des corps de chromite associés. C. R. Acad. Sci. Paris, : 1413-1418.
- Paster T.P. 1968. Petrologic variations within submarine basalt pillows of the South Pacific-Antarctic Ocean. Ph. D., Florida State University, Tallahassee.
- Pearce J.A. et Cann J.R. 1973. Tectonic setting of basic volcanic rocks determined using trace element analyses. Earth Planet. Sci. Lett., 19 : 290-300.
- Pineau F., Javoy M., Hawkins J.W. et Craig H. 1976. Oxygen isotope variations in marginal basin and ocean-ridge basalts. Earth Planet. Sci. Lett., 28 : 299-307.
- Schiffman P. et Smith B. M. 1988. Petrology and oxygen isotope geochemistry of a fossil seawater hydrothermal system within the Solea graben, northern Troodos ophiolite, Cyprus. J. Geophys. Res., 93 : 4612-4624.
- Schiffman P., Williams A.E. et Evarts R.C. 1984. Oxygen isotope evidence for submarine hydrothermal alteration of the Del Puerto ophiolite, California. Earth Planet. Sci. Lett., 70 : 207-220.
- Serri G. 1981. The petrochemistry of ophiolitic gabbroic complex : a key for the classification of ophiolites into low-Ti and high-Ti type. Earth Planet. Sci. Lett., 52 : 203-212.
- Shido F., Miyashiro A. et Ewing M. 1974. Compositional variation in pillow lavas from the Mid-Atlantic Ridge. Mar. Geol., 16 : 177-190.
- Sivell W.J. et Rankin P.C. 1982. Discrimination between ophiolitic metabasalts, north D'Urville Island, New Zealand. N. Z. J. Geol. Geophys., 25 : 275-293.
- Spooner E.T.C., Beckinsale R.D., Fyfe W.S. et Smewing J.D. 1974. O<sup>18</sup> enriched ophiolitic metabasic rocks from E. Liguria (Italy), Pindos (Greece) and Troodos (Cyprus). Contrib. Mineral. Petrol., 47 : 41-62.

- Stern C., de Wit M.J. et Lawrence J.R. 1976. Igneous and metamorphic processes associated with the formation of Chilean ophiolites and their implication for ocean floor metamorphism, seismic layering and magmatism. *J. Geophys. Res.*, 81 : 4370-4380.
- Taylor H.P. 1968. The oxygen isotope geochemistry of igneous rocks. *Contrib. Mineral. Petrol.*, 19 : 1-71.
- Taylor B. E. et South B.C. 1985. Regional stable isotope systematics of hydrothermal alteration and massive sulfide deposition in the West Shasta district, California. *Econom. Geol.*, 80 : 2149-2163.
- Thompson G. 1973. A geochemical study of the low-temperature interaction of seawater and oceanic igneous rocks. *EOS, Trans. Am. Geophys. Union*, 54 : 1015-1019.
- Thompson G. 1983. Basalt-seawater interaction, in "Hydrothermal Processes at Seafloor Spreading Centers", edited by P.A. Rona, K. Bostrom and K.L. Smith, Plenum, New York, pp. 225-278.
- Wenner D.B. et Taylor H.P. 1973. Oxygen and hydrogen isotope studies of the serpentinization of ultramafic rocks in oceanic environments and continental ophiolitic complexes. *Am. J. Sci.*, 273 : 207-239.
- Wolery T.J. et Sleep N.H. 1988. Interactions of geochemical cycles with the mantle. In : *Chemical cycles in the evolution of the Earth*, (Editors) C.B. Gregor, R.M. Garrels, F.T. Mackenzie and J.B. Maynard. John Wiley and sons, New York, 276pp.

## CONCLUSIONS GENERALES

### RAPPELS

1) *objet* : le complexe ophiolitique de Trinity dans les Klamath orientales et les séries volcano-sédimentaires chevauchantes d'Yreka-Callahan (Californie).

2) *intérêt* : étude d'une série ophiolitique complète d'âge silurien représentant une paléoride océanique à expansion lente probablement au voisinage d'un arc insulaire ou dans un domaine océanique de type Mer Rouge (LeSueur et al., 1984; Boudier et Nicolas, 1985/86; Cannat et Boudier, 1986; LeSueur et Boudier, 1986; Lapiere et al., 1987; Brouxel et al., 1988).

3) *but* : mise en évidence des bilans géochimiques (magmatisme et hydrothermalisme) dans une section complète de croûte océanique en relation avec son environnement géotectonique.

### RESULTATS

#### 1) Géologie régionale:

Les nappes volcano-sédimentaires d'âge ordovicien à dévonien d'Yreka-Callahan qui chevauchent le complexe ophiolitique de Trinity correspondent à des dépôts de "seamounts" associés à des sédiments marins profonds qui sont venus s'échouer contre une marge continentale active comme en témoignent la présence d'un volcanisme calco-alcalin d'arc et la présence de dépôts sédimentaires terrigènes. Si les relations spatiales avec le complexe ophiolitique de Trinity mis en place dans un domaine de bassin arrière-arc ou dans un environnement de type Mer Rouge ne sont pas encore précisées; l'existence d'un domaine océanique matérialisé par la présence d'un cortège ophiolitique et de dépôts volcano-sédimentaires d'îles océaniques n'exclut pas le voisinage d'un continent. Les séries ordoviciennes d'Yreka-Callahan sont par contre très bien corrélées avec celles des Roberts Mountain Allochton dans le Nevada et pourraient témoigner d'une continuité paléogéographique au Paléozoïque inférieur.

Le volcanisme d'arc insulaire représente un témoin important dans la reconstruction de l'évolution géodynamique de la marge nord-ouest américaine et plus particulièrement au Permien. Les corrélations stratigraphiques, la distribution des phases tectoniques ainsi que l'examen pétrographique et géochimique du volcanisme contemporain dans des zones clés telles les Klamath orientales, les Blue Mountains et la Sierra Nevada ont pu permettre de retracer des frontières de microplaques avant la constitution du bloc américano-mexicain. En outre, l'existence de sutures ophiolitiques permienues dans la Central Belt de la Sierra Nevada et des formations de Havallah-Pumpnickel dans le Nevada révèle la présence d'anciens domaines océaniques entre les différents segments d'arcs insulaires.

#### 2) Géologie structurale.

Le massif de Trinity comprend une nappe de péridotites mantellaires de 2750Km<sup>2</sup> et une séquence crustale mince en affleurements discontinus. La structure du massif suggère qu'il résulte d'une accréation océanique très lente. L'accent a été mis sur les relations pétrologiques et structurales entre les péridotites et trois affleurements de cumulats gabbroïques (Castle Lake, Toad Lake et Tamarack Lake). Ces affleurements constituent des chambres magmatiques de petite taille (1 km de diamètre) intrusives dans la péridotite mantellaire. Au sein des péridotites mantellaires présentes à Toad Lake, des lentilles feldspathiques se rassemblent en filons gabbroïques. L'orientation moyenne de ces filons est proche de celle des filons de diabase dans la chambre magmatique et sub-parallèle à la direction du flux mantellaire dans la péridotite. Au contact de la base de la chambre, ces filons bréchifient la péridotite et alimentent les premiers niveaux de cumulats lités. Les chambres magmatiques de Trinity peuvent être ainsi alimentées par la fusion partielle de la péridotite associée.

### 3) Activité magmatique.

a) L'étude de l'évolution des éléments traces en roches totales (cumulats de Gray Rock, filons de Toad lake) dans les chambres magmatiques met en évidence une évolution rapide du magma vers un système clos au cours duquel l'évolution de la densité des magmas contrôle les émissions volcaniques.

b) Des bilans de masse effectués à l'aide des éléments majeurs permettent d'estimer à 20% le taux de fusion partielle d'une lherzolite non plagifère pour produire les roches de la séquence ophiolitique de Trinity. La présence de lherzolites plagifères sur le terrain correspond soit à des phénomènes d'imprégnation magmatique soit à des "fenêtres" de péridotites mantellaires fertiles.

c) L'étude des minéraux des péridotites mantellaires et des enclaves de ces péridotites aux parois et planchers des chambres magmatiques a permis de rendre compte des modifications chimiques considérables que subissent les magmas primaires en percolant lentement au sein du manteau supérieur. Ce phénomène peut être assimilé à un véritable "fractionnement mantellique". De tels magmas modifiés chimiquement sont à l'origine de la diversité des ordres de cristallisation observés dans les complexes ophiolitiques voir au sein d'un même complexe ophiolitique (chambres de Gray Rock et Castle lake).

d) La présence d'un magma parent saturé en silice évoluant rapidement dans un système clos a produit de petits volumes (<5%) de magmas acides (plagiogranites) par cristallisation fractionnée de hornblende magmatique.

### 4) Hydrothermalisme.

a) L'étude de l'évolution des paragenèses minérales montre un métamorphisme prograde vers la base de la séquence ophiolitique (avec un maximum au toit de la chambre magmatique) et un métamorphisme rétrograde au cours du temps. La préservation de minéraux très sensibles au métamorphisme comme les céladonites et les adulaires suggère que l'information minéralogique et géochimique contenue dans ce complexe ophiolitique n'a pas été modifiée par un métamorphisme postérieur.

b) Le calcul de flux chimiques élémentaires pour les éléments majeurs (à partir de la connaissance des réactions minéralogiques, la composition chimique des reliques de minéraux primaires et les équations composition-volume de Gresens) a permis de quantifier les transferts chimiques sur roche totale au cours de l'altération hydrothermale.

c) L'intégration des courbes de flux chimiques sur la séquence ophiolitique définit les dimensions du système hydrothermal (les courbes convergent vers les échanges nuls à la transition cumulates mafiques-ultramafiques vers la base de la séquence) ainsi que l'établissement d'un bilan géochimique entre la paléocroûte océanique et l'hydrosphère. Ainsi il apparaît que les flux en Mg et en Na sont susceptibles d'équilibrer les apports des rivières. Une comparaison avec le site 504B dans la ride à expansion rapide de l'Est Pacifique (données de Alt et Emmermann, 1985) suggère que le modèle de ride lente représenté par l'ophiolite de Trinity favorise une activité hydrothermale intense par une durée de vie plus longue du système hydrothermal favorisée par un stade tardif de fracturation.

d) Le budget du K apporté par les rivières est partiellement équilibré au cours du métamorphisme océanique hors-axe de basse température ("oceanic weathering") avec la production de céladonites et adulaires.

L'état d'oxydation de Fe qui évolue jusqu'à un rapport  $Fe^{3+}/Fe_T = 0,3$  pour l'ensemble de la croûte est principalement contrôlé par la formation d'épidote particulièrement riche en Fe dans la partie supérieure de la croûte océanique ( $Ps = 25-28$ ). La variation des rapports  $Fe^{3+}/Fe_T$  qui augmentent depuis le sommet de la croûte océanique jusqu'à l'interface laves en coussins-complexe filonien pour diminuer régulièrement jusqu'à la base de la croûte océanique est un marqueur de l'état de perméabilité de la croûte océanique et de la difficulté pour les fluides hydrothermaux à circuler et à oxyder les couches profondes de la croûte océanique.

L'Al est mobile au sein de la croûte océanique au cours de l'activité hydrothermale sans correspondre à un échange avec l'océan. La capture du Mg par les roches hydrothermalisées est à l'origine de fluides de  $Ph < 4$  (températures  $\geq 250^\circ C$ ) responsables de la mobilité de l'Al au cours de l'albitisation du plagioclase et de la chloritisation de l'actinote.

Le Ti est un élément généralement admis comme immobile au cours des phénomènes d'altération (Pearce et Cann, 1973; Floyd et Winchester, 1975; Tarney et al., 1977; Sivell et Rankin, 1982). La classification des complexes ophiolitiques dans des sites géotectoniques variés (océan ouvert, bassin marginal et arcs) repose principalement sur la concentration en Ti des laves (Miyashiro et Shido, 1975; Bébien, 1980; Serri, 1981; Ohnenstetter, 1982). L'étude des concentrations en Ti dans les basaltes hydrothermalisés suggère la plus grande prudence quant à l'utilisation des teneurs en Ti comme marqueurs pétrogénétiques décisifs. Alt et Emmermann (1985) ont constaté dans certains basaltes hydrothermalisés du site 504B une tendance à perdre du Ti au cours de l'hydratation de ces roches. Une étude minéralogique et de bilan de masses révèle que la transformation des oxydes ferro-titanés en sphène se produit en système ouvert pour Ti; ainsi la production de 2% de sphène est susceptible d'appauvrir la roche initiale de 0.4% en Ti. Le Ti ainsi libéré se retrouve dans les palagonites (jusqu'à 5% de Ti) en remplacement du verre basaltique lors de l'altération de basse température. La présence de telles argiles explique également certaines anomalies positives en Ti dans des basaltes hydrothermalisés indépendamment des processus magmatiques. En effet l'altération de 10% de verre basaltique en palagonite permet de récupérer le Ti fourni par la transformation de 2% d'ilménite en sphène.

e) L'étude isotopique du Sr sur 25 échantillons de la séquence ophiolitique confirme une altération hydrothermale intense avec de l'eau de mer principalement dans la partie supérieure de la croûte océanique (basaltes et complexe filonien; rapports eau-roche autour de 8) avec un maximum dans les gabbros isotropes au toit de la chambre magmatique (rapports eau-roche jusqu'à 16) pour rapidement décroître dans les cumulats (rapports eau-roche  $\leq 1$ ), mafiques et ultramafiques (rapports eau-roche  $\ll 1$ ). La corrélation entre les courbes de flux pour Mg et Na et la courbe des rapports eau-roche (rapports massiques intégrés sur le temps) confirme l'importance de la circulation d'eau marine au sein de la croûte océanique pendant toute la durée du système hydrothermal. Ainsi, le magnésium est capturé par les basaltes hydrothermalisés à haute température (magnésio-hornblende  $\approx 500-600^\circ\text{C}$  puis actinote  $\approx 350^\circ\text{C}$ ) et à plus basse température (chlorite  $\approx 200^\circ\text{C}$ ).

f) L'étude isotopique de l'oxygène en s'appuyant sur les résultats précédents (isotopes du Sr et flux chimiques élémentaires) et l'acquisition de données microthermométriques sur inclusions fluides primaires dans des quartz secondaires ont révélé la complexité de l'activité hydrothermale qui a affecté l'ophiolite de Trinity. La distribution complexe des valeurs de  $\delta^{18}\text{O}$  dans la séquence lithologique résulte du bilan des échanges isotopiques entre croûte océanique et eau de mer au cours du temps. Ainsi le profil isotopique en oxygène résulte de la superposition d'événements hydrothermaux successifs de plus basse température.

Ce bilan révèle un enrichissement global en  $^{18}\text{O}$  en faveur de la croûte océanique. Ce processus a été également reconnu dans le complexe ophiolitique de Xigaze (Tibet, Chine, Agrinier et al., 1988) et semble affecter les domaines océaniques engendrés dans les rides à expansion lente. Un tel modèle doit être opposé à celui des rides à expansion rapide illustré par le complexe ophiolitique de Semail (Oman) dans lequel l'enrichissement des parties supérieures (laves et complexe filonien) de la croûte océanique balance l'appauvrissement des parties inférieures (gabbros isotropes et cumulats, Gregory et Taylor, 1981). Ces auteurs proposent que le  $\delta^{18}\text{O}$  de l'océan est tamponné par l'échange isotopique entre l'eau de mer et la croûte océanique.

La perturbation de cette balance isotopique en oxygène prédite par Gregory et Taylor pour la croûte océanique produite à l'aplomb des rides à expansion lente peut s'expliquer par le développement latéral et profond d'un réseau de failles normales jouant un rôle prépondérant dans la circulation de fluides hydrothermaux de moyenne ou basse température dans la région off-axis de la croûte océanique. La croûte océanique intensément métamorphisée est ainsi enrichie en  $^{18}\text{O}$  aux dépens du réservoir océanique.

La croûte océanique subit ainsi un vieillissement géochimique et isotopique au fur et à mesure qu'elle s'éloigne de la zone axiale et qu'elle se dirige vers les zones de subduction. Ainsi les complexes ophiolitiques représentant des fragments de lithosphère océanique "échoués" sur les continents apparaissent comme les objets appropriés pour établir des bilans géochimiques entre la croûte océanique et l'hydrosphère, mais aussi pour connaître la nature et la variabilité des roches recyclées dans le manteau supérieur via les processus de subduction.

La mise en évidence de la circulation d'eau de mer dans les niveaux profonds de la croûte océanique (flux chimiques élémentaires, Sr et O) confirme l'importance de l'altération hydrothermale de la couche 3 dans la balance du budget de Fe, Mg et Si et de la composition

des fluides hydrothermaux ascendants qui viennent se mélanger dans le réservoir d'eau de mer "pure" susjacent.

L'intervention simultanée de méthodologies indépendantes (données microthermométriques sur inclusions fluides afin de contraindre les températures et isotopes du Sr pour les rapports eau-roche) conduit à estimer la composition isotopique en  $\delta^{18}\text{O}$  de l'océan silurien ( $\delta^{18}\text{O} = 0 \pm 1$ ) qui se révèle voisine de la valeur actuelle (SMOW = 0). Cette nouvelle information offre un jalon supplémentaire dans la connaissance d'une possible évolution séculaire de la composition isotopique en oxygène de l'océan mondial.

g) La comparaison des données minéralogiques et isotopiques (Sr et O) entre le complexe ophiolitique de Trinity (interprété comme un bassin marginal ou un domaine océanique limité produit à l'aplomb d'une ride à expansion lente) et les séries volcaniques du Copley (son arc rémanent d'après Brouxel et al., 1988) suggère les différences de mécanismes de l'altération hydrothermale au sein d'un arc insulaire et d'une croûte océanique. En effet, l'altération hydrothermale qui affecte une séquence océanique produit des profils de flux chimiques et de compositions isotopiques qui sont directement liés à la structuration interne de la croûte océanique (porosité-perméabilité, géométrie des chambres magmatiques, vieillissement et refroidissement de la croûte océanique). Contrastant avec ce modèle, l'altération hydrothermale qui affecte l'arc insulaire de Copley est caractérisé par de très grandes variations de l'intensité du métamorphisme sur de courtes distances au sein d'un édifice volcanique massif et non structuré. Localement, l'altération hydrothermale peut être très intense avec des rapports eau-roche atteignant fréquemment 30. A l'encontre du complexe ophiolitique de Trinity, l'arc du Copley présente des dépôts métallifères exploitables.

Ainsi, non seulement l'étude des magmas peut renseigner sur le site probable dans lequel se sont mis en place les complexes ophiolitiques mais également la connaissance des modalités de l'altération hydrothermale par l'eau de mer peut permettre de lever l'ambiguïté entre les ophiolites mises en place dans un bassin océanique et celles considérées comme des "ophiolites d'arc".

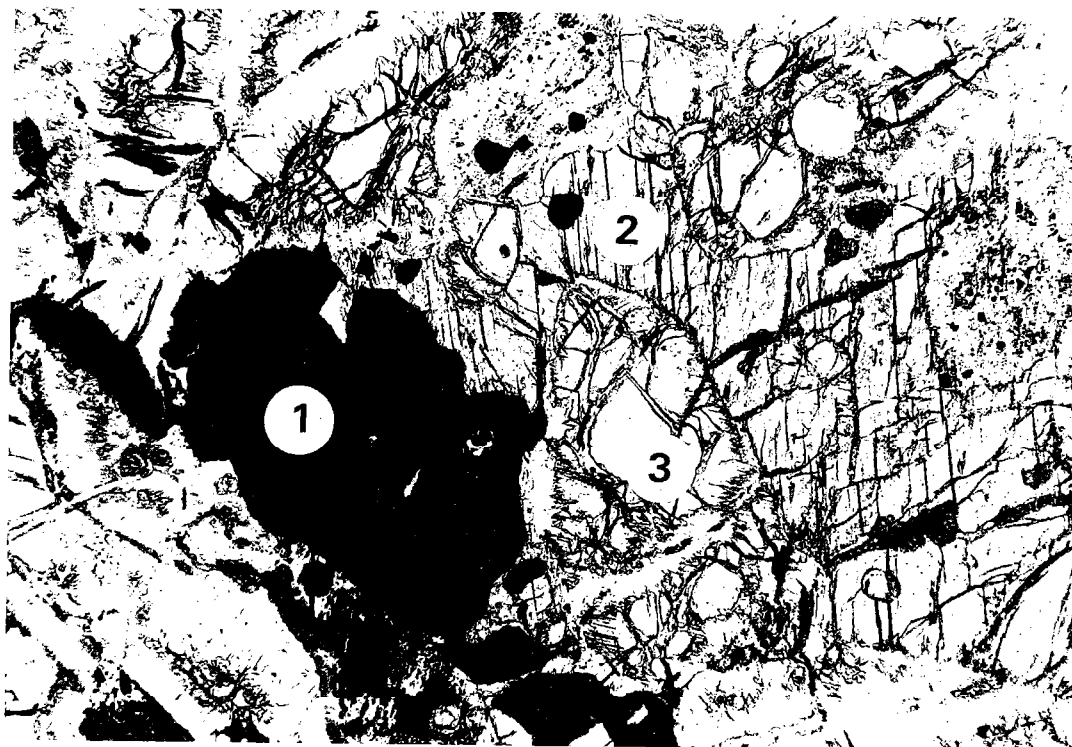


**Microphotographies en lumière transmise des xénolites  
mantelliques de la chambre magmatique de Castle Lake.  
(ophiolite de Trinity).**

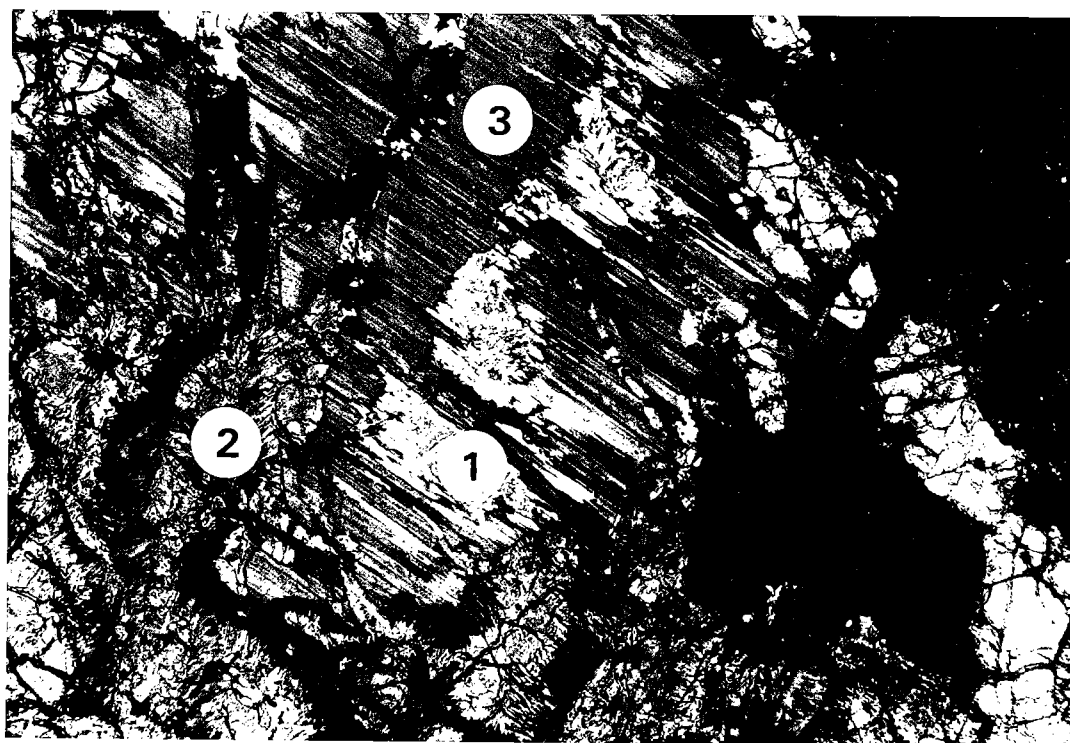
Figure A : spinelle secondaire (1) au contact d'une hornblende pargasitique  
(2) englobant un cristal d'olivine (3).

Figure B : talc magnésien (1) et olivine secondaire (2) en remplacement d'un  
orthopyroxène serpentinisé (3).





0,1mm

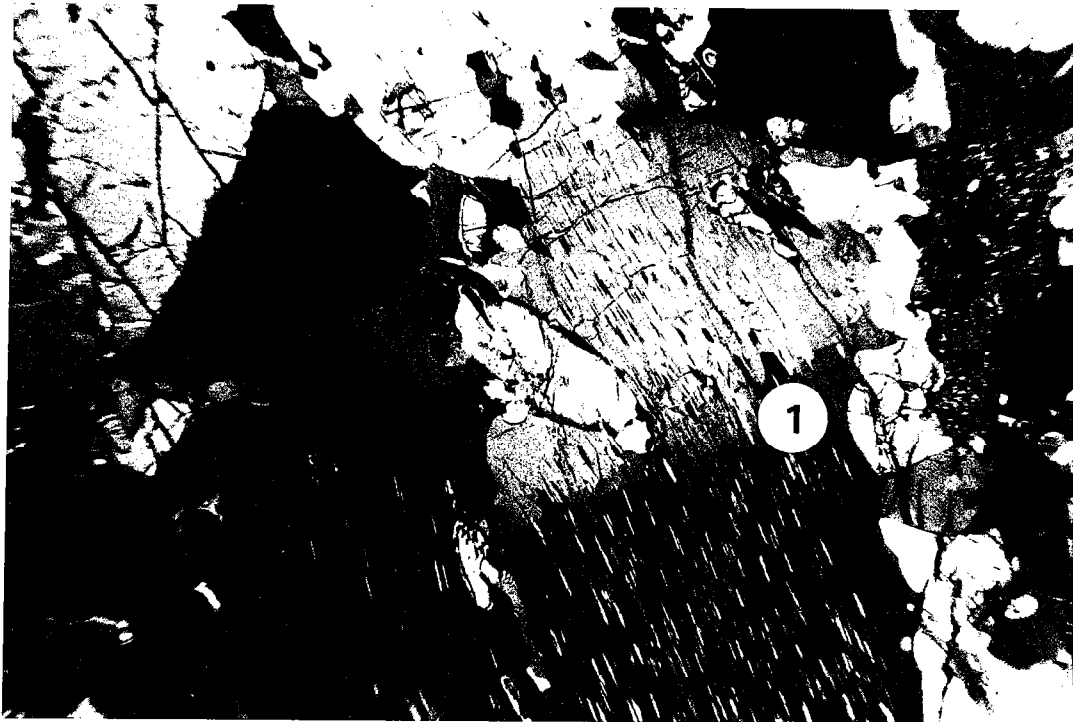


50μm

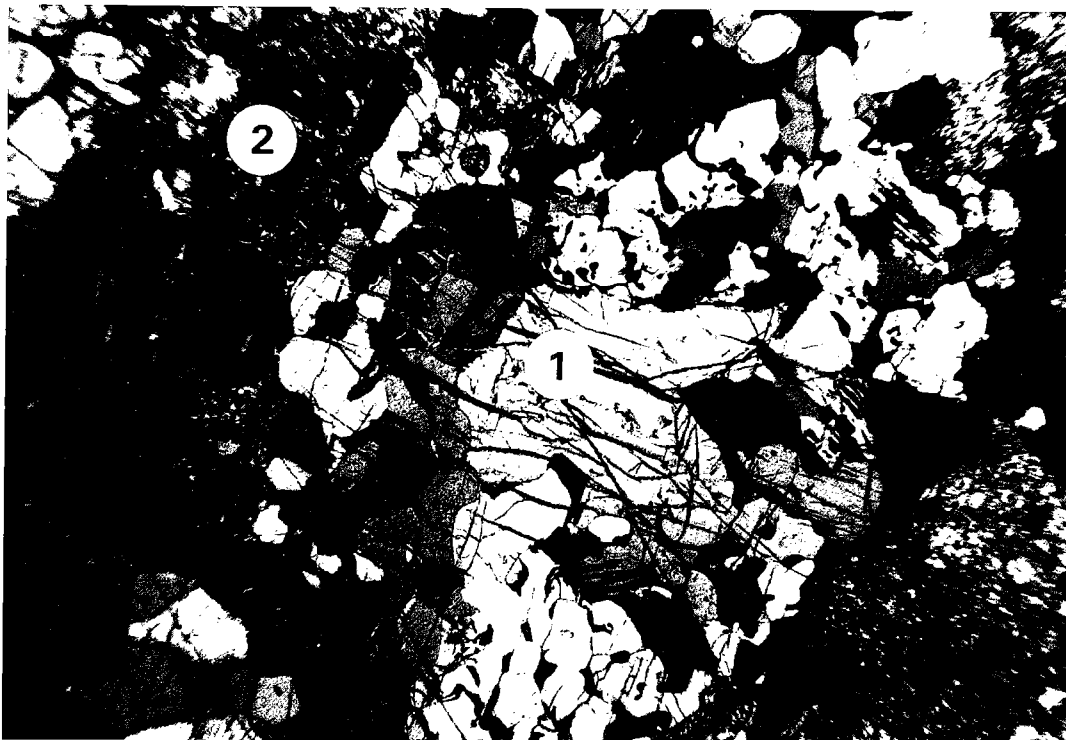
**Microphotographies en lumière transmise des xénolites  
mantelliques de la chambre magmatique de Toad Lake.  
(ophiolite de Trinity).**

Figure C : orthopyroxène avec bandes de pliage (1) et lamelles d'exsolution de clinopyroxène dans le coeur d'une enclave de lherzolite mantellaire centimétrique.

Figure D : xénolite de lherzolite mantellaire (1) inclus dans un cumulat gabbronorite à ilménite (2).



0,25mm

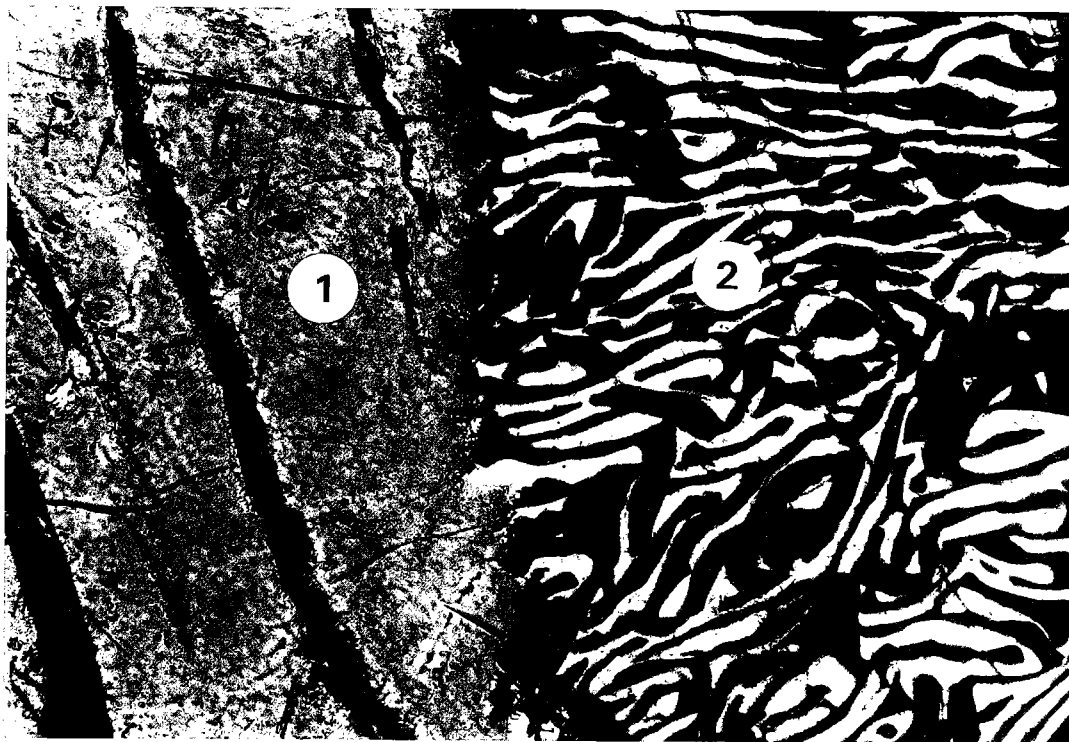
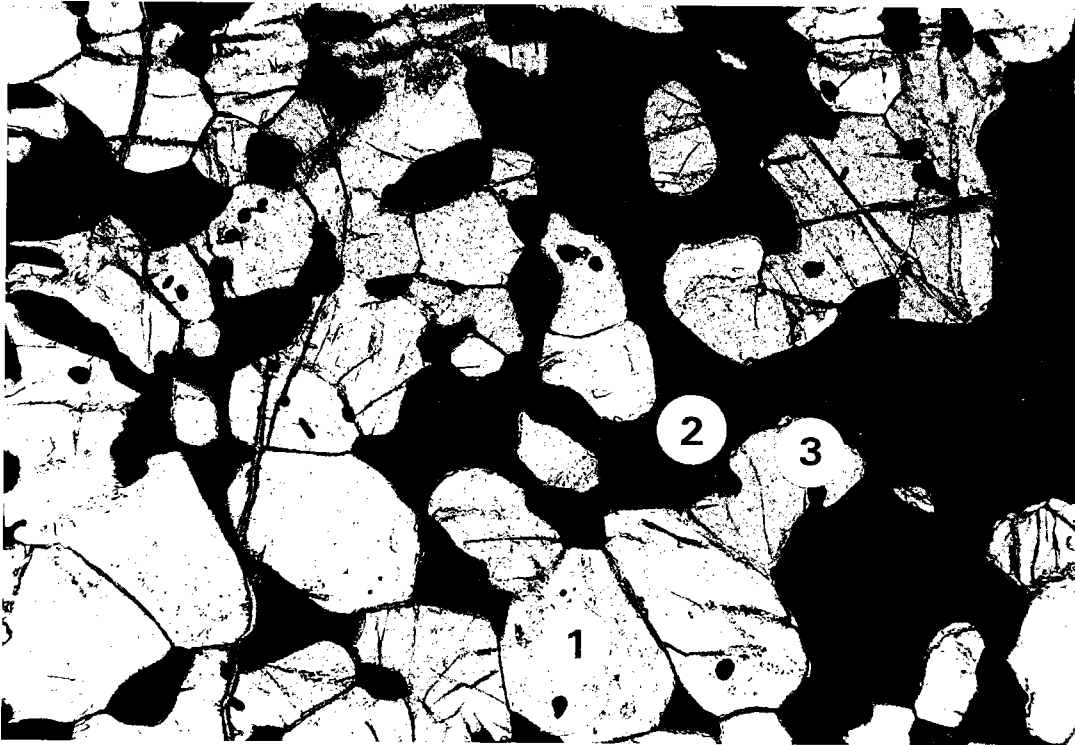


0,25mm

**Microphotographies en lumière transmise des xénolites  
mantelliques de la chambre magmatique de Toad Lake.  
(ophiolite de Trinity).**

Figure E : grains polygonaux d'orthopyroxène (1) et magnétite (2)  
intergranulaire en remplacement partiel ou complet d'olivine (3).

Figure F : déstabilisation d'olivine (1) en symplectite de fins vermicules  
d'orthopyroxène et de magnétite (2).



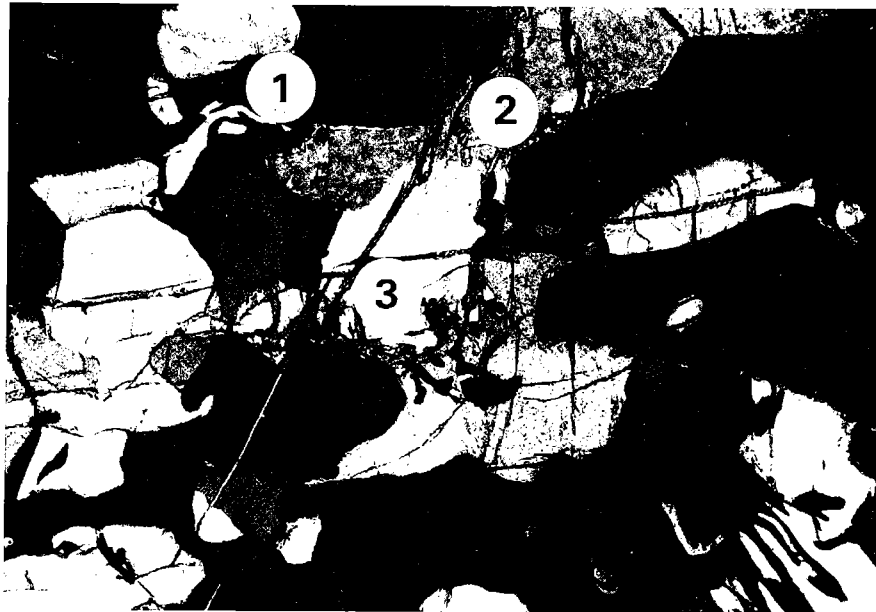
**Microphotographies en lumière transmise des xénolites  
mantelliques de la chambre magmatique de Toad Lake.  
(ophiolite de Trinity).**

Figure G : Développement de la texture symplectite orthopyroxène - magnétite  
(1) aux dépens de l'olivine primaire (2).

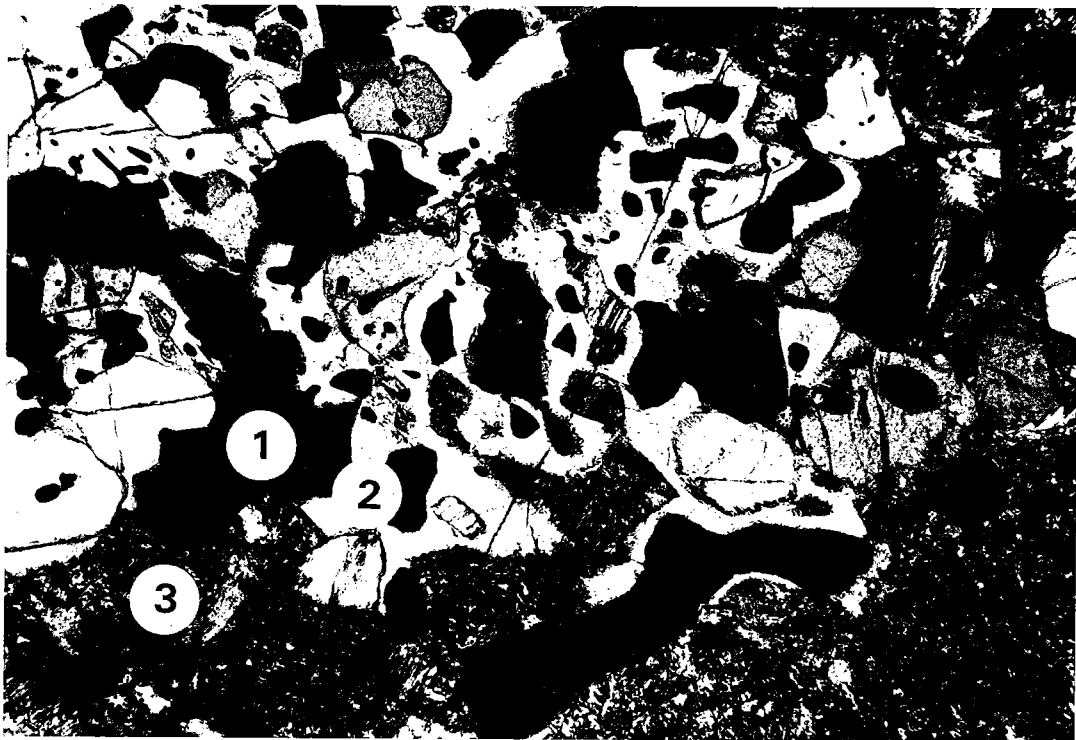
Figure H : réaction coronitique en bordure d'enclave mantellique :

magnétite (1) + plagioclase ———> magnésio-hornblende (2).

Le plagioclase est altéré postérieurement en épidote et albite (3).



0,1mm



0,1mm

**Microphotographies en lumière transmise des filons de  
plagiogranites de la chambre de Gray Rock.  
(ophiolite de Trinity).**

Figure I : texture myrmékitique : association étroite de lamelles de quartz (1) et plagioclase (2).

Figure J : Développement de la texture myrmékitique quartz - plagioclase (1).  
Quartz hypidiomorphe (2) et plagioclase albitisé et séricité (3).





0,1mm



0,1mm

## REMERCIEMENTS

Ce mémoire de thèse est le résultat de 2 ans et demi de travail financé par une allocation de recherche M. R. T. qui m'a été attribuée par l'Académie de Nancy-Metz à la suite du D. E. A. que j'ai effectué à l'Université de Nancy I sous la direction de **H. Lapierre**. Je la remercie vivement pour m'avoir permis l'accès à la géologie des Klamath orientales (Californie) et plus particulièrement au complexe ophiolitique de Trinity qui a servi d'objet de travail au cours de cette thèse. M<sup>lle</sup> H. Lapierre a ainsi largement contribué à ma connaissance générale du terrain et a su me mettre en contact avec des chercheurs américains et français et me faciliter l'approche géologique indispensable en tant que base fondamentale pour toute étude géochimique. Je tiens à remercier également le Professeur **G. Rocci** pour m'avoir accueilli dans son laboratoire pendant la première partie de ma thèse que j'ai effectuée au laboratoire de pétrologie cristalline de l'Université de Nancy I.

J'ai beaucoup apprécié l'encadrement scientifique et les conseils du Professeur **F. Albarède** dans le domaine de l'hydrothermalisme océanique fossile qui représente de loin la partie la plus importante de ce travail. Monsieur F. Albarède a su me guider dans le domaine de l'application des méthodes quantitatives et je lui dois de m'avoir orienté vers le laboratoire de Géochimie et Géochronologie du Professeur **B. M. Jahn** à Rennes où j'ai fini ma thèse sous la direction du Professeur **S. Fourcade**. Je remercie vivement ce dernier pour sa patience lors de mon apprentissage de la théorie et de la technique des isotopes stables. Je lui suis particulièrement reconnaissant pour sa disponibilité de chaque instant et les nombreuses discussions scientifiques qui ont porté sur l'interprétation de nos données. Je tiens également à remercier **M. Cannat** pour son encadrement scientifique sur le terrain et mon initiation à la pétrologie structurale des péridotites mantellaires.

Je remercie **A. M. Boullier**, **W. Brown** et **J. L. Zimmermann** du C. R. P. G. de Nancy, le Professeur **J. Bébian** de l'Université d'Orsay, **J.G. Liou** et **R.G. Coleman** de l'Université de Stanford pour les discussions ou collaborations scientifiques diverses.

J'accorde une mention spéciale à **M. Brouxel** pour l'ensemble du travail que nous avons effectué ensemble sur l'ophiolite de Trinity et à la possibilité qu'il m'a donnée d'utiliser les données analytiques acquises lors de sa thèse. Merci également à **P. Nehlig** de l'Université de Brest qui a bien voulu effectuer des analyses microthermométriques sur inclusions fluides.

Je n'oublierai pas les nombreux amis étudiants nancéiens et rennais qui m'ont soutenu moralement pendant la durée de ce travail. Je pense particulièrement à **P. L. Dupont**, **H. Ouazzani**, **P. Rémy** et **O. Rouer** de Nancy. Merci à **J. de Brémond d'Ars** pour son accueil lors de mon arrivée à Rennes et pour ses conseils "informatiques". Merci à **J. L. Bonjour** pour l'utilisation de son programme d'analyses en composantes principales et à **B. Reynard** pour nos discussions scientifiques et ses conseils de "minéralogiste éclairé". Enfin, je remercie **M. H. Fichet-Delavault** pour son aide à la mise en forme des références bibliographiques... Et un clin d'oeil amical à tous ceux qui ont participé de près ou de loin à l'élaboration de ce travail, je leur fais confiance, ils sauront se reconnaître...

Je réserve les deux dernières lignes de ces remerciements tout spécialement à **mes parents** sans lesquels ce travail n'aurait jamais vu le jour.

## RESUME

Le massif ophiolitique de Trinity comprend une nappe de péridotites mantellaires de 2750Km<sup>2</sup> et une séquence crustale mince en affleurements discontinus (<2Km). Il est chevauché par les nappes volcano-sédimentaires d'âge ordovicien à dévonien d'Yreka-Callahan qui correspondent à des dépôts d'îles océaniques associés à une marge continentale. La structure du massif de Trinity suggère qu'il résulte d'une accréation océanique très lente. Les affleurements de gabbros constituent des chambres magmatiques de petite taille (1 km de diamètre) intrusives dans la péridotite mantellaire. Dans ces chambres, le magma évolue rapidement vers un système clos au cours duquel la densité des magmas contrôle les émissions volcaniques. La présence de lherzolites plagifères correspond soit à des phénomènes d'imprégnation magmatique soit à des "fenêtres" de péridotites mantellaires fertiles. L'étude des minéraux de ces péridotites et des enclaves présentes aux parois et planchers des chambres magmatiques rend compte des modifications chimiques considérables que subissent les magmas primaires en percolant lentement au sein du manteau supérieur. De tels magmas modifiés chimiquement contribuent à l'origine de la diversité des ordres de cristallisation observés dans les complexes ophiolitiques.

L'étude de l'activité hydrothermale fossile révèle un métamorphisme prograde vers la base de la séquence ophiolitique et un métamorphisme rétrograde au cours du temps. Le calcul de flux chimiques élémentaires a permis de quantifier les transferts chimiques au cours de l'altération hydrothermale et de définir les dimensions du système hydrothermal ainsi que l'établissement d'un bilan géochimique entre la paléocroûte océanique et l'hydrosphère. L'étude isotopique du Sr précise une altération hydrothermale intense principalement dans la partie supérieure de la croûte océanique avec un maximum dans les gabbros isotropes au toit de la chambre magmatique et pour rapidement décroître dans les cumulats mafiques et ultramafiques. L'étude isotopique de l'oxygène supportée par des données microthermométriques sur inclusions fluides a révélé la complexité de l'activité hydrothermale qui a affecté l'ophiolite de Trinity et permet de discriminer trois phases hydrothermales de température décroissante au cours du temps. Le bilan établi sur la paléocroûte montre un enrichissement global en <sup>18</sup>O aux dépens du réservoir océanique. Ce processus semble affecter les domaines océaniques engendrés dans les rides à expansion lente et peut s'expliquer par le développement latéral et profond d'un réseau de failles normales jouant un rôle prépondérant dans la circulation de fluides hydrothermaux de moyenne ou basse température dans l'histoire hors axe de la croûte océanique. La composition isotopique de l'océan siluro-ordovicien a été estimée à un  $\delta^{18}\text{O} = 0 \pm 1$  et peut indiquer l'absence d'évolution séculaire de la composition en oxygène de l'océan mondial depuis le Paléozoïque inférieur.



# ANNEXES



## **Liste des tableaux (ANNEXES)**

### ***ANALYSES CHIMIQUES DES ROCHES VOLCANIQUES DES SERIES VOLCANO-SEDIMENTAIRES***

***D'YREKA CALLAHAN ..... page 1***

**Tableau 1 : analyses roches totales des roches  
volcano-sédimentaires d'Yreka-Callahan ..... page 2**

**Tableau 2 : analyses roches totales des roches  
volcaniques de la klippe de Copper Peak ..... page 3**

**Tableau 3 : analyses microsonde des clinopyroxènes  
de Gregg Ranch et Duzel Rock ..... page 4,5**

**Tableau 4 : analyses microsonde des clinopyroxènes  
de la klippe de Copper Peak ..... page 6**

**Tableau 5 : analyses microsonde des amphiboles  
de Negro Gulch ..... page 7**

***ANALYSES CHIMIQUES DE L'OPHIOLITE DE TRINITY  
CHAMBRE MAGMATIQUE DE GRAY ROCK ..... page 8***

**Tableau 6 : analyses roches totales de l'ophiolite  
de Trinity (Gray Rock) ..... pages 9 à 12**

**Tableau 7 : analyses isotopiques du Sr et du Nd  
de l'ophiolite de Trinity ..... page 13**

**Tableau 8 : analyses isotopiques de l'oxygène  
de l'ophiolite de Trinity ..... page 14**

**Tableau 9 : analyses microsonde des olivines  
de Gray Rock ..... page 15**

|  |               |
|--|---------------|
| Tableau 10 : analyses microsonde des pyroxènes<br>de Gray Rock .....   | page 16       |
| Tableau 11 : analyses microsonde des spinelles<br>de Gray Rock .....   | page 17       |
| Tableau 12 : analyses microsonde de titanomagnétites et<br>et ilménites de l'ophiolite de Trinity :<br>Gray Rock (GR), Castle Lake (CL)<br>et Toad Lake (TD) ..... | pages 18, 19  |
| Tableau 13 : analyses microsonde des amphiboles<br>de Gray Rock .....  | pages 21 à 23 |
| Tableau 14 : analyses microsonde des épidotes<br>de Gray Rock .....  | pages 24 à 26 |
| Tableau 15 : analyses microsonde des chlorites<br>de Gray Rock .....   | page 27       |
| <br><i>ANALYSES CHIMIQUES DE L'OPHIOLITE DE TRINITY<br/>CHAMBRES MAGMATIQUES<br/>DE TOAD LAKE ET CASTLE LAKE .....</i>   |               |
| <i>page 28</i>   |               |
| Tableau 16 : analyses roches totales de l'ophiolite<br>de Trinity (Castle Lake et Toad Lake) .....   | page 29       |
| Tableau 17 : analyses microsonde des olivines<br>de Toad Lake et Castle Lake .....   | pages 30 à 32 |
| Tableau 18 : analyses microsonde des clinopyroxènes<br>de Toad Lake et Castle Lake .....   | pages 33, 34  |
| Tableau 19 : analyses microsonde des orthopyroxènes<br>de Toad Lake et Castle Lake .....   | pages 35 à 37 |
| Tableau 20 : analyses microsonde des plagioclases<br>de Toad Lake et Castle Lake .....   | page 38       |



|  |         |
|--|---------|
| Tableau 21 : analyses microsonde des spinelles<br>de Toad Lake .....   | page 39 |
| Tableau 22 : analyses microsonde des spinelles<br>de Castle Lake .....   | page 40 |
| Tableau 23 : analyses microsonde des amphiboles<br>de Toad Lake et Castle Lake .....                                   | page 41 |
| Tableau 24 : analyses microsonde des épidotes, serpentines,<br>chlorites et talcs<br>de Toad Lake et Castle Lake ..... | page 42 |



ANALYSES CHIMIQUES DES ROCHES  
VOLCANIQUES  
DES SERIES VOLCANO-SEDIMENTAIRES  
D'YREKA-CALLAHAN.  
(CHAPITRE 1)

| Echantillons | H 11  | H 12  | H 15  | H 16  | H 17  | BO 9  | BO 13 | BO 15 | DR3A  | DR3B  | DR3C  | DR 4  | DR5A  | DR5B  | DR7   | GR10  | GR12  | GR13  | GR16  | GR19   | GR21  |
|--------------|-------|-------|-------|-------|-------|-------|-------|-------|-------|-------|-------|-------|-------|-------|-------|-------|-------|-------|-------|--------|-------|
| SiO2         | 50,73 | 49,84 | 80,40 | 78,96 | 77,27 | 59,68 | 49,47 | 46,40 | 47,05 | 43,19 | 44,08 | 42,78 | 45,24 | 45,36 | 45,32 | 57,51 | 55,08 | 56,90 | 51,85 | 49,02  | 53,73 |
| TiO2         | 0,61  | 1,44  | 0,23  | 0,23  | 0,11  | 0,60  | 2,16  | 2,14  | 2,49  | 2,80  | 2,24  | 3,08  | 3,02  | 2,81  | 3,17  | 0,55  | 0,61  | 0,65  | 0,49  | 0,55   | 0,50  |
| Al2O3        | 10,17 | 16,05 | 9,70  | 9,38  | 11,10 | 14,05 | 13,88 | 13,34 | 14,21 | 11,92 | 14,01 | 13,09 | 12,93 | 12,79 | 13,82 | 15,79 | 15,76 | 16,11 | 15,79 | 16,80  | 15,84 |
| Fe2O3        | 9,13  | 12,46 | 2,00  | 3,48  | 2,94  | 8,95  | 11,47 | 13,60 | 12,67 | 13,62 | 13,33 | 13,42 | 13,25 | 13,49 | 16,67 | 6,68  | 7,53  | 6,02  | 6,64  | 7,71   | 6,06  |
| MgO          | 11,53 | 5,78  | 0,20  | 0,62  | 1,03  | 3,31  | 5,86  | 5,54  | 4,23  | 4,58  | 5,16  | 5,35  | 4,76  | 4,40  | 5,96  | 5,24  | 5,77  | 5,07  | 6,86  | 7,61   | 6,05  |
| MnO          | 0,18  | 0,20  | 0,04  | 0,05  | 0,05  | 0,18  | 0,20  | 0,21  | 0,18  | 0,19  | 0,19  | 0,19  | 0,19  | 0,20  | 0,19  | 0,16  | 0,15  | 0,15  | 0,16  | 0,15   | 0,15  |
| CaO          | 5,52  | 4,24  | 0,13  | 0,22  | 0,07  | 2,85  | 8,09  | 10,38 | 10,66 | 12,31 | 10,57 | 10,73 | 10,41 | 10,24 | 5,78  | 5,00  | 5,97  | 4,61  | 9,80  | 10,04  | 7,54  |
| Na2O         | 1,05  | 5,45  | 5,65  | 4,69  | 5,10  | 4,53  | 4,89  | 4,23  | 3,42  | 3,35  | 3,61  | 3,94  | 3,96  | 4,00  | 2,71  | 5,72  | 5,79  | 7,18  | 4,34  | 3,94   | 6,12  |
| K2O          | 0,57  | 0,17  | 0,09  | 0,32  | 0,35  | 1,00  | 0,56  | 0,14  | 0,57  | 0,59  | 0,68  | 0,53  | 0,59  | 0,54  | 0,53  | 0,26  | 0,08  | 0,09  | 0,07  | 0,06   | 0,23  |
| P.F.         | 9,98  | 4,20  | 0,96  | 1,47  | 1,57  | 4,73  | 2,86  | 3,84  | 4,41  | 6,94  | 5,82  | 6,66  | 5,23  | 5,45  | 5,57  | 2,91  | 3,17  | 2,75  | 3,68  | 4,24   | 3,66  |
| Total        | 99,47 | 99,93 | 99,40 | 99,42 | 99,59 | 99,88 | 99,44 | 99,82 | 99,89 | 99,49 | 99,69 | 99,77 | 99,58 | 99,28 | 99,72 | 99,82 | 99,91 | 99,51 | 99,68 | 100,12 | 99,98 |
| Cr           | 681   | 149   | 10    | 10    | 12    | 52    | 258   | 129   | 157   | 56    | 134   | 93    | 71    | 64    | 119   | 111   | 123   | 219   | 276   | 267    | 214   |
| Ni           | 129   | 95    | 16    | 14    | 14    | 221   | 112   | 77    | 80    | 72    | 90    | 86    | 90    | 81    | 100   | 62    | 70    | 69    | 92    | 83     | 82    |
| V            | 213   | 247   | 10    | 10    | 0     | 276   | 320   | 338   | 288   | 336   | 323   | 330   | 323   | 318   | 375   | 210   | 236   | 235   | 222   | 267    | 267   |
| Nb           | 2     | 4     | 3     | 2     | 4     | 1     | 9     | 8     | 19    | 22    | 16    | 26    | 26    | 25    | 20    | 0     | 1     | 1     | 1     | 1      | 1     |
| Zr           | 68    | 103   | 60    | 58    | 88    | 60    | 151   | 137   | 164   | 196   | 133   | 221   | 220   | 218   | 187   | 28    | 28    | 34    | 25    | 29     | 25    |
| Y            | 13    | 25    | 19    | 15    | 40    | 10    | 37    | 38    | 32    | 33    | 29    | 36    | 37    | 36    | 40    | 13    | 15    | 15    | 9     | 18     | 11    |
| Sr           | 329   | 194   | 37    | 32    | 22    | 194   | 232   | 113   | 452   | 499   | 456   | 527   | 531   | 487   | 310   | 93    | 27    | 37    | 36    | 27     | 31    |
| Rb           | 9     | 7     | 0     | 5     | 5     | 20    | 16    | 16    | 15    | 16    | 16    | 14    | 14    | 14    | 15    | 5     | 5     | 5     | 8     | 7      | 6     |
| Zr/Nb        | 5,2   | 4,1   | 3,2   | 3,9   | 2,2   | 6     | 4,1   | 3,6   | 5,1   | 5,9   | 4,6   | 6,1   | 5,9   | 6,1   | 4,7   | 2,2   | 1,9   | 2,3   | 2,8   | 1,6    | 2,3   |
| Y/Nb         | 34    | 25,8  | 20    | 29    | 22    | 60    | 16,8  | 17,1  | 8,6   | 8,9   | 8,3   | 8,5   | 8,5   | 8,7   | 9,4   | 2     | 28    | 34    | 25    | 29     | 25    |
| Ti/Nb        | 6,5   | 6,3   | 6,3   | 7,5   | 10    | 10    | 4,1   | 4,8   | 1,7   | 1,5   | 1,8   | 1,4   | 1,4   | 1,4   | 2     | 15    | 15    | 15    | 9     | 18     | 11    |
| Ti/Y         | 1830  | 2160  | 460   | 690   | 165   | 3600  | 1440  | 1605  | 786   | 764   | 840   | 711   | 697   | 674   | 951   | 254   | 3660  | 3900  | 2940  | 3300   | 3000  |
| Ti/Zr        | 282   | 346   | 73    | 92    | 17    | 360   | 350   | 338   | 467   | 509   | 463   | 513   | 490   | 468   | 476   | 118   | 244   | 260   | 327   | 183    | 273   |
|              | 54    | 84    | 23    | 24    | 8     | 60    | 86    | 94    | 91    | 86    | 101   | 84    | 82    | 77    | 102   | 131   | 131   | 115   | 118   | 114    | 120   |
| La           | 11,07 | 7,58  | 3,08  | 3,08  | 7,27  | 7,43  | 5,25  | 5,25  | 17,15 | 19,46 | 19,46 | 19,46 | 19,46 | 19,16 | 18,69 | 0,90  | 0,94  | 1,51  | 1,17  | 1,97   | 0,16  |
| Ce           | 25,39 | 22,80 | 8,12  | 8,12  | 20,54 | 22,36 | 20,53 | 20,53 | 45,15 | 48,08 | 48,08 | 48,08 | 48,08 | 48,69 | 48,32 | 6,11  | 4,77  | 6,14  | 5,24  | 6,72   | 3,16  |
| Nd           | 12,90 | 13,63 | 5,29  | 5,29  | 11,86 | 15,79 | 14,32 | 14,32 | 26,42 | 27,78 | 27,78 | 27,78 | 27,78 | 28,42 | 25,55 | 3,25  | 3,02  | 4,28  | 2,48  | 4,33   | 2,48  |
| Sm           | 3,36  | 4,23  | 1,89  | 1,89  | 4,53  | 5,24  | 5,22  | 5,22  | 7,39  | 7,71  | 7,71  | 7,71  | 7,71  | 7,71  | 7,62  | 1,54  | 1,55  | 1,85  | 1,08  | 1,80   | 1,14  |
| Eu           | 0,87  | 1,29  | 0,53  | 0,53  | 0,94  | 1,64  | 1,76  | 1,76  | 2,49  | 2,54  | 2,54  | 2,54  | 2,54  | 2,53  | 2,52  | 0,53  | 0,55  | 0,73  | 0,45  | 0,62   | 0,33  |
| Gd           | 2,68  | 4,31  | 2,08  | 2,08  | 4,93  | 5,49  | 5,90  | 5,90  | 7,12  | 7,12  | 7,12  | 7,12  | 7,12  | 6,95  | 7,25  | 1,76  | 1,83  | 2,21  | 1,22  | 2,09   | 1,40  |
| Dy           | 2,22  | 4,92  | 2,91  | 2,91  | 6,61  | 6,18  | 7,02  | 7,02  | 6,04  | 6,15  | 6,15  | 6,15  | 6,15  | 6,42  | 7,44  | 2,29  | 2,34  | 2,75  | 1,55  | 2,92   | 1,81  |
| Er           | 1,16  | 2,82  | 2,13  | 2,13  | 4,42  | 3,47  | 4,04  | 4,04  | 2,79  | 2,92  | 2,92  | 2,92  | 2,92  | 3,10  | 3,87  | 1,44  | 1,48  | 1,68  | 0,96  | 1,84   | 1,10  |
| Yb           | 1,19  | 3,01  | 2,88  | 2,88  | 5,47  | 3,75  | 4,39  | 4,39  | 2,47  | 2,80  | 2,80  | 2,80  | 2,80  | 2,87  | 4,08  | 1,55  | 1,72  | 1,81  | 1,16  | 2,11   | 1,23  |
| Lu           | 0,10  | 0,43  | 0,41  | 0,41  | 0,85  | 0,51  | 0,61  | 0,61  | 0,43  | 0,41  | 0,41  | 0,41  | 0,41  | 0,41  | 0,54  | 0,26  | 0,26  | 0,24  | 0,13  | 0,26   | 0,15  |

Tableau 1 : analyses roches totales des roches volcaniques des séries volcano-sédimentaires d'Yreka-Calleahan

| Echantillons | C1    | C4    | C5    | NG3   | NG4   | NG5   | NG8   | NG12  | NG13  | NG14  |
|--------------|-------|-------|-------|-------|-------|-------|-------|-------|-------|-------|
| SiO2         | 54,38 | 65,07 | 48,73 | 66,18 | 62,21 | 48,03 | 49,23 | 43,38 | 51,04 | 52,14 |
| Al2O3        | 16,30 | 14,68 | 18,56 | 17,02 | 17,00 | 17,87 | 15,80 | 12,56 | 17,25 | 15,21 |
| Fe2O3        | 6,78  | 5,61  | 8,70  | 3,11  | 5,08  | 9,58  | 9,54  | 8,20  | 8,79  | 7,97  |
| TiO2         | 0,50  | 0,75  | 0,68  | 0,26  | 0,50  | 0,77  | 0,73  | 0,47  | 0,73  | 0,66  |
| CaO          | 4,74  | 4,83  | 8,17  | 2,10  | 4,45  | 11,24 | 8,58  | 11,90 | 3,15  | 4,98  |
| MgO          | 7,25  | 2,21  | 7,24  | 1,63  | 3,08  | 5,60  | 8,74  | 6,98  | 7,51  | 6,61  |
| MnO          | 0,10  | 0,08  | 0,18  | 0,05  | 0,07  | 0,20  | 0,19  | 0,28  | 0,18  | 0,17  |
| K2O          | 0,05  | 0,57  | 0,11  | 1,57  | 1,09  | 0,23  | 1,64  | 1,09  | 2,33  | 1,55  |
| Na2O         | 6,59  | 4,00  | 3,34  | 5,61  | 4,02  | 2,80  | 2,41  | 0,08  | 0,97  | 1,94  |
| P.F.         | 2,89  | 1,98  | 3,99  | 2,25  | 2,27  | 3,36  | 3,00  | 14,29 | 7,91  | 8,51  |
| Total        | 99,58 | 99,78 | 99,70 | 99,78 | 99,77 | 99,68 | 99,86 | 99,23 | 99,86 | 99,74 |
| Nb           | 1     | 1     | 1     | 3     | 4     | 1     | 3     | 1     | 4     | 2     |
| Zr           | 26    | 41    | 35    | 102   | 102   | 48    | 57    | 43    | 99    | 86    |
| Y            | 16    | 22    | 21    | 8     | 13    | 17    | 19    | 13    | 18    | 15    |
| Sr           | 85    | 68    | 32    | 298   | 398   | 717   | 170   | 48    | 41    | 52    |
| Rb           | 2     | 14    | 7     | 35    | 21    | <1    | 44    | 29    | 59    | 48    |
| Ni           | 58    | 29    | 67    | 16    | 36    | 42    | 112   | 240   | 46    | 56    |
| Cr           | 100   | <10   | 78    | <10   | 102   | 34    | 402   | 766   | 144   | 207   |
| V            | 206   | 274   | 262   | 1     | 76    | 249   | 239   | 203   | 173   | 174   |
| Zr/Nb        | 26    | 41    | 35    | 34,0  | 25,5  | 48,0  | 19,0  | 43,0  | 24,8  | 43,0  |
| Zr/Y         | 1,6   | 1,8   | 1,6   | 12,8  | 7,8   | 2,8   | 3,0   | 3,3   | 5,5   | 5,7   |
| Y/Nb         | 16    | 22    | 21    | 2,7   | 3,3   | 17,0  | 6,3   | 13,0  | 4,5   | 7,5   |
| Ni/Cr        | 0,6   |       | 0,8   |       | 0,4   | 1,2   | 0,3   | 0,3   | 0,3   | 0,3   |
| Ti/Zr        | 115,4 | 109,7 | 116,6 | 15,3  | 29,4  | 96,3  | 76,8  | 65,6  | 44,2  | 46,0  |

Tableau 2 : analyses roches totales des roches volcaniques de la klippe de Copper Peak.



## Echantillons

## DR3A

|       |        |        |        |        |        |        |         |        |        |        |        |        |        |        |        |        |        |        |        |
|-------|--------|--------|--------|--------|--------|--------|---------|--------|--------|--------|--------|--------|--------|--------|--------|--------|--------|--------|--------|
| Fe2O3 | 7.65   | 8.66   | 7.7    | 7.79   | 7.44   | 7.81   | 7.14    | 7.66   | 7.52   | 7.56   | 7.8    | 7.24   | 7.79   | 7.39   | 11.4   | 9.85   | 9.32   | 8.95   | 9.78   |
| Na2O  | 0.28   | 0.28   | 0.27   | 0.29   | 0.3    | 0.28   | 0.27    | 0.28   | 0.3    | 0.28   | 0.3    | 0.3    | 0.28   | 0.25   | 0.35   | 0.41   | 0.4    | 0.41   | 0.35   |
| K2O   | 0      | 0      | 0      | 0      | 0      | 0      | 0       | 0      | 0      | 0      | 0      | 0      | 0      | 0      | 0      | 0      | 0      | 0      | 0.02   |
| MnO   | 0.22   | 0.13   | 0.07   | 0.21   | 0.19   | 0.12   | 0.18    | 0.16   | 0.29   | 0.15   | 0.16   | 0.17   | 0.14   | 0.13   | 0.29   | 0.2    | 0.37   | 0.3    | 0.28   |
| SiO2  | 51.78  | 49.79  | 52.42  | 52     | 52.49  | 50.54  | 51.57   | 51.86  | 51.34  | 52.28  | 51.58  | 51.33  | 51.11  | 51.64  | 53.64  | 51.89  | 51.76  | 51.52  | 51.53  |
| CaO   | 19.43  | 18.62  | 19.41  | 19.67  | 19.58  | 19.03  | 20.41   | 19.79  | 19.81  | 19.79  | 19.91  | 20.28  | 19.58  | 20.12  | 18.2   | 20.51  | 21.93  | 21.69  | 21.33  |
| Cr2O3 | 0.12   | 0.27   | 0.2    | 0.17   | 0.11   | 0.24   | 0.21    | 0.12   | 0.21   | 0.12   | 0.24   | 0.19   | 0.26   | 0.19   | 0.02   | 0      | 0.07   | 0      | 0.06   |
| Al2O3 | 2.4    | 3.9    | 2.77   | 2.39   | 2.48   | 3.25   | 2.84    | 2.48   | 2.93   | 2.2    | 2.96   | 3.04   | 3.06   | 2.64   | 2.61   | 2.07   | 2.64   | 2.1    | 2.59   |
| TiO2  | 0.9    | 1.44   | 0.77   | 0.79   | 0.73   | 1      | 0.95    | 0.88   | 0.98   | 0.72   | 0.92   | 0.96   | 1.03   | 0.93   | 0.38   | 0.29   | 0.33   | 0.35   | 0.54   |
| NiO   | 0.03   | 0      | 0.02   | 0      | 0      | 0.07   | 0       | 0      | 0      | 0      | 0      | 0      | 0      | 0      | 0      | 0      | 0      | 0      | 0      |
| MgO   | 16.53  | 15.88  | 16.78  | 16.59  | 16.64  | 16.53  | 16.1    | 16.51  | 16.39  | 16.93  | 16.29  | 16.43  | 16.27  | 16.32  | 14.36  | 13.94  | 13.46  | 13.83  | 13.79  |
| Total | 99.34  | 99.01  | 99.92  | 99.89  | 99.96  | 99.86  | 99.68   | 99.7   | 99.78  | 99.94  | 100.17 | 99.43  | 99.63  | 99.61  | 101.25 | 99.16  | 100.28 | 99.15  | 100.28 |
| Fe    | 0.2374 | 0.2713 | 0.2373 | 0.2406 | 0.2291 | 0.2439 | 0.2212  | 0.237  | 0.2329 | 0.2332 | 0.2407 | 0.2236 | 0.2418 | 0.2269 | 0.3499 | 0.3101 | 0.2907 | 0.282  | 0.3053 |
| Na    | 0.0201 | 0.0205 | 0.0192 | 0.0207 | 0.0217 | 0.0204 | 0.0195  | 0.0184 | 0.0212 | 0.0208 | 0.0213 | 0.0216 | 0.0212 | 0.018  | 0.0246 | 0.0298 | 0.0298 | 0.0298 | 0.0255 |
| K     | 0      | 0.0012 | 0      | 0      | 0      | 0      | 0       | 0      | 0      | 0      | 0.0006 | 0      | 0      | 0      | 0.0005 | 0      | 0      | 0.0002 | 0.0011 |
| Mn    | 0.007  | 0.004  | 0.0022 | 0.0066 | 0.0059 | 0.0038 | 0.0056  | 0.005  | 0.0091 | 0.0047 | 0.005  | 0.0053 | 0.0043 | 0.0041 | 0.009  | 0.0083 | 0.0115 | 0.0086 | 0.0088 |
| Si    | 1.922  | 1.8643 | 1.9311 | 1.9212 | 1.9315 | 1.888  | 1.9087  | 1.9187 | 1.9078 | 1.9278 | 1.9028 | 1.8968 | 1.8971 | 1.9127 | 1.9683 | 1.9526 | 1.9309 | 1.9408 | 1.9237 |
| Ca    | 0.7728 | 0.747  | 0.768  | 0.7785 | 0.7719 | 0.7618 | 0.8095  | 0.7843 | 0.7859 | 0.7818 | 0.787  | 0.8021 | 0.7788 | 0.7983 | 0.7155 | 0.827  | 0.8767 | 0.8753 | 0.8534 |
| Cr    | 0.0035 | 0.0081 | 0.0059 | 0.005  | 0.0031 | 0.007  | 0.0063  | 0.0034 | 0.0061 | 0.0036 | 0.0069 | 0.0054 | 0.0078 | 0.0057 | 0.0005 | 0      | 0.0021 | 0.0001 | 0.0018 |
| Al    | 0.1049 | 0.1722 | 0.0987 | 0.1042 | 0.1077 | 0.1432 | 0.1238  | 0.1083 | 0.1276 | 0.0957 | 0.1286 | 0.1323 | 0.1337 | 0.1151 | 0.1129 | 0.092  | 0.1159 | 0.0933 | 0.1141 |
| Ti    | 0.0252 | 0.0407 | 0.0214 | 0.0219 | 0.0201 | 0.028  | 0.0285  | 0.0243 | 0.0274 | 0.0189 | 0.0255 | 0.0268 | 0.0288 | 0.0258 | 0.0104 | 0.0082 | 0.0083 | 0.0088 | 0.0152 |
| Ni    | 0.0009 | 0      | 0.0007 | 0      | 0      | 0.0021 | 0       | 0      | 0      | 0      | 0      | 0      | 0      | 0      | 0      | 0      | 0      | 0      | 0      |
| Mg    | 0.8147 | 0.8861 | 0.8218 | 0.8135 | 0.8125 | 0.8205 | 0.888   | 0.9104 | 0.9044 | 0.925  | 0.896  | 0.9049 | 0.9005 | 0.9012 | 0.7852 | 0.7818 | 0.7487 | 0.7766 | 0.7674 |
| Total | 4.0083 | 4.0154 | 4.0044 | 4.0122 | 4.0035 | 4.0187 | 4.00912 | 4.0099 | 4.0153 | 4.0128 | 4.0144 | 4.0184 | 4.0137 | 4.0097 | 3.9768 | 4.016  | 4.015  | 4.0174 | 4.0162 |
| Wo    | 40     | 39.14  | 39.74  | 40.14  | 40.22  | 39.47  | 42.07   | 40.5   | 40.87  | 40.2   | 40.8   | 41.43  | 40.45  | 41.31  | 38.48  | 42.96  | 45.48  | 45.04  | 44.1   |
| En    | 47.35  | 46.43  | 47.93  | 47.11  | 47.54  | 47.7   | 46.15   | 47.01  | 46.8   | 47.57  | 46.48  | 46.74  | 46.77  | 46.63  | 42.22  | 40.81  | 38.84  | 39.66  | 39.66  |
| Fs    | 12.65  | 14.42  | 12.43  | 12.75  | 12.24  | 12.84  | 11.78   | 12.49  | 12.53  | 12.23  | 12.74  | 11.82  | 12.78  | 12.08  | 19.3   | 16.43  | 15.68  | 15     | 16.23  |

## Echantillons

## Upper Peak

|       |        |        |        |        |        |        |        |        |        |        |        |        |        |        |        |        |        |        |        |
|-------|--------|--------|--------|--------|--------|--------|--------|--------|--------|--------|--------|--------|--------|--------|--------|--------|--------|--------|--------|
| Fe2O3 | 3.81   | 3.97   | 3.97   | 3.27   | 3.44   | 2.80   | 2.81   | 2.80   | 2.88   | 2.88   | 2.44   | 3.57   | 3.47   | 3.50   | 5.41   | 4.92   | 4.88   | 4.12   | 2.68   |
| Na2O  | 0.08   | 0.08   | 0.08   | 0.06   | 0.02   | 0.05   | 0.08   | 0      | 0.08   | 0.04   | 0.07   | 0.07   | 0.14   | 0.03   | 0.11   | 0.12   | 0.10   | 0.11   | 0.09   |
| K2O   | 0      | 0      | 0      | 0      | 0.02   | 0.01   | 0      | 0      | 0      | 0      | 0      | 0      | 0.03   | 0      | 0      | 0      | 0      | 0      | 0      |
| MnO   | 0.15   | 0.09   | 0.24   | 0.08   | 0.09   | 0.01   | 0.14   | 0.14   | 0.19   | 0.11   | 0.11   | 0.11   | 0.28   | 0.04   | 0.13   | 0.22   | 0.03   | 0.02   | 0.08   |
| SiO2  | 53.63  | 53.35  | 53.12  | 53.36  | 53.34  | 54.18  | 54.17  | 53.54  | 53.52  | 52.86  | 53.36  | 53.00  | 52.84  | 53.40  | 52.32  | 52.77  | 51.53  | 53.34  | 53.75  |
| CaO   | 21.45  | 21.53  | 21.35  | 21.30  | 21.72  | 21.94  | 21.80  | 21.88  | 21.18  | 21.75  | 21.68  | 21.77  | 21.68  | 21.82  | 20.89  | 20.60  | 21.69  | 21.03  | 21.48  |
| Cr2O3 | 0.16   | 0.09   | 0.07   | 0.15   | 0.28   | 0.38   | 0.31   | 0.51   | 0.64   | 0.39   | 0.80   | 0.47   | 0.51   | 0.33   | 0.08   | 0      | 0.06   | 0.23   | 0.82   |
| Al2O3 | 1.95   | 1.87   | 1.85   | 1.71   | 1.99   | 1.43   | 1.40   | 1.70   | 1.54   | 2.07   | 1.57   | 2.01   | 2.31   | 2.06   | 2.54   | 2.28   | 2.78   | 2.29   | 1.82   |
| TiO2  | 0.03   | 0.14   | 0.17   | 0      | 0.05   | 0      | 0.14   | 0.13   | 0.18   | 0.04   | 0      | 0      | 0.12   | 0.13   | 0.18   | 0.23   | 0.21   | 0.16   | 0.04   |
| NiO   | 0      | 0      | 0.02   | 0      | 0      | 0      | 0      | 0      | 0.02   | 0      | 0.02   | 0.09   | 0.03   | 0      | 0.12   | 0      | 0      | 0      | 0      |
| MgO   | 18.78  | 18.85  | 18.64  | 19.04  | 19.14  | 19.78  | 19.91  | 19.48  | 19.63  | 19.18  | 19.83  | 18.71  | 18.68  | 18.87  | 18.04  | 18.18  | 17.26  | 18.73  | 19.80  |
| Total | 100.04 | 99.97  | 99.48  | 99.95  | 100.09 | 100.55 | 100.62 | 100.19 | 99.66  | 99.31  | 99.77  | 99.78  | 99.88  | 100.19 | 99.83  | 99.32  | 98.55  | 100.03 | 100.38 |
| Fe    | 0.1158 | 0.1208 | 0.1212 | 0.1000 | 0.1042 | 0.0842 | 0.0848 | 0.0848 | 0.0814 | 0.0890 | 0.0742 | 0.1089 | 0.1080 | 0.1060 | 0.1658 | 0.1511 | 0.1515 | 0.1249 | 0.0808 |
| Na    | 0.0055 | 0.0060 | 0.0058 | 0.0041 | 0.0013 | 0.0033 | 0.0053 | 0.0003 | 0.0056 | 0.0029 | 0.0050 | 0.0048 | 0.0101 | 0.0023 | 0.0080 | 0.0083 | 0.0071 | 0.0074 | 0.0063 |
| K     | 0      | 0      | 0      | 0      | 0.0008 | 0.0004 | 0      | 0.0002 | 0      | 0      | 0      | 0      | 0.0012 | 0      | 0      | 0      | 0      | 0      | 0      |
| Mn    | 0.0048 | 0.0028 | 0.0073 | 0.0024 | 0.0028 | 0.0003 | 0.0043 | 0.0043 | 0.0057 | 0.0034 | 0      | 0.0033 | 0.0081 | 0.0012 | 0.0041 | 0.008  | 0.0010 | 0.0008 | 0.0025 |
| Si    | 1.9465 | 1.9404 | 1.9420 | 1.9524 | 1.9348 | 1.9501 | 1.9478 | 1.9370 | 1.9432 | 1.9300 | 1.9360 | 1.9325 | 1.9195 | 1.9355 | 1.9185 | 1.9365 | 1.9138 | 1.9368 | 1.9376 |
| Ca    | 0.8341 | 0.8390 | 0.8362 | 0.8351 | 0.8441 | 0.8459 | 0.8399 | 0.8484 | 0.8240 | 0.8507 | 0.8427 | 0.8508 | 0.8472 | 0.8472 | 0.8209 | 0.8099 | 0.8629 | 0.8178 | 0.8299 |
| Cr    | 0.0047 | 0.0025 | 0.0020 | 0.0042 | 0.0081 | 0.0108 | 0.0088 | 0.0147 | 0.0183 | 0.0112 | 0.0229 | 0.0135 | 0.0146 | 0.0094 | 0.0023 | 0      | 0.0018 | 0.0066 | 0.0178 |
| Al    | 0.0835 | 0.0800 | 0.0797 | 0.0739 | 0.0853 | 0.0607 | 0.0594 | 0.0724 | 0.0681 | 0.0890 | 0.0671 | 0.0882 | 0.0984 | 0.0882 | 0.1098 | 0.0988 | 0.1218 | 0.0981 | 0.0771 |
| Ti    | 0.0007 | 0.0038 | 0.0046 | 0      | 0.0015 | 0      | 0.0039 | 0.0034 | 0.0049 | 0.0011 | 0      | 0      | 0.0034 | 0.0036 | 0.0051 | 0.0064 | 0.0060 | 0.0044 | 0.0010 |
| Ni    | 0      | 0      | 0.0005 | 0      | 0      | 0      | 0      | 0      | 0.0007 | 0      | 0.0006 | 0.0028 | 0.0008 | 0      | 0.0036 | 0      | 0      | 0      | 0      |
| Mg    | 1.0157 | 1.0217 | 1.0156 | 1.0382 | 1.0346 | 1.0599 | 1.0669 | 1.0504 | 1.0623 | 1.0436 | 1.0728 | 1.0172 | 1.0152 | 1.0195 | 0.9958 | 0.9941 | 0.9555 | 1.0135 | 1.0640 |
| Total | 4.0111 | 4.0171 | 4.0150 | 4.0102 | 4.0177 | 4.0157 | 4.0168 | 4.0160 | 4.0122 | 4.0199 | 4.0211 | 4.0197 | 4.0254 | 4.0128 | 4.0238 | 4.0116 | 4.0216 | 4.0101 | 4.0168 |
| Wo    | 42.34  | 42.28  | 42.23  | 42.27  | 42.51  | 42.50  | 42.18  | 42.68  | 41.75  | 42.84  | 42.36  | 42.96  | 42.86  | 42.92  | 41.53  | 41.28  | 43.78  | 41.79  | 41.97  |
| En    | 51.55  | 51.49  | 51.28  | 52.55  | 52.10  | 53.25  | 52.84  | 53.83  | 52.56  | 53.81  | 52.97  | 51.36  | 51.36  | 51.65  | 49.87  | 50.67  | 48.48  | 51.79  | 53.82  |
| Fs    | 6.11   | 6.24   | 6.49   | 5.18   | 5.39   | 4.25   | 4.25   | 4.48   | 4.42   | 4.60   | 3.73   | 5.67   | 5.77   | 5.43   | 8.60   | 7.74   | 6.42   | 6.42   | 4.23   |

Tableau 3 : analyses microsonde des clinopyroxènes de Gregg Ranch et Duzeil Rock

## Echantillons Copper Peak

|       |        |        |        |        |        |        |        |        |        |        |        |        |        |        |        |        |        |        |        |        |        |        |
|-------|--------|--------|--------|--------|--------|--------|--------|--------|--------|--------|--------|--------|--------|--------|--------|--------|--------|--------|--------|--------|--------|--------|
| Fe2O3 | 3,81   | 3,97   | 3,97   | 3,97   | 3,27   | 3,44   | 2,80   | 2,80   | 2,81   | 2,80   | 2,68   | 2,88   | 2,44   | 3,57   | 3,47   | 3,50   | 5,41   | 4,92   | 4,88   | 4,12   | 2,68   | 2,76   |
| Na2O  | 0,08   | 0,08   | 0,08   | 0,08   | 0,06   | 0,02   | 0,05   | 0,05   | 0,08   | 0      | 0,08   | 0,04   | 0,07   | 0,07   | 0,14   | 0,03   | 0,11   | 0,12   | 0,10   | 0,11   | 0,09   | 0,05   |
| K2O   | 0      | 0      | 0      | 0      | 0      | 0,02   | 0,01   | 0,01   | 0      | 0      | 0      | 0      | 0      | 0      | 0,03   | 0      | 0      | 0      | 0      | 0      | 0      | 0      |
| MnO   | 0,15   | 0,09   | 0,24   | 0,08   | 0,08   | 0,09   | 0,01   | 0,01   | 0      | 0,14   | 0,19   | 0,11   | 0      | 0,11   | 0,26   | 0,04   | 0,13   | 0,22   | 0,03   | 0,02   | 0,08   | 0,01   |
| SiO2  | 53,63  | 53,35  | 53,12  | 53,36  | 53,36  | 53,34  | 54,18  | 54,18  | 54,17  | 53,54  | 53,52  | 52,86  | 53,36  | 53,00  | 52,64  | 53,40  | 52,32  | 52,77  | 51,53  | 53,34  | 53,75  | 53,87  |
| CaO   | 21,45  | 21,53  | 21,35  | 21,30  | 21,30  | 21,72  | 21,94  | 21,88  | 21,80  | 21,88  | 21,18  | 21,75  | 21,68  | 21,77  | 21,68  | 21,82  | 20,89  | 20,60  | 21,69  | 21,03  | 21,49  | 21,35  |
| Cr2O3 | 0,16   | 0,09   | 0,07   | 0,15   | 0,15   | 0,28   | 0,38   | 0,38   | 0,31   | 0,51   | 0,64   | 0,39   | 0,80   | 0,47   | 0,51   | 0,33   | 0,08   | 0      | 0,08   | 0,23   | 0,62   | 0,73   |
| Al2O3 | 1,95   | 1,87   | 1,85   | 1,71   | 1,71   | 1,99   | 1,43   | 1,40   | 1,40   | 1,70   | 1,54   | 2,07   | 1,57   | 2,01   | 2,31   | 2,06   | 2,54   | 2,28   | 2,78   | 2,29   | 1,82   | 1,79   |
| TiO2  | 0,03   | 0,14   | 0,17   | 0      | 0      | 0,05   | 0      | 0,14   | 0,14   | 0,13   | 0,18   | 0,04   | 0      | 0      | 0,12   | 0,13   | 0,18   | 0,23   | 0,21   | 0,16   | 0,04   | 0,08   |
| NiO   | 0      | 0      | 0,02   | 0      | 0      | 0      | 0      | 0      | 0      | 0      | 0,02   | 0      | 0,02   | 0,09   | 0,03   | 0      | 0,12   | 0      | 0      | 0      | 0      | 0      |
| MgO   | 18,78  | 18,85  | 18,64  | 19,04  | 19,04  | 19,14  | 19,76  | 19,91  | 19,91  | 19,48  | 19,63  | 19,18  | 19,83  | 18,71  | 18,68  | 18,87  | 18,04  | 18,18  | 17,26  | 18,73  | 19,80  | 19,79  |
| Total | 100,04 | 99,97  | 99,48  | 98,95  | 98,95  | 100,09 | 100,55 | 100,62 | 100,62 | 100,19 | 99,66  | 99,31  | 99,77  | 99,79  | 99,88  | 100,19 | 99,83  | 99,32  | 98,55  | 100,03 | 100,36 | 100,42 |
| Fe    | 0,1158 | 0,1209 | 0,1212 | 0,1000 | 0,1000 | 0,1042 | 0,0842 | 0,0846 | 0,0846 | 0,0848 | 0,0814 | 0,0880 | 0,0742 | 0,1089 | 0,1060 | 0,1060 | 0,1658 | 0,1511 | 0,1515 | 0,1249 | 0,0808 | 0,0832 |
| Na    | 0,0055 | 0,0060 | 0,0058 | 0,0041 | 0,0041 | 0,0013 | 0,0033 | 0,0053 | 0,0053 | 0,0003 | 0,0056 | 0,0029 | 0,0050 | 0,0048 | 0,0101 | 0,0023 | 0,0080 | 0,0083 | 0,0071 | 0,0074 | 0,0063 | 0,0035 |
| K     | 0      | 0      | 0      | 0      | 0      | 0,0009 | 0,0004 | 0      | 0,0002 | 0      | 0      | 0      | 0      | 0      | 0,0012 | 0      | 0      | 0      | 0,0001 | 0      | 0      | 0      |
| Mn    | 0,0046 | 0,0028 | 0,0073 | 0,0024 | 0,0024 | 0,0029 | 0,0003 | 0      | 0,0043 | 0,0043 | 0,0057 | 0,0034 | 0      | 0,0033 | 0,0081 | 0,0012 | 0,0041 | 0,0068 | 0,0010 | 0,0008 | 0,0025 | 0,0002 |
| Si    | 1,9465 | 1,9404 | 1,9420 | 1,9524 | 1,9524 | 1,9349 | 1,9501 | 1,9478 | 1,9478 | 1,9370 | 1,9432 | 1,9300 | 1,9360 | 1,9325 | 1,9195 | 1,9355 | 1,9185 | 1,9365 | 1,9138 | 1,9366 | 1,9376 | 1,9399 |
| Ca    | 0,8341 | 0,8390 | 0,8362 | 0,8351 | 0,8351 | 0,8441 | 0,8459 | 0,8399 | 0,8399 | 0,8484 | 0,8240 | 0,8507 | 0,8427 | 0,8506 | 0,8472 | 0,8472 | 0,8209 | 0,8099 | 0,8629 | 0,8178 | 0,8299 | 0,8236 |
| Cr    | 0,0047 | 0,0025 | 0,0020 | 0,0042 | 0,0042 | 0,0081 | 0,0108 | 0,0088 | 0,0088 | 0,0147 | 0,0183 | 0,0112 | 0,0229 | 0,0135 | 0,0146 | 0,0094 | 0,0023 | 0      | 0,0018 | 0,0066 | 0,0176 | 0,0207 |
| Al    | 0,0835 | 0,0800 | 0,0797 | 0,0739 | 0,0739 | 0,0853 | 0,0607 | 0,0594 | 0,0594 | 0,0724 | 0,0661 | 0,0890 | 0,0671 | 0,0862 | 0,0994 | 0,0882 | 0,1098 | 0,0986 | 0,1218 | 0,0981 | 0,0771 | 0,0759 |
| Ti    | 0,0007 | 0,0038 | 0,0046 | 0      | 0      | 0,0015 | 0      | 0,0039 | 0,0039 | 0,0034 | 0,0049 | 0,0011 | 0      | 0      | 0,0034 | 0,0038 | 0,0051 | 0,0064 | 0,0060 | 0,0044 | 0,0010 | 0,0021 |
| Ni    | 0      | 0      | 0,0005 | 0      | 0      | 0      | 0      | 0      | 0      | 0      | 0,0007 | 0      | 0,0006 | 0,0028 | 0,0008 | 0      | 0,0036 | 0      | 0      | 0      | 0      | 0      |
| Mg    | 1,0157 | 1,0217 | 1,0156 | 1,0382 | 1,0382 | 1,0346 | 1,0599 | 1,0669 | 1,0669 | 1,0504 | 1,0623 | 1,0436 | 1,0726 | 1,0172 | 1,0152 | 1,0195 | 0,9858 | 0,9941 | 0,9555 | 1,0135 | 1,0640 | 1,0620 |
| Total | 4,0111 | 4,0171 | 4,0150 | 4,0102 | 4,0102 | 4,0177 | 4,0157 | 4,0166 | 4,0166 | 4,0160 | 4,0122 | 4,0199 | 4,0211 | 4,0197 | 4,0254 | 4,0128 | 4,0239 | 4,0116 | 4,0216 | 4,0101 | 4,0168 | 4,0111 |
| Wo    | 42,34  | 42,28  | 42,23  | 42,27  | 42,27  | 42,51  | 42,50  | 42,18  | 42,18  | 42,68  | 41,75  | 42,84  | 42,36  | 42,96  | 42,86  | 42,92  | 41,53  | 41,28  | 43,78  | 41,78  | 41,97  | 41,83  |
| En    | 51,55  | 51,49  | 51,28  | 52,55  | 52,55  | 52,10  | 53,25  | 53,58  | 53,58  | 52,84  | 53,83  | 52,56  | 53,91  | 51,37  | 51,36  | 51,65  | 49,87  | 50,67  | 48,48  | 51,79  | 53,82  | 53,94  |
| Fs    | 6,11   | 6,24   | 6,49   | 5,18   | 5,18   | 5,39   | 4,25   | 4,25   | 4,25   | 4,48   | 4,42   | 4,60   | 3,73   | 5,67   | 5,77   | 5,43   | 8,60   | 8,05   | 7,74   | 6,42   | 4,21   | 4,23   |

tableau 4 : analyses microsonde des clinopyroxènes de la klippe de Copper Peak.



| Echantillons | NG4 24 | NG4 26 | NG4 25 | NG4 27 | NG4 28 | NG4 29 | NG4 30 | NG4 31 | NG4 32 | NG4 33 | NG4 34 | NG4 35 |
|--------------|--------|--------|--------|--------|--------|--------|--------|--------|--------|--------|--------|--------|
| FeO          | 14,39  | 14,03  | 13,17  | 14,46  | 14,37  | 13,72  | 11,84  | 13,23  | 11,66  | 12,75  | 11,56  | 13,60  |
| Na2O         | 1,51   | 1,38   | 1,38   | 1,48   | 1,56   | 1,32   | 1,76   | 1,32   | 1,21   | 1,28   | 1,36   | 1,40   |
| K2O          | 0,56   | 0,51   | 0,42   | 0,60   | 0,56   | 0,33   | 0,47   | 0,47   | 0,48   | 0,45   | 0,47   | 0,48   |
| MnO          | 0,40   | 0,37   | 0,10   | 0,31   | 0,23   | 0,25   | 0,23   | 0,22   | 0,14   | 0,19   | 0,25   | 0,15   |
| SiO2         | 45,93  | 46,36  | 46,45  | 45,31  | 44,84  | 47,06  | 44,67  | 47,37  | 47,78  | 45,78  | 46,68  | 47,05  |
| CaO          | 10,90  | 10,90  | 10,89  | 11,02  | 10,41  | 10,83  | 11,06  | 11,07  | 11,77  | 11,50  | 11,28  | 11,23  |
| Cr2O3        | 0,10   | 0,11   | 0,05   | 0,10   | 0,19   | 0,08   | 0      | 0      | 0,14   | 0,14   | 0,07   | 0,05   |
| Al2O3        | 10,90  | 10,01  | 10,49  | 11,26  | 10,52  | 9,51   | 11,48  | 9,67   | 10,74  | 11,61  | 10,58  | 10,27  |
| TiO2         | 1,14   | 0,88   | 0,94   | 1,11   | 1,48   | 0,93   | 1,78   | 0,94   | 0,98   | 1,15   | 1,09   | 0,91   |
| NiO          | 0      | 0      | 0      | 0      | 0      | 0      | 0      | 0      | 0,03   | 0,09   | 0      | 0,04   |
| MgO          | 12,85  | 13,24  | 13,92  | 12,77  | 12,74  | 13,71  | 13,98  | 14,17  | 14,70  | 13,91  | 14,89  | 14,56  |
| Si           | 6,543  | 6,645  | 6,605  | 6,480  | 6,497  | 6,711  | 6,417  | 6,704  | 6,671  | 6,463  | 6,588  | 6,568  |
| AlIV         | 1,456  | 1,354  | 1,394  | 1,519  | 1,502  | 1,288  | 1,582  | 1,295  | 1,328  | 1,536  | 1,411  | 1,431  |
| AlVI         | 0,374  | 0,336  | 0,364  | 0,379  | 0,295  | 0,310  | 0,362  | 0,318  | 0,440  | 0,396  | 0,349  | 0,258  |
| Ti           | 0,122  | 0,094  | 0,100  | 0,119  | 0,161  | 0,099  | 0,192  | 0,100  | 0,102  | 0,122  | 0,115  | 0,095  |
| Cr           | 0,011  | 0,012  | 0,005  | 0,011  | 0,021  | 0,009  | 0      | 0      | 0,015  | 0,015  | 0,007  | 0,005  |
| Fe3          | 0,978  | 0,990  | 1,047  | 0,991  | 1,087  | 1,034  | 0,852  | 0,972  | 0,730  | 0,968  | 0,953  | 1,151  |
| Fe2          | 0,736  | 0,691  | 0,519  | 0,738  | 0,654  | 0,601  | 0,570  | 0,593  | 0,631  | 0,536  | 0,411  | 0,436  |
| Mn           | 0,048  | 0,044  | 0,012  | 0,037  | 0,028  | 0,030  | 0,027  | 0,026  | 0,016  | 0,022  | 0,029  | 0,017  |
| Mg           | 2,728  | 2,828  | 2,950  | 2,722  | 2,751  | 2,914  | 2,993  | 2,989  | 3,059  | 2,927  | 3,132  | 3,029  |
| Ni           | 0      | 0      | 0      | 0      | 0      | 0      | 0      | 0      | 0,003  | 0,010  | 0      | 0,004  |
| Ca           | 1,664  | 1,674  | 1,659  | 1,689  | 1,616  | 1,655  | 1,702  | 1,679  | 1,761  | 1,740  | 1,706  | 1,680  |
| NaB          | 0,081  | 0,057  | 0,040  | 0,099  | 0,055  | 0,020  | 0,193  | 0,041  | 0,089  | 0,090  | 0,078  | 0,059  |
| NaA          | 0,335  | 0,325  | 0,340  | 0,310  | 0,383  | 0,344  | 0,297  | 0,320  | 0,238  | 0,259  | 0,293  | 0,319  |
| K            | 0,101  | 0,093  | 0,076  | 0,109  | 0,103  | 0,060  | 0,086  | 0,084  | 0,085  | 0,081  | 0,084  | 0,085  |

tableau 5 : analyses microsonde des amphiboles de Negro Gulch



**ANALYSES CHIMIQUES  
DE L'OPHIOLITE DE TRINITY  
CHAMBRE MAGMATIQUE DE GRAY ROCK.  
(CHAPITRE 2 et 3)**



| Echantillons                      | Basaltes | TR 45 | TR 47 A | TR 47 B  | TR 49  | TR 51 B | TR 52 B | TR 53 B | TR 55 A | TR 57 B | filons | TR 124 A | TR 124 BC | TR 124 D | TR 127 | TR 128 A | TR 128 E |
|-----------------------------------|----------|-------|---------|----------|--------|---------|---------|---------|---------|---------|--------|----------|-----------|----------|--------|----------|----------|
| SiO <sub>2</sub>                  | 56,01    | 54,45 | 61,61   | 46,34    | 52,71  | 52,75   | 53,10   | 50,59   | 50,43   | 53,81   |        | 54,96    | 51,86     | 50,30    | 53,44  | 56,17    | 55,94    |
| TiO <sub>2</sub>                  | 0,52     | 0,56  | 0,64    | 0,70     | 0,83   | 0,70    | 0,48    | 0,70    | 0,61    | 0,91    |        | 0,94     | 0,53      | 0,52     | 0,82   | 1,06     | 0,66     |
| Al <sub>2</sub> O <sub>3</sub>    | 15,71    | 16,62 | 12,75   | 18,66    | 15,91  | 17,10   | 15,32   | 17,25   | 16,27   | 15,64   |        | 16,49    | 16,84     | 16,56    | 16,56  | 17,73    | 16,05    |
| Fe <sub>2</sub> O <sub>3</sub>    | 6,48     | 7,16  | 6,03    | 9,81     | 8,55   | 7,84    | 7,22    | 8,07    | 7,53    | 7,49    |        | 7,68     | 7,45      | 8,37     | 8,60   | 6,84     | 8,12     |
| (Fe <sub>2</sub> O <sub>3</sub> ) | n.d.     | 3,72  | n.d.    | 3,85     | 3,09   | 1,94    | 2,94    | n.d.    | 1,45    | 1,08    |        | n.d.     | n.d.      | n.d.     | n.d.   | 2,46     | 2,82     |
| (FeO)                             | n.d.     | 3,10  | n.d.    | 5,37     | 4,92   | 5,32    | 3,86    | n.d.    | 5,48    | 5,78    |        | n.d.     | n.d.      | n.d.     | n.d.   | 3,94     | 4,77     |
| MgO                               | 4,46     | 5,08  | 4,18    | 7,84     | 6,33   | 7,10    | 6,94    | 6,63    | 10,28   | 6,76    |        | 5,14     | 7,35      | 8,58     | 5,84   | 3,94     | 5,26     |
| MnO                               | 0,12     | 0,11  | 0,11    | 0,17     | 0,17   | 0,14    | 0,16    | 0,14    | 0,14    | 0,13    |        | 0,15     | 0,14      | 0,16     | 0,13   | 0,12     | 0,14     |
| CaO                               | 13,00    | 12,24 | 10,91   | 9,08     | 10,23  | 6,98    | 13,09   | 7,77    | 5,34    | 8,29    |        | 8,38     | 10,57     | 9,05     | 9,89   | 7,90     | 8,25     |
| Na <sub>2</sub> O                 | 0,87     | 0,53  | 0,00    | 3,07     | 2,12   | 2,82    | 0,10    | 4,58    | 4,18    | 3,64    |        | 3,64     | 2,62      | 3,58     | 2,21   | 3,66     | 2,82     |
| K <sub>2</sub> O                  | 0,16     | 0,18  | 0,10    | 0,14     | 0,29   | 0,65    | 0,12    | 0,26    | 0,06    | 0,11    |        | 0,06     | 0,01      | 0,07     | 0,04   | 0,06     | 0,06     |
| P <sub>2</sub> O <sub>5</sub>     | n.d.     | 0,00  | 0,04    | n.d.     | 0,03   | 0,03    | n.d.    | 0,02    | n.d.    | n.d.    |        | n.d.     | n.d.      | 0,00     | 0,00   | n.d.     | n.d.     |
| P.F.                              | 2,36     | 2,92  | 2,14    | 4,16     | 2,95   | 3,60    | 3,28    | 3,74    | 4,85    | 3,11    |        | 2,13     | 2,42      | 2,57     | 2,95   | 2,38     | 2,54     |
| Total                             | 99,69    | 99,85 | 98,51   | 99,97    | 100,09 | 99,71   | 99,81   | 99,75   | 99,69   | 99,99   |        | 99,57    | 99,79     | 99,76    | 100,48 | 99,86    | 99,84    |
| FeO/MgO                           | 1,31     | 1,27  | 1,29    | 1,13     | 1,22   | 0,99    | 0,94    | 1,09    | 0,66    | 1,00    |        | 1,34     | 0,91      | 0,88     | 1,33   | 1,56     | 1,39     |
| LM.                               | 0,592    | 0,585 | 0,590   | 0,556    | 0,575  | 0,525   | 0,510   | 0,550   | 0,423   | 0,526   |        | 0,599    | 0,503     | 0,494    | 0,596  | 0,635    | 0,607    |
| Cr                                | 237      | 248   | 254     | 342      | 217    | 238     | 428     | 173     | 275     | 143     |        | 42       | 134       | 232      | 108    | 6        | 56       |
| Ni                                | 104      | 109   | 134     | 175      | 188    | 110     | 144     | 106     | 157     | 90      |        | 33       | 85        | 113      | 91     | 40       | 57       |
| Co                                |          | 64    | 80      | 38       | 33     | 83      | 36      | 57      | 30      |         |        |          |           |          | 54     |          |          |
| Sc                                |          |       |         | 35       | 33     |         | 31      |         | 32      |         |        |          |           |          |        |          |          |
| Y                                 |          | 17    | 16      | 16       | 19     | 19      | 16      |         | 13      |         |        |          |           | 14       | 16     | 22       | 17       |
| Zr                                |          | 28    |         | 40       | 42     | 42      |         |         | 45      |         |        |          |           |          | 48     | 61       | 46       |
| Nb                                |          | 1     |         | 1        | 0      | 0       |         |         | 0       |         |        |          |           |          | 1      | 2        | 1,5      |
| Ba                                |          | 10    | 19      | 28       | 46     | 46      | 25      | 37      | 20      |         |        |          |           | 46       | 17     |          |          |
| Sr                                |          | 85    | 51      | 38,5     | 43     | 43      | 38      | 205     | 86      |         |        |          |           | 103      | 131    | 116,9    | 104,9    |
| Rb                                |          | <5    | <10     | 1,9      | 8      | 8       |         | <10     | <5      |         |        |          |           |          | 6      | 0,28     | 0,44     |
| V                                 |          | 322   | 211     |          | 169    | 169     |         | 247     |         |         |        |          |           |          | 276    |          |          |
| Cu                                |          | 24    | 34      |          | <10    | <10     | 0       | 16      |         |         |        |          |           |          | <10    |          |          |
| U                                 |          |       |         | 0        | 0,28   |         |         |         | 0,51    |         |        |          |           | 1,57     |        |          |          |
| Th                                |          |       |         | 0,13     | 0,64   |         | 0,10    |         | 0,60    |         |        |          |           | 3,32     |        | 9,01     | 6,50     |
| Hf                                |          |       |         | 1,22     | 1,48   |         | 0,96    |         | 1,65    |         |        |          |           | 1,15     |        | 7,98     | 6,05     |
| Ta                                |          |       |         | 0,03     | 0,07   |         | 0,04    |         | 0,09    |         |        |          |           | 0,55     |        | 2,62     | 1,98     |
| La                                |          |       |         | 1,55     | 2,95   | 1,29    | 1,20    |         | 1,40    |         |        |          |           | 1,54     |        | 0,838    | 0,718    |
| Ce                                |          | 0,98  |         |          |        |         |         |         |         |         |        |          |           | 1,81     |        | 3,51     | 2,62     |
| Nd                                |          | 3,32  |         | 4,22     | 4,62   | 4,62    | 3,02    |         | 3,28    |         |        |          |           | 1,21     |        | 4,34     | 3,20     |
| Sm                                |          | 1,14  |         | 1,50     | 1,68   | 1,68    | 1,17    |         | 1,13    |         |        |          |           | 1,20     |        | 2,78     | 2,05     |
| Eu                                |          | 0,57  |         | 0,44     | 0,57   | 0,57    | 0,54    |         | 0,36    |         |        |          |           |          |        | 0,704716 | 0,704785 |
| Gd                                |          | 1,53  |         | 2,17     | 2,17   | 2,17    | 1,62    |         | 1,52    |         |        |          |           |          |        | 0,00701  | 0,01216  |
| Dy                                |          | 1,96  |         | 2,68     | 2,68   | 2,68    | 2,07    |         | 1,91    |         |        |          |           |          |        | 0,70467  | 0,70471  |
| Er                                |          | 1,29  |         | 1,75     | 1,75   | 1,75    | 1,37    |         | 1,26    |         |        |          |           |          |        | 9,7      | 10,2     |
| Yb                                |          | 1,28  |         | 1,74     | 1,74   | 1,74    | 1,36    |         | 1,27    |         |        |          |           |          |        |          |          |
| 87Sr/86Sr                         |          |       |         | 0,706548 |        |         |         |         |         |         |        |          |           |          |        |          |          |
| 87Rb/86Rb                         |          |       |         | 0,1425   |        |         |         |         |         |         |        |          |           |          |        |          |          |
| 87Sr/86Sri                        |          |       |         | 0,70567  |        |         |         |         |         |         |        |          |           |          |        |          |          |
| E Sr                              |          |       |         | 23,8     |        |         |         |         |         |         |        |          |           |          |        |          |          |
| 143Nd/144Nd                       |          |       |         | 0,513109 |        |         |         |         |         |         |        |          |           |          |        |          |          |
| 147Sm/144Nd                       |          |       |         | 0,228    |        |         |         |         |         |         |        |          |           |          |        |          |          |
| 143Nd/144Ndi                      |          |       |         | 0,51246  |        |         |         |         |         |         |        |          |           |          |        |          |          |
| Nd                                |          |       |         | 4,14     |        |         |         |         |         |         |        |          |           |          |        |          |          |
| Sm                                |          |       |         | 1,55     |        |         |         |         |         |         |        |          |           |          |        |          |          |
| ENd                               |          |       |         | 7,4      |        |         |         |         |         |         |        |          |           |          |        |          |          |

tableau 6 : analyses roches totales de l'ophiolite de Trinity (Gray Rock)

| Echantillons                      | TR128 F  | TR128 H | TR128 J | TR128 R | TR128 T | TR130 A | TR130 B | TR111 | TR510 A | TR510 B | Peridotites | TR79     | TR423 | Cumulats | TR113  | TR114 | TR222 | TR224 | TR232 |
|-----------------------------------|----------|---------|---------|---------|---------|---------|---------|-------|---------|---------|-------------|----------|-------|----------|--------|-------|-------|-------|-------|
| SiO <sub>2</sub>                  | 56,55    | 54,45   | 52,60   | 52,57   | 52,19   | 49,56   | 56,97   | 52,02 | 50,21   | 56,06   |             | 41,59    | 43,05 |          | 39,58  | 38,43 | 44,72 | 48,05 | 49,56 |
| TiO <sub>2</sub>                  | 0,86     | 0,65    | 0,69    | 0,65    | 0,68    | 0,48    | 0,85    | 0,67  | 0,48    | 0,59    |             | 0,07     | 0,03  |          | 0,18   | 0,12  | 0,09  | 0,13  | 0,14  |
| Al <sub>2</sub> O <sub>3</sub>    | 16,93    | 16,02   | 16,51   | 16,25   | 16,24   | 14,60   | 16,55   | 16,49 | 15,04   | 16,47   |             | 2,16     | 0,93  |          | 2,15   | 5,84  | 1,68  | 1,57  | 6,32  |
| Fe <sub>2</sub> O <sub>3</sub>    | 7,72     | 8,01    | 8,33    | 8,49    | 8,49    | 8,54    | 6,93    | 7,27  | 7,56    | 7,40    |             | 8,10     | 8,91  |          | 11,13  | 10,13 | 8,88  | 8,19  | 6,01  |
| (Fe <sub>2</sub> O <sub>3</sub> ) | 3,36     | 2,31    | 2,08    | 3,16    | n.d.    | n.d.    | n.d.    | n.d.  | n.d.    | n.d.    |             | n.d.     | n.d.  |          | 5,15   | 4,99  | 4,44  | 1,32  | 0,82  |
| (Fe)                              | 3,92     | 5,13    | 5,62    | 4,80    | n.d.    | n.d.    | n.d.    | n.d.  | n.d.    | n.d.    |             | n.d.     | n.d.  |          | 5,39   | 4,63  | 4,00  | 7,09  | 4,68  |
| MgO                               | 3,61     | 5,56    | 6,72    | 6,50    | 6,84    | 10,48   | 4,71    | 7,34  | 10,83   | 5,52    |             | 39,83    | 43,29 |          | 35,82  | 31,41 | 25,75 | 27,24 | 18,97 |
| MnO                               | 0,16     | 0,14    | 0,15    | 0,16    | 0,16    | 0,17    | 0,11    | 0,17  | 0,14    | 0,13    |             | 0,13     | 0,13  |          | 0,20   | 0,13  | 0,14  | 0,14  | 0,11  |
| CaO                               | 8,83     | 9,07    | 9,60    | 10,01   | 10,29   | 10,94   | 10,91   | 10,79 | 10,89   | 9,51    |             | 2,20     | 0,60  |          | 2,56   | 4,18  | 11,93 | 6,59  | 15,56 |
| Na <sub>2</sub> O                 | 2,63     | 2,48    | 2,45    | 2,31    | 2,36    | 1,82    | 0,11    | 2,23  | 1,65    | 0,91    |             | 0,05     | 0,03  |          | 0,20   | 0,00  | 0,01  | 0,04  | 0,12  |
| K <sub>2</sub> O                  | 0,03     | 0,06    | 0,06    | 0,03    | 0,03    | 0,02    | 0,00    | 0,02  | 0,04    | 0,03    |             | 0,06     | 0,02  |          | 0,02   | 0,00  | 0,03  | 0,02  | 0,02  |
| P <sub>2</sub> O <sub>5</sub>     | n.d.     | n.d.    | n.d.    | 0,00    | n.d.    | n.d.    | n.d.    | n.d.  | n.d.    | n.d.    |             | 0,00     | n.d.  |          | 0,08   | 0,05  | 0,00  | n.d.  | n.d.  |
| P.F.                              | 2,49     | 2,64    | 2,98    | 2,13    | 2,54    | 3,07    | 2,89    | 2,88  | 3,15    | 3,32    |             | 4,44     | 2,22  |          | 6,82   | 9,62  | 5,31  | 6,87  | 2,87  |
| Total                             | 99,81    | 99,08   | 100,09  | 99,10   | 99,82   | 99,68   | 100,03  | 99,88 | 99,99   | 99,94   |             | 98,63    | 99,21 |          | 98,74  | 99,91 | 98,54 | 99,84 | 99,68 |
| FeO*/MgO                          | 1,92     | 1,30    | 1,12    | 1,18    | 1,12    | 0,73    | 1,32    | 0,89  | 0,63    | 1,21    |             | 0,18     | 0,19  |          | 0,28   | 0,29  | 0,31  | 0,30  | 0,29  |
| I.M.                              | 0,681    | 0,590   | 0,553   | 0,566   | 0,554   | 0,449   | 0,595   | 0,498 | 0,411   | 0,573   |             | 0,169    | 0,171 |          | 0,237  | 0,244 | 0,256 | 0,252 | 0,241 |
| Cr                                | 27       | 81      | 128     | 131     | 140     | 458     | 17      | 185   | 431     | 46      |             | 2548     | 2402  |          | 3036   | 2606  | 1819  | 1220  | 1253  |
| Ni                                | 26       | 68      | 82      | 95      | 103     | 152     | 39      | 113   | 248     | 65      |             | 2128     | 1696  |          | 1939   | 1253  | 790   | 917   | 401   |
| Co                                | 39       |         |         |         |         |         |         |       |         |         |             | 165      |       |          | 122    | 118   | 70    |       |       |
| Sc                                | 20       | 18      | 18      | 18      | 17      | 12      | 14      |       | 12      | 14      |             |          |       |          | 11     |       | 12    |       |       |
| Y                                 | 50       | 43      | 42      | 40      | 39      | 46      |         |       | 24      | 30      |             |          |       |          | 8      |       | 7     |       |       |
| Nb                                | 2        | 2       | 1       | 2       | 1,5     | 1       |         |       | 0,5     | 0,5     |             |          |       |          | 1      |       | 3     |       |       |
| Ba                                | 24       |         |         | 24      |         | 15      |         |       |         |         |             | 12       |       |          | 34     | 20    | 22    |       |       |
| Sr                                | 121,6    | 117     | 107     | 112     | 106,5   | 109     |         |       | 37      | 50      |             | 0,654    |       |          | 5,21   | 43    | 2     |       |       |
| Rb                                | 0,41     | <10     |         | <10     | 0,26    | <5      |         |       | 6       | 6       |             | 0,117    |       |          | 0,234  | <10   | 16    |       |       |
| V                                 | 273      |         |         |         |         |         |         |       |         |         |             | 73       |       |          | 143    | 140   | 204   |       |       |
| Cu                                | 109      |         |         |         |         |         |         |       |         |         |             | 22       |       |          | 97     | 15    | <10   |       |       |
| Th                                |          |         |         |         |         |         |         |       |         |         |             |          |       |          |        |       |       |       |       |
| Hf                                |          |         |         |         |         |         |         |       |         |         |             |          |       |          |        |       |       |       |       |
| Ta                                |          |         |         |         |         |         |         |       |         |         |             |          |       |          |        |       |       |       |       |
| La                                | 7,28     | 5,82    | 5,57    | 5,29    | 5,06    | 1,40    |         |       |         |         |             | 0,025    |       |          | 0,227  |       |       |       |       |
| Ce                                | 6,52     | 5,19    | 5,01    | 4,73    | 4,50    | 3,36    |         |       |         |         |             | 0,046    |       |          | 0,726  |       |       |       |       |
| Nd                                | 2,15     | 1,72    | 1,68    | 1,58    | 1,53    | 1,13    |         |       |         |         |             | 0,032    |       |          | 0,785  |       |       |       |       |
| Sm                                | 0,784    | 0,661   | 0,641   | 0,614   | 0,601   | 0,43    |         |       |         |         |             | 0,015    |       |          | 0,281  |       |       |       |       |
| Eu                                | 2,91     | 2,31    | 2,26    | 2,19    | 2,12    | 1,53    |         |       |         |         |             | 0,081    |       |          | 0,091  |       |       |       |       |
| Gd                                | 3,57     | 2,87    | 2,79    | 2,70    | 2,59    | 1,91    |         |       |         |         |             | 0,176    |       |          | 0,487  |       |       |       |       |
| Dy                                | 2,30     | 1,83    | 1,78    | 1,73    | 1,67    | 1,25    |         |       |         |         |             | 0,157    |       |          | 0,310  |       |       |       |       |
| Er                                | 2,23     | 1,80    | 1,76    | 1,68    | 1,63    | 1,26    |         |       |         |         |             | 0,147    |       |          | 0,304  |       |       |       |       |
| Yb                                | 0,704622 |         |         |         |         |         |         |       |         |         |             | 0,706066 |       |          | 0,7054 |       |       |       |       |
| 87Sr/86Sr                         | 0,704622 |         |         |         |         |         |         |       |         |         |             | 0,51613  |       |          | 0,1303 |       |       |       |       |
| 87Rb/86Rb                         | 0,009702 |         |         |         |         |         |         |       |         |         |             | 0,70287  |       |          | 0,7046 |       |       |       |       |
| 87Sr/86Sr                         | 0,70456  |         |         |         |         |         |         |       |         |         |             | -15,9    |       |          | 8,6    |       |       |       |       |
| E Sr                              | 8,1      |         |         |         |         |         |         |       |         |         |             |          |       |          |        |       |       |       |       |
| 143Nd/144Nd                       |          |         |         |         |         |         |         |       |         |         |             |          |       |          |        |       |       |       |       |
| 147Sm/144Nd                       |          |         |         |         |         |         |         |       |         |         |             |          |       |          |        |       |       |       |       |
| 143Nd/144Nd                       |          |         |         |         |         |         |         |       |         |         |             |          |       |          |        |       |       |       |       |
| Nd                                |          |         |         |         |         |         |         |       |         |         |             |          |       |          |        |       |       |       |       |
| Sm                                |          |         |         |         |         |         |         |       |         |         |             |          |       |          |        |       |       |       |       |
| ENd                               |          |         |         |         |         |         |         |       |         |         |             |          |       |          |        |       |       |       |       |

Tableau 6 : analyses roches totales de l'ophiolite de Trinity (Gray Rock)

| Echantillons                      | TR 234 | TR 241 | TR 245 | TR 248 | TR 252 | TR 86 | TR 85 | TR 121 | TR 119 | TR 117 | TR 105 | TR 106 | TR 110 | TR 112 AB | TR 523 | Gabbros isotropes | TR 526 | TR 532 | TR 64    |
|-----------------------------------|--------|--------|--------|--------|--------|-------|-------|--------|--------|--------|--------|--------|--------|-----------|--------|-------------------|--------|--------|----------|
| SiO <sub>2</sub>                  | 46,81  | 46,51  | 49,61  | 46,84  | 48,13  | 46,24 | 51,42 | 46,85  | 49,58  | 45,67  | 46,38  | 47,03  | 48,09  | 48,31     | 53,32  |                   | 48,90  | 46,48  | 50,63    |
| TiO <sub>2</sub>                  | 0,02   | 0,07   | 0,12   | 0,10   | 0,16   | 0,18  | 0,19  | 0,19   | 0,15   | 0,12   | 0,13   | 0,13   | 0,19   | 0,20      | 0,52   |                   | 0,26   | 0,92   | 0,42     |
| Al <sub>2</sub> O <sub>3</sub>    | 20,55  | 19,32  | 8,83   | 16,17  | 2,57   | 5,63  | 6,04  | 20,02  | 8,93   | 20,36  | 23,21  | 19,16  | 18,51  | 17,96     | 15,84  |                   | 16,63  | 18,41  | 20,53    |
| Fe <sub>2</sub> O <sub>3</sub>    | 3,39   | 4,08   | 6,33   | 6,05   | 8,24   | 7,14  | 6,86  | 4,49   | 6,72   | 5,28   | 3,58   | 4,87   | 4,97   | 6,43      | 7,12   |                   | 6,33   | 9,60   | 5,49     |
| (Fe <sub>2</sub> O <sub>3</sub> ) | 0,37   | 0,75   | 0,63   | 1,16   | 2,68   | 0,60  | 0,99  | 0,97   | 1,36   | 1,43   | 0,72   | 1,18   | 1,17   | 1,57      | 1,41   |                   | 2,12   | 2,12   | 1,61     |
| (FeO)                             | 2,72   | 3,00   | 5,14   | 4,45   | 5,01   | 5,89  | 5,29  | 3,17   | 4,83   | 3,47   | 2,58   | 3,33   | 3,43   | 4,38      | 5,15   |                   | 6,74   | 6,74   | 3,50     |
| MgO                               | 10,29  | 10,65  | 19,02  | 12,42  | 22,30  | 17,66 | 17,66 | 10,00  | 17,13  | 8,87   | 7,92   | 10,65  | 9,59   | 9,56      | 7,90   |                   | 10,27  | 7,42   | 4,96     |
| MnO                               | 0,08   | 0,07   | 0,15   | 0,11   | 0,15   | 0,19  | 0,12  | 0,08   | 0,14   | 0,11   | 0,08   | 0,10   | 0,11   | 0,13      | 0,12   |                   | 0,14   | 0,16   | 0,09     |
| CaO                               | 14,16  | 15,24  | 12,11  | 13,71  | 15,14  | 16,54 | 14,70 | 13,46  | 11,11  | 13,84  | 14,44  | 13,85  | 13,77  | 14,08     | 9,90   |                   | 13,08  | 13,06  | 10,70    |
| Na <sub>2</sub> O                 | 0,80   | 0,18   | 0,26   | 1,26   | 0,06   | 0,09  | 0,35  | 1,70   | 1,27   | 1,43   | 0,88   | 0,36   | 0,03   | 0,64      | 1,63   |                   | 0,61   | 0,40   | 3,64     |
| K <sub>2</sub> O                  | 0,13   | 0,04   | 0,01   | 0,03   | 0,04   | 0,02  | 0,10  | 0,10   | 0,06   | 0,03   | 0,06   | 0,03   | 0,04   | 0,04      | 0,09   |                   | 0,11   | 0,03   | 0,00     |
| P <sub>2</sub> O <sub>5</sub>     | 0,00   | n.d.   | 0,00   | n.d.   | n.d.   | 0,00  | 0,00  | 0,00   | 0,00   | 0,00   | 0,00   | 0,00   | 0,00   | 0,00      | 0,02   |                   | 0,00   | 0,00   | 0,00     |
| P.F.                              | 2,18   | 3,68   | 2,54   | 3,27   | 2,94   | 2,84  | 2,09  | 3,35   | 3,52   | 3,59   | 3,59   | 3,67   | 3,25   | 3,04      | 2,27   |                   | 2,18   | 2,17   | 2,27     |
| Total                             | 98,51  | 98,84  | 98,98  | 99,96  | 99,73  | 96,53 | 99,53 | 100,24 | 98,61  | 99,30  | 100,27 | 99,81  | 98,55  | 100,39    | 98,73  |                   | 98,51  | 98,65  | 98,73    |
| FeO*/MgO                          | 0,30   | 0,34   | 0,30   | 0,44   | 0,33   | 0,36  | 0,35  | 0,40   | 0,35   | 0,54   | 0,41   | 0,41   | 0,47   | 0,61      | 0,81   |                   | 0,55   | 1,16   | 1,00     |
| I.M.                              | 0,248  | 0,277  | 0,250  | 0,328  | 0,270  | 0,288 | 0,280 | 0,310  | 0,282  | 0,373  | 0,311  | 0,314  | 0,341  | 0,402     | 0,474  |                   | 0,381  | 0,564  | 0,525    |
| Cr                                | 318    | 141    | 1030   | 468    | 1225   | 1524  | 1105  | 315    | 667    | 201    | 83     | 111    | 160    | 140       | 283    |                   | 132    | 51     | 77       |
| Ni                                | 167    | 136    | 315    | 243    | 617    | 442   | 317   | 167    | 381    | 136    | 131    | 142    | 131    | 246       | 182    |                   | 137    | 75     | 76       |
| Co                                | 71     |        | 84     |        |        | 93    | 108   | 77     | 100    | 87     | 111    | 131    | 160    | 312       | 99     |                   | 86     | 88     | 75       |
| Sc                                |        |        |        |        |        |       |       |        |        |        |        |        |        |           |        |                   |        |        |          |
| Y                                 | 11     |        |        |        |        | 14    | 14    | 12     |        |        | 13     | 1      | 5      | 13        |        |                   |        | 14     | 11       |
| Zr                                | 4      |        |        |        |        | 8     | 8     | 6      |        |        | 6      | 6      | 10     | 8         |        |                   |        | 14     | 32       |
| Nb                                | 0      |        |        |        |        | 5     | 4     | 1      |        |        | 1      | 0,5    | 0      | 2         |        |                   |        | 5      | 1        |
| Ba                                | 20     |        | 22     |        |        | 23    | 22    | 24     | 18     | 19     | 12     | 12     | 20     | 14        | 17     |                   | 18     | 19     | 19       |
| Sr                                | 35     |        | 22     |        |        | 4     | 14,8  | 51     | 31     | 59     | 46     | 37,7   | 42,9   | 49        | 40     |                   | 48     | 73     | 122,5    |
| Rb                                | <5     |        | <10    |        |        | <5    | 0,502 | 9      | <10    | <10    | 6      | 0,105  | 0,294  | 10        | <10    |                   | <10    | 24     | 0,136    |
| V                                 | 124    |        | 176    |        |        | 209   | 205   | 124    | 165    | 108    | 95     | 141    | 186    | 183       | 173    |                   | 184    | 425    | 146      |
| Cu                                | <10    |        | <10    |        |        | 12    | <10   | <10    | 15     | <10    | 31     | 18     | <10    | 75        | <10    |                   | 15     | 120    | 39       |
| Th                                |        |        |        |        |        |       |       |        |        |        |        |        |        |           |        |                   |        |        |          |
| Hf                                |        |        |        |        |        |       |       |        |        |        |        |        |        |           |        |                   |        |        |          |
| Ta                                |        |        |        |        |        |       |       |        |        |        |        |        |        |           |        |                   |        |        |          |
| La                                |        |        |        |        |        |       |       |        |        |        |        |        |        |           |        |                   |        |        |          |
| Ce                                |        |        |        |        |        |       |       |        |        |        |        |        |        |           |        |                   |        |        | 0,766    |
| Nd                                |        |        |        |        |        |       |       |        |        |        |        |        |        |           |        |                   |        |        | 2,580    |
| Sm                                |        |        |        |        |        |       |       |        |        |        |        |        |        |           |        |                   |        |        | 3,010    |
| Eu                                |        |        |        |        |        |       |       |        |        |        |        |        |        |           |        |                   |        |        | 1,170    |
| Gd                                |        |        |        |        |        |       |       |        |        |        |        |        |        |           |        |                   |        |        | 0,553    |
| Dy                                |        |        |        |        |        |       |       |        |        |        |        |        |        |           |        |                   |        |        | 1,750    |
| Er                                |        |        |        |        |        |       |       |        |        |        |        |        |        |           |        |                   |        |        | 2,230    |
| Yb                                |        |        |        |        |        |       |       |        |        |        |        |        |        |           |        |                   |        |        | 1,460    |
| 87Sr/86Sr                         |        |        |        |        |        |       |       |        |        |        |        |        |        |           |        |                   |        |        | 1,450    |
| 87Rb/86Rb                         |        |        |        |        |        |       |       |        |        |        |        |        |        |           |        |                   |        |        | 0,705308 |
| 87Sr/86Sr                         |        |        |        |        |        |       |       |        |        |        |        |        |        |           |        |                   |        |        | 0,003225 |
| E Sr                              |        |        |        |        |        |       |       |        |        |        |        |        |        |           |        |                   |        |        | 0,70529  |
| 143Nd/144Nd                       |        |        |        |        |        |       |       |        |        |        |        |        |        |           |        |                   |        |        | 18,4     |
| 147Sm/144Nd                       |        |        |        |        |        |       |       |        |        |        |        |        |        |           |        |                   |        |        | 0,513138 |
| 143Nd/144Nd                       |        |        |        |        |        |       |       |        |        |        |        |        |        |           |        |                   |        |        | 0,2352   |
| Nd                                |        |        |        |        |        |       |       |        |        |        |        |        |        |           |        |                   |        |        | 0,51247  |
| Sm                                |        |        |        |        |        |       |       |        |        |        |        |        |        |           |        |                   |        |        | 2,98     |
| ENd                               |        |        |        |        |        |       |       |        |        |        |        |        |        |           |        |                   |        |        | 1,15     |
|                                   |        |        |        |        |        |       |       |        |        |        |        |        |        |           |        |                   |        |        | 7,6      |

tableau 6 : analyses roches totales de l'ophiolite de Trinity (Gray Rock)

| Echantillons                      | Plagiogranites | TR 524 | TR 109 | TR 70 | TR 74 | TR 368 | Gabbros pegmatiques | PEGM A | PEGM B   | TR 223 | TR 515 | TR 273 | TR 538 |
|-----------------------------------|----------------|--------|--------|-------|-------|--------|---------------------|--------|----------|--------|--------|--------|--------|
| SiO <sub>2</sub>                  |                | 62,59  | 60,47  | 74,54 | 79,67 | 78,16  |                     | 48,09  | 47,74    | 43,81  | 51,77  | 51,98  | 49,79  |
| TiO <sub>2</sub>                  |                | 0,22   | 0,29   | 0,37  | 0,13  | 0,08   |                     | 0,13   | 0,39     | 0,13   | 0,10   | 0,24   | 0,24   |
| Al <sub>2</sub> O <sub>3</sub>    |                | 18,78  | 19,43  | 12,70 | 11,05 | 12,61  |                     | 18,24  | 19,91    | 19,64  | 16,48  | 4,26   | 11,38  |
| Fe <sub>2</sub> O <sub>3</sub>    |                | 1,84   | 1,30   | 2,70  | 0,50  | 0,45   |                     | 5,87   | 4,97     | 5,79   | 4,46   | 6,83   | 6,27   |
| (Fe <sub>2</sub> O <sub>3</sub> ) |                | 0,84   | n.d.   | n.d.  | n.d.  | n.d.   |                     | n.d.   | n.d.     | n.d.   | n.d.   | n.d.   | n.d.   |
| (FeO)                             |                | 4,95   | n.d.   | n.d.  | n.d.  | n.d.   |                     | n.d.   | n.d.     | n.d.   | n.d.   | n.d.   | n.d.   |
| MgO                               |                | 1,96   | 1,20   | 0,56  | 0,00  | 0,13   |                     | 9,03   | 7,94     | 7,08   | 7,78   | 17,36  | 13,49  |
| MnO                               |                | 0,05   | 0,03   | 0,04  | 0,02  | 0,00   |                     | 0,10   | 0,09     | 0,10   | 0,09   | 0,12   | 0,13   |
| CaO                               |                | 10,24  | 3,63   | 3,78  | 2,24  | 0,28   |                     | 14,69  | 14,12    | 19,68  | 15,93  | 16,25  | 14,19  |
| Na <sub>2</sub> O                 |                | 1,34   | 11,54  | 3,15  | 4,57  | 7,21   |                     | 0,69   | 1,86     | 0,18   | 0,89   | 0,55   | 0,61   |
| K <sub>2</sub> O                  |                | 0,05   | 0,08   | 0,22  | 0,03  | 0,08   |                     | 0,02   | 0,03     | 0,05   | 0,05   | 0,06   | 0,06   |
| P <sub>2</sub> O <sub>5</sub>     |                | 0,00   | 0,01   | 0,06  | 0,00  | n.d.   |                     | n.d.   | n.d.     | n.d.   | n.d.   | n.d.   | n.d.   |
| P.F.                              |                | 1,43   | 0,80   | 0,98  | 0,52  | 0,31   |                     | 3,15   | 2,99     | 3,24   | 2,08   | 1,80   | 3,47   |
| Total                             |                | 98,50  | 98,78  | 99,10 | 98,73 | 99,31  |                     | 100,01 | 100,04   | 99,70  | 99,63  | 99,45  | 99,63  |
| FeO*/MgO                          |                | 0,84   | 0,98   | 4,34  |       | 3,12   |                     | 0,59   | 0,56     | 0,74   | 0,51   | 0,35   | 0,42   |
| I.M.                              |                | 0,484  | 0,520  | 0,828 |       | 0,776  |                     | 0,394  | 0,385    | 0,449  | 0,364  | 0,282  | 0,317  |
| Cr                                |                | 92     | <10    | <10   | <10   | 8      |                     | 84     | 47       | 181    | 138    | 1175   | 990    |
| Ni                                |                | 85     | 17     | 31    | 31    | 30     |                     | 102    | 85       | 68     | 97     | 232    | 176    |
| Co                                |                | 87     | <10    | 68    | 48    |        |                     |        |          |        |        |        |        |
| Sc                                |                |        |        |       |       |        |                     |        |          |        |        |        |        |
| Y                                 |                |        | 36     |       | 15    | 23     |                     | 5      | 11       | 6      | 4      | 8      | 9      |
| Zr                                |                |        | 176    |       | 112   | 55     |                     | 9      | 15       | 11     | 9      | 12     | 10     |
| Nb                                |                |        | 0      |       | 3     | 4      |                     | 0,5    | 0        | 2      | 1      | 2      | 1      |
| Ba                                |                | 25     | 17     | 30    | 30    |        |                     |        |          |        |        |        |        |
| Sr                                |                | 53     | 56     | 74    | 81    | 19     |                     | 45     | 50,6     | 81     | 52     | 13     | 31     |
| Rb                                |                | <10    | <5     | <10   | 0     | 1      |                     | 7      | 0,088    | 9      | 6      | 9      | 8      |
| V                                 |                | 101    |        | 39    | <10   |        |                     |        |          | 166    | 187    | 277    | 240    |
| Cu                                |                | <10    |        | <10   | <10   |        |                     |        |          |        |        |        |        |
| U                                 |                |        |        |       |       |        |                     |        |          |        |        |        |        |
| Th                                |                |        |        |       |       |        |                     |        |          |        |        |        |        |
| Hf                                |                |        |        |       |       |        |                     |        |          |        |        |        |        |
| Ta                                |                |        |        |       |       |        |                     |        |          |        |        |        |        |
| La                                |                | 8,22   |        |       | 10,19 | 6,98   |                     | 0,67   | 0,207    |        |        |        |        |
| Ce                                |                | 23,85  |        |       | 24,21 | 18,85  |                     | 1,45   | 0,92     |        |        |        |        |
| Nd                                |                | 15,18  |        |       | 10,26 | 9,14   |                     | 0,66   | 1,80     |        |        |        |        |
| Sm                                |                | 3,74   |        |       | 2,45  | 2,81   |                     | 0,33   | 0,90     |        |        |        |        |
| Eu                                |                | 0,36   |        |       | 0,45  | 0,08   |                     | 0,14   | 0,305    |        |        |        |        |
| Gd                                |                | 3,83   |        |       | 2,66  | 3,16   |                     | 0,56   | 1,55     |        |        |        |        |
| Dy                                |                | 4,44   |        |       | 2,34  | 3,84   |                     | 0,63   | 2,11     |        |        |        |        |
| Er                                |                | 2,89   |        |       | 1,60  | 2,41   |                     | 0,41   | 1,43     |        |        |        |        |
| Yb                                |                | 3,67   |        |       | 2,01  | 3,27   |                     | 0,35   | 1,47     |        |        |        |        |
| 87Sr/86Sr                         |                |        |        |       |       |        |                     |        | 0,704707 |        |        |        |        |
| 87Rb/86Rb                         |                |        |        |       |       |        |                     |        | 0,005065 |        |        |        |        |
| 87Sr/86Sri                        |                |        |        |       |       |        |                     |        | 0,70468  |        |        |        |        |
| E Sr                              |                |        |        |       |       |        |                     |        | 9,8      |        |        |        |        |
| 143Nd/144Nd                       |                |        |        |       |       |        |                     |        | 0,513341 |        |        |        |        |
| 147Sm/144Nd                       |                |        |        |       |       |        |                     |        | 0,3096   |        |        |        |        |
| 143Nd/144Ndi                      |                |        |        |       |       |        |                     |        | 0,51246  |        |        |        |        |
| Nd                                |                |        |        |       |       |        |                     |        | 1,71     |        |        |        |        |
| Sm                                |                |        |        |       |       |        |                     |        | 0,87     |        |        |        |        |
| E Nd                              |                |        |        |       |       |        |                     |        | 7,4      |        |        |        |        |

tableau 6 : analyses roches totales de l'ophiolite de Trinity (Gray Rock)



|          | $^{87}\text{Sr}/^{86}\text{Sr}$ | Sr    | Rb    | $^{87}\text{Rb}/^{86}\text{Sr}$ | $^{87}\text{Sr}/^{86}\text{Sr}$ (i) | $\epsilon_{\text{Sr}}$ (n) | $^{143}\text{Nd}/^{144}\text{Nd}$ | Nd   | Sm   | $^{147}\text{Sm}/^{144}\text{Nd}$ | $^{143}\text{Nd}/^{144}\text{Nd}$ (i) | $\epsilon_{\text{Nd}}$ (n) |
|----------|---------------------------------|-------|-------|---------------------------------|-------------------------------------|----------------------------|-----------------------------------|------|------|-----------------------------------|---------------------------------------|----------------------------|
| TR 55 A  | 0.705182 $\pm$ 35               | 71.3  | 0.829 | 0.0336                          | 0.70497                             | + 14.1                     |                                   |      |      |                                   |                                       |                            |
| TR 53 B  | 0.705467 $\pm$ 40               | 154   | 3.60  | 0.0676                          | 0.70503                             | + 15.1                     |                                   |      |      |                                   |                                       |                            |
| TR 51 B  | 0.708179 $\pm$ 23               | 50.1  | 9.36  | 0.5399                          | 0.70472                             | + 10.6                     | 0.513080 $\pm$ 32                 | 6.53 | 2.35 | 0.2187                            | 0.51244                               | + 7.3                      |
| TR 48    | 0.706548 $\pm$ 35               | 38.5  | 1.90  | 0.1425                          | 0.70563                             | + 23.6                     | 0.513109 $\pm$ 44                 | 4.14 | 1.55 | 0.2280                            | 0.51244                               | + 7.4                      |
| TR 47 A  | 0.705877 $\pm$ 35               | 95.5  | 2.92  | 0.0884                          | 0.70531                             | + 19.0                     |                                   |      |      |                                   |                                       |                            |
| TR 47 B  | 0.705998 $\pm$ 33               | 60.0  |       |                                 |                                     |                            |                                   |      |      |                                   |                                       |                            |
| TR 124 D | 0.705133 $\pm$ 36               | 103   | 0.535 | 0.01508                         | 0.70504                             | + 15.1                     | 0.512931 $\pm$ 32                 | 3.05 | 1.13 | 0.2254                            | 0.51227                               | + 4.1                      |
| TR 127   | 0.704113 $\pm$ 38               | 133   | 0.127 | 0.00277                         | 0.70410                             | + 1.8                      |                                   |      |      |                                   |                                       |                            |
| TR 128 A | 0.704716 $\pm$ 36               | 117   | 0.283 | 0.00701                         | 0.70467                             | + 9.9                      |                                   |      |      |                                   |                                       |                            |
| TR 128 E | 0.704785 $\pm$ 40               | 105   | 0.440 | 0.01216                         | 0.70471                             | + 10.4                     |                                   |      |      |                                   |                                       |                            |
| TR 128 F | 0.704622 $\pm$ 29               | 122   | 0.408 | 0.00970                         | 0.70456                             | + 8.4                      |                                   |      |      |                                   |                                       |                            |
| TR 128 T | 0.704832 $\pm$ 36               | 106   | 0.259 | 0.00704                         | 0.70479                             | + 11.6                     |                                   |      |      |                                   |                                       |                            |
| TR 130 A | 0.704931 $\pm$ 35               | 79.5  | 0.103 | 0.00374                         | 0.70491                             | + 13.3                     | 0.512840 $\pm$ 33                 | 4.57 | 1.58 | 0.2104                            | 0.51222                               | + 3.1                      |
| TR 64    | 0.705308 $\pm$ 46               | 122   | 0.136 | 0.00323                         | 0.70529                             | + 18.7                     | 0.513138 $\pm$ 32                 | 2.98 | 1.15 | 0.2352                            | 0.51244                               | + 7.5                      |
| PGA      | 0.704779 $\pm$ 38               | 37.9  | 0.281 | 0.02143                         | 0.70464                             | + 9.5                      |                                   |      |      |                                   |                                       |                            |
| PGB      | 0.704707 $\pm$ 35               | 50.6  | 0.088 | 0.00507                         | 0.70467                             | + 10.0                     | 0.513341 $\pm$ 23                 | 1.71 | 0.87 | 0.3096                            | 0.51243                               | + 7.2                      |
|          | 0.705073 $\pm$ 52               | 1.55  | 0.108 | 0.20137                         | 0.70378                             | - 2.7                      |                                   |      |      |                                   |                                       |                            |
|          | 0.705334 $\pm$ 40               | 34.1  | 0.115 | 0.00975                         | 0.70527                             | + 18.5                     |                                   |      |      |                                   |                                       |                            |
| TR 532   | 0.704193 $\pm$ 39               | 75.1  | 0.178 | 0.00685                         | 0.70415                             | + 2.5                      |                                   |      |      |                                   |                                       |                            |
| TR 524   | 0.704430 $\pm$ 47               | 60.8  | 0.328 | 0.01559                         | 0.70433                             | + 5.1                      |                                   |      |      |                                   |                                       |                            |
| TR 538   | 0.704183 $\pm$ 36               | 34.0  | 0.251 | 0.02135                         | 0.70405                             | + 1.1                      |                                   |      |      |                                   |                                       |                            |
| TR 515   | 0.704834 $\pm$ 34               | 54.4  | 0.146 | 0.00775                         | 0.70478                             | + 11.5                     |                                   |      |      |                                   |                                       |                            |
| TR 110   | 0.704062 $\pm$ 37               | 42.9  | 0.294 | 0.01980                         | 0.70394                             | - 0.5                      | 0.513145 $\pm$ 28                 | 1.03 | 0.43 | 0.2540                            | 0.51240                               | + 6.6                      |
| TR 109   | 0.705749 $\pm$ 45               | 58.9  | 0.222 | 0.01089                         | 0.70568                             | + 24.3                     | 0.512839 $\pm$ 32                 | 16.5 | 3.86 | 0.1426                            | 0.51242                               | + 7.0                      |
| TR 368   | 0.706078 $\pm$ 40               | 19.0  | 0.217 | 0.03297                         | 0.70587                             | + 26.9                     |                                   |      |      |                                   |                                       |                            |
| TR 106   | 0.704556 $\pm$ 29               | 37.7  | 0.105 | 0.00805                         | 0.70450                             | + 7.6                      |                                   |      |      |                                   |                                       |                            |
|          | 0.704585 $\pm$ 39               |       |       |                                 |                                     |                            |                                   |      |      |                                   |                                       |                            |
| TR 121   | 0.704205 $\pm$ 31               | 14.8  | 0.502 | 0.09822                         | 0.70358                             | - 5.6                      |                                   |      |      |                                   |                                       |                            |
| TR 85    | 0.704122 $\pm$ 37               |       |       |                                 |                                     |                            |                                   |      |      |                                   |                                       |                            |
| TR 248   | 0.704487 $\pm$ 42               | 63.1  | 0.380 | 0.01740                         | 0.70438                             | + 5.7                      |                                   |      |      |                                   |                                       |                            |
| TR 234   | 0.703864 $\pm$ 30               | 50.6  | 0.634 | 0.03621                         | 0.70363                             | - 4.8                      |                                   |      |      |                                   |                                       |                            |
| TR 223   | 0.704151 $\pm$ 35               | 76.6  | 0.635 | 0.02396                         | 0.70400                             | + 0.4                      |                                   |      |      |                                   |                                       |                            |
| TR 222   |                                 |       |       |                                 |                                     |                            |                                   |      |      |                                   |                                       |                            |
| TR 113   | 0.705404 $\pm$ 41               | 5.21  | 0.234 | 0.1303                          | 0.70457                             | + 8.5                      |                                   |      |      |                                   |                                       |                            |
|          | 0.705194 $\pm$ 47               |       |       |                                 |                                     |                            |                                   |      |      |                                   |                                       |                            |
| TR 79    | 0.706066 $\pm$ 47               | 0.654 | 0.117 | 0.51613                         | 0.70276                             | - 17.3                     |                                   |      |      |                                   |                                       |                            |
|          | 0.705513 $\pm$ 52               |       |       |                                 |                                     |                            |                                   |      |      |                                   |                                       |                            |

tableau 7 : analyses isotopiques du Sr et du Nd de l'ophiolite de Trinity (Gray Rock).

Echantillons Type  $\delta^{18}\text{O}$   $\sigma$  n  $t^\circ\text{C}$   $\delta^{13}\text{C}$   $^{87}\text{Sr}/^{86}\text{Sr}(\text{I})$  W/R

### Carbonates

|        |                           |       |  |   |     |       |         |       |
|--------|---------------------------|-------|--|---|-----|-------|---------|-------|
| TR55A  | <i><math>\beta</math></i> | 15.83 |  | 1 | 107 | 1.39  | 0.70497 | 6.50  |
| TR52B  | <i><math>\beta</math></i> | 26.14 |  | 1 | 34  | -2.49 |         |       |
| TR47B  | <i><math>\beta</math></i> | 21.68 |  | 1 | 43  | -3.91 | 0.70546 | 7.60  |
| TR61   | <i>i.g.</i>               | 24.50 |  | 1 | 60  | -5.42 | 0.70556 | 15.90 |
| TR124D | <i>d</i>                  | 27.61 |  | 1 | 26  | -2.19 | 0.70504 | 9.80  |

### Silicates

|        |                           |       |             |   |     |  |         |       |
|--------|---------------------------|-------|-------------|---|-----|--|---------|-------|
| TR55A  | <i><math>\beta</math></i> | 9.60  | $\pm 0.01$  | 4 | 133 |  | 0.70497 | 6.50  |
| TR53B  | <i><math>\beta</math></i> | 9.55  | $\pm 0.01$  | 2 | 139 |  | 0.70503 | 14.60 |
| TR51B  | <i><math>\beta</math></i> | 9.55  | $\pm 0.2$   | 5 | 128 |  | 0.70472 | 3.80  |
| TR48   | <i><math>\beta</math></i> | 8.45  | $\pm 0.1$   | 2 | 153 |  | 0.70563 | 5.40  |
| TR47B  | <i><math>\beta</math></i> | 10.10 | $\pm 0.2$   | 2 | 126 |  | 0.70546 | 7.60  |
| TR47A  | <i><math>\beta</math></i> | 8.95  | $\pm 0.05$  | 2 | 148 |  | 0.70531 | 10.90 |
| TR128F | <i>d</i>                  | 4.80  | $\pm 0.1$   | 2 | 211 |  | 0.70456 | 8.40  |
| TR128H | <i>d</i>                  | 4.80  | $\pm 0.1$   | 3 |     |  |         |       |
| TR127  | <i>d</i>                  | 5.50  | $\pm 0.1$   | 3 | 227 |  | 0.7041  | 6.40  |
| TR124D | <i>d</i>                  | 5.85  | $\pm 0.15$  | 4 | 216 |  | 0.70504 | 9.80  |
| TR130A | <i>d</i>                  | 5.50  | $\pm 0.2$   | 5 |     |  |         |       |
| TR61   | <i>i.g.</i>               | 9.05  | $\pm 0.15$  | 5 | 148 |  | 0.70556 | 15.90 |
| TR64   | <i>i.g.</i>               | 7.30  | $\pm 0.2$   | 6 | 181 |  | 0.70529 | 13.70 |
| TR532  | <i>i.g.</i>               | 5.36  | $\pm 0.2$   | 2 | 288 |  | 0.70415 | 3.80  |
| TR538  | <i>p.g.</i>               | 4.95  | $\pm 0.03$  | 2 | 335 |  | 0.70405 | 1.60  |
| TR526  | <i>i.g.</i>               | 4.00  | $\pm 0.05$  | 5 |     |  |         |       |
| PEGMB  | <i>p.g.</i>               | 5.00  |             | 1 | 319 |  | 0.70467 | 3.80  |
| TR524  | <i>tdj</i>                | 7.43  | $\pm 0.2$   | 4 | 174 |  | 0.70433 | 3.50  |
| TR523  | <i>i.g.</i>               | 6.25  | $\pm 0.02$  | 3 |     |  |         |       |
| TR510A | <i>d</i>                  | 5.85  | $\pm 0.1$   | 3 |     |  |         |       |
| TR112  | <i>lg</i>                 | 5.65  | $\pm 0.1$   | 3 |     |  |         |       |
| TR110  | <i>lg</i>                 | 5.78  | $\pm 0.1$   | 4 | 278 |  | 0.70394 | 1.80  |
| TR121  | <i>lg</i>                 | 6.95  | $\pm 0.2$   | 3 | 231 |  | 0.70411 | 3.30  |
| TR106  | <i>lg</i>                 | 4.93  |             | 1 | 327 |  | 0.7045  | 2.50  |
| TR105  | <i>lg</i>                 | 5.80  | $\pm 0.1$   | 2 |     |  |         |       |
| TR252  | <i>wrh</i>                | 5.45  | $\pm 0.15$  | 2 |     |  |         |       |
| TR248  | <i>lg</i>                 | 5.90  | $\pm 0.15$  | 2 | 274 |  | 0.70438 | 3.80  |
| TR241  | <i>lg</i>                 | 5.75  | $\pm 0.15$  | 2 |     |  |         |       |
| TR234  | <i>lg</i>                 | 6.20  | $\pm 0.2$   | 5 | 255 |  | 0.70363 | 1.60  |
| TR224  | <i>wbs</i>                | 5.48  | $\pm 0.005$ | 2 |     |  |         |       |
| TR223  | <i>p.g.</i>               | 6.00  | $\pm 0.2$   | 2 | 269 |  | 0.70400 | 3.40  |
| TR222  | <i>wrh</i>                | 4.87  | $\pm 0.03$  | 2 |     |  | 0.70276 | 0.00  |

### Quartz

|             |             |       |            |   |  |  |  |  |
|-------------|-------------|-------|------------|---|--|--|--|--|
| TR47B (rim) | <i>b</i>    | 12.73 | $\pm 0.03$ | 2 |  |  |  |  |
| TR532       | <i>i.g.</i> | 11.00 | $\pm 0.02$ | 2 |  |  |  |  |
| TR68        | <i>i.g.</i> | 7.96  | $\pm 0.05$ | 2 |  |  |  |  |

### Amphiboles

|       |             |      |  |   |  |  |  |  |
|-------|-------------|------|--|---|--|--|--|--|
| TR538 | <i>p.g.</i> | 4.54 |  | 1 |  |  |  |  |
| TR223 | <i>p.g.</i> | 5.71 |  | 1 |  |  |  |  |

*$\beta$*  = basalte

*d* = filon

*i.g.* = gabbro isotrope

*p.g.* = gabbro pegmatitique

*tdj* = trondhjemite

*lg* = gabbro lité

*wrh* = werhlite

*wbs* = websterite

| Echantillons                   | cumulats | TR 252 10 | TR 252 11 | TR 252 13 | TR 252 15 | TR 222 10 | TR 222 14 | TR 113 66 | TR 113 70 | TR 113 72 | TR 113 73 | TR 413 36 | TR 413 37 | TR 413 44 | TR 413 45 | TR 413 46 | TR 413 47 | TR 83 107 | TR 83 108 | TR 83 110 |
|--------------------------------|----------|-----------|-----------|-----------|-----------|-----------|-----------|-----------|-----------|-----------|-----------|-----------|-----------|-----------|-----------|-----------|-----------|-----------|-----------|-----------|
| SiO <sub>2</sub>               | 40.1     | 39.93     | 39.99     | 39.99     | 38.41     | 39.27     | 39.35     | 40.80     | 41.22     | 40.66     | 40.54     | 41.75     | 42.11     | 41.70     | 41.51     | 41.46     | 41.33     | 41.33     | 39.79     | 40.49     |
| TiO <sub>2</sub>               | 0        | 0         | 0         | 0         | 0         | 0         | 0         | 0.05      | 0         | 0         | 0         | 0         | 0.02      | 0         | 0         | 0         | 0         | 0         | 0.06      | 0         |
| Al <sub>2</sub> O <sub>3</sub> | 0        | 0.05      | 0         | 0         | 0.30      | 0         | 0.03      | 0.02      | 0.03      | 0.07      | 0         | 0         | 0.01      | 0         | 0         | 0         | 0         | 0         | 0.02      | 0         |
| Fe <sub>2</sub> O <sub>3</sub> | 16.08    | 15.52     | 15.94     | 17.97     | 17.97     | 14.25     | 14.65     | 12.25     | 12.72     | 13.22     | 13.43     | 10.46     | 9.90      | 10.55     | 10.64     | 10.29     | 10.58     | 8.98      | 8.98      | 8.66      |
| MgO                            | 44.55    | 43.77     | 44.19     | 42.20     | 45.08     | 45.08     | 45.36     | 48.09     | 45.52     | 45.18     | 45.55     | 51.31     | 51.64     | 51.41     | 50.43     | 50.93     | 50.65     | 51.98     | 51.32     | 51.28     |
| MnO                            | 0.27     | 0.09      | 0.20      | 0.01      | 0.26      | 0.04      | 0.03      | 0.09      | 0.17      | 0.14      | 0.14      | 0.11      | 0.18      | 0.06      | 0.11      | 0.12      | 0.08      | 0.07      | 0.02      | 0         |
| CaO                            | 0        | 0.01      | 0.09      | 0         | 0         | 0.04      | 0.03      | 0         | 0.02      | 0.01      | 0.01      | 0         | 0         | 0         | 0         | 0.03      | 0         | 0.02      | 0         | 0.02      |
| Na <sub>2</sub> O              | 0        | 0.03      | 0.07      | 0         | 0         | 0         | 0         | 0         | 0.01      | 0         | 0         | 0.01      | 0.03      | 0         | 0.02      | 0.01      | 0         | 0         | 0         | 0         |
| K <sub>2</sub> O               | 0        | 0.03      | 0         | 0         | 0.01      | 0         | 0         | 0         | 0         | 0.01      | 0         | 0         | 0         | 0         | 0         | 0         | 0         | 0         | 0         | 0         |
| Cr                             | 0        | 0         | 0         | 0         | 0         | 0         | 0         | 0         | 0.08      | 0         | 0         | 0         | 0         | 0         | 0         | 0         | 0         | 0         | 0         | 0         |
| N                              | 0.05     | 0.12      | 0.09      | 0.07      | 0.07      | 0.24      | 0.16      | 0.23      | 0.22      | 0.15      | 0.16      | 0.07      | 0.19      | 0.15      | 0.18      | 0.11      | 0.25      | 0.11      | 0.19      | 0.03      |
| Total                          | 101.04   | 99.55     | 100.58    | 98.97     | 99.15     | 99.15     | 99.85     | 99.63     | 99.99     | 99.44     | 99.69     | 103.68    | 104.18    | 103.85    | 102.91    | 102.85    | 102.95    | 102.79    | 100.75    | 100.94    |
| K                              | 0.0001   | 0.0009    | 0         | 0         | 0.0002    | 0         | 0.0032    | 0.0047    | 0.0044    | 0.0003    | 0         | 0.0014    | 0         | 0         | 0.0035    | 0         | 0         | 0         | 0         | 0.0001    |
| N                              | 0.0010   | 0.0025    | 0.0017    | 0.0014    | 0.0014    | 0.0049    | 0.0032    | 0.0047    | 0.0044    | 0.0003    | 0.0033    | 0.0014    | 0.0036    | 0.0028    | 0.0035    | 0.0021    | 0.0048    | 0.0078    | 0.0068    | 0.0088    |
| Na                             | 0        | 0.0016    | 0.0035    | 0         | 0         | 0.0002    | 0         | 0.0001    | 0.0006    | 0         | 0         | 0.0003    | 0.0016    | 0         | 0.0009    | 0.0004    | 0         | 0         | 0         | 0         |
| Ca                             | 0.0001   | 0.0003    | 0.0023    | 0         | 0.0011    | 0.0008    | 0         | 0.0006    | 0.0006    | 0.0004    | 0.0002    | 0.0003    | 0.0001    | 0.0007    | 0.0001    | 0.0007    | 0         | 0.0008    | 0         | 0.0005    |
| Fe                             | 0.3351   | 0.3278    | 0.3342    | 0.3870    | 0.3351    | 0.3014    | 0.3081    | 0.2546    | 0.2637    | 0.2637    | 0.2799    | 0.2071    | 0.1966    | 0.2037    | 0.2127    | 0.2055    | 0.2115    | 0.1767    | 0.1833    | 0.1754    |
| Si                             | 1.0005   | 1.0062    | 1.0002    | 0.9899    | 0.9933    | 0.9933    | 0.9898    | 1.0136    | 1.0213    | 1.0158    | 1.0103    | 0.9898    | 0.9912    | 0.9868    | 0.9921    | 0.9899    | 0.9879    | 0.9834    | 0.9890    | 0.9810    |
| Ti                             | 0        | 0         | 0         | 0         | 0         | 0         | 0         | 0.0010    | 0.0010    | 0         | 0         | 0         | 0.0003    | 0         | 0         | 0         | 0         | 0         | 0.0012    | 0         |
| Mn                             | 0.0058   | 0.0019    | 0.0041    | 0.0002    | 0.0057    | 0.0056    | 0.0056    | 0.0040    | 0.0035    | 0.0029    | 0.0042    | 0.0022    | 0.0035    | 0.0011    | 0.0023    | 0.0025    | 0.0018    | 0.0014    | 0.0005    | 0.0001    |
| Mg                             | 1.8567   | 1.6475    | 1.6515    | 1.6196    | 1.6999    | 1.7006    | 1.7065    | 1.7065    | 1.6811    | 1.6824    | 1.6917    | 1.8133    | 1.8118    | 1.8134    | 1.7864    | 1.8090    | 1.8043    | 1.8435    | 1.8626    | 1.8518    |
| Cr                             | 0        | 0.0015    | 0         | 0.0091    | 0         | 0.0003    | 0         | 0.0003    | 0.0009    | 0.0020    | 0         | 0         | 0.0004    | 0         | 0         | 0         | 0.0011    | 0.0020    | 0.0036    | 0.0007    |
| Al                             | 0        | 0         | 0         | 0.0091    | 0         | 0.0008    | 0.0008    | 0.0005    | 0.0009    | 0.0020    | 0         | 0         | 0.0004    | 0         | 0         | 0         | 0         | 0         | 0.0008    | 0         |
| Total                          | 2.9993   | 2.9921    | 3.0000    | 3.0064    | 3.0065    | 3.0094    | 3.0094    | 2.9850    | 2.9775    | 2.9830    | 2.9895    | 3.0111    | 3.0098    | 3.0129    | 3.0081    | 3.0101    | 3.0113    | 3.0153    | 3.0275    | 3.0184    |
| Fo                             | 82.89    | 83.22     | 82.92     | 80.65     | 84.49     | 84.29     | 84.29     | 86.63     | 86.09     | 85.64     | 85.48     | 89.58     | 89.89     | 89.50     | 89.15     | 89.6      | 89.22     | 90.85     | 90.72     | 90.95     |

| Echantillons                   | TR 83 111 | TR 79 6 | TR 79 7 | TR 79 12 | TR 79 1 | TR 79 3 | TR 79 6 | TR 79 7 | TR 79 10 | TR 79 11 | TR 81 32 | TR 81 34 | TR 423 16 | TR 423 21 | TR 423 24 | TR 423 27 | TR 423 29 |
|--------------------------------|-----------|---------|---------|----------|---------|---------|---------|---------|----------|----------|----------|----------|-----------|-----------|-----------|-----------|-----------|
| SiO <sub>2</sub>               | 40.38     | 40.27   | 40.79   | 40.58    | 41.16   | 41.47   | 41.13   | 40.79   | 40.85    | 40.67    | 40.44    | 39.96    | 41.00     | 40.77     | 40.38     | 40.74     | 41.56     |
| TiO <sub>2</sub>               | 0         | 0       | 0       | 0.06     | 0       | 0       | 0       | 0.01    | 0        | 0        | 0        | 0        | 0.02      | 0.03      | 0.01      | 0         | 0         |
| Al <sub>2</sub> O <sub>3</sub> | 0         | 0       | 0       | 0        | 0.04    | 0.04    | 0       | 0.03    | 0        | 0        | 0.02     | 0        | 0.01      | 0         | 0.18      | 0.01      | 0         |
| Fe <sub>2</sub> O <sub>3</sub> | 8.87      | 8.87    | 8.85    | 8.77     | 8.59    | 7.45    | 8.86    | 8.64    | 8.43     | 8.55     | 8.30     | 8.29     | 8.87      | 8.08      | 8.13      | 8.38      | 7.93      |
| MgO                            | 51.37     | 51.39   | 50.82   | 50.96    | 48.86   | 50.19   | 50.59   | 48.56   | 49.31    | 49.11    | 48.84    | 48.93    | 49.36     | 49.51     | 49.02     | 49.46     | 50.1      |
| MnO                            | 0.04      | 0.04    | 0.20    | 0.19     | 0.09    | 0.11    | 0.06    | 0.20    | 0.14     | 0.08     | 0.04     | 0.18     | 0.11      | 0.05      | 0.15      | 0.15      | 0.09      |
| CaO                            | 0         | 0       | 0       | 0        | 0       | 0       | 0       | 0.02    | 0        | 0        | 0        | 0        | 0         | 0         | 0         | 0         | 0.01      |
| Na <sub>2</sub> O              | 0         | 0       | 0       | 0.02     | 0       | 0       | 0       | 0       | 0        | 0        | 0        | 0        | 0         | 0         | 0         | 0         | 0         |
| K <sub>2</sub> O               | 0         | 0       | 0       | 0        | 0       | 0       | 0.02    | 0       | 0        | 0        | 0.02     | 0        | 0         | 0         | 0         | 0         | 0         |
| Cr                             | 0.03      | 0       | 0.07    | 0.30     | 0       | 0.22    | 0.07    | 0       | 0        | 0        | 0.02     | 0        | 0         | 0         | 0         | 0         | 0         |
| N                              | 0.19      | 0.28    | 0.29    | 0.32     | 0.29    | 0.27    | 0.25    | 0.23    | 0.15     | 0.25     | 0.26     | 0.29     | 0.31      | 0.28      | 0.28      | 0.51      | 0.07      |
| Total                          | 100.90    | 100.85  | 101.02  | 101.06   | 99.04   | 99.74   | 98.99   | 98.47   | 98.88    | 98.67    | 97.91    | 97.64    | 99.67     | 98.73     | 98.13     | 99.25     | 100.08    |
| K                              | 0.0002    | 0       | 0.0057  | 0.0052   | 0       | 0       | 0.0007  | 0       | 0.0029   | 0.0051   | 0.0051   | 0.0058   | 0.0061    | 0.0056    | 0.0055    | 0         | 0         |
| N                              | 0.0038    | 0.0054  | 0.0057  | 0.0063   | 0.0058  | 0.0053  | 0.0050  | 0.0045  | 0.0029   | 0.0051   | 0.0051   | 0.0058   | 0.0061    | 0.0056    | 0.0055    | 0.0100    | 0.0063    |
| Na                             | 0         | 0       | 0       | 0.0007   | 0       | 0       | 0       | 0       | 0        | 0        | 0        | 0        | 0         | 0         | 0         | 0.0002    | 0.0002    |
| Ca                             | 0         | 0       | 0       | 0        | 0       | 0       | 0       | 0.0005  | 0        | 0        | 0        | 0        | 0         | 0         | 0         | 0         | 0         |
| Fe                             | 0.1799    | 0.1800  | 0.1792  | 0.1775   | 0.1767  | 0.1513  | 0.1402  | 0.1768  | 0.1735   | 0.1766   | 0.1725   | 0.1731   | 0.1816    | 0.1663    | 0.1687    | 0.1722    | 0.1610    |
| Si                             | 0.9790    | 0.9773  | 0.9875  | 0.9827   | 1.0118  | 1.0076  | 1.0046  | 1.0094  | 1.0056   | 1.0045   | 1.0052   | 0.9978   | 1.0038    | 1.0041    | 1.0009    | 1.0012    | 1.0083    |
| Ti                             | 0         | 0       | 0       | 0.0010   | 0       | 0       | 0       | 0.0002  | 0        | 0        | 0.0001   | 0        | 0.0004    | 0.0006    | 0.0003    | 0         | 0         |
| Mn                             | 0.0009    | 0.0009  | 0.0041  | 0.0038   | 0.0019  | 0.0022  | 0.0012  | 0.0041  | 0.0029   | 0.0016   | 0.0009   | 0.0038   | 0.0022    | 0.0011    | 0.0031    | 0.0031    | 0.0018    |
| Mg                             | 1.8563    | 1.8598  | 1.8338  | 1.8357   | 1.7902  | 1.8177  | 1.8417  | 1.7912  | 1.8091   | 1.8075   | 1.8093   | 1.8214   | 1.8012    | 1.8174    | 1.8121    | 1.8115    | 1.8119    |
| Cr                             | 0.0005    | 0       | 0.0013  | 0.0057   | 0       | 0.0043  | 0.0013  | 0       | 0        | 0        | 0.0003   | 0        | 0.0001    | 0         | 0         | 0         | 0.0013    |
| Al                             | 0         | 0       | 0       | 0        | 0.0011  | 0.0011  | 0.0013  | 0.0008  | 0        | 0        | 0.0005   | 0        | 0.0001    | 0         | 0.0054    | 0.0002    | 0         |
| Total                          | 3.0206    | 3.0225  | 3.0116  | 3.0135   | 2.9874  | 2.9895  | 2.9849  | 2.9897  | 2.9942   | 2.9953   | 2.9941   | 3.0019   | 2.9955    | 2.9951    | 2.9959    | 2.9985    | 2.9909    |
| Fo                             | 90.86     | 90.89   | 90.66   | 90.72    | 90.68   | 91.97   | 92.63   | 90.53   | 90.98    | 90.79    | 91.02    | 90.88    | 90.46     | 91.31     | 91.09     | 90.72     | 91.46     |

Tableau 9 : analyses microsonde des olivines de Gray Rock.

**Tableau 10 : analyses microsonde des pyroxènes de Gray Rock.**

| N°Analyses                     | cumulats | TR413.38 | TR413.39 | TR413.40 | TR413.41 | TR413.42 | TR413.43 | TR379.63 | TR379.64 | TR379.65 | peridotites | TR83.109 | TR83.112 | TR83.114 |
|--------------------------------|----------|----------|----------|----------|----------|----------|----------|----------|----------|----------|-------------|----------|----------|----------|
| TiO <sub>2</sub>               |          | 0,28     | 0,35     | 0,28     | 0,28     | 0,40     | 0,43     | 0        | 0,04     | 0        | 0           | 0,21     | 0,07     | 0,16     |
| Al <sub>2</sub> O <sub>3</sub> |          | 21,06    | 20,14    | 19,82    | 19,33    | 20,54    | 19,57    | 0,18     | 0,36     | 0,23     |             | 17,75    | 18,79    | 18,40    |
| Cr <sub>2</sub> O <sub>3</sub> |          | 42,06    | 43,60    | 44,29    | 44,94    | 42,56    | 44,54    | 21,98    | 24,16    | 23,42    |             | 40,10    | 41,50    | 42,77    |
| FeO*                           |          | 24,34    | 26,33    | 28,16    | 28,32    | 25,05    | 26,78    | 77,86    | 71,28    | 74,38    |             | 28,58    | 27,98    | 26,31    |
| MnO                            |          | 0,81     | 0,69     | 0,43     | 0,43     | 0,66     | 0,73     | 1,05     | 1,33     | 1,14     |             | 0,25     | 0,38     | 0,31     |
| MgO                            |          | 12,12    | 9,60     | 8,39     | 8,29     | 10,24    | 8,74     | 1,06     | 1,55     | 1,52     |             | 7,84     | 8,49     | 9,09     |
| Total*                         |          | 100,67   | 100,71   | 101,37   | 101,59   | 99,45    | 100,79   | 102,13   | 98,72    | 100,69   |             | 94,73    | 97,21    | 97,04    |
| Ti                             |          | 0,052    | 0,066    | 0,053    | 0,053    | 0,076    | 0,082    | 0        | 0,009    | 0        |             | 0,043    | 0,014    | 0,032    |
| Al                             |          | 6,118    | 5,974    | 5,902    | 5,761    | 6,121    | 5,850    | 0,060    | 0,123    | 0,077    |             | 5,669    | 5,817    | 5,693    |
| Cr                             |          | 8,192    | 8,671    | 8,843    | 8,981    | 8,505    | 8,927    | 4,895    | 5,548    | 5,275    |             | 8,588    | 8,615    | 8,873    |
| Fe <sup>3+</sup>               |          | 1,586    | 1,223    | 1,148    | 1,152    | 1,222    | 1,059    | 11,045   | 10,311   | 10,648   |             | 1,658    | 1,541    | 1,370    |
| Fe <sup>2+</sup>               |          | 3,430    | 4,318    | 4,801    | 4,837    | 4,075    | 4,621    | 7,304    | 7,010    | 7,079    |             | 4,819    | 4,605    | 4,406    |
| Mn                             |          | 0,169    | 0,147    | 0,092    | 0,092    | 0,141    | 0,157    | 0,251    | 0,327    | 0,275    |             | 0,085    | 0,085    | 0,069    |
| Mg                             |          | 4,453    | 3,601    | 3,160    | 3,125    | 3,860    | 3,304    | 0,445    | 0,671    | 0,646    |             | 3,167    | 3,324    | 3,557    |
| Total                          |          | 24,000   | 24,000   | 23,999   | 24,001   | 24,000   | 24,000   | 24,000   | 23,999   | 24,000   |             | 24,001   | 24,001   | 24,000   |
| Fe <sub>2</sub> O <sub>3</sub> |          | 8,55     | 6,46     | 6,04     | 6,05     | 6,42     | 5,55     | 52,09    | 47,16    | 49,65    |             | 8,13     | 7,80     | 6,94     |
| FeO                            |          | 16,64    | 20,52    | 22,73    | 22,87    | 19,27    | 21,79    | 30,99    | 28,85    | 28,70    |             | 21,26    | 20,97    | 20,07    |
| Total                          |          | 101,52   | 101,36   | 101,98   | 102,19   | 100,09   | 101,35   | 107,35   | 103,45   | 105,66   |             | 95,54    | 98,00    | 97,74    |
| % Magn                         |          | 10       | 7,7      | 7,2      | 7,2      | 7,7      | 6,7      | 69       | 64,5     | 66,6     |             | 10,4     | 9,6      | 8,6      |
| % Herc                         |          | 38,5     | 37,6     | 37,1     | 36,2     | 38,6     | 36,9     | 0,4      | 0,8      | 0,5      |             | 35,6     | 36,4     | 35,7     |
| % Chro                         |          | 51,5     | 54,7     | 55,7     | 56,6     | 53,7     | 56,4     | 30,6     | 34,7     | 32,9     |             | 54       | 54       | 55,7     |

| N°Analyses                     | TR81.42 | TR79.1 | TR79.2 | TR79.4 | TR79.5 | TR79.8 | TR423.15 | TR423.16 | TR423.17 | TR423.18 | TR423.20 | TR423.22 | TR423.23 | TR423.25 | TR423.26 |
|--------------------------------|---------|--------|--------|--------|--------|--------|----------|----------|----------|----------|----------|----------|----------|----------|----------|
| TiO <sub>2</sub>               | 0,21    | 0,21   | 0,09   | 0,18   | 0,18   | 0,22   | 0,17     | 0,10     | 0        | 0,11     | 0,14     | 0,11     | 0,08     | 0,12     | 0,06     |
| Al <sub>2</sub> O <sub>3</sub> | 33,10   | 29,54  | 30,10  | 28,96  | 29,65  | 29,36  | 35,13    | 34,25    | 33,19    | 33,41    | 33,46    | 34,06    | 35,75    | 34,04    | 34,56    |
| Cr <sub>2</sub> O <sub>3</sub> | 34,23   | 37,42  | 33,11  | 35,07  | 34,96  | 34,57  | 33,10    | 34,85    | 31,08    | 32,31    | 33,50    | 32,02    | 30,90    | 31,99    | 31,74    |
| FeO*                           | 15,56   | 20,35  | 21,77  | 20,36  | 21,40  | 20,31  | 17,93    | 18,77    | 20,15    | 18,50    | 17,93    | 19,01    | 17,01    | 18,64    | 17,43    |
| MnO                            | 0,20    | 0,19   | 0,29   | 0,27   | 0,28   | 0,18   | 0,26     | 0,01     | 0,09     | 0,27     | 0,19     | 0,25     | 0,15     | 0,27     | 0,19     |
| MgO                            | 15,67   | 13,29  | 11,82  | 12,72  | 12,82  | 12,90  | 14,58    | 13,59    | 12,89    | 14,58    | 14,49    | 13,29    | 14,90    | 13,80    | 14,43    |
| Total*                         | 98,97   | 101,00 | 97,18  | 97,56  | 99,29  | 97,54  | 101,17   | 101,57   | 97,40    | 99,18    | 99,71    | 98,74    | 98,79    | 98,86    | 98,41    |
| Ti                             | 0,037   | 0,037  | 0,017  | 0,033  | 0,033  | 0,040  | 0,029    | 0,017    | 0        | 0,019    | 0,025    | 0,020    | 0,014    | 0,021    | 0,011    |
| Al                             | 9,111   | 8,230  | 8,708  | 8,342  | 8,391  | 8,435  | 9,497    | 9,320    | 9,405    | 9,227    | 9,210    | 9,497    | 9,801    | 9,451    | 9,574    |
| Cr                             | 6,318   | 6,990  | 6,423  | 6,774  | 6,634  | 6,660  | 6,000    | 6,359    | 5,905    | 5,983    | 6,183    | 5,986    | 5,680    | 5,956    | 5,896    |
| Fe <sup>3+</sup>               | 0,497   | 0,706  | 0,837  | 0,818  | 0,910  | 0,824  | 0,445    | 0,286    | 0,689    | 0,752    | 0,559    | 0,478    | 0,491    | 0,551    | 0,509    |
| Fe <sup>2+</sup>               | 2,542   | 3,317  | 3,632  | 3,343  | 3,387  | 3,316  | 2,994    | 3,338    | 3,362    | 2,874    | 2,943    | 3,283    | 2,818    | 3,122    | 2,917    |
| Mn                             | 0,040   | 0,038  | 0,060  | 0,056  | 0,057  | 0,037  | 0,051    | 0,002    | 0,018    | 0,054    | 0,038    | 0,050    | 0,030    | 0,054    | 0,038    |
| Mg                             | 5,455   | 4,682  | 4,324  | 4,634  | 4,588  | 4,687  | 4,985    | 4,677    | 4,620    | 5,092    | 5,044    | 4,686    | 5,166    | 4,846    | 5,056    |
| Total                          | 24,000  | 24,000 | 24,001 | 24,000 | 24,000 | 23,999 | 24,001   | 23,999   | 23,999   | 24,001   | 24,002   | 24,000   | 24,000   | 24,001   | 24,001   |
| Fe <sub>2</sub> O <sub>3</sub> | 2,83    | 3,97   | 4,53   | 4,45   | 5,04   | 4,49   | 2,58     | 1,65     | 3,81     | 4,26     | 3,18     | 2,68     | 2,80     | 3,11     | 2,88     |
| FeO                            | 13,02   | 16,78  | 17,69  | 16,36  | 16,87  | 16,27  | 15,61    | 17,29    | 16,72    | 14,66    | 15,07    | 16,60    | 14,49    | 15,85    | 14,84    |
| Total                          | 99,26   | 101,40 | 97,63  | 98,01  | 99,80  | 97,99  | 101,43   | 101,74   | 97,78    | 99,60    | 100,03   | 99,01    | 99,07    | 99,18    | 98,70    |
| % Magn                         | 3,1     | 4,4    | 5,2    | 5,1    | 5,7    | 5,2    | 2,8      | 1,8      | 4,3      | 4,7      | 3,5      | 3        | 3,1      | 3,5      | 3,2      |
| % Herc                         | 57,2    | 51,7   | 54,5   | 52,4   | 52,7   | 53     | 59,6     | 58,4     | 58,8     | 57,8     | 57,7     | 59,5     | 61,4     | 59,2     | 59,9     |
| % Chro                         | 39,7    | 43,9   | 40,3   | 42,5   | 41,6   | 41,8   | 37,6     | 39,8     | 36,9     | 37,5     | 38,8     | 37,5     | 35,5     | 37,3     | 36,9     |

tableau 11 : analyses microsonde des spiralles de Gray Rock.

| N°Echantillons<br>N°Analyses | TR 68<br>2 | TR 68<br>3 | TR 68<br>4 | TR 68<br>9 | TR 68<br>10 | CL5<br>12 | CL5<br>13 | TOAD 20<br>6 | TOAD 20<br>7 | TOAD 20<br>8 | TOAD 21<br>67 | TOAD 21<br>68 | TOAD 21<br>69 | TOAD 21<br>74 | TOAD 21<br>76 |
|------------------------------|------------|------------|------------|------------|-------------|-----------|-----------|--------------|--------------|--------------|---------------|---------------|---------------|---------------|---------------|
| TiO2                         | 52,27      | 51,32      | 52,01      | 51,16      | 52,70       | 51,13     | 49,55     | 2,19         | 10,11        | 1,28         | 52,76         | 51,96         | 51,29         | 51,74         | 52,17         |
| Al2O3                        | 0          | 0          | 0,28       | 0          | 0           | 0,01      | 0,03      | 1,01         | 1,70         | 1,73         | 0,24          | 0,04          | 0,35          | 0             | 0,06          |
| Cr2O3                        | 0          | 0,02       | 0,02       | 0,05       | 0           | 0,36      | 0,38      | 6,49         | 6,45         | 6,15         | 0             | 0,06          | 0             | 0,02          | 0,09          |
| FeO*                         | 46,22      | 45,51      | 45,06      | 43,99      | 44,21       | 41,35     | 43,74     | 80,39        | 72,86        | 80,57        | 44,23         | 44,87         | 45,02         | 45,42         | 45,03         |
| MnO                          | 2,30       | 2,20       | 2,26       | 2,45       | 2,63        | 5,08      | 3,06      | 0,10         | 0,29         | 0,01         | 1,69          | 1,35          | 1,47          | 1,70          | 1,57          |
| MgO                          | 0,15       | 0,16       | 0,28       | 0,12       | 0,18        | 0,12      | 0,21      | 0,11         | 0,41         | 0,21         | 0,20          | 0,16          | 0,10          | 0,05          | 0,07          |
| Total*                       | 100,94     | 99,21      | 99,91      | 97,77      | 99,72       | 98,05     | 96,97     | 90,29        | 91,82        | 89,95        | 99,12         | 98,44         | 98,23         | 98,93         | 98,99         |
| Ti                           | 1,962      | 1,960      | 1,969      | 1,984      | 2,003       | 1,977     | 1,934     | 0,087        | 0,398        | 0,051        | 2,009         | 2,000         | 1,977         | 1,985         | 1,999         |
| Al                           | 0          | 0          | 0,017      | 0          | 0           | 0,001     | 0,002     | 0,063        | 0,105        | 0,108        | 0,014         | 0,002         | 0,021         | 0             | 0,004         |
| Cr                           | 0          | 0,001      | 0,001      | 0,002      | 0           | 0,015     | 0,016     | 0,272        | 0,267        | 0,257        | 0             | 0,002         | 0             | 0,001         | 0,004         |
| Fe3+                         | 0,076      | 0,080      | 0,045      | 0,029      | 0           | 0,031     | 0,115     | 3,490        | 2,833        | 3,533        | 0             | 0             | 0,024         | 0,030         | 0             |
| Fe2+                         | 1,854      | 1,853      | 1,851      | 1,868      | 1,868       | 1,746     | 1,783     | 0,074        | 0,353        | 0,034        | 1,873         | 1,921         | 1,906         | 1,907         | 1,919         |
| Mn                           | 0,097      | 0,095      | 0,096      | 0,107      | 0,113       | 0,221     | 0,134     | 0,004        | 0,013        | 0,000        | 0,072         | 0,059         | 0,064         | 0,073         | 0,068         |
| Mg                           | 0,011      | 0,012      | 0,021      | 0,009      | 0,014       | 0,009     | 0,016     | 0,009        | 0,032        | 0,017        | 0,015         | 0,012         | 0,008         | 0,004         | 0,005         |
| Total                        | 4,000      | 4,001      | 4,000      | 3,999      | 3,998       | 4,000     | 4,000     | 3,999        | 4,001        | 4,000        | 3,983         | 3,996         | 4,000         | 4,000         | 3,999         |
| Fe2O3                        | 2,01       | 2,08       | 1,20       | 0,76       | 0           | 0,81      | 2,95      | 87,48        | 72,01        | 88,69        | 0             | 0             | 0,63          | 0,78          | 0             |
| FeO                          | 44,41      | 43,64      | 43,98      | 43,31      | 44,21       | 40,62     | 41,08     | 1,67         | 8,07         | 0,77         | 44,23         | 44,87         | 44,46         | 44,72         | 45,03         |
| Total                        | 101,14     | 99,42      | 100,03     | 97,85      | 99,72       | 98,13     | 97,26     | 99,05        | 99,04        | 98,84        | 99,12         | 98,44         | 98,30         | 99,01         | 98,99         |
| % Ilm                        | 97,40      | 97,30      | 97,70      | 98,80      | 99,30       | 98,60     | 96,00     | 4,00         | 19,60        | 1,90         | 99,20         | 99,40         | 99,00         | 99,00         | 99,70         |
| % Gai                        | 0,60       | 0,60       | 1,10       | 0,50       | 0,70        | 0,50      | 0,90      | 0,50         | 1,80         | 0,90         | 0,80          | 0,60          | 0,40          | 0,20          | 0,30          |
| % Hém                        | 2,00       | 2,10       | 1,20       | 0,70       | 0           | 0,90      | 3,10      | 95,50        | 78,60        | 97,20        | 0             | 0             | 0,60          | 0,80          | 0             |
| % Hém                        | 26,00      | 27,20      | 16,10      | 11,10      | 0           | 6,30      | 27,70     | 99,30        | 96,90        | 99,00        | 0             | 0             | 14,30         | 16,30         | 0             |
| % Gai                        | 7,50       | 8,20       | 15,10      | 6,90       | 11,00       | 3,70      | 7,70      | 0,50         | 2,20         | 1,00         | 17,20         | 16,90         | 9,50          | 4,30          | 6,80          |
| % Pyr                        | 66,50      | 64,60      | 68,80      | 82,00      | 89,00       | 90,00     | 64,60     | 0,20         | 0,90         | 0            | 82,80         | 83,10         | 76,20         | 79,40         | 93,20         |

tableau 12 : analyses microsonde de titanomagnétites et ilménites de l'ophiolite de Trinity : Gray Rock (GR), Castle Lake (CL) et Toad Lake (TD).

| N°Echantillons<br>N°Analyses | TOAD 21<br>78 | TOAD 21<br>79 | TOAD 21<br>80 | TOAD 12<br>51 | TOAD 12<br>52 | TOAD 12<br>60 | TOAD 12<br>61 | TOAD 12<br>62 | TOAD 12<br>66 | TOAD 12<br>5 | TOAD 12<br>10 | TOAD 12<br>17 | TOAD 17<br>6 | TOAD 22<br>24 | TOAD 22<br>25 | TOAD 22<br>31 |
|------------------------------|---------------|---------------|---------------|---------------|---------------|---------------|---------------|---------------|---------------|--------------|---------------|---------------|--------------|---------------|---------------|---------------|
| TiO2                         | 51,83         | 52,27         | 52,01         | 52,75         | 51,52         | 1,05          | 0,92          | 0,86          | 1,91          | 0,67         | 0,33          | 0,78          | 0,82         | 51,77         | 51,10         | 3,22          |
| Al2O3                        | 0,04          | 0             | 0,04          | 0,76          | 2,84          | 1,29          | 5,51          | 0,65          | 0,67          | 0,62         | 4,29          | 0,67          | 0            | 0,07          | 0             | 0,51          |
| Cr2O3                        | 0,07          | 0,02          | 0,35          | 0             | 0             | 3,37          | 3,48          | 3,32          | 1,47          | 2,73         | 1,79          | 2,76          | 0,12         | 0             | 0,01          | 0,16          |
| FeO *                        | 44,87         | 44,87         | 45,23         | 45,21         | 43,61         | 82,80         | 79,07         | 85,73         | 85,65         | 88,36        | 83,60         | 84,90         | 90,18        | 44,83         | 44,46         | 83,72         |
| MnO                          | 1,27          | 1,40          | 1,34          | 0,54          | 0,48          | 0,13          | 0,04          | 0,12          | 0,01          | 0,08         | 0             | 0             | 0,22         | 1,05          | 0,90          | 0,16          |
| MgO                          | 0,11          | 0,09          | 0,07          | 0,81          | 0,86          | 0,30          | 1,29          | 0,19          | 0,20          | 0,20         | 0,18          | 0,09          | 0,28         | 0,03          | 0,03          | 0,34          |
| Total *                      | 98,19         | 98,65         | 99,04         | 100,07        | 99,31         | 88,94         | 90,31         | 90,87         | 89,91         | 92,66        | 90,19         | 89,20         | 91,62        | 97,75         | 96,50         | 88,11         |
| Ti                           | 2,001         | 2,008         | 1,993         | 1,981         | 1,926         | 0,042         | 0,035         | 0,034         | 0,076         | 0,026        | 0,013         | 0,031         | 0,032        | 2,007         | 2,007         | 0,131         |
| Al                           | 0,002         | 0             | 0,002         | 0,045         | 0,166         | 0,081         | 0,329         | 0,040         | 0,042         | 0,038        | 0,263         | 0,042         | 0            | 0,004         | 0             | 0,033         |
| Cr                           | 0,003         | 0,001         | 0,014         | 0             | 0             | 0,142         | 0,139         | 0,138         | 0,062         | 0,111        | 0,074         | 0,117         | 0,005        | 0             | 0             | 0,007         |
| Fe3+                         | 0             | 0             | 0             | 0             | 0             | 3,692         | 3,418         | 3,754         | 3,744         | 3,799        | 3,637         | 3,778         | 3,931        | 0             | 0             | 3,698         |
| Fe2+                         | 1,926         | 1,916         | 1,927         | 1,888         | 1,813         | 0,012         | 0,000         | 0,014         | 0,060         | 0,007        | 0,000         | 0,024         | 0,001        | 1,932         | 1,942         | 0,096         |
| Mn                           | 0,055         | 0,061         | 0,058         | 0,023         | 0,020         | 0,006         | 0,002         | 0,005         | 0,000         | 0,003        | 0,000         | 0,000         | 0,010        | 0,046         | 0,040         | 0,007         |
| Mg                           | 0,008         | 0,007         | 0,005         | 0,060         | 0,064         | 0,024         | 0,098         | 0,015         | 0,016         | 0,015        | 0,014         | 0,007         | 0,022        | 0,002         | 0,002         | 0,027         |
| Total                        | 3,995         | 3,993         | 3,999         | 3,997         | 3,989         | 3,999         | 4,021         | 4,000         | 4,000         | 3,999        | 4,001         | 3,999         | 4,001        | 3,991         | 3,991         | 3,999         |
| Fe2O3                        | 0             | 0             | 0             | 0             | 0             | 91,71         | 89,55         | 94,93         | 93,69         | 98,01        | 92,94         | 93,75         | 100,20       | 0             | 0             | 90,68         |
| FeO                          | 44,87         | 44,87         | 45,23         | 45,21         | 43,61         | 0,28          | 0             | 0,31          | 1,35          | 0,16         | 0             | 0,54          | 0,02         | 44,83         | 44,46         | 2,13          |
| Total                        | 98,19         | 98,65         | 99,04         | 100,07        | 99,31         | 98,13         | 100,79        | 100,38        | 99,30         | 102,47       | 99,53         | 98,59         | 101,66       | 97,75         | 96,50         | 97,20         |
| % Ilm                        | 99,60         | 99,60         | 99,70         | 96,90         | 96,60         | 0,60          | 0             | 0,70          | 3,10          | 0,40         | 0,00          | 1,30          | 0,10         | 99,90         | 99,90         | 4,90          |
| % Gei                        | 0,40          | 0,40          | 0,30          | 3,10          | 3,40          | 1,30          | 5,40          | 0,80          | 0,80          | 0,80         | 0,80          | 0,40          | 1,10         | 0,10          | 0,10          | 1,40          |
| % Hém                        | 0             | 0             | 0             | 0             | 0             | 98,10         | 94,60         | 98,50         | 96,10         | 98,80        | 99,20         | 98,30         | 98,80        | 0             | 0             | 93,70         |
| % Hém                        | 0             | 0             | 0             | 0             | 0             | 98,40         | 94,50         | 98,90         | 99,20         | 99,10        | 99,20         | 99,60         | 98,40        | 0             | 0             | 98,20         |
| % Gei                        | 12,70         | 10,30         | 7,90          | 72,30         | 76,20         | 1,30          | 5,40          | 0,80          | 0,80          | 0,80         | 0,80          | 0,40          | 1,10         | 4,20          | 4,80          | 1,40          |
| % Pyr                        | 87,30         | 89,70         | 92,10         | 27,70         | 23,80         | 0,30          | 0,10          | 0,30          | 0             | 0,10         | 0             | 0             | 0,50         | 95,80         | 95,20         | 0,40          |

tableau 12 : analyses microsonde de titanomagnétites et ilménites de l'ophiolite de Trinity : Gray Rock (GR), Castle Lake (CL) et Toad Lake (TD).

| Echantillons                   | TR 113 | TR 113 | TR 113 | TR 113 | TR 113 | TR 248 | TR 85  | TR 85  | TR 85  | TR 121 | TR 121 | TR 121 | TR 106 |
|--------------------------------|--------|--------|--------|--------|--------|--------|--------|--------|--------|--------|--------|--------|--------|
| SiO <sub>2</sub>               | 45,33  | 52,61  | 48,47  | 44,81  | 44,49  | 44,71  | 45,16  | 57,12  | 56,53  | 57,27  | 53,37  | 53,92  | 54,34  |
| Al <sub>2</sub> O <sub>3</sub> | 11,58  | 5,30   | 7,69   | 11,17  | 11,70  | 11,78  | 11,03  | 1,17   | 1,62   | 1,16   | 5,24   | 4,96   | 3,78   |
| FeO                            | 5,27   | 4,18   | 4,14   | 4,62   | 5,15   | 5,04   | 4,67   | 5,46   | 6,67   | 4,25   | 6,16   | 6,75   | 6,09   |
| MgO                            | 18,33  | 20,96  | 19,67  | 17,87  | 18,25  | 18,44  | 18,15  | 21,00  | 20,36  | 21,37  | 18,71  | 19,53  | 20,16  |
| MnO                            | 0,05   | 0,09   | 0      | 0      | 0,13   | 0,07   | 0,19   | 0,16   | 0,29   | 0,30   | 0,12   | 0,08   | 0      |
| TiO <sub>2</sub>               | 0,68   | 0,09   | 0,25   | 0,90   | 0,94   | 0,53   | 0,38   | 0      | 0      | 0      | 0      | 0,06   | 0,39   |
| Cr <sub>2</sub> O <sub>3</sub> | 0      | 0      | 0      | 0      | 0      | 0      | 0      | 0,12   | 0,26   | 0      | 0,19   | 0,42   | 0,03   |
| NiO                            | 1,00   | 0,24   | 0,32   | 1,30   | 1,35   | 1,14   | 1,24   | 0      | 0      | 0,09   | 0,02   | 0      | 0      |
| CaO                            | 11,91  | 12,73  | 12,48  | 11,82  | 11,35  | 12,02  | 12,39  | 12,79  | 12,64  | 12,83  | 12,29  | 12,00  | 12,09  |
| Na <sub>2</sub> O              | 2,77   | 1,05   | 1,45   | 2,69   | 2,79   | 2,72   | 2,48   | 0,16   | 0,22   | 0,18   | 0,79   | 0,51   | 0,57   |
| K <sub>2</sub> O               | 0,18   | 0,03   | 0,05   | 0,10   | 0,12   | 0,19   | 0,14   | 0      | 0      | 0      | 0,02   | 0,03   | 0,02   |
| Total                          | 97,10  | 97,28  | 94,52  | 95,28  | 96,27  | 96,64  | 95,71  | 97,98  | 98,59  | 97,45  | 96,91  | 97,48  | 97,48  |
| Si                             | 6,49   | 7,335  | 6,981  | 6,533  | 6,425  | 6,414  | 6,529  | 7,888  | 7,794  | 7,919  | 7,442  | 7,493  | 7,524  |
| AlIV                           | 1,52   | 0,665  | 1,019  | 1,467  | 1,575  | 1,586  | 1,471  | 0,198  | 0,205  | 0,080  | 0,557  | 0,506  | 0,475  |
| AlVI                           | 0,44   | 0,205  | 0,286  | 0,453  | 0,416  | 0,405  | 0,408  | 0,059  | 0,057  | 0,108  | 0,304  | 0,192  | 0,142  |
| Ti                             | 0,07   | 0,009  | 0,027  | 0,098  | 0,102  | 0,057  | 0,041  | 0      | 0      | 0      | 0      | 0,006  | 0,040  |
| Cr                             | 0      | 0      | 0      | 0      | 0      | 0      | 0      | 0,013  | 0,028  | 0      | 0,020  | 0,046  | 0,003  |
| Fe <sup>3+</sup>               | 0,126  | 0,149  | 0,262  | 0,035  | 0,149  | 0,273  | 0,257  | 0,064  | 0,178  | 0,019  | 0,441  | 0,472  | 0,397  |
| Fe <sup>2+</sup>               | 0,503  | 0,338  | 0,235  | 0,527  | 0,227  | 0,331  | 0,307  | 0,567  | 0,590  | 0,471  | 0,276  | 0,325  | 0,306  |
| Mn                             | 0,006  | 0,010  | 0      | 0      | 0,015  | 0,008  | 0,008  | 0,018  | 0,033  | 0,035  | 0,014  | 0,009  | 0      |
| Mg                             | 3,909  | 4,356  | 4,223  | 3,885  | 3,928  | 3,943  | 3,911  | 4,212  | 4,184  | 4,404  | 3,889  | 3,886  | 4,161  |
| Ni                             | 0,115  | 0,026  | 0,037  | 0,152  | 0,156  | 0,131  | 0,144  | 0      | 0      | 0,010  | 0,002  | 0      | 0      |
| Ca                             | 1,826  | 1,902  | 1,926  | 1,847  | 1,756  | 1,847  | 1,919  | 1,892  | 1,867  | 1,901  | 1,836  | 1,798  | 1,794  |
| NaA                            | 0      | 0      | 0      | 0      | 0      | 0      | 0      | 0,042  | 0,058  | 0,048  | 0,213  | 0,215  | 0,153  |
| NaB                            | 0,768  | 0,283  | 0,405  | 0,760  | 0,781  | 0,756  | 0,695  | 0      | 0      | 0      | 0      | 0      | 0      |
| K                              | 0,032  | 0,005  | 0,009  | 0,018  | 0,022  | 0,034  | 0,025  | 0      | 0      | 0      | 0,003  | 0,005  | 0,003  |
| Total                          | 15,796 | 15,283 | 15,410 | 15,775 | 15,552 | 15,785 | 15,715 | 14,993 | 14,994 | 14,995 | 14,997 | 15,002 | 15,130 |

tableau 13 : analyses microsonde des amphiboles de Gray Rock.



**tableau 13 : analyses microsonde des amphiboles de Gray Rock.**

**tableau 13 : analyses microsonde des amphiboles de Gray Rock.**

[illegible]

| Echantillons                   | b      | b      | b      | V      | c      | TR 53B | TR 53B | TR 53B | TR 53B | TR 53B | TR 53B | TR 128F | TR 128F | TR 124D | TR 124D | TR 124D |
|--------------------------------|--------|--------|--------|--------|--------|--------|--------|--------|--------|--------|--------|---------|---------|---------|---------|---------|
| SiO <sub>2</sub>               | 46,26  | 48,02  | 47,82  | 45,97  | 46,27  | 55,37  | 54,22  | 53,41  | 54,53  | 54,67  | 55,05  | 53,03   | 54,09   | 51,73   | 52,14   | 53,02   |
| Al <sub>2</sub> O <sub>3</sub> | 8,89   | 6,51   | 7,33   | 8,96   | 8,53   | 1,51   | 2,23   | 1,82   | 1,97   | 1,07   | 1,58   | 4,00    | 3,61    | 5,48    | 4,25    | 3,70    |
| FeO                            | 15,54  | 16,03  | 15,59  | 14,80  | 14,17  | 7,20   | 7,36   | 10,23  | 7,18   | 6,82   | 6,93   | 9,58    | 9,57    | 5,98    | 4,25    | 4,06    |
| MgO                            | 12,09  | 12,52  | 13,02  | 11,64  | 13,28  | 18,61  | 18,71  | 16,36  | 18,47  | 19,13  | 18,60  | 16,26   | 16,81   | 15,20   | 11,02   | 10,38   |
| MnO                            | 0,25   | 0,35   | 0,26   | 0,28   | 0,24   | 0,19   | 0,28   | 0,43   | 0,25   | 0,17   | 0,36   | 0,25    | 0,41    | 0,36    | 0,31    | 0,24    |
| TiO <sub>2</sub>               | 1,73   | 1,14   | 1,38   | 1,64   | 1,62   | 0,03   | 0      | 0      | 0,07   | 0      | 0      | 0,18    | 0,07    | 0,10    | 0,59    | 0,27    |
| Cr <sub>2</sub> O <sub>3</sub> | 0,04   | 0      | 0      | 0      | 0,02   | 0,03   | 0,18   | 0,10   | 0,32   | 0,28   | 0,13   | 0,28    | 0,29    | 0       | 0,05    | 0       |
| NiO                            | 0      | 0      | 0      | 0      | 0      | 0      | 0      | 0,07   | 0      | 0      | 0      | 0,18    | 0,01    | 0       | 0       | 0       |
| CaO                            | 10,79  | 10,73  | 10,39  | 11,16  | 10,63  | 13,57  | 13,51  | 12,85  | 13,35  | 13,14  | 13,39  | 11,68   | 11,62   | 12,21   | 11,98   | 12,44   |
| Na <sub>2</sub> O              | 1,47   | 1,23   | 1,28   | 1,62   | 1,37   | 0,08   | 0,17   | 0,10   | 0,16   | 0,06   | 0,14   | 0,57    | 0,46    | 0,68    | 0,63    | 0,46    |
| K <sub>2</sub> O               | 0,03   | 0,25   | 0,05   | 0,07   | 0,09   | 0      | 0,05   | 0,05   | 0,01   | 0,04   | 0,02   | 0,04    | 0,04    | 0,07    | 0,09    | 0,06    |
| Total                          | 97,09  | 96,78  | 97,12  | 96,14  | 96,22  | 96,56  | 96,71  | 95,42  | 96,31  | 95,38  | 96,20  | 96,05   | 96,98   | 95,41   | 96,58   | 96,78   |
| Si                             | 6,733  | 7,020  | 6,911  | 6,811  | 6,727  | 7,850  | 7,666  | 7,780  | 7,751  | 7,831  | 7,829  | 7,624   | 7,698   | 7,486   | 7,497   | 7,584   |
| AlIV                           | 1,267  | 0,980  | 1,089  | 1,189  | 1,273  | 0,149  | 0,333  | 0,219  | 0,248  | 0,168  | 0,170  | 0,375   | 0,301   | 0,513   | 0,502   | 0,415   |
| AlVI                           | 0,258  | 0,141  | 0,159  | 0,375  | 0,188  | 0,103  | 0,038  | 0,093  | 0,081  | 0,012  | 0,094  | 0,302   | 0,304   | 0,421   | 0,218   | 0,208   |
| Ti                             | 0,189  | 0,125  | 0,150  | 0,182  | 0,177  | 0,003  | 0      | 0      | 0,007  | 0      | 0      | 0,019   | 0,007   | 0,010   | 0,063   | 0,029   |
| Cr                             | 0,004  | 0      | 0      | 0      | 0,002  | 0      | 0,020  | 0,011  | 0,035  | 0,031  | 0,014  | 0,031   | 0,032   | 0       | 0,005   | 0       |
| Fe <sup>3+</sup>               | 0,835  | 0,828  | 0,977  | 0,423  | 1,010  | 0,061  | 0,312  | 0,132  | 0,158  | 0,134  | 0,095  | 0,154   | 0,069   | 0,247   | 0,309   | 0,265   |
| Fe <sup>2+</sup>               | 1,056  | 1,131  | 0,906  | 1,411  | 0,712  | 0,792  | 0,558  | 1,113  | 0,695  | 0,682  | 0,728  | 0,997   | 1,069   | 0,911   | 1,016   | 0,976   |
| Mn                             | 0,030  | 0,043  | 0,031  | 0,035  | 0,029  | 0,022  | 0,033  | 0,053  | 0,030  | 0,020  | 0,043  | 0,030   | 0,049   | 0,044   | 0,037   | 0,029   |
| Mg                             | 2,623  | 2,728  | 2,804  | 2,570  | 2,878  | 3,933  | 3,943  | 3,552  | 3,913  | 4,084  | 3,943  | 3,484   | 3,566   | 3,278   | 3,326   | 3,456   |
| Ni                             | 0      | 0      | 0      | 0      | 0      | 0      | 0      | 0,008  | 0      | 0      | 0      | 0,020   | 0,001   | 0       | 0       | 0       |
| Ca                             | 1,683  | 1,681  | 1,609  | 1,772  | 1,656  | 2,061  | 2,046  | 2,005  | 2,032  | 2,016  | 2,040  | 1,799   | 1,772   | 1,893   | 1,845   | 1,906   |
| NaA                            | 0,317  | 0,319  | 0,358  | 0,228  | 0,344  | 0,021  | 0,046  | 0,028  | 0,044  | 0,016  | 0,038  | 0,158   | 0,126   | 0,190   | 0,175   | 0,127   |
| NaB                            | 0,097  | 0,028  | 0      | 0,236  | 0,041  | 0      | 0      | 0      | 0      | 0      | 0      | 0       | 0       | 0       | 0       | 0       |
| K                              | 0,005  | 0,046  | 0,009  | 0,013  | 0,016  | 0      | 0,009  | 0,009  | 0,001  | 0,007  | 0,003  | 0,007   | 0,007   | 0,012   | 0,016   | 0,010   |
| Total                          | 15,097 | 15,070 | 15,003 | 15,245 | 15,053 | 14,995 | 15,004 | 15,003 | 14,995 | 15,001 | 14,997 | 15,000  | 15,001  | 15,005  | 15,009  | 15,005  |
|                                |        |        |        |        |        |        |        |        |        |        |        |         |         |         |         | 0,012   |
|                                |        |        |        |        |        |        |        |        |        |        |        |         |         |         |         | 15,006  |

tableau 13 : analyses microsonde des amphiboles de Gray Rock.

| Echantillons         | gabbros | TR64  | PEGMA | PEGMA | PEGMA | PEGMB | PEGMB | TR532 | TR532 | TR532 | TR110 | TR110 | TR110 | TR110 | TR110 | TR110 | TR110 |       |
|----------------------|---------|-------|-------|-------|-------|-------|-------|-------|-------|-------|-------|-------|-------|-------|-------|-------|-------|-------|
| Echantillons gabbros | SiO2    | 42,96 | 41,08 | 40,11 | 42,01 | 40,17 | 39,82 | 40,28 | 39,75 | 37,72 | 38,28 | 38,12 | 41,56 | 40,58 | 40,17 | 40,11 | 42,01 |       |
|                      | Al2O3   | 31,22 | 29,50 | 32,50 | 32,05 | 32,71 | 30,17 | 29,59 | 29,88 | 28,86 | 32,18 | 31,91 | 31,53 | 32,95 | 32,71 | 32,50 | 32,05 |       |
|                      | Fe2O3t  | 1,18  | 3,44  | 1,07  | 0,49  | 0,52  | 2,88  | 3,16  | 2,74  | 4,03  | 0,69  | 0,41  | 0,69  | 0,42  | 0,52  | 1,07  | 0,49  |       |
|                      | MgO     | 0,30  | 0,01  | 0,00  | 0,00  | 0,02  | 0,00  | 0,01  | 0,00  | 0,00  | 0,00  | 0,03  | 0,01  | 0,02  | 0,02  | 0,00  | 0,00  |       |
|                      | MnO     | 0,13  | 0,06  | 0,09  | 0,04  | 0,00  | 0,13  | 0,08  | 0,00  | 0,00  | 0,00  | 0,11  | 0,03  | 0,00  | 0,13  | 0,09  | 0,04  |       |
|                      | TiO2    | 0,00  | 0,00  | 0,00  | 0,00  | 0,00  | 0,01  | 0,00  | 0,00  | 0,10  | 0,00  | 0,00  | 0,06  | 0,00  | 0,00  | 0,00  | 0,00  |       |
|                      | Cr2O3   | 0,00  | 0,00  | 0,00  | 0,00  | 0,00  | 0,00  | 0,00  | 0,00  | 0,00  | 0,00  | 0,00  | 0,00  | 0,01  | 0,00  | 0,00  | 0,00  |       |
|                      | NiO     | 0,00  | 0,01  | 0,00  | 0,00  | 0,00  | 0,02  | 0,00  | 0,00  | 0,00  | 0,00  | 0,00  | 0,00  | 0,02  | 0,00  | 0,00  | 0,00  |       |
|                      | CaO     | 21,28 | 21,80 | 24,58 | 22,19 | 24,16 | 24,39 | 25,03 | 24,66 | 24,40 | 23,11 | 22,82 | 23,42 | 20,68 | 24,16 | 24,39 | 24,58 | 22,19 |
|                      | Na2O    | 1,09  | 0,88  | 0,09  | 0,76  | 0,05  | 0,19  | 0,05  | 0,00  | 0,01  | 0,01  | 0,02  | 0,00  | 1,67  | 0,05  | 0,19  | 0,09  | 0,76  |
| K2O                  | 0,00    | 0,00  | 0,02  | 0,00  | 0,00  | 0,00  | 0,02  | 0,01  | 0,00  | 0,00  | 0,02  | 0,01  | 0,00  | 0,00  | 0,00  | 0,02  | 0,00  |       |
| Total                | 98,16   | 96,78 | 98,46 | 97,54 | 98,18 | 98,15 | 97,98 | 97,79 | 96,78 | 93,83 | 94,01 | 94,07 | 96,20 | 98,18 | 98,15 | 98,46 | 97,54 |       |
| Echantillons gabbros | Si      | 3,226 | 3,182 | 3,039 | 3,172 | 3,062 | 3,043 | 3,190 | 3,215 | 3,048 | 3,020 | 3,011 | 3,183 | 3,062 | 3,043 | 3,039 | 3,172 |       |
|                      | AlVI    | 2,758 | 2,688 | 2,897 | 2,847 | 2,925 | 2,915 | 2,848 | 2,847 | 2,744 | 2,987 | 2,965 | 2,841 | 2,925 | 2,915 | 2,897 | 2,847 |       |
|                      | Ti      | 0     | 0     | 0     | 0     | 0     | 0     | 0,001 | 0     | 0,006 | 0     | 0,003 | 0     | 0     | 0     | 0     | 0     |       |
|                      | Fe3+    | 0,064 | 0,193 | 0,059 | 0,027 | 0,023 | 0,028 | 0,193 | 0,212 | 0,236 | 0,013 | 0,023 | 0,038 | 0,023 | 0,028 | 0,059 | 0,027 |       |
|                      | Fe2+    | 0     | 0     | 0     | 0     | 0     | 0     | 0     | 0     | 0     | 0,052 | 0     | 0     | 0     | 0     | 0     | 0     |       |
|                      | Mg      | 0,033 | 0,001 | 0     | 0     | 0,002 | 0,002 | 0     | 0,001 | 0     | 0     | 0,003 | 0,001 | 0,001 | 0,002 | 0     | 0     |       |
|                      | Mn      | 0,008 | 0,003 | 0,005 | 0,002 | 0     | 0,008 | 0     | 0,005 | 0     | 0     | 0,007 | 0,001 | 0,001 | 0     | 0,005 | 0,002 |       |
|                      | Cr      | 0     | 0     | 0     | 0     | 0     | 0     | 0     | 0     | 0     | 0     | 0     | 0     | 0     | 0     | 0     | 0     |       |
|                      | Ni      | 0     | 0     | 0     | 0     | 0     | 0,001 | 0     | 0     | 0     | 0     | 0     | 0,001 | 0     | 0,001 | 0     | 0     |       |
|                      | Ca      | 1,712 | 1,809 | 1,995 | 1,795 | 1,953 | 1,980 | 2,148 | 2,119 | 2,113 | 2,001 | 1,929 | 1,982 | 1,697 | 1,953 | 1,980 | 1,995 | 1,795 |
| Na                   | 0,158   | 0,131 | 0,013 | 0,111 | 0,007 | 0,027 | 0,008 | 0     | 0,002 | 0,001 | 0,003 | 0     | 0,247 | 0,007 | 0,027 | 0,013 | 0,111 |       |
| K                    | 0       | 0     | 0,001 | 0     | 0     | 0     | 0,002 | 0,001 | 0     | 0     | 0,002 | 0,001 | 0     | 0     | 0     | 0,001 | 0     |       |
| Total                | 7,959   | 8,007 | 8,009 | 7,954 | 7,972 | 8,004 | 8,390 | 8,368 | 8,362 | 8,036 | 8,006 | 7,995 | 8,009 | 7,972 | 8,004 | 8,009 | 7,954 |       |

tableau 14 : analyses microsonde des épidotes de Gray Rock.

| Echantillons                    | TR106 | TR106 | TR106 | TR121 | TR121 | TR121 | TR121 | TR121 | TR85  | TR85  | TR85  | TR85  | TR85  | TR85  | TR248 | TR234 | TR234 |
|---------------------------------|-------|-------|-------|-------|-------|-------|-------|-------|-------|-------|-------|-------|-------|-------|-------|-------|-------|
| SiO <sub>2</sub>                | 40,94 | 40,62 | 40,54 | 38,06 | 39,13 | 40,09 | 40,26 | 41,18 | 40,04 | 39,49 | 39,22 | 39,94 | 40,06 | 40,29 | 40,76 | 39,46 | 40,15 |
| Al <sub>2</sub> O <sub>3</sub>  | 32,29 | 31,15 | 31,82 | 31,81 | 31,48 | 32,62 | 31,00 | 31,93 | 31,30 | 32,41 | 30,87 | 32,94 | 32,42 | 32,61 | 32,30 | 32,04 | 33,59 |
| Fe <sub>2</sub> O <sub>3t</sub> | 0,46  | 0,95  | 0,73  | 0,93  | 1,46  | 0,81  | 2,39  | 0,85  | 1,72  | 1,26  | 3,60  | 0,42  | 0,75  | 0,55  | 1,02  | 1,88  | 0,47  |
| MgO                             | 0,04  | 0,01  | 0,06  | 0,01  | 0,04  | 0,00  | 0,05  | 0,03  | 0,04  | 0,01  | 0,00  | 0,00  | 0,00  | 0,05  | 0,01  | 0,08  | 0,00  |
| MnO                             | 0,13  | 0,00  | 0,24  | 0,00  | 0,00  | 0,03  | 0,01  | 0,09  | 0,09  | 0,00  | 0,14  | 0,00  | 0,02  | 0,00  | 0,13  | 0,11  | 0,00  |
| TiO <sub>2</sub>                | 0,00  | 0,05  | 0,00  | 0,00  | 0,04  | 0,00  | 0,00  | 0,02  | 0,00  | 0,00  | 0,00  | 0,01  | 0,01  | 0,00  | 0,00  | 0,00  | 0,00  |
| Cr <sub>2</sub> O <sub>3</sub>  | 0,00  | 0,00  | 0,00  | 0,00  | 0,00  | 0,00  | 0,00  | 0,00  | 0,00  | 0,02  | 0,02  | 0,00  | 0,00  | 0,00  | 0,00  | 0,00  | 0,00  |
| NiO                             | 0,00  | 0,00  | 0,00  | 0,00  | 0,00  | 0,00  | 0,00  | 0,00  | 0,00  | 0,00  | 0,09  | 0,02  | 0,00  | 0,01  | 0,00  | 0,00  | 0,00  |
| CaO                             | 24,35 | 24,69 | 24,42 | 23,98 | 23,15 | 24,67 | 24,15 | 23,41 | 24,03 | 23,80 | 23,50 | 24,46 | 24,64 | 24,46 | 23,91 | 24,30 | 25,37 |
| Na <sub>2</sub> O               | 0,05  | 0,12  | 0,05  | 0,00  | 0,21  | 0,05  | 0,04  | 0,39  | 0,13  | 0,23  | 0,00  | 0,07  | 0,01  | 0,00  | 0,17  | 0,00  | 0,04  |
| K <sub>2</sub> O                | 0,00  | 0,00  | 0,00  | 0,00  | 0,00  | 0,00  | 0,00  | 0,00  | 0,00  | 0,00  | 0,00  | 0,00  | 0,00  | 0,00  | 0,00  | 0,00  | 0,00  |
| Total                           | 98,27 | 97,59 | 97,85 | 94,79 | 95,51 | 98,27 | 97,90 | 97,90 | 97,35 | 97,22 | 97,44 | 97,86 | 97,91 | 97,97 | 98,30 | 97,86 | 99,64 |
| Si                              | 3,213 | 3,225 | 3,205 | 2,997 | 3,054 | 3,038 | 3,083 | 3,119 | 3,075 | 3,028 | 3,039 | 3,031 | 3,045 | 3,054 | 3,082 | 3,140 | 3,122 |
| AlVI                            | 2,986 | 2,915 | 2,964 | 2,943 | 2,890 | 2,908 | 2,793 | 2,845 | 2,828 | 2,924 | 2,814 | 2,941 | 2,900 | 2,908 | 2,873 | 3,004 | 3,055 |
| Ti                              | 0     | 0,003 | 0     | 0     | 0,002 | 0     | 0     | 0,001 | 0     | 0     | 0     | 0     | 0     | 0     | 0     | 0     | 0     |
| Fe <sub>3+</sub>                | 0,030 | 0,063 | 0,048 | 0,053 | 0,083 | 0,044 | 0,133 | 0,047 | 0,096 | 0,070 | 0,186 | 0,023 | 0,041 | 0,030 | 0,056 | 0,125 | 0,031 |
| Fe <sub>2+</sub>                | 0     | 0     | 0     | 0     | 0     | 0     | 0     | 0     | 0     | 0     | 0,032 | 0     | 0     | 0     | 0     | 0     | 0,014 |
| Mg                              | 0,005 | 0,001 | 0,007 | 0,001 | 0,004 | 0     | 0,005 | 0,003 | 0,004 | 0,001 | 0     | 0     | 0     | 0,005 | 0,001 | 0,009 | 0     |
| Mn                              | 0,009 | 0     | 0,016 | 0     | 0     | 0,001 | 0     | 0,005 | 0,005 | 0     | 0,009 | 0     | 0,001 | 0     | 0,008 | 0,007 | 0     |
| Cr                              | 0     | 0     | 0     | 0     | 0     | 0     | 0     | 0     | 0     | 0,001 | 0,001 | 0     | 0     | 0     | 0     | 0     | 0     |
| Ni                              | 0     | 0     | 0     | 0     | 0     | 0     | 0     | 0     | 0     | 0,001 | 0,001 | 0     | 0     | 0     | 0     | 0     | 0     |
| Ca                              | 2,047 | 2,100 | 2,068 | 2,023 | 1,935 | 2,003 | 1,981 | 1,899 | 1,977 | 1,955 | 1,951 | 0,001 | 2,007 | 1,986 | 1,937 | 2,071 | 2,104 |
| Na                              | 0,008 | 0,018 | 0,008 | 0     | 0,031 | 0,007 | 0,005 | 0,057 | 0,019 | 0,034 | 0     | 0,010 | 0,001 | 0     | 0,024 | 0     | 0,006 |
| K                               | 0     | 0     | 0     | 0     | 0     | 0     | 0     | 0     | 0     | 0     | 0     | 0     | 0     | 0     | 0     | 0     | 0     |
| Total                           | 8,298 | 8,325 | 8,316 | 8,017 | 7,999 | 8,001 | 8     | 7,976 | 8,004 | 8,013 | 8,037 | 7,995 | 7,995 | 7,983 | 7,981 | 8,356 | 8,336 |

tableau 14 : analyses microsonde des épidotes de Gray Rock.

| Echantillons | basaltes | TR47  | TR47  | TR47  | TR47  | TR47  | TR47  | TR48  | TR48  | TR48  | fions | TR128E | TR128E | TR128J | TR128J | TR128K |
|--------------|----------|-------|-------|-------|-------|-------|-------|-------|-------|-------|-------|--------|--------|--------|--------|--------|
| SiO2         | 38,66    | 39,21 | 39,81 | 39,45 | 39,88 | 38,95 | 40,71 | 38,76 | 39,79 | 39,24 | 39,51 | 39,29  | 39,47  | 39,11  | 39,22  | 39,43  |
| Al2O3        | 24,34    | 25,46 | 29,98 | 29,65 | 30,24 | 24,92 | 29,98 | 23,02 | 30,25 | 25,95 | 27,35 | 26,85  | 27,97  | 25,66  | 26,51  | 25,30  |
| Fe2O3t       | 11,61    | 10,49 | 4,83  | 5,58  | 4,86  | 10,64 | 4,27  | 12,89 | 4,85  | 10,20 | 7,80  | 8,89   | 7,18   | 9,17   | 8,10   | 9,64   |
| MgO          | 0,00     | 0,00  | 0,00  | 0,02  | 0,00  | 0,00  | 0,55  | 0,00  | 0,00  | 0,00  | 0,00  | 0,00   | 0,00   | 0,02   | 0,04   | 0,02   |
| MnO          | 0,00     | 0,03  | 0,12  | 0,00  | 0,10  | 0,29  | 0,09  | 0,18  | 0,15  | 0,41  | 0,08  | 0,08   | 0,10   | 0,31   | 0,19   | 0,04   |
| TiO2         | 0,00     | 0,00  | 0,00  | 0,00  | 0,00  | 0,00  | 0,00  | 0,00  | 0,00  | 0,00  | 0,00  | 0,00   | 0,00   | 0,15   | 0,10   | 0,06   |
| Cr2O3        | 0,00     | 0,00  | 0,00  | 0,00  | 0,00  | 0,00  | 0,00  | 0,00  | 0,00  | 0,00  | 0,00  | 0,00   | 0,00   | 0,18   | 0,00   | 0,05   |
| NiO          | 0,00     | 0,00  | 0,00  | 0,00  | 0,00  | 0,00  | 0,00  | 0,00  | 0,00  | 0,00  | 0,00  | 0,00   | 0,00   | 0,03   | 0,04   | 0,04   |
| CaO          | 22,72    | 23,17 | 23,52 | 23,48 | 23,84 | 23,29 | 23,52 | 22,87 | 23,90 | 23,22 | 23,86 | 23,65  | 23,27  | 23,64  | 23,64  | 23,37  |
| Na2O         | 0,00     | 0,00  | 0,00  | 0,00  | 0,00  | 0,00  | 0,00  | 0,00  | 0,00  | 0,00  | 0,00  | 0,00   | 0,00   | 0,01   | 0,02   | 0,00   |
| K2O          | 0,00     | 0,00  | 0,00  | 0,00  | 0,00  | 0,00  | 0,00  | 0,00  | 0,00  | 0,00  | 0,00  | 0,00   | 0,00   | 0,00   | 0,00   | 0,00   |
| Total        | 97,33    | 98,36 | 98,26 | 98,18 | 98,92 | 98,09 | 98,12 | 97,72 | 98,94 | 99,02 | 98,60 | 98,76  | 97,99  | 98,28  | 97,88  | 97,95  |
| Si           | 3,132    | 3,122 | 3,074 | 3,061 | 3,062 | 3,122 | 3,103 | 3,155 | 3,056 | 3,060 | 3,060 | 3,050  | 3,070  | 3,109  | 3,108  | 3,142  |
| AlVI         | 2,319    | 2,385 | 2,723 | 2,707 | 2,731 | 2,350 | 2,688 | 2,204 | 2,733 | 2,370 | 2,500 | 2,450  | 2,560  | 2,399  | 2,471  | 2,372  |
| Ti           | 0,674    | 0     | 0     | 0     | 0     | 0     | 0     | 0     | 0     | 0     | 0     | 0      | 0      | 0,008  | 0,005  | 0,003  |
| Fe3+         | 0        | 0,600 | 0,270 | 0,293 | 0,269 | 0,613 | 0,236 | 0,751 | 0,267 | 0,520 | 0,410 | 0,410  | 0,290  | 0,525  | 0,463  | 0,553  |
| Fe2+         | 0        | 0     | 0     | 0,042 | 0,002 | 0     | 0     | 0     | 0,006 | 0,080 | 0,050 | 0,120  | 0,140  | 0      | 0      | 0      |
| Mg           | 0        | 0     | 0     | 0,002 | 0     | 0     | 0,062 | 0     | 0     | 0     | 0     | 0      | 0      | 0,002  | 0,002  | 0,002  |
| Mn           | 0        | 0,002 | 0,007 | 0     | 0,006 | 0,019 | 0,005 | 0,012 | 0,009 | 0,030 | 0     | 0      | 0      | 0,002  | 0,012  | 0,002  |
| Cr           | 0        | 0     | 0     | 0     | 0     | 0     | 0     | 0     | 0     | 0     | 0     | 0      | 0      | 0,011  | 0      | 0,003  |
| Ni           | 0        | 0     | 0     | 0     | 0     | 0     | 0     | 0     | 0     | 0     | 0     | 0      | 0      | 0,001  | 0,002  | 0,002  |
| Ca           | 1,972    | 1,977 | 1,946 | 1,952 | 1,961 | 2,000 | 1,920 | 1,994 | 1,966 | 1,940 | 1,980 | 1,970  | 1,940  | 2,013  | 2,007  | 1,995  |
| Na           | 0        | 0     | 0     | 0     | 0     | 0     | 0     | 0     | 0     | 0     | 0     | 0      | 0      | 0,001  | 0,003  | 0      |
| K            | 0        | 0     | 0     | 0     | 0     | 0     | 0     | 0     | 0     | 0     | 0     | 0      | 0      | 0      | 0      | 0      |
| Total        | 8,097    | 8,086 | 8,020 | 8,057 | 8,031 | 8,104 | 8,014 | 8,116 | 8,037 | 8,000 | 8,000 | 8,000  | 8,000  | 8,089  | 8,075  | 8,074  |

**Tableau 14 : analyses microsonde des épidotes de Gray Rock.**

| Echantillons                   | TR 128J | TR 128J | TR 128R | TR 128R | TR 128R | TR 128R | TR 128R | TR 128T | TR 128T | TR 128T | TR 532 | TR 234 |
|--------------------------------|---------|---------|---------|---------|---------|---------|---------|---------|---------|---------|--------|--------|
| SiO <sub>2</sub>               | 26,96   | 26,07   | 26,95   | 27,54   | 27,39   | 26,63   | 27,45   | 26,86   | 26,65   | 26,11   | 27,15  | 27,85  |
| Al <sub>2</sub> O <sub>3</sub> | 21,61   | 21,59   | 22,24   | 22,05   | 22,12   | 22,27   | 22,08   | 20,57   | 21,65   | 21,52   | 21,28  | 22,96  |
| TiO <sub>2</sub>               | 0,00    | 0,00    | 0,00    | 0,10    | 0,08    | 0,08    | 0,00    | 0,01    | 0,05    | 0,03    | 0,00   | 0,00   |
| FeO                            | 17,69   | 19,55   | 17,35   | 15,89   | 16,15   | 16,98   | 15,71   | 17,15   | 17,16   | 17,62   | 18,72  | 9,11   |
| MgO                            | 19,59   | 19,20   | 20,29   | 20,24   | 20,45   | 20,11   | 20,49   | 20,72   | 20,39   | 19,91   | 18,67  | 25,99  |
| MnO                            | 0,37    | 0,42    | 0,41    | 0,25    | 0,17    | 0,21    | 0,31    | 0,32    | 0,29    | 0,24    | 0,18   | 0,01   |
| CaO                            | 0,01    | 0,03    | 0,06    | 0,01    | 0,00    | 0,00    | 0,21    | 0,08    | 0,03    | 0,00    | 0,08   | 0,10   |
| Na <sub>2</sub> O              | 0,01    | 0,00    | 0,00    | 0,00    | 0,06    | 0,04    | 0,00    | 0,00    | 0,00    | 0,11    | 0,00   | 0,00   |
| K <sub>2</sub> O               | 0,00    | 0,00    | 0,06    | 0,01    | 0,03    | 0,00    | 0,04    | 0,00    | 0,00    | 0,03    | 0,00   | 0,00   |
| Cr <sub>2</sub> O <sub>3</sub> | 0,27    | 0,20    | 0,19    | 0,37    | 0,33    | 0,26    | 0,25    | 0,34    | 0,03    | 0,24    | 0,00   | 0,00   |
| Total                          | 86,51   | 87,06   | 87,55   | 86,46   | 86,78   | 86,58   | 86,54   | 86,05   | 86,25   | 85,81   | 86,08  | 86,02  |
| Si                             | 5,519   | 5,371   | 5,442   | 5,574   | 5,533   | 5,424   | 5,552   | 5,526   | 5,458   | 5,402   | 5,604  | 5,462  |
| Al                             | 5,214   | 5,243   | 5,294   | 5,260   | 5,267   | 5,347   | 5,264   | 4,988   | 5,226   | 5,248   | 5,177  | 5,307  |
| Ti                             | 0       | 0       | 0       | 0,015   | 0,012   | 0,012   | 0       | 0,002   | 0,008   | 0,005   | 0      | 0      |
| Fe                             | 3,029   | 3,368   | 2,930   | 2,690   | 2,728   | 2,893   | 2,658   | 2,951   | 2,939   | 3,049   | 3,232  | 1,494  |
| Mg                             | 5,978   | 5,897   | 6,108   | 6,107   | 6,158   | 6,106   | 6,178   | 6,355   | 6,225   | 6,140   | 5,745  | 7,598  |
| Mn                             | 0,064   | 0,073   | 0,070   | 0,043   | 0,029   | 0,036   | 0,053   | 0,056   | 0,050   | 0,042   | 0,031  | 0,002  |
| Ca                             | 0,002   | 0,007   | 0,013   | 0,002   | 0       | 0       | 0,046   | 0,018   | 0,007   | 0       | 0,018  | 0,021  |
| Na                             | 0,004   | 0       | 0       | 0       | 0,024   | 0,016   | 0       | 0       | 0       | 0,044   | 0      | 0      |
| K                              | 0       | 0       | 0,015   | 0,003   | 0,008   | 0       | 0,010   | 0       | 0       | 0,008   | 0      | 0      |
| Cr                             | 0,044   | 0,033   | 0,030   | 0,059   | 0,053   | 0,042   | 0,040   | 0,055   | 0,005   | 0,039   | 0      | 0      |
| Total                          | 19,854  | 19,992  | 19,902  | 19,753  | 19,812  | 19,876  | 19,801  | 19,951  | 19,918  | 19,977  | 19,807 | 19,884 |
| XFe                            | 33,60   | 36,40   | 32,40   | 30,60   | 30,70   | 32,10   | 30,10   | 31,70   | 32,10   | 33,20   | 36,00  | 16,40  |
| Al <sub>4</sub>                | 2,481   | 2,629   | 2,558   | 2,426   | 2,467   | 2,576   | 2,448   | 2,474   | 2,542   | 2,598   | 2,396  | 2,538  |
| Al <sub>6</sub>                | 2,733   | 2,614   | 2,736   | 2,834   | 2,800   | 2,771   | 2,816   | 2,514   | 2,684   | 2,650   | 2,781  | 2,769  |

tableau 15 : analyses microsonde des chlorites de Gray Rock.





ANALYSES CHIMIQUES  
DE L'OPHIOLITE DE TRINITY

CHAMBRES MAGMATIQUES  
DE TOAD LAKE et CASTLE LAKE.

(CHAPITRE 2 et 3)



| ECHANTILLONS | SiO <sub>2</sub> | Al <sub>2</sub> O <sub>3</sub> | Fe <sub>2</sub> O <sub>3</sub> | MnO  | MgO   | CaO   | Na <sub>2</sub> O | K <sub>2</sub> O | TiO <sub>2</sub> | P <sub>2</sub> O <sub>5</sub> | P.F.  | Total  | Nb | Zr  | Y  | Sr  | Rb | Co  | V     | Ni   | Cr   | Ba  |
|--------------|------------------|--------------------------------|--------------------------------|------|-------|-------|-------------------|------------------|------------------|-------------------------------|-------|--------|----|-----|----|-----|----|-----|-------|------|------|-----|
| CL5          | 45,18            | 13,29                          | 10,82                          | 0,24 | 12,24 | 14,33 | 0,33              | 0,09             | 0,38             | 0,01                          | 2,62  | 99,54  | 3  | 13  | 5  | 79  | 3  | 48  | 319   | 265  | 656  | 8   |
| CL6          | 41,65            | 4,72                           | 9,03                           | 0,14 | 30,09 | 4,01  | 0,12              | 0,01             | 0,18             | 0,02                          | 9,29  | 99,27  | 3  | 14  | 3  | 13  | 1  | 91  | 93    | 1644 | 1991 | 0   |
| CL14         | 39,18            | 18,91                          | 14,30                          | 0,19 | 10,33 | 10,48 | 0,89              | 0,17             | 1,30             | 0,04                          | 4,15  | 99,94  | 4  | 19  | 12 | 118 | 7  | 59  | 821   | 274  | 76   | 25  |
| CL15         | 41,67            | 16,48                          | 14,78                          | 0,20 | 9,91  | 10,97 | 1,14              | 0,27             | 1,44             | 0,00                          | 2,90  | 99,76  | 2  | 15  | 6  | 89  | 12 | 60  | 1130* | 188  | 200  | 47  |
| CL19         | 45,77            | 18,16                          | 8,06                           | 0,15 | 9,45  | 12,66 | 1,26              | 0,75             | 0,21             | 0,00                          | 3,17  | 99,64  | 3  | 13  | 5  | 125 | 36 | 38  | 203   | 117  | 282  | 345 |
| TOAD8        | 46,70            | 22,12                          | 5,21                           | 0,10 | 7,14  | 14,66 | 1,01              | 0,09             | 0,10             | 0,00                          | 2,43  | 99,56  | 2  | 17  | 3  | 105 | 5  | 27  | 127   | 64   | 128  | 163 |
| TOAD11       | 41,79            | 1,78                           | 8,45                           | 0,12 | 38,32 | 2,04  | 0,02              | 0,01             | 0,06             | 0,01                          | 6,92  | 99,53  | 3  | 11  | 1  | 9   | 1  | 102 | 70    | 2163 | 3062 | 0   |
| TOAD15       | 46,01            | 11,75                          | 8,27                           | 0,18 | 15,47 | 13,96 | 0,81              | 0,03             | 0,24             | 0,00                          | 2,95  | 99,67  | 2  | 17  | 6  | 102 | 3  | 48  | 195   | 380  | 825  | 12  |
| TOAD17       | 39,03            | 0,72                           | 7,97                           | 0,11 | 38,91 | 0,89  | 0,00              | 0,01             | 0,02             | 0,01                          | 11,43 | 99,09  | 3  | 10  | 0  | 0   | 1  | 107 | 43    | 2287 | 2360 | 0   |
| TOAD19       | 29,14            | 17,00                          | 8,89                           | 0,17 | 20,46 | 9,10  | 0,02              | 0,07             | 0,20             | 0,00                          | 14,02 | 99,07  | 3  | 11  | 3  | 35  | 4  | 52  | 224   | 258  | 230  | 11  |
| TOAD21       | 40,98            | 2,62                           | 8,21                           | 0,11 | 36,89 | 2,27  | 0,05              | 0,00             | 0,10             | 0,01                          | 7,90  | 99,15  | 3  | 12  | 1  | 0   | 1  | 97  | 73    | 2049 | 2318 | 0   |
| TOAD22       | 42,77            | 14,44                          | 12,13                          | 0,21 | 11,46 | 13,32 | 0,60              | 0,26             | 0,63             | 0,01                          | 4,40  | 100,23 | 3  | 11  | 5  | 53  | 5  | 48  | 548   | 225  | 465  | 18  |
| TOAD23       | 42,35            | 19,77                          | 11,84                          | 0,16 | 7,39  | 13,34 | 0,64              | 0,15             | 1,02             | 0,01                          | 2,78  | 99,45  | 4  | 11  | 2  | 36  | 3  | 47  | 1128  | 62   | 50   | 18  |
| TOAD24       | 46,17            | 18,43                          | 9,13                           | 0,17 | 9,11  | 13,20 | 0,71              | 0,24             | 0,25             | 0,01                          | 2,66  | 100,08 | 3  | 11  | 3  | 30  | 4  | 43  | 292   | 58   | 47   | 8   |
| TOAD27       | 48,47            | 12,89                          | 7,09                           | 0,13 | 15,16 | 11,57 | 0,71              | 0,00             | 0,23             | 0,00                          | 3,81  | 99,50  | 3  | 13  | 5  | 16  | 3  | 46  | 209   | 411  | 980  | 4   |
| TOAD28       | 46,13            | 19,46                          | 5,89                           | 0,11 | 9,61  | 14,41 | 0,30              | 0,01             | 0,09             | 0,01                          | 3,54  | 99,56  | 4  | 11  | 1  | 29  | 1  | 35  | 167   | 67   | 36   | 0   |
| TOAD29       | 53,45            | 14,73                          | 12,41                          | 0,21 | 3,77  | 8,05  | 3,04              | 0,75             | 1,19             | 0,21                          | 1,54  | 99,35  | 6  | 85  | 27 | 311 | 23 | 33  | 372*  | 10   | 30   | 447 |
| TOAD35       | 42,59            | 1,16                           | 8,60                           | 0,21 | 0,09  | 4,19  | 3,59              | 0,24             | 0,18             | 0,03                          | 0,60  | 99,00  | 4  | 130 | 18 | 65  | 4  | 2   | 4     | 0    | 15   | 44  |
| TOAD40       | 41,03            | 2,54                           | 8,49                           | 0,12 | 37,32 | 2,21  | 0,02              | 0,00             | 0,04             | 0,00                          | 7,09  | 99,18  | 3  | 10  | 0  | 10  | 0  | 104 | 65    | 2165 | 2847 | 0   |
| GR           | 76,84            | 12,64                          | 0,78                           | 0,02 | 37,70 | 2,40  | 0,05              | 0,01             | 0,10             | 0,01                          | 6,76  | 99,21  | 3  | 11  | 1  | 1   | 1  | 102 | 74    | 2090 | 2452 | 0   |
| KO           | 78,27            | 11,76                          | 0,92                           | 0,01 | 0,80  | 3,27  | 4,00              | 0,08             | 0,18             | 0,03                          | 0,81  | 99,01  | 4  | 146 | 12 | 91  | 1  | 2   | 4     | 12   | 18   | 35  |
|              |                  |                                |                                |      |       | 1,39  | 5,14              | 0,19             | 0,14             | 0,05                          | 0,89  | 99,57  | 4  | 79  | 16 | 42  | 1  | 2   | 12    | 10   | 17   | 17  |

Tableau 16 : analyses roches totales de l'ophiolite de Trinity (Castle Lake et Toad Lake).

| N°Echantillons<br>N°Analyses | TOAD 19<br>3 | TOAD 19<br>4 | TOAD 19<br>5 | TOAD 19<br>9 | TOAD 19<br>10 | TOAD 19<br>11 | TOAD 19<br>15 | TOAD 19<br>16 | TOAD 19<br>17 | TOAD 19<br>19 | TOAD 19<br>23 | TOAD 19<br>24 | TOAD 19<br>26 | TOAD 15<br>38 | TOAD 15<br>40 | TOAD 15<br>44 | TOAD 15<br>45 | TOAD 15<br>46 | TOAD 15<br>50 |
|------------------------------|--------------|--------------|--------------|--------------|---------------|---------------|---------------|---------------|---------------|---------------|---------------|---------------|---------------|---------------|---------------|---------------|---------------|---------------|---------------|
| SiO2                         | 41,21        | 42,22        | 41,26        | 41,52        | 41,39         | 41,70         | 41,93         | 41,55         | 41,20         | 41,18         | 41,17         | 41,90         | 41,55         | 41,53         | 41,74         | 41,72         | 41,50         | 41,74         | 42,36         |
| Al2O3                        | 0            | 0            | 0            | 0,01         | 0             | 0             | 0             | 0             | 0,01          | 0             | 0,08          | 0             | 0             | 0,03          | 0,06          | 0,07          | 0             | 0,03          | 0             |
| TiO2                         | 0            | 0            | 0            | 0            | 0,28          | 0             | 0             | 0,02          | 0,22          | 0             | 0,10          | 0             | 0             | 0             | 0             | 0,08          | 0             | 0             | 0             |
| FeO                          | 9,94         | 9,95         | 9,97         | 9,77         | 9,39          | 9,11          | 9,43          | 9,58          | 9,27          | 9,29          | 11,02         | 10,23         | 10,07         | 8,47          | 8,73          | 7,17          | 9,43          | 9,01          | 8,63          |
| MgO                          | 48,39        | 48,74        | 48,54        | 48,72        | 49,00         | 48,82         | 49,17         | 49,36         | 47,84         | 48,70         | 47,89         | 48,83         | 48,87         | 49,36         | 47,86         | 50,32         | 48,84         | 49,20         | 49,58         |
| MnO                          | 0,07         | 0,10         | 0,09         | 0,14         | 0,12          | 0,26          | 0,14          | 0,12          | 0,12          | 0,07          | 0             | 0,23          | 0,12          | 0,10          | 0,10          | 0,06          | 0,04          | 0,41          | 0,10          |
| Cr2O3                        | 0,19         | 0            | 0            | 0            | 0,06          | 0,41          | 0,10          | 0,54          | 0             | 0             | 0             | 0             | 0,01          | 0             | 0             | 0,07          | 0             | 0,08          | 0             |
| NiO                          | 0,22         | 0,38         | 0,44         | 0,35         | 0,42          | 0,41          | 0,32          | 0,49          | 0,25          | 0,23          | 0,24          | 0,34          | 0,34          | 0,40          | 0,32          | 0,56          | 0,31          | 0,36          | 0,34          |
| Total                        | 100,02       | 101,39       | 100,44       | 100,51       | 100,66        | 100,51        | 101,09        | 101,66        | 99,91         | 99,47         | 100,31        | 101,53        | 100,76        | 99,89         | 98,81         | 100,05        | 100,12        | 100,83        | 101,01        |
| Si                           | 1,009        | 1,019        | 1,007        | 1,011        | 1,008         | 1,014         | 1,013         | 1,002         | 1,017         | 1,011         | 1,009         | 1,012         | 1,011         | 1,012         | 1,027         | 1,010         | 1,012         | 1,011         | 1,019         |
| Al                           | 0            | 0            | 0            | 0            | 0             | 0             | 0             | 0             | 0             | 0             | 0,003         | 0             | 0             | 0,001         | 0,002         | 0,002         | 0             | 0,001         | 0             |
| Ti                           | 0            | 0            | 0            | 0            | 0,005         | 0             | 0             | 0             | 0,004         | 0             | 0,002         | 0             | 0             | 0             | 0             | 0,001         | 0             | 0             | 0             |
| Fe                           | 0,204        | 0,201        | 0,204        | 0,199        | 0,191         | 0,185         | 0,191         | 0,193         | 0,191         | 0,191         | 0,226         | 0,207         | 0,205         | 0,173         | 0,180         | 0,145         | 0,192         | 0,183         | 0,174         |
| Mg                           | 1,767        | 1,753        | 1,766        | 1,789        | 1,775         | 1,762         | 1,771         | 1,775         | 1,760         | 1,782         | 1,743         | 1,758         | 1,765         | 1,793         | 1,755         | 1,815         | 1,776         | 1,776         | 1,779         |
| Mn                           | 0,001        | 0,002        | 0,002        | 0,003        | 0,002         | 0,005         | 0,003         | 0,002         | 0,003         | 0,001         | 0,000         | 0,005         | 0,002         | 0,002         | 0,002         | 0,001         | 0,001         | 0,008         | 0,002         |
| Cr                           | 0,004        | 0            | 0            | 0            | 0,001         | 0,008         | 0,002         | 0,010         | 0             | 0             | 0             | 0             | 0             | 0             | 0             | 0,001         | 0             | 0,002         | 0             |
| N                            | 0,004        | 0,007        | 0,009        | 0,007        | 0,008         | 0,008         | 0,006         | 0,010         | 0,005         | 0,005         | 0,005         | 0,007         | 0,007         | 0,008         | 0,006         | 0,011         | 0,006         | 0,007         | 0,007         |
| Total                        | 2,989        | 2,982        | 2,991        | 2,989        | 2,988         | 2,982         | 2,986         | 2,992         | 2,980         | 2,990         | 2,988         | 2,989         | 2,990         | 2,989         | 2,972         | 2,986         | 2,987         | 2,988         | 2,981         |
| XFe                          | 0,103        | 0,103        | 0,103        | 0,101        | 0,097         | 0,095         | 0,097         | 0,098         | 0,098         | 0,097         | 0,115         | 0,105         | 0,104         | 0,088         | 0,093         | 0,074         | 0,098         | 0,093         | 0,089         |
| XMg                          | 0,897        | 0,897        | 0,897        | 0,899        | 0,903         | 0,905         | 0,903         | 0,902         | 0,902         | 0,903         | 0,885         | 0,895         | 0,896         | 0,912         | 0,907         | 0,926         | 0,902         | 0,907         | 0,911         |

tableau 17 : analyses microsonde des olivines de Toad Lake et Castle Lake.

| N°Echantillons<br>N°Analyses | TOAD 12<br>63 | TOAD 12<br>64 | TOAD 12<br>65 | TOAD 12<br>2 | TOAD 12<br>1 | TOAD 12<br>20 | TOAD 12<br>21 | TOAD 12<br>22 | TOAD 12<br>23 | TOAD 8<br>2 | TOAD 8<br>5 | TOAD 20<br>15 | TOAD 20<br>16 | TOAD 20<br>23 | TOAD 20<br>24 | TOAD 20<br>27 | TOAD 40<br>41 | TOAD 40<br>42 | TOAD 40<br>43 |
|------------------------------|---------------|---------------|---------------|--------------|--------------|---------------|---------------|---------------|---------------|-------------|-------------|---------------|---------------|---------------|---------------|---------------|---------------|---------------|---------------|
| SiO2                         | 39,47         | 39,64         | 39,91         | 40,13        | 41,14        | 39,31         | 39,17         | 39,74         | 39,31         | 41,20       | 41,52       | 40,01         | 40,16         | 39,77         | 39,49         | 39,88         | 40,87         | 41,08         | 41,26         |
| Al2O3                        | 0             | 0,02          | 0,31          | 0,03         | 0            | 0             | 0             | 0,08          | 0             | 0           | 0           | 0             | 0             | 0             | 0,02          | 0,20          | 0             | 0             | 0             |
| TiO2                         | 0             | 0             | 0,01          | 0            | 0            | 0             | 0             | 0             | 0             | 0,01        | 0           | 0             | 0,03          | 0             | 0             | 0             | 0             | 0             | 0             |
| FeO                          | 20,79         | 20,45         | 20,75         | 14,12        | 10,87        | 19,67         | 19,07         | 19,90         | 20,15         | 9,51        | 9,12        | 18,05         | 17,78         | 17,70         | 18,23         | 14,06         | 9,83          | 9,74          | 9,99          |
| MgO                          | 39,71         | 40,31         | 39,23         | 44,01        | 46,98        | 41,18         | 41,48         | 41,43         | 40,68         | 48,30       | 48,88       | 42,73         | 42,72         | 41,97         | 42,64         | 44,62         | 48,71         | 49,42         | 48,98         |
| MnO                          | 0,21          | 0,22          | 0,40          | 0,20         | 0,12         | 0,33          | 0,39          | 0,28          | 0,28          | 0,04        | 0,03        | 0,21          | 0,21          | 0,38          | 0,19          | 0,23          | 0,13          | 0,16          | 0,08          |
| Cr2O3                        | 0             | 0             | 0             | 0            | 0            | 0             | 0             | 0             | 0,05          | 0,02        | 0           | 0             | 0             | 0             | 0             | 0             | 0             | 0             | 0             |
| NiO                          | 0,24          | 0,17          | 0,11          | 0,32         | 0,37         | 0,30          | 0,32          | 0,20          | 0,20          | 0,45        | 0,31        | 0,17          | 0,32          | 0,09          | 0,26          | 0,17          | 0,28          | 0,20          | 0,36          |
| Total                        | 100,42        | 100,81        | 100,62        | 98,81        | 99,58        | 100,79        | 100,43        | 101,63        | 100,65        | 100,53      | 99,86       | 101,17        | 101,20        | 99,91         | 100,88        | 99,16         | 98,82         | 100,58        | 100,87        |
| Si                           | 1,013         | 1,011         | 1,018         | 1,015        | 1,017        | 1,002         | 1,000         | 1,003         | 1,004         | 1,003       | 1,014       | 1,006         | 1,008         | 1,011         | 0,998         | 1,005         | 1,004         | 1,000         | 1,005         |
| Al                           | 0             | 0,001         | 0,008         | 0,001        | 0            | 0             | 0             | 0,002         | 0             | 0           | 0           | 0             | 0             | 0             | 0,001         | 0,006         | 0             | 0             | 0             |
| Ti                           | 0             | 0             | 0             | 0            | 0            | 0             | 0             | 0             | 0             | 0           | 0           | 0             | 0,001         | 0             | 0             | 0             | 0             | 0             | 0             |
| Fe                           | 0,446         | 0,436         | 0,444         | 0,299        | 0,227        | 0,419         | 0,407         | 0,420         | 0,431         | 0,194       | 0,186       | 0,378         | 0,373         | 0,376         | 0,385         | 0,296         | 0,202         | 0,198         | 0,203         |
| Mg                           | 1,519         | 1,533         | 1,495         | 1,659        | 1,730        | 1,584         | 1,578         | 1,559         | 1,549         | 1,789       | 1,779       | 1,801         | 1,599         | 1,581         | 1,807         | 1,676         | 1,783         | 1,784         | 1,778         |
| Mn                           | 0,005         | 0,005         | 0,009         | 0,004        | 0,003        | 0,007         | 0,008         | 0,006         | 0,006         | 0,001       | 0,001       | 0,004         | 0,004         | 0,008         | 0,004         | 0,005         | 0,003         | 0,003         | 0,002         |
| Cr                           | 0             | 0             | 0             | 0            | 0            | 0             | 0             | 0             | 0,001         | 0           | 0           | 0             | 0             | 0             | 0             | 0             | 0             | 0             | 0             |
| N                            | 0,005         | 0,003         | 0,002         | 0,007        | 0,007        | 0,006         | 0,007         | 0,004         | 0,004         | 0,009       | 0,006       | 0,003         | 0,006         | 0,002         | 0,005         | 0,003         | 0,006         | 0,004         | 0,007         |
| Total                        | 2,988         | 2,989         | 2,977         | 2,985        | 2,984        | 2,988         | 3,000         | 2,994         | 2,985         | 2,986       | 2,988       | 2,993         | 2,991         | 2,988         | 3,001         | 2,991         | 2,998         | 2,999         | 2,995         |
| X Fe                         | 0,227         | 0,222         | 0,229         | 0,153        | 0,116        | 0,211         | 0,205         | 0,212         | 0,217         | 0,098       | 0,095       | 0,192         | 0,189         | 0,191         | 0,193         | 0,150         | 0,102         | 0,100         | 0,103         |
| X Mg                         | 0,773         | 0,778         | 0,771         | 0,847        | 0,884        | 0,789         | 0,795         | 0,788         | 0,783         | 0,902       | 0,905       | 0,808         | 0,811         | 0,809         | 0,807         | 0,850         | 0,898         | 0,900         | 0,897         |

tableau 17 : analyses microsonde des olivines de Toad Lake et Castle Lake.

| N°Echantillons<br>N°Analyses | TOAD 40<br>44 | TOAD 40<br>53 | TOAD 40<br>54 | TOAD 35<br>83 | TOAD 35<br>82 | TOAD 35<br>93 | TOAD 35<br>101 | CL6<br>6 | CL6<br>11 | CL6<br>12 | CL6<br>16 | CL6<br>24 | CL6<br>88 | CL6<br>89 | CL6<br>91 | CL6<br>94 | CL6<br>96 | CL6<br>97 | CL6<br>100 | CL6<br>110 | CL6<br>111 | CL6<br>120 | CL6<br>121 |
|------------------------------|---------------|---------------|---------------|---------------|---------------|---------------|----------------|----------|-----------|-----------|-----------|-----------|-----------|-----------|-----------|-----------|-----------|-----------|------------|------------|------------|------------|------------|
| SiO2                         | 41,28         | 41,40         | 41,44         | 40,48         | 41,07         | 40,98         | 41,28          | 39,99    | 40,18     | 40,27     | 40,18     | 40,79     | 41,64     | 41,30     | 40,88     | 41,60     | 41,41     | 40,81     | 41,09      | 40,44      | 40,48      | 41,32      | 41,21      |
| Al2O3                        | 0,04          | 0             | 0             | 0             | 0,01          | 0             | 0,01           | 0        | 0,11      | 0,01      | 0         | 0         | 0,04      | 0         | 0         | 0,13      | 0,02      | 0,15      | 0,08       | 0,02       | 0          | 0,08       | 0          |
| TiO2                         | 0,02          | 0             | 0,03          | 0,02          | 0             | 0             | 0              | 0        | 0         | 0         | 0         | 0         | 0         | 0,03      | 0         | 0         | 0         | 0         | 0          | 0          | 0,06       | 0          | 0          |
| FeO                          | 9,69          | 9,73          | 9,81          | 8,90          | 9,51          | 9,58          | 10,00          | 18,30    | 11,14     | 11,11     | 13,27     | 10,77     | 10,44     | 11,51     | 11,29     | 11,47     | 11,91     | 11,93     | 18,03      | 11,38      | 11,95      | 11,91      | 11,75      |
| MgO                          | 49,44         | 48,95         | 48,84         | 48,93         | 48,84         | 49,25         | 49,24          | 41,81    | 48,46     | 49,04     | 47,12     | 49,02     | 48,36     | 47,76     | 47,74     | 47,71     | 47,78     | 46,95     | 40,85      | 47,24      | 47,04      | 47,34      | 49,20      |
| MnO                          | 0,05          | 0,03          | 0,09          | 0,17          | 0,15          | 0,17          | 0,07           | 0,35     | 0,20      | 0,08      | 0,11      | 0,06      | 0,21      | 0,21      | 0,15      | 0,14      | 0,15      | 0,17      | 0,37       | 0,13       | 0,05       | 0,16       | 0,10       |
| Cr2O3                        | 0             | 0,03          | 0             | 0             | 0,32          | 0             | 0,13           | 0        | 0         | 0         | 0         | 0         | 0         | 0         | 0         | 0         | 0         | 0,03      | 0,02       | 0          | 0,05       | 0          | 0          |
| NiO                          | 0,23          | 0,17          | 0,45          | 0,23          | 0,41          | 0,25          | 0,27           | 0,40     | 0,40      | 0,35      | 0,27      | 0,42      | 0,36      | 0,35      | 0,41      | 0,39      | 0,28      | 0,21      | 0,20       | 0,28       | 0,41       | 0,32       | 0,33       |
| Total                        | 100,75        | 100,31        | 100,46        | 98,73         | 100,31        | 100,21        | 101,00         | 100,85   | 100,49    | 100,86    | 100,95    | 101,08    | 101,05    | 101,16    | 100,47    | 101,44    | 101,55    | 100,25    | 100,84     | 99,49      | 100,04     | 101,11     | 101,59     |
| Si                           | 1,003         | 1,009         | 1,009         | 1,001         | 1,003         | 1,001         | 1,002          | 1,011    | 0,988     | 0,986     | 0,992     | 0,995     | 1,012     | 1,008     | 1,004     | 1,011     | 1,008     | 1,006     | 1,035      | 1,004      | 1,002      | 1,010      | 1,002      |
| Al                           | 0,001         | 0             | 0             | 0             | 0             | 0             | 0              | 0        | 0,003     | 0         | 0         | 0         | 0,001     | 0         | 0         | 0,004     | 0,001     | 0,004     | 0,002      | 0,001      | 0          | 0,002      | 0          |
| Ti                           | 0             | 0             | 0,001         | 0             | 0             | 0             | 0              | 0        | 0         | 0         | 0         | 0         | 0         | 0,001     | 0         | 0         | 0         | 0         | 0          | 0          | 0,001      | 0          | 0          |
| Fe                           | 0,197         | 0,198         | 0,196         | 0,184         | 0,194         | 0,195         | 0,203          | 0,387    | 0,229     | 0,228     | 0,274     | 0,220     | 0,212     | 0,235     | 0,232     | 0,233     | 0,242     | 0,246     | 0,380      | 0,236      | 0,247      | 0,243      | 0,239      |
| Mg                           | 1,790         | 1,779         | 1,774         | 1,804         | 1,778         | 1,794         | 1,782          | 1,576    | 1,777     | 1,791     | 1,734     | 1,782     | 1,751     | 1,737     | 1,748     | 1,729     | 1,733     | 1,728     | 1,534      | 1,748      | 1,736      | 1,725      | 1,748      |
| Mn                           | 0,001         | 0,001         | 0,002         | 0,004         | 0,003         | 0,004         | 0,001          | 0,007    | 0,004     | 0,002     | 0,002     | 0,001     | 0,004     | 0,004     | 0,003     | 0,003     | 0,003     | 0,004     | 0,008      | 0,003      | 0,001      | 0,003      | 0,002      |
| Cr                           | 0             | 0,001         | 0             | 0             | 0,006         | 0             | 0,002          | 0        | 0         | 0         | 0         | 0         | 0         | 0         | 0         | 0         | 0         | 0,001     | 0          | 0          | 0,001      | 0          | 0          |
| N                            | 0,004         | 0,003         | 0,009         | 0,005         | 0,008         | 0,005         | 0,005          | 0,008    | 0,008     | 0,007     | 0,005     | 0,008     | 0,007     | 0,007     | 0,008     | 0,008     | 0,005     | 0,004     | 0,004      | 0,008      | 0,008      | 0,006      | 0,006      |
| Total                        | 2,986         | 2,991         | 2,991         | 2,988         | 2,992         | 2,999         | 2,985          | 2,989    | 3,009     | 3,014     | 3,007     | 3,006     | 2,987     | 2,992     | 2,995     | 2,988     | 2,992     | 2,991     | 2,963      | 2,998      | 2,996      | 2,989      | 2,987      |
| X Fe                         | 0,099         | 0,100         | 0,099         | 0,093         | 0,098         | 0,098         | 0,102          | 0,197    | 0,114     | 0,113     | 0,136     | 0,110     | 0,108     | 0,119     | 0,117     | 0,119     | 0,123     | 0,125     | 0,198      | 0,119      | 0,125      | 0,124      | 0,120      |
| X Mg                         | 0,801         | 0,900         | 0,901         | 0,907         | 0,902         | 0,902         | 0,998          | 0,903    | 0,886     | 0,887     | 0,864     | 0,890     | 0,892     | 0,881     | 0,893     | 0,881     | 0,877     | 0,875     | 0,802      | 0,881      | 0,875      | 0,876      | 0,880      |

tableau 17 : analyses microsonde des olivines de Toad Lake et Caselle Lake.

| N°Echantillon | TOAD 15 | TOAD 15 | TOAD 15 | TOAD 15 | TOAD 15 | TOAD 15 | TOAD 12 | TOAD 12 | TOAD 12 | TOAD 8 | TOAD 8 | TOAD 40 | TOAD 40 | TOAD 40 | TOAD 40 | TOAD 40 | TOAD 40 | TOAD 40 | TOAD 21 |
|---------------|---------|---------|---------|---------|---------|---------|---------|---------|---------|--------|--------|---------|---------|---------|---------|---------|---------|---------|---------|
| N°Analyse     | 31      | 32      | 33      | 34      | 35      | 37      | 53      | 54      | 55      | 3      | 4      | 31      | 32      | 33      | 34      | 38      | 39      | 45      | 59      |
| SiO2          | 54,08   | 54,28   | 54,20   | 54,10   | 54,38   | 54,15   | 52,78   | 52,77   | 53,19   | 52,71  | 52,71  | 51,72   | 52,30   | 51,78   | 52,41   | 52,29   | 52,69   | 52,57   | 52,14   |
| Al2O3         | 2,47    | 2,58    | 2,40    | 2,31    | 2,35    | 2,99    | 1,83    | 1,71    | 1,29    | 3,18   | 3,35   | 3,11    | 2,99    | 2,77    | 2,66    | 2,99    | 3,24    | 3,10    | 1,96    |
| TiO2          | 0,11    | 0,07    | 0,10    | 0,07    | 0       | 0       | 0,38    | 0,49    | 0,12    | 0,26   | 0,22   | 0,29    | 0,33    | 0,30    | 0,29    | 0,39    | 0,34    | 0,52    | 0,35    |
| FeO           | 2,08    | 2,21    | 2,32    | 2,18    | 2,15    | 1,97    | 7,59    | 8,18    | 7,83    | 2,19   | 2,08   | 2,43    | 2,48    | 2,52    | 2,45    | 2,18    | 2,61    | 2,69    | 8,21    |
| MgO           | 17,69   | 17,30   | 17,38   | 17,53   | 17,37   | 17,02   | 14,53   | 14,02   | 14,63   | 16,32  | 16,32  | 16,53   | 16,44   | 16,66   | 16,49   | 16,63   | 16,50   | 16,78   | 14,54   |
| CaO           | 23,70   | 23,11   | 23,69   | 23,16   | 24,19   | 23,67   | 22,22   | 21,80   | 21,92   | 24,14  | 23,32  | 23,71   | 23,77   | 23,67   | 24,48   | 23,80   | 23,91   | 23,49   | 22,08   |
| MnO           | 0,03    | 0,05    | 0       | 0,05    | 0,12    | 0,04    | 0,21    | 0,18    | 0,20    | 0,03   | 0,06   | 0,13    | 0,09    | 0,05    | 0,01    | 0,04    | 0       | 0,13    | 0,18    |
| Cr2O3         | 0,42    | 0,51    | 0,36    | 0,41    | 0,35    | 1,13    | 0,12    | 0       | 0,06    | 0,81   | 1,12   | 1,07    | 1,10    | 1,01    | 0,82    | 1,04    | 1,15    | 0,87    | 0,06    |
| NiO           | 0       | 0,07    | 0,11    | 0,11    | 0,06    | 0       | 0       | 0,02    | 0       | 0,05   | 0,05   | 0       | 0,19    | 0,10    | 0,10    | 0       | 0,12    | 0,02    | 0,13    |
| Na2O          | 0,16    | 0,17    | 0,19    | 0,22    | 0,18    | 0,16    | 0,23    | 0,13    | 0,21    | 0,09   | 0,14   | 0,26    | 0,24    | 0,12    | 0,22    | 0,27    | 0,19    | 0,25    | 0,18    |
| Total         | 100,74  | 100,35  | 100,75  | 100,14  | 101,15  | 101,13  | 99,89   | 99,40   | 99,45   | 99,78  | 99,37  | 99,25   | 99,93   | 98,98   | 99,93   | 99,63   | 100,75  | 100,43  | 99,81   |
| Si            | 1,944   | 1,958   | 1,951   | 1,956   | 1,951   | 1,940   | 1,958   | 1,969   | 1,981   | 1,922  | 1,925  | 1,903   | 1,911   | 1,910   | 1,916   | 1,912   | 1,908   | 1,909   | 1,944   |
| Al            | 0,105   | 0,110   | 0,102   | 0,098   | 0,099   | 0,128   | 0,080   | 0,075   | 0,057   | 0,137  | 0,144  | 0,135   | 0,129   | 0,120   | 0,115   | 0,129   | 0,138   | 0,133   | 0,088   |
| Ti            | 0,003   | 0,002   | 0,003   | 0,002   | 0       | 0       | 0,011   | 0,014   | 0,003   | 0,007  | 0,006  | 0,008   | 0,009   | 0,008   | 0,008   | 0,011   | 0,009   | 0,014   | 0,010   |
| Fe            | 0,063   | 0,067   | 0,070   | 0,066   | 0,064   | 0,059   | 0,235   | 0,255   | 0,244   | 0,067  | 0,064  | 0,075   | 0,076   | 0,078   | 0,075   | 0,067   | 0,079   | 0,082   | 0,256   |
| Mg            | 0,948   | 0,929   | 0,932   | 0,945   | 0,929   | 0,909   | 0,804   | 0,780   | 0,812   | 0,887  | 0,889  | 0,907   | 0,896   | 0,918   | 0,899   | 0,906   | 0,891   | 0,909   | 0,808   |
| Ca            | 0,813   | 0,892   | 0,813   | 0,897   | 0,930   | 0,909   | 0,883   | 0,876   | 0,875   | 0,943  | 0,913  | 0,935   | 0,931   | 0,936   | 0,959   | 0,932   | 0,928   | 0,914   | 0,881   |
| Mn            | 0,001   | 0,002   | 0       | 0,002   | 0,004   | 0,001   | 0,007   | 0,006   | 0,006   | 0,001  | 0,002  | 0,004   | 0,003   | 0,002   | 0       | 0,001   | 0       | 0,004   | 0,008   |
| Cr            | 0,012   | 0,015   | 0,010   | 0,012   | 0,010   | 0,032   | 0,004   | 0       | 0,002   | 0,023  | 0,032  | 0,031   | 0,032   | 0,029   | 0,024   | 0,030   | 0,033   | 0,025   | 0,002   |
| N             | 0       | 0,002   | 0,003   | 0,003   | 0,002   | 0       | 0       | 0,001   | 0       | 0,001  | 0,001  | 0       | 0,006   | 0,003   | 0,003   | 0       | 0,003   | 0,001   | 0,004   |
| Na            | 0,011   | 0,012   | 0,013   | 0,015   | 0,013   | 0,011   | 0,017   | 0,009   | 0,015   | 0,006  | 0,010  | 0,019   | 0,017   | 0,009   | 0,016   | 0,019   | 0,013   | 0,018   | 0,013   |
| Total         | 4,000   | 3,987   | 3,997   | 3,996   | 4,002   | 3,987   | 3,999   | 3,985   | 3,995   | 3,994  | 3,986  | 4,017   | 4,010   | 4,011   | 4,015   | 4,007   | 4,002   | 4,008   | 4,010   |
| %En           | 49,30   | 49,20   | 48,70   | 49,50   | 48,20   | 48,40   | 41,70   | 40,70   | 41,90   | 46,70  | 47,60  | 47,20   | 47,00   | 47,40   | 46,50   | 47,50   | 48,90   | 47,60   | 41,40   |
| %Fs           | 3,30    | 3,60    | 3,60    | 3,50    | 3,50    | 3,20    | 12,60   | 13,60   | 12,90   | 3,60   | 3,50   | 4,10    | 4,10    | 4,10    | 3,90    | 3,60    | 4,20    | 4,50    | 13,40   |
| %Wo           | 47,40   | 47,20   | 47,70   | 47,00   | 48,30   | 48,40   | 45,70   | 45,70   | 45,20   | 49,70  | 48,90  | 48,70   | 48,90   | 48,50   | 49,60   | 48,90   | 48,90   | 47,90   | 45,20   |
| Al4           | 0,056   | 0,044   | 0,049   | 0,044   | 0,049   | 0,060   | 0,042   | 0,031   | 0,019   | 0,078  | 0,075  | 0,097   | 0,089   | 0,090   | 0,084   | 0,088   | 0,092   | 0,091   | 0,056   |
| Al6           | 0,049   | 0,066   | 0,053   | 0,054   | 0,050   | 0,068   | 0,038   | 0,044   | 0,038   | 0,059  | 0,069  | 0,038   | 0,040   | 0,030   | 0,031   | 0,041   | 0,046   | 0,042   | 0,030   |

tableau 18 : analyses microsonde des clinopyroxènes de Toad Lake.

| N°Echantillon<br>N°Analyse     | TOAD 21<br>60 | TOAD 21<br>61 | TOAD 35<br>87 | TOAD 35<br>88 | TOAD 35<br>96 | TOAD 35<br>97 | TOAD 35<br>98 | TOAD 17<br>1 | TOAD 17<br>4 | TOAD 17<br>7 | TOAD 17<br>8 | TOAD 17<br>9 | TOAD 17<br>10 | TOAD 17<br>12 | TOAD 17<br>13 | TOAD 17<br>14 | TOAD 17<br>15 |
|--------------------------------|---------------|---------------|---------------|---------------|---------------|---------------|---------------|--------------|--------------|--------------|--------------|--------------|---------------|---------------|---------------|---------------|---------------|
| SiO <sub>2</sub>               | 52,18         | 52,38         | 53,03         | 53,52         | 52,36         | 52,51         | 52,73         | 54,55        | 54,37        | 55,29        | 54,58        | 54,05        | 54,19         | 54,47         | 53,91         | 54,00         | 54,05         |
| Al <sub>2</sub> O <sub>3</sub> | 1,77          | 1,61          | 2,55          | 2,03          | 2,84          | 3,00          | 2,95          | 2,20         | 2,41         | 1,02         | 0,90         | 1,82         | 2,03          | 1,94          | 1,79          | 2,03          | 1,80          |
| TiO <sub>2</sub>               | 0,24          | 0,50          | 0,08          | 0             | 0,25          | 0,29          | 0             | 0,14         | 0,10         | 0,07         | 0,06         | 0,15         | 0,08          | 0,06          | 0,12          | 0             | 0,12          |
| FeO                            | 8,50          | 8,21          | 2,40          | 2,37          | 2,33          | 2,52          | 2,21          | 3,91         | 3,53         | 3,01         | 3,02         | 3,43         | 3,61          | 3,63          | 3,92          | 3,36          | 3,69          |
| MgO                            | 14,35         | 14,51         | 16,91         | 16,94         | 16,64         | 16,52         | 17,39         | 17,39        | 17,26        | 17,24        | 17,49        | 17,33        | 17,39         | 17,50         | 17,55         | 17,21         | 17,18         |
| CaO                            | 22,58         | 22,37         | 23,99         | 23,93         | 24,03         | 23,66         | 23,78         | 22,76        | 23,03        | 24,34        | 24,30        | 23,06        | 23,53         | 23,04         | 22,82         | 23,24         | 23,22         |
| MnO                            | 0,26          | 0,20          | 0,04          | 0,17          | 0,07          | 0,08          | 0,10          | 0,08         | 0,13         | 0,18         | 0,12         | 0,01         | 0,19          | 0             | 0,10          | 0             | 0,17          |
| Cr <sub>2</sub> O <sub>3</sub> | 0             | 0             | 0,64          | 0,34          | 1,10          | 1,17          | 0,72          | 0,11         | 0,20         | 0,14         | 0,08         | 0,09         | 0,06          | 0,21          | 0,15          | 0,19          | 0,04          |
| NiO                            | 0             | 0             | 0,03          | 0             | 0,19          | 0,02          | 0,08          | 0            | 0,02         | 0,01         | 0            | 0,05         | 0             | 0,15          | 0,05          | 0,13          | 0             |
| Na <sub>2</sub> O              | 0,22          | 0,19          | 0,29          | 0,22          | 0,31          | 0,33          | 0,20          | 0,19         | 0,22         | 0,06         | 0,08         | 0,13         | 0,16          | 0,06          | 0,22          | 0,16          | 0,16          |
| Total                          | 100,10        | 99,97         | 99,96         | 99,52         | 100,12        | 100,12        | 99,29         | 101,33       | 101,27       | 101,36       | 100,63       | 100,12       | 101,24        | 101,06        | 100,63        | 100,32        | 100,43        |
| Si                             | 1,945         | 1,950         | 1,932         | 1,955         | 1,911         | 1,913         | 1,931         | 1,958        | 1,952        | 1,984        | 1,976        | 1,963        | 1,951         | 1,961         | 1,954         | 1,958         | 1,961         |
| Al                             | 0,078         | 0,071         | 0,109         | 0,087         | 0,122         | 0,129         | 0,127         | 0,093        | 0,102        | 0,043        | 0,038        | 0,078        | 0,086         | 0,082         | 0,076         | 0,087         | 0,077         |
| Ti                             | 0,007         | 0,014         | 0,002         | 0             | 0,007         | 0,008         | 0             | 0,004        | 0,003        | 0,002        | 0,002        | 0,004        | 0,002         | 0,002         | 0,003         | 0             | 0,003         |
| Fe                             | 0,265         | 0,258         | 0,073         | 0,072         | 0,071         | 0,077         | 0,068         | 0,117        | 0,106        | 0,090        | 0,091        | 0,104        | 0,109         | 0,109         | 0,119         | 0,102         | 0,112         |
| Mg                             | 0,797         | 0,805         | 0,918         | 0,922         | 0,905         | 0,898         | 0,902         | 0,930        | 0,924        | 0,922        | 0,944        | 0,938        | 0,933         | 0,939         | 0,948         | 0,930         | 0,929         |
| Ca                             | 0,902         | 0,892         | 0,936         | 0,937         | 0,940         | 0,924         | 0,933         | 0,875        | 0,886        | 0,936        | 0,943        | 0,897        | 0,908         | 0,889         | 0,886         | 0,903         | 0,903         |
| Mn                             | 0,008         | 0,006         | 0,001         | 0,005         | 0,002         | 0,002         | 0,003         | 0,002        | 0,004        | 0,005        | 0,004        | 0            | 0,006         | 0             | 0,003         | 0             | 0,005         |
| Cr                             | 0             | 0             | 0,018         | 0,010         | 0,032         | 0,034         | 0,021         | 0,003        | 0,006        | 0,004        | 0,002        | 0,003        | 0,002         | 0,006         | 0,004         | 0,005         | 0,001         |
| Ni                             | 0             | 0             | 0,001         | 0             | 0,006         | 0,001         | 0,002         | 0            | 0,001        | 0            | 0            | 0,001        | 0             | 0,004         | 0,001         | 0,004         | 0             |
| Na                             | 0,016         | 0,014         | 0,020         | 0,016         | 0,022         | 0,023         | 0,014         | 0,013        | 0,015        | 0,004        | 0,008        | 0,009        | 0,011         | 0,004         | 0,015         | 0,011         | 0,011         |
| Total                          | 4,018         | 4,008         | 4,010         | 4,004         | 4,018         | 4,009         | 4,001         | 3,995        | 3,999        | 3,990        | 4,006        | 3,997        | 4,008         | 3,986         | 4,008         | 4,000         | 4,002         |
| %En                            | 40,40         | 41,10         | 47,60         | 47,60         | 47,20         | 47,20         | 47,30         | 48,30        | 48,10        | 47,20        | 47,60        | 48,40        | 47,70         | 48,50         | 48,50         | 48,10         | 47,70         |
| %Fs                            | 13,90         | 13,40         | 3,90          | 4,00          | 3,80          | 4,20          | 3,70          | 6,20         | 5,70         | 4,90         | 4,80         | 5,40         | 5,80          | 5,60          | 6,20          | 5,30          | 6,00          |
| %Wo                            | 45,70         | 45,50         | 48,50         | 48,40         | 49,00         | 48,60         | 49,00         | 45,50        | 46,20        | 47,90        | 47,60        | 46,20        | 46,40         | 45,90         | 45,30         | 46,60         | 46,30         |
| Al <sub>4</sub>                | 0,055         | 0,050         | 0,068         | 0,045         | 0,069         | 0,087         | 0,069         | 0,042        | 0,048        | 0,016        | 0,024        | 0,037        | 0,049         | 0,039         | 0,046         | 0,042         | 0,039         |
| Al <sub>6</sub>                | 0,023         | 0,021         | 0,041         | 0,042         | 0,033         | 0,042         | 0,058         | 0,051        | 0,054        | 0,027        | 0,014        | 0,041        | 0,037         | 0,043         | 0,030         | 0,045         | 0,038         |

tableau 18 : analyses microsonde des clinopyroxènes de Toad Lake.



| N°Echantillons<br>N°Analyses | TOAD 19<br>1 | TOAD 19<br>2 | TOAD 19<br>6 | TOAD 19<br>8 | TOAD 19<br>18 | TOAD 19<br>22 | TOAD 19<br>26 | TOAD 19<br>27 | TOAD 19<br>28 | TOAD 15<br>30 | TOAD 15<br>47 | TOAD 15<br>48 | TOAD 15<br>49 | TOAD 12<br>57 | TOAD 12<br>58 | TOAD 12<br>59 | TOAD 12<br>-1 | TOAD 12<br>1 | TOAD 12<br>2 | TOAD 12<br>3 |
|------------------------------|--------------|--------------|--------------|--------------|---------------|---------------|---------------|---------------|---------------|---------------|---------------|---------------|---------------|---------------|---------------|---------------|---------------|--------------|--------------|--------------|
| SiO2                         | 56,05        | 57,23        | 56,82        | 56,58        | 56,73         | 57,27         | 56,49         | 56,14         | 56,06         | 57,12         | 56,65         | 57,72         | 57,08         | 54,53         | 54,29         | 54,10         | 55,67         | 55,00        | 54,91        | 55,38        |
| Al2O3                        | 2,39         | 1,92         | 2,54         | 2,58         | 1,94          | 1,89          | 2,39          | 2,39          | 3,08          | 2,47          | 3,48          | 2,12          | 2,23          | 0,80          | 1,03          | 1,11          | 2,54          | 1,94         | 1,61         | 1,53         |
| TiO2                         | 0,20         | 0,05         | 0,21         | 0,30         | 0,15          | 0             | 1,05          | 0,40          | 0,14          | 0             | 0,01          | 0,25          | 0,10          | 0,28          | 0             | 0,20          | 0,19          | 0,18         | 0,16         | 0,23         |
| FeO                          | 6,60         | 6,53         | 6,35         | 6,01         | 6,39          | 6,42          | 6,05          | 5,75          | 6,26          | 5,62          | 5,54          | 6,10          | 5,98          | 18,71         | 18,78         | 18,57         | 30,75         | 28,98        | 28,65        | 29,37        |
| MgO                          | 33,41        | 33,66        | 32,80        | 32,30        | 33,42         | 33,87         | 32,90         | 33,56         | 33,15         | 33,98         | 32,30         | 33,64         | 33,89         | 24,80         | 24,65         | 24,34         | 30,75         | 28,98        | 28,65        | 29,37        |
| CaO                          | 0,74         | 0,39         | 1,78         | 1,62         | 0,19          | 0,37          | 1,68          | 0,52          | 0,60          | 0,82          | 1,67          | 0,67          | 0,61          | 1,00          | 0,73          | 0,97          | 0,72          | 0,55         | 0,81         | 0,56         |
| MnO                          | 0,21         | 0            | 0,10         | 0,10         | 0,11          | 0,23          | 0,05          | 0,13          | 0,13          | 0,26          | 0,11          | 0,18          | 0,15          | 0,41          | 0,44          | 0,28          | 0,15          | 0,37         | 0,40         | 0,40         |
| Cr2O3                        | 0,36         | 0,45         | 0,64         | 0,67         | 0             | 0,40          | 0,40          | 0,69          | 1,19          | 0,49          | 0,47          | 0,49          | 0,52          | 0             | 0             | 0             | 0             | 0            | 0,04         | 0            |
| NiO                          | 0,06         | 0,08         | 0,09         | 0,13         | 0             | 0,11          | 0,10          | 0             | 0             | 0,12          | 0,11          | 0,21          | 0,15          | 0,07          | 0             | 0,05          | 0,05          | 0,06         | 0            | 0,08         |
| Na2O                         | 0            | 0,02         | 0,01         | 0            | 0,05          | 0             | 0             | 0             | 0             | 0             | 0,01          | 0             | 0,02          | 0,06          | 0             | 0             | 0             | 0,01         | 0            | 0,01         |
| Total                        | 100,02       | 100,33       | 101,34       | 100,29       | 98,98         | 100,56        | 101,11        | 99,58         | 100,61        | 100,88        | 100,35        | 101,38        | 100,71        | 100,68        | 99,92         | 99,63         | 99,27         | 100,87       | 100,48       | 100,36       |
| Si                           | 1,939        | 1,967        | 1,943        | 1,950        | 1,972         | 1,965         | 1,934         | 1,942         | 1,927         | 1,950         | 1,945         | 1,963         | 1,953         | 1,982         | 1,986         | 1,984         | 1,958         | 1,948        | 1,955        | 1,963        |
| Al                           | 0,087        | 0,078        | 0,102        | 0,105        | 0,079         | 0,078         | 0,096         | 0,097         | 0,125         | 0,099         | 0,141         | 0,085         | 0,090         | 0,034         | 0,044         | 0,048         | 0,105         | 0,081        | 0,088        | 0,084        |
| Ti                           | 0,005        | 0,001        | 0,005        | 0,008        | 0,004         | 0             | 0,027         | 0,010         | 0,004         | 0             | 0             | 0,006         | 0,003         | 0,008         | 0             | 0,006         | 0,005         | 0,005        | 0,004        | 0,006        |
| Fe                           | 0,191        | 0,188        | 0,182        | 0,173        | 0,186         | 0,184         | 0,173         | 0,166         | 0,180         | 0,160         | 0,159         | 0,173         | 0,171         | 0,569         | 0,575         | 0,570         | 0,271         | 0,409        | 0,414        | 0,379        |
| Mg                           | 1,723        | 1,724        | 1,672        | 1,660        | 1,732         | 1,732         | 1,679         | 1,731         | 1,698         | 1,729         | 1,653         | 1,705         | 1,729         | 1,344         | 1,344         | 1,331         | 1,612         | 1,529        | 1,521        | 1,552        |
| Ca                           | 0,027        | 0,014        | 0,065        | 0,060        | 0,007         | 0,014         | 0,062         | 0,019         | 0,022         | 0,030         | 0,061         | 0,024         | 0,022         | 0,039         | 0,029         | 0,038         | 0,027         | 0,021        | 0,031        | 0,021        |
| Mn                           | 0,006        | 0            | 0,003        | 0,003        | 0,003         | 0,007         | 0,001         | 0,004         | 0,004         | 0,008         | 0,003         | 0,005         | 0,004         | 0,013         | 0,014         | 0,009         | 0,004         | 0,011        | 0,012        | 0,012        |
| Cr                           | 0,010        | 0,012        | 0,017        | 0,018        | 0             | 0,011         | 0,003         | 0,018         | 0,032         | 0,013         | 0,013         | 0,013         | 0,014         | 0             | 0             | 0             | 0             | 0            | 0,001        | 0            |
| Ni                           | 0,002        | 0,002        | 0,002        | 0,004        | 0             | 0,003         | 0,003         | 0             | 0             | 0,003         | 0,003         | 0,006         | 0,004         | 0,002         | 0             | 0,001         | 0,001         | 0,002        | 0            | 0,002        |
| Na                           | 0            | 0,001        | 0,001        | 0            | 0,003         | 0             | 0             | 0             | 0             | 0             | 0,001         | 0             | 0,001         | 0,004         | 0             | 0             | 0             | 0,001        | 0            | 0,001        |
| Total                        | 4,000        | 3,987        | 3,992        | 3,981        | 3,986         | 3,992         | 3,986         | 3,988         | 3,992         | 3,992         | 3,979         | 3,980         | 3,991         | 3,995         | 3,992         | 3,987         | 3,983         | 4,007        | 4,006        | 4,000        |
| %En                          | 88,50        | 89,50        | 87,00        | 87,60        | 89,80         | 89,40         | 87,70         | 89,10         | 88,20         | 89,70         | 88,10         | 89,40         | 89,70         | 68,40         | 68,50         | 68,30         | 84,20         | 77,60        | 76,90        | 79,00        |
| %Fs                          | 10,10        | 9,70         | 9,60         | 9,30         | 8,80          | 8,90          | 9,10          | 8,90          | 9,60          | 8,70          | 9,60          | 9,40          | 9,10          | 29,60         | 30,00         | 29,70         | 14,40         | 21,30        | 21,50        | 18,90        |
| %Wo                          | 1,40         | 0,80         | 3,40         | 3,10         | 0,40          | 0,70          | 3,20          | 1,00          | 1,20          | 1,60          | 3,30          | 1,20          | 1,20          | 2,00          | 1,50          | 2,00          | 1,40          | 1,10         | 1,60         | 1,10         |
| Al4                          | 0,061        | 0,033        | 0,057        | 0,050        | 0,028         | 0,035         | 0,068         | 0,058         | 0,073         | 0,050         | 0,055         | 0,037         | 0,047         | 0,018         | 0,014         | 0,016         | 0,042         | 0,052        | 0,045        | 0,037        |
| Al6                          | 0,036        | 0,045        | 0,045        | 0,055        | 0,051         | 0,041         | 0,030         | 0,039         | 0,052         | 0,049         | 0,086         | 0,048         | 0,043         | 0,016         | 0,030         | 0,032         | 0,063         | 0,029        | 0,023        | 0,027        |

tableau 19 : analyses microsonde des orthopyroxènes de Toad Lake et Castile Lake.

| N°Echantillons<br>N°Analyses | TOAD12<br>4 | TOAD12<br>8 | TOAD12<br>9 | TOAD12<br>13 | TOAD12<br>18 | TOAD12<br>19 | TOAD12<br>29 | TOAD 8<br>6 | TOAD 8<br>13 | TOAD 8<br>14 | TOAD 20<br>1 | TOAD 20<br>3 | TOAD 20<br>4 | TOAD 20<br>5 | TOAD 20<br>10 | TOAD 20<br>17 | TOAD 20<br>18 | TOAD 20<br>20 | TOAD 20<br>21 | TOAD 20<br>30 |
|------------------------------|-------------|-------------|-------------|--------------|--------------|--------------|--------------|-------------|--------------|--------------|--------------|--------------|--------------|--------------|---------------|---------------|---------------|---------------|---------------|---------------|
| SiO2                         | 55,34       | 55,29       | 54,32       | 54,29        | 53,36        | 53,78        | 55,68        | 56,05       | 55,73        | 56,25        | 55,32        | 55,79        | 55,35        | 56,38        | 54,86         | 55,28         | 55,48         | 55,84         | 55,36         | 54,84         |
| Al2O3                        | 1,72        | 1,98        | 1,83        | 1,52         | 1,96         | 2,18         | 1,48         | 2,87        | 2,89         | 3,06         | 2,36         | 1,88         | 1,42         | 1,18         | 1,10          | 2,24          | 2,09          | 3,03          | 2,29          | 1,91          |
| TiO2                         | 0,21        | 0,28        | 0,20        | 0,21         | 0,17         | 0,03         | 0,16         | 0,10        | 0,07         | 0,07         | 0,03         | 0,08         | 0,15         | 0,05         | 0,18          | 0,10          | 0,07          | 0,09          | 0,10          | 0,10          |
| FeO                          | 12,71       | 13,39       | 14,29       | 13,72        | 14,81        | 14,43        | 13,59        | 6,35        | 6,14         | 6,08         | 12,90        | 14,85        | 13,91        | 13,54        | 18,92         | 10,94         | 10,76         | 10,55         | 11,01         | 13,35         |
| MgO                          | 29,24       | 28,27       | 27,91       | 27,57        | 27,53        | 27,59        | 28,79        | 32,48       | 32,48        | 32,77        | 28,95        | 28,49        | 28,68        | 29,16        | 25,63         | 29,50         | 30,07         | 29,88         | 28,70         | 28,48         |
| CaO                          | 0,58        | 0,67        | 0,78        | 0,94         | 0,74         | 0,77         | 0,59         | 0,56        | 0,61         | 0,65         | 0,67         | 1,31         | 0,96         | 0,64         | 0,71          | 0,87          | 0,79          | 0,77          | 0,77          | 0,52          |
| MnO                          | 0,39        | 0,25        | 0,32        | 0,21         | 0,52         | 0,50         | 0,33         | 0,12        | 0,12         | 0,22         | 0,22         | 0,31         | 0,28         | 0,42         | 0             | 0,28          | 0,24          | 0,21          | 0,21          | 0,42          |
| Cr2O3                        | 0,09        | 0           | 0           | 0,07         | 0,25         | 0,35         | 0,05         | 0,82        | 0,52         | 0,54         | 0,40         | 0,27         | 0,03         | 0,07         | 0,03          | 0,37          | 0,35          | 0,35          | 0,47          | 0,17          |
| NiO                          | 0,09        | 0           | 0           | 0,05         | 0            | 0,16         | 0            | 0,07        | 0,07         | 0,10         | 0,08         | 0            | 0,07         | 0,03         | 0,07          | 0,04          | 0,04          | 0,14          | 0,06          | 0,01          |
| Na2O                         | 0,01        | 0,01        | 0           | 0            | 0            | 0            | 0,02         | 0           | 0,01         | 0            | 0,04         | 0            | 0            | 0,01         | 0             | 0,02          | 0             | 0             | 0,03          | 0             |
| Total                        | 100,38      | 100,14      | 99,65       | 98,58        | 99,34        | 98,79        | 100,69       | 99,23       | 98,68        | 98,74        | 100,97       | 100,99       | 100,86       | 101,48       | 101,50        | 99,64         | 99,89         | 100,79        | 100,00        | 99,78         |
| Si                           | 1,960       | 1,965       | 1,953       | 1,969        | 1,936        | 1,939        | 1,971        | 1,949       | 1,947        | 1,945        | 1,949        | 1,981        | 1,963        | 1,980        | 1,973         | 1,957         | 1,957         | 1,948         | 1,953         | 1,960         |
| Al                           | 0,072       | 0,083       | 0,078       | 0,065        | 0,084        | 0,093        | 0,062        | 0,118       | 0,123        | 0,125        | 0,098        | 0,079        | 0,059        | 0,049        | 0,047         | 0,093         | 0,087         | 0,125         | 0,095         | 0,080         |
| Ti                           | 0,006       | 0,007       | 0,005       | 0,006        | 0,005        | 0,001        | 0,004        | 0,003       | 0            | 0,002        | 0,001        | 0,002        | 0,004        | 0,001        | 0,005         | 0,003         | 0,002         | 0,002         | 0,003         | 0,003         |
| Fe                           | 0,377       | 0,388       | 0,430       | 0,416        | 0,448        | 0,435        | 0,402        | 0,185       | 0,179        | 0,176        | 0,380        | 0,441        | 0,413        | 0,398        | 0,569         | 0,324         | 0,317         | 0,308         | 0,325         | 0,399         |
| Mg                           | 1,544       | 1,498       | 1,498       | 1,490        | 1,489        | 1,483        | 1,519        | 1,684       | 1,691        | 1,689        | 1,521        | 1,402        | 1,517        | 1,528        | 1,374         | 1,557         | 1,581         | 1,554         | 1,562         | 1,516         |
| Ca                           | 0,022       | 0,026       | 0,030       | 0,037        | 0,029        | 0,030        | 0,022        | 0,021       | 0,023        | 0,024        | 0,025        | 0,050        | 0,036        | 0,024        | 0,027         | 0,033         | 0,030         | 0,029         | 0,029         | 0,020         |
| Mn                           | 0,012       | 0,008       | 0,010       | 0,006        | 0,016        | 0,015        | 0,01         | 0,004       | 0,004        | 0,006        | 0,007        | 0,008        | 0,008        | 0,012        | 0             | 0,008         | 0,007         | 0,004         | 0,008         | 0,013         |
| Cr                           | 0,003       | 0           | 0           | 0,002        | 0,007        | 0,010        | 0,001        | 0,017       | 0,014        | 0,015        | 0,011        | 0,008        | 0,001        | 0,002        | 0,001         | 0,010         | 0,010         | 0,010         | 0,013         | 0,005         |
| N                            | 0,003       | 0           | 0           | 0,001        | 0            | 0,005        | 0            | 0,002       | 0,002        | 0,003        | 0,003        | 0            | 0,002        | 0,001        | 0,002         | 0,001         | 0,001         | 0,004         | 0,002         | 0             |
| Na                           | 0,001       | 0,001       | 0           | 0            | 0            | 0            | 0,001        | 0           | 0,001        | 0            | 0,003        | 0            | 0            | 0,001        | 0             | 0,001         | 0             | 0             | 0,002         | 0             |
| Total                        | 4,000       | 3,986       | 4,002       | 3,992        | 4,015        | 4,011        | 3,992        | 3,983       | 3,984        | 3,985        | 3,997        | 3,972        | 4,003        | 3,994        | 3,998         | 3,987         | 3,992         | 3,984         | 3,990         | 3,996         |
| %En                          | 79,00       | 77,70       | 76,10       | 76,50        | 75,10        | 75,50        | 77,80        | 89,00       | 89,20        | 89,10        | 78,70        | 73,70        | 76,80        | 77,90        | 69,70         | 81,00         | 81,70         | 82,00         | 81,30         | 77,80         |
| %Fs                          | 19,90       | 21,00       | 22,40       | 21,70        | 23,50        | 22,90        | 21,10        | 9,80        | 9,60         | 9,60         | 20,00        | 23,70        | 21,30        | 20,90        | 28,90         | 17,30         | 16,80         | 16,50         | 17,20         | 21,10         |
| %Wo                          | 1,10        | 1,30        | 1,50        | 1,80         | 1,40         | 1,60         | 1,10         | 1,10        | 1,20         | 1,30         | 1,30         | 2,60         | 1,90         | 1,20         | 1,40          | 1,70          | 1,50          | 1,50          | 1,50          | 1,10          |
| Al4                          | 0,040       | 0,035       | 0,047       | 0,031        | 0,064        | 0,061        | 0,029        | 0,051       | 0,053        | 0,055        | 0,051        | 0,019        | 0,037        | 0,020        | 0,027         | 0,043         | 0,043         | 0,052         | 0,047         | 0,040         |
| Al6                          | 0,032       | 0,048       | 0,031       | 0,034        | 0,020        | 0,032        | 0,033        | 0,067       | 0,070        | 0,070        | 0,047        | 0,060        | 0,022        | 0,029        | 0,020         | 0,050         | 0,044         | 0,073         | 0,048         | 0,040         |

tableau 19 : analyses microsonde des orthopyroxènes de Toad Lake et Casile Lake.

| N°Echantillons<br>N°Analyses | TOAD 40<br>35 | TOAD 40<br>36 | TOAD 40<br>37 | TOAD 21<br>62 | TOAD 21<br>64 | TOAD 21<br>72 | TOAD 21<br>73 | TOAD 21<br>77 | TOAD 35<br>81 | TOAD 35<br>82 | TOAD 35<br>88 | TOAD 35<br>89 | TOAD22<br>21 | TOAD22<br>23 | TOAD22<br>27 | TOAD22<br>32 | CL29<br>59 | CL29<br>60 | CL29<br>61 | CL29<br>63 |
|------------------------------|---------------|---------------|---------------|---------------|---------------|---------------|---------------|---------------|---------------|---------------|---------------|---------------|--------------|--------------|--------------|--------------|------------|------------|------------|------------|
| SiO2                         | 56,57         | 56,74         | 56,49         | 54,00         | 53,71         | 53,93         | 53,55         | 53,98         | 56,42         | 56,24         | 57,04         | 56,29         | 54,69        | 54,16        | 55,15        | 53,87        | 55,95      | 56,84      | 56,26      | 56,49      |
| Al2O3                        | 2,80          | 2,51          | 2,61          | 1,18          | 1,09          | 1,19          | 1,06          | 0,99          | 2,42          | 2,20          | 2,07          | 2,48          | 1,32         | 1,25         | 1,27         | 1,35         | 1,35       | 1,41       | 1,43       | 1,81       |
| TiO2                         | 0,08          | 0,21          | 0,17          | 0,23          | 0,10          | 0             | 0,06          | 0             | 0             | 0,35          | 0,03          | 0,30          | 0,15         | 0,12         | 0,14         | 0,30         | 0          | 0,09       | 0          | 0,10       |
| FeO                          | 6,50          | 6,49          | 6,09          | 20,33         | 19,89         | 19,98         | 20,21         | 19,87         | 6,30          | 6,22          | 6,01          | 6,10          | 19,29        | 18,56        | 18,14        | 18,49        | 13,27      | 11,97      | 12,31      | 15,03      |
| MgO                          | 33,56         | 33,03         | 32,78         | 23,70         | 23,86         | 23,61         | 23,54         | 23,98         | 33,27         | 33,33         | 33,70         | 33,41         | 24,75        | 25,37        | 25,00        | 23,88        | 28,30      | 29,43      | 28,79      | 23,31      |
| CaO                          | 0,50          | 0,68          | 0,58          | 0,81          | 1,21          | 1,25          | 0,84          | 0,95          | 0,54          | 0,91          | 0,49          | 0,63          | 0,95         | 0,81         | 0,92         | 1,65         | 1,35       | 0,97       | 0,99       | 1,19       |
| MnO                          | 0,22          | 0,11          | 0,13          | 0             | 0,44          | 0,46          | 0,48          | 0,43          | 0,19          | 0,05          | 0,11          | 0,17          | 0,36         | 0,33         | 0,31         | 0,40         | 0,16       | 0,28       | 0,37       | 0,28       |
| Cr2O3                        | 0,69          | 0,78          | 0,67          | 0,12          | 0,17          | 0             | 0             | 0,12          | 0,47          | 0,94          | 0,28          | 0,39          | 0,05         | 0,02         | 0            | 0,01         | 0          | 0          | 0,06       | 0          |
| Na2O                         | 0             | 0             | 0,02          | 0,01          | 0,07          | 0,14          | 0,02          | 0,02          | 0,05          | 0,10          | 0,13          | 0             | 0,08         | 0            | 0            | 0,12         | 0          | 0,03       | 0,01       | 0          |
| Total                        | 100,92        | 100,63        | 99,76         | 100,38        | 100,54        | 100,58        | 99,76         | 100,34        | 99,66         | 100,36        | 99,88         | 99,77         | 101,64       | 100,63       | 100,83       | 101,07       | 100,38     | 101,02     | 101,22     | 98,51      |
| Si                           | 1,937         | 1,949         | 1,951         | 1,978         | 1,969         | 1,976         | 1,979         | 1,980         | 1,953         | 1,939         | 1,966         | 1,945         | 1,972        | 1,967        | 1,988        | 1,963        | 1,985      | 1,989      | 1,972      | 2,049      |
| Al                           | 0,113         | 0,102         | 0,114         | 0,051         | 0,047         | 0,051         | 0,046         | 0,043         | 0,099         | 0,089         | 0,084         | 0,101         | 0,056        | 0,054        | 0,054        | 0,058        | 0,058      | 0,058      | 0,059      | 0,077      |
| Ti                           | 0,002         | 0,005         | 0,004         | 0,008         | 0,003         | 0             | 0,002         | 0             | 0             | 0,009         | 0,001         | 0,008         | 0,004        | 0,004        | 0,004        | 0,008        | 0          | 0,002      | 0          | 0,003      |
| Fe                           | 0,186         | 0,186         | 0,178         | 0,623         | 0,610         | 0,612         | 0,625         | 0,609         | 0,192         | 0,179         | 0,173         | 0,176         | 0,582        | 0,564        | 0,547        | 0,594        | 0,394      | 0,350      | 0,381      | 0,456      |
| Mg                           | 1,713         | 1,691         | 1,688         | 1,294         | 1,304         | 1,290         | 1,297         | 1,311         | 1,717         | 1,713         | 1,731         | 1,721         | 1,330        | 1,373        | 1,343        | 1,297        | 1,496      | 1,535      | 1,556      | 1,260      |
| Ca                           | 0,018         | 0,025         | 0,021         | 0,032         | 0,048         | 0,049         | 0,033         | 0,037         | 0,020         | 0,034         | 0,018         | 0,023         | 0,037        | 0,032        | 0,036        | 0,064        | 0,051      | 0,036      | 0,037      | 0,046      |
| Mn                           | 0,006         | 0,003         | 0,004         | 0             | 0,014         | 0,014         | 0,015         | 0,013         | 0,006         | 0,001         | 0,003         | 0,005         | 0,011        | 0,010        | 0,009        | 0,012        | 0,005      | 0,008      | 0,011      | 0,009      |
| Cr                           | 0,019         | 0,021         | 0,018         | 0,003         | 0,005         | 0             | 0             | 0,003         | 0,013         | 0,026         | 0,008         | 0,011         | 0,001        | 0,001        | 0            | 0            | 0          | 0          | 0,002      | 0          |
| N                            | 0             | 0,002         | 0,001         | 0             | 0,002         | 0,004         | 0,001         | 0,001         | 0,001         | 0,003         | 0,004         | 0             | 0,002        | 0            | 0            | 0,004        | 0          | 0,001      | 0          | 0          |
| Na                           | 0             | 0             | 0,001         | 0             | 0             | 0,001         | 0             | 0             | 0             | 0,001         | 0,001         | 0             | 0            | 0,001        | 0            | 0            | 0          | 0          | 0          | 0          |
| Total                        | 3,994         | 3,984         | 3,978         | 3,987         | 4,002         | 3,997         | 3,998         | 3,997         | 3,991         | 3,994         | 3,989         | 3,990         | 3,995        | 4,005        | 3,981        | 4,000        | 3,987      | 3,979      | 3,988      | 3,921      |
| %En                          | 89,00         | 88,70         | 89,30         | 68,40         | 68,00         | 65,60         | 65,80         | 68,50         | 89,20         | 88,90         | 88,90         | 89,40         | 67,90        | 68,40        | 69,40        | 65,90        | 76,90      | 79,50      | 79,20      | 71,20      |
| %Fs                          | 10,00         | 9,90          | 9,50          | 32,00         | 31,60         | 31,90         | 32,50         | 31,60         | 9,80          | 9,40          | 9,20          | 9,40          | 30,20        | 29,00        | 28,70        | 30,80        | 20,50      | 18,80      | 18,90      | 26,20      |
| %Wo                          | 1,00          | 1,40          | 1,20          | 1,80          | 2,40          | 2,50          | 1,70          | 1,90          | 1,00          | 1,70          | 0,80          | 1,20          | 1,90         | 1,60         | 1,90         | 3,30         | 2,80       | 1,90       | 1,90       | 2,60       |
| Al4                          | 0,063         | 0,051         | 0,049         | 0,022         | 0,031         | 0,024         | 0,021         | 0,020         | 0,047         | 0,061         | 0,034         | 0,055         | 0,028        | 0,033        | 0,012        | 0,037        | 0,015      | 0,011      | 0,028      | 0,000      |
| Al6                          | 0,050         | 0,051         | 0,065         | 0,029         | 0,016         | 0,027         | 0,025         | 0,023         | 0,052         | 0,028         | 0,050         | 0,046         | 0,028        | 0,021        | 0,042        | 0,021        | 0,041      | 0,047      | 0,031      | 0,077      |

tableau 19 : analyses microsonde des orthopyroxènes de Toad Lake et Castile Lake.

| N°Echantillons<br>N°Analyses | TOAD22<br>16 | TOAD22<br>17 | TOAD22<br>18 | TOAD22<br>19 | TOAD22<br>20 | TOAD22<br>34 | TOAD22<br>35 | TOAD22<br>36 | CL28<br>39 | CL28<br>41 | CL28<br>43 | CL28<br>44 | CL28<br>51 | CL28<br>53 |
|------------------------------|--------------|--------------|--------------|--------------|--------------|--------------|--------------|--------------|------------|------------|------------|------------|------------|------------|
| SiO2                         | 45,80        | 45,78        | 45,68        | 45,93        | 42,92        | 46,27        | 44,90        | 45,08        | 45,95      | 46,78      | 45,38      | 45,32      | 45,53      | 45,24      |
| Al2O3                        | 35,39        | 35,59        | 34,96        | 34,91        | 31,82        | 35,23        | 35,20        | 34,93        | 35,65      | 34,70      | 35,56      | 35,43      | 35,72      | 35,24      |
| FeO                          | 0,16         | 0,27         | 0,20         | 0,29         | 0,66         | 0,31         | 0,35         | 0,50         | 0,06       | 0,15       | 0,19       | 0,22       | 0,07       | 0,07       |
| CaO                          | 19,40        | 19,00        | 19,19        | 17,64        | 23,13        | 18,66        | 19,37        | 19,27        | 18,99      | 18,35      | 18,85      | 18,92      | 19,21      | 18,53      |
| Na2O                         | 0,64         | 0,66         | 0,73         | 1,03         | 0,81         | 0,96         | 0,66         | 0,62         | 0,70       | 1,30       | 0,54       | 0,74       | 0,78       | 0,91       |
| K2O                          | 0            | 0,01         | 0,07         | 0,16         | 0,01         | 0            | 0            | 0,12         | 0          | 0          | 0          | 0          | 0          | 0          |
| Total                        | 101,39       | 101,31       | 100,83       | 99,96        | 99,35        | 101,43       | 100,48       | 100,52       | 101,35     | 101,28     | 100,52     | 100,63     | 101,31     | 99,99      |
| Si                           | 2,085        | 2,084        | 2,092        | 2,114        | 2,041        | 2,103        | 2,068        | 2,077        | 2,089      | 2,127      | 2,080      | 2,078      | 2,074      | 2,085      |
| Al                           | 1,899        | 1,910        | 1,898        | 1,894        | 1,784        | 1,887        | 1,911        | 1,897        | 1,910      | 1,860      | 1,921      | 1,915      | 1,918      | 1,914      |
| Fe                           | 0,006        | 0,010        | 0,008        | 0,011        | 0,026        | 0,012        | 0,013        | 0,019        | 0,002      | 0,006      | 0,007      | 0,008      | 0,003      | 0,003      |
| Ca                           | 0,946        | 0,927        | 0,942        | 0,870        | 1,179        | 0,909        | 0,956        | 0,951        | 0,925      | 0,894      | 0,926      | 0,930      | 0,938      | 0,915      |
| Na                           | 0,056        | 0,058        | 0,065        | 0,092        | 0,075        | 0,085        | 0,059        | 0,055        | 0,062      | 0,115      | 0,048      | 0,066      | 0,069      | 0,081      |
| K                            | 0            | 0,001        | 0,004        | 0,009        | 0,001        | 0            | 0            | 0,007        | 0          | 0          | 0          | 0          | 0          | 0          |
| Total                        | 4,992        | 4,990        | 4,999        | 4,990        | 5,106        | 4,996        | 5,007        | 5,006        | 4,988      | 5,002      | 4,982      | 4,997      | 5,002      | 4,998      |
| %An                          | 94,40        | 94,00        | 93,20        | 89,60        | 94,00        | 91,50        | 94,20        | 93,80        | 93,70      | 88,60      | 95,10      | 93,40      | 93,20      | 91,80      |
| %Ab                          | 5,60         | 5,90         | 6,40         | 9,50         | 6,00         | 8,50         | 5,80         | 5,50         | 6,30       | 11,40      | 4,90       | 6,60       | 6,80       | 8,20       |
| %Or                          | 0            | 0,10         | 0,40         | 0,90         | 0            | 0            | 0            | 0,70         | 0          | 0          | 0          | 0          | 0          | 0          |

03  
00

N°Echantillons  
N°Analyses

| N°Echantillons<br>N°Analyses | CL28<br>54 | CL28<br>55 | CL29<br>67 | CL29<br>68 | CL29<br>69 | CL29<br>70 | CL30<br>75 | CL30<br>76 | CL30<br>77 | CL30<br>78 |
|------------------------------|------------|------------|------------|------------|------------|------------|------------|------------|------------|------------|
| SiO2                         | 46,11      | 45,35      | 45,48      | 45,85      | 45,59      | 45,77      | 58,70      | 59,76      | 59,55      | 59,58      |
| Al2O3                        | 35,52      | 35,03      | 35,36      | 35,32      | 35,18      | 35,28      | 27,07      | 26,41      | 26,23      | 25,86      |
| FeO                          | 0,15       | 0,19       | 0,23       | 0,18       | 0,28       | 0,47       | 0          | 0,02       | 0,01       | 0          |
| CaO                          | 19,00      | 19,08      | 19,10      | 19,06      | 18,97      | 18,68      | 8,89       | 8,43       | 8,30       | 8,06       |
| Na2O                         | 0,79       | 0,86       | 0,79       | 0,74       | 0,69       | 0,94       | 6,86       | 6,92       | 6,85       | 7,34       |
| K2O                          | 0,03       | 0          | 0,01       | 0          | 0,01       | 0,05       | 0,04       | 0,03       | 0,01       | 0,04       |
| Total                        | 101,6      | 100,51     | 100,97     | 101,15     | 100,72     | 101,19     | 101,56     | 101,57     | 100,95     | 100,88     |
| Si                           | 2,092      | 2,084      | 2,080      | 2,091      | 2,089      | 2,089      | 2,588      | 2,627      | 2,632      | 2,638      |
| Al                           | 1,900      | 1,898      | 1,906      | 1,898      | 1,900      | 1,898      | 1,407      | 1,368      | 1,366      | 1,350      |
| Fe                           | 0,006      | 0,007      | 0,009      | 0,007      | 0,011      | 0,018      | 0          | 0,001      | 0          | 0          |
| Ca                           | 0,924      | 0,940      | 0,936      | 0,931      | 0,931      | 0,914      | 0,420      | 0,397      | 0,393      | 0,382      |
| Na                           | 0,070      | 0,077      | 0,070      | 0,065      | 0,061      | 0,083      | 0,586      | 0,590      | 0,587      | 0,630      |
| K                            | 0,002      | 0          | 0,001      | 0          | 0,001      | 0,003      | 0,002      | 0,002      | 0,001      | 0,002      |
| Total                        | 4,994      | 5,006      | 5,002      | 4,992      | 4,993      | 5,005      | 5,003      | 4,985      | 4,979      | 5,002      |
| %An                          | 92,80      | 92,50      | 93,00      | 93,40      | 93,80      | 91,40      | 41,60      | 40,20      | 40,1       | 37,7       |
| %Ab                          | 7,00       | 7,50       | 7,00       | 6,60       | 6,20       | 8,30       | 58,10      | 59,70      | 59,9       | 62,1       |
| %Or                          | 0,20       | 0          | 0          | 0          | 0          | 0,30       | 0,30       | 0,10       | 0          | 0,20       |

tableau 20 : analyses microsonde des plagioclases de Toad Lake et Castle Lake.

| N°Echantillons<br>N°Analyses | TOAD 19<br>12 | TOAD 19<br>13 | TOAD 19<br>14 | TOAD 19<br>20 | TOAD 8<br>7 | TOAD 8<br>9 | TOAD 8<br>10 | TOAD 8<br>12 | TOAD 20<br>22 | TOAD 20<br>29 | TOAD 40<br>46 | TOAD 40<br>47 | TOAD 40<br>48 | TOAD 40<br>49 | TOAD 40<br>50 | TOAD 40<br>52 | TOAD 35<br>84 | TOAD 35<br>85 | TOAD 35<br>90 | TOAD 35<br>91 | TOAD 35<br>100 |
|------------------------------|---------------|---------------|---------------|---------------|-------------|-------------|--------------|--------------|---------------|---------------|---------------|---------------|---------------|---------------|---------------|---------------|---------------|---------------|---------------|---------------|----------------|
| TO2                          | 0.36          | 0.29          | 0.54          | 0.43          | 0.09        | 0.18        | 0.08         | 0.09         | 1.74          | 0.67          | 0             | 0.37          | 0.53          | 0.54          | 0.53          | 0.54          | 0.13          | 0.13          | 0             | 0.44          | 0              |
| Al2O3                        | 28.23         | 28.40         | 28.61         | 30.94         | 34.40       | 34.88       | 35.05        | 34.63        | 7.84          | 20.82         | 29.25         | 29.50         | 28.79         | 29.21         | 28.91         | 29.05         | 31.51         | 33.04         | 33.45         | 36.11         | 33.99          |
| Cr2O3                        | 34.99         | 35.32         | 33.70         | 32.66         | 29.16       | 29.29       | 29.80        | 29.41        | 22.23         | 28.37         | 35.39         | 34.62         | 34.99         | 34.97         | 34.77         | 34.97         | 34.75         | 33.83         | 31.86         | 30.93         | 32.50          |
| FeO*                         | 23.28         | 22.92         | 25.02         | 24.18         | 20.59       | 20.20       | 19.84        | 20.62        | 58.96         | 42.53         | 22.03         | 22.51         | 21.54         | 22.32         | 22.02         | 20.90         | 20.04         | 21.16         | 20.53         | 19.75         | 19.07          |
| MnO                          | 0.23          | 0.23          | 0.32          | 0.28          | 0.18        | 0.24        | 0.23         | 0.12         | 0.33          | 0.43          | 0.20          | 0.35          | 0.11          | 0.17          | 0.25          | 0.18          | 0.21          | 0.19          | 0             | 0.17          | 0.13           |
| MgO                          | 12.37         | 12.27         | 10.91         | 11.23         | 13.63       | 13.85       | 14.12        | 13.63        | 1.32          | 4.97          | 13.13         | 12.82         | 12.80         | 12.56         | 12.68         | 13.18         | 12.50         | 12.85         | 12.99         | 13.27         | 13.45          |
| Total*                       | 99.36         | 99.43         | 99.10         | 99.73         | 98.05       | 98.65       | 98.22        | 98.50        | 92.42         | 97.89         | 100.00        | 99.97         | 98.76         | 99.77         | 99.16         | 98.82         | 98.14         | 101.20        | 98.83         | 100.87        | 99.14          |
| Ti                           | 0.065         | 0.053         | 0.098         | 0.078         | 0.016       | 0.032       | 0.014        | 0.016        | 0.394         | 0.133         | 0             | 0.067         | 0.096         | 0.097         | 0.096         | 0.098         | 0.023         | 0.023         | 0             | 0.077         | 0              |
| Al                           | 8.048         | 8.094         | 8.240         | 8.769         | 9.602       | 9.662       | 9.716        | 9.624        | 2.784         | 6.509         | 8.224         | 8.316         | 8.212         | 8.262         | 8.221         | 8.254         | 8.889         | 9.093         | 9.358         | 9.843         | 9.440          |
| Cr                           | 6.670         | 6.749         | 6.508         | 6.207         | 5.457       | 5.439       | 5.353        | 5.480        | 5.292         | 6.818         | 6.672         | 6.544         | 6.692         | 6.633         | 6.629         | 6.662         | 6.573         | 6.243         | 5.975         | 5.653         | 6.052          |
| Fe3+                         | 1.151         | 1.051         | 1.054         | 0.869         | 0.909       | 0.838       | 0.903        | 0.864        | 7.136         | 3.307         | 1.104         | 1.006         | 0.903         | 0.910         | 0.958         | 0.888         | 0.490         | 0.619         | 0.669         | 0.351         | 0.508          |
| Fe2+                         | 3.558         | 3.583         | 4.059         | 3.993         | 3.189       | 3.133       | 3.018        | 3.202        | 7.717         | 6.081         | 3.291         | 3.498         | 3.456         | 3.570         | 3.485         | 3.325         | 3.521         | 3.513         | 3.405         | 3.469         | 3.250          |
| Mn                           | 0.047         | 0.047         | 0.068         | 0.059         | 0.038       | 0.048       | 0.046        | 0.024        | 0.084         | 0.086         | 0.040         | 0.071         | 0.023         | 0.035         | 0.051         | 0.037         | 0.043         | 0.038         | 0.000         | 0.033         | 0.026          |
| Mg                           | 4.460         | 4.422         | 3.974         | 4.025         | 4.811       | 4.851       | 4.950        | 4.790        | 0.593         | 1.958         | 4.669         | 4.499         | 4.817         | 4.493         | 4.560         | 4.738         | 4.460         | 4.472         | 4.595         | 4.575         | 4.724          |
| Total                        | 23.999        | 23.999        | 24.000        | 24.000        | 24.000      | 24.001      | 24.000       | 24.000       | 24.000        | 24.000        | 24.000        | 23.999        | 23.999        | 24.000        | 24.000        | 24.000        | 23.999        | 24.001        | 24.000        | 24.001        | 24.000         |
| Fe2O3                        | 6.32          | 5.78          | 5.73          | 4.80          | 5.10        | 4.73        | 5.10         | 4.87         | 31.48         | 16.65         | 6.15          | 5.59          | 4.96          | 5.04          | 5.27          | 4.90          | 2.72          | 3.52          | 3.75          | 2.02          | 2.88           |
| FeO                          | 17.59         | 17.72         | 19.88         | 19.86         | 16.00       | 15.95       | 15.35        | 16.24        | 30.83         | 27.55         | 16.50         | 17.48         | 17.08         | 17.79         | 17.27         | 16.49         | 17.59         | 17.99         | 17.16         | 17.93         | 18.49          |
| Total                        | 99.99         | 100.01        | 99.67         | 100.21        | 98.56       | 99.13       | 98.73        | 98.99        | 95.57         | 98.56         | 100.82        | 100.53        | 98.26         | 100.28        | 99.88         | 99.31         | 99.41         | 101.55        | 99.21         | 100.87        | 99.42          |
| % Magn                       | 7.30          | 6.80          | 6.70          | 5.50          | 5.70        | 5.20        | 5.70         | 5.40         | 46.90         | 21.00         | 6.90          | 6.30          | 5.70          | 5.80          | 6.10          | 5.80          | 3.10          | 3.90          | 4.20          | 2.20          | 3.20           |
| % Herc                       | 50.70         | 50.90         | 52.10         | 55.30         | 60.10       | 60.60       | 60.80        | 60.30        | 18.30         | 41.40         | 51.40         | 52.40         | 52.00         | 52.30         | 52.00         | 52.20         | 55.70         | 57.00         | 58.50         | 62.10         | 59.00          |
| % Chro                       | 42.00         | 42.50         | 41.20         | 39.20         | 34.20       | 34.20       | 33.50        | 34.30        | 34.80         | 37.60         | 41.70         | 41.30         | 42.30         | 41.90         | 41.90         | 42.20         | 41.20         | 39.10         | 37.30         | 35.70         | 37.80          |

tableau 21 : analyses microonde des spinelles de Toad Lake.

| N°Echantillons<br>N°Analyses | CL6<br>9 | CL6<br>17 | CL6<br>21 | CL6<br>23 | CL6<br>101 | CL6<br>102 | CL6<br>103 | CL6<br>104 | CL6<br>105 | CL6<br>106 | CL6<br>107 | CL6<br>108 |
|------------------------------|----------|-----------|-----------|-----------|------------|------------|------------|------------|------------|------------|------------|------------|
| TiO2                         | 1,15     | 0,77      | 0,46      | 0,58      | 0,45       | 0,54       | 0,54       | 0,28       | 0,34       | 0,30       | 0,36       | 0,40       |
| Al2O3                        | 10,52    | 18,99     | 20,50     | 21,70     | 22,66      | 23,63      | 21,72      | 25,16      | 24,54      | 24,17      | 23,29      | 23,21      |
| Cr2O3                        | 30,67    | 39,34     | 35,97     | 38,50     | 38,61      | 36,92      | 35,18      | 36,33      | 37,29      | 38,04      | 37,82      | 37,54      |
| FeO *                        | 48,40    | 33,10     | 35,03     | 30,05     | 30,83      | 28,23      | 33,86      | 26,16      | 26,96      | 26,78      | 27,24      | 27,36      |
| MnO                          | 0,65     | 0,31      | 0,59      | 0,31      | 0,53       | 0,39       | 0,38       | 0,29       | 0,34       | 0,38       | 0,35       | 0,14       |
| MgO                          | 1,86     | 5,75      | 3,89      | 8,71      | 5,16       | 8,76       | 6,19       | 10,12      | 10,03      | 10,68      | 9,50       | 9,00       |
| Total *                      | 93,25    | 98,26     | 96,44     | 99,85     | 98,24      | 98,47      | 97,87      | 98,34      | 99,50      | 100,35     | 98,56      | 97,65      |
| Ti                           | 0,255    | 0,153     | 0,094     | 0,110     | 0,089      | 0,103      | 0,106      | 0,053      | 0,064      | 0,056      | 0,069      | 0,077      |
| Al                           | 3,660    | 5,931     | 6,550     | 6,474     | 7,007      | 7,078      | 6,702      | 7,430      | 7,198      | 7,019      | 6,946      | 7,004      |
| Cr                           | 7,155    | 8,239     | 7,707     | 7,702     | 8,005      | 7,416      | 7,279      | 7,194      | 7,334      | 7,407      | 7,563      | 7,596      |
| Fe3+                         | 4,674    | 1,523     | 1,556     | 1,603     | 0,811      | 1,299      | 1,807      | 1,270      | 1,340      | 1,464      | 1,354      | 1,246      |
| Fe2+                         | 7,274    | 5,813     | 6,386     | 4,758     | 5,953      | 4,701      | 5,606      | 4,211      | 4,271      | 4,054      | 4,410      | 4,612      |
| Mn                           | 0,163    | 0,070     | 0,135     | 0,066     | 0,118      | 0,084      | 0,084      | 0,062      | 0,072      | 0,079      | 0,075      | 0,030      |
| Mg                           | 0,818    | 2,271     | 1,572     | 3,286     | 2,018      | 3,319      | 2,416      | 3,780      | 3,721      | 3,922      | 3,583      | 3,435      |
| Total                        | 23,999   | 24,000    | 24,000    | 23,999    | 24,001     | 24,000     | 24,000     | 24,000     | 24,000     | 24,001     | 24,000     | 24,000     |
| Fe2O3                        | 21,04    | 7,64      | 7,63      | 8,42      | 4,11       | 6,79       | 9,17       | 6,74       | 7,16       | 7,89       | 7,11       | 6,47       |
| FeO                          | 29,47    | 26,23     | 28,17     | 22,48     | 27,13      | 22,12      | 25,61      | 20,10      | 20,52      | 19,68      | 20,84      | 21,54      |
| Total                        | 95,36    | 99,03     | 97,21     | 100,70    | 98,65      | 99,15      | 98,79      | 99,02      | 100,22     | 101,14     | 99,27      | 98,30      |
| % Magn                       | 30,20    | 9,70      | 9,80      | 10,20     | 5,10       | 8,20       | 11,40      | 8,00       | 8,40       | 9,20       | 8,50       | 7,90       |
| % Herc                       | 23,60    | 37,80     | 41,40     | 41,00     | 44,30      | 44,80      | 42,40      | 46,70      | 45,40      | 44,20      | 43,80      | 44,20      |
| % Chro                       | 46,20    | 52,50     | 48,80     | 48,80     | 50,60      | 47,00      | 46,20      | 45,30      | 46,20      | 46,60      | 47,70      | 47,90      |

tableau 22 : analyses microsonde des spinelles de Castle Lake.

| Echantillons | CL6 2 | CL6 13 | CL6 86 | CL6 87 | CL6 92 | CL6 93 | CL6 112 | CL6 113 | CL6 114 | CL6 118 | TOAD12 6 | TOAD12 11 | TOAD12 14 | TOAD20 | TOAD21 | TOAD21 | TOAD22 28 |
|--------------|-------|--------|--------|--------|--------|--------|---------|---------|---------|---------|----------|-----------|-----------|--------|--------|--------|-----------|
| SiO2         | 46,22 | 47,14  | 46,19  | 49,24  | 47,19  | 47,19  | 46,36   | 46,26   | 45,58   | 47,40   | 44,79    | 46,24     | 46,54     | 57,11  | 56,82  | 52,97  | 54,69     |
| TiO2         | 1,26  | 1,32   | 1,30   | 0,89   | 0,82   | 0,87   | 1,33    | 1,25    | 1,48    | 1,21    | 1,06     | 1,41      | 1,30      | 0,01   | 0,60   | 0      | 0,12      |
| Al2O3        | 11,62 | 10,98  | 11,20  | 9,09   | 11,97  | 11,30  | 11,42   | 11,61   | 11,59   | 11,62   | 13,29    | 11,92     | 10,44     | 1,14   | 1,48   | 3,05   | 1,81      |
| FeO          | 3,84  | 4,33   | 4,52   | 3,86   | 3,78   | 4,15   | 4,53    | 4,47    | 4,36    | 4,60    | 7,67     | 6,71      | 7,53      | 2,59   | 2,90   | 12,79  | 10,91     |
| MnO          | 0     | 0,09   | 0,05   | 0      | 0,07   | 0,15   | 0,04    | 0,15    | 0       | 0,07    | 0,10     | 0,07      | 0,17      | 0,05   | 0      | 0,19   | 0,16      |
| MgO          | 18,38 | 18,55  | 18,14  | 19,10  | 18,49  | 18,54  | 18,40   | 18,42   | 18,26   | 18,64   | 15,96    | 17,13     | 16,96     | 22,14  | 22,63  | 15,65  | 17,12     |
| CaO          | 12,31 | 12,90  | 12,52  | 12,78  | 12,54  | 12,26  | 12,24   | 12,62   | 12,35   | 12,15   | 11,69    | 11,41     | 11,67     | 13,06  | 13,30  | 10,74  | 11,97     |
| Na2O         | 2,18  | 2,07   | 2,14   | 1,68   | 2,21   | 2,01   | 2,11    | 2,08    | 2,04    | 1,97    | 1,65     | 1,51      | 1,54      | 0,19   | 0,19   | 0,59   | 0,39      |
| K2O          | 0,11  | 0,10   | 0,18   | 0,09   | 0,07   | 0,06   | 0,09    | 0,08    | 0,08    | 0,10    | 0,02     | 0         | 0         | 0      | 0      | 0      | 0,03      |
| NiO          | 0     | 0,10   | 0,07   | 0,05   | 0,11   | 0,01   | 0,14    | 0,13    | 0,12    | 0,09    | 0,11     | 0         | 0         | 0      | 0,30   | 0,02   | 0         |
| Cr2O3        | 1,70  | 1,70   | 1,63   | 1,65   | 1,14   | 0,83   | 1,58    | 1,69    | 1,59    | 0,94    | 0,02     | 0         | 0,03      | 0,35   | 0,07   | 0,08   | 0,07      |

| Echantillons | TOAD22 28 | TOAD22 37 | CL28 45 | CL28 46 | CL28 47 | CL28 48 | CL28 49 | CL28 50 | CL28 56 | CL28 57 | CL28 62 | CL28 66 | CL28 73 | CL30 79 | CL30 80 | CL30 81 | CL30 82 | CL30 83 | CL30 84 |
|--------------|-----------|-----------|---------|---------|---------|---------|---------|---------|---------|---------|---------|---------|---------|---------|---------|---------|---------|---------|---------|
| SiO2         | 51,36     | 50,03     | 53,17   | 53,79   | 53,32   | 54,25   | 53,02   | 51,33   | 53,05   | 53,06   | 53,67   | 48,14   | 52,55   | 51,57   | 51,28   | 50,13   | 51,45   | 48,24   | 50,59   |
| TiO2         | 0,86      | 1,20      | 0,21    | 0,09    | 0,13    | 0,27    | 0,34    | 0,99    | 0,30    | 0,33    | 0,34    | 1,98    | 0,50    | 0,91    | 0,97    | 0,97    | 0,99    | 1,87    | 1,10    |
| Al2O3        | 6,28      | 7,06      | 4,72    | 4,12    | 4,28    | 4,26    | 4,86    | 6,38    | 4,77    | 4,98    | 4,52    | 8,70    | 5,21    | 5,75    | 6,16    | 6,69    | 5,84    | 8,90    | 6,62    |
| FeO          | 9,14      | 11,43     | 9,57    | 10,25   | 10,05   | 9,78    | 9,42    | 9,61    | 9,24    | 9,51    | 9,28    | 10,15   | 9,44    | 11,35   | 11,31   | 11,23   | 11,62   | 12,00   | 11,22   |
| MnO          | 0,15      | 0,11      | 0,18    | 0,14    | 0,22    | 0,19    | 0,16    | 0,15    | 0,11    | 0,18    | 0,13    | 0,14    | 0,20    | 0,23    | 0,20    | 0,25    | 0,23    | 0,19    | 0,14    |
| MgO          | 17,93     | 16,35     | 18,00   | 18,07   | 17,69   | 17,90   | 18,18   | 16,65   | 18,52   | 17,78   | 18,58   | 15,64   | 17,81   | 16,20   | 16,62   | 16,05   | 15,82   | 14,37   | 15,81   |
| CaO          | 11,76     | 10,99     | 11,42   | 11,15   | 11,25   | 11,63   | 11,53   | 12,17   | 11,64   | 11,42   | 11,56   | 11,33   | 11,94   | 11,31   | 10,27   | 11,31   | 11,00   | 11,55   | 11,05   |
| Na2O         | 0,78      | 0,95      | 0,64    | 0,51    | 0,57    | 0,62    | 0,64    | 0,78    | 0,66    | 0,64    | 0,68    | 1,42    | 0,68    | 0,74    | 0,86    | 0,62    | 0,63    | 0,83    | 0,72    |
| K2O          | 0,02      | 0,03      | 0,08    | 0,06    | 0,05    | 0,01    | 0,02    | 0,05    | 0,02    | 0,01    | 0       | 0,03    | 0,04    | 0,12    | 0,06    | 0,03    | 0,16    | 0,11    | 0,07    |
| NiO          | 0,03      | 0         | 0,05    | 0,04    | 0       | 0,15    | 0       | 0       | 0,03    | 0       | 0,11    | 0       | 0       | 0,04    | 0       | 0,02    | 0       | 0,08    | 0       |
| Cr2O3        | 0         | 0,04      | 0       | 0       | 0       | 0       | 0,10    | 0,11    | 0       | 0       | 0       | 0,07    | 0       | 0,03    | 0,27    | 0,06    | 0,01    | 0       | 0,11    |

tableau 23 : analyses microsonde des amphiboles de Castile Lake et Toad Lake.

| Echantillons | epidote | TOAD12 | TOAD12 | TOAD12 | TOAD21 | TOAD21 | TOAD22 | TOAD40 | TOAD40 | TOAD40 | CL28 42 | CL30 85 | serpentine | CL19 3 | CL6 4 | CL6 5 | CL6 28 | CL6 27 | CL6 28 | CL6 98 |
|--------------|---------|--------|--------|--------|--------|--------|--------|--------|--------|--------|---------|---------|------------|--------|-------|-------|--------|--------|--------|--------|
| SiO2         | 43,38   | 40,79  | 37,71  | 44,96  | 42,79  | 39,59  | 35,25  | 37,70  | 40,87  | 40,16  | 44,23   | 40,14   | 40,83      | 45,23  | 45,22 | 43,23 | 43,36  |        |        |        |
| TiO2         | 0       | 0      | 0      | 0      | 0      | 0      | 0,11   | 0,12   | 0      | 0      | 0       | 0,04    | 0          | 0      | 0,01  | 0     | 0,07   |        |        |        |
| Al2O3        | 31,67   | 32,56  | 29,98  | 36,81  | 28,89  | 31,30  | 28,86  | 30,26  | 32,62  | 33,13  | 0,65    | 1,02    | 3,08       | 0,06   | 0,51  | 2,43  | 3,25   |        |        |        |
| MnO          | 0,02    | 0,08   | 0,08   | 0      | 0      | 0,04   | 0,08   | 0,20   | 0,01   | 0      | 0       | 0,26    | 0,03       | 0      | 0,12  | 0,04  | 0,08   |        |        |        |
| FeO          | 1,21    | 1,14   | 2,83   | 0,48   | 0,21   | 3,47   | 1,77   | 3,78   | 0,62   | 0,84   | 4,81    | 13,28   | 7,01       | 4,77   | 4,83  | 5,16  | 4,78   |        |        |        |
| MgO          | 0,01    | 0,06   | 0,05   | 0,07   | 0,01   | 0,02   | 0,09   | 1,38   | 0      | 0      | 37,65   | 39,10   | 37,44      | 38,85  | 39,10 | 37,24 | 37,77  |        |        |        |
| CaO          | 16,29   | 17,74  | 21,53  | 9,01   | 19,35  | 24,43  | 30,24  | 23,89  | 24,22  | 23,99  | 0,02    | 0,01    | 0,04       | 0      | 0,02  | 0     | 0      |        |        |        |
| Na2O         | 2,78    | 1,44   | 0,59   | 4,09   | 1,13   | 0,08   | 0,04   | 0,02   | 0,23   | 0,05   | 0       | 0,03    | 0,03       | 0      | 0     | 0     | 0      |        |        |        |
| K2O          | 0,09    | 0,01   | 0,14   | 1,13   | 1,13   | 0      | 0      | 0,01   | 0,02   | 0      | 0,14    | 0,37    | 0,21       | 0,01   | 0,01  | 0     | 0,02   |        |        |        |
| NiO          | 0       | 0,01   | 0,15   | 0,02   | 0      | 0,04   | 0      | 0      | 0,09   | 0      | 0,01    | 0       | 0          | 0,17   | 0,11  | 0     | 0,10   |        |        |        |
| Cr2O3        | 0       | 0,05   | 0      | 0      | 0      | 0      | 0      | 0      | 0      | 0      | 0,01    | 0       | 0          | 0      | 0     | 0,55  | 0,59   |        |        |        |
| Total        | 95,45   | 83,88  | 83,07  | 96,57  | 94,51  | 98,95  | 96,44  | 97,29  | 98,68  | 98,17  | 87,51   | 94,25   | 88,66      | 89,09  | 89,93 | 88,65 | 90,02  |        |        |        |

| Echantillons | CL6 99 | CL6 109 | TOAD17 5 | TOAD15 | TOAD15 | TOAD35 | Chlorite | TOAD21 | laac  | CL6 8 | CL6 10 | CL6 14 | CL6 15 | CL6 20 | CL6 22 | CL6 25 |
|--------------|--------|---------|----------|--------|--------|--------|----------|--------|-------|-------|--------|--------|--------|--------|--------|--------|
| SiO2         | 45,00  | 42,18   | 42,73    | 42,33  | 42,52  | 37,66  | 38,71    | 23,27  | 60,23 | 58,09 | 60,23  | 62,09  | 61,86  | 60,16  | 58,58  |        |
| TiO2         | 0,04   | 0       | 0        | 0      | 0,03   | 0,37   | 0        | 1,29   | 0     | 0     | 0      | 0,05   | 0,11   | 0,04   | 0      |        |
| Al2O3        | 2,24   | 2,47    | 1,71     | 0,93   | 0,96   | 0,04   | 0,07     | 14,57  | 1,48  | 2,10  | 1,48   | 0,80   | 1,88   | 0,89   | 1,65   |        |
| MnO          | 0,01   | 0,08    | 0,25     | 0      | 0,09   | 0,14   | 0,10     | 0,21   | 0,06  | 0,10  | 0,06   | 0      | 0,05   | 0,05   | 0      |        |
| FeO          | 4,98   | 4,83    | 4,67     | 2,41   | 2,12   | 6,89   | 5,97     | 44,95  | 2,63  | 2,63  | 2,22   | 2,35   | 2,49   | 3,70   | 2,59   |        |
| MgO          | 39,00  | 36,78   | 36,09    | 41,00  | 34,89  | 36,23  | 36,98    | 0,54   | 31,07 | 30,74 | 31,07  | 29,66  | 29,87  | 29,92  | 31,75  |        |
| CaO          | 0,04   | 0,07    | 0,19     | 3,28   | 3,28   | 0,18   | 0,07     | 0      | 0,01  | 0,01  | 0      | 0,02   | 0,04   | 0      | 0      |        |
| Na2O         | 0      | 0       | 0,02     | 0,02   | 0      | 2,00   | 0        | 0,03   | 0,04  | 0,04  | 0,02   | 0,04   | 0,19   | 0,08   | 0,05   |        |
| K2O          | 0      | 0,03    | 0        | 0      | 0      | 0      | 0        | 0,06   | 0     | 0     | 0      | 0      | 0,01   | 0      | 0      |        |
| NiO          | 0,21   | 0,13    | 0,09     | 0,06   | 0      | 0,30   | 0,23     | 0      | 0,02  | 0,02  | 0,08   | 0,08   | 0,13   | 0,24   | 0,05   |        |
| Cr2O3        | 0,52   | 0,56    | 0,10     | 0,70   | 0,27   | 0      | 0,14     | 0,21   | 0,48  | 0,48  | 0,25   | 0,29   | 0,53   | 0,32   | 0,35   |        |
| Total        | 92,04  | 87,11   | 85,85    | 87,54  | 84,17  | 83,81  | 82,27    | 85,13  | 94,21 | 94,91 | 95,41  | 95,38  | 96,76  | 95,38  | 95,02  |        |

tableau 24 : analyses de microsonde des épidotes, serpentines, chlorites et talcs de Toad Lake et Castle Lake.



Dans la même collection :

- N°1 - H. MARTIN - Nature, origine et évolution d'un segment de croûte continentale archéenne : contraintes chimiques et isotopiques. Exemple de la Finlande orientale. 392 p., 183 fig., 51 tabl., 4 pl. (1985). 140F.
- N°2 - G. QUERRE - Paléogénèse de la croûte continentale à l' archéen : les granitoïdes tardifs (2,5-2,4 Ga) de Finlande Orientale. Pétrologie et géochimie. 226 p., 74 fig., 41 tabl., 3 pl.(1985). 85F.
- N°3 - J. DURAND - Le Grès Armoricaïn. Sédimentologie. Traces fossiles. Milieux de dépôt. 150 p., 76 fig., 9 tabl., 19 pl. (1985). EPUISE
- N°4 - D. PRIOUR - Genèse des zones de cisaillement : Application de la méthode des éléments finis à la simulation numérique de la déformation des roches. 157 p., 106 fig., 7 tabl., (1985). 55F.
- N°5 - V. NGAKO - Evolution métamorphique et structurale de la bordure sud-ouest de la "série de Poli". Segment camerounais de la chaîne panafricaine. 185 p., 76 fig., 16 tabl., 12 pl. (1986). 70F.
- N°6 - J. DE POULPIQUET - Etude géophysique d'un marqueur magnétique situé sur la marge continentale sud-armoricaine. 159 p., 121 fig., 5 tabl. (1986). 55F.
- N°7 - P. BARBEY - Signification géodynamique des domaines granulitiques. La ceinture des granulites de Laponie : une suture de collision continentale d'âge Protérozoïque inférieur (1.9-2.4 Ga). 324 p., 89 fig., 46 tabl., 11 pl. (1986). 115F.

- N°8 - Ph. DAVY - Modélisation thermo-mécanique de la collision continentale. 233 p., 72 fig., 2 tabl. (1986). EPUISÉ
- N°9 - Y. GEORGET - Nature et origine des granites peralumineux à cordiérite et des roches associées. Exemples des granitoïdes du Massif Armoricaïn (France) : Pétrologie et géochimie. 250 p., 140 fig., 67 tabl., (1986).  
EPUISÉ
- N°10 - D. MARQUER - Transfert de matière et déformation progressive des granitoïdes. Exemple des massifs de l'Aar et du Gothard (Alpes centrales Suisses). 287 p., 134 fig., 52 tabl., 5 cartes hors-texte (1987).  
EPUISÉ
- N°11 - J.S. SALIS - Variation séculaire du champ magnétique terrestre. Direction et Paléointensité sur la période 7.000 - 70.000 BP dans la chaîne des Puys. 190 p., 73 fig., 28 tabl., 1 carte hors-texte (1987).  
90F.
- N°12 - Y. GERARD - Etude expérimentale des interactions entre déformation et transformation de phase. Exemple de la transition calcite-aragonite. 126 p., 42 fig., 3 tabl., 10 pl. (1987).  
75F.
- N°13 - H. TATTEVIN - Déformation et transformation de phases induites par ondes de choc dans les silicates. Caractérisation par la microscopie électronique en transmission. 150 p., 50 fig., 1 tabl., 13 pl. (1987).  
95F.
- N°14 - J.L. PAQUETTE - Comportement des systèmes isotopiques U-Pb et Sm-Nd dans le métamorphisme éclogitique. Chaîne Hercynienne et chaîne Alpine. 190 p., 88 fig., 39 tabl., 2 pl. (1987).  
95F.
- N°15 - B. VENDEVILLE - Champs de failles et tectonique en extension : modélisation expérimentale. 392 p., 181 fig., 1 tabl., 82 pl. (1987).  
265F.

N°16 - E. TAILLEBOIS - Cadre géologique des indices sulfurés à Zn, Pb, Cu, Fe du secteur de Gouézec-St-Thois : Dévono-Carbonifère du flanc Sud du Bassin de Châteaulin (Finistère). 195 p., 64 fig., 41 tabl., 8 pl. photo., 8 pl. h.texte. (1987). 110F.

N°17 - J.P. COGNE - Contribution à l'étude paléomagnétique des roches déformées. 204 p., 86 fig., 17 tabl., (1987). 90F.

N°18 - E. DENIS - Les sédiments briovériens ( Protérozoïque supérieur ) de Bretagne septentrionale et occidentale : Nature, mise en place et évolution. 263 p., 148 fig., 26 tab., 8 pl. (1988). 140F.

N°19 - M. BALLEVRE - Collision continentale et chemins P-T : l'unité pennique du Grand Paradis (Alpes Occidentales). 340 p., 146 fig., 10 tabl., (1988). 145F.

N°20 - J.P. GRATIER - L'équilibrage des coupes géologiques. Buts, méthodes et applications. Atelier du Groupe d'Etudes Tectoniques le 8 Avril 1987 à Rennes. 165 p., 82 fig., 2 tabl. (1988). 85F.

N°21 - R.P. MENOT - Magmatismes paléozoïques et structuration carbonifère du Massif de Belledonne (Alpes Françaises). Contraintes nouvelles pour les schémas d'évolution de la chaîne varisque ouest-européenne. 465 p., 101 fig., 31 tab., 6 pl., (1988). 200F.

N°22 - S. BLAIS - Les ceintures de roches vertes archéennes de Finlande Orientale : Géologie, pétrologie, géochimie et évolution géodynamique. 312 p., 107 fig., 98 tab., 11 pl. photo, 1 pl. h.texte, (1989). 160F.

- N°23 - A. CHAUVIN - Intensité du champ magnétique terrestre en période stable de transition, enregistrée par des séquences de coulées volcaniques du quaternaire. 217 p., 100 fig., 13 tab. (1989). 100F.
- N°24 - J.P. VUICHARD - La marge austroalpine durant la collision alpine : évolution tectonométamorphique de la zone de Sesia-Lanzo. 307 p., 143 fig., 26 tab., 6 pl. hors-texte. (1989). 170F.
- N°25 - C. GUERROT - Archéen et Protérozoïque dans la chaîne hercynienne ouest-européenne : géochimie isotopique (Sr-Nd-Pb) et géochronologie U-Pb sur zircons. 180 p., 68 fig., 29 tab., 1 pl. (1989). 90F.
- N°26 - J.L. LAGARDE - Granites tardi carbonifères et déformation crustale. L'exemple de la Méséta marocaine. 353 p., 244 fig., 15 pl. (1989). 210F.
- N°27 - Ph. BARDY - L'orogène cadomien dans le Nord-Est du Massif Armoricaïn et en Manche Occidentale. Etude tectonométamorphique et géophysique. 395 p., 142 fig., 7 tab., 1 pl. hors-texte. (1989). 175F.
- N°28 - D. GAPAIS - Les Orthogneiss : Structures, mécanismes de déformation et analyse cinématique. 377 p., 184 fig., 3 tab., (1989). 275F.
- N°29 - E. LE GOFF - Conditions pression-température de la déformation dans les orthogneiss : Modèle thermodynamique et exemples naturels. 321 p., 146 fig., 42 tab. (1989). 150F.
- N°30 - D. KHATTACH - Paléomagnétisme de formations paléozoïques du Maroc. 220 p., 97 fig., 35 tab., (1989). 100F.

- N°31 - A. HAIDER - Géologie de la formation ferrifère précambrienne et du complexe granulitique encaissant de Buur (Sud de la Somalie). Implications sur l'évolution crustale du socle de Buur. 215 p., 18 fig., 42 tab., 7 pl. 130 F. (1989).
- N°32 - T. DANIEL - Traitement numérique d'image appliqué à l'analyse texturale de roches déformées. 186 p., 121 fig., 4 tab., (1989). 210 F.
- N°33 - C. LECUYER - Hydrothermalisme fossile dans une paléocroûte océanique associée à un centre d'expansion lent : Le complexe ophiolitique de Trinity (N. Californie, U.S.A). 342 p., 109 fig., 73 tab., (1989). 200 F.
- N°34 - P. RICHARD - Champs de failles au dessus d'un décrochement de socle: modélisation expérimentale. 382 p., 137 fig., (1989). 400 F.
- N°35 - J. de BREMOND d'ARS - Estimation des propriétés rhéologiques des magmas par l'étude des instabilités gravitaires. Pétrologie du complexe plutonique lité de Guernesey. 370 p., 128 fig., 64 tabl., (1989). 180 F.
- N°36 - A. LE CLEAC'H - Contribution à l'étude des propriétés physiques des minéraux à haute pression : Spectroscopie et calcul des grandeurs thermodynamiques de la lawsonite, des épidotes et des polymorphes de SiO<sub>2</sub>. 190 p., 72 fig., 37 tabl., (1989). 100 F.



## BON DE COMMANDE

A retourner à :

Centre Armoricaïn d'Etude Structurale des Socles  
Mémoires et documents du CAESS  
Université de Rennes I - Campus de Beaulieu  
35042 - RENNES Cédex (France).

NOM .....  
ORGANISME .....  
ADRESSE .....

Veuillez me faire parvenir les ouvrages suivants :

| N°                 | Auteur | Nb Exemplaires | Prix Unitaire | TOTAL |
|--------------------|--------|----------------|---------------|-------|
|                    |        |                |               |       |
|                    |        |                |               |       |
|                    |        |                |               |       |
|                    |        |                |               |       |
|                    |        |                |               |       |
| Frais d'envoi :    |        |                |               |       |
| 1 volume : 20,00 F |        |                |               |       |
| Total              |        |                |               |       |
| Frais d'envoi      |        |                |               |       |
| Montant total      |        |                |               |       |

Veuillez établir votre chèque au nom de l' Agent comptable de l'Université de Rennes I et le joindre au bon de commande.





## RESUME

Le massif ophiolitique de Trinity comprend une nappe de péridotites mantellaires de  $2750\text{Km}^2$  et une séquence crustale mince en affleurements discontinus ( $<2\text{Km}$ ). Il est chevauché par les nappes volcano-sédimentaires d'âge ordovicien à dévonien d'Yreka-Callahan qui correspondent à des dépôts d'îles océaniques associés à une marge continentale. La structure du massif de Trinity suggère qu'il résulte d'une accréation océanique très lente. Les affleurements de gabbros constituent des chambres magmatiques de petite taille (1 km de diamètre) intrusives dans la péridotite mantellaire. Dans ces chambres, le magma évolue rapidement vers un système clos au cours duquel la densité des magmas contrôle les émissions volcaniques. La présence de lherzolites plagifères correspond soit à des phénomènes d'imprégnation magmatique soit à des "fenêtres" de péridotites mantellaires fertiles. L'étude des minéraux de ces péridotites et des enclaves présentes aux parois et planchers des chambres magmatiques rend compte des modifications chimiques considérables que subissent les magmas primaires en percolant lentement au sein du manteau supérieur. De tels magmas modifiés chimiquement contribuent à l'origine de la diversité des ordres de cristallisation observés dans les complexes ophiolitiques.

L'étude de l'activité hydrothermale fossile révèle un métamorphisme prograde vers la base de la séquence ophiolitique et un métamorphisme rétrograde au cours du temps. Le calcul de flux chimiques élémentaires a permis de quantifier les transferts chimiques au cours de l'altération hydrothermale et de définir les dimensions du système hydrothermal ainsi que l'établissement d'un bilan géochimique entre la paléocroûte océanique et l'hydrosphère.

L'étude isotopique du Sr précise une altération hydrothermale intense principalement dans la partie supérieure de la croûte océanique avec un maximum dans les gabbros isotropes au toit de la chambre magmatique et pour rapidement décroître dans les cumulats mafiques et ultramafiques. L'étude isotopique de l'oxygène supportée par des données microthermométriques sur inclusions fluides a révélé la complexité de l'activité hydrothermale qui a affecté l'ophiolite de Trinity et permet de discriminer trois phases hydrothermales de température décroissante au cours du temps. Le bilan établi sur la paléocroûte montre un enrichissement global en  $^{18}\text{O}$  aux dépens du réservoir océanique. Ce processus semble affecter les domaines océaniques engendrés dans les rides à expansion lente et peut s'expliquer par le développement latéral et profond d'un réseau de failles normales jouant un rôle prépondérant dans la circulation de fluides hydrothermaux de moyenne ou basse température dans l'histoire hors axe de la croûte océanique. La composition isotopique de l'océan siluro-ordovicien a été estimée à un  $\delta^{18}\text{O} = 0 \pm 1$  et peut indiquer l'absence d'évolution séculaire de la composition en oxygène de l'océan mondial depuis le Paléozoïque inférieur.